Beyond Click Chemistry: Ruthenium(II) Complexes of Tridentate Ligands Featuring 1,2,3-Triazole-derived Donors

Dissertation

zur Erlangung des akademischen Grades
doctor rerum naturalium (Dr. rer. nat.)

seit 1558

vorgelegt dem Rat der
Chemisch-Geowissenschaftlichen Fakultät
der Friedrich-Schiller-Universität Jena

von Diplom-Chemiker Benjamin Schulze
geboren am 10.07.1983 in Weimar

Gutachter:

1. Prof. Dr. Ulrich S. Schubert (Friedrich-Schiller-Universität Jena)
2. Prof. Dr. Benjamin Dietzek (Friedrich-Schiller-Universität Jena)
3. Prof. Dr. Stefan Hecht (Humboldt-Universität zu Berlin)

Tag der öffentlichen Verteidigung: 05.03.2014

„Ein gerader Weg führt immer nur ans Ziel." André Gide

Table of Contents

Documentation of Authorship

This section contains a list of the individual authors' contributions to the publications reprinted in this thesis.

A1)   B. Schulze, U. S. Schubert, "Beyond click chemistry – Supramolecular interactions of 1,2,3-triazoles", *Chem. Soc. Rev.* **2014**, *43*, 2522−2571.

B. Schulze:	preparation of the manuscript
U. S. Schubert:	correction of the manuscript, supervision

A2)   B. Schulze, C. Friebe, M. D. Hager, W. Günther, U. Köhn, B. O. Jahn, H. Görls, U. S. Schubert, "Anion complexation by triazolium 'ligands': Mono- and bis-tridentate complexes of sulfate", *Org. Lett.* **2010**, *12*, 2710−2713.

B. Schulze:	conception, synthesis and characterization of compounds, preparation of the manuscript
C. Friebe:	UV−vis absorption and emission measurements, assistance with the binding studies, correction of the manuscript
M. D. Hager:	correction of the manuscript
W. Günther:	assistance with NMR measurements
U. Köhn:	computational calculations
B. O. Jahn:	computational calculations
H. Görls:	single-crystal X-ray diffraction analysis
A. Winter:	correction of the manuscript
U. S. Schubert:	correction of the manuscript, supervision

A3)   B. Schulze, D. Escudero, C. Friebe, R. Siebert, H. Görls, U. Köhn, E. Altuntaş, A. Baumgaertel, M. D. Hager, A. Winter, B. Dietzek, J. Popp, L. González, U. S. Schubert, "A heteroleptic *bis*(tridentate) ruthenium(II) complex of a click-derived abnormal carbene pincer ligand with potential for photosensitizer application", *Chem. Eur. J.* **2011**, *17*, 5494−5498.

B. Schulze:	conception, synthesis and characterization of compounds, preparation of the manuscript
D. Escudero:	computational calculations, contribution to the manuscript preparation
C. Friebe:	UV−vis absorption and emission measurements, electrochemistry, spectroelectrochemistry, contribution to the manuscript preparation
R. Siebert:	excited-state lifetime measurements
H. Görls:	single-crystal X-ray diffraction analysis
U. Köhn:	computational calculations
E. Altuntas:	ESI MS measurements
A. Baumgaertel:	MALDI MS measurements
M. D. Hager, A. Winter:	correction of the manuscript
B. Dietzek, J. Popp:	correction of the manuscript, supervision
L. González:	correction of the manuscript, supervision
U. S. Schubert:	correction of the manuscript, supervision

A4)   S. Sinn, B. Schulze, C. Friebe, D. G. Brown, M. Jäger, E. Altuntaş, J. Kübel, O. Guntner, B. Dietzek, C. P. Berlinguette, U. S. Schubert, "Physicochemical analysis of ruthenium(II) sensitizers of 1,2,3-triazole-derived mesoionic carbene and cyclometalating ligands", *Inorg. Chem.* **2014**, *53*, 2083−2095.

S. Sinn	synthesis and characterization of compounds, contribution to the manuscript preparation
B. Schulze:	conception, manuscript preparation, supervision, construction and investigation of the dye-sensitized solar cells
C. Friebe:	UV−vis absorption and emission measurements, electrochemistry, spectroelectrochemistry, correction of the manuscript preparation
D. G. Brown:	assistance with the construction and investigation of the dye-sensitized solar cells, correction of the manuscript
M. Jäger:	computational calculations, correction of the manuscript
E. Altuntas:	ESI MS measurements
J. Kübel, O. Guntner:	lifetime measurements
B. Dietzek:	correction of the manuscript, supervision
C. P. Berlinguette:	correction of the manuscript, supervision
U. S. Schubert:	correction of the manuscript, supervision

A5)   B. Schulze, D. Escudero, C. Friebe, R. Siebert, H. Görls, S. Sinn, M. Thomas, S. Mai, J. Popp, B. Dietzek, L. González, U. S. Schubert, "Ruthenium(II) photosensitizers of tridentate click-derived cyclometalating ligands: A joint experimental and computational study", *Chem. Eur. J.* **2012**, *18*, 4010−4025.

B. Schulze:	conception, synthesis and characterization of compounds, preparation of the manuscript
D. Escudero:	computational calculations, contribution to the manuscript preparation
C. Friebe:	UV−vis absorption and emission measurements, electrochemistry, spectroelectrochemistry, contribution to the manuscript preparation
R. Siebert:	temperature-dependent excited-state lifetime measurements, contribution to the manuscript preparation
H. Görls:	single-crystal X-ray diffraction analysis
S. Sinn:	synthesis of compounds
M. Thomas, S. Mai:	computational calculations
J. Popp, B. Dietzek:	correction of the manuscript, supervision
L. González:	correction of the manuscript, supervision
U. S. Schubert:	correction of the manuscript, supervision

A6)   S. Sinn,[#] B. Schulze,[#] C. Friebe, D. G. Brown, M. Jäger, J. Kübel, B. Dietzek, C. P. Berlinguette, U. S. Schubert, "A heteroleptic *bis*(tridentate) ruthenium(II) platform featuring an anionic 1,2,3-triazolate-based ligand for application in the dye-sensitized solar cell", *Inorg. Chem.* **2014**, *53*, 1637−1645.

S. Sinn	synthesis and characterization of compounds, contribution to the manuscript preparation
B. Schulze:	conception, manuscript preparation, supervision, synthesis and characterization of compounds, construction and investigation of the dye-sensitized solar cells

C. Friebe:	UV–vis absorption and emission measurements, electrochemistry, spectroelectrochemistry, correction of the manuscript preparation
D. G. Brown:	assistance with the construction and investigation of the dye-sensitized solar cells, correction of the manuscript
M. Jäger:	computational calculations, correction of the manuscript
J. Kübel:	lifetime measurements
B. Dietzek:	correction of the manuscript, supervision
C. P. Berlinguette:	correction of the manuscript, supervision
U. S. Schubert:	correction of the manuscript, supervision

A7)   B. Schulze, D. G. Brown, K. C. D. Robson, C. Friebe, M. Jäger, E. Birckner, C. P. Berlinguette, U. S. Schubert, "Cyclometalated ruthenium(II) complexes featuring tridentate click-derived ligands for dye-sensitized solar cell applications", *Chem. Eur. J.* **2013**, *19*, 14171−14180.

B. Schulze:	conception, synthesis of characterization of compounds, construction and investigation of the dye-sensitized solar cells, manuscript preparation
D. G. Brown:	assistance with the construction and investigation of the dye-sensitized solar cells, correction of the manuscript
K. C. D. Robson:	assistance with the construction and investigation of the dye-sensitized solar cells
C. Friebe:	UV–vis absorption and emission measurements, electrochemistry, correction of the manuscript
M. Jäger	computational calculations, correction of the manuscript
E. Birckner:	lifetime measurements
C. P. Berlinguette:	correction of the manuscript, supervision
U. S. Schubert:	correction of the manuscript, supervision

A8)   C. Friebe,[#] B. Schulze,[#] H. Görls, M. Jäger, U. S. Schubert, "Designing cyclometalated ruthenium(II) complexes for anodic electropolymerization", *Chem. Eur. J.* **2014**, *20*, 2357−2366.

C. Friebe:	conception, electropolymerization, UV–vis absorption and emission measurements , electrochemistry, spectroelectrochemistry, manuscript preparation
B. Schulze:	conception, synthesis and characterization of compounds, manuscript preparation
H. Görls:	single-crystal X-ray diffraction analysis
M. Jäger:	computational calculations, contribution to the manuscript preparation
U. S. Schubert:	correction of the manuscript, supervision

Signature of the supervisor: ⎯⎯⎯⎯⎯⎯⎯⎯⎯⎯⎯⎯

Prof. Dr. Ulrich S. Schubert

[#]Equal author contribution

1   Introduction

The increasing global energy consumption[1] as well as the ecological and ethical consequences associated with fossil and nuclear fuels constitute an imperative to harness sustainable energy sources – ideally, the practically inexhaustible solar energy.[2−6] Promising approaches are to develop an artificial photosynthesis[5, 7−10] as well as efficient photovoltaic devices.[11−13] The fundamental requirement to convert solar energy to chemical or electric energy is to achieve a light-driven charge separation.[13−14] Ruthenium(II) complexes of suitable ligands can be considered as minimalistic entities that allow a charge separation upon the absorption of visible light.[15−18] Successful applications as sensitizers in photo-redox catalysis[19] and in dye-sensitized solar cells (DSSC)[12, 20−21] emphasize their potential to act as "molecular heterojunction". In contrast to most, purely organic sensitizers, these metal complexes exhibit a high (redox)stability.[13, 21] Notably, the photophysical and electrochemical properties of ruthenium(II) complexes can be tailored *via* ligand modifications. Additionally, to enable the construction of, *e.g.*, photo-redox active (supramolecular) assemblies,[22−25] a facile preparation of highly functional ligands is desirable. A concept that addresses this demand is "click chemistry", which deals with chemical reactions that are, amongst other, wide in scope, modular, stereospecific, chemoselective, and highly efficient.[26] Interestingly, the copper(I)-catalyzed azide−alkyne cycloaddition, the prime example for the concept of click chemistry, provides ready access to 1,2,3-triazoles, which are able to serve as pyridine surrogates.[27−29] Accordingly, virtually unlimited ligand architectures based on 1,2,3-triazoles are available and myriads of applications of the triazole's coordination chemistry have been reported, covering metal ion sensing, medicinal chemistry, catalysis, magnetic materials, and photovoltaic as well as electroluminescent devices.[27−34] Moreover, 1,2,3-triazoles are highly functional molecules offering various supramolecular interactions ranging from anion complexation *via* (charge-assisted) hydrogen and halogen bonds to metal coordination by anionic, neutral or cationic nitrogen donors as well as anionic and mesoionic carbon donors (Figure 1.1).[29]
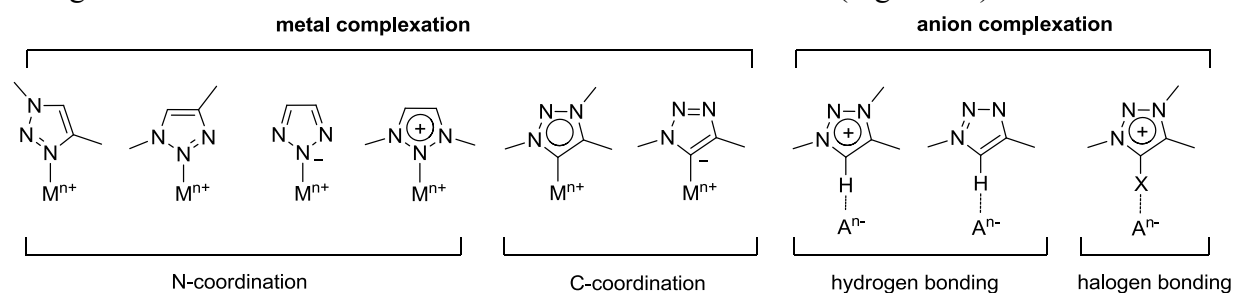

Figure 1.1. Schematic representation of selected supramolecular interactions of 1,2,3-triazoles and its derivatives.[29]

The goal of this thesis is to develop *bis*(tridentate) ruthenium(II) complexes featuring readily functionalized ligands based on 1,2,3-triazole or 1,2,3-triazole-derived donors for photosensitizer applications. The *bis*(tridentate) complex platform was chosen as it precludes the formation of isomers[21−23] and provides an increased stability by virtue of the chelate effect. As *bis*(tridentate) ruthenium(II) complexes often suffer from short excited-state lifetimes,[35−36] an important task is to impede their fast deactivation by the help of a judicious ligand design and, thereby, allow the exploitation of the charge-separated excited-state in terms of an artificial photosynthesis or photocatalysis. In this regard, the use of strongly σ-donating *N*-heterocyclic carbenes was proven to be successful.[37] On the other hand, for the purpose of

applications in DSSCs, a panchromatic absorption is most important, requiring strongly σ- *and* π-donating ligands. While the suppression of the radiationless deactivation is less pronounced in this case, excited-state lifetimes of moderate length are sufficient as the sensitizer is immobilized on the semiconductor surface and the electron injection into the conduction band is very fast. Accordingly, ruthenium(II) complexes relying on anionic chelates, for instance cyclometalating ligands,[38] were elected as they are known to rival the performance of famous ruthenium(II) polypyridyl sensitizers featuring monodentate thiocyanato ligands[20, 39–41] in the DSSC, while offering an enhanced complex stability and the potential to further optimize the efficiency *via* functionalization of the anionic chelating ligands.[42–45]

2   Theoretical Background

2.1   Ruthenium(II) polypyridyl complexes

Ruthenium(II) polypyridyl complexes[15–17, 22] show a great potential for the utilization of solar energy by means of photo-redox catalysis,[19] artificial photosynthesis,[7−10] and photovoltaic applications like dye-sensitized solar cells (DSSCs)[21, 42–43, 46] as they undergo a charge separation upon visible light absorption.[18] To exploit the charge-separated excited state, photo and redox stability as well as long excited-state lifetimes are required. A central dilemma is that *tris*(bidentate) ruthenium(II) complexes (*e.g.*, [Ru(bpy)$_3$](PF$_6$)$_2$, bpy = 2,2′-bipyridine) show long excited-state lifetimes at room temperature, while *bis*(tridentate) ruthenium(II) complexes (*e.g*, [Ru(tpy)$_2$](PF$_6$)$_2$, tpy = 2,2′:6′,2″-terpyridine) enable an isomer-free functionalization of the complexes (Figure 2.1).[21−23, 35−36, 47] Moreover, *bis*(tridentate) ruthenium(II) complexes offer an increased (photo)stability if the population of σ-antibonding orbitals in the excited state is avoided (*vide infra*).[48−51] To allow the design of *bis*(tridentate) ruthenium(II) complexes with improved photophysical properties, the electronic structure of the prototypical [Ru(tpy)$_2$](PF$_6$)$_2$ is discussed in the following.

[Ru(bpy)$_3$](PF$_6$)$_2$ [Ru(tpy)$_2$](PF$_6$)$_2$

− isomers formed with functionalized ligands   + isomer-free functionalization
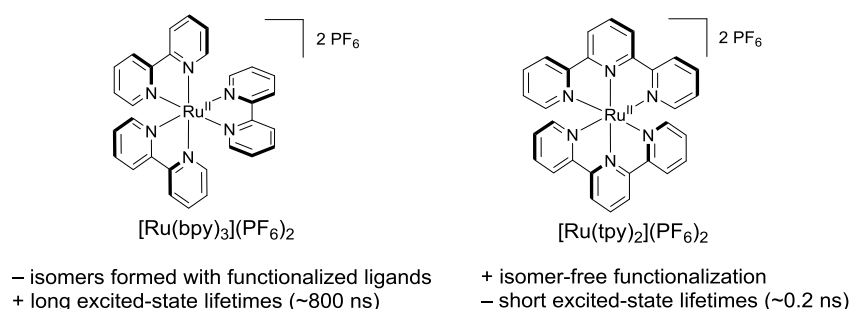+ long excited-state lifetimes (~800 ns)   − short excited-state lifetimes (~0.2 ns)

Figure 2.1. Schematic representation of well-known ruthenium(II) polypyridyl complexes. The excited-state lifetimes at room temperature are reported in refs. [48, 52−53].

In case of a virtual ruthenium(II) polypyridyl complex of ideal octahedral symmetry (O$_h$), the five d orbitals of the ruthenium(II) center are destabilized due to electrostatic repulsion mostly with the σ lone pairs of the six pyridine rings, resulting in two sets of d orbitals, namely the e$_g$ (d$_{z^2}$, d$_{x^2-y^2}$) orbitals, which are of σ symmetry and therefore more destabilized, and the t$_{2g}$ (d$_{xy}$, d$_{xz}$, d$_{yz}$) orbitals, which are less destabilized as they are of π symmetry (Figure 2.2). Furthermore, the 4d (e$_g$), 5s (a$_{1g}$), and 5p (t$_{1u}$) orbitals of the ruthenium(II) center can undergo strong σ interactions with ligand group orbitals of appropriate symmetry, leading to the formation of σ-antibonding and σ-bonding molecular orbitals (MOs). Due to the energy difference between the involved ligand and metal orbitals, the destabilized σ-antibonding orbitals are predominantly of metal character, *i.e.* the energy separation between e$_g$ and t$_{2g}$ orbitals is increased. If this ligand field splitting is sufficiently strong, the six valence electrons of the ruthenium(II) center will occupy the lower-lying t$_{2g}$ orbitals, while the e$_g$ orbitals remain unoccupied resulting in a singlet ground state (^{1}GS). In addition, ligand π and π* orbitals of appropriate symmetry can undergo a π donation and π back-donation, respectively, with the t$_{2g}$ orbitals, depending on the orbital overlap and energy of the interacting orbitals. Notably, in case of ruthenium(II), the π donation is repulsive and gives rise to a destabilization of the

occupied metal t_{2g} orbitals, while a stabilization of the latter can occur *via* π back-donation into low-lying π* orbitals of the ligand.[54−56]

In contrast, in *bis*(tridentate) ruthenium(II) complexes like [Ru(tpy)$_2$](PF$_6$)$_2$ the bite angle of about 158° of the tridentate ligands enforces a z compression/xy elongation of the octahedron[22, 47, 57−58] resulting in a lowered symmetry (D$_{2d}$).[59] Consequently, the degeneracy of the metal-d orbitals (t_{2g} and e_g) is reduced as the electrostatic repulsion is enhanced for orbitals with a z component and lowered for orbitals within the xy plane.[54] Likewise, the σ interaction with $d_{x^2-y^2}$ (b$_1$) and the π interactions with the d_{xy} orbital of the metal (b$_2$) are weakened and, as a consequence, the metal d_{xy} orbital represents the highest occupied molecular orbital (HOMO). On the other hand, in case of [Ru(tpy)$_2$](PF$_6$)$_2$, the (doubly degenerate) lowest unoccupied molecular orbital (LUMO) receives a major contribution from a π* (e) orbital of the tpy and, due to the π back-donation, a minor contribution from a d_{xz} (e) / d_{yz} (e) orbital of the metal.[60] The lowest-energy electronic excitations (b$_2$→e, e→e) are thus of MLCT character. At higher excitation energies, additional MLCT transitions as well as ligand-centered (LC) and metal-centered (MC) transitions can occur; however, after internal conversion (IC), ultrafast intersystem crossing (ISC), and intramolecular vibrational relaxation (IVR),[61−62] the excited electron will occupy the tpy-based LUMO and the corresponding excited state can thus be described as triplet MLCT excited state (^{3}MLCT).
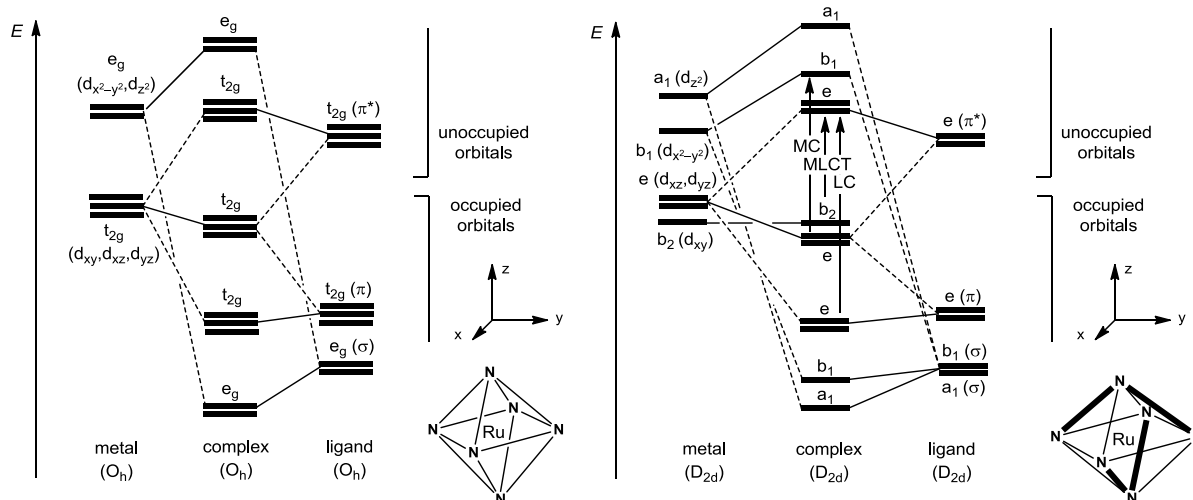

Figure 2.2. Simplified qualitative MO scheme for a virtual, octahedral ruthenium(II) polypyridyl complex (left) and [Ru(tpy)$_2$](PF$_6$)$_2$ (right).[60, 63] The σ interactions with 5s and 5p orbitals of the metal and weakly or non-interacting ligand orbitals are omitted for clarity.

The ^{3}MLCT can undergo a direct radiative and radiationless deactivation to the ^{1}GS or a radiationless deactivation *via* upper-lying excited states that are thermally accessible at room temperature, namely a ^{3}MLCT with a slightly increased singlet character (^{3}MLCT′)[51, 64−66] and, more importantly, a triplet MC excited state (^{3}MC). In case of [Ru(tpy)$_2$](PF$_6$)$_2$, the ^{3}MC, associated with the occupation of a σ-antibonding molecular orbital of predominant $d_{x^2-y^2}$ character (b$_1$), is low in energy due to the unfavorable bite angle (*vide supra*).[22, 58, 63] While for the vertical excitation at the ground-state nuclear coordinates (Born−Oppenheimer approximation), a large energy separation between the ^{3}MLCT and the ^{3}MC can be calculated ($\Delta E \sim$ 3,000 cm^{-1}), the nuclear reorganization upon the ^{3}MLCT→^{3}MC transition has to be considered (Figure 2.3).[52] As a σ*($d_{x^2-y^2}$) orbital is occupied in the ^{3}MC, this state features significantly elongated Ru−N bonds in the xy plane at its energy minimum.[63] Accordingly, the ^{3}MLCT and ^{3}MC potential energy curves are offset and almost isoenergetic,[67] resulting in a

significantly lower barrier for the ^{3}MLCT→^{3}MC transition ($\Delta E \sim 1{,}700$ cm^{-1}).[52, 58] Importantly, the nuclear coordinates in the vibrational ground state of the ^{3}MC coincide to a large extent with coordinates of the vibrationally excited ^{1}GS, *i.e.* a large Franck−Condon overlap is given, which implies a high probability for the ^{3}MC→^{1}GS ISC.[8, 68−72] Furthermore, as any radiationless transition between electronic states is formally forbidden, the rate of the radiationless deactivation depends on the availability of "promoting modes", which enable a mixing between the initial and the final state.[8, 18, 69, 71, 73−76] In case of an ISC, the radiationless deactivation additionally depends on the extent of spin−orbit coupling.[18, 68-69, 77] Ultimately, the ^{3}MC is the main deactivation pathway in case of [Ru(tpy)$_2$](PF$_6$)$_2$[52, 78] and, due to the weakened coordination, the ^{3}MC also gives rise to photodecomposition.[8, 49, 51]
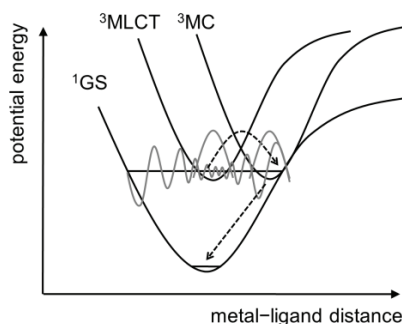

Figure 2.3. Potential energy curves of ground and relevant excited states of ruthenium(II) polypyridyl complexes (the ^{3}MLCT′ is omitted for clarity) and illustration of the significant Franck−Condon overlap between ^{3}MC and ^{1}GS vibrational wavefunctions.[8, 72]

Accordingly, a major strategy to obtain *bis*(tridentate) ruthenium(II) complexes with long-excited state lifetimes focusses on the destabilization of the ^{3}MC and/or the stabilization of the ^{3}MLCT.[35−36] The former can be achieved by increasing the σ donor strength of the ligands for instance by the incorporation of *N*-heterocyclic carbenes, which allows to achieve excited-state lifetimes in the μs range.[37] An alternative strategy is to increase the bite angle of the ligands in order to achieve a more octahedral coordination environment.[47] In analogy to [Ru(bpy)$_3$](PF$_6$)$_2$,[79] the LUMO is thus exclusively a ligand π* orbital and the removal of the metal contribution to the LUMO is assumed to impede the ^{3}MLCT→^{3}MC transition.[63] A fundamentally different strategy – the bichromophoric approach – relies on the sensitization of a long-lived triplet excited state (usually a ^{3}ππ) of an organic chromophore, which is attached to the ruthenium(II) complex. If the ^{3}ππ is energetically close to the ^{3}MLCT, both states can equilibrate and the ^{3}MLCT→^{1}GS decay is delayed.[35−36] A combination of the latter strategies, *i.e.* a bichromophoric system with expanded bite angles, yielded a *bis*(tridentate) ruthenium(II) complex with an excited-state lifetime of 42 μs.[80] However, the extrinsic optimization *via* additional chromophores restricts the possibility to functionalize the ruthenium(II) complexes and hence their versatility. Furthermore, the ^{3}ππ is not a charge-separated excited state, which compromises the most interesting feature of this kind of complexes.

When introducing strong σ- *and* π-donors, *e.g.* carbanions[81] or anionic *N*-heterocycles,[82] into *bis*(tridentate) ruthenium(II) complexes, beside the ^{3}MC destabilization, the ^{3}MLCT and, in particular, the ^{1}GS are destabilized, resulting in a moderate ^{3}MC−^{3}MLCT energy separation as well as a small ^{3}MLCT−^{1}GS energy gap. The latter increases the probability for a direct ^{3}MLCT→^{1}GS radiationless transition due to a larger corresponding Franck−Condon overlap integral (energy gap law).[8, 18, 68−69, 83−84] As a result, the corresponding ruthenium(II)

complexes show a panchromatic absorption, which is crucial for a successful application in DSSCS, while the excited-state lifetimes are typically within the range of 1 to 100 ns.[35-36]

2.2   Electronic properties of 1,2,3-triazoles and 1,2,3-triazolylidenes

While the thermal (3+2) $[_\pi 4_s +_\pi 2_s]$ 1,3-dipolar cycloaddition between an organic azide and an alkyne, resulting in the formation of functionalized 1,2,3-triazoles, requires elevated temperatures and shows only a low regioselectivity, Meldal *et al.*[85] and Fokin, Sharpless *et al.*[86] independently reported that both the reactivity and regioselectivity of the reaction can be dramatically enhanced by the addition of catalytic amounts of copper(I).[87−88] In fact, the copper(I)-catalyzed azide−alkyne cycloaddition (CuAAC) is one of the most efficient chemical reactions in organic chemistry and has become the prime example for the concept of click chemistry.[26]

In order to obtain ruthenium(II) complexes of readily synthesized and highly functionalized polypyridyl-analogous ligands, the pyridine rings of the chelating ligands can be partially or entirely replaced by 1,2,3-triazoles (Figure 2.4).[89−94] To enable the design of electronically tailored ruthenium(II) complexes, the electronic consequences of ligand modifications need to be known. Conversely, ruthenium(II) complexes are predestinated to investigate the electronic properties of new ligands.[95]
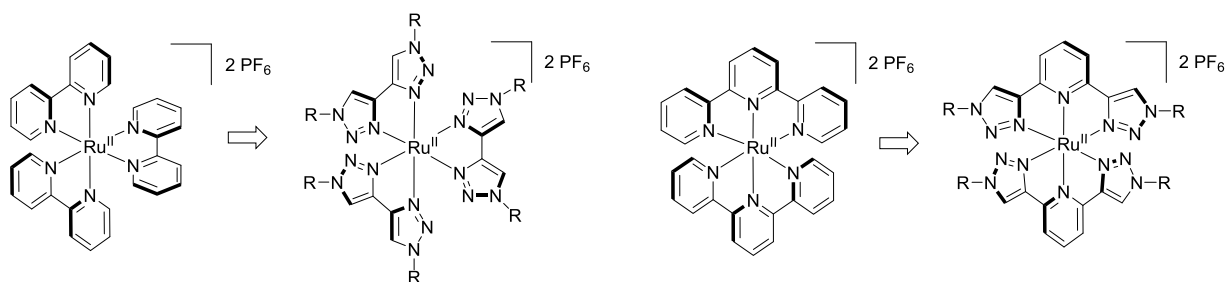

Figure 2.4. Schematic representation of ruthenium(II) polypyridyl complexes and their 1,2,3-triazole-based counterparts.[89−90, 93−94]

As basis for the interpretation of the properties of the resulting complexes, diagnostic parameters of the 1,2,3-triazole and pyridine ring should be compared first (Figure 2.5). The proton affinity (PA),[96−97] which correlates well with the energy of a σ lone pair,[98−100] is higher in case of pyridine. Furthermore, the σ donor strength of the 3-nitrogen of the 1,2,3-triazole depends on the electronic nature of the substituents.[97, 101−103] Notably, the 2-nitrogen of the 1,2,3-triazole is an even weaker σ donor and its coordination is usually not observed unless it is supported by a pendant donor.[104−106] The increased electron density of the pyridine nitrogen relative to the 3-nitrogen of the 1,2,3-triazole is also reflected in the calculated natural bond orbital (NBO) charges of −0.48 and −0.29, respectively.[103, 106] Accordingly, the 1,2,3-triazole is of weaker σ-donor strength than pyridine, which is reasonable regarding its high degree of *aza* substitution.[98]

Furthermore, although the orbital coefficients will also play a role, the relative π donor and π acceptor properties of 1,2,3-triazole and pyridine can be estimated by comparing the π and π* orbital energies (Figure 2.5).[98, 107] Accordingly, pyridine is expected to be both a stronger π acceptor and π donor than the 1,2,3-triazole. For ligands containing both 1,2,3-triazole and pyridine, an intermediate π acceptor and π donor strength compared to the ligands consisting of either 1,2,3-triazoles or pyridines is expected.[108] This depends, however, on the extent of π conjugation within a multidentate ligand. 1,2,3-Triazoles are known to interrupt the π

conjugation between the 1,4-substituents,[109–114] which is attributed to the presence of the lone pair of the 1-nitrogen enforcing a cross-conjugation.[115–117] As a result, the π system of 1,2,3-triazole-containing multidentate ligands might be less efficiently delocalized giving rise to an increased π donor strength, while the π acceptor strength is further diminished.[89, 93]
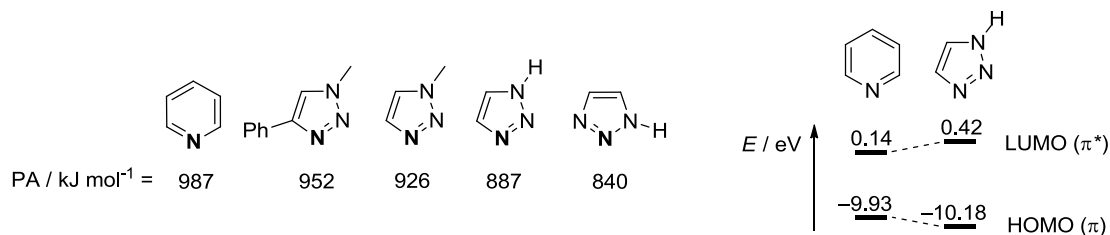

PA / kJ mol^{-1} =   987   952   926   887   840

Figure 2.5. Comparison of the electronic properties of pyridine and selected 1,2,3-triazoles. Left: Calculated proton affinity (PA, *N*-donor atom in boldface).[96–97] Right: Selected AM1 frontier orbital energies.[98, 107]

In practice, when comparing the homoleptic *bis*(tridenate) ruthenium(II) complexes of either tpy or 2,6-*bis*(1*H*-1,2,3-triazol-4-yl)pyridine (*cf.* Figure 2.4), the replacement of pyridines by triazoles leads to a slight stabilization of the HOMO and a pronounced destabilization of the LUMO causing (Figure 2.6) an increased energy of the ^{3}MLCT in the triazole complex. Experimentally, this is manifest in the shifts of the corresponding redox potentials, *i.e.* a slightly more positive potential for the metal-based oxidation and a more negative potential for the ligand-based reduction, and in a spectral blue-shift of the MLCT absorption band.[89–94] The destabilization of the LUMO can be rationalized by the higher energy of the π* orbitals of the triazole-based ligand as well as by a diminished π conjugation within the chelating ligand system (*vide supra*).[89] On the other hand, the lowered energy of the almost entirely metal-based HOMO can be ascribed to a weaker electrostatic repulsion with the less electron-rich σ lone pair of the 1,2,3-triazoles (*vide supra*).[93] As a further consequence of the reduced σ donation by the triazole, the σ-antibonding orbitals within the metal complex are energetically lowered associated with a lower energy of the ^{3}MC. In view of the concomitant ^{3}MLCT destabilization, the ^{3}MLCT–^{3}MC energy separation is expected to be lowered in the 1,2,3-triazole-containing complex, which is corroborated by the observation of a more efficient radiationless deactivation.[90–91, 93] Ultimately, if all pyridines are replaced by triazoles in *tris*(bidentate) ruthenium(II) complexes (*cf.* Figure 2.4), the lowest-energy excited state is no longer of ^{3}MLCT but of ^{3}MC character.[93]
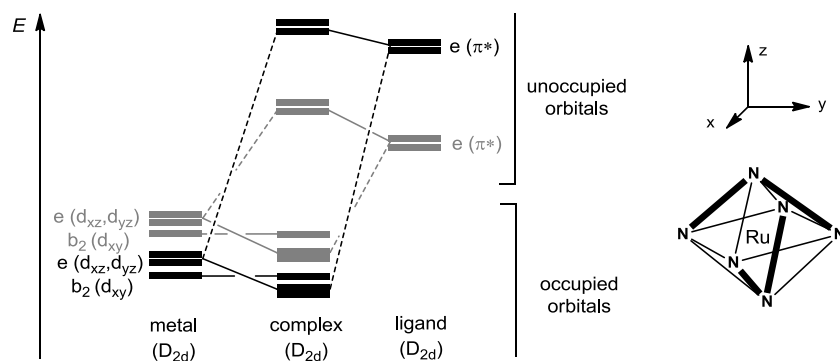
Figure 2.6. Simplified qualitative MO scheme of a *bis*(tridenate) ruthenium(II) complex of tpy (black) or 2,6-*bis*(1*H*-1,2,3-triazol-4-yl)pyridine (grey) illustrating the differences in π back-donation between the pyridine- and triazole-based ligands (σ interactions omitted for clarity). (Note that the ruthenium(II) d orbitals are energetically lowered due to a weakened electrostatic repulsion with the triazole ligand. See text for details.)

13

While the use of 1,2,3-triazoles as pyridine surrogates in ruthenium(II) polypyridyl complexes can have a detrimental effect on their photophysical properties, 1,2,3-triazoles offer alternative, more strongly σ-donating coordination modes. For instance, *N*-unsubstituted 1,2,3-triazoles can be deprotonated to serve as anionic nitrogen donors.[118] Moreover, the deprotonation of 1,2,3-triazolium salts affords 1,2,3-triazolylidenes, which are abnormal or mesoionic carbenes (MICs).[29, 119−125] While conventional *N*-heterocyclic carbenes (NHCs) are represented best by a neutral structure featuring a divalent carbon formally bearing an electron sextet with only minor contribution of an ylidic (zwitterionic) structure,[126] no reasonable charge-neutral structure can be drawn for MICs (Figure 2.7).[125] Nonetheless, the zwitterionic character is diminished *via* delocalization within the aromatic system and, on account of the electron-withdrawing ring heteroatoms, significant contribution of a carbene structure can be expected (Figure 2.7).
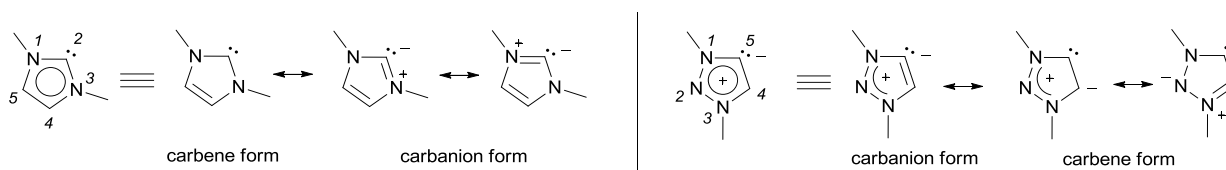

Figure 2.7. Schematic representation of an *N*-Heterocyclic carbene (left) and a mesoionic carbene (right).

Similar to classical NHCs like imidazol-2-ylidenes, MICs can be considered as heteroatom-stabilized, nucleophilic singlet carbenes. Indeed, DFT calculations predict a highly aromatic character and a large singlet−triplet energy gap (230 to 250 kJ mol^{-1}) for 1,2,3-triazolylidenes.[127] Moreover, in comparison to most common imidazol-2-ylidenes, the σ donor strength of 1,2,3-triazolylidenes is significantly increased, which is rather attributed to the reduced heteroatom stabilization of the carbene center due to the remote positioning of nitrogen ring atoms[128−129] than to the mesoionic character.[130] According to DFT calculations, the HOMO of 1,2,3-triazolylidenes (−4.44 to −4.48 eV, depending on the substituent) is energetically well above the HOMO of imidazol-2-ylidene (−5.00 eV).[127] Furthermore, abnormal/mesoionic carbenes are slightly stronger π donors and slightly weaker π acceptors.[131] Thus, 1,2,3-triazolylidenes appear to be highly attractive ligands as they offer a rapid and modular synthesis as well as a superior σ donor strength.

2.3   Dye-sensitized solar cells

Photoelectrochemical cells[13] employing a wide-bandgap semiconductor that is sensitized with dye molecules as photoactive electrode are called dye-sensitized solar cells (DSSCs).[12, 14, 132−135] In case of DSSCs based on *n*-type semiconductors, the electronically excited sensitizer injects an electron into the conduction band of the semiconductor and is regenerated *via* the electrolyte.[12] The DSSC relies on kinetic competition between charge-injection and charge-recombination dynamics at the dye−semiconductor interface (*vide infra*),[136−138] while light-driven charge separation and subsequent charge transport are spatially separated.[133−134, 139] In 1991, Grätzel and O'Regan reported a significant improvement in efficiency by using a mesoporous network of TiO$_2$ nanoparticles as semiconducting material, a ruthenium(II)-containing charge-transfer dye, and a I$_3^-$/I$^-$-based redox electrolyte.[139] This seminal report has motivated extensive research efforts and, currently, record power conversion efficiencies (PCEs) of up to 13% have been achieved with both inorganic and organic sensitizers, and Co(III)/Co(II)-based redox electrolytes under optimized conditions.[140−141] Prospectively,

PCEs of about 15% appear to be realistic[12, 142−144] and strategies have been presented to further improve the long-term stability of DSSCs.[42, 44, 145] Among the distinct advantages of DSSCs, compared to conventional silicon-based solar cells, are a better relative performance under diffuse light conditions, the potential for lower production costs, and the opportunity to construct flexible and transparent devices.[12]

A schematic representation of a Grätzel-type DSSC is depicted in Figure 2.8. The photoactive anode consists of a glass substrate coated with a transparent conducting oxide (TCO) on which a layer (~ 10 μm thick) of sintered TiO_2 nanoparticles (~ 20 nm in diameter), covered with a monolayer of sensitizer molecules, is deposited.[12] The electrolyte typically consists of an acetonitrile solution containing the I_3^-/I^--based redox mediator as well as further additives, which determine the energy of the conduction band of the semiconductor (*vide infra*).[146] The counter electrode is a TCO-coated glass slide covered with platinum to catalyze the triiodide reduction. Upon light-excitation of the dye molecules, an electron is injected into the TiO_2 conduction band, diffuses through the mesoporous TiO_2 network (porosity of 50 to 60%),[12] passes an external circuit, and is captured by the triiodide at the cathode. Reduction of the photo-oxidized dye by iodide closes the circuit.

In order to achieve a sufficiently stable anchoring as well as a good electronic coupling with the TiO_2, the sensitizer is most commonly functionalized with carboxy groups.[12] Upon anchoring, the proton of a carboxy group is transferred to the TiO_2 and the resulting carboxylate coordinates to Ti(IV) in various binding modes (unidentate, chelating, and bridging).[147−149]
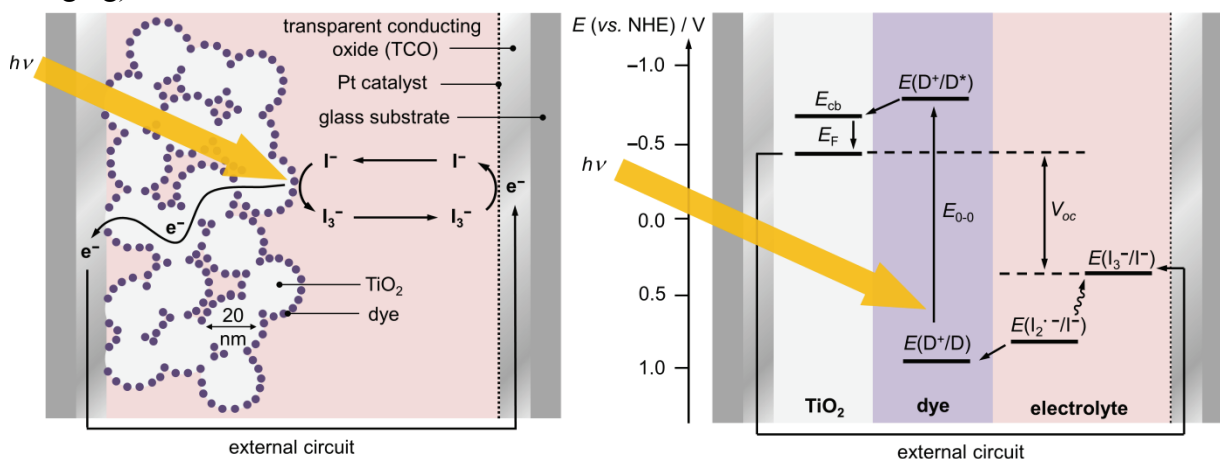

Figure 2.8. Building (left) and working principle (right) of a dye-sensitized solar cell.[12, 136, 143−144]

In Figure 2.8, the DSSC working principle from an energy perspective is outlined. While a DSSC based on a TiO_2 semiconductor and a I_3^-/I^- redox mediator typically affords an open-circuit voltage (V_{oc}) of about 700 mV, the energy gap of the sensitizer has to be at least 1.5 eV (*vide infra*). Beside several energy losses that are required to drive the electron transfer steps,[136−137] a considerable energy loss is associated with the I_3^-/I^--based electrolyte, as the photo-oxidized dye is regenerated by the $I_2^{\cdot-}/I^-$ redox couple (0.79 V *vs.* NHE), while, after disproportionation ($2\,I_2^{\cdot-} \rightarrow I_3^- + I^-$), the I_3^-/I^- redox couple (0.35 *vs.* NHE) determines the V_{oc} (Figure 2.8).[12, 144, 150] Consequently, a major opportunity to improve the efficiency of DSSCs is to use alternative redox couples, for instance Co(III)/Co(II).[142, 146, 151] On the other hand, under illumination at open-circuit conditions, the voltage is limited by the quasi Fermi level (E_F), which, in turn, depends on the competition between electron injection and recombination.[152−154] In this regard, a major challenge is to replace the I_3^-/I^--based electrolyte since the performance of DSSCs employing Co(III)/Co(II)-based redox shuttles suffers from

mass transport limitations and enhanced recombination reactions.[146, 151, 155] A key strategy to lower the recombination tendency when using the latter electrolytes is to place alkyl chains on the sensitizer in order to physically protect the TiO_2 surface from the redox shuttle.[156] Moreover, the hydrophobic alkyl chains suppress the water-induced dye desorption and thereby improve the long-term stability of a DSSC.[157]

In Figure 2.9, the typical electron transfer dynamics in a Grätzel-type DSSC employing a ruthenium(II) sensitizer are detailed.[12, 136] After electronic excitation of the sensitizer, electron injection into TiO_2 can occur either from an initially populated, short-lived Franck−Condon state of ^{1}MLCT character (S_1 or higher[158]) or, after ultrafast ISC and IVR,[62] from the longer-lived ^{3}MLCT.[136] For model systems, a ^{1}MLCT lifetime of ~ 30 fs has been determined, resulting from two parallel, almost equally contributing processes, namely electron injection and ISC.[136, 159−160] However, in contrast to dye-sensitized TiO_2 films that have been used as model systems, the injection kinetics in a complete and optimized DSSC are typically significantly slower (~ 100 ps, *vide infra*).[136, 161] Importantly, the injection dynamics depend, amongst others, on the injection driving force resulting from the potential difference between the excited-state redox potential of the sensitizer and the redox potential of the conduction band of the semiconductor (about −0.7 V *vs*. NHE).[136] As the conduction band energy can be lowered and raised with cationic and basic additives, respectively, the injection rate can be adapted for a given sensitizer.[153−154, 161−162] Ideally, a conduction band energy as high as possible to sustain efficient electron injection is desirable, as this allows a maximization of the V_{oc} while maintaining a high J_{sc}. In other words, the injection should be just fast enough to enable a high injection yield, while a faster injection is kinetically redundant and associated with an unnecessary loss in efficiency.[161,163] As the ^{3}MLCT lifetime is about five orders of magnitude longer than the ^{1}MLCT lifetime, injection form the ^{3}MLCT allows a significantly lower driving force and, thus, a substantially higher V_{oc}.[163] For instance, a ^{3}MLCT lifetime of about 10 ns, which is a typical value for ruthenium(II) sensitizers, only requires electron injection within ~ 100 ps in order to achieve an injection yield near unity.[136] Ultimately, an opportunity to further increase the PCE of a DSSC is to use ruthenium(II) sensitizers with significantly longer excited-state lifetimes.[136]
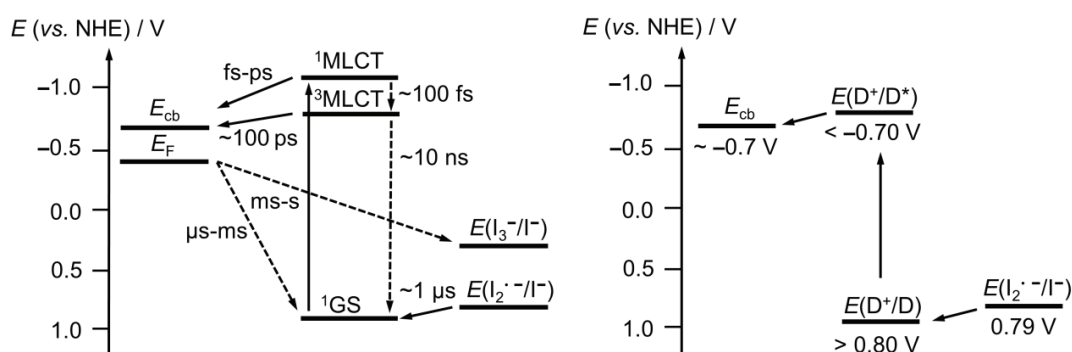
Figure 2.9. Electron transfer kinetics (left) and energetics (right) within a typical DSSC.[12, 136]

Analogously, the efficiency of the dye regeneration depends, amongst others, on the regeneration driving force. For a I_3^-/I^--based electrolyte, the redox potential of the sensitizer should be sufficiently more positive than the value of the crucial redox couple, $I_2^{\cdot-}/I^-$ (0.79 V *vs*. NHE).[42−43, 150] While an efficient regeneration of the oxidized dye is required to minimize electron recapture from the TiO_2, a too positive redox potential of the sensitizers would again lead to a kinetic redundancy. Also the molecular design of the dye influences the extent of

recombination reactions with the photo-oxidized dye: For instance, an intramolecular hole transfer away from the TiO$_2$ surface lowers the recombination tendency[164−166] and an exposure of the hole towards the electrolyte, offering an intimate contact between the oxidized dye and iodide, is known to facilitate the regeneration.[167−169] On the other hand, the sensitizer should neither interact with iodine nor allow iodine to reach the TiO$_2$ surface, which would provoke recombination reactions.[170−173] To improve the shielding of the TiO$_2$ surface, the dye can be co-sensitized with, *e.g.*, chenodeoxycholic acid (cheno).[174−175] Furthermore, high iodide[176−177] and moderate lithium concentrations[178] in the electrolyte are known to accelerate the regeneration.

Ultimately, for a DSSC based on TiO$_2$ and I$_3^-$/I$^-$ as the respective electron and hole transporting medium, the sensitizer should ideally exhibit an excited-state redox potential more negative than −0.7 V *vs*. NHE as well as a ground-state redox potential more positive than 0.8 V *vs*. NHE (Figure 2.9), corresponding to an energy gap of at least 1.5 eV (*vide supra*).[77, 179] Notably, [Ru(Htctpy)(NCS)$_3$](NBu$_4$)$_3$ (**N749** or black dye; Htctpy = 2,2′:6′,2″-terpyridine-4′-carboxylic acid-4,4″-dicarboxylate),[40−41] which is one of the benchmark ruthenium(II) sensitizers and achieves PCEs of up to 11.4% in optimized DSSCs,[143, 180] matches these values very well.[115] However, while the thiocyanato ligands enable a panchromatic MLCT absorption and mediate the dye regeneration, they preclude the optimization of the sensitizer *via* ligand functionalization, *e.g.* with additional chromophores and alkyl chains, and limit the lifetime of DSSCs as they can decoordinate easily.[45, 181] A promising strategy to further improve both the PCE and the long-term stability of DSSCs is to replace the thiocyanato ligands with anionic multidentate ligands[42−43] including anionic phenyl rings,[182−188] and anionic *N*-heterocycles.[44, 189−193] Indeed, judicious molecular engineering afforded *bis*(tridentate) ruthenium(II) sensitizers that rival or beat the performance of **N749** in the DSSC and, moreover, enable an improved DSSC long-term stability.[44, 190]

3 *Bis*(tridentate) Ruthenium(II) Complexes Featuring Mesoionic Carbenes

The quest to suppress the fast radiationless deactivation of the [3]MLCT of *bis*(tridentate) ruthenium(II) polypyridyl complexes *via* a thermally accessible [3]MC[52, 78] has stimulated considerable research efforts.[35−36, 47] One of the most promising approaches is to enhance the [3]MC destabilization *via* an increased σ donor strength of the ligand, while leaving the [3]MLCT nearly unaffected and therefore preserving the energy that is stored in the excited state in order to drive photochemical reactions.[19] For instance, the incorporation of imidazol-2-ylidenes (Figure 3.1), which are strong σ donors and moderate π acceptors,[194] causes a strong [3]MC destabilization, while the [3]MLCT and [1]GS are only marginally affected, resulting in significantly prolonged excited-state lifetimes (*e.g.*, τ = 500 ns to 3 μs).[37] In view of this strategy, 1,2,3-triazolylidenes are particularly attractive as they are stronger σ donors than imidazol-2-ylidenes and can be modularly synthesized by employing the CuAAC.[34, 120, 122]
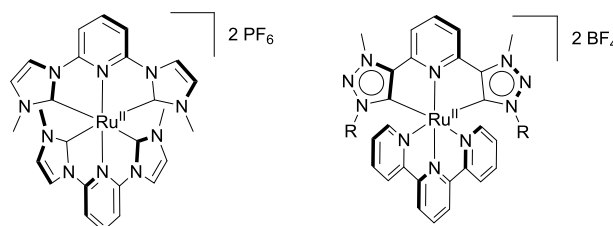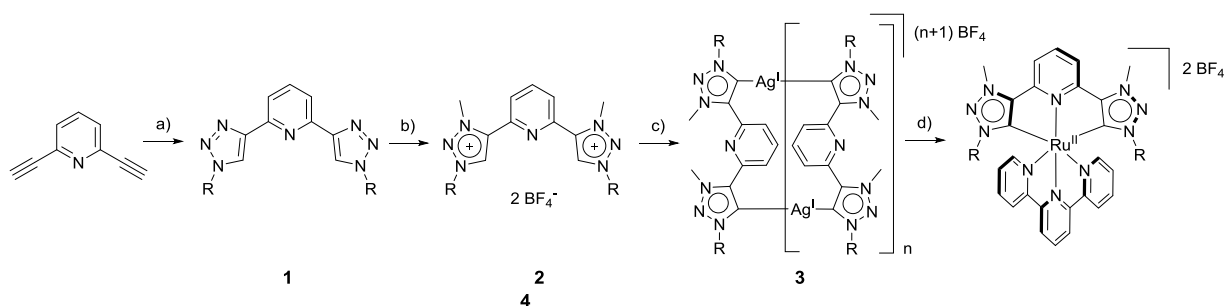

Figure 3.1. Schematic representation of *bis*(tridentate) ruthenium(II) complexes featuring NHC (left) and MIC donors (right).[37, 195]

To allow the ruthenium(II) coordination of a tridentate ligand featuring two 1,2,3-triazolylidenes donors, a corresponding triazolium salt was prepared first (**2**, Scheme 3.1). Accordingly, **1** was methylated using an excess of trimethyloxonium tetrafluoroborate,[196] which allowed the selective N3-methylation of the 1,2,3-triazoles without affecting the pyridine as proven, amongst others, by single crystal X-ray diffraction analysis.[195, 197] Because free 1,2,3-triazolylidenes are known to undergo a 3,5-methyl shift,[127] a stable silver(I)-precursor (**3**) was prepared using silver(I) oxide.[124] The successful silver(I) complexation was confirmed by the absence of the 1,2,3-triazolium protons in the ^{1}H NMR spectrum and the presence of carbon resonances at around 170 ppm with a characteristic coupling to the [107/109]Ag nucleus[198] in the ^{13}C NMR spectrum. On the basis of mass spectrometry (MS) and diffusion-ordered NMR-spectroscopy (DOSY) experiments, the formation of higher aggregates, most likely cyclic tetramers, is assumed (*cf.* Scheme 3.1).[199] For the subsequent transmetalation of the 1,2,3-triazolylidene ligand to the ruthenium(II) center, the viability of common ruthenium(II) and ruthenium(III) monocomplexes of tpy as precursor was tested, but only [Ru(tpy)(DMSO)Cl₂][200−201] proved to be a sufficiently selective and reactive, allowing the synthesis of **4** under mild reaction conditions and with a reasonable yield. This is rationalized by the presence of ruthenium(II), the weakly coordinated DMSO, and the chloro ligands, which

provide an additional driving force for the transmetallation as they give rise to the formation of the silver(I) chloride with the silver(I) carbene complex.

Scheme 3.1. Schematic representation of the synthesis of the *bis*(tridentate) ruthenium(II) 1,2,3-triazolylidene complex **4** (R = mesityl): a) RN_3, $CuSO_4$, sodium ascorbate, $EtOH/H_2O$ (3:1 *v/v*), 60 °C, 36 h, 90%; b) $Me_3O^+BF_4^-$, CH_2Cl_2, rt, 12 h, 90%; c) fresh Ag_2O, molecular sieves, MeCN, 80 °C, 12 h, 90%; d) *cis*-[Ru(tpy)(DMSO)Cl_2], CH_2Cl_2, 70 °C (closed vial), 5 d , 40%.

The identity and purity of **4** were proven by MS and various NMR techniques. The triazolium protons are absent and characteristic high-field shifts due to the π stacking were visible in the ^{1}H NMR spectrum. Furthermore, a low-field shift to around 185 ppm can be observed for the ruthenium(II)-coordinated carbon atoms in the ^{13}C NMR spectrum. Single crystals of **4** suitable for X-ray diffraction were grown by vapor diffusion of diethyl ether into a methanol solution (Figure 3.2). The desired C^N^C-coordination as well as an intramolecular tweezer-like π stacking are confirmed. In comparison to the tpy ligand, the bite angle of the carbene ligand is more acute and the central Ru−N bond is elongated, which is a consequence of the short Ru–C bonds rather than of the introduction of 5-membered rings.[90] The Ru–C bond lengths are identical to those reported for an analogous heteroleptic ruthenium(II) complex featuring imidazol-2-ylidene donors, while the bite angle of the carbene-containing ligand, ∠C−Ru−C, is marginally smaller for **4**.[202] The averaged bond angle at the carbene center, ∠C−C−N, is 102.2°, which is a typical value for metal-coordinated 1,2,3-triazolylyidenes and larger than for free 1,2,3-triazolylidenes (99.7°).[34, 125, 127] For comparison, the angle for free and ruthenium(II)-coordinated imidazol-2-ylidenes are on average 101.4° and 103.6°, respectively.[126, 202] Presumably, the σ lone pair of the 1,2,3-triazolylidene features a higher s orbital contribution to allow a better stabilization of the excessive charge.[203]
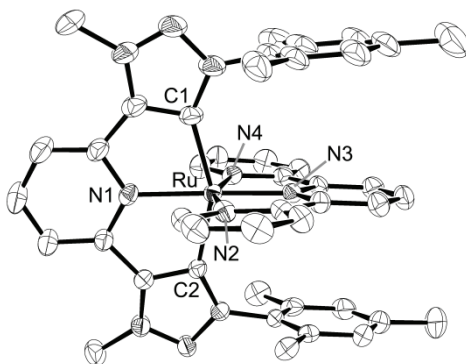
Figure 3.2. Solid-state structure of **4** (ellipsoids at 50% probability level; hydrogen atoms, solvents molecules, and tetrafluoroborate anions are omitted for clarity). Selected bond lengths (Å) and angles (°): Ru−C1, 2.058(4); Ru−C2, 2.051(4); Ru−N1, 2.083(4); Ru−N2, 2.068(4); Ru−N3, 1.962(4); Ru−N4, 2.052(4); ∠C1−Ru−C2, 154.34(17); ∠N2−Ru−N4, 158.25(15); ∠N1−Ru−N3, 178.48(15).

To better understand the electronic properties of the novel ruthenium(II) complex, density functional theory (DFT) and time-dependent DFT (TD-DFT) calculations as well as an energy-

decomposition analysis (EDA)[204] have been performed. The EDA calculation revealed a substantial binding energy between the carbene-containing ligand and the ruthenium(II)–tpy fragment ($-1,070$ kJ mol^{-1}) resulting from both strong covalent interactions and electrostatic attraction. The covalent contribution is mainly due to strong σ interactions (Figure 3.3), but also a π back-donation with the mesoionic carbenes as well as with the central pyridine ring of the carbene-containing ligand contributes to the attractive interactions (*vide infra*). Also the electrostatic interactions mainly depend on the electron density within the σ lone pairs, which penetrate the metal's valence shell.[55] For comparison, the overall binding energy for [Ru(tpy)]$^{2+}$ and [Os(tpy)]$^{2+}$ was calculated to be $-1,950$ and $-2,150$ kJ mol^{-1}, respectively, corresponding to -975 and $-1,075$ kJ mol^{-1}, respectively, per metal−tpy interaction.[205] Consequently, the binding strength of the tridentate ligand is significantly enhanced by the 1,2,3-triazolylidenes, which is mostly attributed to their strongly σ-donating character.
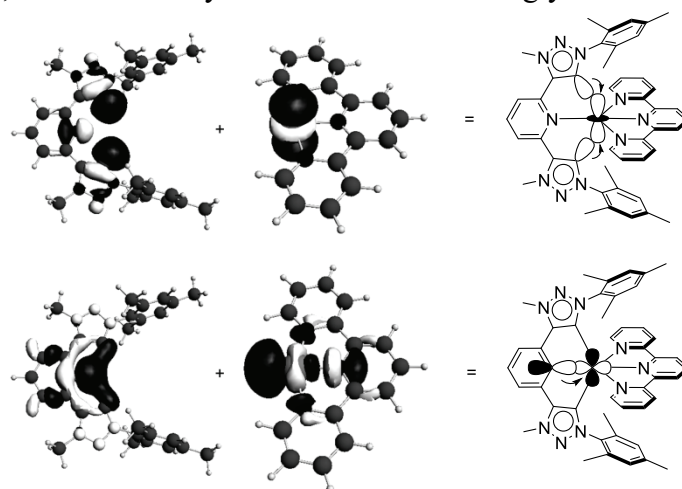
Figure 3.3. Main σ interactions between the 1,2,3-triazolylidene-containing ligand and the [Ru(tpy)]$^{2+}$ fragment according to EDA (BP86-ZORA/TZP).

The main π interactions are illustrated in a simplified MO scheme depicted in Figure 3.3. Owing to repulsive interactions with the electron-rich σ lone pairs of the carbene ligand, metal orbitals aligned with the y-axis are more strongly destabilized. Furthermore, due to the partial anionic character of the mesoionic carbene,[131] the π and π* orbitals of the triazolylidene are relatively high in energy resulting in both a weak π repulsion and π back-donation with the metal-d_{xy} (a_2) orbital. Accordingly, the HOMO receives a major contribution from the d_{xy} orbital, but also features a non-negligible contribution from the carbene-containing ligand. Nonetheless, an energetically low π* orbital located on the central pyridine ring of the C^N^C-ligand can undergo a π back-donation with the metal-d_{xz} (b_1) orbital. On the other hand, the tpy ligand can undergo a π back-donation with the metal-d_{yz} (b_2) orbital, which is expected to be more pronounced, not least because the interacting orbitals are more similar in energy. Ultimately, the LUMO is mostly represented by π* orbitals of the tpy, while the LUMO+1, which is only slightly higher in energy, receives a major contribution from a π* orbital localized on the central pyridine ring of the C^N^C-ligand.
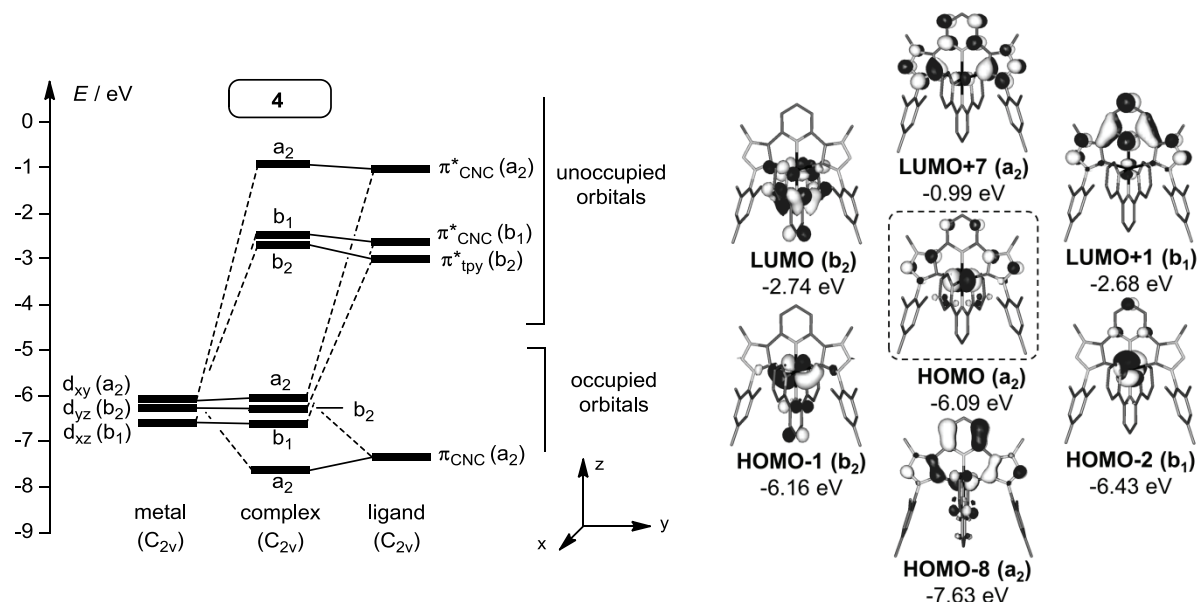
Figure 3.4. Part of an MO scheme illustrating the main π interactions within **4** (left) and corresponding Kohn−Sham orbitals (PCM-B3LYP/6-31G* in MeCN, right). Ligand π orbitals with little overlap (*cf.* Figure S 1) and σ interactions are not shown for clarity. Note that the energies of the complex orbitals were calculated, while the orbital energies for the metal fragment and the free ligand are estimated.

According to the TD-DFT calculations (Table S 1), the lowest-energy, symmetry-allowed electronic excitation is the HOMO→LUMO transition, which is clearly of MLCT character and directed towards the tpy ligand. On the other hand, also the HOMO→LUMO+1 transition is symmetry-allowed and of MLCT character, but directed towards the C^N^C-ligand. While both transitions are of low intensity, also the more intense electronic excitations at shorter wavelengths are of MLCT character and involve the π* system of either the tpy or the C^N^C-ligand. In the UV region, additional MLCT, LC and ligand-to-ligand charge-transfer (LLCT) transitions are predicted. The calculated UV−vis spectrum is slightly blue-shifted in comparison to the experimental spectrum, but both are consistent in band shape (Figure 3.5). In comparison to [Ru(tpy)$_2$](PF$_6$)$_2$ and [Ru(bpy)$_3$](PF$_6$)$_2$, **4** shows an MLCT maximum at a very similar wavelength, but with a lowered extinction coefficient (Table 3.1). As intended, **4** is emissive at room temperature (Figure 3.5) with quantum yields comparable to [Ru(bpy)$_3$](PF$_6$)$_2$, albeit at longer wavelengths (Table 3.1). Also, the computed emission maximum at 652 nm is in good agreement with the experimental value of 643 nm (both in acetonitrile). The emission showed a monoexponential decay on the μs timescale, thus arising from a single phosphorescent triplet state (Figure 3.5). In acetonitrile, the excited-state lifetime of 633 ns measured for **4** approaches the lifetime of [Ru(bpy)$_3$](PF$_6$)$_2$ of 860 ns,[48] while both complexes exhibit a comparable lifetime in dichloromethane (Table 3.1). In comparison to the excited-state lifetime of [Ru(tpy)$_2$](PF$_6$)$_2$ (0.21 ns),[52] the value of **4** is about 3,000 times longer, which is ascribed to the strong destabilization of the ^{3}MC in the presence of the 1,2,3-triazolylidenes. This is corroborated by the calculated vertical excitation energies at the ground-state nuclear coordinates, which reveal a ^{3}MC−^{3}MLCT energy difference of 7,900 cm^{-1}, while the corresponding value for [Ru(tpy)$_2$](PF$_6$)$_2$ is only 2,900 cm^{-1}.[52] Although these energies are overestimated as nuclear reorganization is not considered (*vide supra*), they support the substantial ^{3}MC destabilization in **4**.
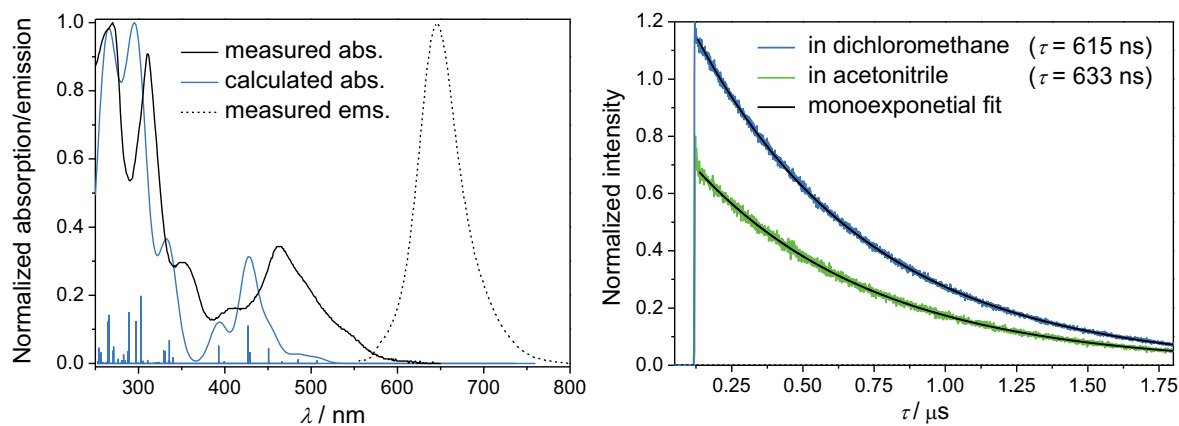
Figure 3.5. Calculated (PCM-TD-B3LYP/6-31G*) and measured UV−vis absorption as well as measured emission spectrum (all in MeCN, left). Emission decay curves in MeCN and CH$_2$Cl$_2$ (right).

Table 3.1. Photophysical and electrochemical properties of **4** and prototypical ruthenium(II) polypyridyl complexes.

Complex	[Ru(tpy)$_2$](PF$_6$)$_2$	[Ru(bpy)$_3$](PF$_6$)$_2$	**4**
λ_{max}^{Abs} / nm (ε /10^4 M^{-1} cm^{-1})[a,b]	474 (1.8)	450 (1.4)	463 (1.0)
λ_{max}^{Em} / nm[a]	−	597	643
τ / ns	0.21[c] (0.25[d])	860;[e] 680[e,f]	633; 615[f]
Φ_{PL} / %	−	6.2[g]	4.4[h]; 5.5[f,h]
$E_{1/2}^{Ox}$ / V[i]	0.90	0.90	0.60
$E_{1/2}^{Red}$ / V[i]	−1.64	−1.71	−1.95 (irrev.)
E_{0-0} / eV	−	2.13[j]	2.09[k]
$E^*_{1/2}^{Ox}$ / V[l]	−	−1.20	−1.49

[a] Measured in deaerated MeCN at 298 K, unless stated otherwise. [b] Maximum of the MLCT band. [c] Measured in butyronitrile at 290 K; taken from ref. [52]. [d] Measured in H$_2$O at 298 K with [Ru(tpy)$_2$](ClO$_4$)$_2$; taken from ref. [53]. [e] Taken from ref. [48]. [f] Measured in deaerated CH$_2$Cl$_2$. [g] Taken from ref. [206]. [h] Measured against [Ru(bpy)$_3$](PF$_6$)$_2$ as standard. [i] Measured in MeCN containing 0.1 M NBu$_4$PF$_6$ and using Fc$^+$/Fc as reference. [j] Taken from ref. [207]. [k] Determined at the intersection of the absorption and emission with the latter being normalized to the lowest-energy absorption. [l] Calculated using $E^*_{1/2}^{Ox} = E_{1/2}^{Ox} - E_{0-0}$.[12]

Also the electrochemical properties are consistent with the computational results. In comparison to ruthenium(II) complexes of charge-neutral polypyridyl ligands like [Ru(tpy)$_2$](PF$_6$)$_2$ and [Ru(bpy)$_3$](PF$_6$)$_2$, the redox potentials of **4** are cathodically shifted, while the electrochemical energy gap remains constant (Table 3.1). Furthermore, the oxidation is reversible, while the reduction process is irreversible. To obtain a more detailed insight into the oxidation process, UV−vis spectroelectrochemical experiments were executed. Several isosbestic points suggest the presence of only two species and, thus, a well-defined oxidation process. The most prominent spectral change is the decrease of the absorption bands at 463, 410, and 352 nm, consistent with a metal-based HOMO (*vide supra*). Additionally, a weak and broad band between 600 and 800 nm appears, most likely due to a ligand-to-metal charge transfer (LMCT), whereas the bands below 330 nm, in the region dominated by LC transitions, appear essentially unchanged. Remarkably, the reduction of the oxidized species regenerates the parent complex quantitatively. As the excited-state redox potential of **4** is more negative than the one of [Ru(bpy)$_3$](PF$_6$)$_2$ (Table 3.1), *i.e.* **4** is a more effective reducing agent in the excited state, **4** shows potential for application to act as an efficient electron donor in photovoltaic devices or in photo-redox catalysis.[12, 19, 208]

In subsequent work, the groups of Schubert and Berlinguette demonstrated that an additional electronic fine tuning by the attachment of electron-withdrawing or electron-releasing substituents on the tpy ligand as well as by a modification of the *N*-substituent of the 1,2,3-triazolylidenes affords even longer excited-state lifetimes of up to 7.9 μs.[201]

In conclusion, a readily synthesized tridentate ligand based upon 1,2,3-triazolylidenes donors was utilized to destabilize the deactivating ^{3}MC in the corresponding *bis*(tridentate) ruthenium(II) complex. By virtue of the exceptionally strong σ donation from the mesoionic carbene ligand, the radiationless deactivation of the ^{3}MLCT is efficiently suppressed allowing substantially prolonged excited-state lifetimes relative to the parent $[Ru(tpy)_2](PF_6)_2$. The promising photophysical properties of **4** suggest applications as photosensitizer or as photo-redox catalyst. As a *bis*(tridentate), heteroleptic system, **4** represents a valuable building block for the construction of structurally-defined electron-transfer assemblies.[209] Moreover, **4** emits red light with a relatively high photoluminescence quantum yield, which is attractive for applications in light-emitting electrochemical cells[210–211] and sensing.[212]

As an outlook, besides utilizing 1,2,3-triazolium salts as 1,2,3-triazolylidene precursors, they can be employed to bind anions *via* charge-assisted hydrogen bonds.[29, 32, 213] Exemplarily, it was demonstrated that simple cleft-type receptors featuring one or two 1,2,3-triazolium units (Figure 3.6) strongly bind the dianion sulfate in acetonitrile ($K_{a1}K_{a2} \approx 7 \cdot 10^6$ M^{-2}) or acetonitrile/methanol (4:1 *v/v*, $K_{a1} > 2.4 \cdot 10^4$ M^{-1}) solution, respectively. Notably, the singly charged receptor featuring one 1,2,3-triazolium ring enables the formation of a charge-neutral 2:1 host–guest complex ($K_{a2} \approx 1.3 \cdot 10^3$ M^{-1}) beside a 1:1 complex ($K_{a1} \approx 5.4 \cdot 10^3$ M^{-1}) with the dianion. Accordingly to NMR studies, the receptors bind the anion in a tridentate fashion and, in case of the 2:1 stoichiometry, an "octahedral" *bis*(tridentate) complex is formed.
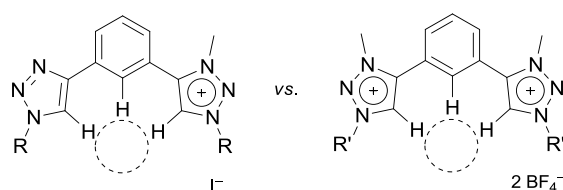

Figure 3.6. Schematic representation of cleft-type, 1,2,3-triazolium-based anion receptors (R = 4-tolyl, R' = 4-bromo-2,6-dimethylphenyl), the anion cavity is indicated by a dashed circle.

4 *Bis*(tridentate) Ruthenium(II) Complexes Featuring Anionic Chelates

Parts of this chapter have been or will be published: A5) B. Schulze, D. Escudero, C. Friebe, R. Siebert, H. Görls, S. Sinn, M. Thomas, S. Mai, J. Popp, B. Dietzek, L. González, U. S. Schubert, *Chem. Eur. J.* **2012**, *18*, 4010−4025; A6) S. Sinn, B. Schulze, C. Friebe, D. G. Brown, M. Jäger, J. Kübel, B. Dietzek, C. P. Berlinguette, U. S. Schubert, *Inorg. Chem.* **2014**, *53*, 1637−1645.

Cyclometalated ruthenium(II) complexes

A prominent approach to overcome the short excited-state lifetimes of [Ru(tpy)$_2$](PF$_6$)$_2$ is the replacement of a pyridyl ring by a phenyl ring leading to the establishment of a strong, organometallic Ru−C bond upon chelation-assisted C−H activation.[81, 214−218] This cyclometalation[38] affords complexes that feature a strongly electron-donating carbanion, which is supposed to increase the energy separation between the ^{3}MLCT and the short-lived ^{3}MC.[81, 219] While cyclometalated ruthenium(II) complexes were reported long ago[81, 215, 219−220] and received considerable attention,[221] their viability for application in DSSCs was demonstrated only recently by the groups of van Koten,[183] Grätzel,[182, 222] Berlinguette,[184, 186, 223] and Ghaddar.[187] Accordingly, the cyclometalating ligands can mimic the electronic properties of the monodentate thiocyanato ligands of classical ruthenium(II) sensitizers and furthermore enable the accurate optimization of the photophysical and electrochemical properties *via* the substituents attached to the cyclometalating phenyl ring.[224] Moreover, the anionic chelates provide an enhanced stability[44, 219] as well as the potential to further improve the light harvesting *via* installation of additional chromophores.[42−43] Recently, spurred by the efficiency of CuAAC, 1,2,3-triazole-containing ligands have emerged including analogs of famous polypyridyl ligands.[27−29] We were interested in extending this analogy to tridentate cyclometalating polypyridyl ligands, namely 1,3-di(2-pyridyl)benzene (dpbH), and examine the viability of the corresponding 1,2,3-triazole-containing ruthenium(II) complexes (**6**, Figure 4.1) for applications in DSSCs. To better understand the electronic consequences of the cyclometalation as well as the replacement of a pyridine by a 1,2,3-triazole ring, a heteroleptic ruthenium(II) complex featuring a non-cyclometalating 2,6-*bis*(1*H*-1,2,3-triazol-4-yl)pyridine ligand was also investigated (**5**, Figure 4.1).[90]

[Ru(tpy)$_2$][PF$_6$]$_2$ [Ru(tpy)(dpb)][PF$_6$]   **5**   **6**
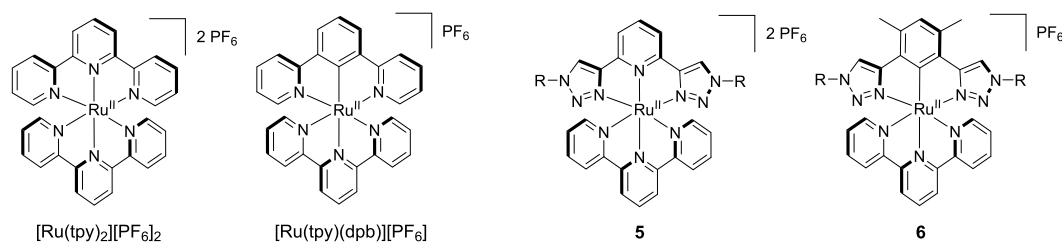
Figure 4.1. Schematic representation of the cyclometalated and non-cyclometalated *bis*(tridentate) polypyridyl-type ruthenium(II) complexes as well as their 1,2,3-triazole-containing analogs (R = mesityl).

The 1,2,3-triazole-based ligands were obtained from aryl azides and diethynylbenzene building blocks in good yields using standard CuAAC conditions.[86] For the sake of blocking an alternative, bidentate coordination, which was observed in an initial attempt, methyl groups were placed at strategic positions (Figure 4.2). For this purpose, *o*-xylene was chosen as the central ring[225−226] as well as mesityl rings as the triazole's *N*-substituents. The diethynylbenzene building blocks were synthesized *via* a Sonogashira cross-coupling reaction

using 1,5-dibromo-2,4-dimethylbenzene or, to additionally lower the electron donation from the carbanion,[182, 227] 1,5-dibromo-2,4-difluorobenzene as starting materials (*cf.* **7**, Figure 4.3).
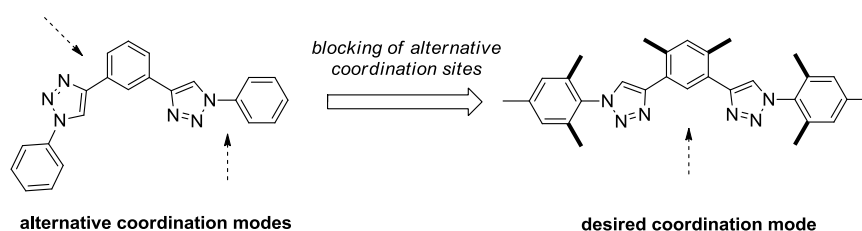
Figure 4.2. Schematic illustration of the optimization strategy.

To allow the installation of a thiophene ring on the central phenyl ring *via* a Suzuki cross-coupling reaction, a bromo-functionalized ligand was synthesized starting from 1,3,5-tribromobenzene. Additional methyl groups were omitted in this case to enable an extended conjugation and, thus, an enhanced molar absorptivity of the corresponding ruthenium(II) complex (*cf.* **9**, Figure 4.2). Alternatively, 9-(4-azidophenyl)-3,6-di-*tert*-butyl-9*H*-carbazole was used to build up a cyclometalating ligand functionalized with peripheral chromophores (*cf.* **10**, Figure 4.3).[228] In this case, the chromophores are expected to act as light-harvesting antennas, as the conjugation is usually interrupted by the 1,2,3-triazole ring.[29] For all other ligands, the mesityl moiety was kept as a reference.
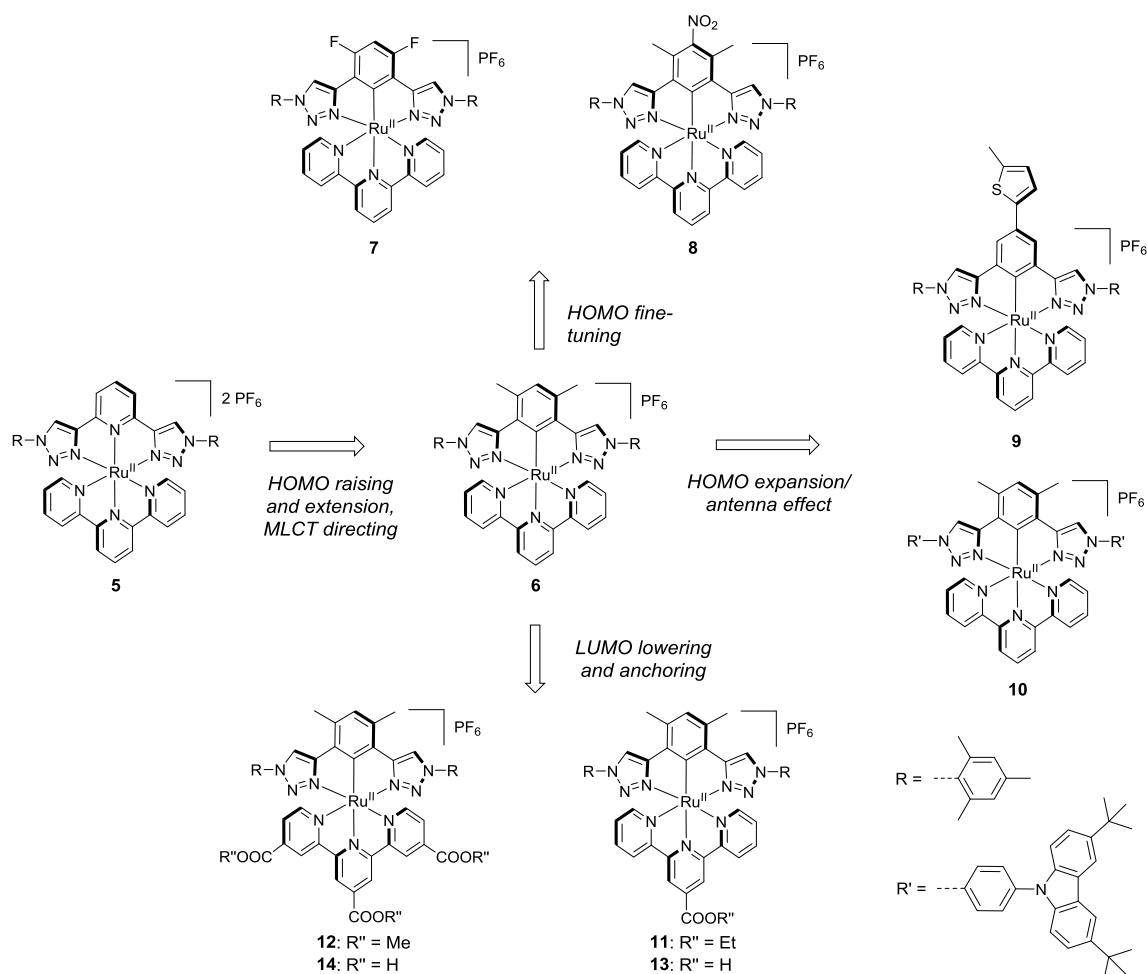
Figure 4.3. Schematic representation of the design strategy and overview of the synthesized ruthenium(II) complexes.

In initial cyclometalation attempts, the use of a common [Ru[III](tpy)(acetone)$_3$](BF$_4$)$_3$ precursor, obtained after activation of [Ru[III](tpy)Cl$_3$][229] with AgBF$_4$ in acetone and removal of the resulting AgCl by filtration,[60, 230] resulted in poor yields due to excessive side reactions, which was also observed by others in the course of our investigations.[231] Notably, the anionic ring of cyclometalated ruthenium(III) complexes show a significant radical character in the *para* position with respect to the Ru−C bond, which gives rise to, for instance, homocoupling reactions.[218, 232−233] When using a ruthenium(III) precursor, the initially formed *bis*(tridentate) ruthenium(III) polypyridyl complex is strongly oxidizing and will be reduced by an alcoholic solvent or a sacrificial amine.[234] However, in case of cyclometalating ligands, the initially formed ruthenium(III) complex will be less efficiently reduced and remains prone to side reactions. This drawback was overcome by employing [Ru[II](tpy)(MeCN)$_3$](PF$_6$)$_2$ as precursor (Scheme 4.1),[235] which is easily synthesized by refluxing [Ru[III](tpy)Cl$_3$] in acetonitrile/ethanol/water in the presence of AgNO$_3$.[236] As a further benefit, in contrast to [Ru[III](tpy)Cl$_3$], the acetonitrile-containing precursor can be purified completely by column chromatography and crystallization, thus simplifying the subsequent complexation. Ultimately, the cyclometalation was performed under oxygen-free conditions in a closed vial using an alcohol as solvent and microwave heating to 160 °C for 30 min. Isolation of the product by a combination of column chromatography and crystallization afforded the desired complexes, in most cases as X-ray-quality crystals and in reasonable yields varying from 35 to 68%, with higher yields in cases where all strategic methyl groups were present. The installation of the anchoring carboxy groups (*cf*. **13** and **14**, Figure 4.3) for the prospective DSSC application was achieved by using the corresponding ester-functionalized ruthenium(II) precursor. While the subsequent saponification was readily achieved at elevated temperatures in DMF/triethylamine/water,[184, 227, 237] the ester-functionalized complexes (**11** and **12**, Figure 4.3) were studied in more detail as they provide a higher solubility and are considered as models for the TiO$_2$-anchored sensitizers.[237]
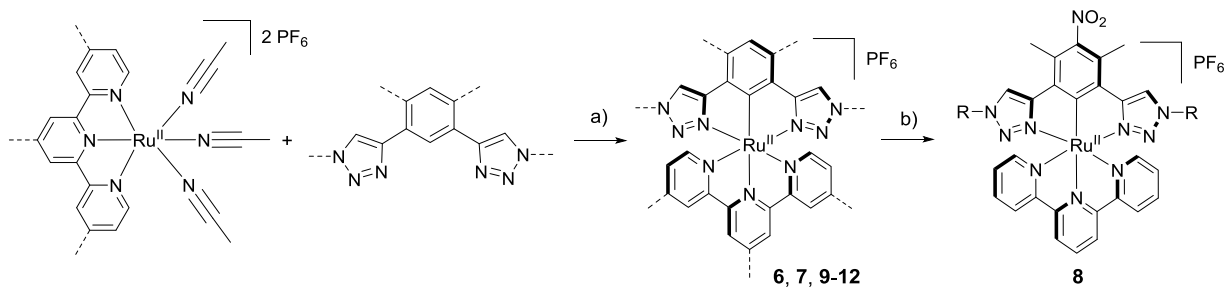
Scheme 4.1. Schematic representation of the generalized synthesis of the cyclometalated ruthenium(II) complexes (*cf*. Figure 4.3, R = mesityl): a) alcohol, microwave irradiation, 30 min., 160 °C, 35 to 68%; b) Cu(NO$_3$)$_2$, Ac$_2$O, 0 °C, 60%.

The cyclometalating phenyl ring of ruthenium(II) complexes features a high electron density in the position *para* to the Ru−C bond (*vide infra*) and is thus highly reactive against electrophiles.[238] Accordingly, a nitro group could be successfully introduced under Menke conditions (*cf*. **8**, Figure 4.3 and Scheme 4.1)[238] allowing, conversely, the manipulation of the carbanion donation by the σ- and π-accepting nitro group.[224, 239]

Two selected solid state structures are displayed in Figure 4.4. As intended, the dihedral angle between the cyclometalated phenyl ring and the thiophene ring of **9** is small (30.7°) enabling an extended conjugation (*vide infra*). On the other hand, the nitro group of **8** is

twisted out of plane by 51.8° (Figure 4.4, right), which is expected to lower the π-accepting character (*vide infra*).
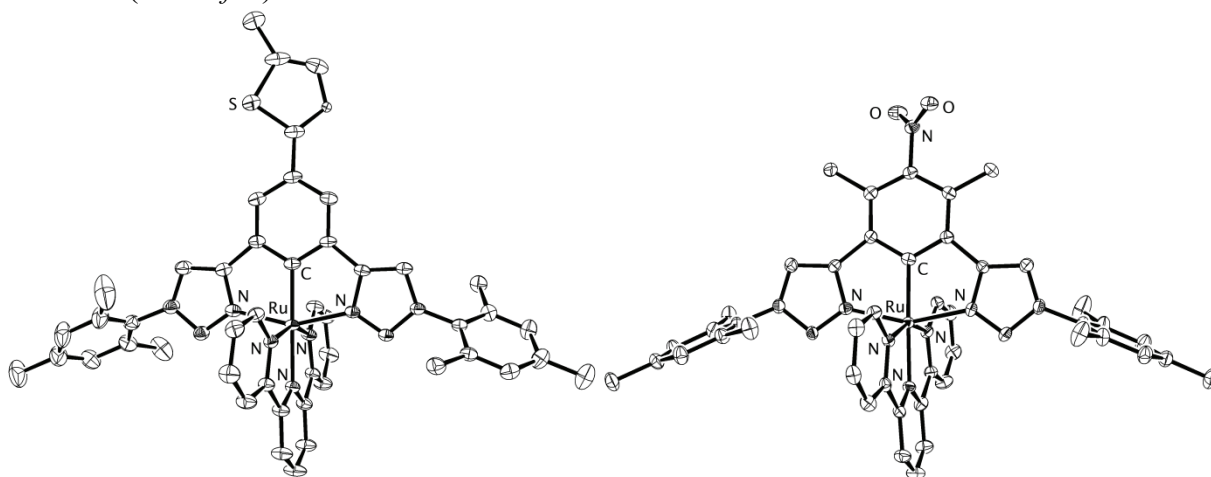
Figure 4.4. Solid-state structures of **9** (left) and **8** (right, 50% probability level; counterions, hydrogen atoms and solvent molecules omitted for clarity). The dihedral angle between the cyclometalating phenyl ring and the thiophene ring as well as the nitro groups is 30.7° and 51.8°, respectively.

To gain deeper understanding of the photophysical and electrochemical properties of the presented ruthenium(II) complexes, DFT calculations have been performed. The differences in metal−ligand π interactions within **5** and **6** are illustrated in the partial molecular orbital (MO) scheme depicted in Figure 4.5.[184, 223] Both heteroleptic, *bis*(tridentate) complexes belong to the C_{2v} point group, thus the ruthenium(II) d_{xy}, d_{xz}, and d_{yz} orbitals transform as a_2, b_1, and b_2, respectively. By combining the metal d orbitals with ligand group orbitals of appropriate symmetry, the b_1 (d_{xz}) and b_2 (d_{yz}) orbitals of the metal interact with the b_1 (π and π*) orbitals of the 1,2,3-triazole-containing ligand and the b_2 (π and π*) orbitals of the tpy ligand, respectively, while the metal-a_2 (d_{xy}) orbital can simultaneously interact with the π systems of both ligands (a_2). In the latter case, however, the interaction involves the outer 1,2,3-triazole and pyridine rings and is only weak, presumably due to the typically longer Ru−N bond lengths brought about by structural restrictions imposed by the tridentate chelation.[89−90] Furthermore, the strength of the orbital interaction depends on the energy difference and spatial overlap.

In case of **5**, the d_{xz} and d_{yz} orbitals each undergo a π back-donation with the energetically low π* orbitals of one of the tridentate ligand leading to a stabilization of both metal d orbitals. As the π* orbitals of the 1,2,3-triazole-containing ligand are higher in energy,[29, 93, 98] the π back-donation is more pronounced in case of the tpy and the LUMO is essentially located on the tpy ligand. As a result of the increasing π back-donation, the weakly interacting d_{xy} orbital represents the HOMO, while the d_{xz} and d_{yz} orbitals mostly contribute to the HOMO−1 and HOMO−2, respectively (Figure 4.5, left).
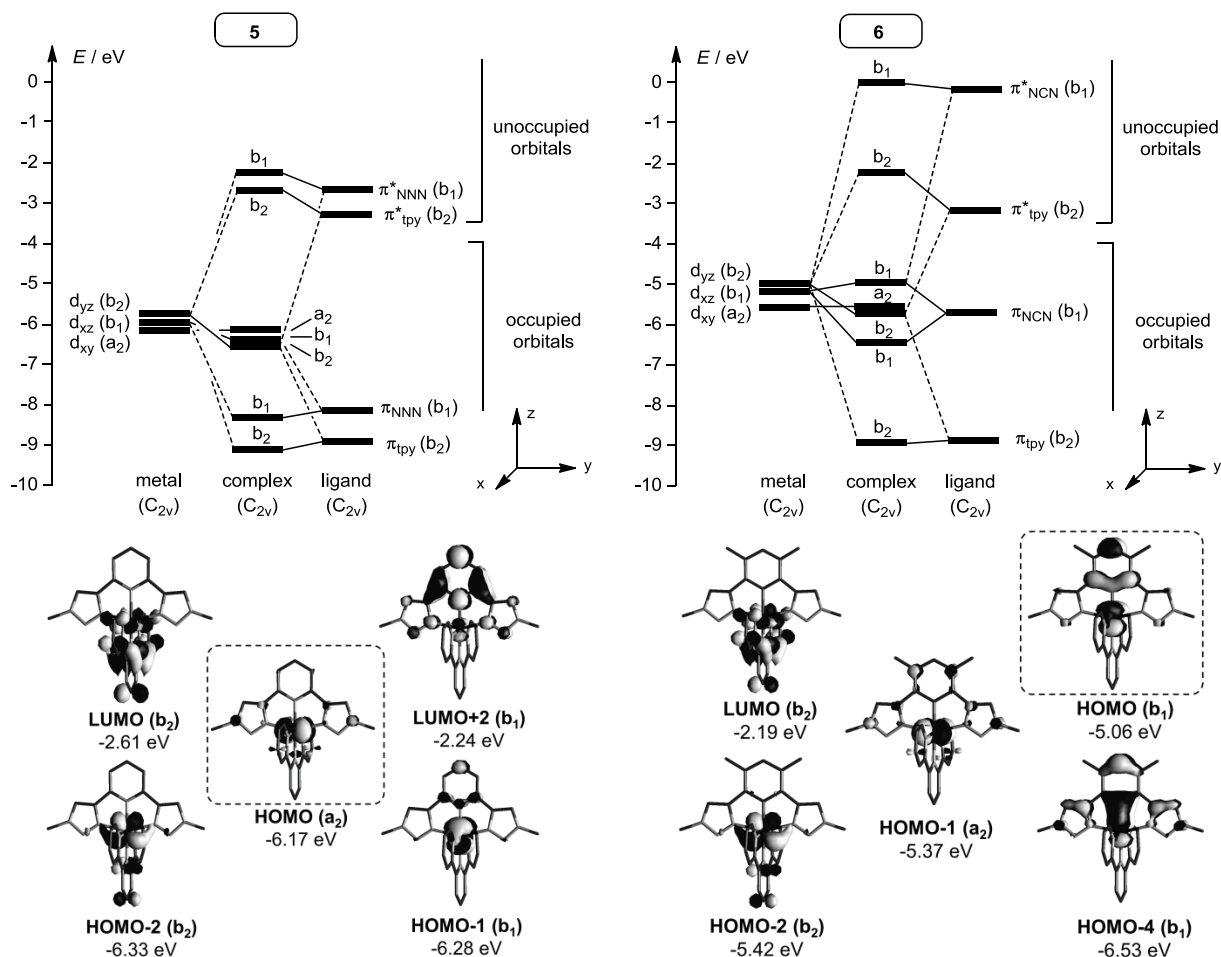
Figure 4.5. Part of an MO scheme illustrating the main π interactions within the *bis*(tridentate) ruthenium(II) complexes (top) and corresponding Kohn−Sham orbitals (PCM-B3LYP/6-31G* in MeCN, bottom) for **5** (left) and **6** (right). The mesityl moieties, ligand π orbitals with little overlap (*cf.* Figure S 2 in case of **6**) and σ interactions omitted for clarity. Note that the energies of the complex orbitals were calculated, while the orbital energies for the metal fragment and the free ligand are estimated.

While the orbital interactions within **6** are in principle the same as discussed above, the π and π* orbitals of the anionic ligand are raised in energy leading to a significant interaction between the occupied metal-d_{xz} (b_1) orbital and the π (b_1) orbital of the cyclometalating ligand (Figure 4.5, right). As a result of this repulsive interaction, the HOMO of **6** involves a different metal d-orbital than in **5** (d_{xz} instead of d_{xy}) and is strongly destabilized. Moreover, the HOMO of **6** is a π-antibonding orbital located on the metal center and essentially the cyclometalating phenyl ring. Importantly, the HOMO energy can thus be directly influenced *via* substituents attached to the cyclometalating phenyl ring.[223−224, 240] Additionally, the delocalization of the HOMO onto the ligand is postulated to facilitate the regeneration of the photo-oxidized sensitizer by the electrolyte in the DSSC.[168−169] Furthermore, the very electron-rich σ lone pair of the carbanion leads to a strong σ interaction with, amongst others, the metal-d_{z^2} (a_1) orbital and, hence, the corresponding σ-antibonding orbital is strongly destabilized. In addition, stronger electrostatic interactions within **6** raise in particular the energy of the d_{xz} and d_{yz} orbitals resulting in an enhanced π back-donation between the metal-d_{yz} orbital and the π* orbitals of the tpy ligand. Consequently, the tpy-based LUMO is more destabilized than for **5**. Furthermore, while the weakly interacting d_{xy} orbital represent the HOMO−1, the d_{yz} orbital is stabilized through π back-donation and essentially constitutes the HOMO−2.

The experimental photophysical properties are consistent with the computational results. The electronic excitations for **5** and **6** obtained *via* TD-DFT calculations are displayed in Figure 4.6 together with the measured UV−vis absorption spectra (see Table S 2 for the electronic excitations of **6**). In line with the group-theoretical considerations, the HOMO−1→LUMO transition of **5** and the HOMO→LUMO transition of **6** are not allowed as these transitions (b_1→b_2) do not feature a transition dipole moment. Accordingly, only a weak low-energy tailing is observed in the experimental spectrum, in particular for **6**. Instead, for **6** and **5**, the more intense low-energy electronic excitations involve a charge transfer directed from the metal-d_{xy} and/or the metal d_{yz} orbital towards the π^* system of the tpy ligand and are thus of MLCT character. In case of **5**, an MLCT transition directed towards the π^* system of the 1,2,3-triazole-containing ligand is predicted at about 420 nm, while, for **6**, a charge transfer towards the π^* system of the anionic ligand is expected in the UV region. Consequently, the MLCT transitions at wavelengths relevant to light harvesting applications in a DSSC (> 400 nm) are exclusively directed towards the prospective anchoring ligand in case of **6**, which is a prerequisite for fast electron injection into TiO_2. Furthermore, owing to the destabilization of the metal d-orbitals in the cyclometalated complex (*vide supra*), the MLCT maxima are significantly bathochromically shifted relative to those of **5** (Figure 4.6, left). In comparison to [Ru(tpy)(dpb)]PF$_6$,[60, 223] the absorption maxima are slightly hypsochromically shifted and the extinction coefficients are lowered for **6**. The latter is attributed to the shorter conjugation within the 1,2,3-triazole-containing cyclometalating ligand.[29, 89]
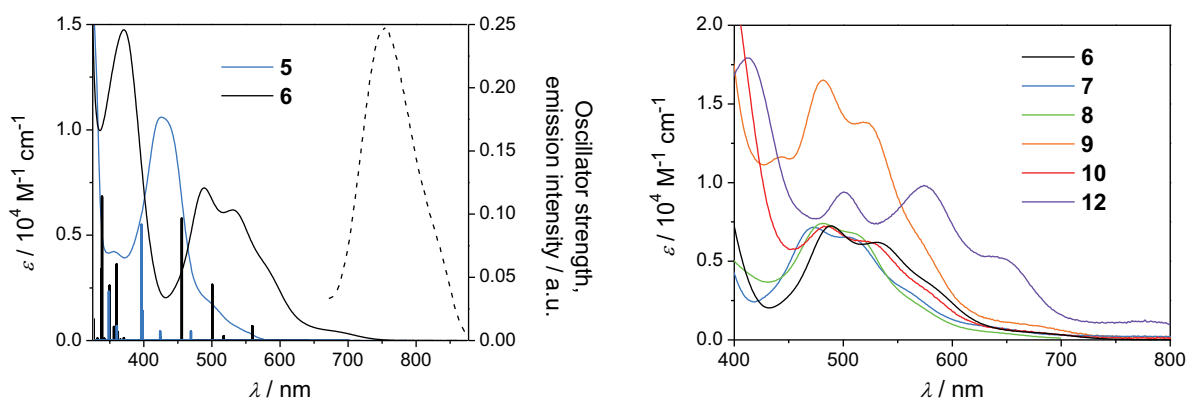
Figure 4.6. Left: Measured UV−vis absorption and emission spectra as well as computed vertical excitations (PCM-TD-B3LYP/6-31G*) of **5** and **6**. Right: Measured UV−vis absorption spectra of selected cyclometalated ruthenium(II) complexes (right, all in MeCN).

For **7** and **8**, a hypsochromic shift of the MLCT maxima relative to **6** is observed (Figure 4.6, right). According to the DFT calculations, the installation of an electron-withdrawing fluoro or nitro group on the cyclometalating phenyl ring leads to a HOMO stabilization, since the electron donation from the carbanion donor is tempered, but also because the aromatic system, which forms a part of the HOMO itself, is stabilized. In case of **10**, additional transition located on the carbazole fragment enhance the molar absorptivity at lower wavelengths (Figure 4.6, right), which is expected based on the interruption of the π-conjugation by the 1,2,3-triazoles. In contrast, for **9**, also the extinction coefficients in the region of the MLCT transitions are enhanced (Figure 4.6, right). According to the DFT calculations and X-ray crystallography (Figure 4.4), the dihedral angle between the phenyl and thienyl ring is 30.2 and 30.7°, respectively, which enables an extended conjugation of the HOMO and lower occupied molecular orbitals onto the thiophene. Additionally, an increased polarizability has been proposed for analogous complexes.[240] For the ester-functionalized

complexes, the LUMO level is strongly stabilized owing to the presence of the electron-withdrawing groups and the HOMO is slightly stabilized because of the increased π acidity of the tpy ligand, which results in smaller energy gaps than for **6**, in particular in case of **12** (Figure 4.6, right). In addition, due to the extension of, *e.g.*, the LUMO onto the conjugated acceptor, the extinction coefficients are increased.

In contrast to [Ru(tpy)$_2$](PF$_6$)$_2$ and **5**, which are practically non-emissive at room temperature,[52, 90] **6** exhibits a weak room-temperature emission in acetonitrile solution at 751 nm (Figure 4.6, left, Table 4.1) similar to [Ru(tpy)(dpb)]PF$_6$.[60] The excited-state lifetime of **6** at room temperature of 4.1 ns is significantly prolonged relative to the 0.2 ns measured for [Ru(tpy)$_2$](PF$_6$)$_2$[52–53] and comparable to the 4.5 ns observed for a derivative of [Ru(tpy)(dpb)]PF$_6$.[215] Typically, the emission of ruthenium(II) polypyridyl complexes originates from a ^{3}MLCT, which is populated after light excitation *via* IC, ISC, and vibrational relaxation.[16, 62] To confirm the MLCT nature of the lowest-energy triplet excited state of **6**, the corresponding spin density distribution has been calculated. According to the unpaired electrons within the metal-d$_{xz}$ orbital and a π^* orbital of the tpy ligand, this state can be characterized as a ^{3}MLCT.

As the radiationless deactivation of ruthenium(II) polypyridyl complexes usually proceeds *via* thermal population of short-lived ^{3}MC states,[22, 35–36, 47, 241] the excited-state lifetimes of the selected complexes were measured at variable temperatures (160 to 300 K). By the help of an Arrhenius analysis (equation 1), the sum of temperature-independent rate constants ($k_r + k_0$) as well as pre-exponential factors (A) and activation barriers (ΔE) of up to two thermally activated non-radiative deactivation pathways (k_1, k_2) were determined (Table 4.1).[52, 78, 82, 119, 219, 242–248] Beside the direct, non-activated radiative (k_r) and radiationless (k_0) ^{3}MLCT decay, the radiationless deactivation of the ^{3}MLCT can proceed *via* the ^{3}MC (A_1, ΔE_1) or a ^{3}MLCT featuring a slightly increased singlet character (^{3}MLCT$'$, A_2, ΔE_2) after thermal activation.[65, 78, 243, 248]

$$\tau(T) = \frac{1}{k_r + \sum k_{nr}} = \frac{1}{k_r + k_0 + A_1 \exp\left(-\Delta E_1 / k_B T\right) + A_2 \exp\left(-\Delta E_2 / k_B T\right)} \quad (1)$$

As the potential energy curves of the ^{3}MLCT$'$ and the ^{3}MLCT exhibit almost no horizontal displacement, the ^{3}MLCT→^{3}MLCT$'$ transition is barrierless and both states are in thermal equilibrium. Consequently, ΔE_2 represents the ^{3}MLCT–^{3}MLCT$'$ energy difference while the ^{3}MLCT$'$→^{1}GS transition, characterized by A_2, is the rate-limiting step.[78] In contrast, due to the significant reorganization associated with the population of the ^{3}MC (Figure 2.3) and the strong ^{3}MC–^{1}GS coupling, the rate-determining step for the radiationless ^{3}MLCT→^{1}GS transition *via* the ^{3}MC is usually the ^{3}MLCT→^{3}MC transition with A_1 and ΔE_1 representing the corresponding pre-exponential factor and activation energy, respectively (Figure 4.7, left).[58, 78, 210, 244–246] Nonetheless, the ^{3}MC–^{1}GS coupling might be weak, enabling a repopulation of the ^{3}MLCT from the ^{3}MC, *i.e.* ^{3}MLCT and ^{3}MC are in thermal equilibrium.[210, 245, 246] In this case, which is indicated by a relatively small A_1 ($\leq 10^{12}$ s^{-1}),[58, 245, 246] the ^{3}MC→^{1}GS transition becomes the rate-determining step instead and ΔE_1 corresponds to the ^{3}MLCT–^{3}MC energy difference (Figure 4.7, middle).[210, 245, 246] Additionally, also the ^{3}MC→^{1}GS transition can be interpreted as an activated process[8, 241] so that ΔE_1 corresponds to the energy difference between the ^{3}MLCT minimum and the ^{3}MC–^{1}GS potential-energy surface crossing (Figure 4.7, right);[58, 247] nonetheless, A_1 still corresponds to the ^{3}MC→^{1}GS transition in this case.
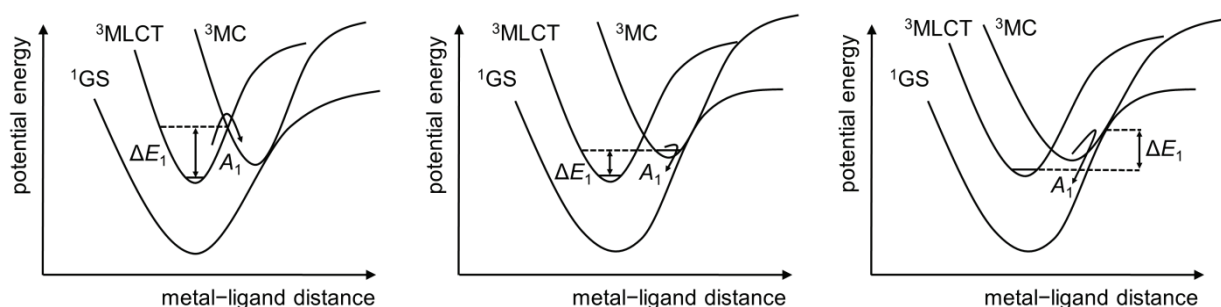
Figure 4.7. Illustration of the limiting cases of the non-radiative ^{3}MLCT deactivation *via* the ^{3}MC (^{3}MLCT$'$ omitted for clarity): The ^{3}MLCT→^{3}MC transition is the rate-limiting step in case of a strong ^{3}MC−^{1}GS coupling (left), while the ^{3}MC→^{1}GS transition is the rate-limiting step in case of a weak ^{3}MC−^{1}GS coupling (middle and right).[58, 78, 210, 245−247]

Despite the reasonably long excited-state lifetimes, the activation barrier for the ^{3}MLCT→^{1}GS transition (ΔE_1) of the cyclometalated complexes is, depending on the substitution pattern, comparable or even smaller than for [Ru(tpy)$_2$](PF$_6$)$_2$ (Table 4.1). On the other hand, the pre-exponential factor for the deactivation *via* the ^{3}MC (A_1) is significantly smaller than for [Ru(tpy)$_2$](PF$_6$)$_2$, which is the origin of the prolonged excited-state lifetimes observed for the cyclometalated complexes. Furthermore, also the activation barrier for the ^{3}MLCT$'$ population (ΔE_2) is comparable or lower relative to [Ru(tpy)$_2$](PF$_6$)$_2$; however, this parallel deactivation pathway exhibits a small pre-exponential factor (A_2) and does therefore not determine the excited-state lifetime of the cyclometalated complexes. In some cases, the corresponding parameters are not even required to reproduce the temperature dependence of the excited-state lifetimes. Notably, the room-temperature excited-state lifetimes of the studied ruthenium(II) complexes are not compromised by the different substituents, except for **7**, which exhibits a very small ΔE_1 in line with the weakest electron donation from the carbanion within series (*vide infra*). For **13** an even smaller ΔE_1 was determined,[248] but A_1 is lowered at the same time enabling an excited-state lifetime longer than 10 ns, which is promising in view of the aspired application in DSSCs.[136] Note that no emission was detected for **11**, **12**, and **14** presumably due to the low sensitivity of the used detector at $\lambda > 800$ nm.

In contrast, the deactivation for [Ru(bpy)$_3$](PF$_6$)$_2$ and ruthenium(II) complexes featuring thiocyanato ligands, *e.g.*, the fully deprotonated form of **N719**, is fundamentally different, as a high activation barrier for the ^{3}MC population ($\Delta E_1 > 4,000$ cm^{-1}) was reported (Table 4.1).[119] While A_1 is large in these cases ($> 10^{14}$ s^{-1}), the high ΔE_1 gives rise to a decelerated deactivation *via* the ^{3}MC. Beside the direct decay to the ^{1}GS,[83] the ^{3}MLCT lifetime is only limited by the deactivation *via* the ^{3}MLCT$'$ in these cases, which explains the longer excited-state lifetimes than for the cyclometalated complexes.

The reason for the stronger ^{3}MC destabilization in complexes like [Ru(bpy)$_3$](PF$_6$)$_2$ and **N719** is the equal destabilization of both the d$_{z^2}$ and the d$_{x^2−y^2}$ orbital. In contrast, *bis*(tridentate) ruthenium(II) complexes like [Ru(tpy)$_2$](PF$_6$)$_2$ exhibit a weakened coordination of the outer pyridine rings due to the non-ideal bite angle of the tpy ligand (~ 158°).[22, 57] The σ*(d$_{x^2−y^2}$) orbital is thus lowered in energy enabling an efficient deactivation *via* the corresponding ^{3}MC state.[52, 60, 63] In line with an increased σ*(d$_{x^2−y^2}$) destabilization, an excited-state lifetime of 60 ns was measured for N^N^C-cyclometalated *bis*(tridentate) ruthenium(II) complexes.[81] However, for the N^C^N-cyclometalated congeners, mainly the σ*(d$_{z^2}$) orbital is destabilized, while the σ*(d$_{x^2−y^2}$) orbital remains relatively low in energy[60, 63] resulting in a small ^{3}MLCT−^{3}MC energy separation. Despite the small energy barrier for the non-radiative

^{3}MLCT→^{1}GS transition *via* the ^{3}MC ($\Delta E_1 \leq 1{,}830$ cm^{-1}), the deactivation of the presented N^C^N-cyclometalated complexes is decelerated by means of a smaller pre-exponential factor A_1 (10^{12} to 10^{10} s^{-1}), which suggests a reduced ^{3}MC−^{1}GS coupling (*vide supra*, *cf.* Figure 4.7, right).[245] The latter appears to be a general feature of cyclometalated ruthenium(II) complexes, as also *tris*(bidentate) ruthenium(II) complexes bearing cyclometalating ligands show very similar deactivation parameters (*cf.* Table 4.1).[219]

Table 4.1. Photophysical data of selected ruthenium(II) complexes.

Complex	λ_{max}^{Em} / nm [a]	Φ_{PL} 10^{-4} [a]	τ / ns [a]	k_r+k_0 / s^{-1} [b]	A_1 / s^{-1} [b]	A_2 / s^{-1} [b]	ΔE_1 / cm^{-1} [b]	ΔE_2 / cm^{-1} [b]
[Ru(tpy)$_2$]$^{2+}$[c]	–	–	0.21[d]	6.5·10^4	2.0·10^{13}	2.1·10^7	1,700	720
[Ru(bpy)$_3$]$^{2+}$[e]	615	620	825	7.8·10^5	4.4·10^{14}	–	4,240	–
[Ru(bpy)$_2$(NO$_2$-ppy)]$^{+}$[f]	–	–	–	1.2·10^6	2.6·10^{11}	–	956	–
[Ru(dcbpy)$_2$(NCS)$_2$]$^{2-}$[e]	723	35	27	5.5·10^6	1.7·10^{15}	1.3·10^8	4,620	750
6	751	0.6[g]	4.1	2.44·10^5	1.1·10^{12}	3.11·10^8	1,830	350
7	–	–	0.5[h]	1.72·10^5	9.74·10^{11}	–	1,290	–
8	705	1.0[g]	5.3	1.92·10^5	6.63·10^{11}	–	1,395	–
9	745	0.5[g]	4.1[h]	2.33·10^5	1.89·10^{11}	1.42·10^8	1,452	240
10	750	2.5[g]	6.7[h]	2.22·10^5	2.04·10^{11}	1.33·10^8	1,570	270
13	–	–	12.3[h]	1.75·10^5	2.02·10^{10}	–	1,135	–

[a] Measured at 298 K in deaerated MeCN unless stated otherwise. [b] The corresponding measurements were conducted in deaerated *n*-butyronitrile unless stated otherwise. [c] Counterion = PF$_6^-$; taken from ref. [78]. [d] Measured at 290 K; taken from ref. [52]. [e] Counterion = PF$_6^-$ or NBu$_4^+$; dcbpy = 2,2′-bipyridine-4,4'-dicarboxylate; measured in MeCN; taken from ref. [119]. [f] Counterion = BF$_4^-$; NO$_2$-ppy = 4-nitro-2-(pyridin-2-yl)benzen-1-ide; measured in EtOH/MeOH (4:1 *v/v*); taken from ref. [219]. [g] Determined using [Ru(dqp)$_2$](PF$_6$)$_2$ in MeOH/EtOH (1:4 *v/v*; Φ_{PL} = 2.0%) as a reference.[50] [h] Extrapolated from the temperature-dependent lifetime measurements conducted in *n*-butyronitrile.

The experimental electrochemical properties of the studied complexes (Figure 4.8, Table 4.2) corroborate the theoretical analysis of their electronic structure (*vide supra*). As a consequence of the cyclometalation, the Ru(III)/Ru(II)-based redox potential of **6** is lowered by 900 mV relative to **5**. The first reduction process of **6** is cathodically shifted by 260 mV in comparison to **5**, as the more electron-rich metal center allows a stronger π back-donation, which raises the LUMO energy. Upon the installation of electron-withdrawing fluoro and nitro groups on the cyclometalating phenyl ring, the Ru(III)/Ru(II)-based redox potential is increased by 230 and 180 mV, respectively. In contrast, for a related series of cyclometalated *tris*(bidentate) ruthenium(II) complexes bearing the same substitution patterns except for the methyl groups adjacent to the nitro group, the HOMO stabilization was more pronounced for the nitro substituent than for the fluoro substituents.[224] The different behavior is ascribed to the dihedral angle between the nitro group and the phenyl ring of about 51.8° (*vide supra*, DFT-calculated value: 51.6°) enforced by the methyl groups, which lowers the effective π-accepting character of the nitro group. For the ester-substituted complexes, **11** and **12**, significant anodic shifts of about 190 and 430 mV, respectively, were observed for the reduction, while the oxidation process is anodically shifted by 80 and 180 mV, respectively. This is in line with a direct stabilization of the tpy-based LUMO, which, in turn, allows an indirect HOMO stabilization *via* an enhanced π back-donation with the tpy (*vide supra*). For **9** and **10**, the redox potentials are nearly unchanged, but the reduction process becomes irreversible.
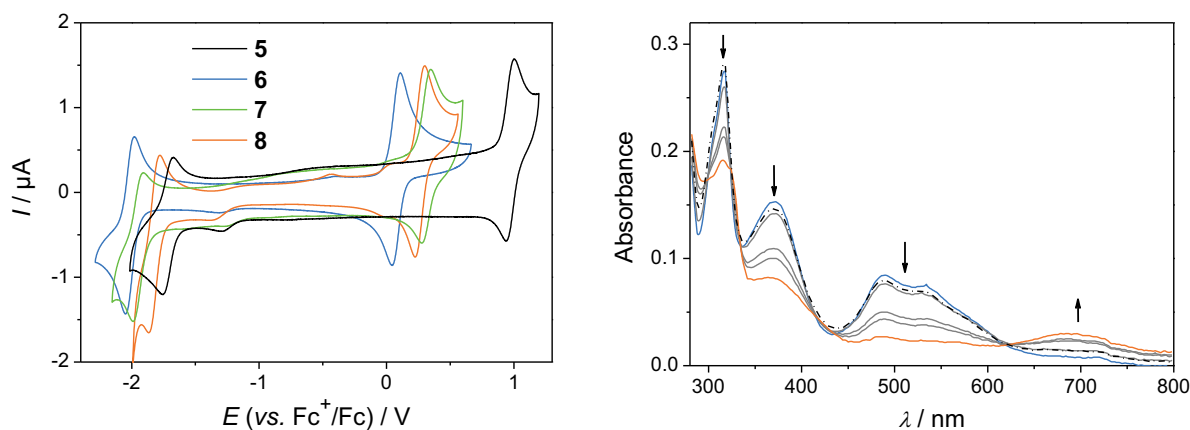
Figure 4.8. Left: Cyclic voltammetry spectra of selected ruthenium(II) complexes (10^{-5} M in MeCN with 0.1 M Bu$_4$NPF$_6$). Right: Change of the UV−vis absorption spectrum of **6** during the oxidation (solid lines) and after the re-reduction (dashed line) process (10^{-5} M in MeCN with 0.1 M Bu$_4$NPF$_6$).

Table 4.2. Electrochemical data of selected ruthenium(II) complexes.

Complex	$E_{1/2}^{Ox}$ / V (i_{pa}/i_{pc}, ΔE_p / mV)[a]	$E_{1/2}^{Red}$ / V (i_{pa}/i_{pc}, ΔE_p / mV)[a]
5	0.98 (1.1, 74)	−1.72 (0.9, 80)
[Ru(tpy)$_2$](PF$_6$)$_2$[b]	0.89 (64)	−1.66 (63)
6	0.08 (1.0, 67)	−1.98 (1.0, 71)
[Ru(tpy)(dpb)]PF$_6$[b]	0.12 (62)	−1.95 (63)
7	0.31 (1.0, 74)	−1.95 (1.0, 79)
8	0.26 (1.0, 76)	−1.82 (1.0, 88)
9	0.07 (1.0, 69)	−1.97[c]
10	0.10 (1.0, 83)	−1.97[c]
11	0.16 (1.0, 70)	−1.79 (1.1, 80)
12	0.26 (1.0, 71)	−1.56 (1.0, 71)

[a] Measured in MeCN with 0.1 M Bu$_4$NPF$_6$ using Fc$^+$/Fc as reference. [b] Taken from ref. [60]. [c] Irreversible process.

A comparison of **5** and **6** with [Ru(tpy)$_2$](PF$_6$)$_2$ and [Ru(tpy)(dpb)]PF$_6$, respectively, reveals the influence of the 1,2,3-triazole. For the non-cyclometalated complexes, the substitution of a tpy ligand by the 2,6-*bis*(1,2,3-triazol-4-yl)pyridine leads to a metal-based HOMO of lower energy and a tpy-based LUMO of higher energy, indicating a weaker σ-donor and π-acceptor strength of the triazole-containing ligand that would allow the tpy to predominate the π back-donation.[29] When comparing [Ru(tpy)(dpb)]PF$_6$ and **6**, for the latter complex the oxidation and reduction potentials are cathodically shifted. Consequently, the triazole-containing cyclometalating ligand is a stronger effective π donor than its pyridine-counterpart increasing the energy of the HOMO, based on a metal d-orbitals and π orbitals of the central phenyl ring, and, through increased π back-donation from the more electron-rich metal center, the energy of the tpy-based LUMO. The former is most likely caused by a weaker π back-donation into the peripheral triazole as well as by a weaker stabilization of the carbanion by the adjacent triazoles due to a less extended conjugation.[29, 89]

The oxidation process of **6** was studied in more detail by spectroelectrochemical experiments (Figure 4.8). The most obvious changes during oxidation are the decrease of the MLCT bands between 350 and 600 nm corroborating the assumption of a significant metal contribution to the HOMO. In line with that, additional, broad peaks between 600 and 850 nm appear upon oxidation, which are tentatively assigned to an LMCT transition. The observation of several isosbestic points indicates a well-defined conversion from the ruthenium(II) to the

ruthenium(III) species. Remarkably, the reduction of the oxidized species recreates the original spectra almost completely, thus approving the oxidation processes to be fully reversible even under these demanding conditions where the complexes are oxidized for hours. Notably, a C−C homocoupling of the complexes in their oxidized state[232] was not observed, which is ascribed to the placement of the methyl groups on the cyclometalating phenyl ring.

In conclusion, a series of 1,2,3-triazole-containing cyclometalated ruthenium(II) complexes is presented. The functionalized, cyclometalating ligands are readily assembled by means of click chemistry and the corresponding complexes are easily synthesized *via* an optimized protocol. Regarding the photophysical and electrochemical properties, the cyclometalated complexes resemble ruthenium(II) polypyridyl complexes featuring thiocyanato ligands, *i.e.* the carbanionic chelating ligand mimic the electronic function of multiple monodentate thiocyanates. Accordingly, the new complexes meet several requirements for an application in DSSCs: 1) The metal-based d-orbital are raised in energy causing a small energy gap and, therefore, a strongly red-shifted absorption, 2) the HOMO is extended to the ligand, which is postulated to facilitate the dye regeneration, 3) the MLCT transitions are directed towards the anchoring tpy ligand enabling electron injection into TiO_2, and 4) the excited-state lifetimes are sufficiently long to allow efficient electron injection. Moreover, the cyclometalated complexes offer an electrochemical fine-tuning, to ensure efficient dye regeneration by the electrolyte, and the optimization of the light harvesting capability *via* functionalization of the cyclometalating ligand. A further advantage of the cyclometalated complexes is their increased stability by virtue of the tridentate chelates and the presence of a strong organometallic bond. Ultimately, these promising electronic properties and structural benefits strongly suggest their application in DSSCs. Importantly, the replacement of pyridines by 1,2,3-triazoles does not compromise the photophysical and electrochemical properties of the cyclometalated ruthenium(II) complexes, thus allowing a more flexible and facile functionalization of the sensitizers.

Ruthenium(II) complexes featuring 1,2,3-triazolate donors

Apart from the above discussed cyclometalation, the poor photophysical properties of $[Ru(tpy)_2](PF_6)_2$ can be improved by replacement of the outer pyridine rings of the tpy ligand by, *e.g.*, carbenes[37, 195, 201] or anionic nitrogen donors.[82, 188] The viability of the latter approach was demonstrated by Vos and co-workes, who employed 1,2,4-triazolate donors to suppress the radiationless deactivation *via* the ^{3}MC.[82, 188] The use of analogous 1,2,3-triazolate-based ligands is expected to result in similar electronic properties of the corresponding ruthenium(II) complexes (**15** and **16**, Figure 4.9), while the formation of coordination isomers is precluded (*cf.* Figure 4.9) and a facile ligand synthesis *via* an azide−alkyne cycloaddition is enabled.

15: R = H
16: R = n-hexyl
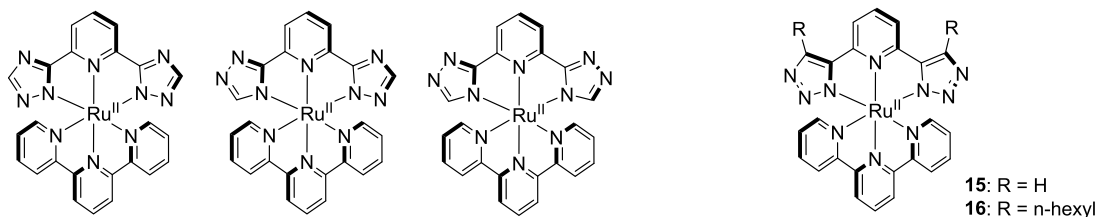
Figure 4.9. Schematic representation of ruthenium(II) complexes featuring 1,2,4-triazolates (left) and 1,2,3-triazolates (right).

The unsubstituted 2,6-*bis*(2*H*-1,2,3-triazol-4-yl)pyridine ligand (*cf.* **15**, Figure 4.9) was synthesized *via* a copper(I)-catalyzed cycloaddition between 2,6-diethynylpyridine and *in situ* formed azidomethanol followed by a base-induced cleavage of formaldehyde.[249] Alternatively, an alkyl-functionalized ligand (*cf.* **16**, Figure 4.9) was synthesized *via* a thermal azide−alkyne cycloaddition between 2,6-di(oct-1-yn-1-yl)pyridine and azidomethyl pivalate followed by a base-induced saponification−elimination sequence to cleave off the *N*-substituent.[250] The corresponding charge-neutral metal complexes, **15** and **16**, were obtained in good yields after conversion of the respective 1,2,3-triazole ligands with [Ru(tpy)(MeCN)$_3$](PF$_6$)$_2$[251] at elevated temperatures and after treatment of the reaction mixture with a base.

To better understand the electronic properties of the new complex, DFT and TD-DFT calculations have been carried out for **16** (note that the hexyl chains have been replaced by methyl groups for the calculations). The main π interactions are illustrated in a simplified MO scheme depicted in Figure 4.10. Firstly, in comparison to the analogous ruthenium(II) complex featuring neutral 1,2,3-triazole donors (**5**, *vide supra*), the anionic 1,2,3-triazolates cause a destabilization of the d$_{xz}$ and, in particular, the d$_{yz}$ and d$_{xy}$ orbitals *via* electrostatic repulsion. Secondly, the π system of the 1,2,3-triazolate is raised causing a repulsive π interaction with the metal-d$_{xy}$ (a$_2$) orbital. As a result, the HOMO is located mainly on the metal center and the 1,2,3-triazolates. On account of the increased electron density on the metal center, the d$_{yz}$ (b$_2$)→π* (b$_2$) back-donation is enhanced, lifting the tpy-based LUMO level. As the energy of the π* (b$_1$) orbital of the anionic ligand is significantly higher, only a weak stabilization of the metal-d$_{xz}$ (b$_1$) orbital though π back-donation is expected. Furthermore, the σ*(d$_{x^2-y^2}$) orbital is more destabilized in the triazolate complex due to the increased σ donor strength relative to **5**. Ultimately, similar to the cyclometalated ruthenium(II) complexes, the strong anionic donors result in a HOMO and LUMO destabilization with the former effect being more pronounced, *i.e.* the HOMO−LUMO gap is smaller.
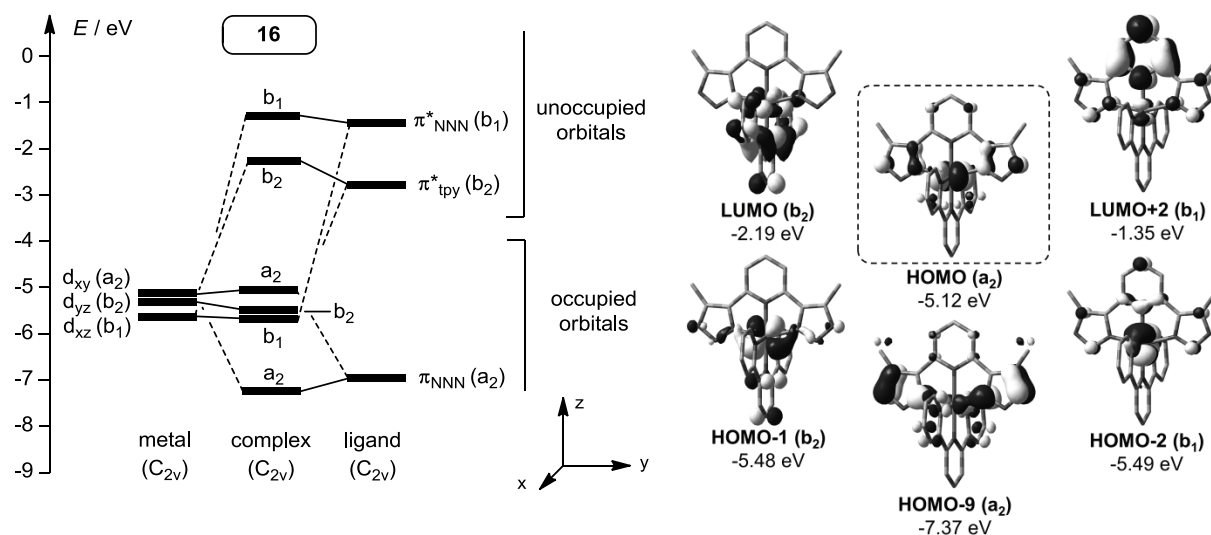
Figure 4.10. Part of an MO scheme illustrating the main π interactions within the 1,2,3-triazolate complex **16** (left) and corresponding Kohn−Sham orbitals (PCM-B3LYP/6-31G* in MeCN, right). The hexyl chains have been replaced by methyl groups, ligand π orbitals with little overlap (*cf.* Figure S 3) and σ interactions omitted for clarity. Note that the energies of the complex orbitals were calculated, while the orbital energies for the metal fragment and the free ligand are estimated.
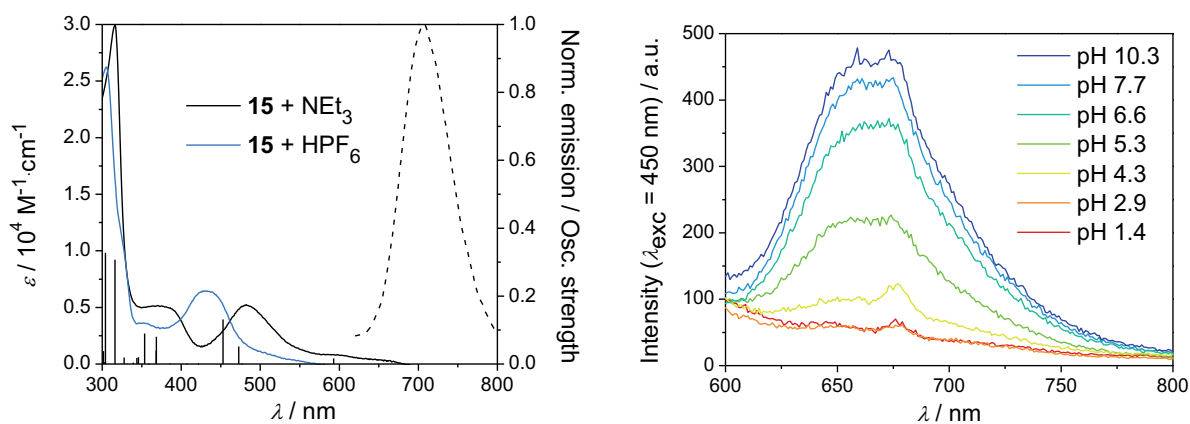
Figure 4.11. UV−vis absorption and emission spectrum of the deprotonated and protonated form of **15** as well as the calculated vertical excitations of **16** (PCM-TD-B3LYP/6-31G* in MeCN, left). Emission spectra at different pH values for **15** (right).

The photophysical and electrochemical properties (Figure 4.11, Table 4.3) support the computational results: Relative to its 1,2,3-triazole counterpart, a cathodic shift of the redox potentials as well as a bathochromically shifted absorption is observed for the 1,2,3-triazolate ruthenium(II) complex. Furthermore, a weak, plateau-like absorption band extends to very long wavelengths, which is a typical feature of *bis*(tridentate) ruthenium(II) complexes featuring azolate donors.[82, 188, 190, 193] According to the TD-DFT calculations (Table S 3), the longest-wavelength absorption corresponds to the HOMO→LUMO transition, which is allowed for this kind of complex (a_2→b_2), but only of moderate oscillator strength. Due to the participation of the 1,2,3-triazolates, this transition is of metal−ligand-to-ligand (MLLCT) character. Further transitions at longer wavelengths are either of weak intensity or symmetry-forbidden, *e.g.* HOMO−2(b_1)→LUMO(b_2), which explains the plateau in the absorption spectrum. More intense electronic transitions are predicted at 470 and 450 nm and involve a charge transfer from the d_{yz} and d_{xy} orbitals of the metal towards π^* orbitals located on the tpy ligand. An MLCT transition associated with a charge transfer towards the central pyridine ring of the anionic ligand is expected to occur in the UV region.

As the 1,2,3-triazolate rings of the ruthenium(II) complexes feature additional nitrogen donors, the complexes can be protonated (Figure 4.11). By using UV−vis acid−base titration, the pK_a value of the corresponding ruthenium(II)-coordinated 1,2,3-triazoles was determined to be about 4.7. As expected, the electronic properties of the fully protonated form bearing two charge-neutral 1,2,3-triazole donors resemble the ones of **5** (Table 4.3). In contrast, the 1,2,3-triazolate complex **15** is weakly emissive in solution at room temperature (Figure 4.11), which is ascribed to a diminished radiationless deactivation of the ^{3}MLCT *via* the ^{3}MC in line with the increased donors strength of the 1,2,3-triazolates.[82, 188] This is corroborated by the relatively long excited-state lifetime of 54 ns measured for **16**.

Table 4.3. Selected data of the studied ruthenium(II) complexes.

complex	λ_{max}^{Abs} / nm (ε / 10^3 M^{-1} cm^{-1})[a]	λ_{max}^{Em} / nm[a]	τ / ns[a]	$E_{1/2}^{Ox}$ / V[b] (i_{pa}/i_{pc}, ΔE_p / mV)	$E_{1/2}^{Red}$ / V[b] (i_{pa}/i_{pc}, ΔE_p / mV)
15	661 (sh, 0.3), 600 (sh, 0.8), 482 (5.2)	705	_[d]	_[d]	_[d]
15H[c]	503 (sh, 1.0), 430 (br, 6.4)	–	_[e]	_[e]	_[e]
16	662 (0.7), 608 (0.9), 487 (5.6)	719	54	0.20 (1.1, 74)	−2.01 (1.0, 71)
5	500 (1.8), 428 (br, 10.6)	–	–	0.98 (1.1, 74)	−1.72 (0.9, 80)

[a] Measured in deaerated MeCN unless stated otherwise; br = broad, sh = shoulder. [b] Measured in MeCN with 0.1 M Bu$_4$NPF$_6$ using Fc$^+$/Fc as reference. [c] **15** in the presence of an excess of HPF$_6$. [d] Not measured due to low solubility. [e] Not determined.

In conclusion, the new 1,2,3-triazolate ruthenium(II) complexes are readily synthesized and show a broad absorption of visible light resulting in charge-separated excited states with long lifetimes. Furthermore, in the excited-state, an electron is transferred to the tpy ligand, while the resulting hole is shared by the metal and the ligand, rendering the new complexes promising candidates for applications in DSSCs.

5   Dye-sensitized Solar Cell Application and Anodic Electropolymerization

Parts of this chapter have been or will be published: A4) S. Sinn, B. Schulze, C. Friebe, D. G. Brown, M. Jäger, E. Altuntaş, J. Kübel, O. Guntner, B. Dietzek, C. P. Berlinguette, U. S. Schubert, *Inorg. Chem.* **2014**, *53*, 2083−2095; A6) B. Schulze, D. G. Brown, K. C. D. Robson, C. Friebe, M. Jäger, E. Birckner, C. P. Berlinguette, U. S. Schubert, *Chem. Eur. J.* **2013**, *19*, 14171−14180; A7) S. Sinn, B. Schulze, C. Friebe, D. G. Brown, M. Jäger, J. Kübel, B. Dietzek, C. P. Berlinguette, U. S. Schubert, *Inorg. Chem.* **2014**, *53*, 1637−1645; A9) C. Friebe, B. Schulze, H. Görls, M. Jäger, U. S. Schubert, *Chem. Eur. J.* **2014**, *20*, 2357−2366.

Cyclometalated ruthenium(II) photosensitizers

Among the most efficient dyes for application in DSSCs are the thiocyanate-containing ruthenium(II) complexes $[Ru(Hdcbpy)_2(NCS)_2](NBu_4)_2$ (**N719**; Hdcbpy = 2,2′-bipyridine-4-carboxylic acid-4′-carboxylate)[252] and **N749** (Figure 5.1).[41] Enormous research efforts have been made in the last years to improve both the PCE as well as the long-term stability of devices based on these prototypical sensitizers.[21, 42−43] The most promising approach is the replacement of the monodentate thiocyanato ligands with anionic aromatic chelates, which improves the complex stability and allows the installation of additional chromophores in order to optimize the light harvesting capability.[184, 186, 190, 193, 253] In addition, the electrochemical properties of the cyclometalated ruthenium(II) complexes can be adjusted by the attachment of electron-donating or -withdrawing substituents to the anionic phenyl ring.[224, 227, 251, 254] Moreover, the sensitizers can be easily equipped with hydrophobic alkyl chains, which are known to enhance the thermal and long-term stability of a DSSC by preventing water-induced dye desorption[145, 157, 255−256] and enable the use of alternative electrolytes,[142, 156, 257] which are crucial for the further improvement of the efficiency of DSSCs.[140] While the vast majority of DSSC sensitizers has focused on polypyridyl ligands, it has been demonstrated that 1,2,3-triazoles can serve as pyridine surrogates offering readily functionalized ligands.[29, 251, 258] Motivated by a high PCE of 8.3% (*vs.* 9.0% achieved with **N719** under identical conditions) for **T4** (Figure 5.1),[222] we sought to examine the viability of triazole-based analogues as useful sensitizer platforms.
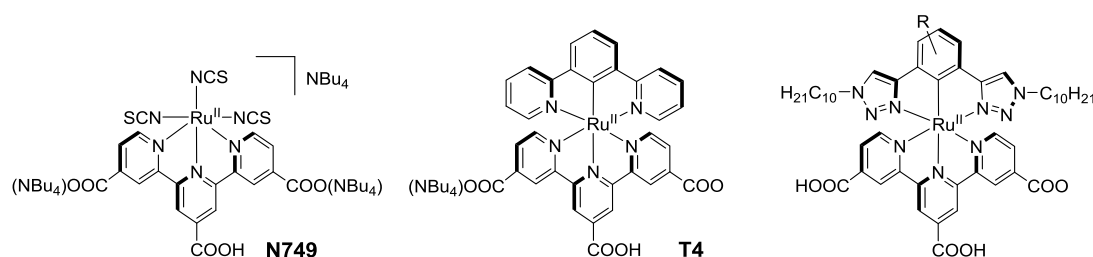
Figure 5.1. Schematic representation of the benchmark dye **N749**, of a related cyclometalated ruthenium(II) sensitizer, **T4**, and of a 1,2,3-triazole-analog of the latter. Note that the cyclometalated complexes are zwitterionic with one carboxylate compensating the positive charge of the ruthenium(II) complex fragment.

The synthesis of the 1,2,3-triazole-based tridentate ligands (**17** and **18**, Scheme 5.1) was readily achieved *via* CuAAC using functionalized 1,3-diethynylbenzenes as well as *n*-decyl azide as building blocks. The *n*-decyl chain was chosen in view of the successful DSSC application of ruthenium(II) sensitizers bearing alkyl chains of similar length.[145, 156] Furthermore, a fluoro-substituted ligand was prepared in order to increase the Ru(III)/Ru(II) redox potential of the corresponding ruthenium(II) complex and thereby ensure efficient

regeneration of the photo-oxidized sensitizer by the I_3^-/I^--based electrolyte.[182, 227] The subsequent cyclometalation step was conducted with $[Ru(tcmtpy)(MeCN)_3](PF_6)_2$ (tcmtpy = 4,4′,4″-tricarboxymethyl-2,2′:6′,2″-terpyridine) in either methanol or *N,N*-dimethylformamide (DMF) at elevated temperatures under microwave irradiation (Scheme 5.1) to afford the desired cyclometalated product with fair yields after a simple chromatographic purification. Notably, methanol was the solvent of choice to avoid transesterification/saponification and to promote the cyclometalation;[60, 259] however, in case of **18** a partial replacement by a methoxy group was observed leading to inseparable mixtures and DMF was thus used instead. As the anionic aryl ring enables a facile post-complexation functionalization in the position opposite to the Ru−C bond,[238] a nitro group was introduced using $Cu(NO_3)_2$ in order to attenuate the electron donation from the carbanion.[251] Furthermore, bromo and iodo substituents were installed at the cyclometalated phenyl ring using *N*-bromo- and *N*-iodosuccinimide, respectively, which enables prospective cross-coupling reactions,[260−261] *e.g.*, to attach electron donors that allow intramolecular hole transfer.[164, 166, 184, 262−263] The saponification of the ester-functionalized ruthenium(II) complexes was conducted at elevated temperatures in DMF/water/triethylamine (3:1:1 *v/v/v*).[184, 237] After washing with dichloromethane, the cyclometalated sensitizers were obtained as zwitterionic species (featuring two carboxy groups and one carboxylate) as confirmed by elemental analyses. The solubility of the complexes was sufficient to prepare a 0.25 mM staining solution in DMF/methanol (4:1 *v/v*).
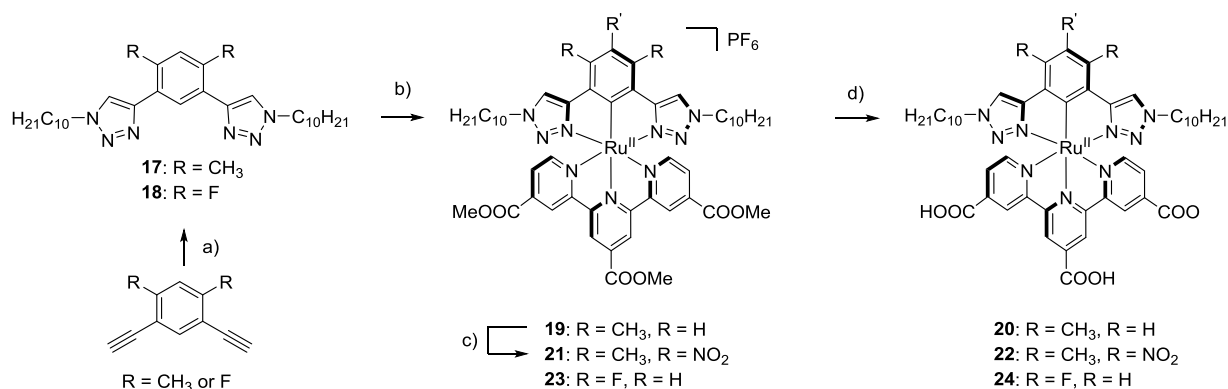
Scheme 5.1. Schematic representation of the syntheses of the ruthenium(II) sensitizers: a) $C_{10}H_{21}N_3$, $CuSO_4 \cdot 5H_2O$, sodium ascorbate, EtOH/H_2O (2:1 *v/v*), 50 °C, 12 h, 81 to 85%; b) $[Ru(tcmtpy)(MeCN)_3](PF_6)_2$, MeOH or DMF, 150 to 160 °C, 30 to 60 min., 56 to 60%; c) $Cu(NO_3)_2$, CH_2Cl_2/MeOH (2:1 *v/v*), 40 °C, 18 h, 87%; d) DMF/NEt_3/H_2O (3:1:1 *v/v/v*), 80 °C, 24 h, 95 to 98%.

To allow a deeper understanding of the photophysical properties of the presented ruthenium(II) complexes, DFT and TD-DFT calculations were performed. The calculated vertical singlet−singlet transitions, exemplarily shown for **20** in Figure 5.2, are in reasonable agreement with the experimental absorption spectra (*vide infra*). For **20** and **24**, all vertical singlet transitions in the visible light region are mainly of MLCT character with varying ligand-to-ligand-charge-transfer (LLCT) contributions (MLLCT), *i.e.* they essentially involve a charge transfer from the metal center (and in some cases the cyclometalating ligand) towards the carboxy-functionalized tpy ligand. Notably, the lowest-energy transition ($S_0 \rightarrow S_1$), which is an almost pure HOMO→LUMO transition, is symmetry-forbidden and only a weak shoulder is observed in the experimental spectrum. In case of **22**, the LUMO+2 features significant contribution from the nitro group resulting in an intense MLCT transition at about 470 nm, directed from the metal center towards both the tpy ligand and the nitro group. However,

generally all electronic excitations result in the population of the lowest-energy excited state, which is typically a ^{3}MLCT for ruthenium(II) complexes.[16] For all three complexes studied herein, a significant portion of spin density is localized on the carboxy-functionalized tpy in the T_1 state (Figure 5.2), *i.e.* the excited electron is transferred to the anchoring ligand awaiting injection into TiO_2.
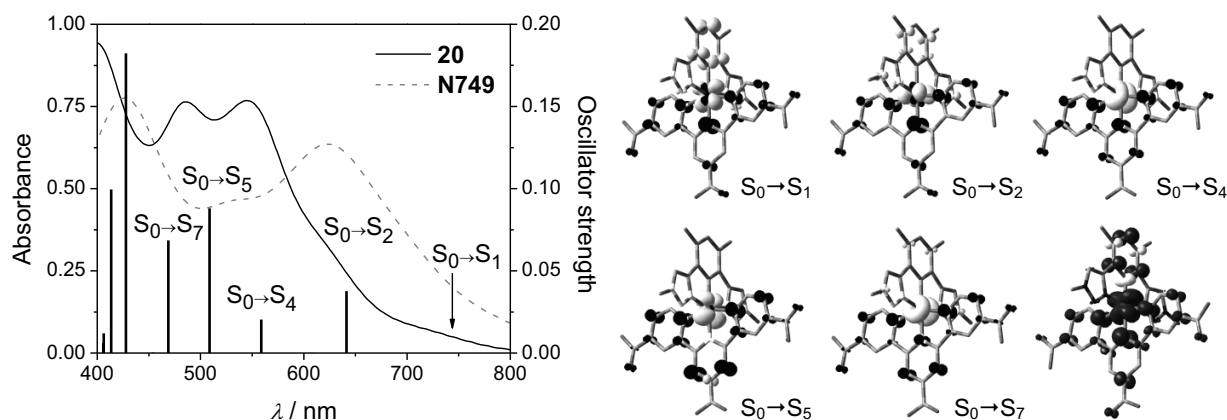
Figure 5.2. Left: Experimental UV−vis absorption spectrum of **20** and **N749** adsorbed on TiO_2 (12 μm thick, transparent film, active area of 0.88 cm^2) and calculated vertical singlet−singlet transitions (PCM-TD-B3LYP/6-31G* in MeCN) of **20**. Right: Selected corresponding electron-density difference maps (white = depletion, black = accumulation, isovalue 0.004) as well as spin density distribution of the ^{3}MLCT of **20** (bottom right, isovalue 0.004). Note that, for the DFT calculations, the *n*-decyl chains have been replaced by methyl groups and that the tpy ligand is functionalized with carboxy groups, which are known to electronically resemble the Ti(IV)-coordinated carboxylates.[147]

The experimental UV−vis absorption and emission spectra of the title complexes are displayed in Figure 5.3 and summarized in Table 5.1. The **20** and **24** complexes show moderate extinction coefficients in the MLCT region (about 9,000 and 8,000 M^{-1} cm^{-1}, respectively), while the extinction coefficient in the MLCT maximum of **22** (about 12,000 M^{-1} cm^{-1}) is increased by about 30% relative to **20** in line with the DFT-predicted participation of the nitro group to the HOMO and, in particular, the LUMO+2 (*vide supra*). Upon functionalization of the central cyclometalating phenyl ring with electron withdrawing groups, the HOMO destabilization by the carbanion is reduced resulting in a hypsochromic shift of the MLCT features corresponding to 0.07 to 0.10 eV.
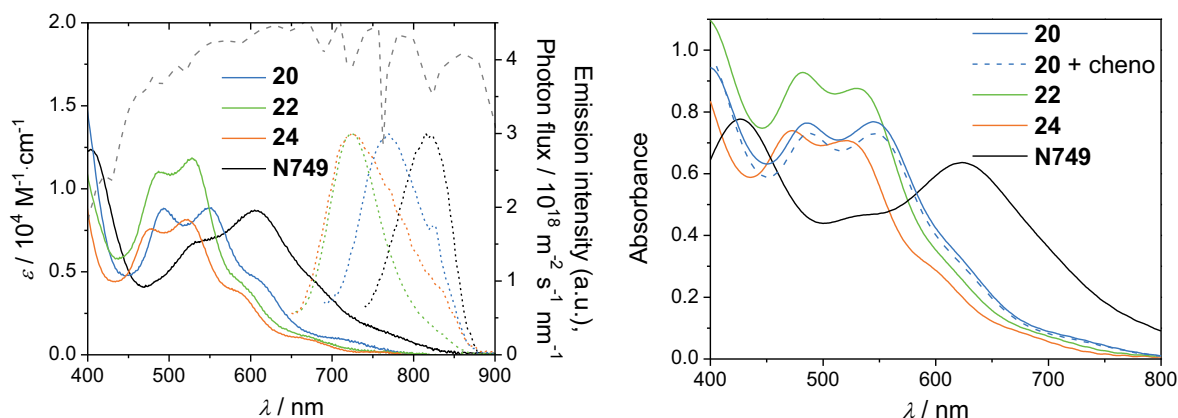
Figure 5.3. Left: UV−vis absorption (solid) and emission (dotted) spectra of selected complexes recorded in DMF/MeOH (4:1 *v/v*) as well as the AM1.5 solar photon flux (dashed). Right: UV−vis absorption of the complexes adsorbed on TiO_2 (12 μm thick, transparent film, active area of 0.88 cm^2).

In comparison to **N749**, the MLCT maximum of **20** has a comparable extinction coefficient but is hypsochromically shifted from 605 to 552 nm (corresponding to 0.2 eV) in

DMF/methanol (4:1 *v/v*). To assess the light-harvesting capabilities of the new dyes relative to **N749**, the product of $\varepsilon(\lambda)$ (with $\lambda > 400$ nm) and the AM1.5 solar photon flux was integrated.[264] Ideally, **20** and **22** would allow for 80% of the theoretical current achievable with **N749**, while **24** would only allow about 60%. The optical energy gap (E_{0-0}), which is required to determine the excited-state redox potentials (*vide infra*), was estimated from the intersection of the absorption and emission with the latter being normalized to the lowest-energy absorption shoulder, which presumably corresponds to the HOMO→LUMO transition (*vide supra*). The energy gap of 1.58 eV for **N749** is the smallest, while for **20**, **22**, and **24** energy gaps of 1.68, 1.78, and 1.79 eV, respectively, were determined. The absorption profiles of the complexes anchored to transparent TiO_2 anodes are also provided in Figure 5.3. Assuming that the extinction coefficients do not change upon anchoring of the dyes onto TiO_2, the dye uptake of the cyclometalated dyes is comparable to **N749**, even when **20** is coadsorbed with chenodeoxycholic acid (cheno).

Table 5.1. Selected data of the studied ruthenium(II) complexes.

complex	λ_{max}^{Abs} / nm (ε / 10^3 M^{-1} cm^{-1})[a]	λ_{max}^{Em}/ nm[a]	τ / ns[a]	E_{0-0} / eV[b]	$E_{1/2}^{Ox}$ / V vs. Fc$^+$/Fc (vs. NHE)[c]	$E^*_{1/2}^{Ox}$ / V vs. Fc$^+$/Fc (vs. NHE)[d]
20	493 (8.9), 552 (8.9), 610 (sh, 4.5)	768	16.1,[e] 16.7[f]	1.68	0.11 (0.80)	−1.57 (−0.88)
22	487 (11.0), 528 (11.9), 591 (sh, 4.2)	725	11.0,[e] 11.7[f]	1.78	0.30 (0.99)	−1.48 (−0.79)
24	477 (7.6), 522 (8.1), 580 (sh, 3.8)	723	4.5,[e] 4.9[f]	1.79	0.37 (1.06)	−1.42 (−0.73)
N749	528 (sh, 6.7), 605 (8.7)	820	30[g]	1.58	0.16 (0.85)	−1.42 (−0.73)

[a] Measured in DMF/MeOH (4:1 *v/v*) unless stated otherwise; sh = shoulder. [b] Determined at the intersection of the absorption and emission with the latter being normalized to the lowest-energy absorption. [c] Determined by cyclic voltammetry using NBu_4PF_6 as supporting electrolyte; Fc$^+$/Fc was used as internal standard; conversion to NHE scale by addition of 0.69 V.[265] [d] Calculated using $E^*_{1/2}^{Ox} = E_{1/2}^{Ox} - E_{0-0}$.[12] [e] Air-equilibrated solution. [f] Nitrogen-sparged solution. [g] Measured in EtOH, taken from ref. [41].

The new cyclometalated ruthenium(II) complexes show a weak photoluminescence in DMF/methanol (4:1 *v/v*) at room temperatures with emission maxima of about 770 nm for **20** and about 725 nm for **24** as well as **22** (Table 5.1). Excited-state lifetimes of 4.9, 11.7, and 16.7 ns were determined for **24**, **22**, and **20**, respectively, which are typical values for cyclometalated *bis*(tridentate) ruthenium(II) complexes[215] and are attributed to a phosphorescence from a ^{3}MLCT excited state (*vide supra*). The observation of the shortest lifetime for **24** is attributed to a small energy separation between the ^{3}MLCT state and the deactivating ^{3}MC state.[251] All lifetimes are shorter than for **N749** (30 ns), but, except for **24**, sufficiently long to allow almost quantitative electron injection if the injection occurs within 100 ps.[136] Nonetheless, provided that the injection driving force is high, the injection can be much faster and even with an excited-state lifetime of 1 ns, apparently no injection problems were encountered in a series of related complexes.[266]

Cyclic voltammetry (CV) experiments in DMF/methanol (4:1 *v/v*) revealed a reversible oxidation at 0.80, 0.99, and 1.06 V *vs.* NHE for **20**, **22**, and **24**, respectively, (Table 5.1), which is attributed to a Ru(III)/Ru(II)-based redox process in line with the bleaching of the MLCT absorption band observed in spectroelectrochemistry experiments upon oxidation.[251] The low redox potential for the parent complex **20**, which is cathodically shifted by 50 mV relative to the redox potential of **N749**, is a consequence of the strong electron donation by the carbanion and might impede efficient regeneration of the photo-oxidized sensitizer by the relevant $I_2^{•-}$/I^--

redox couple located at 0.79 V *vs.* NHE (Figure 5.4).[44, 151] While there are examples of well-performing dyes with even 50 mV less positive redox potentials than **N749**,[267] electron-withdrawing substituents were installed at the cyclometalated phenyl ring to increase the Ru(III)/Ru(II) redox potential and thereby ensure a sufficiently high regeneration driving force.[182, 224, 227]

The excited-state redox potentials were calculated from the Ru(III)/Ru(II) redox potentials and the optical energy gap, E_{0-0} (Table 5.1).[12] Accordingly, **20** and **22** show excited-state redox potentials significantly more negative than the conduction band edge of TiO_2 located at about −0.7 V *vs.* NHE (Figure 5.4),[136] while a value close to the conduction band edge has been determined for **24** implying a low driving force for the electron injection. Notably, an equal excited-state redox potential has been determined for **24** and **N749**, but the excited-state lifetime of **24** is significantly shorter, which might compromise the injection efficiency.
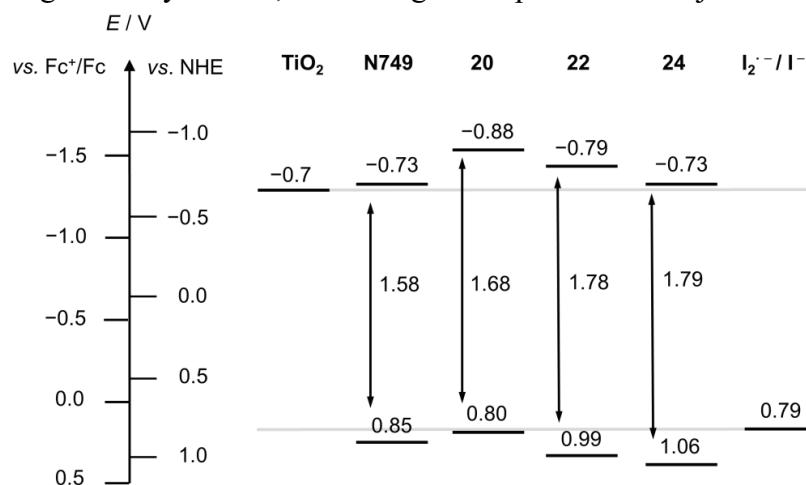
Figure 5.4. Comparison of the excited-state and ground-state redox potentials (values refer to the NHE scale)[268] with the relevant redox potential of the electrolyte and the conduction band edge of TiO_2.

To test the PCE of the presented sensitizers in the DSSC, commercially available test cells with transparent TiO_2 anodes (20 nm particles, 12 μm thickness, 0.28 or 0.88 cm^2 active area) were used and assembled according to standard literature procedures,[269] and directly compared to **N749**. Notably, although cell types with different areas were used, which leads to higher fill factors (FF) in case of a smaller areas, the short-circuit photocurrent densities (J_{sc}) and open-circuit voltages (V_{oc}) are comparable. An established acetonitrile-based electrolyte solution was chosen, containing 0.05 M iodine, 0.1 M guanidinium thiocyanate (GuSCN), 0.5 M 4-*tert*-butylpyridine (TBP), and varying concentrations of 1,3-dimethylimidazolium iodide (DMII) and lithium or sodium iodide (Table 5.2, Figure 5.2).[146] Initially, a sodium-containing electrolyte (0.6 M NaI, El 1a) was employed,[184, 270] which allowed a PCE of about 2% throughout the series. As regeneration problems were suspected for **20**, the effective iodide concentration was increased (1.0 M DMII, El 1b),[44, 176] which significantly improved the J_{sc} resulting in a PCE of 3.0%. Subsequently, an electrolyte with a high lithium concentration (1.0 M, El 2) was used to facilitate both electron injection[153] and dye regeneration,[178] which would provide an estimation of the attainable photocurrents of the new dyes. Additionally, the high lithium concentration improves the charge-collection efficiency, which has been confirmed by electrochemical impedance spectroscopy (EIS). For **20**, the J_{sc} was again significantly improved relative to the sodium-containing electrolytes (9.2 mA cm^{-2}), while for **22** and **24**, only a slight improvement in J_{sc} was achieved resulting in much inferior values (6.3 and 5.8 mA cm^{-2}, respectively). The extent of current improvement for the latter complexes is

in the range observed for benchmark dyes,[153] which suggests that injection problems are not the main origin of the inferior performance of **24** and **22**. For **24**, the low photocurrents are mainly ascribed to the lower light harvesting ability that was estimated to be only 75% of **20** (*vide supra*). In contrast, **22** should be a light harvester as good as **20** and the lower photocurrents as well as the comparatively lower V_{oc} values (about 80 mV less than for **20** and **24**) are attributed to enhanced recombination reactions (*vide infra*),[38] which was corroborated by EIS experiments.[256, 271−272]

Table 5.2. Selected data of the ruthenium(II) complexes measured under AM1.5 light conditions.

complex	area /cm^{2} [a]	electrolyte[b]	cheno	V_{oc} / V	J_{sc} /mA cm^{-2}	FF	η / %
	0.88	El 1a	No	0.62	5.7	0.61	2.2
	0.88	El 1b	No	0.62	7.4	0.62	3.0
20	0.88	El 2	No	0.57	9.2	0.61	3.4
	0.28	El 3	No	0.66	8.1	0.70	4.0
	0.28	El 3	Yes	0.65	9.4	0.70	4.5
22	0.88	El 1a	No	0.57	5.5	0.56	1.8
	0.88	El 2	No	0.49	6.3	0.58	1.9
24	0.88	El 1a	No	0.63	5.4	0.56	2.0
	0.28	El 2	No	0.57	5.8	0.70	2.5
N749	0.88	El 3	No	0.69	11.6	0.62	5.1
	0.28	El 3	No	0.69	10.7	0.69	5.2

[a] TiO$_2$ layer thickness of 12 μm (20 nm particles). [b] Electrolyte abbreviations: El 1a: 0.6 M NaI, 0.6 M DMII, El 1b: 0.6 M NaI, 1.0 M DMII; El 2: 1.0 M LiI, 0.6 M DMII; El 3: 0.1 M LiI, 0.6 M DMII.

As internal reference, the performance of **N749** was measured using a typical electrolyte composition containing 0.1 M LiI (El 3, Table 5.2).[273] The same electrolyte was tested for **20** as this dye clearly shows the best performance within the series. In Figure 5.5, the $J{-}V$ curves and the incident photon-to-current efficiency (IPCE) spectra for **20** and **N749** measured under identical conditions are provided. In this direct comparison, two benefits of **N749** become obvious: Firstly, **N749** produces a higher current (10.7 *vs.* 8.1 mA cm^{-2}), which is ascribed mainly to the better red to near-IR response as evident from the IPCE traces (Figure 5.5, right). Note that the estimated light harvesting ability of **20** amounts to 80% of the one of **N749** (*vide supra*). Secondly, **N749** allows for a higher voltage (0.69 *vs.* 0.66 V), which is attributed to its doubly deprotonated form and anionic charge leading to a higher TiO$_2$ conduction band.[147−149] Consequently, **N749** achieves a PCE of 5.1%, while **20** affords 4.0% under identical conditions. Apparently, the PCE for **20** is not limited by an inefficient regeneration under these conditions. The superior performance achieved with electrolytes containing Li$^+$ instead of Na$^+$ (Table 5.2) indicates that the dye regeneration kinetics need to be enhanced by increasing the near-surface iodide concentration with the help of charge-dense cations.[178] However, a 0.1 M lithium concentration is sufficient,[274] which still allows reasonably high voltages and commonly results in the best overall performance as the electron injection is facilitated as well.[163]

For **20**, using the best electrolyte composition (El 3), the influence of the cheno coadsorbent was tested (Table 5.2, Figure 5.5) to gain information about the dye's ability to protect the TiO$_2$ surface from the electrolyte and thereby prevent recombination reactions.[174] The J_{sc} values could be further improved (9.4 *vs.* 8.1 mA cm^{-2}), although the V_{oc} decreased slightly (0.65 *vs.* 0.66 V). The observed improvement in the IPCE spectrum (Figure 5.5) suggests that the charge collection efficiency is enhanced by the help of cheno. Similarly, it was reported that the PCE achieved with **N749** could be increased from 4.3 to 4.7% by coadsorption with cheno.[175] The effect of the coadsorbent on the performance of **20** was also

studied by the help of EIS. Accordingly, the conduction band lifting effect of the TBP additive[163] is attenuated in the presence of cheno. Apart from the slightly lowered V_{oc}, the electron transport within TiO_2 is thus improved and recombination reactions of injected electron with the electrolyte are diminished leading to an increased charge-collection efficiency[272] in line with the higher J_{sc} and IPCE values.
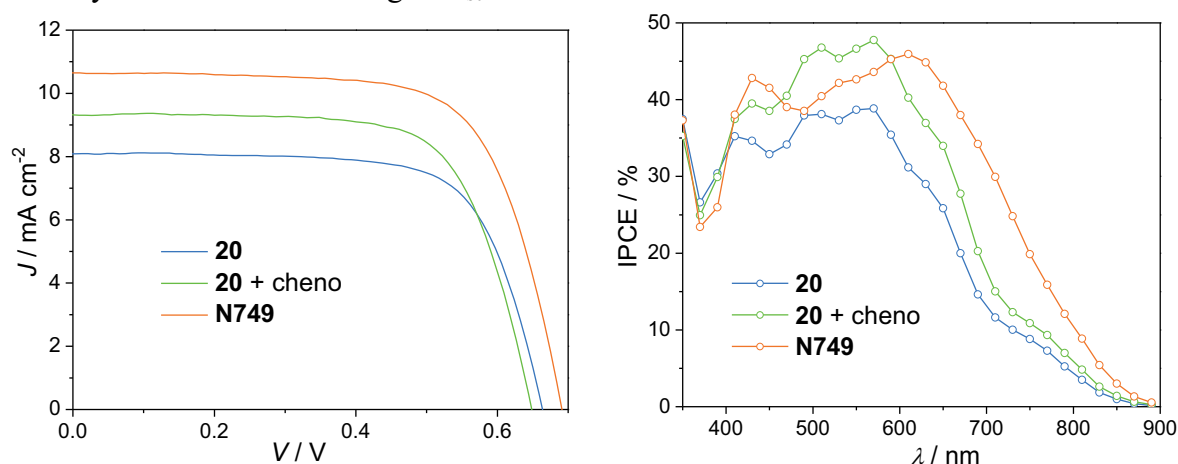
Figure 5.5. Left: $J-V$ curves of **20** without and with cheno coadsorbent as well as of **N749** without cheno under otherwise identical conditions (El 3, active area of 0.28 cm^2, *cf.* Table 5.2). Right: Corresponding photocurrent action spectra.

In conclusion, the DSSC performance of a series of *bis*(tridentate) ruthenium(II) complexes featuring 1,2,3-triazole-containing cyclometalating ligands has been investigated. The parent dye devoid of electron-withdrawing groups (**20**) revealed the best results by achieving a PCE that corresponds to 80% of the value of **N749**, which correlates well with the individual light-harvesting capabilities. Despite the low Ru(III)/Ru(II) redox potential of the parent photosensitizer, its regeneration appeared to be efficient when lithium-containing electrolytes are used. In contrast, the *meta*-difluoro substitution pattern, which is commonly used to lower the HOMO energy of the sensitizer,[182, 227] showed a detrimental effect on the light harvesting properties and, thus, resulted in an inferior performance. Alternatively, a nitro groups was installed at the cyclometalated phenyl ring, but the DSSC performance of the corresponding sensitizer was only modest due to enhanced recombination reactions. Ultimately, in view of the performance of **20**, a promising thiocyanate-free ruthenium(II) photosensitizer platform is presented, which shows great potential for further improvement since the employed cyclometalating ligand is amenable to functionalization, *e.g.*, with additional chromophores. As demonstrated, hydrophobic alkyl chains can be introduced most easily, which is expected to improve the long-term stability and allow the use of alternative electrolytes. Additional chromophores can, in principle, be attached to the cyclometalated phenyl ring to further optimize the light harvesting in the future.

Ruthenium(II) photosensitizers featuring 1,2,3-triazolate donors

Apart from ruthenium(II) sensitizers featuring carbanionic donors, Chou and coworkers presented ruthenium(II) dyes bearing functionalized dianionic 2,6-*bis*(5-pyrazolyl)pyridine ligands (Figure 5.6), which achieved remarkable PCEs of 9.1% (**TF-1**) and 10.7% (**TF-2**, *vs.* 9.2% for **N749**) in the DSSC.[193] Building on these promising results, the viability of 1,2,3-triazolates as thiocyanate surrogates was examined. Again, this approach benefits from a very simple ligand synthesis *via* an azide−alkyne cycloaddition, which also allows the ready installation of alkyl chains.[156, 186] Furthermore, in contrast to 1,2,4-triazolates,[82, 188] the use of

1,2,3-triazolates circumvents the formation of coordination isomers and, due to the higher degree of *aza* substitution when compared with pyrazolates, no electron-withdrawing groups need to be installed to increase the Ru(III)/Ru(II) redox potential of the corresponding ruthenium(II) complexes and thereby ensure efficient dye regeneration.[193]
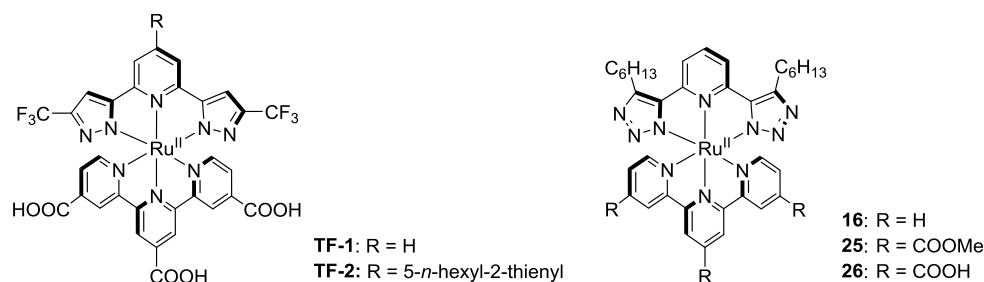
Figure 5.6. Schematic representation of ruthenium(II) sensitizers featuring azolate donors.

The synthesis of the 2,6-*bis*(1,2,3-triazole)pyridine ligand was described in the previous chapter. The metal coordination was achieved utilizing [Ru(tcmtpy)(MeCN)$_3$](PF$_6$)$_2$[251] as precursor and, after the subsequent saponification, the carboxy-functionalized sensitizer **26** was obtained in good overall yields.

To allow a deeper understanding of the electronic properties of the new ruthenium(II) sensitizer, DFT and TD-DFT calculations were carried out for **26**. Accordingly, the HOMO is composed of a metal d orbital and π orbitals located on the 1,2,3-triazolate, which is expected in view of the energetically high π system of the anionic ring. The LUMO is mainly composed of π* orbitals of the carboxy-functionalized tpy ligand. Consequently, the lowest-energy absorption, which is an almost pure HOMO→LUMO transition, can be assigned as an MLCT transition with some LLCT character, *i.e.* an MLLCT transition (S$_0$→S$_1$, Figure 5.7). Also the other relevant computed electronic excitations in the visible light region are mainly of MLCT character with varying LLCT contributions. As the electron transfer is directed towards the anchoring ligand in each case, **26** features an excited-state electronic structure suitable for electron injection into TiO$_2$.
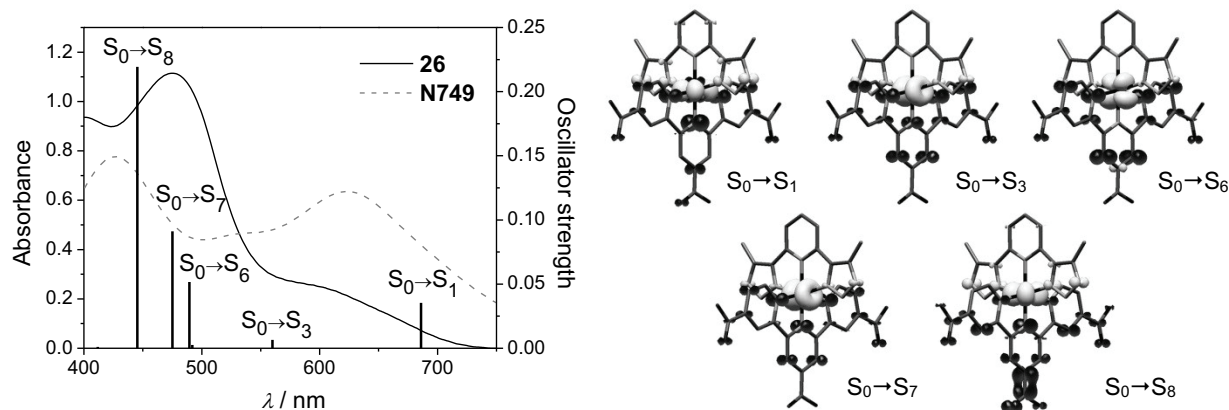
Figure 5.7. Left: Experimental UV−vis absorption spectrum of **26** and **N749** adsorbed on TiO$_2$ (12 μm thick, transparent film, active area of 0.88 cm^2) and calculated vertical singlet−singlet transitions (PCM-TD-B3LYP/6-31G* in MeCN) of **26**. Right: Selected corresponding electron-density difference maps of **26** (white = depletion, black = accumulation, isovalue 0.004). Note that, for the DFT calculations, the *n*-hexyl chains have been replaced by methyl groups and that the tpy ligand is functionalized with carboxy groups, which are known to electronically resemble the Ti(IV)-coordinated carboxylates.[147]

The fundamental properties of a simple model complex of sensitizer **26** were discussed in the previous chapter. In view of the pK_a values of the corresponding ruthenium(II)-coordinated 1,2,3-triazoles (pK_{a1} and p$K_{a2} \approx 4.7$) and the pK_a values for the three deprotonation steps of the

carboxy-functionalized tpy ligand determined for similar ruthenium(II) complexes ($pK_{a1} = 1.2$, $pK_{a2} = 3.1$, and $pK_{a3} = 5.5$),[41, 251] **26** is expected to form a zwitterion in solution (two 1,2,3-triazole rings, two carboxylates, one carboxy group). Consequently, the photophysical properties were determined in methanol solution containing 0.5 M NEt$_3$ in order to ensure the complete deprotonation of the 1,2,3-triazolates. Under these conditions, also the three carboxy groups are deprotonated giving rise to a LUMO destabilization, which is reflected by the hypsochromically shifted UV−vis absorption and emission maxima relative to the complex featuring an unsubstituted tpy ligand (**2a**, Table 5.3). Accordingly, the energy gap of **26** in solution (1.86 eV, Table 5.3) is overestimated when compared to the energy gap of **26** within a working DSSC, as the Ti(IV)-coordination of the carboxylates will result in a LUMO stabilization (*vide infra*). Furthermore, due to the presence of 0.5 M TBP in the DSSC electrolyte,[146] the two triazolates of **26** are deprotonated under working conditions. This is corroborated by the measurement of the Ru(III)/Ru(II) redox potential of **26** by square-wave voltammetry in acetonitrile containing 0.5 M pyridine with a dye-loaded TiO$_2$ anode as the working electrode. The measured potential of 0.86 V *vs.* NHE is almost identical to the redox potential of **N749** (0.85 V *vs.* NHE) and, thus, sufficiently high to ensure efficient regeneration by the relevant $I_2^{-\cdot}/I^-$-redox couple (0.79 V *vs.* NHE).[151] Furthermore, in comparison to the redox potential of an analogous complex featuring two neutral 1,2,3-triazole donors (**5**, 1.61 V *vs.* NHE),[251] the considerable cathodic shift observed for **26** suggests the presence of two anionic 1,2,3-triazolate donors under the conditions of the measurement.

Table 5.3. Photophysical and electrochemical data of the selected ruthenium(II) complexes.

Complex	λ_{max}^{Abs} / nm (ε /10^3 M^{-1} cm^{-1})	λ_{max}^{Em} / nm	Φ_{PL} / %[a]	τ / ns	$E_{1/2}^{Ox}$ / V *vs.* Fc$^+$/Fc (*vs.* NHE)[b]	$E^*_{1/2}^{Ox}$ / V *vs.* Fc$^+$/Fc (*vs.* NHE)[c]	E_{0-0} / eV[d]
16[e]	662 (0.7), 608 (0.9), 487 (5.6)	719	0.35	54	0.20 (0.83)	−1.60 (−0.97)	1.80
25[e]	742 (2.3), 673 (2.7), 507 (8.9), 448 (10.7)	_[f]	_[f]	_[f]	0.46 (1.09)	–	–
26	651(1.2), 602(2.1), 479(11.0)[g,h]	698[g,h]	–	83[g,h]	0.23 (0.86)[i]	−1.63 (−1.00)	1.86[h]
N749	620(6.5), 585(6.0), 420(10.5)[j]	820[j]	–	30[k]	0.16 (0.85)[j]	−1.40 (−0.71)	1.58

[a] Determined using [Ru(dqp)$_2$](PF$_6$)$_2$ in MeOH/EtOH (1:4 *v/v*, Φ_{PL} = 2.0%) as reference.[50] [b] Determined by cyclic voltammetry experiments using NBu$_4$PF$_6$ as supporting electrolyte, unless stated otherwise; Fc$^+$/Fc was used as internal standard; conversion to NHE scale by addition of 0.63 V[275] and 0.69 V[265] when the measurement was done in MeCN and DMF/MeOH (4:1 *v/v*), respectively. [c] Calculated using $E^*_{1/2}^{Ox} = E_{1/2}^{ox} - E_{0-0}$.[12] [d] Determined at the intersection of the absorption and emission with the latter being normalized to the lowest-energy absorption. [e] Measured in MeCN containing 0.5 M NEt$_3$. [f] Not observed. [g] Measured in MeOH containing 0.5 M NEt$_3$. [h] Fully deprotonated species, see text. [i] Determined by square-wave voltammetry with the complex-anchored TiO$_2$ anode as the working electrode immersed in MeCN containing 0.5 M pyridine and 0.1 M NBu$_4$PF$_6$ as supporting electrolyte; Fc$^+$/Fc was used as internal standard. [j] Measured in DMF/MeOH (4:1 *v/v*). [k] Measured in EtOH, taken from ref. [41].

Despite the aforementioned difficulties to accurately determine the energy gap of **26**, a lower limit of the excited-state redox potential of **26** can be calculated from the ground-state redox potential and the minimal energy gap taken from the onset in the IPCE spectrum (750 nm or 1.65 eV, *vide infra*). Accordingly, the excited-state redox potential of the TiO$_2$-coordinated **26** is at least −0.79 V *vs.* NHE, which is sufficiently more negative than the conduction band edge of TiO$_2$ (ca. −0.7 V *vs.* NHE)[136] and, thus, enables efficient electron injection into the semiconductor. In comparison, the energy gap and excited-state redox

potential of **N749** are 1.58 eV and −0.73 V *vs*. NHE, respectively, which implies a larger driving force for the electron injection but an inferior absorption at longer wavelengths in case of **26**. The light harvesting capability of **26** is further diminished by the relatively low extinction coefficients of the plateau-like low-energy absorption band (Figure 5.7, Table 5.3), which is typical for *bis*(tridentate) ruthenium(II) complexes featuring azolate donors.[82, 188, 190, 193] The excited-state lifetimes of 54 and 83 ns determined for **2a** and **26**, respectively, at room temperature in acetonitrile solution are slightly longer than for **N749**[41] and sufficiently long to permit a highly efficient electron injection into TiO_2 given that the electron injection occurs on the picosecond timescale.[136]

To evaluate the performance of **26** in the DSSC, commercially available test cells were assembled according to literature procedures (TiO_2 layer thickness of 12 μm (20 nm particles) + 3 μm (400 nm particles), active area of 0.28 cm^2)[269] and an electrolyte composition typically used for **N749** was chosen.[273] The obtained parameters are reported in Table 5.4. Under identical conditions, the PCEs of **26** and **N749** are 4.0% and 6.1%, respectively. Compared to **N749**, **26** achieves a lower V_{oc} (0.61 *vs*. 0.69 V), which is attributed to its higher degree of protonation lowering the TiO_2 conduction band,[147] and a lower J_{sc} (8.9 *vs*. 12.7 mA cm^{-2}), which reflects, amongst others, the inferior light harvesting capability of **26** associated with the larger energy gap mentioned above. In line with the latter, the onset in the IPCE spectrum of **26** is significantly hypsochromically shifted (Figure 5.8). Moreover, the maximum in the IPCE spectrum is lower for **26**.

Table 5.4. Selected DSSC data for the ruthenium(II) complexes measured under AM1.5 light conditions.[a]

Dye	Electrolyte[b]	cheno	V_{oc}/ V	J_{sc}/ mA cm^{-2}	FF	PCE/ %
26	El 1	No	0.61	8.9	0.70	4.0
26	El 1	Yes	0.62	11.8	0.63	4.9
26	El 2	No	0.70	6.2	0.58	2.7
N749	El 1	No	0.69	12.7	0.66	6.1

[a] AM1.5 light conditions; TiO_2 layer thickness of 12 μm (20 nm particles) + 3 μm (400 nm particles), active area of 0.28 cm^2; MeCN-based electrolyte containing 0.6 M DMII, 0.06 M I_2, 0.1 M LiI, 0.5 M TBP and 0.1 M GuSCN. [b] El 1: 0.6 M DMII, 0.06 M I_2, 0.1 M LiI, 0.5 M TBP and 0.1 M GuSCN; El 2: 0.21 M $[Co^{II}(bpy)_3](PF_6)_2$, 0.033 M $[Co^{III}(bpy)_3](PF_6)_3$, 0.1 M LiClO$_4$, 0.5 M TBP.

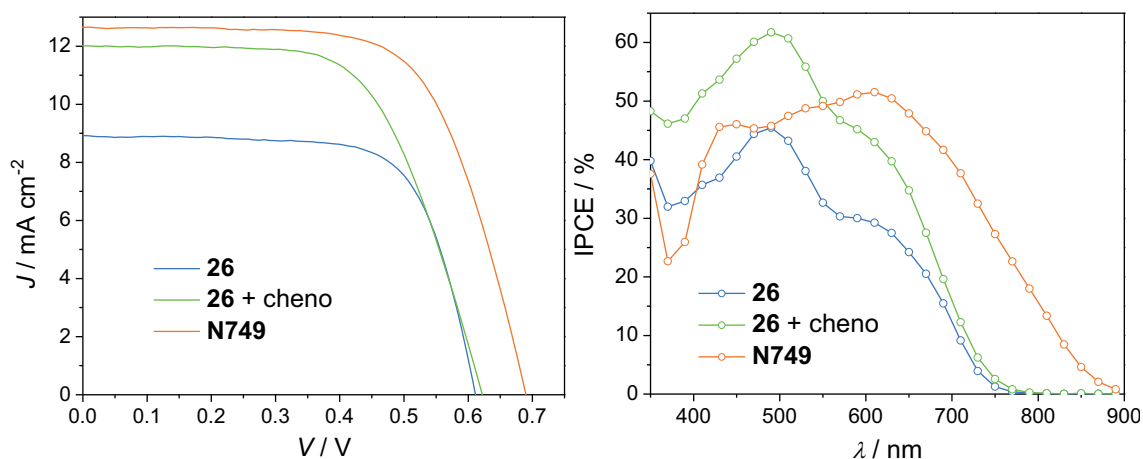**Figure 5.8.** Left: *J−V* curves of **26** without and with cheno coadsorbent as well as of **N749** without cheno under otherwise identical conditions (El 1, *cf*. Table 5.4). Right: Corresponding photocurrent action spectra.

It was reported in the literature that the PCE achieved with **N749** increased from 4.3 to 4.7% by co-adsorption with cheno,[175] presumably because **N749** is unable to create a

complete monolayer when adsorbed onto TiO$_2$[41] thus giving rise to recombination reactions. Similarly, when **26** is co-adsorbed with cheno, the V_{oc} value is slightly increased (0.62 *vs*. 0.61 V) and the J_{sc} value is significantly improved (11.8 *vs*. 8.9 mA cm^{-2}) in line with much higher IPCE values resulting in a promising PCE of 4.9%. The significant enhancement of the photocurrent in the presence of cheno suggests that the relatively low IPCE values observed in the absence of cheno are not caused by inefficient regeneration or injection but rather by recombination reactions due to interactions between TiO$_2$ and the electrolyte. A more detailed investigation of the devices by EIS corroborated the assumption of enhanced recombination reactions in case of **26** in the absence of cheno. Accordingly, the TiO$_2$ surface passivation is improved in the presence of cheno and the charge-collection efficiency is enhanced. Furthermore, when comparing **N749** and **26** without cheno, a slightly higher recombination tendency in case of **26** suggests a lower TiO$_2$ surface coverage and/or unfavorable interactions between the sensitizer and iodine.[170−172] Nonetheless, **26** is not expected to leave larger voids on the TiO$_2$ surface, since, even in the absence of cheno, a PCE of 2.7% was achieved in an initial attempt employing a [Co^{III}(bpy)$_3$](PF$_6$)$_3$/[Co^{II}(bpy)$_3$](PF$_6$)$_2$-containing electrolyte.[142, 186] This result is promising as thiocyanate-based benchmark dyes typically afford significantly lower PCE values (~ 1%) when using the same Co(III)/Co(II)-based redox shuttle,[155, 186] which is ascribed to the decoration of **26** with hexyl chains allowing a more efficient protection of the TiO$_2$ surface from the bulky redox mediator and, thus, diminished recombination reactions.[156]

In conclusion, a heteroleptic *bis*(tridentate) ruthenium(II) complex bearing a 1,2,3-triazolate-containing ligand, which offers a simple and modular synthesis. Owing to the anionic triazolate donors, the corresponding ruthenium(II) complex features photophysical and electrochemical properties suitable for DSSC application. Accordingly, a promising DSSC performance has been achieved with different types of electrolytes. Prospectively, the thiocyanate-free, *bis*(tridenate) sensitizer platform is expected to enable an extended DSSC life span[44] and offers the potential to optimize the light-harvesting capability *via* attachment of additional chromophores at the central pyridine ring of the anionic ligand.[184, 193]

Design of cyclometalated ruthenium(II) complexes for anodic electropolymerization

As demonstrated above, cyclometalated *bis*(tridentate) ruthenium(II) complexes featuring 1,2,3-triazole-containing N^C^N-coordinating are efficient sensitizers for DSSC applications.[115] By making use of click-chemistry,[26, 87] a facile access to highly functionalized ligand systems is given.[251] For instance, the sensitizer can be equipped with hydrophobic alkyl chains, which, amongst others, are known to suppress the water-induced dye desorption and thereby improve the DSSC long-term stability.[157] An alternative strategy, which would even allow the use of water as electrolyte,[276] is the formation of an insoluble polymer network on the semiconductor surface *via* electropolymerization.[277−278] While the cathodic electropolymerization of cyclometalated ruthenium(II) complexes functionalized with vinyl groups was demonstrated,[279] the anodic electropolymerization relying on thiophenes as a typical electropolymerizable unit was only reported for non-cyclometalated ruthenium(II) complexes.[280−281] A distinct advantage of the anodic electropolymerization is that it results in π-conjugated systems thus allowing, in principle, the formation of photo-redox-active, conducting metallopolymers.[278, 282−283] However, this method appears to be particularly challenging for cyclometalated ruthenium(II) complexes, as the very electron-rich complexes have to withstand highly positive potentials. Nonetheless, motivated by the high stability of

complexes like **5** (*vide supra*) in the oxidized state as well as by the flexible synthesis and great potential for photovoltaic applications of this type of complex, we were interested in its viability for the formation of photo-redox-active films *via* for anodic electropolymerization.

In order to allow a rapid and modular access to the thiophene-functionalized cyclometalating ligands, the 2-thienyl moiety was attached to an aryl azide *via* a Suzuki cross-coupling reaction first (Scheme 5.2). Interestingly, the Suzuki coupling tolerated the presence of aryl azides despite their known tendency to form phosphazides and phosphimines with free or coordinated phosphines of the palladium catalyst.[284] Subsequently, the thiophene-containing 1,3-*bis*(1,2,3-triazolyl)benzene ligands were readily built up *via* CuAAC in good yields. Thereby, two ligands, **27** and **28**, were synthesized that differ in the substitution pattern of the phenyl spacer between the thiophene and the triazole ring (Scheme 5.2), which is expected to affect the π conjugation. Additionally, as a coplanarization is prevented, an intermolecular π stacking is precluded as well and the solubility is thus higher for **28**. Notably, an alternative approach *via* Suzuki coupling between 2-thienylboronic acid and a bromo-functionalized cyclometalating ligand resulted in low conversions and inseparable reaction mixtures under various conditions. For both cyclometalating ligands, the corresponding ruthenium(II) complexes, **29** and **30**, were obtained in fair yields using [Ru^{II}(tpy)(MeCN)$_3$](PF$_6$)$_2$ as precursor (Scheme 5.2).
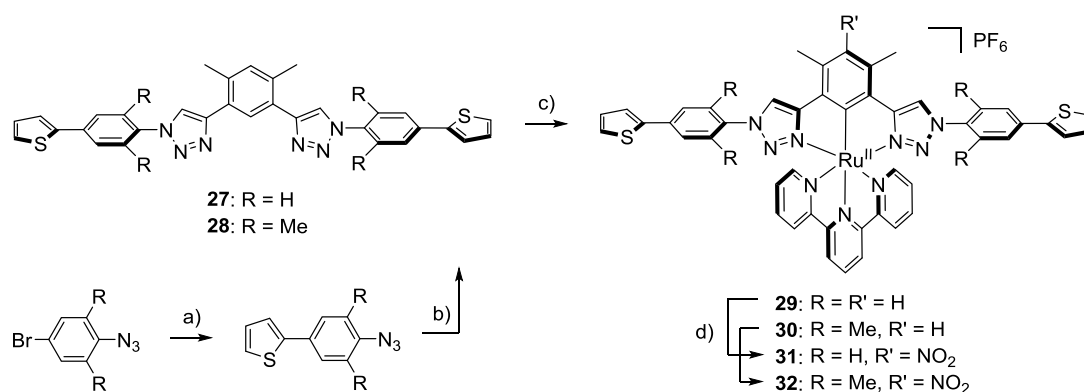
Scheme 5.2. Schematic representation of the synthesis of the thiophene-containing cyclometalated ruthenium(II) complexes: a) 2-Thienylboronic acid, Pd(PPh$_3$)$_4$, K$_2$CO$_3$, DMF, 50 °C, 12 h, 40 to 41%; b) 1,3-diethynyl-4,6-dimethylbenzene, CuSO$_4$, sodium ascorbate, CH$_2$Cl$_2$/EtOH/H$_2$O (1:2:1 *v/v/v*), 50 °C, 12 h, 70 to 73%; c) [Ru^{II}(tpy)(MeCN)$_3$](PF$_6$)$_2$, EtOH/toluene (1:1 *v/v*) or DMF, 140 to 160 °C, 30 to 120 min., 50 to 52%; d) Cu(NO$_3$)$_2$, CH$_2$Cl$_2$/MeOH (2:1 to 3:1 *v/v*), rt, 96 h, 67 to 85%.

In view of the highly positive potentials that are required for the later thiophene oxidation and since the cyclometalated ruthenium(II) complexes offer a facile post-complexation functionalization in the *para* position of the ruthenium(II)-coordinated phenyl ring,[238] nitro-functionalized derivatives, **31** and **32**, were prepared in order to anodically shift the Ru(III)/Ru(II) redox potential.[251] Notably, to circumvent a nitration of the thiophene moieties,[285] the commonly applied Menke conditions (Cu(NO$_3$)$_2$ and acetic anhydride)[238] were attenuated. Using Cu(NO$_3$)$_2$ and a dichloromethane/methanol solvent mixture, solely the nitration on the cyclometalated phenyl ring is observed, even if a high excess of Cu(NO$_3$)$_2$ is used. The desired complexes were obtained after counterion exchange and crystallization by vapor diffusion of diethyl ether into a concentrated DMF solution, which was confirmed by MS and several NMR techniques. Additionally, in case of **32**, the nitro-functionalization was proven by single crystal X-ray diffraction (Figure 5.9). As expected, due to the presence of the methyl groups, the nitro group and the peripheral phenyl rings are twisted out of plane by 52.1° and 62.4/71.6°, respectively. On the other hand, a small torsion between the thiophene and the

peripheral phenyl ring (15.3/25.1°) is observed in the solid state, which may give rise to the formation of an additional chromophore after the electropolymerization (*vide infra*).
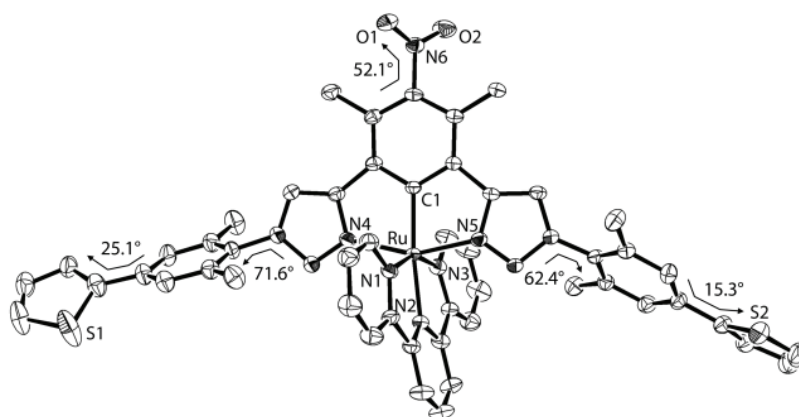
Figure 5.9. Solid-state structure of **32** (thermal ellipsoids drawn at 50% probability level, solvent molecules, counterion, hydrogen atoms, and disorder of a thiophene rings omitted for clarity).

The electrochemical properties of the new ruthenium(II) complexes are in line with the respective model complexes, **6** and **8** (see the previous chapter),[251] except for the additional oxidation process associated with the thiophene ring. The CV spectra of **29** and **30** reveal a reversible metal-based redox process with a half-wave potential of 0.10 V *vs*. Fc$^+$/Fc, while the corresponding Ru(III)/Ru(II) redox potentials of **31** and **32** are anodically shifted by 200 mV. In the region around 1.1 to 1.4 V *vs*. Fc$^+$/Fc, further oxidation processes appear, including the thienyl radical cation formation, which is crucial for the electropolymerization process.[277−278] A closer inspection of the CV spectra at high potentials (> 1 V *vs*. Fc$^+$/Fc) of **29** and **30** reveals a second, irreversible oxidation process, which is assigned to the complex fragment as it is also observed with the model complex **6** (exemplarily shown for **30** in Figure 5.10). This detrimental oxidation process occurs at slightly lower potentials than the thiophene-based oxidation process. Importantly, for **8** also the second, irreversible oxidation processes are anodically shifted. As the nitro-group mainly affects the electronic properties of the complex fragment, the irreversible oxidation of the complex is shifted beyond the thiophene-based oxidation in case of **31** and **32** (exemplarily shown for **32** in Figure 5.10), which is expected to be a prerequisite for the success of the electropolymerization.

The photophysical properties of the thiophene-equipped complexes resemble the ones of the corresponding model complexes **6** and **8** (see the previous chapter). The introduction of a nitro group at the anionic phenyl ring causes a hypsochromic shift as well as slightly increased extinction coefficients for the MLCT bands (*vide supra*). Likewise, the emission is hypsochromically shifted due to the reduced destabilization of metal-based orbitals. In the presence of the thiophene rings, absorption bands associated with LC transitions are bathochromically shifted and strongly enhanced, which is attributed to an extended conjugation in the peripheral 2-thienylphenyl moiety. The effect is particularly pronounced for **29** and **31**, which indicates a partially extended π conjugation into the 1,2,3-triazoles in the absence of the methyl groups on the phenyl spacer. Notably, 1,2,3-triazoles are known to interrupt the π conjugation between their substituents,[29, 110−112] and it is thus expected that the ruthenium(II) complex is electronically separated from the 2-thienylphenyl moieties.
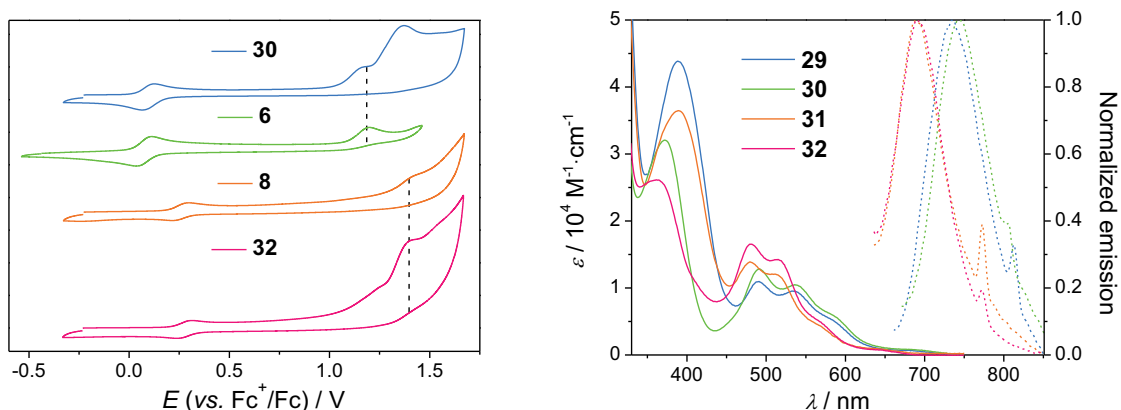
Figure 5.10. Left: Comparison of selected CV spectra illustrating the effect of the nitro group on the second, irreversible oxidation process. Right: UV−vis absorption and emission spectra in CH_2Cl_2.

Subsequently, electropolymerization experiments with either a glassy carbon disk electrode as the working electrode were carried out in dichloromethane containing 0.1 M Bu_4NPF_6. Therefore, the potential was cycled between −0.2 and 1.2 V *vs*. Fc^+/Fc with a scan rate of 200 mV s^{-1}, which is expected to result in a homocoupling of the thiophene moieties. During the potentiodynamic cycling, for **29** and **30**, the metal-based redox signals first undergo a cathodic shift and decreases afterwards, indicating side reactions as well as decomposition. In contrast, for **31** and **32**, the peak current of the first oxidation of the complex rises during the potentiodynamic cycling (exemplarily shown for **31** in Figure 5.11), as expected for a successful electropolymerization (Scheme 5.3). The obtained polymer films of **31** and **32** deposited on the working electrode were characterized by CV (Figure 5.11): In both cases, a reversible first, Ru(III)/Ru(II)-based oxidation was observed, which is slightly cathodically shifted relative to the dissolved monomer complexes. The latter is ascribed to a slightly increased electron donation from the 1,2,3-triazoles on account of the bithiophene formation. Furthermore, the peak current grows linearly with increasing scan rate up to 500 mV s^{-1}, indicating the formation of conductive films with only weakly diffusion-controlled charge migration.[278]
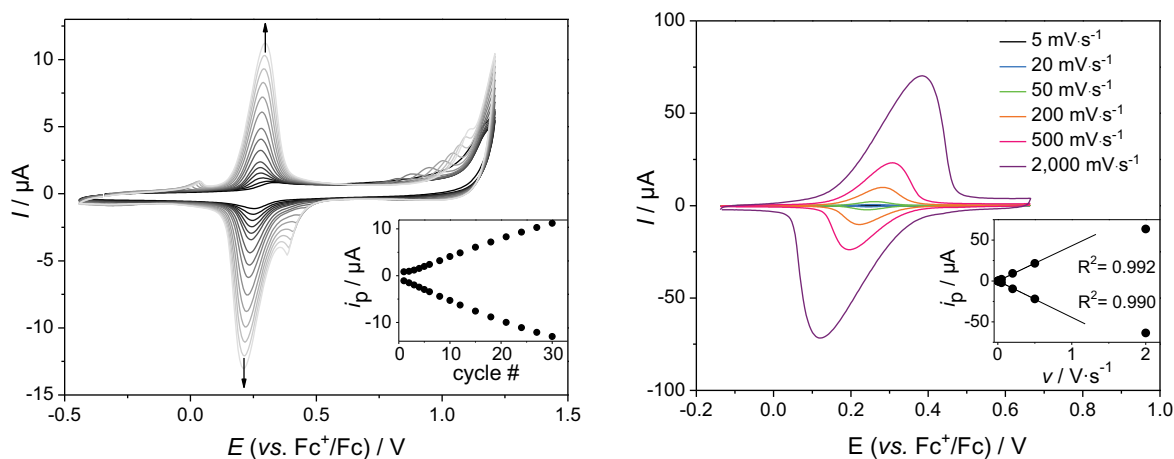
Figure 5.11. Left: Development of the CV spectrum during the potentiodynamic cycling of **31** in CH_2Cl_2 (10^{-5} M with 0.1 M Bu_4NPF_6); inset: Development of the peak current of the first oxidation process. Right: CV spectrum of **31** showing the first oxidation process at different scan rates; inset: Relationship between peak current and applied scan rate. Film on glassy-carbon disk electrode in CH_2Cl_2 with 0.1 M Bu_4NPF_6. Note that the additional signals at 0.45 and −0.05 V *vs*. Fc^+/Fc are only observed during the electropolymerization but not in the CV of the resulting film, thus being tentatively assigned to non-reacted radicals; similar effects have also been observed in other electropolymerization studies.[286]
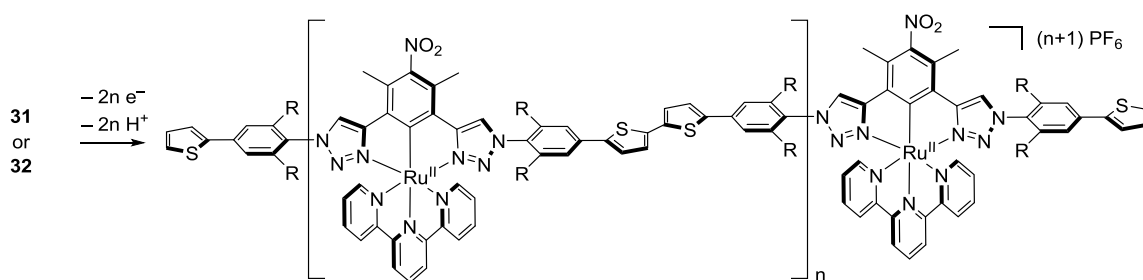
Scheme 5.3. Schematic representation of the anodic electropolymerization (R = H or Me).

Accordingly, the experiments support the assumption that the electron density on the metal center needs to lowered, *e.g.* by installing an electron-withdrawing group at the cyclometalating phenyl ring, to allow a successful electropolymerization. It is important to note that this is not simply due to the concomitant blocking of a reactive position. This claim is corroborated by two control experiments: Firstly, a bromo-functionalized complex was synthesized in order to block the reactive position opposite to the Ru−C bond without affecting the redox potential; however, the same signs of decomposition were observed as with **29** and **30**. Secondly, also **31** and **32** undergo side reactions and decomposition when the electropolymerization is conducted at more positive potentials. While it is reported in the literature that cyclometalated complexes undergo a C−C homocoupling in their oxidized state,[232] this behavior was not observed during the presented studies, which is ascribed to the placement of the methyl groups on the cyclometalating phenyl ring.

For the determination of the photophysical properties of electropolymerized films of **31** and **32**, the electropolymerization was conducted with a glass slide coated with indium tin oxide (ITO) as the working electrode. In comparison to drop-casted films of the monomer on an ITO substrate, the MLCT bands of the polymer films are almost unaffected, while an additional, intense absorption band at about 350 nm emerges, which is assigned to LC transitions located on the phenyl-substituted 2,2'-bithiophene spacer formed during the electropolymerization.[287] Although the MLCT absorption is essentially unchanged after the electropolymerization, in line with the expected electronic decoupling of the complex (*vide supra*), both the MLCT and the aforementioned LC transitions are slightly bathochromically shifted for the polymer derived from **31**, suggesting at least a weak π conjugation through the 1,2,3-triazoles[112] if coplanarization is not prevented by the methyl groups of the spacer.

For the polymer film obtained with **31**, UV−vis−NIR spectroelectrochemical studies were carried out. The first, metal-based oxidation process is accompanied by the typical spectral changes that have been observed also for the **6** model complex (Figure 4.8), *i.e.* the MLCT absorption bleaches, while a broad and weak LMCT band between 700 and 900 nm arises (Figure 5.12). Repeated switching between the initial and the oxidized state turned out to be reversible for at least the 30 cycles that were run, proving the redox stability of the prepared polymer film. Furthermore, a switching time, which is defined by the time that is necessary to undergo 95% of the full transmission change,[288] of 1.8 s was determined.

Subsequent work focused on copolymers containing the nitro-functionalized, cyclometalated ruthenium(II) complexes, **31** and **32**, and 3,4-ethylenedioxythiophene (EDOT) in varying ratios. The obtained *co*-polymer films exhibit a UV−vis absorption that is expanded to the NIR region, which is attributed to the incorporated *oligo-/poly*-EDOT chains, as well as a reversible electrochemical behavior, reflecting the mixed characteristics of the ruthenium(II) and the EDOT moieties.
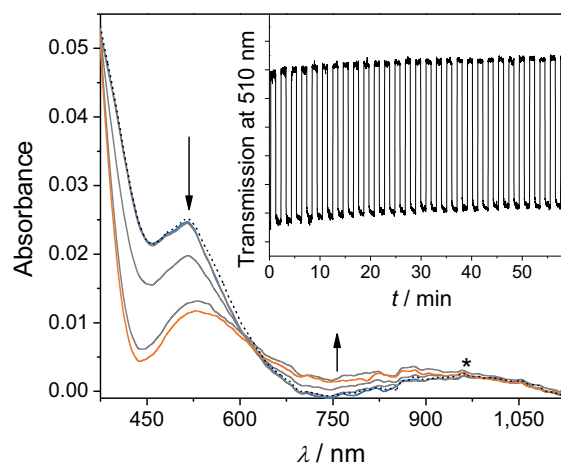
Figure 5.12. Change of the UV−vis−NIR absorption spectrum of an electropolymerized film of **31** during the oxidation (solid lines) and after the re-reduction (dashed line) process (film on ITO-coated glass in CH_2Cl_2 with 0.1 M Bu_4NPF_6). Note that the underlying absorbance between 800 and 1,100 nm (*) is attributed to the ITO substrate. Inset: Change of transmission at 510 nm over 30 cycles of switching between initial and oxidized state.

In conclusion, while the anodic electropolymerization of electron-rich, cyclometalated ruthenium(II) complexes prove to be challenging, a slight lowering of the electronic donation from the cyclometalating ligands was sufficient to allow a successful electropolymerization. Exemplarily, a *bis*(tridentate) ruthenium(II) complexes featuring a readily synthesized, triazole-containing cyclometalating ligand was used, but this strategy is believed to be more general. Alternatively, the ruthenium(II) complexes might be equipped with more electron-rich oxidatively polymerizable units (*e.g.* EDOT), which would allow the use of milder potentials in the electropolymerization. Accordingly, very recently, the anodic electropolymerization of cyclometalated ruthenium(II) complexes equipped triarylamines as eletropolymerizable units was reported.[289] Ultimately, thin films of conductive photo-redox-active and -stable metallopolymers featuring a low energy gap were obtained, which show potential for applications in electrochromic and photovoltaic devices. In case of the latter, the insoluble polymer would allow the use of aqueous electrolytes.[276] Moreover, depending on the used electropolymerizable units,[277] the extended π system that emerges during the oxidative electropolymerization might act as light harvesting antenna[290] and/or enable an intramolecular hole transfer after photo-oxidation of the complex.[164]

6 Summary

Ruthenium(II) polypyridyl complexes are well-suited building blocks for the construction of photo-redox active (supramolecular) assemblies[9, 22–25] and "molecular photovoltaics",[20] namely dye-sensitized solar cells,[12] as they undergo a light-driven charge separation upon visible-light absorption[16] and exhibit a high redox stability. While *bis*(tridentate) ruthenium(II) complexes are robust complex platforms and excellent building blocks for the construction of electron-transfer assemblies,[22–23] their typically short-lived charge-separated excited states represent a major drawback in further exploiting these coordination compounds in solar energy conversion.[35–36, 47]

This thesis aimed on the design of tridentate ligands based on 1,2,3-triazoles, which are readily prepared and functionalized by making use of azide−alkyne cycloaddition reactions and afford ruthenium(II) complexes with optimized photophysical properties. In order to extend the excited-state lifetimes of *bis*(tridentate) ruthenium(II) complexes, a tridentate ligand featuring 1,2,3-triazolylidene donors was synthesized *via* further transformations of the 1,2,3-triazoles. The corresponding heteroleptic, *bis*(tridentate) ruthenium(II) complex (Figure 6.1) showed a substantially prolonged excited-state lifetime (up to 633 ns) as well as much higher photoluminescence quantum yields (up to 11.4%)[201] than the parent [Ru(tpy)$_2$](PF$_6$)$_2$ complex, which exhibits an excited-state lifetime of about 0.2 ns[52–53] and is practically non-luminescent. This difference is attributed to the enhanced σ-donor strength of the mesoionic carbenes, which leads to a suppression of the radiationless deactivation within the corresponding ruthenium(II) complex. Despite the strong electron donation from the 1,2,3-triazolylidenes, the energy, which is stored in the excited-state of the complex and which represents the driving force for subsequent chemical reactions, is relatively high, suggesting prospective applications of the new complex in electron-transfer assemblies or as photocatalyst. Furthermore, materials featuring an intense emission of red light are attractive for applications in light-emitting electrochemical cells[210–211] and sensing.[212]
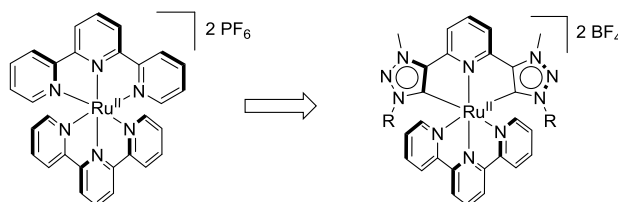
Figure 6.1. Schematic representation of a prototypical *bis*(tridentate) ruthenium(II) complexes (left) and a 1,2,3-triazolylidene-containing analogue (right).

While ruthenium(II) complexes bearing functionalized polypyridyl ligands as well as thiocyanato ligands (*e.g.* **N749**, Figure 6.2) represent prime examples for the efficient sensitization of a semiconductor in terms of a DSSC,[40–41, 273] the monodentate NCS⁻ ligands compromise the complex stability[45] and preclude further optimization of the sensitizers *via* ligand functionalization. It has been demonstrated during the last years that the replacement of the thioyanato ligands of ruthenium(II) sensitizers by anionic chelating ligands allows comparable or even improved power conversion efficiencies in the DSSC,[42–43] while the long-term stability is improved.[44]

Aiming at application in the DSSC, different types of *bis*(tridentate) ruthenium(II) complexes featuring anionic 1,2,3-triazole-derived ligands were readily prepared (Figure 6.2). The metal is either coordinated by an N^C^N-cyclometalating ligand, *i.e.* by an anionic phenyl

ring equipped with peripheral 1,2,3-triazole donors, or by a tridentate ligand consisting of two anionic 1,2,3-triazolates and a central pyridine ring (*cf.* Figure 6.2). In both cases, the ruthenium(II) complexes exhibit narrow energy gaps allowing light absorption throughout the visible region. Upon light absorption, a charge transfer directed towards the anchoring ligand is induced with the lifetimes of the charge-separated excited state being sufficiently long to enable efficient electron injection into TiO_2. Accordingly, the new sensitizers achieved PCEs in the DSSC approaching the values obtained with the thiocyanate-containing benchmark dye **N749** under identical conditions. Moreover, the presented thiocyanate-free, *bis*(tridentate) ruthenium(II) complex platform is expected to provide an enhanced long-term stability of the corresponding DSSCs[44] as the tridentate chelates increase the complex stability and since the dyes are decorated with hydrophobic alkyl chains, which is known to impede a water-induced dye desorption.[145, 157] Additionally, the alkyl chains are expected to better isolate the TiO_2 surface from the electrolyte thereby enabling the use of alternative, for instance Co(III)/Co(II)-based redox shuttles.[142, 156] Prospectively, the power conversion efficiencies can be further optimized *via* attachment of additional chromophores at the tridentate anionic ligands of the presented sensitizers.[42−43]
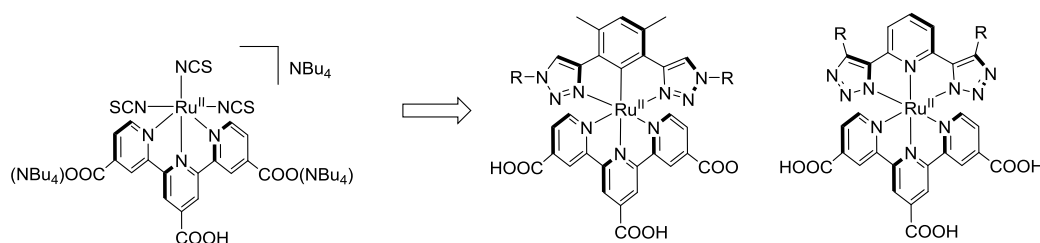
Figure 6.2. Schematic representation of a prototypical ruthenium(II)-based, thiocyanate-containing sensitizer (**N749**, left) and related thiocyanate-free ruthenium(II) complexes featuring anionic tridentate ligands (right).

Moreover, conducting, photo-redox active metallopolymer films were successfully prepared *via* anodic electropolymerization of ruthenium(II) complexes featuring a 1,2,3-triazole-containing N^C^N-cyclometalating ligand equipped with thiophene moieties. For this purpose, the electron donation from the carbanion had to be attenuated by installing suitable substituents at the cyclometalating phenyl ring. Prospectively, the electropolymerization may be applied to TiO_2-anchored cyclometalated dyes in order to form an insoluble sensitizer network. The latter is expected to prevent water-induced dye desorption, which limits amongst others the long-term and thermal stability of a DSSC,[145, 157] and even allow the use of benign, aqueous electrolytes.[276]

Ultimately, by employing 1,2,3-triazoles, 1,2,3-triazolates, and 1,2,3-triazolylidenes as alternative donors in *bis*(tridentate) ruthenium(II) polypyridyl complexes, rapid access to highly functionalized complexes, which are suitable for applications in, *e.g.*, photovoltaic devices, is provided.

7   Zusammenfassung

Ruthenium(II)-Polypyridylkomplexe sind prädestinierte Bausteine für den Aufbau photo-redoxaktiver (supramolekularer) Strukturen[9, 22−25] und „molekularer Photovoltaik",[20] d.h. farbstoffsensibilisierte Solarzellen,[12] da sie unter Absorption von sichtbarem Licht eine Ladungsseparation vollführen und zudem elektrochemisch reversibel schaltbar sind.[16] Während Ruthenium(II)-Komplexe mit zwei dreizähnigen Liganden, sogenannte *bis*(tridentate) Komplexe, eine hohe Stabilität aufweisen und die Konstruktion von strukturell definierten Elektrontransferaggregaten erlauben,[22−23] ist der ladungsgetrennte angeregte Zustand dieser Komplexe typischerweise äußerst kurzlebig, was einen entscheidenden Nachteil in der Nutzbarmachung von Sonnenenergie darstellt.[35−36, 47]

Ziel dieser Arbeit war es, dreizähnige Liganden basierend auf 1,2,3-Triazolen zu entwickeln, die zum einen mittels Cycloadditionsreaktionen zwischen organischen Aziden und Alkinen sehr leicht zugänglich und funktionalisierbar sind und zum anderen eine Verbesserung der photophysikalischen Eigenschaften entsprechendener Ruthenium(II)-Komplexe erreichen. Um die Lebenszeiten der elektronisch angeregten Zustände von *bis*(tridentaten) Ruthenium(II)-Komplexen zu verlängern, wurde mittels Funktionalisierung der 1,2,3-Triazolringe ein dreizähniges Ligandsystem mit 1,2,3-Triazolylidendonoren aufgebaut. Der entsprechenden heteroleptische Ruthenium(II)-Komplex (Abbildung 7.1) zeigte eine wesentlich längere Lebenszeit des angeregten Zustands (bis zu 633 ns) sowie eine deutlich höhere Photolumineszenzquantenausbeute (bis zu 11.4%)[201] als der zugrundeliegende homoleptische *Bis*(2,2′:6′,2″-Terpyridin)-Ruthenium(II)-Komplex, [Ru(tpy)$_2$](PF$_6$)$_2$, welcher eine Lebenszeit von etwa 0.2 ns aufweist[52−53] und praktisch nicht photolumineszent ist. Dieser Unterschied ist auf die hohe σ-Donorstärke der mesoionischen Carbene zurückzuführen, welche zu einer Unterdrückung der strahlungslosen Deaktivierung innerhalb des entsprechenden Ruthenium(II)-Komplexes führt. Trotz der hohen Donorstärke der 1,2,3-Triazolylidene ist die Energie, die im angeregten Zustand im Komplex gespeichert ist und die Triebkraft für anschließende chemische Reaktionen darstellt, relativ hoch, was eine Anwendung des neuen Komplexes in Elektrontransferaggregaten oder als Photokatalysator nahelegt. Aufgrund der relativ intensiven Emission von rotem Licht sind diese Komplexe zudem interessant für die Anwendung in lichtemittierenden Dioden[210−211] und Sensoren.[212]
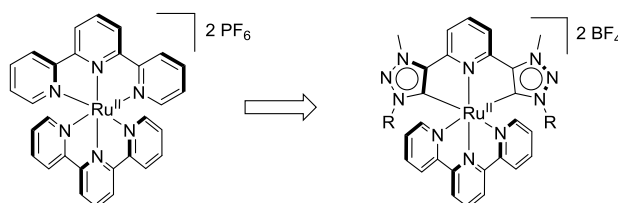
Abbildung 7.1. Schematische Darstellung eines prototypischen *bis*(tridentaten) Ruthenium(II)-Komplexes (links) und eines 1,2,3-Triazolyliden-basierten Analogons (rechts).

Obwohl Ruthenium(II)-Komplexe mit funktionalisierten Polypyridylliganden und Thiocyanato-Liganden (z.B. **N749**, Abbildung 7.2) Paradebeispiele für die effiziente Sensibilisierung eines Halbleiters in farbstoffsensibilisierten Solarzellen darstellen,[40−41, 273] beeinträchtigen die einzähnigen NCS⁻-Liganden zugleich die Komplexstabilität[45] und verhindern eine weitere Verbesserung der Farbstoffe durch Ligandfunktionalisierungen. Während der letzten Jahre wurde gezeigt, dass die Ersetzung der Thiocyanato-Liganden der Ruthenium(II)-Farbstoffe durch anionische Chelatliganden zu ähnlichen oder sogar höheren

Effizienzen[42–43] der entsprechenden Solarzellen bei gleichzeitig verbesserter Langzeitstabilität führt.[44]

Für die Anwendung in Farbstoffsolarzellen wurden zwei verschiedene Typen von Ruthenium(II)-Komplexen basierend auf anionischen, dreizähnigen Chelatliganden mit 1,2,3-Triazoldonoren entwickelt (Abbildung 7.2). Dabei erfolgt die Metallkoordination entweder durch einen N^C^N-cyclometallierenden Liganden, d.h. durch einen anionischer Phenylring und zwei periphere 1,2,3-Triazolringe, oder durch einen dreizähnigen Liganden bestehend aus zwei anionische 1,2,3-Triazolatringen und einem zentralen Pyridinring (vgl. Abbildung 7.2).

In beiden Fällen weisen die entsprechenden Ruthenium(II)-Komplexe eine enge Energielücke auf, welche die Absorption von Licht im gesamten sichtbaren Spektrum erlaubt. Die Lichtabsorption wird von einem Ladungstransfer vom Metall zum Ankerliganden begleitet und die Ladungsrekombination ist langsam genug, um eine effiziente Übertragung von Elektronen in das Leitungsband des TiO_2-Halbleiters zu erlauben. Dementsprechend ermöglichen diese Farbstoffe Energieumwandlungseffizienzen, die vergleichbar mit denen des Thiocyanat-basierten Referenzfarbstoffes **N749** unter identischen Bedingungen sind. Darüber hinaus wird erwartet, dass Solarzellen basierend auf den neuen Komplexen eine erhöhte Langzeitstabilität erreichen, da die dreizähnigen Liganden zu einer erhöhten Komplexstabilität führen.[44] Zusätzlich wurden die Farbstoffe mit hydrophoben Alkylketten funktionalisiert, was die Wahrscheinlichkeit einer Ablösung vom Halbleiter durch Wasser verringert.[145, 157] Aufgrund der besseren Isolierung des Halbleiters vom Elektrolyten durch die Alkylketten besteht zudem die Möglichkeit, alternative Elektrolytsysteme, z.B. basierend auf dem Co(III)/Co(II)-Redoxpaar, zu nutzen.[142, 156] Weiterhin kann die Energieumwandlungseffizienz durch Funktionalisierung der anionischen Chelatliganden der untersuchten Farbstoffe mit zusätzlichen Chromophoren noch gesteigert werden.[42–43]
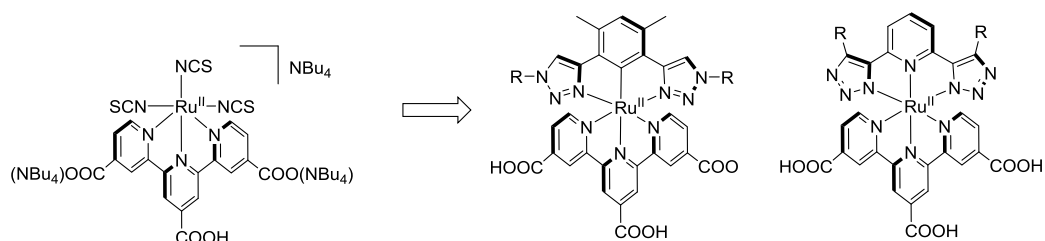
Abbildung 7.2. Schematische Darstellung eines prototypischen Ruthenium(II)-basierten Sensibilisators mit Thiocyanato-Liganden (**N749**, links) und verwandte, thiocyanatfreie Ruthenium(II)-Komplexe mit anionischen, dreizähnigen Liganden (rechts).

Darüber hinaus konnten erfolgreich leitfähige, photo-redoxaktive Metallopolymere durch anodische Elektropolymerisation von cyclometallierten Ruthenium(II)-Komplexen mit Thiophen-funktionalisierten, 1,2,3-Triazol-basierten Liganden hergestellt werden. Um dies zu erreichen, war es nötig, die Donorstärke des Carbanions durch die Anbringung geeigneter Substituenten am cyclometallierenden Phenylring zu verringern. Perspektivisch kann die Elektropolymerisation angewandt werden, um an TiO_2 gebundene cyclometallierte Farbstoffe zu verbinden und somit ein unlösliches Netzwerk aus Sensibilisatoren zu bilden. Dies würde eine Farbstoffdesorption durch Wasser unterbinden, welche unter anderem die Lebensdauer und thermische Stabilität von Farbstoffsolarzellen limitiert,[145, 157] und sogar die Nutzung von umweltfreundlichen Elektrolyten basierend auf Wasser ermöglichen.[276]

Letztlich konnte gezeigt werden, dass die Verwendung von 1,2,3-Triazolen, 1,2,3-Triazolaten und 1,2,3-Triazolylidenen als alternative Donoren in *bis*(tridentaten) Ruthenium(II)-Polypyridylkomplexen einen schnellen synthetischen Zugang zu

hochfunktionalisierten Komplexen ermöglicht, welche sich für Anwendungen beispielsweise in Farbstoffsolarzellen eignen.

References

[1]   N. S. Lewis, D. G. Nocera, *Proc. Natl. Acad. Sci. USA* **2006**, *103*, 15729−15735.
[2]   Q. Schiermeier, J. Tollefson, T. Scully, A. Witze, O. Morton, *Nature* **2008**, *454*, 816−823.
[3]   R. F. Service, *Science* **2005**, *309*, 548−551.
[4]   T. R. Cook, D. K. Dogutan, S. Y. Reece, Y. Surendranath, T. S. Teets, D. G. Nocera, *Chem. Rev.* **2010**, *110*, 6474−6502.
[5]   J. Barber, *Chem. Soc. Rev.* **2009**, *38*, 185−196.
[6]   N. Armaroli, V. Balzani, *Angew. Chem. Int. Ed.* **2007**, *46*, 52−66.
[7]   T. J. Meyer, *Acc. Chem. Res.* **1989**, *22*, 163−170.
[8]   J. H. Alstrum-Acevedo, M. K. Brennaman, T. J. Meyer, *Inorg. Chem.* **2005**, *44*, 6802−6827.
[9]   W. Song, Z. Chen, M. K. Brennaman, J. J. Concepcion, A. O. T. Patrocinio, N. Y. Murakami Iha, T. J. Meyer, *Pure Appl. Chem.* **2011**, *83*, 749−768.
[10]   K. S. Joya, Y. F. Joya, K. Ocakoglu, R. van de Krol, *Angew. Chem. Int. Ed.* **2013**, *52*, 10426−10437.
[11]   A. W. Hains, Z. Liang, M. A. Woodhouse, B. A. Gregg, *Chem. Rev.* **2010**, *110*, 6689−6735.
[12]   A. Hagfeldt, G. Boschloo, L. Sun, L. Kloo, H. Pettersson, *Chem. Rev.* **2010**, *110*, 6595−6663.
[13]   M. Grätzel, *Nature* **2001**, *414*, 338−344.
[14]   M. Grätzel, *J. Photoch. Photobio. C* **2003**, *4*, 145−153.
[15]   K. Kalyanasundaram, *Coord. Chem. Rev.* **1982**, *46*, 159−244.
[16]   A. Juris, V. Balzani, F. Barigelletti, S. Campagna, P. Belser, A. von Zelewsky, *Coord. Chem. Rev.* **1988**, *84*, 85−277.
[17]   S. Campagna, F. Puntoriero, F. Nastasi, G. Bergamini, V. Balzani, *Top. Curr. Chem.* **2007**, *280*, 117−214.
[18]   D. W. Thompson, A. Ito, T. J. Meyer, *Pure Appl. Chem.* **2013**, *85*, 1257−1305.
[19]   C. K. Prier, D. A. Rankic, D. W. C. MacMillan, *Chem. Rev.* **2013**, *113*, 5322−5363.
[20]   A. Hagfeldt, M. Grätzel, *Acc. Chem. Res.* **2000**, *33*, 269−277.
[21]   A. Reynal, E. Palomares, *Eur. J. Inorg. Chem.* **2011**, 4509−4526.
[22]   J.-P. Sauvage, J.-P. Collin, J.-C. Chambron, S. Guillerez, C. Coudret, V. Balzani, F. Barigelletti, L. De Cola, L. Flamigni, *Chem. Rev.* **1994**, *94*, 993−1019.
[23]   E. Baranoff, J.-P. Collin, L. Flamigni, J.-P. Sauvage, *Chem. Soc. Rev.* **2004**, *33*, 147−155.
[24]   V. Balzani, *Pure Appl. Chem.* **1990**, *62*, 1099−1102.
[25]   V. Balzani, A. Juris, M. Venturi, S. Campagna, S. Serroni, *Chem. Rev.* **1996**, *96*, 759−834.
[26]   H. C. Kolb, M. G. Finn, K. B. Sharpless, *Angew. Chem. Int. Ed.* **2001**, *40*, 2004−2021.
[27]   H. Struthers, T. L. Mindt, R. Schibli, *Dalton Trans.* **2010**, *39*, 675−696.
[28]   J. Crowley, D. McMorran, *Top. Heterocycl. Chem.* **2012**, *28*, 31−83.
[29]   B. Schulze, U. S. Schubert, *Chem. Soc. Rev.* **2014**, *43*, 2522−2571.
[30]   S. Lee, A. Flood, *Top. Heterocycl. Chem.* **2012**, *28*, 85−107.
[31]   M. Watkinson, *Top. Heterocycl. Chem.* **2012**, *28*, 109−136.
[32]   K. P. McDonald, Y. Hua, A. H. Flood, *Top. Heterocycl. Chem.* **2010**, *24*, 341−366.
[33]   Y. Hua, A. H. Flood, *Chem. Soc. Rev.* **2010**, *39*, 1262−1271.
[34]   K. F. Donnelly, A. Petronilho, M. Albrecht, *Chem. Commun.* **2013**, *49*, 1145−1159.
[35]   E. A. Medlycott, G. S. Hanan, *Chem. Soc. Rev.* **2005**, *34*, 133−142.
[36]   E. A. Medlycott, G. S. Hanan, *Coord. Chem. Rev.* **2006**, *250*, 1763−1782.
[37]   S. U. Son, K. H. Park, Y.-S. Lee, B. Y. Kim, C. H. Choi, M. S. Lah, Y. H. Jang, D.-J. Jang, Y. K. Chung, *Inorg. Chem.* **2004**, *43*, 6896−6898.
[38]   Throughout this thesis, the term cyclometalation implies a metal-mediated, donor-assisted C−R bond activation at RC^E (R = e.g. H; E = donor atom) yielding a metalacycle featuring a M−C σ bond. As a result, a carbanion is coordinated to the metal complex, which is often part of an aromatic system and usually of strong σ- and π-donating character. While the coordination of a chelating ligand bearing an anionic nitrogen donor, such as an azolate, is synthetically and electronically closely related, the term cyclometalation is generally restricted to carbon atoms. See M. Albrecht, *Chem. Rev.* **2010**, *110*, 576−623 and M. I. Bruce, *Angew. Chem. Int. Ed.* **1977**, *16*, 73−86. Note that also carbenes are excluded from the above definition, which require in most cases different synthetic strategies to be coordinated to a metal center and, moreover, possess fundamentally different electronic properties.

[39] M. K. Nazeeruddin, A. Kay, I. Rodicio, R. Humphry-Baker, E. Mueller, P. Liska, N. Vlachopoulos, M. Grätzel, *J. Am. Chem. Soc.* **1993**, *115*, 6382−6390.

[40] M. K. Nazeeruddin, P. Péchy, M. Grätzel, *Chem. Commun.* **1997**, 1705−1706.

[41] M. K. Nazeeruddin, P. Péchy, T. Renouard, S. M. Zakeeruddin, R. Humphry-Baker, P. Comte, P. Liska, L. Cevey, E. Costa, V. Shklover, L. Spiccia, G. B. Deacon, C. A. Bignozzi, M. Grätzel, *J. Am. Chem. Soc.* **2001**, *123*, 1613−1624.

[42] P. G. Bomben, K. C. D. Robson, B. D. Koivisto, C. P. Berlinguette, *Coord. Chem. Rev.* **2012**, *256*, 1438−1450.

[43] K. C. D. Robson, P. G. Bomben, C. P. Berlinguette, *Dalton Trans.* **2012**, *41*, 7814−7829.

[44] C.-W. Hsu, S.-T. Ho, K.-L. Wu, Y. Chi, S.-H. Liu, P.-T. Chou, *Energy Environ. Sci.* **2012**, *5*, 7549−7554.

[45] F. Nour-Mohhamadi, S. D. Nguyen, G. Boschloo, A. Hagfeldt, T. Lund, *J. Phys. Chem. B* **2005**, *109*, 22413−22419.

[46] J.-F. Yin, M. Velayudham, D. Bhattacharya, H.-C. Lin, K.-L. Lu, *Coord. Chem. Rev.* **2012**, *256*, 3008−3035.

[47] L. Hammarström, O. Johansson, *Coord. Chem. Rev.* **2010**, *254*, 2546−2559.

[48] B. Durham, J. V. Caspar, J. K. Nagle, T. J. Meyer, *J. Am. Chem. Soc.* **1982**, *104*, 4803−4810.

[49] J. R. Kirchhoff, D. R. McMillin, P. A. Marnot, J. P. Sauvage, *J. Am. Chem. Soc.* **1985**, *107*, 1138−1141.

[50] M. Abrahamsson, M. Jäger, R. J. Kumar, T. Österman, P. Persson, H.-C. Becker, O. Johansson, L. Hammarström, *J. Am. Chem. Soc.* **2008**, *130*, 15533−15542.

[51] T. J. Meyer, *Pure Appl. Chem.* **1986**, *58*, 1193−1206.

[52] A. Amini, A. Harriman, A. Mayeux, *Phys. Chem. Chem. Phys.* **2004**, *6*, 1157−1164.

[53] J. R. Winkler, T. L. Netzel, C. Creutz, N. Sutin, *J. Am. Chem. Soc.* **1987**, *109*, 2381−2392.

[54] J. E. Huheey, E. A. Keiter, R. L. Keiter, in *Inorganic Chemistry: Principles of Structure and Reactivity*, 4th ed., HarperCollins College Publishers, New York, **1993**.

[55] G. Frenking, N. Fröhlich, *Chem. Rev.* **2000**, *100*, 717−774.

[56] G. Frenking, K. Wichmann, N. Fröhlich, C. Loschen, M. Lein, J. Frunzke, V. M. Rayón, *Coord. Chem. Rev.* **2003**, *238–239*, 55−82.

[57] K. Lashgari, M. Kritikos, R. Norrestam, T. Norrby, *Acta Crystallogr. C* **1999**, *55*, 64−67.

[58] A. Islam, N. Ikeda, A. Yoshimura, T. Ohno, *Inorg. Chem.* **1998**, *37*, 3093−3098.

[59] M. Ziegler, V. Monney, H. Stoeckli-Evans, A. Von Zelewsky, I. Sasaki, G. Dupic, J.−C. Daran, G. G. A. Balavoine, *J. Chem. Soc., Dalton Trans.* **1999**, 667−676.

[60] S. H. Wadman, M. Lutz, D. M. Tooke, A. L. Spek, F. Hartl, R. W. A. Havenith, G. P. M. van Klink, G. van Koten, *Inorg. Chem.* **2009**, *48*, 1887−1900.

[61] J. K. McCusker, *Acc. Chem. Res.* **2003**, *36*, 876−887.

[62] N. H. Damrauer, G. Cerullo, A. Yeh, T. R. Boussie, C. V. Shank, J. K. McCusker, *Science* **1997**, *275*, 54−57.

[63] O. A. Borg, S. S. M. C. Godinho, M. J. Lundqvist, S. Lunell, P. Persson, *J. Phys. Chem. A* **2008**, *112*, 4470−4476.

[64] G. H. Allen, R. P. White, D. P. Rillema, T. J. Meyer, *J. Am. Chem. Soc.* **1984**, *106*, 2613−2620.

[65] E. M. Kober, T. J. Meyer, *Inorg. Chem.* **1984**, *23*, 3877−3886.

[66] A. Harriman, G. Izzet, *Phys. Chem. Chem. Phys.* **2007**, *9*, 944−948.

[67] A. Breivogel, M. Meister, C. Förster, F. Laquai, K. Heinze, *Chem. Eur. J.* **2013**, *19*, 13745−11376.

[68] R. Englman, J. Jortner, *Mol. Phys.* **1970**, *18*, 145−164.

[69] K. F. Freed, J. Jortner, *J. Chem. Phys.* **1970**, *52*, 6272−6291.

[70] P. S. Wagenknecht, P. C. Ford, *Coord. Chem. Rev.* **2011**, *255*, 591−616.

[71] W. R. Browne, J. G. Vos, *Coord. Chem. Rev.* **2001**, *219–221*, 761−787.

[72] C. E. Wayne, R. P. Wayne, in *Photochemistry*, Oxford University Press, Oxford, U. K., **1996**.

[73] D. J. Robbins, A. J. Thomson, *Mol. Phys.* **1973**, *25*, 1103−1119.

[74] L. S. Forster, *Coord. Chem. Rev.* **2002**, *227*, 59−92.

[75] J. P. Claude, T. J. Meyer, *J. Phys. Chem.* **1995**, *99*, 51−54.

[76] S. H. Lin, R. Bersohn, *J. Chem. Phys.* **1968**, *48*, 2732−2736.

[77] T. Kinoshita, J. T. Dy, S. Uchida, T. Kubo, H. Segawa, *Nat. Photonics* **2013**, *7*, 535−539.

[78] A. C. Benniston, G. Chapman, A. Harriman, M. Mehrabi, C. A. Sams, *Inorg. Chem.* **2004**, *43*, 4227−4233.

[79] F. Alary, J. L. Heully, L. Bijeire, P. Vicendo, *Inorg. Chem.* **2007**, *46*, 3154−3165.

[80] G. Ragazzon, P. Verwilst, S. Denisov, A. Credi, G. Jonusauskas, N. D. McClenaghan, *Chem. Commun.* **2013**, *49*, 9110−9112.

[81] J.-P. Collin, M. Beley, J.-P. Sauvage, F. Barigelletti, *Inorg. Chim. Acta* **1991**, *186*, 91−93.

[82] M. Duati, S. Tasca, F. C. Lynch, H. Bohlen, J. G. Vos, S. Stagni, M. D. Ward, *Inorg. Chem.* **2003**, *42*, 8377−8384.

[83] J. V. Caspar, B. P. Sullivan, E. M. Kober, T. J. Meyer, *Chem. Phys. Lett.* **1982**, *91*, 91−95.

[84] P.-T. Chou, Y. Chi, M.-W. Chung, C.-C. Lin, *Coord. Chem. Rev.* **2011**, *255*, 2653−2665.

[85] C. W. Tornøe, C. Christensen, M. Meldal, *J. Org. Chem.* **2002**, *67*, 3057−3064.

[86] V. V. Rostovtsev, L. G. Green, V. V. Fokin, K. B. Sharpless, *Angew. Chem. Int. Ed.* **2002**, *41*, 2596−2599.

[87] M. Meldal, C. W. Tornøe, *Chem. Rev.* **2008**, *108*, 2952−3015.

[88] J. E. Hein, V. V. Fokin, *Chem. Soc. Rev.* **2010**, *39*, 1302−1315.

[89] Y. Li, J. C. Huffman, A. H. Flood, *Chem. Commun.* **2007**, 2692−2694.

[90] B. Schulze, C. Friebe, M. D. Hager, A. Winter, R. Hoogenboom, H. Görls, U. S. Schubert, *Dalton Trans.* **2009**, 787−794.

[91] B. Happ, C. Friebe, A. Winter, M. D. Hager, R. Hoogenboom, U. S. Schubert, *Chem. Asian J.* **2009**, *4*, 154−163.

[92] J. T. Fletcher, B. J. Bumgarner, N. D. Engels, D. A. Skoglund, *Organometallics* **2008**, *27*, 5430−5433.

[93] C. E. Welby, S. Grkinic, A. Zahid, B. S. Uppal, E. A. Gibson, C. R. Rice, P. I. P. Elliott, *Dalton Trans.* **2012**, *41*, 7637−7646.

[94] B. Schulze, C. Friebe, S. Hoeppener, G. M. Pavlov, A. Winter, M. D. Hager, U. S. Schubert, *Macromol. Rapid Commun.* **2012**, *33*, 597−602.

[95] A. B. P. Lever, *Inorg. Chem.* **1990**, *29*, 1271−1285.

[96] J. Catalán, M. Sánchez-Cabezudo, J. L. G. De Paz, J. Elguero, R. W. Taft, F. Anvia, *J. Comput. Chem.* **1989**, *10*, 426−433.

[97] J.-Luis M. Abboud, C. Foces-Foces, R. Notario, Rostislav E. Trifonov, Anna P. Volovodenko, Vladimir A. Ostrovskii, I. Alkorta, J. Elguero, *Eur. J. Org. Chem.* **2001**, 3013−3024.

[98] A. R. Katritzky, C. A. Ramsden, J. A. Joule, V. V. Zhdankin, in *Handbook of Heterocyclic Chemistry (Third Edition)*, Elsevier, Amsterdam, **2010**, pp. 139−209.

[99] I. Jano, *J. Phys. Chem.* **1991**, *95*, 7694−7699.

[100] R. Vianello, Z. B. Maksić, *Mol. Phys.* **2005**, *103*, 209−219.

[101] B. M. J. M. Suijkerbuijk, B. N. H. Aerts, H. P. Dijkstra, M. Lutz, A. L. Spek, G. van Koten, R. J. M. Klein Gebbink, *Dalton Trans.* **2007**, 1273−1276.

[102] M. Ostermeier, M.-A. Berlin, R. M. Meudtner, S. Demeshko, F. Meyer, C. Limberg, S. Hecht, *Chem. Eur. J.* **2010**, *16*, 10202−10213.

[103] A. Maisonial, P. Serafin, M. Traïkia, E. Debiton, V. Théry, D. J. Aitken, P. Lemoine, B. Viossat, A. Gautier, *Eur. J. Inorg. Chem.* **2008**, 298−305.

[104] T. L. Mindt, H. Struthers, L. Brans, T. Anguelov, C. Schweinsberg, V. Maes, D. Tourwé, R. Schibli, *J. Am. Chem. Soc.* **2006**, *128*, 15096−15097.

[105] K. J. Kilpin, E. L. Gavey, C. J. McAdam, C. B. Anderson, S. J. Lind, C. C. Keep, K. C. Gordon, J. D. Crowley, *Inorg. Chem.* **2011**, *50*, 6334−6346.

[106] D. Urankar, B. Pinter, A. Pevec, F. De Proft, I. Turel, J. Košmrlj, *Inorg. Chem.* **2010**, *49*, 4820−4829.

[107] A. R. Katritzky, C. A. Ramsden, J. A. Joule, V. V. Zhdankin, in *Handbook of Heterocyclic Chemistry (Third Edition)*, Elsevier, Amsterdam, **2010**, pp. 37−86.

[108] A. Ajayaghosh, *Chem. Soc. Rev.* **2003**, *32*, 181−191.

[109] S. Bakbak, P. J. Leech, B. E. Carson, S. Saxena, W. P. King, U. H. F. Bunz, *Macromolecules* **2006**, *39*, 6793−6795.

[110] A. Wild, C. Friebe, A. Winter, M. D. Hager, U.-W. Grummt, U. S. Schubert, *Eur. J. Org. Chem.* **2010**, 1859−1868.

[111] I. Stengel, C. A. Strassert, E. A. Plummer, C.-H. Chien, L. De Cola, P. Bäuerle, *Eur. J. Inorg. Chem.* **2012**, 1795−1809.

[112] S. Potratz, A. Mishra, P. Bäuerle, *Beilstein J. Org. Chem.* **2012**, *8*, 683−692.

[113] P. D. Zoon, I. H. M. van Stokkum, M. Parent, O. Mongin, M. Blanchard-Desce, A. M. Brouwer, *Phys. Chem. Chem. Phys.* **2010**, *12*, 2706−2715.

[114] P. D. Jarowski, Y.-L. Wu, W. B. Schweizer, F. Diederich, *Org. Lett.* **2008**, *10*, 3347−3350.

[115] B. Schulze, D. G. Brown, K. C. D. Robson, C. Friebe, E. Birckner, C. P. Berlinguette, U. S. Schubert, *Chem. Eur. J.* **2013**, *19*, 14171−14180.

[116] M. Gholami, R. R. Tykwinski, *Chem. Rev.* **2006**, *106*, 4997−5027.

[117] A. R. Waterloo, S. Kunakom, F. Hampel, R. R. Tykwinski, *Macromol. Chem. Phys.* **2012**, *213*, 1020−1032.

[118] G. Aromí, L. A. Barrios, O. Roubeau, P. Gamez, *Coord. Chem. Rev.* **2011**, *255*, 485−546.

[119] R. M. O'Donnell, P. G. Johansson, M. Abrahamsson, G. J. Meyer, *Inorg. Chem.* **2013**, *52*, 6839−6848.

[120] J. D. Crowley, A.-L. Lee, K. J. Kilpin, *Aust. J. Chem.* **2011**, *64*, 1118−1132.

[121] M. Albrecht, *Chem. Commun.* **2008**, 3601−3610.

[122] A. Krüger, M. Albrecht, *Aust. J. Chem.* **2011**, *64*, 1113−1117.

[123] R. H. Crabtree, *Coord. Chem. Rev.* **2013**, *257*, 755−766.

[124] P. Mathew, A. Neels, M. Albrecht, *J. Am. Chem. Soc.* **2008**, *130*, 13534−13535.

[125] G. Guisado-Barrios, J. Bouffard, B. Donnadieu, G. Bertrand, *Angew. Chem. Int. Ed.* **2010**, *49*, 4759−4762.

[126] T. Dröge, F. Glorius, *Angew. Chem. Int. Ed.* **2010**, *49*, 6940−6952.

[127] J. Bouffard, B. K. Keitz, R. Tonner, G. Guisado-Barrios, G. Frenking, R. H. Grubbs, G. Bertrand, *Organometallics* **2011**, *30*, 2617−2627.

[128] G. Heydenrych, M. von Hopffgarten, E. Stander, O. Schuster, H. G. Raubenheimer, G. Frenking, *Eur. J. Inorg. Chem.* **2009**, 1892−1904.

[129] D. G. Gusev, *Organometallics* **2009**, *28*, 6458−6461.

[130] L.-A. Schaper, K. Ofele, R. Kadyrov, B. Bechlars, M. Drees, M. Cokoja, W. A. Herrmann, F. E. Kuhn, *Chem. Commun.* **2012**, *48*, 3857−3859.

[131] R. Tonner, G. Heydenrych, G. Frenking, *Chem. Asian J.* **2007**, *2*, 1555−1567.

[132] M. Grätzel, *J. Photochem. Photobio. A* **2004**, *164*, 3−14.

[133] M. Grätzel, *Inorg. Chem.* **2005**, *44*, 6841−6851.

[134] M. Grätzel, *Acc. Chem. Res.* **2009**, *42*, 1788−1798.

[135] J. M. Kroon, N. J. Bakker, H. J. P. Smit, P. Liska, K. R. Thampi, P. Wang, S. M. Zakeeruddin, M. Grätzel, A. Hinsch, S. Hore, U. Würfel, R. Sastrawan, J. R. Durrant, E. Palomares, H. Pettersson, T. Gruszecki, J. Walter, K. Skupien, G. E. Tulloch, *Prog. Photovoltaics* **2007**, *15*, 1−18.

[136] A. Listorti, B. O'Regan, J. R. Durrant, *Chem. Mater.* **2011**, *23*, 3381−3399.

[137] B. C. O'Regan, J. R. Durrant, *Acc. Chem. Res.* **2009**, *42*, 1799−1808.

[138] S. Ardo, G. J. Meyer, *Chem. Soc. Rev.* **2009**, *38*, 115−164.

[139] B. O'Regan, M. Grätzel, *Nature* **1991**, *353*, 737−740.

[140] A. Yella, H.-W. Lee, H. N. Tsao, C. Yi, A. K. Chandiran, M. K. Nazeeruddin, E. W.-G. Diau, C.-Y. Yeh, S. M. Zakeeruddin, M. Grätzel, *Science* **2011**, *334*, 629−634.

[141] P. Wang, M. Zhang, Y. Wang, M. Xu, W. Ma, R. Li, *Energy Environ. Sci.* **2013**, *6*, 2944−2949.

[142] T. W. Hamann, *Dalton Trans.* **2012**, *41*, 3111−3115.

[143] S. Zhang, X. Yang, Y. Numata, L. Han, *Energy Environ. Sci.* **2013**, *6*, 1443−1464.

[144] B. E. Hardin, H. J. Snaith, M. D. McGehee, *Nat. Photonics* **2012**, *6*, 162−169.

[145] P. Wang, S. M. Zakeeruddin, J. E. Moser, M. K. Nazeeruddin, T. Sekiguchi, M. Grätzel, *Nat. Mater.* **2003**, *2*, 402−407.

[146] Z. Yu, N. Vlachopoulos, M. Gorlov, L. Kloo, *Dalton Trans.* **2011**, *40*, 10289−10303.

[147] M. K. Nazeeruddin, R. Humphry-Baker, P. Liska, M. Grätzel, *J. Phys. Chem. B* **2003**, *107*, 8981−8987.

[148] F. De Angelis, S. Fantacci, A. Selloni, M. K. Nazeeruddin, M. Grätzel, *J. Phys. Chem. C* **2010**, *114*, 6054−6061.

[149] S.-H. Liu, H. Fu, Y.-M. Cheng, K.-L. Wu, S.-T. Ho, Y. Chi, P.-T. Chou, *J. Phys. Chem. C* **2012**, *116*, 16338−16345.

[150] G. Boschloo, E. A. Gibson, A. Hagfeldt, *J. Phys. Chem. Lett.* **2011**, *2*, 3016−3020.

[151] P. J. Cameron, L. M. Peter, S. M. Zakeeruddin, M. Grätzel, *Coord. Chem. Rev.* **2004**, *248*, 1447−1453.

[152] Q. Wang, S. Ito, M. Grätzel, F. Fabregat-Santiago, I. Mora-Seró, J. Bisquert, T. Bessho, H. Imai, *J. Phys. Chem. B* **2006**, *110*, 25210−25221.

[153] Y. Bai, J. Zhang, Y. Wang, M. Zhang, P. Wang, *Langmuir* **2011**, *27*, 4749−4755.

[154] Y. Shi, Y. Wang, M. Zhang, X. Dong, *Phys. Chem. Chem. Phys.* **2011**, *13*, 14590−14597.

[155] B. M. Klahr, T. W. Hamann, *J. Phys. Chem. C* **2009**, *113*, 14040−14045.

[156] L. E. Polander, A. Yella, B. F. E. Curchod, N. Ashari Astani, J. Teuscher, R. Scopelliti, P. Gao, S. Mathew, J.-E. Moser, I. Tavernelli, U. Rothlisberger, M. Grätzel, M. K. Nazeeruddin, J. Frey, *Angew. Chem. Int. Ed.* **2013**, *52*, 8731−8735.

[157] S. M. Zakeeruddin, M. K. Nazeeruddin, R. Humphry-Baker, P. Péchy, P. Quagliotto, C. Barolo, G. Viscardi, M. Grätzel, *Langmuir* **2002**, *18*, 952−954.

[158] A. R. Srimath Kandada, S. Fantacci, S. Guarnera, D. Polli, G. Lanzani, F. De Angelis, A. Petrozza, *ACS Appl. Mater. Inter.* **2013**, *5*, 4334−4339.

[159] J. Kallioinen, G. Benkö, V. Sundström, J. E. I. Korppi-Tommola, A. P. Yartsev, *J. Phys. Chem. B* **2002**, *106*, 4396−4404.

[160] G. Benkö, J. Kallioinen, J. E. I. Korppi-Tommola, A. P. Yartsev, V. Sundström, *J. Am. Chem. Soc.* **2001**, *124*, 489−493.

[161] S. A. Haque, E. Palomares, B. M. Cho, A. N. M. Green, N. Hirata, D. R. Klug, J. R. Durrant, *J. Am. Chem. Soc.* **2005**, *127*, 3456−3462.

[162] X. Yang, S. Zhang, K. Zhang, J. Liu, C. Qin, H. Chen, A. Islam, L. Han, *Energy Environ. Sci.* **2013**, *6*, 3637−3645.

[163] S. E. Koops, B. C. O'Regan, P. R. F. Barnes, J. R. Durrant, *J. Am. Chem. Soc.* **2009**, *131*, 4808−4818.

[164] K. Hu, K. C. D. Robson, P. G. Johansson, C. P. Berlinguette, G. J. Meyer, *J. Am. Chem. Soc.* **2012**, *134*, 8352−8355.

[165] S. A. Haque, S. Handa, K. Peter, E. Palomares, M. Thelakkat, J. R. Durrant, *Angew. Chem. Int. Ed.* **2005**, *44*, 5740−5744.

[166] S. Handa, H. Wietasch, M. Thelakkat, J. R. Durrant, S. A. Haque, *Chem. Commun.* **2007**, 1725−1727.

[167] K. C. D. Robson, K. Hu, G. J. Meyer, C. P. Berlinguette, *J. Am. Chem. Soc.* **2013**, *135*, 1961−1971.

[168] J. Jeon, W. A. Goddard, H. Kim, *J. Am. Chem. Soc.* **2013**, *135*, 2431−2434.

[169] T. Privalov, G. Boschloo, A. Hagfeldt, P. H. Svensson, L. Kloo, *J. Phys. Chem. C* **2008**, *113*, 783−790.

[170] A. Reynal, A. Forneli, E. Martinez-Ferrero, A. Sánchez-Díaz, A. Vidal-Ferran, B. C. O'Regan, E. Palomares, *J. Am. Chem. Soc.* **2008**, *130*, 13558−13567.

[171] X. Li, A. Reynal, P. Barnes, R. Humphry-Baker, S. M. Zakeeruddin, F. De Angelis, B. C. O'Regan, *Phys. Chem. Chem. Phys.* **2012**, *14*, 15421−15428.

[172] C. E. Richards, A. Y. Anderson, S. Martiniani, C. Law, B. C. O'Regan, *J. Phys. Chem. Lett.* **2012**, *3*, 1980−1984.

[173] E. M. Barea, J. Bisquert, *Langmuir* **2013**, *29*, 8773−8781.

[174] T. Daeneke, T.-H. Kwon, A. B. Holmes, N. W. Duffy, U. Bach, L. Spiccia, *Nat. Chem.* **2011**, *3*, 211−215. Additionally, cheno may suppress the formation of aggregates, which can potentially lower the J_{sc}, see: Z.-S. Wang, Y. Cui, Y. Dan-oh, C. Kasada, A. Shinpo, K. Hara, *J. Phys. Chem. C* **2007**, *2111*, 7224−7230. However, this effect is rather unlikely given the bulkieness of the studied ruthenium(II) complexes.

[175] K.-M. Lee, V. Suryanarayanan, K.-C. Ho, K. R. Justin Thomas, J. T. Lin, *Sol. Energy Mater. Sol. Cells* **2007**, *91*, 1426−1431.

[176] A. C. Onicha, F. N. Castellano, *J. Phys. Chem. C* **2010**, *114*, 6831−6840.

[177] J. R. Jennings, Y. Liu, Q. Wang, *J. Phys. Chem. C* **2011**, *115*, 15109−15120.

[178] S. Pelet, J.-E. Moser, M. Grätzel, *J. Phys. Chem. B* **2000**, *104*, 1791−1795.

[179] K.-L. Wu, S.-T. Ho, C.-C. Chou, Y.-C. Chang, H.-A. Pan, Y. Chi, P.-T. Chou, *Angew. Chem. Int. Ed.* **2012**, *51*, 5642−5646.

[180] L. Han, A. Islam, H. Chen, C. Malapaka, B. Chiranjeevi, S. Zhang, X. Yang, M. Yanagida, *Energy Environ. Sci.* **2012**, *5*, 6057−6060.

[181] J. T. Manka, V. C. McKenzie, P. Kaszynski, *J. Org. Chem.* **2004**, *69*, 1967−1971.

[182] T. Bessho, E. Yoneda, J.-H. Yum, M. Guglielmi, I. Tavernelli, H. Imai, U. Rothlisberger, M. K. Nazeeruddin, M. Grätzel, *J. Am. Chem. Soc.* **2009**, *131*, 5930−5934.

[183] S. H. Wadman, J. M. Kroon, K. Bakker, M. Lutz, A. L. Spek, G. P. M. van Klink, G. van Koten, *Chem. Commun.* **2007**, 1907−1909.

[184] K. C. D. Robson, B. D. Koivisto, A. Yella, B. Sporinova, M. K. Nazeeruddin, T. Baumgartner, M. Grätzel, C. P. Berlinguette, *Inorg. Chem.* **2011**, *50*, 5494−5508.

[185] D. V. Pogozhev, M. J. Bezdek, P. A. Schauer, C. P. Berlinguette, *Inorg. Chem.* **2013**.

[186] P. G. Bomben, T. J. Gordon, E. Schott, C. P. Berlinguette, *Angew. Chem. Int. Ed.* **2011**, *50*, 10682−10685.

[187] H. Kisserwan, T. H. Ghaddar, *Dalton Trans.* **2011**, *40*, 3877−3884.

[188] M. Duati, S. Fanni, J. G. Vos, *Inorg. Chem. Commun.* **2000**, *3*, 68−70.

[189] S.-W. Wang, K.-L. Wu, E. Ghadiri, M. G. Lobello, S.-T. Ho, Y. Chi, J.-E. Moser, F. De Angelis, M. Grätzel, M. K. Nazeeruddin, *Chem. Sci.* **2013**, *4*, 2423−2433.

[190] K.-L. Wu, C.-H. Li, Y. Chi, J. N. Clifford, L. Cabau, E. Palomares, Y.-M. Cheng, H.-A. Pan, P.-T. Chou, *J. Am. Chem. Soc.* **2012**, *134*, 7488−7496.

[191] Y. Chi, J. N. Clifford, P.-T. Chou, *Energy Environ. Sci.* **2012**, *6*, 859−870.

[192] K.-L. Wu, H.-C. Hsu, K. Chen, Y. Chi, M.-W. Chung, W.-H. Liu, P.-T. Chou, *Chem. Commun.* **2010**, *46*, 5124−5126.

[193] C.-C. Chou, K.-L. Wu, Y. Chi, W.-P. Hu, S. J. Yu, G.-H. Lee, C.-L. Lin, P.-T. Chou, *Angew. Chem. Int. Ed.* **2011**, *50*, 2054−2058.

[194] G. Frenking, M. Solà, S. F. Vyboishchikov, *J .Organomet. Chem.* **2005**, *690*, 6178−6204.

[195] B. Schulze, D. Escudero, C. Friebe, R. Siebert, H. Görls, U. Köhn, E. Altuntas, A. Baumgaertel, M. D. Hager, A. Winter, B. Dietzek, J. Popp, L. González, U. S. Schubert, *Chem. Eur. J.* **2011**, *17*, 5494−5498.

[196] K. M. Mullen, J. Mercurio, C. J. Serpell, P. D. Beer, *Angew. Chem. Int. Ed.* **2009**, *48*, 4781−4784.

[197] B. Schulze, C. Friebe, M. D. Hager, W. Günther, U. Köhn, B. O. Jahn, H. Görls, U. S. Schubert, *Org. Lett.* **2010**, *12*, 2710−2713.

[198] J. C. Garrison, W. J. Youngs, *Chem. Rev.* **2005**, *105*, 3978−4008.

[199] C. Radloff, H.-Y. Gong, C. Schulte to Brinke, T. Pape, V. M. Lynch, J. L. Sessler, F. E. Hahn, *Chem. Eur. J.* **2010**, *16*, 13077−13081.

[200] R. Ziessel, V. Grosshenny, M. Hissler, C. Stroh, *Inorg. Chem.* **2004**, *43*, 4262−4271.

[201] D. G. Brown, N. Sanguantrakun, B. Schulze, U. S. Schubert, C. P. Berlinguette, *J. Am. Chem. Soc.* **2012**, *134*, 12354−12357.

[202] H.-J. Park, K. H. Kim, S. Y. Choi, H.-M. Kim, W. I. Lee, Y. K. Kang, Y. K. Chung, *Inorg. Chem.* **2010**, *49*, 7340−7352.

[203] A. J. Arduengo, *Acc. Chem. Res.* **1999**, *32*, 913−921.

[204] M. Lein, G. Frenking, in *Theory and Applications of Computational Chemistry: The First 40 Years* (Eds.: E. D. Clifford, F. Gernot, S. K. Kwang, G. E. Scuseria), Elsevier, Amsterdam, **2005**, pp. 291−372.

[205] C. Morari, *Phys. Lett. A* **2008**, *372*, 1885−1889.

[206] J. M. Calvert, J. V. Caspar, R. A. Binstead, T. D. Westmoreland, T. J. Meyer, *J. Am. Chem. Soc.* **1982**, *104*, 6620−6627.

[207] A. Juris, V. Balzani, P. Belser, A. von Zelewsky, *Helv. Chim. Acta* **1981**, *64*, 2175−2182.

[208] D. G. Brown, P. A. Schauer, J. Borau-Garcia, B. R. Fancy, C. P. Berlinguette, *J. Am. Chem. Soc.* **2013**, *135*, 1692−1695.

[209] R. J. Kumar, S. Karlsson, D. Streich, A. Rolandini Jensen, M. Jäger, H.-C. Becker, J. Bergquist, O. Johansson, L. Hammarström, *Chem. Eur. J.* **2010**, *16*, 2830−2842.

[210] R. D. Costa, E. Ortí, H. J. Bolink, F. Monti, G. Accorsi, N. Armaroli, *Angew. Chem. Int. Ed.* **2012**, *51*, 8178−8211.

[211] P.-T. Chou, Y. Chi, *Chem. Eur. J.* **2007**, *13*, 380−395.

[212] D.-L. Ma, V. P.-Y. Ma, D. S.-H. Chan, K.-H. Leung, H.-Z. He, C.-H. Leung, *Coord. Chem. Rev.* **2012**, *256*, 3087−3113.

[213] J. M. Aizpurua, R. M. Fratila, Z. Monasterio, N. Perez-Esnaola, E. Andreiev, A. Irastorza, M. Sagartzazu-Aizpurua, *New J. Chem.* **2014**, *38*, 474−480.

[214] F. Barigelletti, B. Ventura, J.-P. Collin, R. Kayhanian, P. Gaviña, J.-P. Sauvage, *Eur. J. Inorg. Chem.* **2000**, 113−119.

[215] M. Beley, S. Chodorowski, J.-P. Collin, J.-P. Sauvage, L. Flamigni, F. Barigelletti, *Inorg. Chem.* **1994**, *33*, 2543−2547.

[216] M. Beley, J.-P. Collin, J.-P. Sauvage, *Inorg. Chem.* **1993**, *32*, 4539−4543.

[217] C. Patoux, J.-P. Launay, M. Beley, S. Chodorowski-Kimmes, J.-P. Collin, S. James, J.-P. Sauvage, *J. Am. Chem. Soc.* **1998**, *120*, 3717−3725.

[218] M. Beley, J.-P. Collin, R. Louis, B. Metz, J.-P. Sauvage, *J. Am. Chem. Soc.* **1991**, *113*, 8521−8522.

[219] P. Reveco, R. H. Schmehl, W. R. Cherry, F. R. Fronczek, J. Selbin, *Inorg. Chem.* **1985**, *24*, 4078−4082.

[220] E. C. Constable, J. M. Holmes, *J .Organomet. Chem.* **1986**, *301*, 203−208.

[221] J.-P. Djukic, J.-B. Sortais, L. Barloy, M. Pfeffer, *Eur. J. Inorg. Chem.* **2009**, 817−853.

[222] E. Yoneda, M. Grätzel, M. K. Nazeeruddin, Eur. Pat. Appl. (2009), EP 2036955.

[223] P. G. Bomben, K. C. D. Robson, P. A. Sedach, C. P. Berlinguette, *Inorg. Chem.* **2009**, *48*, 9631−9643.

[224] P. G. Bomben, B. D. Koivisto, C. P. Berlinguette, *Inorg. Chem.* **2010**, *49*, 4960−4971.

[225] A. J. Wilkinson, H. Puschmann, J. A. K. Howard, C. E. Foster, J. A. G. Williams, *Inorg. Chem.* **2006**, *45*, 8685−8699.

[226] M. Jäger, A. Smeigh, F. Lombeck, H. Görls, J.-P. Collin, J.-P. Sauvage, L. Hammarström, O. Johansson, *Inorg. Chem.* **2009**, *49*, 374−376.

[227] P. G. Bomben, K. D. Thériault, C. P. Berlinguette, *Eur. J. Inorg. Chem.* **2011**, 1806−1814.

[228] C.-Y. Chen, J.-G. Chen, S.-J. Wu, J.-Y. Li, C.-G. Wu, K.-C. Ho, *Angew. Chem. Int. Ed.* **2008**, *47*, 7342−7345.

[229] B. P. Sullivan, J. M. Calvert, T. J. Meyer, *Inorg. Chem.* **1980**, *19*, 1404−1407.

[230] F. Barigelletti, L. Flamigni, V. Balzani, J.-P. Collin, J.-P. Sauvage, A. Sour, E. C. Constable, A. M. W. C. Thompson, *J. Am. Chem. Soc.* **1994**, *116*, 7692−7699.

[231] W.-W. Yang, L. Wang, Y.-W. Zhong, J. Yao, *Organometallics* **2011**, *30*, 2236−2240.

[232] W.-W. Yang, J. Yao, Y.-W. Zhong, *Organometallics* **2012**, *31*, 1035−1041.

[233] S. H. Wadman, R. W. A. Havenith, M. Lutz, A. L. Spek, G. P. M. van Klink, G. van Koten, *J. Am. Chem. Soc.* **2010**, *132*, 1914−1924.

[234] M. Maestri, N. Armaroli, V. Balzani, E. C. Constable, A. M. W. C. Thompson, *Inorg. Chem.* **1995**, *34*, 2759−2767.

[235] H. F. Suen, S. W. Wilson, M. Pomerantz, J. L. Walsh, *Inorg. Chem.* **1989**, *28*, 786−791.

[236] M. Jäger, R. J. Kumar, H. Görls, J. Bergquist, O. Johansson, *Inorg. Chem.* **2009**, *48*, 3228−3238.

[237] S. H. Wadman, J. M. Kroon, K. Bakker, R. W. A. Havenith, G. P. M. van Klink, G. van Koten, *Organometallics* **2010**, *29*, 1569−1579.

[238] M. Gagliardo, D. J. M. Snelders, P. A. Chase, R. J. M. Klein Gebbink, G. P. M. van Klink, G. van Koten, *Angew. Chem. Int. Ed.* **2007**, *46*, 8558−8573.

[239] C. Hansch, A. Leo, R. W. Taft, *Chem. Rev.* **1991**, *91*, 165−195.

[240] B. D. Koivisto, K. C. D. Robson, C. P. Berlinguette, *Inorg. Chem.* **2009**, *48*, 9644−9652.

[241] J.-L. Heully, F. Alary, M. Boggio-Pasqua, *J. Chem. Phys.* **2009**, *131*, 184308−184309.

[242] L. Hammarström, F. Barigelletti, L. Flamigni, M. T. Indelli, N. Armaroli, G. Calogero, M. Guardigli, A. Sour, J.-P. Collin, J.-P. Sauvage, *J. Phys. Chem. A* **1997**, *101*, 9061−9069.

[243] M. Sykora, J. R. Kincaid, *Inorg. Chem.* **1995**, *34*, 5852−5856.

[244] C. R. Hecker, A. K. I. Gushurst, D. R. McMillin, *Inorg. Chem.* **1991**, *30*, 538−541.

[245] F. Barigelletti, A. Juris, V. Balzani, P. Belser, A. Von Zelewsky, *J. Phys. Chem.* **1987**, *91*, 1095−1098.

[246] F. Monti, F. Kessler, M. Delgado, J. Frey, F. Bazzanini, G. Accorsi, N. Armaroli, H. J. Bolink, E. Ortí, R. Scopelliti, M. K. Nazeeruddin, E. Baranoff, *Inorg. Chem.* **2013**, *52*, 10292−10305.

[247] D. Escudero, E. Heuser, R. J. Meier, M. Schäferling, W. Thiel, E. Holder, *Chem. Eur. J.* **2013**, *19*, 15639−15644.

[248] W. F. Wacholtz, R. A. Auerbach, R. H. Schmehl, *Inorg. Chem.* **1986**, *25*, 227−234.

[249] J. Kalisiak, K. B. Sharpless, V. V. Fokin, *Org. Lett.* **2008**, *10*, 3171−3174.

[250] J. C. Loren, A. Krasiński, V. V. Fokin, K. B. Sharpless, *Synlett* **2005**, *2005*, 2847−2850.

[251] B. Schulze, D. Escudero, C. Friebe, R. Siebert, H. Görls, S. Sinn, M. Thomas, S. Mai, J. Popp, B. Dietzek, L. González, U. S. Schubert, *Chem. Eur. J.* **2012**, *18*, 4010−4025.

[252] M. K. Nazeeruddin, S. M. Zakeeruddin, R. Humphry-Baker, M. Jirousek, P. Liska, N. Vlachopoulos, V. Shklover, C.-H. Fischer, M. Grätzel, *Inorg. Chem.* **1999**, *38*, 6298−6305.

[253] K. C. D. Robson, B. D. Koivisto, T. J. Gordon, T. Baumgartner, C. P. Berlinguette, *Inorg. Chem.* **2010**, *49*, 5335−5337.

[254] M. L. Muro-Small, J. E. Yarnell, C. E. McCusker, F. N. Castellano, *Eur. J. Inorg. Chem.* **2012**, 4004−4011.

[255] C. Klein, M. K. Nazeeruddin, D. Di Censo, P. Liska, M. Grätzel, *Inorg. Chem.* **2004**, *43*, 4216−4226.

[256] Q. Wang, J.-E. Moser, M. Grätzel, *J. Phys. Chem. B* **2005**, *109*, 14945−14953.

[257] S. Yanagida, Y. Yu, K. Manseki, *Acc. Chem. Res.* **2009**, *42*, 1827−1838.

[258] I. Stengel, A. Mishra, N. Pootrakulchote, S.-J. Moon, S. M. Zakeeruddin, M. Grätzel, P. Bäuerle, *J. Mater. Chem.* **2011**, *21*, 3726−3734.

[259] E. C. Constable, M. J. Hannon, *Inorg. Chim. Acta* **1993**, *211*, 101−110.

[260] V. L. Whittle, J. A. G. Williams, *Dalton Trans.* **2009**, 3929−3940.

[261] C. Coudret, S. Fraysse, J.-P. Launay, *Chem. Commun.* **1998**, 663−664.

[262] P. Bonhôte, J.-E. Moser, R. Humphry-Baker, N. Vlachopoulos, S. M. Zakeeruddin, L. Walder, M. Grätzel, *J. Am. Chem. Soc.* **1999**, *121*, 1324−1336.

[263] K. C. D. Robson, B. D. Koivisto, C. P. Berlinguette, *Inorg. Chem.* **2012**, *51*, 1501–1507.

[264] K. Hasan, E. Zysman-Colman, *Inorg. Chem.* **2012**, *51*, 12560−12564.

[265] N. G. Connelly, W. E. Geiger, *Chem. Rev.* **1996**, *96*, 877−910.

[266] H. Kisserwan, A. Kamar, T. Shoker, T. H. Ghaddar, *Dalton Trans.* **2012**, *41*, 10643−10651.

[267] S.-H. Yang, K.-L. Wu, Y. Chi, Y.-M. Cheng, P.-T. Chou, *Angew. Chem. Int. Ed.* **2011**, *50*, 8270−8274.

[268] In the DSSC literature, redox potentials are often referenced to the (aqueous) NHE scale, while the experiments were mostly conducted in organic solvents using Fc^+/Fc as an internal reference. Notably, the Fc^+/Fc couple is widely solvent independent and inconsistent conversion numbers to the NHE scale are applied, which makes it reasonable to compare directly the experimental values referring to Fc^+/Fc in line with IUPAC recommendations. However, the potentials refering to the traditional NHE scale are provided here as well. See ref. [275, 265] and G. Gritzner, J. Kuta, *Pure Appl. Chem.* **1984**, *1956*, 1461−1466.

[269] P. G. Bomben, J. Borau-Garcia, C. P. Berlinguette, *Chem. Commun.* **2012**, *48*, 5599−5601.

[270] H. Wang, L. M. Peter, *J. Phys. Chem. C* **2012**, *116*, 10468−10475.

[271] F. Fabregat-Santiago, G. Garcia-Belmonte, I. Mora-Seró, J. Bisquert, *Phys. Chem. Chem. Phys.* **2011**, *13*, 9083−9118.

[272] F. Fabregat-Santiago, J. Bisquert, G. Garcia-Belmonte, G. Boschloo, A. Hagfeldt, *Sol. Energy Mater. Sol. Cells* **2005**, *87*, 117−131.

[273] Y. Chiba, A. Islam, Y. Watanabe, R. Komiya, N. Koide, L. Han, *Jpn. J. Appl. Phys.* **2006**, *45*, L638−L640.

[274] It has been reported that the reversal of the TiO_2 ζ-potential from negative to positive values occurs at concentrations one order of magnitude lower for the more charge-dense Li^+ when compared to Na^+ (see ref. [178]). As a result of the positively charged surface, the near-surface concentration of iodide is increased and the dye regeneration kinetics are improved abruptly. A potential coordination of Li^+ to the vacant 2-nitrogen of the 1,2,3-triazole and a concomitant increase of the redox potential can be excluded since no changes in the Ru(III)/Ru(II) couple were observed for **12** in the presence of 0.1 M Li^+ in acetonitrile (0.1 M $LiClO_4$ *vs.* 0.1 M NBu_4ClO_4 as supporting electrolyte). Notably, the ester derivative was used to avoid interactions with the carboxy groups/carboxylates and provide sufficient solubility in acetonitrile.

[275] V. V. Pavlishchuk, A. W. Addison, *Inorg. Chim. Acta* **2000**, *298*, 97−102.

[276] J. A. Moss, J. C. Yang, J. M. Stipkala, X. Wen, C. A. Bignozzi, G. J. Meyer, T. J. Meyer, *Inorg. Chem.* **2004**, *43*, 1784−1792.

[277] C. Friebe, M. D. Hager, A. Winter, U. S. Schubert, *Adv. Mater.* **2012**, *24*, 332−345.

[278] J. Heinze, B. A. Frontana-Uribe, S. Ludwigs, *Chem. Rev.* **2010**, *110*, 4724−4771.

[279] Y.-W. Zhong, C.-J. Yao, H.-J. Nie, *Coord. Chem. Rev.* **2013**, *257*, 1357−1372.

[280] J. Hjelm, E. C. Constable, E. Figgemeier, A. Hagfeldt, R. Handel, C. E. Housecroft, E. Mukhtar, E. Schofield, *Chem. Commun.* **2002**, 284−285.

[281] J. Hjelm, R. W. Handel, A. Hagfeldt, E. C. Constable, C. E. Housecroft, R. J. Forster, *Inorg. Chem.* **2005**, *44*, 1073−1081.

[282] X. J. Zhu, B. J. Holliday, *Macromol. Rapid Commun.* **2010**, *31*, 904−909.

[283] C. Friebe, M. Jäger, U. S. Schubert, *RSC Advances* **2013**, *3*, 11686−11690.

[284] M. Lamberti, G. C. Fortman, A. Poater, J. Broggi, A. M. Z. Slawin, L. Cavallo, S. P. Nolan, *Organometallics* **2012**, *31*, 756−767.

[285] A. R. Katritzky, E. F. V. Scriven, S. Majumder, R. G. Akhmedova, N. G. Akhmedov, A. V. Vakulenko, *ARKIVOC* **2005**, *iii*, 179−191.

[286] C. Friebe, H. Görls, M. Jäger, U. S. Schubert, *Eur. J. Inorg. Chem.* **2013**, 4191−4202.

[287] J. J. Apperloo, L. B. Groenendaal, H. Verheyen, M. Jayakannan, R. A. J. Janssen, A. Dkhissi, D. Beljonne, R. Lazzaroni, J.-L. Brédas, *Chem. Eur. J.* **2002**, *8*, 2384−2396.

[288] C. L. Gaupp, D. M. Welsh, R. D. Rauh, J. R. Reynolds, *Chem. Mater.* **2002**, *14*, 3964−3970.
[289] C.-J. Yao, Y.-W. Zhong, J. Yao, *Inorg. Chem.* **2013**, *52*, 10000−10008.
[290] X. Yu, X. Jin, G. Tang, J. Zhou, W. Zhang, D. Peng, J. Hu, C. Zhong, *Eur. J. Org. Chem.* **2013**, 5893−5901.

Publication List

Refereed publications in scientific journals

12. <u>B. Schulze</u>, U. S. Schubert, "Beyond click chemistry – Supramolecular interactions of 1,2,3-triazoles", *Chem. Soc. Rev.* **2014**, *43*, 2522−2571.

11. S. Sinn, <u>B. Schulze</u>, C. Friebe, D. G. Brown, M. Jäger, E. Altuntaş, J. Kübel, O. Guntner, B. Dietzek, C. P. Berlinguette, U. S. Schubert, "Physicochemical analysis of ruthenium(II) sensitizers of 1,2,3-triazole-derived mesoionic carbene and cyclometalating ligands", *Inorg. Chem.* **2014**, *53*, 2083−2095.

10. S. Sinn, <u>B. Schulze</u>, C. Friebe, D. G. Brown, M. Jäger, J. Kübel, O. Guntner, B. Dietzek, C. P. Berlinguette, U. S. Schubert, "A heteroleptic *bis*(tridentate) ruthenium(II) platform featuring an anionic 1,2,3-triazolate-based ligand for application in the dye-sensitized solar cell", *Inorg. Chem.* **2014**, *53*, 1637−1645.

9. C. Friebe, <u>B. Schulze</u>, H. Görls, M. Jäger, U. S. Schubert, "Designing cyclometalated ruthenium(II) complexes for anodic electropolymerization", *Chem. Eur. J.* **2014**, *20*, 2357−2366.

8. <u>B. Schulze</u>, D. G. Brown, K. C. D. Robson, C. Friebe, E. Birckner, C. P. Berlinguette, U. S. Schubert, "Cyclometalated ruthenium(II) complexes featuring tridentate click-derived ligands for dye-sensitized solar cell applications", *Chem. Eur. J.* **2013**, *19*, 14171−14180.

7. D. G. Brown, N. Sanguantrakun, <u>B. Schulze</u>, U. S. Schubert, C. P. Berlinguette, "*Bis*(tridentate) ruthenium-terpyridine complexes featuring microsecond excited-state lifetimes", *J. Am. Chem. Soc.* **2012**, *134*, 12354−12357.

6. <u>B. Schulze</u>, C. Friebe, S. Hoeppener, G. M. Pavlov, A. Winter, M. D. Hager, U. S. Schubert, "Ruthenium(II) metallo-supramolecular polymers of click-derived tridentate ditopic ligands", *Macromol. Rapid Commun.* **2012**, *33*, 597−602.

5. <u>B. Schulze</u>, D. Escudero, C. Friebe, R. Siebert, H. Görls, S. Sinn, M. Thomas, S. Mai, J. Popp, B. Dietzek, L. González, U. S. Schubert, "Ruthenium(II) photosensitizers of tridentate click-derived cyclometalating ligands: A joint experimental and computational study", *Chem. Eur. J.* **2012**, *18*, 4010−4025.

4. A. Malassa, <u>B. Schulze</u>, B. Stein-Schaller, H. Görls, B. Weber, M. Westerhausen, "Influence of *N*-substitution on the oxidation of 2-pyridylmethylamines with *bis*(trimethylsilyl)amides of iron(III) – Synthesis of heteroleptic iron(II) 2-pyridylmethylamides", *Eur. J. Inorg. Chem.* **2011**, 1584−1592.

3. <u>B. Schulze</u>, D. Escudero, C. Friebe, R. Siebert, H. Görls, U. Köhn, E. Altuntaş, A. Baumgaertel, M. D. Hager, A. Winter, B. Dietzek, J. Popp, L. González, U. S. Schubert, "A heteroleptic *bis*(tridentate) ruthenium(II) complex of a click-derived abnormal carbene pincer ligand with potential for photosensitizer application", *Chem. Eur. J.* **2011**, *17*, 5494−5498.

2. <u>B. Schulze</u>, C. Friebe, M. D. Hager, W. Günther, U. Köhn, B. O. Jahn, H. Görls, U. S. Schubert, "Anion complexation by triazolium "ligands": Mono- and bis-tridentate complexes of sulfate", *Org. Lett.* **2010**, *12*, 2710−2713.

1. <u>B. Schulze</u>, C. Friebe, M. D. Hager, A. Winter, R. Hoogenboom, H. Görls, U. S. Schubert, "2,2′:6′,2″-Terpyridine meets 2,6-*bis*(1*H*-1,2,3-triazol-4-yl)pyridine: Tuning the electro-optical properties of ruthenium(II) complexes", *Dalton Trans.* **2009**, 787−794.

Non-refereed publications

3. <u>B. Schulze</u>, C. Friebe, S. Hoeppener, G. M. Pavlov, M. D. Hager, A. Winter, U. S. Schubert, "Ruthenium(II) and platinum(II) metallopolymers of ditopic π-conjugated clicked ligands − Towards printable optoelectronics", *Polym. Prepr. (Am. Chem. Soc., Div. Polym. Chem.)* **2011**, *52*, 917−918.

2. <u>B. Schulze</u>, C. Friebe, M. D. Hager, A. Winter, U. S. Schubert, "π-Conjugated spacer bridged ditopic 2′,6′-*bis*(1*H*-1,2,3-triazol-4-yl)pyridines", *Polym. Prepr. (Am. Chem. Soc., Div. Polym. Chem.)* **2009**, *50*, 575−576.

1. <u>B. Schulze</u>, C. Friebe, M. D. Hager, A. Winter, R. Hoogenboom, H. Görls, U. S. Schubert, "2,2′:6′,2″-Terpyridine meets 2,6-*bis*(1*H*-1,2,3-triazol-4-yl)pyridine: Tuning the optical properties of ruthenium(II) complexes", *Polym. Prepr. (Am. Chem. Soc., Div. Polym. Chem.)* **2009**, *50*, 252−253.

Posters

7. <u>B. Schulze</u>, S. Sinn, C. Friebe, M. Jäger, D. G. Brown, J. Kübel, B. Dietzek, C. P. Berlinguette, U. S. Schubert, "Heteroleptic *Bis*(tridentate) Ruthenium(II) Complexes Featuring 1,2,3-Triazole-Derived Ligand Platforms as Efficient Photosensitizers", European Symposium (COST Action): Current Challenges in Supramolecular Artificial Photosynthesis, Jena, Germany, 03/12/14−03/13/14.

6. <u>B. Schulze</u>, C. Friebe, D. Escudero, M. D. Hager, H Görls, U. Köhn, W. Günther, L. González, U. S. Schubert, "Pincer-type triazolium and triazolylidene ligands – Complexes of sulfate and ruthenium(II) ions", 242nd ACS National Meeting, Denver, Colorado, U.S., 08/28/11−09/01/11.

5. <u>B. Schulze</u>, C. Friebe, D. Escudero, R. Siebert, U. Köhn, W. Günther, H. Görls, S. Hoeppener, A. Winter, M. D. Hager, B. Dietzek, L. Gonzáles, U. S. Schubert, "Pincer-type triazolium and triazolylidene ligands − Complexes of sulfate and ruthenium(II) ions", Gordon Research Conference on Physical Organic Chemistry, Holderness, New Hampshire, U.S., 06/26/11−07/01/11.

4. <u>B. Schulze</u>, C. Friebe, D. Escudero, R. Siebert, U. Köhn, B. O. Jahn, W. Günther, H. Görls, M. D. Hager, B. Dietzek, L. Gonzáles, U. S. Schubert, "Pincer-type triazolium and triazolylidene ligands − Complexes of sulfate and ruthenium(II) ions" Orchem, Weimar, Germany, 09/13/10−09/15/10.

3. B. Beyer, B. Happ, <u>B. Schulze</u>, A. Winter, M. D. Hager, C. Friebe, C. Ulbricht, R. Hoogenboom, U. S. Schubert, "1*H*-[1,2,3]-Triazole based ligands", 238th ACS National Meeting, Washington, D. C., U. S., 08/16/09−08/20/09.

2. <u>B. Schulze</u>, C. Friebe, M. D. Hager, A. Winter, U. S. Schubert, "π-Conjugated spacer bridged ditopic 2′,6′-*bis*(1*H*-1,2,3-triazol-4-yl)pyridines", 238th ACS National Meeting, Washington, D. C., U. S., 08/16/09−08/20/09.

1. <u>B. Schulze</u>, C. Friebe, M. D. Hager, A. Winter, U. S. Schubert, "2,2′:6′,2″-Terpyridine (tpy) meets 2′,6′-*bis*(triazol-4-yl)pyridines (tripy)" ORCHEM, Weimar, Germany, 09/01/08−09/03/08.

Oral presentations

5. <u>B. Schulze</u>, S. Sinn, C. Friebe, M. Jäger, D. G. Brown, J. Kübel, B. Dietzek, C. P. Berlinguette, U. S. Schubert, "Heteroleptic *Bis*(tridentate) Ruthenium(II) Complexes Featuring 1,2,3-Triazole-Derived Ligand Platforms as Efficient Photosensitizers", Young-Researcher-Meeting (COST Action): Current Challenges in Supramolecular Artificial Photosynthesis, Jena, Germany, 03/09/14−03/11/14.

4. <u>B. Schulze</u>, C. Friebe, M. D. Hager, W. Günther, U. Köhn, B. O. Jahn, H. Görls, U. S. Schubert, "Anion complexation by triazolium 'ligands': Mono- and bis-tridentate complexes of sulfate", 242nd ACS National Meeting, Denver, Colorado, U.S., 08/28/11−09/01/11.

3. <u>B. Schulze</u>, D. Escudero, C Friebe, R. Siebert, H. Görls, U. Köhn, E. Altuntas, A. Baumgaertel, M. D. Hager, A. Winter, B. Dietzek, J. Popp, L. González, U. S. Schubert, "Click-derived abnormal carbene and cyclometallated pincer ligands: New heteroleptic bis-tridentate ruthenium(II) complexes for potential applications in artificial photosynthesis and dye sensitized solar cells," 242nd ACS National Meeting, Denver, Colorado, U.S., 08/28/11−09/01/11.

2. <u>B. Schulze</u>, C. Friebe, S. Hoeppener, G. M. Pavlov, M. D. Hager, A. Winter, U. S. Schubert, "Ruthenium(II) and platinum(II) metallopolymers of ditopic π-conjugated clicked ligands – Towards printable optoelectronics", ACS National Meeting, Denver, Colorado, U.S., 08/28/11−09/01/11.

1. <u>B. Schulze</u>, C. Friebe, M. D. Hager, A. Winter, R. Hoogenboom, H. Görls, U. S. Schubert, "2,2′:6′,2″-Terpyridine meets 2,6-*bis*(1*H*-1,2,3-triazol-4-yl)pyridine: Tuning the optical properties of ruthenium(II) complexes", 238th ACS National Meeting, Washington, D. C., U. S., 08/16/09−08/20/09.

Curriculum Vitae

Personal Data

Date of birth:	July, 10th 1983
Place of birth:	Weimar
Researcher-ID:	B-8266-2012

University Education

09/2012:	Research activities in the group of Prof. Dr. C. P. Berlinguette at the *University of Calgary*, Canada
03/2009–03/2014:	PhD student in the group of Prof. Dr. U. S. Schubert at the *Institute of Organic and Macromolecular Chemistry* of the *Friedrich Schiller University Jena*, Germany, thesis title: "Beyond Click Chemistry: Ruthenium(II) Complexes of Tridentate Ligands Featuring 1,2,3-Triazole-derived Donors"
09/2008	Diploma (equivalent to M.Sc., grade: 1.0, with distinction)
11/2007–07/2008	Diploma thesis in the group of Prof. Dr. U. S. Schubert at the *Institute of Organic and Macromolecular Chemistry* of the *Friedrich Schiller University Jena*, Germany (the practical work has been conducted at the *Technical University Eindhoven*, The Netherlands), thesis title: "1,4′,1″-Functionalized 2′,6′-*bis*(1*H*-1,2,3-triazol-4-yl)pyridines (tripy) – Synthesis of quasi-2,2′:6′,2″-terpyridines by 'click' reactions"
10/2003–09/2008:	Studies of Chemistry at the *Friedrich Schiller University Jena*, Germany

Civilian Service

09/2002–06/2003:	Civilian service at the *Thüringisches Landesamt für Denkmalpflege und Archäologie*, Weimar, Germany

Schooling

04/2002:	Abitur (grade: 1.1) at the *Hoffmann-von-Fallersleben Gymnasium*, Weimar, Germany

Fellowships/Awards

03/2009–02/2011:	PhD fellowship of the *Fonds der Chemischen Industrie*
2011:	Travel grant of the *Liebig Vereinigung für Organische Chemie* of the *Gesellschaft Deutscher Chemiker* to attend the "Gordon Research

Conference on Physical Organic Chemistry", Holderness, New Hampshire, U.S., 06/26/11–07/01/11

Travel grant of the *Divison of Inorganic Chemistry* of the *American Chemical Society* to attend the "ACS National Meeting", Denver, Colorado, U.S., 08/28/11–09/01/11

04/2009: Exam prize of the *Faculty of Chemistry and Earth Sciences* of the *Friedrich Schiller University Jena*

01/2007–07/2008: Scholarship of the *Studienstiftung des deutschen Volkes*

Jena, den 20.05.2014

Benjamin Schulze

Acknowledgements

Christian, Michael, Uli M., and Stephan, it was a pleasure to grow together as friends during the years.

Last but not least, my deepest gratitude goes to my family, my friends, and my beloved girlfriend Iris.

Declaration of Authorship / Selbstständigkeitserklärung

Ich erkläre, dass ich die vorliegende Arbeit selbstständig und unter Verwendung der angegebenen Hilfsmittel, persönlichen Mitteilungen und Quellen angefertigt habe.

I certify that the work presented here is, to the best of my knowledge and belief, original and the result of my own investigations, except as acknowledged, and has not been submitted, either in part or whole, for a degree at this or any other university.

Jena, den 20.05.2014

Supplementary Information

Table S 1. Selected theoretical electronic singlet−singlet transitions for **4**.

tran-sition	ΔE / nm	f	participating MOs (contribution)	assignment
$S_0 \rightarrow S_1$	507	0.007	HOMO(a_2)→LUMO(b_2) (0.69)	$d_{xy} \rightarrow \pi^*_{tpy}$ (MLCT)
$S_0 \rightarrow S_2$	485	0.011	HOMO(a_2)→LUMO+1(b_1) (0.68)	$d_{xy} \rightarrow \pi^*_{CNC}$ (MLCT)
$S_0 \rightarrow S_3$	473	0.000	HOMO−1(b_2)→LUMO+1(b_1) (0.61)	$d_{yz} \rightarrow \pi^*_{CNC}$ (MLCT)
$S_0 \rightarrow S_4$	466	0.052	HOMO−1(b_2)→LUMO(b_2) (-0.46)	$d_{yz} \rightarrow \pi^*_{tpy}$ (MLCT)
			HOMO(a_2)→LUMO+2(a_2) (0.50)	$d_{xy} \rightarrow \pi^*_{tpy}$ (MLCT)
$S_0 \rightarrow S_5$	460	0.000	HOMO−2(b_1)→LUMO(b_2) (0.62)	$d_{xz} \rightarrow \pi^*_{tpy}$ (MLCT)
$S_0 \rightarrow S_6$	451	0.044	HOMO−1(b_2)→LUMO+2(a_2) (0.67)	$d_{yz} \rightarrow \pi^*_{tpy}$ (MLCT)
$S_0 \rightarrow S_7$	430	0.001	HOMO−1(b_2)→LUMO+3(a_2) (0.69)	$d_{yz} \rightarrow \pi^*_{CNC}$ (MLCT)
$S_0 \rightarrow S_8$	429	0.031	HOMO−2(b_1)→LUMO+1(b_1) (0.39)	$d_{xz} \rightarrow \pi^*_{CNC}$ (MLCT)
			HOMO(a_2)→LUMO+3(a_2) (0.48)	$d_{xy} \rightarrow \pi^*_{CNC}$ (MLCT)
$S_0 \rightarrow S_9$	427	0.110	HOMO−1(b_2)→LUMO(b_2) (0.34)	$d_{yz} \rightarrow \pi^*_{tpy}$ (MLCT)
			HOMO(a_2)→LUMO+2(a_2) (0.45)	$d_{xy} \rightarrow \pi^*_{tpy}$ (MLCT)
			HOMO(a_2)→LUMO+3(a_2) (-0.36)	$d_{xy} \rightarrow \pi^*_{CNC}$ (MLCT)
$S_0 \rightarrow S_{11}$	400	0.051	HOMO−2(b_1)→LUMO+3(a_2) (0.68)	$d_{xz} \rightarrow \pi^*_{CNC}$ (MLCT)

(For $S_0 \rightarrow S_{10}$: $f = 0.0001$)

LUMO+7 (a_2) -0.99 eV

LUMO (b_2) -2.74 eV   **LUMO+2 (a_2)** -2.66 eV   **LUMO+3 (a_2)** -2.59 eV   **LUMO+1 (b_1)** -2.68 eV

HOMO-1 (b_2) -6.16 eV   **HOMO (a_2)** -6.09 eV   **HOMO-2 (b_1)** -6.43 eV

HOMO-8 (a_2) -7.63 eV
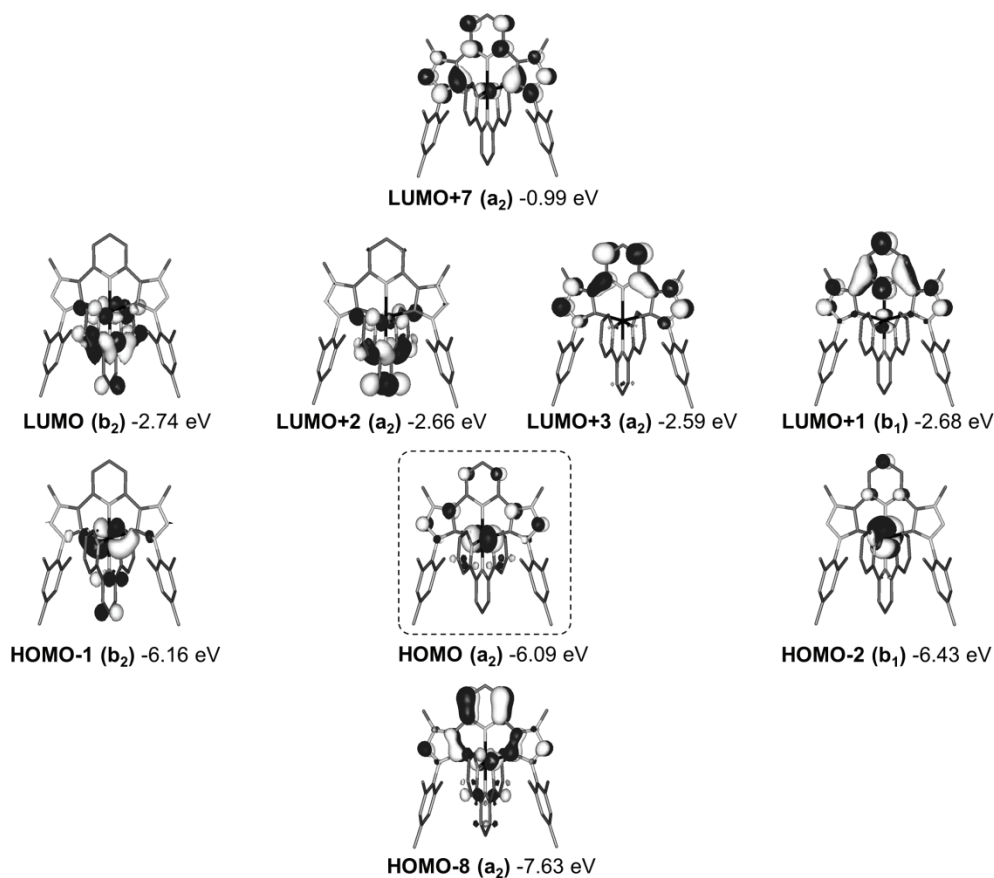
Figure S 1. Relevant Kohn−Sham orbitals (PCM-B3LYP/6-31G*) of **4**.

Table S 2. Selected theoretical electronic singlet−singlet transitions for **6**.

tran-sition	ΔE / nm	f	participating MOs (contribution)	assignment
$S_0 \rightarrow S_1$	639	0.0000	HOMO(b_1)→LUMO(b_2) (0.69)	$d_{xz}+\pi_{NCN}\rightarrow\pi^*_{tpy}$ (MLLCT)
$S_0 \rightarrow S_2$	571	0.0001	HOMO(b_1)→LUMO+1(a_2) (0.70)	$d_{xz}\rightarrow\pi^*_{tpy}$ (MLCT)
$S_0 \rightarrow S_3$	557	0.0124	HOMO−1(a_2)→LUMO(b_2) (0.67)	$d_{xy}\rightarrow\pi^*_{tpy}$ (MLCT)
$S_0 \rightarrow S_4$	515	0.0038	HOMO−2(b_2)→LUMO(b_2) (0.46)	$d_{yz}\rightarrow\pi^*_{tpy}$ (MLCT)
			HOMO−1(a_2)→LUMO+1(a_2) (0.52)	$d_{xy}\rightarrow\pi^*_{tpy}$ (MLCT)
$S_0 \rightarrow S_5$	499	0.0479	HOMO−2(b_2)→ LUMO+1(a_2) (0.68)	$d_{yz}\rightarrow\pi^*_{tpy}$ (MLCT)
$S_0 \rightarrow S_6$	454	0.1048	HOMO−2(b_2)→LUMO(a_2) (0.45)	$d_{yz}\rightarrow\pi^*_{tpy}$ (MLCT)
			HOMO−1(a_2)→LUMO+1(a_2) (-0.45)	$d_{xy}\rightarrow\pi^*_{tpy}$ (MLCT)
$S_0 \rightarrow S_{10}$	369	0.0021	HOMO−3(a_2)→LUMO+1(a_2) (0.69)	$\pi_{NCN}\rightarrow\pi^*_{tpy}$ (LLCT)
$S_0 \rightarrow S_{11}$	364	0.0000	HOMO−1(a_2)→LUMO+14(a_1) (0.51)	$d_{xy}\rightarrow d_{x^2-y^2}$ (MC)
$S_0 \rightarrow S_{13}$	360	0.0073	HOMO−2(b_2)→LUMO+2(b_2) (0.68)	$d_{yz}\rightarrow\pi^*_{tpy}$ (MLCT)
$S_0 \rightarrow S_{14}$	358	0.0654	HOMO(b_1)→LUMO+4(a_2) (0.63)	$d_{xz}+\pi_{NCN}\rightarrow\pi^*_{NCN}$ (MLLCT)
$S_0 \rightarrow S_{15}$	358	0.0620	HOMO−1(a_2)→ LUMO+2(b_2) (0.60)	$d_{xy}\rightarrow\pi^*_{tpy}$ (MLCT)

(For $S_0 \rightarrow S_7$, $S_0 \rightarrow S_8$, $S_0 \rightarrow S_9$, and $S_0 \rightarrow S_{12}$: $f \leq 0.0008$)

LUMO+2 (b_2) -1.17 eV

LUMO+4 (a_2) -0.89 eV

LUMO+14 (a_1) 0.10 eV

LUMO (b_2) -2.19 eV

LUMO+1 (a_2) -2.11 eV

HOMO-2 (b_2) -5.42 eV

HOMO-1 (a_2) -5.37 eV

HOMO (b_1) -5.06 eV

HOMO-3 (a_2) -6.05 eV

HOMO-4 (b_1) -6.53 eV
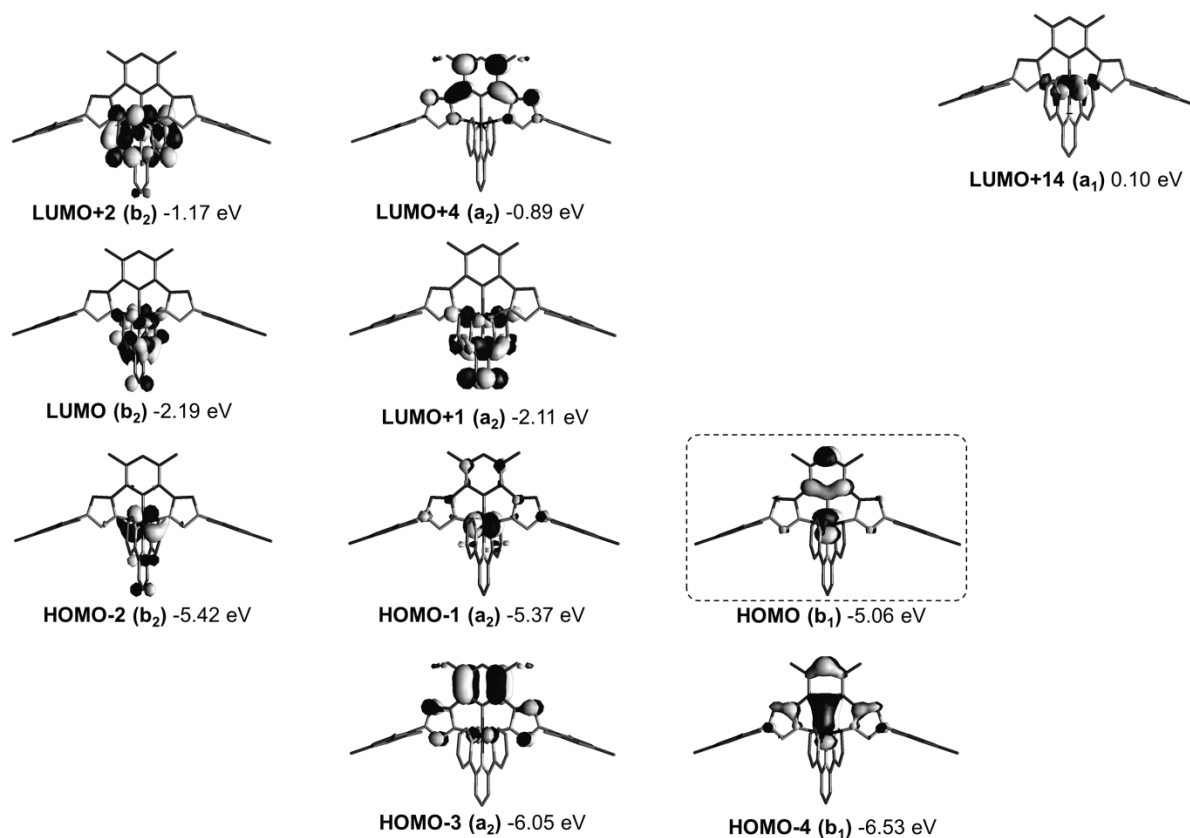
Figure S 2. Relevant Kohn−Sham orbitals (B3LYP/6-31G*) of **6**.

Table S 3. Selected theoretical electronic singlet−singlet transitions for **16**.

transition	ΔE / nm	f	participating MOs (contribution)	assignment
$S_0 \rightarrow S_1$	593	0.0162	HOMO(a_2)→LUMO(b_2) (0.70)	$d_{xy}+\pi_{NNN}\rightarrow\pi^*_{tpy}$ (MLLCT)
$S_0 \rightarrow S_2$	539	0.0000	HOMO−2(b_1)→LUMO(b_2) (0.69)	$d_{xz}\rightarrow\pi^*_{tpy}$ (MLCT)
$S_0 \rightarrow S_3$	522	0.0003	HOMO(a_2)→LUMO+1(a_2) (0.63)	$d_{xy}+\pi_{NNN}\rightarrow\pi^*_{tpy}$ (MLCT)
$S_0 \rightarrow S_4$	476	0.0001	HOMO−2(b_1)→LUMO+1(a_2) (0.69)	$d_{xz}\rightarrow\pi^*_{tpy}$ (MLCT)
$S_0 \rightarrow S_5$	473	0.0514	HOMO−1(b_2)→LUMO+1(a_2) (0.69)	$d_{yz}\rightarrow\pi^*_{tpy}$ (MLCT)
$S_0 \rightarrow S_6$	453	0.1315	HOMO−1(b_2)→LUMO(b_2) (0.59)	$d_{yz}\rightarrow\pi^*_{tpy}$ (MLCT)
			HOMO(a_2)→LUMO+1(a_2) (0.31)	$d_{xy}\rightarrow\pi^*_{tpy}$ (MLCT)
$S_0 \rightarrow S_9$	386	0.0016	HOMO−3(a_2)→LUMO+1(a_2) (0.70)	$\pi_{NNN}\rightarrow\pi^*_{tpy}$ (LLCT)
$S_0 \rightarrow S_{11}$	368	0.0802	HOMO(a_2)→LUMO+3(b_2) (0.69)	$d_{xy}\rightarrow\pi^*_{tpy}$ (MLCT)
$S_0 \rightarrow S_{12}$	368	0.0395	HOMO−2(b_1)→LUMO+2(b_1) (0.55)	$d_{xz}\rightarrow\pi^*_{NNN}$ (MLCT)
			HOMO(a_2)→LUMO+5(a_2) (0.36)	$d_{xy}\rightarrow\pi^*_{NNN}$ (MLCT)
$S_0 \rightarrow S_{13}$	358	0.0000	HOMO(a_2)→LUMO+8(a_1) (0.36)	$d_{xy}\rightarrow d_{x^2-y^2}$ (MC)

(For transitions $S_0 \rightarrow S_7$, $S_0 \rightarrow S_8$, and $S_0 \rightarrow S_{10}$: $f \leq 0.0002$)

LUMO+3 (b_2) -1.16 eV   **LUMO+4 (a_2)** -1.08 eV   **LUMO+5 (a_2)** -0.98 eV   **LUMO+2 (b_1)** -1.35 eV   **LUMO+8 (a_1)** 0.28 eV

LUMO (b_2) -2.19 eV   **LUMO+1 (a_2)** -2.10 eV

HOMO-1 (b_2) -5.48 eV   **HOMO (a_2)** -5.12 eV   **HOMO-3 (a_2)** -5.82 eV   **HOMO-2 (b_1)** -5.49 eV

HOMO-9 (a_2) -7.37 eV
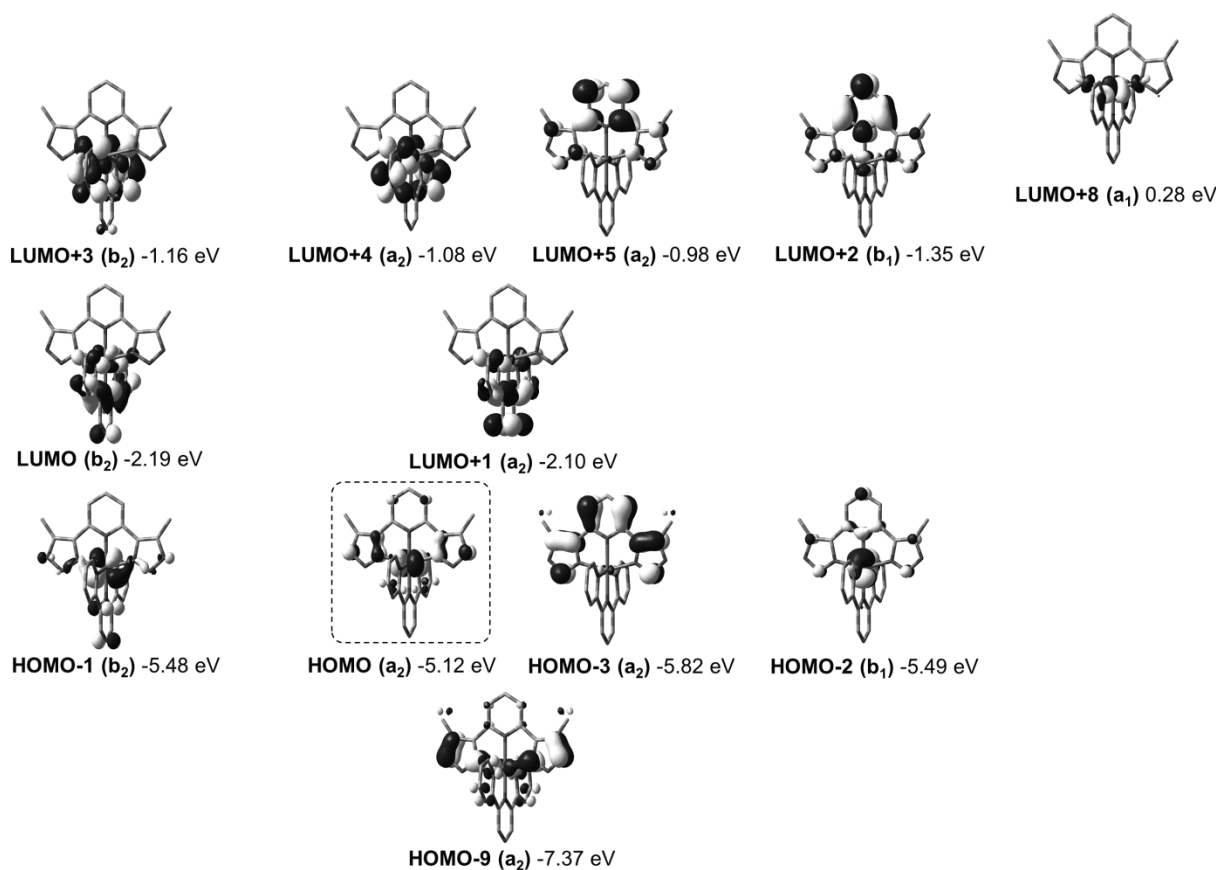
Figure S 3. Relevant Kohn−Sham orbitals (B3LYP/6-31G*) of **16**.

List of Abbreviations

A	pre-exponential factor
Abs	absorption
a.u.	arbitrary units
bpy	2,2′-bipyridine
cheno	chenodeoxycholic acid
CuAAC	copper(I)-catalyzed azide–alkyne cycloaddition
CV	cyclic voltammetry
dcbpy	2,2′-bipyridine-4,4'-dicarboxylate
DOSY	diffusion-ordered NMR spectroscopy
DFT	density functional theory
DMF	N,N-dimethyl formamide
DMII	1,3-dimethylimidazolium iodide
DMSO	dimethyl sulfoxide
dpbH/dpb	1,3-di(2-pyridyl)benzene/1,3-di(2-pyridyl)benzen-2-ide
dqp	2,6-di(quinoline-8-yl)pyridine
DSSC	dye-sensitized solar cell
E	energy
$E_{0\text{-}0}$	optical energy gap
$E_{1/2}$	half-wave redox potential
$E^*_{1/2}$	excited-state half-wave redox potential
E_{cb}	conduction band energy
EDA	energy-decomposition analysis
EDOT	3,4-ethylenedioxythiophene
E_F	quasi Fermi level
EIS	electrochemical impedance spectroscopy
El	electrolyte
Ems	emission
E_p	peak potential
EtOH	ethanol
ε	extinction coefficient
Fc^+/Fc	ferrocenium/ferrocene
FF	fill factor
^1GS	singlet electronic ground state
GuSCN	guanidinium thiocyanate
HOMO	highest occupied molecular orbital
Htctpy	2,2′:6′,2″-terpyridine-4′-carboxylic acid-4,4″-dicarboxylate
Hdcbpy	2,2′-bipyridine-4-carboxylic acid-4′-carboxylate

IC	internal conversion
i_{pa}/i_{pc}	ratio of anodic and cathodic peak current
IPCE	incident photon-to-current efficiency
IR	infra-red
ISC	intersystem crossing
ITO	indium-doped tin oxide
IVR	intramolecular vibrational relaxation
J_{sc}	short-circuit photocurrent density
k	rate constant
K_a	association constant
LC	ligand-centered
LLCT	ligand-to-ligand charge transfer
LMCT	ligand-to-metal charge transfer
LUMO	lowest unoccupied molecular orbital
λ_{max}	wavelength of the maximum
MeCN	acetonitrile
MeOH	methanol
MIC	mesoionic carbene
MC	metal-centered
^{3}MC	triplet metal-centered excited state
MLCT	metal-to-ligand charge transfer
^{3}MLCT	triplet metal-to-ligand charge-transfer excited state
MLLCT	metal−ligand-to-ligand charge transfer
MO	molecular orbital
MS	mass spectrometry
N719	$[Ru(Hdcbpy)_2(NCS)_2](NBu_4)_2$
N749	$[Ru(Htctpy)(NCS)_3](NBu_4)_3$
NBO	natural bond orbital
NEt$_3$	triethylamine
NIR	near infra-red
NHC	*N*-heterocyclic carbene
NHE	normal hydrogen electrode
NMR	nuclear magnetic resonance
NO$_2$-ppy	4-nitro-2-(pyridin-2-yl)benzen-1-ide
Ox	oxidation
Φ_{PL}	photoluminescence quantum yield
PA	proton affinity
PCE	power conversion efficiency

PCM	polarizable continuum model
pK_a	negative decadic logarithm of the acid dissociation constant
Red	reduction
sh	shoulder
NBu_4^+	tetra-*n*-butylammonium cation
TBP	4-*tert*-butylpyridine
tcmtpy	4,4′,4″-tricarboxymethyl-2,2′:6′,2″-terpyridine
TCO	transparent conducting oxide
TD-DFT	time-dependent density functional theory
tpy	2,2′:6′,2″-terpyridine
τ	excited-state lifetime
UV–vis	ultra-violet and visible
v	volume
V_{oc}	open-circuit voltage
ZORA	zero-order regular approximation

Publications A1–A8

The Supplementary Information of each publication can be downloaded at the publisher's site.

Publication A1:

"Beyond click chemistry – Supramolecular interactions of 1,2,3-triazoles"

B. Schulze, U. S. Schubert

Chem. Soc. Rev. **2014**, *43*, 2522−2571.

Featuring work from the Schubert group at the Friedrich Schiller University Jena, Jena, Germany.

Beyond click chemistry – supramolecular interactions of 1,2,3-triazoles

The readily generated 1,2,3-triazole ring is by far more than just the sum of azide and alkyne – it is shown that the 1,2,3-triazole framework offers an intriguing diversity of interactions with both metal ions and anions.

As featured in:
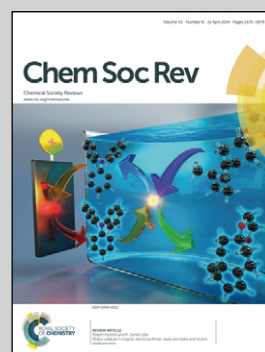
See Benjamin Schulze
and Ulrich S. Schubert,
Chem. Soc. Rev., 2014, **43**, 2522.

ROYAL SOCIETY
OF CHEMISTRY

www.rsc.org/chemsocrev

Chem Soc Rev

REVIEW ARTICLE

Beyond click chemistry – supramolecular interactions of 1,2,3-triazoles

Benjamin Schulze[ab] and Ulrich S. Schubert*[ab]

The research on 1,2,3-triazoles has been lively and ever-growing since its stimulation by the advent of click chemistry. The attractiveness of 1*H*-1,2,3-triazoles and their derivatives originates from their unique combination of facile accessibility *via* click chemistry and truly diverse supramolecular interactions, which enabled myriads of applications in supramolecular and coordination chemistry. The nitrogen-rich triazole features a highly polarized carbon atom allowing the complexation of anions by hydrogen and halogen bonding or, in the case of the triazolium salts, *via* charge-assisted hydrogen and halogen bonds. On the other hand, the triazole offers several N-coordination modes including coordination *via* anionic and cationic nitrogen donors of triazolate and triazolium ions, respectively. After CH-deprotonation of the triazole and the triazolium, powerful carbanionic and mesoionic carbene donors, respectively, are available. The latter coordination mode even features non-innocent ligand behavior. Moreover, these supramolecular interactions can be combined, *e.g.*, in ion-pair recognition, preorganization by intramolecular hydrogen bond donation and acceptance, and in bimetallic complexes. Ultimately, by clicking two building blocks into place, the triazole emerges as a most versatile functional unit allowing very successful applications, *e.g.*, in anion recognition, catalysis, and photochemistry, thus going far beyond the original purpose of click chemistry. It is the intention of this review to provide a detailed analysis of the various supramolecular interactions of triazoles in comparison to established functional units, which may serve as guidelines for further applications.

1. Introduction

1.1. Motivation

"*. . . the totality is not, as it were, a mere heap, but the whole is something besides the parts. . .*" (*Aristotle, Metaphysics*)

The concept of click chemistry was established by Sharpless *et al.* and deals with reaction types that are wide in scope and modular, stereospecific, chemoselective and highly efficient, that offer simple purification methods and benign reaction conditions, and which are therefore particularly suited to link building blocks as the name suggests.[1] While this concept is certainly of general interest to a chemist, one can easily notice that the Cu(ɪ)-catalyzed azide–alkyne cycloaddition (CuAAC)[2,3] has become the prime example of click reactions, being even used synonymously with click chemistry,[4] and that, more importantly, many applications thereof not only aimed to link two units together but also to synthesize the triazole moiety.

In fact, the 1,2,3-triazole is an intriguing heterocycle offering various supramolecular interactions[5] ranging from anion complexation *via* (charge-assisted) hydrogen and halogen bonds to metal coordination by anionic, neutral, or cationic nitrogen donors as well as carbanionic and mesoionic carbene donors (Fig. 1). Importantly, these diverse functions are all provided by a single heterocyclic scaffold and some of them can even be employed simultaneously resulting in virtually unlimited
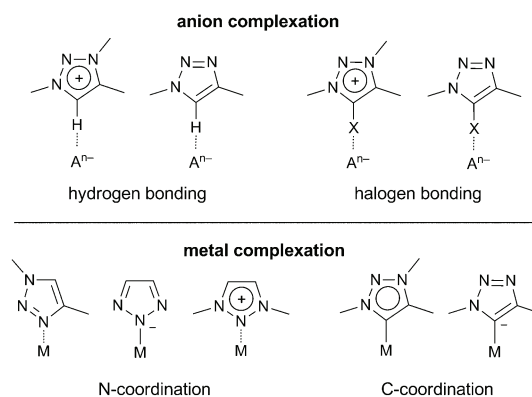
[a] *Laboratory of Organic and Macromolecular Chemistry (IOMC), Friedrich Schiller University Jena, Humboldtstraße 10, 07743 Jena, Germany.*
E-mail: ulrich.schubert@uni-jena.de; Fax: +49(0) 3641 9482 02;
Tel: +49(0) 3641 9482 00
[b] *Jena Center for Soft Matter (JCSM), Friedrich Schiller University Jena, Philosophenweg 7, 07743 Jena, Germany*

Fig. 1 Selected supramolecular interactions of 1,2,3-triazoles and their derivatives.

2522 | *Chem. Soc. Rev.*, 2014, 43, 2522–2571

This journal is © The Royal Society of Chemistry 2014

applications in supramolecular and coordination chemistry. Thus, while it is acknowledged that the popularity of 1,2,3-triazoles is largely driven by their facile and modular synthesis *via* click chemistry, the expanding use of CuAAC in turn is stimulated by the rich potential of the 1,2,3-triazole, which is more than just the sum of its parts, the azide and alkyne.

1.2. Scope

This review is dedicated to the unique variety of supramolecular interactions offered by 1,2,3-triazoles. Our intention is to provide a differentiated analysis of these interactions serving as guidelines for their applications in the complexation of anions and metal cations. We therefore focused on fundamental aspects and general trends. On account of the mutual dependence of the different types of interactions and the potential to employ them simultaneously, we sought to discuss them in context rather than providing a complete literature collection on a particular aspect. Owing to this premise, only selected references were used to compose this review and the reader is referred to individual reviews when particular applications are of interest.[6,7] Furthermore, references that solely use the triazole as a linker (in the original spirit of click chemistry[1]) are generally beyond the scope of this review except for literature specifically reporting the synthesis of triazoles, which is also outlined in this review.

2. Synthesis of 1,2,3-triazoles

In the following chapter, the different synthesis routes towards 1,2,3-triazoles are discussed to allow a full exploitation of the potential of this heterocycle in practice.

2.1. 1,3-Dipolar cycloaddition

Already in 1893, Michael discovered a synthesis of 1,2,3-triazoles (also *v*-triazole for vicinal)[8–10] by reacting phenyl azide with dimethyl acetylenedicarboxylate.[11] This type of reaction was later classified by Huisgen as (3+2) 1,3-dipolar cycloaddition, *i.e.* the concerted addition of a 1,3-dipole to a multiple bond.[12–19] The 1,3-dipole is characterized by the presence of an electrophilic atom, having an electron sextet and a formal positive charge, as well as a nucleophilic atom, having an electron octet and a formal negative charge, with one in the 1-position and the other one in the 3-position (**1c**, Fig. 2).[13] The azide belongs to the propargyl-allenyl type of 1,3-dipoles and is thus almost linear.[19]

Later, Woodward and Hoffmann in turn classified the 1,3-dipolar cycloaddition as an example of pericyclic reactions, which is thermally allowed due to symmetrically and geometrically favorable $[_\pi 4_s + _\pi 2_s]$ interactions.[20] Nonetheless, reaction rates and regioselectivity remained unexplained until Sustmann *et al.*[21–23] and Houk *et al.*[24–26] applied a frontier molecular orbital (FMO) model to the reaction.[27,28] This model is based on the perturbation theory[29–32] and is widely used in textbooks but uses many simplifications.[33] Briefly, it implies that the reaction between the 1,3-dipole and the 1,3-dipolarophile proceeds essentially *via* interaction of the highest occupied
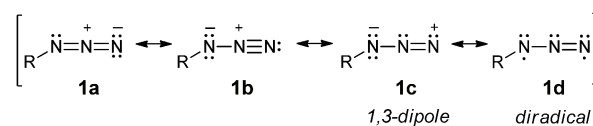
Fig. 2 Selected contributing structures of an organic azide.

Benjamin Schulze was born in Weimar (Germany) in 1983. He studied chemistry at the Friedrich Schiller University Jena (Germany) and the Eindhoven University of Technology (The Netherlands). Since 2009 he is a PhD student in the group of Prof. U. S. Schubert at the Friedrich Schiller University Jena (Germany). His research interests cover supramolecular chemistry and organometallic chemistry, in particular energy-conversion applications of transition-metal complexes.

Benjamin Schulze

Ulrich S. Schubert studied chemistry at the Universities of Frankfurt and Bayreuth (Germany) and the Virginia Commonwealth University, Richmond (USA). His PhD work was performed under the supervision of Prof. C. D. Eisenbach (Bayreuth, Germany) and Prof. G. R. Newkome (Florida, USA). After postdoctoral training with Prof. J.-M. Lehn at the Université Strasbourg (France), he moved to the Munich University of Technology (Germany) to obtain his habilitation in 1999 (with Prof. O. Nuyken). From 1999 to spring 2000, he held a temporary position as a professor at the Center for NanoScience (CeNS) at the LMU Munich (Germany). From June 2000 to March 2007, he was Full-Professor at the Eindhoven University of Technology (Chair for Macromolecular Chemistry and Nanoscience), the Netherlands. Since April 2007, he has been Full-Professor at the Friedrich-Schiller-University Jena (Chair of Organic and Macromolecular Chemistry), Germany.

Ulrich S. Schubert
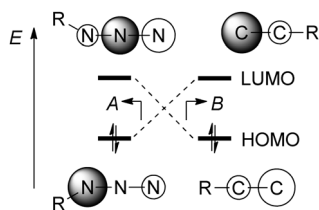
Fig. 3 FMO interactions between azide and alkyne (R = Ph).[23,39]

molecular orbital (HOMO) of one reactant and the lowest unoccupied molecular orbital (LUMO) of the other reactant with the reaction rate depending on the corresponding energy gap. Therefore, a HOMO-raising electron-donating group (EDG) as well as a LUMO-lowering electron-withdrawing group (EWG) will increase the reaction rate.[22,23] Additionally, EDGs and EWGs will polarize particularly the π system, which influences the regioselectivity because the interaction occurs in such a way that the orbitals with larger orbital coefficients overlap (Fig. 3). Accordingly, the cycloaddition of phenyl azide and phenylacetylene yields the 1,4- and 1,5-substituted 1,2,3-triazoles in roughly a 1:1 ratio,[34] while electron-deficient and electron-excessive alkynes favor the formation of the 1,4-regioisomer (dipole-HOMO control, A) and the 1,5-regioisomer (dipole-LUMO control, B), respectively.[9,19,35–38]

Remarkably, cycloaddition reactions between aryl azides and α-keto phosphorous ylides as alkyne equivalents followed by elimination of phosphine oxide afford 1,5-disubstituted 1,2,3-triazoles exclusively (Scheme 1).[40] In line with a concerted cycloaddition, the reaction rate hardly depends on the solvent, and, as the reaction is apparently dipole-LUMO controlled, electron-poor azides give shorter reaction times. Importantly, this reaction allows a reasonably free choice of substituents at the 1,2,3-triazole as they do not control the regioselectivity.

Furthermore, ynamines (NR$_2$–C≡CR) were reported to allow the exclusive formation of 1,5-disubstituted 1,2,3-triazoles.[9] It should be noted that the resulting 1,2,3-triazole, in particular if an EWG is positioned at C5,[41] undergoes reversible ring opening at the N1–N2 bond (*vide infra*, Scheme 7).[42] In the case of (primary) amines as C5-substituents, this ring-chain equilibrium allows 1,2,3-triazole interconversion with the exocyclic and cyclic nitrogen changing place (Dimroth rearrangement).[8,9,43,44]

In general, only a few substituents at the azide and alkyne allow the exclusive formation of one 1,2,3-triazole regioisomer[9] and, moreover, the observed regioselectivity is frequently in opposition to expectations based on the FMO model, in particular for varying azide substituents.[37] Obviously, 1,3-dipolar cycloaddition reactions
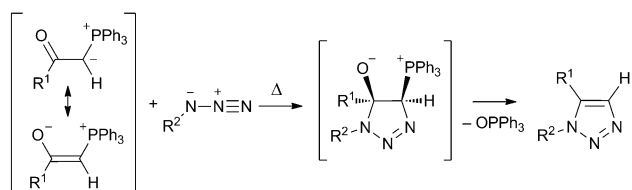
cannot be described adequately when being reduced to frontier-orbital interactions only.[33] With the development of more sophisticated computational methods, a series of alternative approaches has been proposed and the debate is ongoing.[45] For example, application of Pearson's concept of hard and soft acids and bases (HSAB)[46] on the basis of density functional theory (DFT), *i.e.* conceptual DFT,[47,48] leads to the Fukui function as a reactivity descriptor.[45,49] This model is related to the FMO model, but not restricted to frontier *orbitals*, as local softness within a molecule is identified and the regioselectivity is determined by softness matching between reactants.[45] Although the predicted regioselectivities were in better accord with experimental data,[37,38,50] it remained unexplained why the activation barriers for the cycloaddition of alkynes and alkenes with azides are very similar although the reaction exothermicities and FMO energy gaps are very different. While the former models first consider the isolated reactants in the ground state and subsequently include mutual perturbation, *i.e.* only little perturbation can be covered, Houk *et al.* recently proposed a distortion/interaction model based on high-accuracy quantum chemical methods (Fig. 4).[51,52] Accordingly, the activation energy ($\Delta E^{\ddagger}$) is largely determined by the energy that is required to transform the reactants into their transition-state geometries; in other words, the reactivity is controlled by the stability of the dipolarophile and, in particular, of the 1,3-dipole. The distortion, in turn, alters the electronic properties, *e.g.* the HOMO–LUMO gap of the 1,3-dipole is significantly narrowed, which greatly enhances charge-transfer interactions in comparison to the ground state. At the transition state, the destabilizing distortion ($\Delta E_{\mathrm{d}}^{\ddagger}$) is compensated by the stabilizing orbital interactions ($\Delta E_{\mathrm{i}}^{\ddagger}$) enabling the formation of the cycloadduct upon further movement along the reaction coordinate.[51] If the distortion energy is comparable for the formation of both regioisomers, orbital interactions might control the regioselectivity.[51,52] An alternative interpretation has been reported by Braida, Hiberty *et al.*: upon distortion, the singlet diradical character of the azide (1d, Fig. 2) is increased to a critical level, which is still far from a pure diradical, giving rise to a nearly barrierless concerted cycloaddition.[53] Again, in the case of comparable distortion energies, maximized orbital interactions may account for any regiopreference.

Scheme 1 1,3-Dipolar cycloaddition with α-keto phosphorous ylides.[40]
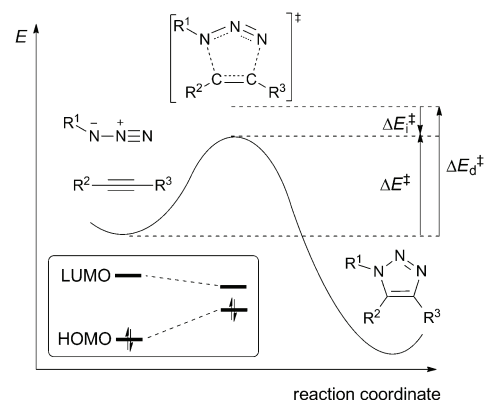
Fig. 4 The distortion/interaction model.[51]

2524 | *Chem. Soc. Rev.*, 2014, **43**, 2522–2571

This journal is © The Royal Society of Chemistry 2014

In view of Houk's distortion/interaction model, it is plausible that the introduction of strain to the alkyne ground state (*e.g.* cyclooctyne, benzyne) causes a rate enhancement in 1,3-dipolar cycloadditions (strain-promoted azide–alkyne cycloaddition, SPAAC).[4,54,55] However, while these alkyne building blocks are spring-loaded, thus allowing a facile linking in the original sense of click chemistry, they induce only low regioselectivities, their synthesis is rather demanding, and their substitution pattern is fixed.

In marked contrast to terminal alkynes, the cycloaddition of organic azides with trimethylsilyl-substituted alkynes shows generally a very high selectivity for the 4-silylated 1,5-regioisomer.[9,36,56–58] Fortunately, the trimethylsilyl group is a common protecting group for the introduction of alkynes *via* Sonogashira cross coupling and it can be cleaved off after the triazole synthesis. Like other thermal cycloadditions, the reaction requires elevated temperatures (85 to 110 °C) and prolonged reaction times but affords high yields and is ideally conducted in water[59] (Scheme 2).[60] Importantly, the very high regioselectivity is only marginally affected when azide and alkyne are substituted with sterically demanding or electron-withdrawing/ donating groups with the lowest 1,5-regioselectivity being about 90% when strong EWGs are present.[36] In addition, the trimethylsilyl group is considered to have a rather little electronic influence, which suggests that the high regiopreference does not primarily originate from electronic effects. Indeed, according to DFT calculations, the trimethylsilyl-group causes a total destabilization of the transition state for the 1,4-attack by about 15 to 25 kJ mol^{-1}, while the transition state for the 1,5-attack is similar in energy to the one of the cycloaddition with the corresponding terminal alkyne. In line with the distortion/interaction model, this is mainly due to an increased distortion energy of the alkyne for the 1,4-attack and electronic effects of the substituents are of minor influence.[36] Consequently, the trimethylsilyl-directed azide–alkyne cycloaddition (SiAAC) represents an elegant method to selectively synthesize 1,5-disubstituted triazoles by making use of the distortion energy and thereby screening out electronic influences, which offers variable substitution patterns.

Alternatively, in the course of the development of powerful organocatalytic methods[61] it became possible to make use of electronic influences of substituents that are only intermediately present, *i.e.* they do not limit the substrate variability. The use of ketones as alkyne surrogates (considering ketones as hydrates of alkynes) allows the regioselective 1,2,3-triazole formation with aryl azides *via* intermediate enamine formation (Scheme 3).[62–68] The enamine-type activation (HOMO raising) and polarization (increased β-nucleophilicity) significantly increases both the reaction rate and the regioselectivity of the cycloaddition. As the reaction is dipole-LUMO-controlled (*vide supra*) in this case,
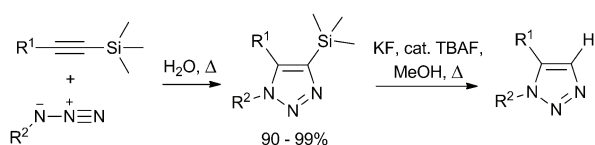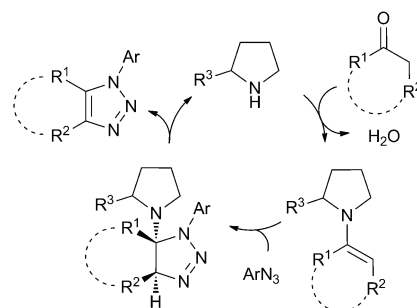
conditions:
A) 20 mol-% L-proline, 2 eq. ketone, CH$_2$Cl$_2$, 80 °C, 1 h, microwave
B) 20 mol-% pyrrolidine, 2 eq. ketone, DMSO, 80 °C, 12–24 h, oilbath

Scheme 3   Organocatalytic azide–alkyne cycloaddition.[62,65]

the amine substituent is exclusively incorporated in the 5-position of the intermediately formed 1,2,3-triazoline (Scheme 3).[23] Spontaneous aromatization *via* elimination of the amine base affords the corresponding 1,5-disubstituted 1,2,3-triazole.[62] Notably, the use of a tertiary amine base does not significantly accelerate the reaction suggesting only a minor contribution of an alternative enolate cycloaddition pathway.[65] Regarding the substrate scope, aromatic azides are required, but the presence of EDGs and EWGs is tolerated in most cases.[62,63,65,68] Furthermore, the ketone is ideally alkyl-substituted (including cyclo-alkanones), while the conversion of phenones requires an EWG on the α-carbon of the ketone (Scheme 3, R^2).[63,65,68] Of course, the more stable enamine will form preferentially, which implies an additional regioselectivity.[62] For the organocatalyst–solvent system, two general procedures (Scheme 3) have been presented, both providing moderate to good yields.[62,65]

Apart from the thermally induced, concerted 1,3-dipolar cycloaddition, a stepwise, base-promoted version has been developed.[69,70] Originally, this method uses halomagnesium acetylides, which are sufficiently nucleophilic to attack the electrophilic terminal nitrogen of an organic azide (Scheme 4). After subsequent spontaneous cyclization by nucleophilic attack of the internal azide nitrogen on the remote alkyne carbon, the corresponding triazolide is formed, which can be hydrolyzed, trapped by appropriate (non-oxidizing) electrophiles, or trans-metalated to other metal centers for further use (*vide infra*).[69] Besides this versatility, the required stoichiometric amounts of Grignard reagents might be a drawback in terms of functional group tolerance. Alternatively, a catalytic version has been presented[70] that relies on the increased acidity of aryl acetylenes in dimethyl sulfoxide (DMSO).[71] This allows the use of catalytic

Scheme 2   Trimethylsilyl-directed azide–alkyne cycloaddition (SiAAC).[36]

Scheme 4   Base-catalyzed azide–alkyne cycloaddition.[69,70]

This journal is © The Royal Society of Chemistry 2014

Chem. Soc. Rev., 2014, **43**, 2522–2571 | **2525**

amounts of hydroxide bases (*e.g.* aqueous tetramethylammonium hydroxide) or, if a base-labile group is present, of less nucleophilic potassium *tert*-butoxide under anhydrous conditions. However, in contrast to the original protocol, the catalytic version requires aromatic substituents on both azide and alkyne. In either case, the reaction affords solely the 1,5-disubstituted triazole in high yields at room temperature, as long as the nucleophilicity of the alkyne is not lowered too strongly by electron acceptors.[70] Notably, the DMSO participates in the protonation of the triazolide, which was proven by the formation of 4-deutero-1,2,3-triazole when conducting the reaction in deuterated DMSO.[70,72] Furthermore, an excess of azide might provoke the formation of 4-triazenyl-1,2,3-triazole *via* nucleophilic attack of a triazolide at an azide.[69,70] In conclusion, if strong bases can be tolerated, the base-catalyzed, stepwise azide–alkyne cycloaddition is an efficient synthesis of 1,5-disubstituted triazoles and offers functionalization in the 4-position *via* the intermediate triazolide.

2.2. Copper-catalyzed azide–alkyne cycloaddition

The prominent Cu(I)-catalyzed azide–alkyne cycloaddition (CuAAC), discovered independently by Meldal *et al.*[3] and Fokin, Sharpless *et al.*,[2] yields 1,2,3-triazoles most efficiently and with a very high regioselectivity for the 1,4-regioisomer.[73–76] A collection of mechanistic key aspects based on computational[77–79] and experimental studies[80–82] is collected in Scheme 5. Firstly, a Cu(I) species undergoes π coordination of an alkyne (**A**), which greatly increases the CH-acidity of the terminal alkyne (pK_a drops from ∼25 to ∼15) and allows the subsequent formation of a σ-coordinated Cu(I) acetylide with the activated alkyne (**B**) in aqueous media even without an additional amine base.[78] DFT calculations suggest that a second Cu(I) remains π-coordinated at the α-carbon of the σ-bound acetylide resembling the known

μ-coordination mode of Cu(I) acetylides.[77,83] In the next step, coordination of an azide at the π-coordinated Cu(I) center occurs (**C**). This is corroborated by the absence of the subsequent cycloaddition when using a preformed σ-bound Cu(I) acetylide without additional Cu(I).[82] In principle, coordination of the organic azide can occur *via* both the substituted or the terminal nitrogen, but, in contrast to the π-accepting, terminal nitrogen, the π-donating, substituted nitrogen is expected to increase the electron density on the metal center,[84] which would facilitate the subsequent oxidative coupling (**D**). The observed selectivity for the 1,4-regioisomer may be explained by the preference for Cu(I) π coordination at the α-carbon of the acetylide,[77,83] which directs a nucleophilic attack of the β-carbon at the terminal, electrophilic nitrogen[16] of the coordinated azide upon oxidative coupling.[85] As a result of the latter, rate-limiting step,[2,73,77–79] a six-membered metalacycle is formed including a μ-alkenylidene.[79] According to computational methods, this intermediate is stabilized by a geminal bimetallic coordination,[77,79,86,87] while a potential monometallic cupra-cycle, which was postulated earlier, would represent an unfavorably strained structure possessing excessive electron density.[78] Recently, the transient formation of the bimetallic cupra-cycle was corroborated by a Cu[63]/Cu[65] crossover experiment, which implies that the six-membered ring can isomerize.[82] It should be noted that the formal oxidation states of the two Cu centers are not given as it remains unclear whether Cu(III)[88] is intermediately formed or if both metal centers cooperate in the oxidation step. Furthermore, improved activity has been observed when using a bimetallic, mixed-valent Cu(II)/Cu(I) catalytic system.[89] Ultimately, ring contraction and Cu(I) extrusion *via* reductive elimination (**E**) affords the Cu(I)-bound triazolide in a highly exothermic process.[79,81] In aqueous media, the Cu(I) triazolide then readily undergoes protonolysis (**F**)

Scheme 5 Proposed mechanism of the CuAAC (top) and CuAXAC (bottom).[73,75,82,92] ([Cu] denotes a copper fragment that varies in the number of ligands and in the formal oxidation state.)

2526 | *Chem. Soc. Rev.*, 2014, **43**, 2522–2571

This journal is © The Royal Society of Chemistry 2014

liberating the free triazole and allowing the Cu(I) to re-enter the catalytic cycle.

In line with the aforementioned involvement of a second Cu(I) center, a second-order rate dependence on the Cu(I) concentration has been observed under catalytic conditions.[80] By the use of bridging ligands, e.g., tris((1-benzyl-1H-1,2,3-triazol-4-yl)methyl)amine (TBTA),[90] the formation of hemilabile, bimetallic Cu(I) complexes[91] enables cooperativity between the Cu(I) centers resulting in rate acceleration with a first-order (but also more complex) dependence on the concentration of the bimetallic complex.[73,74,93] Nonetheless, also monometallic Cu(I) complexes with high catalytic activity have been reported[73,74,94] and already in the absence of a Cu(I)-stabilizing ligand, for instance when using CuSO$_4$/sodium ascorbate as a Cu(I) source in aqueous media, the CuAAC is highly efficient in most cases.[2,73,75] It should be noted, however, that Cu(I) acetylides tend to aggregate, which not only provides a resting state for the catalyst but can also stall the catalytic cycle.[73,95] Thus, the Cu(I) acetylides should be prepared in the presence of the organic azide and the addition of catalytic amounts of a polydentate, hemilabile ligand may be advisable.[73,90,94] The latter also helps to avoid the formation of an inactive Cu(I) complex, if the desired product is a strongly binding ligand.[90] Furthermore, if Cu(II) is generated via oxidation or disproportionation of Cu(I), for instance bis(triazoles) can be formed (Scheme 5), which is promoted by carbonates as well as hydroxides[96,97] and prevented by addition of a sacrificial reducing agent (sodium ascorbate),[2,73] Cu(I)-stabilizing ligands[90] (including amine bases[75,96]), and the exclusion of oxygen.

The formation of a Cu(I) triazolide (E, Scheme 5) in the course of the CuAAC gives rise to valuable modifications of the catalytic cycle: in aprotic media, the triazolide protonolysis might become rate-limiting[79] allowing subsequent cross-coupling reactions,[98,99] while, in the absence of protons and when using stoichiometric amounts of Cu(I), the Cu(I) triazolide is obtained as product[81] allowing the subsequent transmetalation of the triazolide to other metal centers (vide infra).[100] Furthermore, the Cu(I) triazolide may be trapped with electrophiles, which can be added directly (e.g. N-chlorosuccinimide[101]) or generated in situ via oxidation of a halide (e.g. by using NaI–Cu(ClO$_4$)$_2$,[102] CuI–N-bromosuccinimide,[103] CuBr–N-chlorosuccinimide[104]) to yield 5-halogenated triazoles.[74,105]

Alternatively, metallo- and haloalkynes can be converted directly with organic azides via Cu(I)-catalyzed cycloaddition to afford the corresponding 1,4-disubstituted 5-metallo- or 5-halo-1,2,3-triazoles, thus being named CuAXAC here, with X = AlL$_2$,[106] AuL,[107,108] BiL$_3$,[109] Br,[110] I.[92,102,111,112] In fact, if a Cu(I)-supporting ligand such as TBTA is present, iodoalkynes react even faster than terminal alkynes.[92] The conversion of bromoalkynes is achieved at elevated temperatures using 20 mol% of CuBr/Cu(OAc)$_2$ (1:1) in tetrahydrofuran (THF).[110] For the latter, as reported for the original CuAAC, cooperativity between Cu(I) and Cu(II) within an acetate-bridged, bimetallic complex is most likely responsible for the enhanced catalytic performance.[89,113,114] The tentative CuAXAC mechanism (Scheme 5, bottom) is closely related to the CuAAC mechanism,

i.e. stable, σ-bound metal acetylides as well as haloalkynes can undergo an analogous stepwise cycloaddition if the alkyne is reasonably electron-rich and sterically open to allow π coordination of a Cu(I) center.[82] Similarly, it has been reported that certain Cu(I) complexes enable the CuAAC with a symmetrical internal alkyne (3-hexyne).[115,116]

2.3. Ruthenium-catalyzed azide–alkyne cycloaddition

Building on the known ability of the [Ru(Cp)Cl] (Cp = cyclopentadienyl) fragment to catalyze alkyne cyclotrimerization,[117] its catalytic activity in the azide–alkyne cycloaddition was anticipated by Jia, Fokin et al.[118] The strongly electron donating, anionic Cp ligand is required to facilitate the intermediate ruthenium oxidation.[119] Although [Ru(Cp)Cl] only showed modest reactivity and regioselectivity, the use of the pentamethylcyclopentadienyl (Cp*) derivative greatly improved both the activity and, remarkably, the selectivity for the formation of 1,5-disubstituted 1,2,3-triazoles.[118–120] Interestingly, while only a few examples for the conversion of internal alkynes have been reported for the CuAAC,[115,116] both terminal and internal alkynes are in principle equally suited substrates for the RuAAC.[119,121–124] Based on DFT calculations, a potential RuAAC mechanism was formulated by Lin, Jia, Fokin et al.[119] and further detailed by Nolan et al.[125] (Scheme 6, exemplarily shown for a terminal alkyne). Initially, a coordinatively unsaturated 16-electron species can be used directly or has to be generated by ligand dissociation. Subsequently, ligand substitution via an addition–elimination sequence (G, H) provides the catalytically active species featuring a π-coordinated alkyne.[125] Then, coordination of the azide via the substituted nitrogen (I) is energetically favored in this case[125] and the resulting π donation may facilitate the subsequent oxidative coupling (J). Accordingly, nucleophilic attack of the alkyne at the terminal nitrogen of the azide proceeds with a small activation barrier and affords a six-membered ruthenacycle.[125] Based on the computations,[119,125] this species involves a metala-cyclopropene,[126] which is in equilibrium with a vinyl complex. The latter is slightly more stable due to reduced strain but not prone to reductive elimination (K) and, therefore, represents a resting state.[119] In the subsequent, rate-limiting step (K),[119,125] the six-membered ruthenacycle contracts upon reductive elimination with the extruded Ru(II) remaining π-coordinated to the triazole. After isomerization to the N-bound complex (L), the triazole is liberated by substitution with an alkyne (M, N) and the catalytic cycle can start anew.[125]

The regioselectivity of the reaction is determined in the C–N bond-forming step (J) by the spatial and electronic structure of the alkyne (Scheme 6, in the box). In line with the much improved regioselectivity when using Cp* instead of Cp as an auxiliary ligand, the more bulky group (or the substituent of a terminal alkyne) preferentially points away from the Cp* plane, thus being incorporated in the 5-position. While complete 1,5-regioselectivity was observed for terminal alkynes, for internal alkynes only a moderate regioselectivity was achieved based on differences in bulkiness of the substituents.[119,122,125] In contrast, the electronic structure of the alkyne has a more pronounced effect on the regioselectivity in that the more nucleophilic carbon

This journal is © The Royal Society of Chemistry 2014

Chem. Soc. Rev., 2014, 43, 2522–2571 | 2527
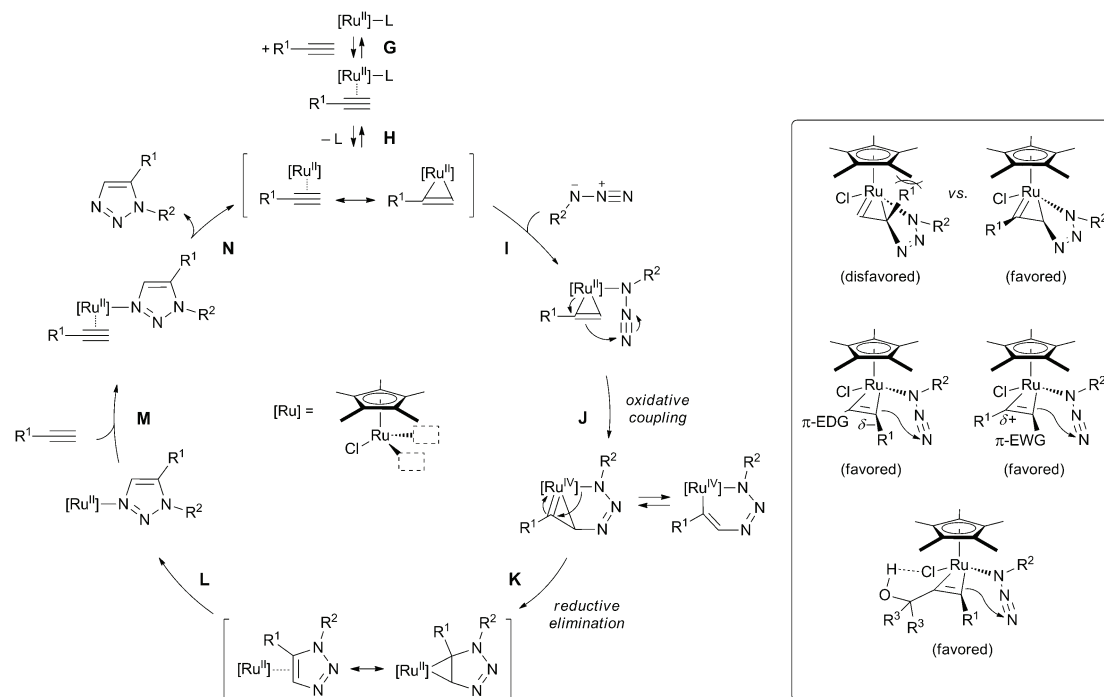
Scheme 6 Proposed mechanism of the RuAAC and explanation of the observed 1,5-regioselectivity. (Note that the ruthenium oxidation states in the mesomeric forms of π-coordinated ligands are based on a neutral and not on an ionic formalism to avoid additional changes in the formal oxidation state.)[119,125]

of the alkyne attacks the electrophilic terminal nitrogen of the azide.[121–124] Accordingly, a π-electron-donating group (π-EDG) generally increases the reactivity and will direct a β-attack to give the final product with the donor in the 5-position.[119,121] In contrast, a π-electron-withdrawing group (π-EWG) reduces the β-nucleophilicity and, thus, the nucleophilic attack will occur *via* the α-carbon to leave the acceptor in the 4-position.[122] However, it should be noted that the polarization of the π system of the alkyne also directly influences the π bonding with the Ru(II) fragment giving rise to an additional orientational preference.[127] Furthermore, for certain (terminal and internal) propargylic alcohols a very high reactivity and selectivity was observed, which was attributed to intramolecular hydrogen bonding with the chloro-ligand resulting in 5-positioning of the hydrogen-bond donor (*cf.* Scheme 6).[119,122,124,125]

It is important to note that the RuAAC depends on a subtle interplay of competing steps and that the suitable conditions are narrower than for the CuAAC, which is almost "unstoppable".[2] Already the order of educt addition is crucial for the success of the RuAAC. When [RuCp*(PR$_3$)Cl] is subjected solely to azides, a Ru(II) phosphazide complex can form either with the free or coordinated phosphine (Fig. 5).[125] While this labile complex was proven to be still catalytically active, it eventually affords a stable and catalytically inactive Ru(IV) tetrazenide or Ru(II) tetraazadiene complex (Fig. 5) *via* an intermediately formed Ru(IV) imido complex.[119,125] The latter is formed by phosphazide cleavage and can also form directly by nitrogen loss from an azide ligand, in particular at elevated temperatures and when using aromatic azides, which are prone to nitrogen loss. On the other hand,
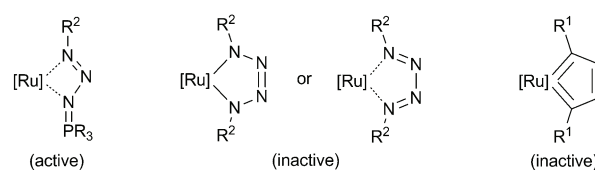
Fig. 5 Possible side products formed under RuAAC conditions and their activity in RuAAC.[119,125]

if solely the alkyne is present, coordination of two alkynes and subsequent oxidative coupling results in the formation of a ruthenacyclopentatriene (Fig. 5),[117] which was proven to be catalytically inactive in terms of RuAAC.[119,125] Importantly, both deactivation processes are suppressed if alkyne *and* azide are present as both substrates show a synergistic effect: initial phosphine replacement by an alkyne favors subsequent azide coordination thus allowing the RuAAC to proceed.[125] Consequently, it is recommended to add a mixture of azide and alkyne to the catalyst solution and to avoid a high excess of either azide or alkyne.[119]

Furthermore, also the selection of the precatalyst significantly influences the success of the RuAAC. While various alkynes are efficiently converted with alkyl azides in the presence of 1 to 2 mol% [Ru(Cp*)(PPh$_3$)$_2$Cl] in aprotic solvents at elevated temperatures (80 °C), aryl azides are hardly tolerated.[118] The latter may be attributed to a higher propensity of aryl azides for phosphazide cleavage (*vide supra*). Alternatively, aryl azides are converted at elevated temperatures (90 to 110 °C) when using phosphine-free [RuCp*Cl]$_4$ as a precatalyst and

2528 | *Chem. Soc. Rev.*, 2014, **43**, 2522–2571

This journal is © The Royal Society of Chemistry 2014

N,N-dimethylformamide (DMF) as solvent.[120] Under these conditions, an increased catalyst loading (10 mol%) is required, presumably due to catalyst poisoning caused by incipient azide decomposition (*vide supra*). As another alternative, [RuCp*-(COD)Cl][119] (COD = 1,5-cyclooctadiene), which features a readily displaced ligand, and coordinatively unsaturated [RuCp*(P^{i}Pr$_3$)Cl][125] show a significantly higher reactivity. Consequently, even aryl azides are efficiently converted at ambient temperature with low catalyst loadings in toluene[119] or dichloromethane.[125] Still, the RuAAC's azide scope is limited to azides devoid of high steric demand (such as tertiary alkyl azides and *ortho*-substituted aryl azides) and strongly π-accepting substituents.[119,120] Similarly, highly sterically demanding and electron-deficient alkynes are less reactive in RuAAC (*vide supra*).[121,122]

3. Fundamental properties of 1,2,3-triazoles

This paragraph is dedicated to fundamental properties of 1,2,3-triazoles, in particular in comparison to other aromatics such as benzene, pyridine, and other azoles, to allow a deeper understanding of the various supramolecular interactions offered by 1,2,3-triazoles.

3.1. Building principles

When comparing benzene and pyridine, the isoelectronic replacement of a methine group by nitrogen (aza substitution) results in a deficit of π electrons due to the higher electronegativity of a ring atom that donates a single π electron. This pyridine-type nitrogen (–N=), featuring an additional σ lone pair, is weakly σ-donating and strongly π-accepting with respect to the other ring atoms.[128–130] Notably, protonation of the σ lone pair does not compromise the aromatic character. In contrast, the five-membered pyrrole (–CH=CH– replaced by –NH–) offers an amine-like nitrogen whose lone pair is part of the aromatic π sextet. This pyrrole-type nitrogen is σ-accepting and π-donating, causing an aromatic system of π-electron excess.[129,130] Furthermore, pyrrole does not behave like an amine base but is NH-acidic instead. 1,2,3-Triazoles (Fig. 6) feature both pyridine- and pyrrole-type nitrogen atoms and are, thus, acidic and basic. With respect to the carbon atoms, the 1*H*-1,2,3-triazole is weakly π-excessive (note that the 2*H*-1,2,3-triazole is π-deficient).[131] These features will be discussed in more detail in the following paragraphs.

3.2. Aromaticity

To assess the aromatic character of 1,2,3-triazoles, it has to be noted first that two orthogonal types of aromaticity and their corresponding indices are distinguished, namely classical (energetic
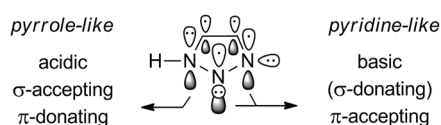

pyrrole-like   *pyridine-like*

acidic   basic
σ-accepting   (σ-donating)
π-donating   π-accepting

Fig. 6 Features of the electronic structure of 1*H*-1,2,3-triazole.[131]

and structural) and magnetic aromaticity.[132–135] Classically, aromaticity refers to bond-length equalization and is described either by the aromatic stabilization energy (ASE) or by the harmonic oscillator model of aromaticity (HOMA). Accordingly, the energy difference between delocalized and isolated bonds (ASE) or the deviation of actual bond lengths from ideal values for full delocalization (HOMA, the optimal value is 1) is used as a measure of aromaticity. Alternatively, the delocalization of π electrons is assessed by calculation of the nucleus-independent chemical shift (NICS) at the center of a ring (NICS(0)) or, to exclude σ effects, 1 Å above the center (NICS(1)).[136–138] Referring to the experimental nuclear magnetic resonance, the NICS is given in ppm and negative values indicate magnetic shielding by an aromatic ring current, *i.e.* magnetic aromaticity.

In comparison to selected aromatics (Table 1), all three indices display a high degree of aromaticity for the 1,2,3-triazole. Notably, the ASE corresponds to a few percent of the molecule's energy only and heavily depends on the used computational method thus being hardly comparable for different series.[135,139] HOMA and NICS represent more robust indices and display a different trend when comparing the five- and six-membered ring aromatics. According to the HOMA values, benzene features ideal structural aromaticity and the slightly lower value of pyridine is still higher than the ones of the azoles. In contrast, the azole's NICS(1) values are higher than for benzene and pyridine. On the other hand, HOMA and NICS(1) (and essentially the ASE) agree in the consequences of successive aza substitution: while pyridine has a marginally lower aromaticity than benzene, the aromatic character generally increases for the azoles though with a pronounced dependency on the positioning of the heteroatoms.[133]

To understand the highly aromatic nature of 1,2,3-triazole, it is helpful to consider the contributing structures of pyrrole (Fig. 7). Due to the π excess of pyrrole, a more negative NICS than for benzene is reasonable, while the predominance of a neutral contributing structure (**2a**), causing more localized bonds and thus a lowered HOMA value, is plausible in view of the electronegativity of the ring atoms. Introduction of a heteroatom in the α-position increases the relevance of structures **2b/2c**, which feature a complementary bond order, and, thereby,

Table 1 Selected properties of different aromatics

Compound	HOMA^a [eV]	LUMO^a [eV]	NICS(1) [ppm]	ASE^e [kJ mol^{-1}]	HOMA	μ [D]
Benzene	−9.65^b	0.56^b	−10.21^d	^{f}	1^b	0
Pyridine	−9.93^b	0.14^b	−10.12^d	^{f}	0.998^g	2.22^b
Pyrrole	−8.66^c	1.38^c	−10.60^e	86.1	0.876^e	1.94^h
Pyrazole	−9.71^c	0.96^c	−11.93^e	99.2	0.926^e	2.33^h
Imidazole	−9.16^c	0.98^c	−10.83^e	78.6	0.908^e	3.84^h
1*H*-1,2,3-Triazole	−10.18^c	0.42^c	−13.51^e	102.0	0.931^e	4.55^h
2*H*-1,2,3-Triazole	−10.33^c	0.55^c	−13.61^e	111.6	0.960^e	0.12^h

^{a} Energies obtained by semi-empirical AM1 calculations.[131,140] ^{b} From ref. 140. ^{c} From ref. 131. ^{d} From ref. 141. ^{e} From ref. 132. ^{f} The ASE strongly depends on the computational level and calculation method[135,142] and, hence, values other than from the same series were omitted. ^{g} From ref. 134. ^{h} Calculated values from ref. 143.

This journal is © The Royal Society of Chemistry 2014

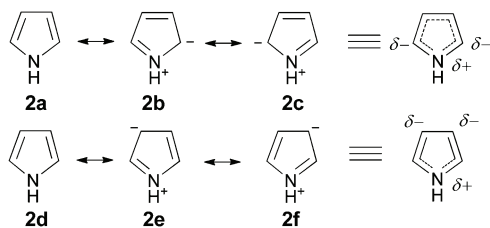*Chem. Soc. Rev.*, 2014, **43**, 2522–2571 | **2529**

Fig. 7 Contributing structures of pyrrole and the corresponding bond-length equalization.[133]

enhances delocalization (cf. HOMA and NICS of pyrazole and 2H-1,2,3-triazole).[133] In contrast, aza substitution in the β-position supports 2e/2f, which only partially enhances delocalization. Additionally, aromaticity increases with decreasing electronegativity difference between adjacent atoms.[142] Thus, a cumulative (pyrazole, 1,2,3-triazole) instead of an alternating (imidazole) arrangement of heteroatoms is beneficial. Furthermore, the aromaticity is essentially preserved upon protonation at pyridine-type- and deprotonation at pyrrole-type nitrogen atoms.[144]

3.3. Electronic structure

The three nitrogen atoms of the 1H-1,2,3-triazole cause a strong polarization of the aromatic π system and the σ framework.[129,130] When considering the relevant contributing structures (Fig. 8) as well as inductive effects, the carbon atoms and the nitrogen atom in the 1-position are expected to be positively charged, while the 2- and 3-nitrogen atoms should show negative partial charges. This is corroborated by computational data,[129] which, in turn, are consistent with experimental results (e.g. ^{1}H and ^{13}C NMR shifts).[129,131,145] Accordingly, a very large dipole moment was measured (4.38 D)[146] and calculated (4.55 D,[143] Fig. 8 and Table 1). Furthermore, two forms of annular tautomerism are observed: firstly, a degenerate tautomerism, with both tautomers formally being 1H-1,2,3-triazoles, and, secondly, interconversion to the 2H-1,2,3-triazole (Fig. 8). According to computational results, all three tautomers, the 1H-, 2H-, and 3H-form, readily equilibrate with low activation energies via an intermolecular double proton transfer,[147] while an intramolecular proton shift is unlikely.[148–150] In line with a higher calculated stability of the 2H-1,2,3-triazole,[149,151,152] which can be rationalized by the alternating order of pyridine- and pyrrole-type nitrogen atoms (cf. Fig. 8) and the absence of electrostatic repulsion between
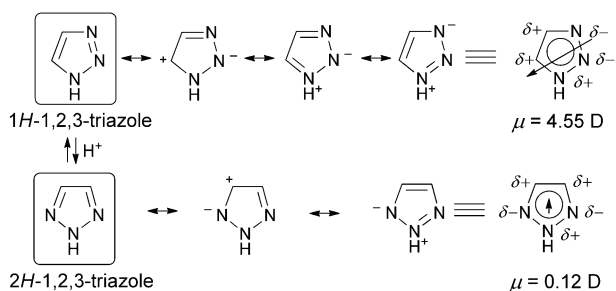
adjacent σ lone pairs, a large excess of this tautomer is observed in the gas phase.[146,151,153] Due to the more balanced charge distribution, the dipole moment of the 2H-1,2,3-triazole is strongly reduced (0.12 D).[143] In solution, the 1H-form is stabilized by dipole interactions and, thus, both tautomers are observed in varying ratios depending on the concentration, solvent polarity, and temperature.[151,154] When the triazole is N1-substituted, conversion to the N2-substituted triazole is blocked, except for hemiaminales, which are in equilibrium with the corresponding aldehyde and free triazole.[155]

Considering the frontier molecular orbitals (Table 1),[131,140] which are π and π* orbitals in this case,[144] the π deficient pyridine features an energetically lower π system, while the π excess of pyrrole causes a destabilized π system relative to benzene. For the azole series, with increasing number of nitrogen atoms, both HOMO and LUMO are gradually stabilized. Furthermore, in comparison to imidazole, the contiguous nitrogen atoms of pyrazole cause a strong HOMO stabilization. When comparing the 1H- and 2H-tautomer of triazole, the alternation of π-accepting, pyridine-type and π-donating, pyrrole-type nitrogen atoms causes a HOMO stabilization as well as a LUMO destabilization (Table 1).

3.4. π Conjugation

In general, π conjugation through 1H-1,2,3-triazoles is not observed.[156–158] This can be rationalized by the presence of a p lone pair (pyrrole-type nitrogen in the 1-position, Fig. 6) within the conjugation pathway[159–162] causing a formal cross conjugation between the triazole's substituents.[163] The lone pair cannot mediate π-electron delocalization leading to consecutive "single bonds" at the substituted nitrogen atom.[159–161] Similarly, the nitrogen lone pair in polyanilines acts as an insulator in the electronic ground state. This effect may be visualized using potential contributing structures (Fig. 9). In view of the experimental bond lengths within the 1H-1,2,3-triazole ring, the neutral representation 3a should predominate, but significant contributions from structures 3c and 3d are expected in line with the large dipole moment of the molecule (vide supra). Accordingly, all bond lengths within the triazole ring are significantly shorter than C–C, C–N, or N–N single bonds,[164] and π bond orders between 0.5 and 0.7 have been calculated with the N2–N3 and the C4–C5 bond showing the highest values.[144]

Upon quarternization, protonation or metal coordination at N3, the polarization in terms of structure 3d should be enhanced.[158] Accordingly, partial bond-length equalization between the three nitrogen atoms by virtue of an aza-allylic resonance (3a and 3d) is observed for the triazolium cation (Fig. 9). Likewise, partial bond-length equalization is observed upon metal coordination via N3, which may additionally be attributed to back-donation into triazole π* orbitals (vide infra).[165,168,169] On the other hand, the electronic properties of the triazole's nitrogen atoms in 2- and 3-positions can be manipulated by (de)stabilization of structures 3b to 3e via suitable substituents (see the following chapters).[170] In the case of the N-substituent, π acceptors are expected to have a stronger influence on the electronic structure of the triazole
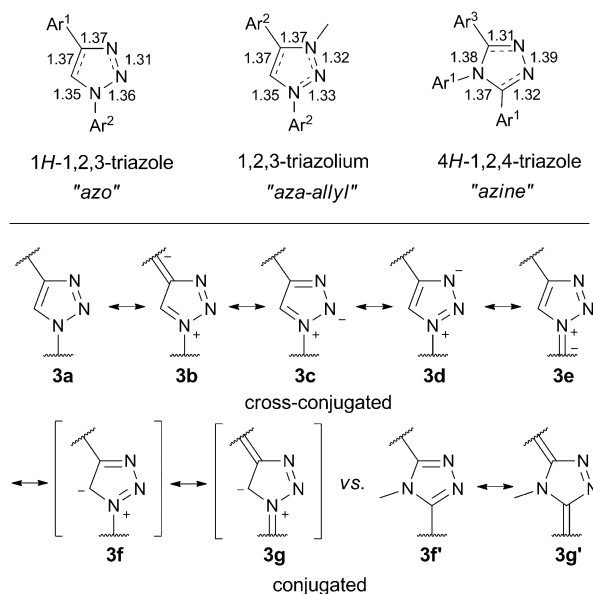

Fig. 8 Selected contributing structures, tautomerism, partial charges, and dipole moments of the 1H and 2H 1,2,3-triazole.[143]

1H-1,2,3-triazole
"azo"

1,2,3-triazolium
"aza-allyl"

4H-1,2,4-triazole
"azine"

3a   3b   3c   3d   3e

cross-conjugated

3f   3g   vs.   3f'   3g'

conjugated

Fig. 9   Selected bond lengths (in Å) of 1H-1,2,3-triazole,[165] 1,2,3-triazolium,[166] and 4H-1,2,4-triazole[128] (Ar[1] = 2-pyridyl, Ar[2] = substituted phenyl rings, Ar[3] = 3-pyridyl) including structural features[165,167] (top) and selected contributing structures (bottom).

Scheme 7   Valence tautomerism of 1H-1,2,3-triazoles.[131]

than π donors as the nitrogen p lone pair cannot be delocalized away from N1.[160]

Importantly, the structures 3a–3e do not show a delocalization between the 1,4-substituents, but each substituent is at least in partial conjugation with the triazole (3b and 3e). Provided that the triazole is reasonably coplanar with its substituents, it can contribute to one or both frontier orbitals.[171] By tendency, for 1,4-diaryl-1,2,3-triazoles, the HOMO is expected to reside on the former alkyne part, while the LUMO is predicted to be located on the former azide part,[158,171–173] in other words, extended π-electron delocalization beyond the 1-position of the triazole may be enabled in the excited state.[174–176] However, this situation may be reversed by electron-donating and -withdrawing substituents.[162,177] Moreover, charge-transfer chromophores with low energy gaps can be obtained when applying a push–pull substitution pattern to the triazole[162,173,177,178] or, alternatively, by metal coordination or protonation.[158,179]

Conversely, when considering the 1,2,3-triazole as a substituent, it acts as a donor if it is attached via C4,[168,180–182] while connection via N1 reveals an (inductive) electron-accepting character (relative to the organic azide precursor, which is already an acceptor[16,183]).[184]

Despite the formal cross-conjugation, a weak electronic communication through 1,4-disubstituted 1,2,3-triazoles is apparently operative.[185] Notably, the electronic structure of 1,2,3-triazoles may not be adequately described by classical valence bond structures using localized two-center, two-electron bonds.[186,187] Tentatively, this may be rationalized with the help of dipolar/ylidic contributing structures 3f and 3g (Fig. 9), which would enable a chinoid conjugation pathway. Given the charges and the electronegativities of the corresponding atoms, this structure should be of minor relevance but may become more important if supported by appropriate substituents at the triazole.[162] Accordingly, the
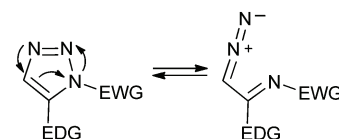
4H-1,2,4-triazole enables π conjugation, although delocalization is still limited most likely due to the electronegative nitrogen atoms, which cause a predominance of structure 3f' in line with the observed alternating bond lengths (Fig. 9).[128] Similar considerations may be applied to 1,5-disubstituted 1,2,3-triazoles; however, these sterically crowded systems often lack coplanarity.[162]

Notably, while the 1H-1,2,3-triazole ring can be considered as highly stable,[188,189] strongly electron-withdrawing N-substituents (nitro, cyano, sulfonyl) provoke a scission of the N1–N2 bond giving rise to the establishment of a ring-chain equilibrium, in particular if an electron-donating group is installed at C5 or if the triazole is metalated in the 5-position (Scheme 7).[41,42,131] Thereby, C5-metalated N-sulfonyl-1,2,3-triazoles tend to undergo nitrogen loss.[188–191] Even without strongly electron-withdrawing N-substituents, Dimroth rearrangement may be observed in the case of 5-amino-substituted 1,2,3-triazoles.[9,43]

3.5.   Acid–base behavior

Acid and base strength are directly correlated with the electronic structure. Firstly, due to the strong polarization within the 1H-1,2,3-triazole, each position is either acidic or basic to an extent that is practically relevant. Again, comparison with benzene, pyridine, and other azoles (Table 2) is of interest for later discussions as both acidity and basicity allow a first assessment of the potential of triazoles to undergo hydrogen bonding and metal coordination, respectively.

For a series of selected azoles (Table 2), successive aza substitution causes increasing polarization of C–H and N–H bonds, i.e. the CH- and NH-acidity increases. The CH-acidity is the highest in the position adjacent to the σ-accepting, pyrrole-type nitrogen. Accordingly, the pK_a values for CH-deprotonation of 1-methyl-1H-1,2,3-triazole are 35.0 for C4 and 27.8 for C5, which are significantly lower than the pK_a of 44.7 of benzene.[192,193] Consequently, 1-phenyl-1H-1,2,3-triazole is readily deprotonated in the 5-position by, e.g., n-butyl lithium[44] and able to undergo direct cross coupling by C–H activation.[105] Furthermore, the NH-acidity in solution (pK_a) mainly depends on the total number of nitrogen ring atoms.[44] Note that the NH-acidity in the gas phase is unexpectedly low for the pyrazole anion (cf. the high proton affinity, PA, of the corresponding azolate, Table 2), which can be explained by enhanced intramolecular electron repulsion between adjacent nitrogen lone pairs of the anionic form, which is reduced in solution due to stabilizing solvent interactions.[44,194]

On the other hand, for the azole series, the base strength (Table 2, cf. the pK_a of the corresponding azolium) of a pyridine-type nitrogen depends on the proximity, number, and type of additional nitrogen ring atoms and is particularly low if a pyrrole-type nitrogen is placed in an adjacent position (cf. pyrazole vs. imidazole). The increasing stabilization of the

Table 2 Acid–base properties of selected aromatics

Compound	pK_a (azole, CH) in DMSO	pK_a (azole, NH) in water	PA (azolate) [kJ mol^{-1}]	pK_a (azolium) in water	PA (azole) [kJ mol^{-1}]
Benzene	44.7[a]	—	—	—	—
Pyridine	40.3 (C4),[a] 43.6 (C2)[a]	—	—	5.2[d]	924,[h] 987[h,i]
Pyrrole	38.8 (C2)[b,c]	16.5[d]	1501[f]	—	—
Pyrazole	33.8 (C5)[b,c]	14.2[d]	1481[f]	2.5[d]	891,[h] 950[h,i]
Imidazole	34.1 (C2)[b,c]	14.4[d]	1468[f]	7.0[d]	936,[h] 1005[h,i]
1H-1,2,3-Trz.	35.0 (C4),[b,c] 27.8 (C5)[b,c]	(9.3)[d,e]	(1439)[g]	1.3[c,d]	915 (N3),[c,j] 887 (N3),[h,i] 839 (N2)[h,i]
2H-1,2,3-Trz.	—	(9.3)[d,e]	1452[f]	<1[c,d]	823[h,i]

[a] Calculated value, taken from ref. 193. [b] Calculated value, taken from ref. 192. [c] Value for the N-methyl derivative. [d] Taken from ref. 44. [e] Mixture of tautomers most likely with a predominance of the 1H-form.[151,154] [f] Taken from ref. 195. [g] Not observable as the 2H-1,2,3-triazole is predominantly formed in the gas phase, but the 1H-1,2,3-triazole was calculated to be 62 kJ mol^{-1} more stable than pyrrole, see ref. 151. [h] Taken from ref. 151. [i] Calculated value. [j] Taken from ref. 152.

σ lone pair upon progressive aza substitution is reflected by an increasing σ ionization potential and, thus, a decreasing proton affinity of the azole (Table 2).[131,144,153,196–198] Accordingly, the base strength is the highest for imidazole, modest for pyrazole and lowest for 1,2,3-triazole, while the electron-deficient pyridine lies in between pyrazole and imidazole (Table 2). Notably, the 1,2,3-triazole offers two basic pyridine-type nitrogen atoms, either in the 2,3-position for the 1H-tautomer or in the 1,3-position for the 2H-tautomer (Fig. 8). For the 1H-1,2,3-triazole, the base strength of N2 and N3 is increased by virtue of the π-donating, pyrrole-type nitrogen in the 1-position (cf. Fig. 8). Furthermore, N2 features two adjacent nitrogen atoms thus showing a lower base strength, which is also reflected by the natural population analysis (NBO) charges of −0.08 for N2 and −0.28 for N3.[199] Regarding the 1,3H-triazolium resulting from N3-protonation, a beneficial alternating arrangement of pyrrole-type and pyridine-type nitrogen atoms (cf. the 2H-1,2,3-triazole, vide supra) is established and potential electrostatic repulsion between adjacent protons ("electrostatic proximity"[194]) is avoided (Fig. 10), which is in contrast to N2-protonation. Additionally, N3-protonation allows an enhanced ion–dipole interaction (cf. Fig. 8).[149] Consequently, while for 1,2,3-triazoles, a higher stability was calculated for the 2H-tautomer (ΔG = 18 kJ mol^{-1}, vide supra),[148,149,151,152] for the corresponding triazolium, the 1,3H-tautomer is much more stable than the 1,2H-tautomer (ΔG = 51 kJ mol^{-1}).[149,152] The more stable 1,3H-1,2,3-triazolium can, however, be formed only via formation of the less stable 1H-1,2,3-triazole or 1,2H-1,2,3-triazolium salt, which precludes the experimental determination of the N3 base strength of 1H-1,2,3-triazole (Scheme 5, left,

and Table 2).[149,151,153] Interestingly, as a result of the interplay of the tautomers of triazole and triazolium, a proton conductivity superior than that of the imidazole–imidazolium pair is observed.[200,201] By using 1-methyl-1H-1,2,3-triazole, tautomerization is prevented allowing the direct formation of the most stable N3-protonated triazolium cation. The gas-phase basicity (corresponding to ΔG) of 882 kJ mol^{-1} determined by mass spectrometry is in good agreement with the DFT-calculated value of 901 kJ mol^{-1} (Fig. 10, right).[152] Furthermore, the calculated gas-phase basicities given in Fig. 10 demonstrate the much weaker base strength of N2 of the 1H-1,2,3-triazole as well as of the degenerated nitrogen donors of the 2H-1,2,3-triazole. The corresponding proton affinities (corresponding to ΔH) are given in Table 2.[152] It should be noted that N-methylation slightly increases the base strength (cf. Table 2).[195,202] Consequently, in line with the pK_a values for proton loss of azolium ions, the following order of increasing proton affinity results: 2H-1,2,3-triazole < 1H-1,2,3-triazole (N3) < pyrazole < pyridine < imidazole.

4. 1,2,3-Triazoles and 1,2,3-triazolium salts in hydrogen and halogen bonding

Relatively weak yet directional supramolecular interactions like the hydrogen bond (and, more recently, the halogen bond) have attracted significant interest as they enable dynamic processes at ambient temperature, thus being suitable for applications in molecular machines,[203,204] organocatalysis,[205,206] and anion receptors/sensors.[207,208] The latter applications are motivated
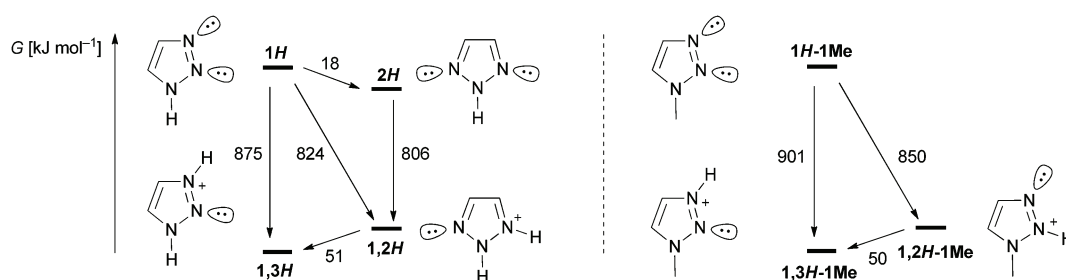

Fig. 10 Calculated gas-phase basicities of the tautomers of the 1,2,3-triazole and the 1,2,3-triazolium cation as well as of their N-methyl derivatives.[151,152]

2532 | Chem. Soc. Rev., 2014, 43, 2522–2571

This journal is © The Royal Society of Chemistry 2014

by the biological relevance of anions but also by the structure that anions can have (*e.g.* linear, trigonal planar, tetrahedral, octahedral), which suggests their use as templating ions.[207,209,210] Not least in view of the efficient synthesis by CuAAC, triazole and triazolium are valuable building blocks for these applications. In the following, we want to focus on the potential of triazoles and triazolium salts as C–H hydrogen bond donors for the design of anion receptors and provide a comparison to established hydrogen-bonding units such as pyrroles, amides, and imidazolium salts. Due to their pivotal role in anion receptor design, preorganization effects will be briefly discussed as well. At the end, also the potential of halo-triazoles and halo-triazolium salts to bind anions *via* (charge-assisted) halogen bonds is demonstrated.

4.1. Hydrogen bonds

According to a recently released IUPAC definition, a hydrogen bond is an attractive interaction between a hydrogen atom that is positively polarized by a more electronegative element or group R, and an atom, ion or molecule Y with electron-rich regions (*e.g.* lone pairs) resulting in a three-center, four-electron system, R–H···Y.[211,212] Importantly, the hydrogen bond is not a unique interaction but the sum of different interactions in varying contributions, namely electrostatic forces between di- and multipoles, London dispersion forces, and charge-transfer interactions (covalency).[211,213–216] The hydrogen bond energy typically ranges from below 20 to 25 kJ mol^{-1} and depends also on the bond angle ($\angle$ RHY), which is ideally 180° and preferentially above 110°.[211,212,217] Furthermore, cooperativity between several hydrogen bond donors and/or acceptors (bi- and oligofurcated hydrogen bonds)[217,218] as well as additional ionic interactions (charge-assisted hydrogen bonds)[214,219] might reinforce the binding.

In practice, host–guest interactions in solution based on hydrogen bonding are usually analyzed by titration experiments (^{1}H NMR, UV-vis, or isothermal titration calorimetry, ITC). To allow a reliable determination of the binding constants by fitting of the titration isotherms, the analytical method has to be chosen according to the binding strength.[220,221] Strong binding requires UV-vis titrations ($K_a = 10^3$ to 10^7 M^{-1}, $c = 10^{-4}$ to 10^{-6} M) and moderate to weak binding is examined by ^{1}H NMR titrations ($K_a = 1$ to 10^3 M^{-1}, $c = 10^{-1}$ to 10^{-3} M), while ITC has a wider operational range ($K_a = 10$ to 10^6 M^{-1}) and additionally allows to distinguish between enthalpic and entropic contributions.[220,222–224] In addition, as binding in solution implies preferential binding over the solvent background,[225] the hydrogen bond strength strongly depends on the donor and acceptor characteristics of the solvent (Gutmann acceptor and donor number, AN and DN, respectively)[226] as well as on the solvent polarity.

4.2. 1,2,3-Triazoles

It has been shown that extrinsic polarization of a carbon atom affords hydrogen bonds involving C–H groups that are as strong as for classical, intrinsically polarized hydrogen bond donors (N–H and O–H).[227–229] This is plausible in view of the widely tunable CH-acidity and the correlation between

hydrogen-bond-donor strength and the pK_a value (*vide infra*).[214,230,231] In combination with the large dipole moment, which is almost aligned with the C–H bond, the relatively high CH-acidity in the 5-position (Table 3) qualifies the 1,2,3-triazole as a potent hydrogen bond donor. The computed gas-phase binding energy for a triazole–chloride hydrogen bond ranges from −64 kJ mol^{-1} for 1,4-dimethyl-1*H*-1,2,3-triazole[232] to −79 kJ mol^{-1} for 1*H*-1,2,3-triazole,[233] while about −89 kJ mol^{-1} [234] and −94 kJ mol^{-1} [233,235] have been calculated for the chloride complexes with *N*-methylacetamide and pyrrole, respectively (Table 3). Accordingly, depending on the substitution pattern, the triazole approaches the hydrogen-bond-donor strength of the prototypical amide.

Importantly, the hydrogen bonds established with the above donors are composed differently with respect to covalent and electrostatic contributions (Table 3 and Fig. 11). On the one hand, the electrostatic interactions depend on the magnitude and alignment of the dipole moment ($E \sim \mu \cos \theta$) and therefore descend in the order triazole > amide > pyrrole. On the other hand, the covalent contribution to a hydrogen bond correlates with the acidity of the hydrogen bond donor since polarization of the R–H bond is required for both hydrogen bond donation (R$^{\delta-}$–H$^{\delta+}$) as well as heterolytic bond dissociation (R$^-$H$^+$). As a result of a strong R–H bond polarization, the σ⋆(R–H) orbital becomes available for a hyperconjugative n(Y) → σ⋆(R–H) charge-transfer interaction (*vide infra*),[239] *i.e.* a three-center, four-electron system (R–H···Y). Accordingly, the covalent character of a hydrogen bond increases upon equalization between the acidity of the hydrogen bond donor and the basicity of the hydrogen bond acceptor.[214,215,230] For a negative-charge-assisted hydrogen bond (−CAHB) between a

Table 3 Selected hydrogen-bonding parameters

Compound	μ [D]	pK_a (DMSO)	r(H···Cl$^-$)^f [Å]	ΔE(H···Cl$^-$)^k [kJ mol^{-1}]
1*H*-1,2,3-Triazole	4.38 (4.55)^a	27.8^c	2.24,^{g} 2.33^h	−79,^{g} −64^h
N-Methylacetamide	3.9^b	25.9^d	2.10 (2.14)^i	−89 (−88)^i
Pyrrole	1.74 (1.9)^a	23.0^e	2.02 (2.05)^j	−94 (97)^j

^{a} Calculated value in brackets, taken from ref. 143. ^{b} Taken from ref. 236. ^{c} Calculated value for 1-methyl-1*H*-1,2,3-triazole, taken from ref. 192. ^{d} Taken from ref. 237. ^{e} Taken from ref. 238. ^{f} Calculated hydrogen bond distance in the gas phase. ^{g} MP2/aug-cc-pVDZ, taken from ref. 233. ^{h} For 1,4-dimethyl-1*H*-1,2,3-triazole, B3LYP/6-31++G(3df,2p), taken from ref. 232. ^{i} MP2/6-31+G(d,p) (B3LYP/6-31+G(d,p)), taken from ref. 234. ^{j} MP2/aug-cc-pVDZ (B3LYP/DZVP2), taken from ref. 235. ^{k} Calculated binding energy in the gas phase.
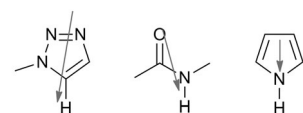
increasing hydrogen-bond-donor strength
(decreasing dipole moment but increasing acidity)

Fig. 11 Comparison of the hydrogen-bond-donor strength of 1,2,3-triazole, *N*-methylacetamide, and pyrrole (the dipole moments are indicated as grey arrows, *cf.* Table 3).

neutral hydrogen bond donor and, *e.g.*, chloride, the hydrogen bond is considered as proton-sharing equilibrium ([R···H···Y]$^{-}$) and the pK_a values for the proton loss (*cf.* Table 3 and pK_a (HCl) = 1.8 in DMSO)[238] have to be compared.[214] With a decreasing pK_a difference, the covalent character of the hydrogen bond increases in the order 1-methyl-1,2,3-triazole < *N*-methylacetamide < pyrrole. Consequently, triazoles are expected to show hydrogen bonds that are mostly electrostatic in origin (dipole–ion interaction), while the stronger hydrogen bond donation from pyrrole is ascribed to a significant covalent contribution, which overcompensates the energy loss caused by the lower dipole moment. Amides are within an intermediate range and *N*-methylacetamide is rather similar to the 1*H*-1,2,3-triazole; however, the acidity of amides strongly depends on their substituents, in particular at the nitrogen atom (*e.g.* pK_a = 21.5 in DMSO for *N*-phenylacetamide[240]).

In practice, due to counterion and solvent competition, a single hydrogen bond will hardly allow a significant anion binding and, thus, several hydrogen bond donors are commonly arranged within a chelating system allowing a cooperatively strengthened binding.[218] For this purpose, the receptor design is crucially important (*vide infra*).[224,225,241–244] For isophthalamide **4** (Scheme 8), a simple representative of the widely used family of cleft-form receptors, a significantly larger chloride affinity was found ($\Delta G = -26.8$ kJ mol^{-1})[245] in comparison to 1,3-bis(1,2,3-triazol-4-yl)benzene **5** ($\Delta G = -17.1$ kJ mol^{-1}).[246] Notably, both ^{1}H NMR titrations were performed with dichloromethane as solvent but with different chloride salts (tetraphenylphosphonium chloride, TPhPCl, *vs.* tetra-*n*-butylammonium chloride, TBACl), which show differences in ion pairing;[223] however, a high degree of dissociation is expected for TPhPCl and the strong ion pairing known for TBACl (in dichloromethane) can be included in the analysis of the titration data.[246] On the other hand, Beer *et al.* observed a more balanced binding strength in the formation of chloride-templated pseudorotaxanes between an isophthalamide macrocycle (Scheme 8) and either a bis(amide)-pyridinium thread **6** (K_{obs} = 420 M^{-1}, $\Delta G = -14.7$ kJ mol^{-1}) or a triazole-analog thread **7** (K_{obs} = 800 M^{-1}, $\Delta G = -16.3$ kJ mol^{-1}) under otherwise identical conditions (in chloroform/acetone 1:1).[247] The more similar behavior in this example may, in part, be explained by the

N-alkyl substituent of the amide, which renders its NH-acidity more comparable to the CH-acidity of the triazole (*vide supra*). Alkene-functionalized derivatives of the amide- and triazole-based pseudorotaxane templates were then ring-closed to yield the corresponding [2]catenanes with strongly increased (as a result of the interlocked structure) but also equalized chloride affinity for amide and triazole-containing catenanes ($K_a \approx 700$ M^{-1}, $\Delta G \approx -16$ kJ mol^{-1} in chloroform/methanol 1:1). In accord with the larger chloride affinity of the pseudorotaxane precursor, the yield of [2]catenane was higher in the case of the triazole-containing system.[247]

4.3. Cooperativity and preorganization

To create a significant affinity for a certain binding partner in competition with the solvent, multiple hydrogen bond interactions are commonly combined within a receptor, which, in turn, requires a careful consideration of enthalpic and entropic effects.[224,225] A flexible structure may allow an adaptive binding and, if flexibility is preserved in the resulting complex, the binding is associated with a low entropic penalty; however, this usually implies a low selectivity. Alternatively, the entropic penalty can be lowered by introducing structural restrictions to the receptor *via* preorganization, which may additionally lead to a strained receptor resulting in an enthalpic relief upon binding. In this case, selectivity is achieved by means of complementarity between the rigid host and the guest. Furthermore, a sophisticated receptor design enables positive cooperativity between the employed binding sites, *i.e.* the binding is stronger than the sum of the individual interactions (synergy). The triazole offers various binding sites that give rise to cooperativity and preorganization. Additionally, the CuAAC is particularly suited to synthesize triazole-containing oligomers and macrocycles. These features are discussed in the following paragraph. For a more detailed description of the fundamental importance of entropic effects, the reader is referred to the reviews by Schmidtchen.[224,225]

The triazole's ambivalent character allows simultaneous metal coordination and hydrogen bond donation (Fig. 12), *e.g.* in ion-pair recognition. Thereby, a synergistic increase of both CH-acidity and N-donor strength is expected. Beer *et al.*
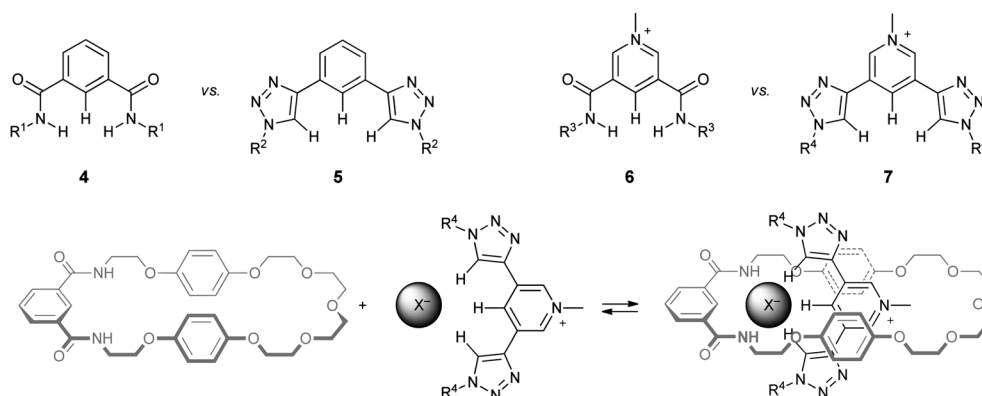
Scheme 8 Tridentate triazole- and amide-based hydrogen bond donors (R^1 = 4-(*n*-butyl)phenyl; R^2 = 4-*tert*-butylphenyl; R^3 = R^4 = *n*-hexyl) and pseudorotaxane formation.[245–247]

2534 | *Chem. Soc. Rev.*, 2014, **43**, 2522–2571

This journal is © The Royal Society of Chemistry 2014

recently demonstrated the viability of this effect for a triazole-containing heteroditopic calix[4]diquinone isophthalamide macrocycle and found cooperativity factors of up to 11 in the case of the NaCl ion pair, *i.e.* titration of a solution (acetonitrile/water 98 : 2) of the host and NaPF$_6$ with TBACl resulted in eleven times stronger binding than for the control experiment without additional NaPF$_6$.[248] Likewise, the triazole can function simultaneously as a hydrogen bond acceptor and donor with both interactions mutually strengthening each other,[246] which has also been observed for amides (Fig. 12).[249] The latter feature allows a further enhancement of the binding by pre-organization *via* intramolecular hydrogen bonding, which is discussed in the following.

The groups of Flood and Hecht independently demonstrated that 2,6-bis(1*H*-1,2,3-triazol-4-yl)pyridines can serve as analogs to well-known 2,2′:6′,2″-terpyridine (terpy or tpy) ligands.[250,251] Meanwhile, 2,6-bis(1*H*-1,2,3-triazol-1-yl)pyridines, which feature a reversed connectivity, have been presented, although the synthesis of the required 2,6-diazidopyridine represents a hurdle.[252] As for terpy, the free bis(triazolyl)pyridine triad adopts a planar *anti–anti* conformation with respect to the nitrogen lone pairs to avoid repulsive interactions and allow intramolecular hydrogen bonds, while a *syn–syn* conformation is enforced upon protonation or metal coordination (see, *e.g.*, Section 5.1.2).[251,253] Given the modular and facile synthesis of triazoles, Hecht *et al.* synthesized bis(triazolyl)pyridine oligomers as well as polymers and explored their potential as responsive helical foldamers.[254,255] Similarly, Jiang *et al.* observed helical folding in oligo(aryl-triazole)s.[256] Furthermore, Hecht *et al.*[257] as well as Zhao, Li *et al.*[258–261] systematically investigated the preorganization *via* intramolecular hydrogen bonds in 1,4-diaryl-1,2,3-triazole model systems. For a 1,4-bis(2-pyridyl)-1,2,3-triazole triad (8, Fig. 13), intramolecular five-membered-ring hydrogen bonds are established between the triazole and both pyridines with both heterocycles serving as a hydrogen bond donor and acceptor, which results in a coplanar structure that shows a stabilization by about 25 to 28 kJ mol^{-1} relative to alternative conformations for each side.[257] A similar relative stabilization (20 to 31 kJ mol^{-1}) was calculated for 9 (X = F or OMe), albeit with a deviation from coplanarity in the case of the C–N bond ($\psi = 34°$ for X = F, $\psi = 42°$ for X = OMe), while the C-bound phenyl ring was found to be coplanar with the triazole ($\phi = 0$–3°).[257,258,260] Triads built with two adjacent phenol rings (10) have been synthesized although the preorganization thereof has not been discussed.[262] In principle,
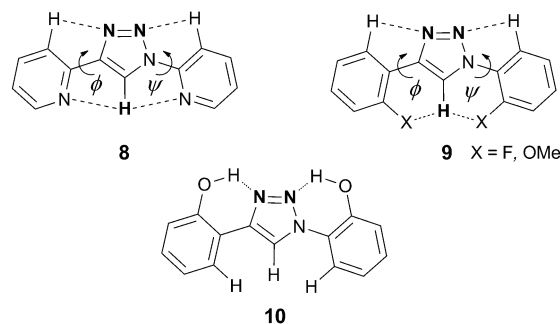
Fig. 13 Preorganization *via* intramolecular hydrogen bonds in 1,4-diaryl-1,2,3-triazoles.[257,258,260,262]

twofold hydrogen bond acceptance by the triazole with dihedral angles close to planarity is expected (*vide infra*).[246]

Apart from the design of responsive macromolecules with defined secondary structures, intramolecular hydrogen bonding with the triazole can be used to preorganize anion receptors (Fig. 14). Flood *et al.* employed auxiliary phenolic[246] (and amide-based[232]) hydrogen bond donors to preorganize three hydrogen bond donors of a bis(triazolyl)benzene cleft receptor (11).[246] ^{1}H NMR titration experiments with TBACl in dichloromethane at 298 K revealed a much higher chloride affinity for 11 (K_a = 46 800 M^{-1}, $\Delta G = -26.6$ kJ mol^{-1}) when compared with the flexible analog 5 (K_a = 1000 M^{-1}, $\Delta G = -17.1$ kJ mol^{-1}).[246,263] The preorganization fulfills two functions: firstly, the rotational freedom of the free receptor is restricted reducing its conformational entropy.[264] Secondly, the receptor is prevented from adopting a relaxed *syn–anti* conformation[263] in the uncomplexed state. Consequently, entropic and enthalpic penalties that occur upon binding are neutralized resulting in a larger binding Gibbs energy (ΔG, Fig. 14). In addition, the auxiliary hydrogen bonds may cooperatively enhance the triazole's hydrogen-bond-donor strength by further polarization of the triazole (an increased dipole moment of 6 D has been calculated).[246]

In parallel, the groups of Flood and Craig reported on shape-persistent [3$_4$]-triazolophanes[228,265–273] and reconfigurizable oligo(aryl-triazole)s,[263,274] respectively, as anion receptors (Fig. 14). Detailed analysis of the ^{1}H NMR titration of the triazolophane (13) with TBACl in dichloromethane revealed an impressive binding constant of $K_a = 5 \times 10^6$ M^{-1}, corresponding to $\Delta G = -38$ kJ mol^{-1}, for the formation of a 1 : 1 complex with chloride.[268] Notably, four equilibria were considered including ion paring and formation of a 2 : 1 complex and the results were confirmed by UV-vis titration. Moreover, chloride and bromide were bound much stronger than fluoride and iodide due to the complementary size of the former anions and the cavity of the receptor.[270] In contrast, a much lower chloride affinity of K_a = 80 M^{-1}, corresponding to $\Delta G = -11$ kJ mol^{-1}, was obtained for the triazole foldamer (12) under the same conditions considering three equilibria (the formation of a 2 : 1 complex was not observed in the case of 12).[267] This striking difference is a consequence of the high degree of preorganization or shape-persistence of the rigid macrocycle (*cf.* the above-mentioned cleft receptors 5 and 11): while a similar sum of hydrogen bond energies was calculated for both,
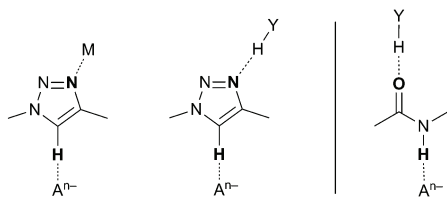

Fig. 12 Cooperativity by hydrogen bonding with the 5-proton and metal coordination/hydrogen bonding with the 3-nitrogen of the 1,4-disubstituted triazole as well as analogy with amides.

This journal is © The Royal Society of Chemistry 2014

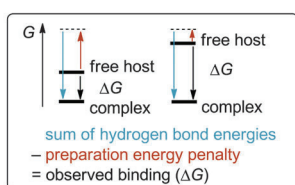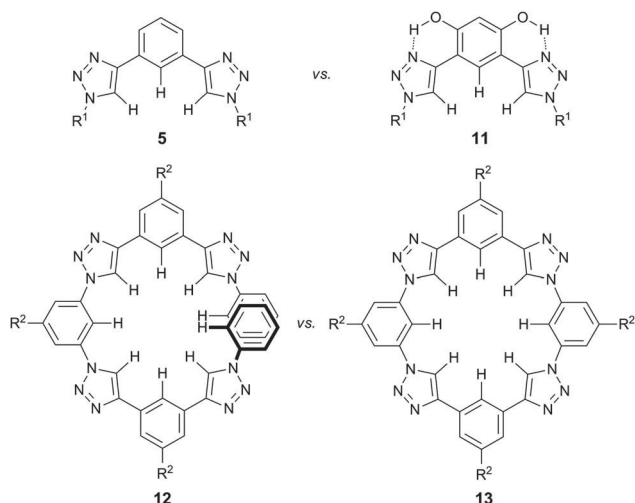*Chem. Soc. Rev.*, 2014, 43, 2522–2571 | 2535

Fig. 14 Flexibility *vs.* preorganization for triazole clefts (**5** and **11**), triazole foldamer (**12**), and triazolophane (**13**) (R^1 = 4-*tert*-butylphenyl, R^2 = *tert*-butyl, note that the receptors are drawn as if complexed).[246,267]

12 and **13**, the flexible triazole-foldamer **12** has to pay a large enthalpic and entropic penalty upon chloride binding – a penalty that the rigid triazolophane **13** has already paid during its synthesis. This intrinsic penalty of **13** stems from repulsive dipole contacts and an entropically unfavorable conformational restriction providing an electropositive cavity that is almost ideally aligned for the binding of an incoming chloride anion (*cf.* the entatic state model[275]).[276] In contrast, the uncomplexed and flexible **12** adopts an open zigzag structure, enabling the partial compensation of the triazole's dipole moments and the rotation around the eight single bonds connecting the aromatic rings, which strongly stabilizes the free **12** resulting in a much lower anion affinity.[263,267,274] Ultimately, the shape-persistent triazolophane allows a much stronger binding permitting application as ionophores,[277] while the triazole oligomers represent molecular switches showing anion-induced folding[274] or helicity inversion.[254]

Very recently, Leigh *et al.* presented an acid–base-switchable hydrogen bond donor based on a 1,2,3-triazole-functionalized guanidine (**14**, Scheme 9).[278] Upon protonation, the degree of preorganization and polarization within the quadruple hydrogen bond donor is enhanced and the hydrogen bonding with a complementary, charge-neutral hydrogen bond acceptor is strengthened.

For more information on the applications of triazoles in hydrogen bonding, the reader is referred to the reviews by Flood *et al.*[228,266,269,272] and Haridas *et al.*[279]

4.4. 1,2,3-Triazolium salts

1,2,3-Triazolium salts[280] can be readily obtained from the corresponding 1,2,3-triazoles by alkylation using alky halides,[166,281–285]
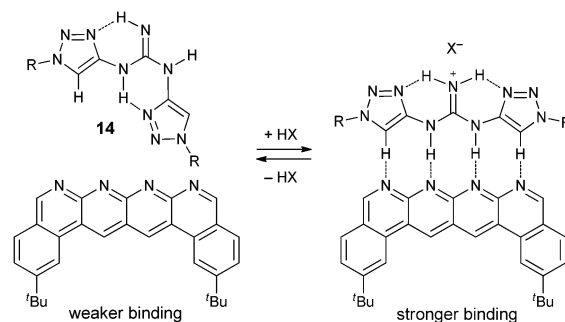
Scheme 9 Acid–base switchable quadruple hydrogen-bonding array (R = *n*-hexyl).[278]

tosylates or triflates,[286–288] or trimethyloxonium tetrafluoroborate (Meerwein's reagent).[166,289–294] Notably, milder alkylation conditions (methyl iodide in dichloromethane) require elevated temperatures and prolonged reaction times, which allows a single alkylation of bis(triazole)benzene (**5**, Fig. 14), while Meerwein's reagent readily achieves the twofold methylation at room temperature.[166] Furthermore, even arylation by nucleophilic aromatic substitution with electron-deficient aryl halides can be achieved under forcing conditions.[295] Alternatively, 1,2,3-triazolium salts can be obtained directly by (3+2) cycloaddition between alkynes and 1,3-diaza-2-azoniaallene salts, which allows the synthesis of 1,3-diaryl-1,2,3-triazolium salts (see Section 5.4.2).[296]

On account of the introduction of an electron-withdrawing iminium-type nitrogen, the CH-acidity of the triazolium ring is increased relative to the parent triazole. The pK_a value of N3-alkylated 1,2,3-triazolium salts is about 24[297] and even lower for 1,3-diaryl-substituted triazolium salts as the latter can be deprotonated using KO^{t}Bu (pK_a = 22).[296,297] In comparison, the imidazolium ring is more acidic (pK_a ~ 20 to 23)[298–300] since two strongly electron-withdrawing nitrogen atoms are placed adjacent to the 2-carbon. For the same reason and because of the additional ring nitrogen, the 1,2,4-triazolium is even more acidic (pK_a ~ 17–19).[301] In a first approximation, a complementary trend to the corresponding carbene donor strength is thus established (Fig. 15, see Section 5.4.1), which is governed by the number of iminium-type nitrogen atoms and their proximity to the CH-group.

The higher CH-acidity of the 1,2,3-triazolium salt relative to the parent triazole increases the covalent contribution of the hydrogen bond in line with the above mentioned pK_a equalization principle.[214,216] As the C–H bond polarization is enhanced, the σ*(R–H) orbital is lowered in energy and more localized at the acidic hydrogen atom (Fig. 16) thus enabling a stronger hyperconjugative interaction, n(Y) → σ*(R–H).[302,303] Depending on the base strength of the anion, the increased electron-accepting/proton-donating character of the 1,2,3-triazolium eventually allows a proton transfer. Accordingly, a doubly charge-assisted hydrogen bond (±CAHB) is considered as proton-transfer equilibrium ([R$^+$–H···Y$^-$] → [R···H–Y]).[214] When comparing the pK_a values of the triazolium and, *e.g.*, fluoride (pK_a (HF) ~ 15 in DMSO[238]), the low pK_a difference (~9) indicates a significant covalent character of the hydrogen bond
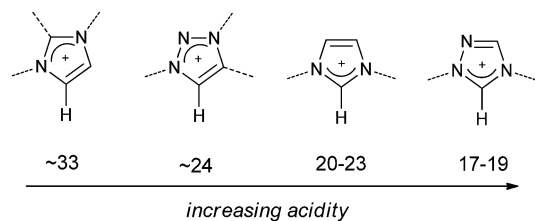
2536 | *Chem. Soc. Rev.*, 2014, **43**, 2522–2571

This journal is © The Royal Society of Chemistry 2014

Fig. 15 pK_a ranges for selected azoliums.[297,299–301]

Fig. 17 Influences of inductive substituent effects (σ_m)[183] on the relative CH-acidity determined by H/D-exchange kinetics.[305]

between triazolium and fluoride, and even deprotonation of 1,2,3-triazolium salts by fluoride was observed, most likely additionally driven by the formation of $[F \cdots H \cdots F]^-$.[285,304] Similarly, for 1,2,3-triazolium salts and even for 1,2,3-triazoles, a H/D-exchange has been observed in the presence of sulfate[166] and fluoride,[263] respectively.

Furthermore, Begtrup investigated the effect of the substituents of 1,2,3-triazolium salts on the base-catalyzed H/D-exchange kinetics (Fig. 17) and observed a mostly inductive influence.[305] Taking the C-unsubstituted 1,3-dimethyl-1,2,3-triazolium as a reference, replacement of the 4-proton by a methyl group retards the exchange rate to a tenth due to the inductive electron donating effect. Conversely, the rate is enhanced by a factor of 2 and 450 when introducing σ-electron withdrawing methoxy and bromo substituents, respectively. Apparently, the effect of the methoxy group is partially compensated by π-electron donation, which lowers the electron deficit of the cationic ring. Furthermore, replacement of a methyl N-substituent by a σ-electron withdrawing phenyl ring increases the acidity, in particular for the adjacent carbon atom. As mentioned above, the acidity can be further increased if both nitrogen atoms are substituted with an aryl ring.[296]

Concerning the dipole interactions of the triazolium cation, it first has to be noted that, in contrast to neutral molecules, the dipole moment of a monopole depends on its positioning, which is usually either the center of mass or the geometrical center.[306,307] The latter is certainly more useful when designing anion receptors from individual building blocks and artifacts can be produced by the former approach in larger molecules. Given the polarization within the 1,2,3-triazolium, even though ill-defined, one can still expect an equivalent to an electric dipole moment. The calculated dipole moment shows a less beneficial alignment for the desired hydrogen bonding with the 5-proton and it amounts to 1.2 D only (Fig. 18),[303] which is very

similar to the value reported for imidazolium cations (1.1 D)[306] and plausible in view of the introduction of a carbocation in the region of the negative pole of the triazole's dipole. Nonetheless, this result has to be taken with caution since unusually high fluctuations of the electrostatic interactions by mutual polarization between anion and imidazolium cations have been reported.[307–311] Although studied in the context of ionic liquids and still under debate, this behavior was suggested to result from π interactions and hydrogen bonding rather than being a bulk effect. Ultimately, the dipole interactions with an anion offered by the 1,2,3-triazolium are certainly lower in comparison to triazoles, while, on the other hand, ion–ion interactions are enabled, which is discussed in the following.

4.5. Coulomb interactions vs. hydrogen bonding

A question that immediately arises for the cationic hydrogen bond donors concerns the role of the ionic interactions. It is of importance to consider the characteristics of the main stabilizing interactions of hydrogen bonds first: (i) electrostatic interactions, which are directed and of long range (dipole–dipole, $E \sim r^{-3}$, dipole–ion, $E \sim r^{-2}$), (ii) dispersion (London) forces, which are isotropic and of shorter range ($E \sim r^{-6}$), and (iii) covalent (charge-transfer) interactions, which are directed and of very short range.[217] In contrast, ion–ion (Coulomb) interactions are exceedingly strong, isotropic, and of very long range ($E \sim r^{-1}$). In the following, fundamental differences in binding of anions by 1,2,3-triazoles and 1,2,3-triazolium cations are discussed as they have important implications for the design of anion receptors.

Recently, the groups of Sessler and Hay evaluated the binding of chloride by simple triazole and triazolium models. According to their calculations, the triazolium chloride complex is much
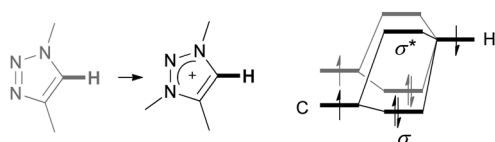

Fig. 16 Simplified molecular orbital scheme qualitatively demonstrating the electronic differences between 1,2,3-triazole (grey) and 1,2,3-triazolium (black). The σ^*(C–H) orbital is able to establish a hypercongugative three-center, four-electron bond with an electron donor, C–H$\cdots$Y. Additionally, the hydrogen bond can be accompanied by in-plane π interactions directly between C(π^*) and Y(n) (not shown).[302]
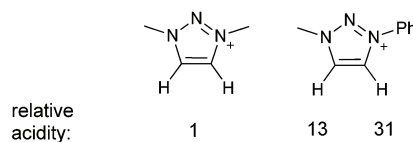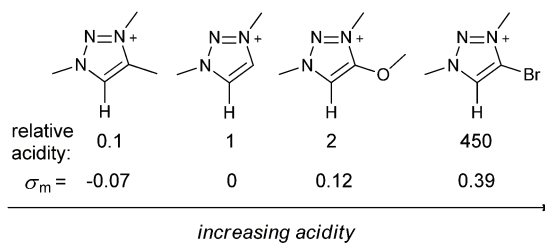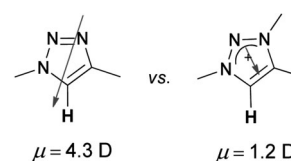

Fig. 18 Calculated (B3LYP/6-31G(d)) dipole moments for 1,2,3-triazole and the corresponding 1,2,3-triazolium salt.[303]

more stable ($\Delta G = -373.5$ kJ mol^{-1}) than the corresponding triazole chloride complex ($\Delta G = -51.9$ kJ mol^{-1}, Fig. 19) in vacuum.[312] Importantly, based on Coulomb's law, one can assess that both interactions with chloride are strongly dominated by electrostatic attraction (ion–ion and dipole–ion interactions in the case of the triazolium and the triazole, respectively).† In practice, however, the weakening of the electric field by alignment of solvent dipoles has to be considered, which strongly reduces the electrostatic interaction ($E \sim \varepsilon_r^{-1}$ with ε_r being the relative dielectric constant of the solvent).[313] In addition, competitive hydrogen bonding of the solvent molecules with the hydrogen bond donor and/or the anion further reduces the effective binding energy. In other words, the binding modes offered by a receptor are available for the solvent, too. As a result, the ΔG values for the formation of the triazolium chloride and triazole chloride complex are strongly reduced already in moderately competitive and less polar solvents like chloroform, but, according to computations, still the triazolium complex is more favorable than the triazole counterpart (Fig. 19).[312] Eventually, in highly polar media like acetonitrile, the complex formation with chloride suffers from extensive solvation, in particular in the case of the triazolium, which offers isotropic and long-range interactions with its monopol.[314] On the other hand, the solvent interaction may give rise to entropically driven complexation (*vide infra*).

Notably, the above calculations[312] should serve only to demonstrate the difference in solvent dependency between triazolium and triazole. However, this does not imply that chloride binding by a triazolium cation will not occur in acetonitrile solution, which is deduced from the reasonably strong binding that was found experimentally for the triazolium congener 1,3-dimethylimidazolium.[315] This difference may be rationalized by the use of a minimalistic triazolium model equipped with hydrogen atoms only. The resulting triazolium cation thus features alternative, even more acidic hydrogen-bonding sites, which required a restriction of the C–H⋯Cl$^-$ angle to 180° in the energy optimization[312] and leads to an overestimation of the solvation enthalpy of the molecule. In practice, the facile functionalizability of the 1,2,3-triazolium will be exploited and the most acidic protons at the nitrogen atoms will be replaced by substituents. Still, by tendency, the solvophilic behavior or "stickiness"[224] remains as also aliphatic substituents at the iminium nitrogen atoms are polarized[302] and thus prone to participation in bifurcated hydrogen bonding (Fig. 20).[316] Additionally, the anion can be bound by direct charge-transfer interaction with the electron-deficient π system of the triazolium cation (n → π*).[229,303,312] These alternative binding modes are well-known for the imidazolium cation[302,309,317–319] and cause a relatively low orientational preference, while a moderate to strong overall hydrogen-bonding capability is given. In theory, the larger variety of potential

in vacuum: −373.5 kJ mol^{-1} −51.9 kJ mol^{-1}
in chloroform: −16.7 kJ mol^{-1} 10.5 kJ mol^{-1}
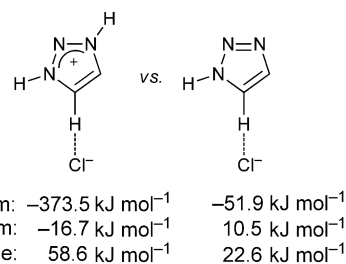in acetonitrile: 58.6 kJ mol^{-1} 22.6 kJ mol^{-1}

Fig. 19 Comparison of the calculated (MP2/aug-cc-pVDZ) Gibbs energies, ΔG, for the formation of a chloride complex with the triazolium cation and triazole (notably, the C–H⋯Cl$^-$ hydrogen bond was restricted to 180° as it does not represent the global minimum for the NH-triazole and its protonated form).[233,312]

interactions gives rise to a low orientational preference, but, at the same time, a favorable contribution to the binding by an increase in configurational entropy.[225]

Ultimately, even in highly competitive solvents, charged receptors are not *per se* counterproductive; in fact, charge assistance is required in most cases to enable anion binding in aqueous solutions.[219,243] As for hydrogen bonding, multiple interactions can cooperatively strengthen the binding.[218] Accordingly, the use of multiply charged receptors based on, for instance, imidazolium cations has become a successful strategy to achieve strong anion binding.[320] Thereby, the local charge density is increased, while the cavity of the receptor will only provide a limited volume, which leads to a preference for the anions over solvent molecules, in particular in the case of multiply charged anions ($E \sim q_{\text{cation}}\,q_{\text{anion}}$), in order to maximize the Coulomb interactions.[321] Furthermore, charged receptors necessarily carry an original counteranion, which is usually of low charge density, *e.g.* BF$_4^-$ or PF$_6^-$, and preferential binding thus results from the closer contact ($E \sim r^{-1}$) enabled by a more charge-dense anion, which will allow a stronger hydrogen bonding as well. Besides, structural restrictions within interlocked structures[208,210] or cleft and macrocyclic receptors may induce

† Using the Coulomb equation, stabilization energies (ignoring entropic contributions) were estimated to be about −330 kJ mol^{-1} for the ion–ion interaction and about −70 kJ mol^{-1} for the ion–dipole interaction in vacuum (a distance of 4.25 Å between the center of the heterocycle and chloride, corresponding to a H⋯Cl$^-$ distance of 2.25 Å,[233] and an ideally aligned ($\theta = 180°$) dipole moment of 4.5 D in the case of the triazole was assumed).

non-furcated   anion–π
hydrogen bonding   interaction

bifurcated
hydrogen bonding

Fig. 20 Selected potential triazolium–anion interactions.

2538 | *Chem. Soc. Rev.*, 2014, **43**, 2522–2571

This journal is © The Royal Society of Chemistry 2014

selectivity by means of complementarity with the anion's size and structure. In this regard, the preparation of macrocycles *via* the highly efficient CuAAC is particularly attractive as the cyclization usually requires pseudo-high-dilution conditions.[271,293]

Accordingly, Beer *et al.* reported a tight binding of halides and, in particular, of sulfate by a flexible macrocyclic tetrakis-(triazolium) host (**16**) in highly competitive solvents (Fig. 21).[293] A preference for larger halides was observed, which was attributed to a better matching with the size of the cavity. Detailed investigations by molecular dynamics (MD) and quantum mechanics/molecular mechanics (QM/MM) simulations including an appropriate modeling of the solvent interactions have been performed and nicely revealed how the solvent and receptor compete in the complexation of, *e.g.*, sulfate within a dynamic ensemble.[293] This scenario reflects how the interaction with the solvent and the flexibility of the receptor in conjunction with the various binding sites provided by the polyatomic sulfate lead to a spreading of energy over a larger number of microstates, *i.e.* a lowering of structural definition associated with a gain in entropy.[224,225] Additionally, in polar/protic solvents the binding partners are highly solvated, in particular sulfate,[243,322] and the liberation of a large number of solvent molecules upon binding of a single anion by the receptor is usually driven entropically, enabling the binding even if it is an endothermic process.[225,243] Still, this requires significant binding enthalpies to at least partially compensate the enthalpic loss required for the desolvation and, thus, to render the binding event an exergonic process. Accordingly, a much stronger binding of chloride by the tetrakis(triazolium) macrocycle **16** relative to the parent tetrakis(triazole) macrocycle **15** is observed in d$_6$-DMSO (Fig. 21). While the binding strength for the triazolium host is of course strongly enhanced by ion–ion interactions, electrostatic and dispersion interactions alone are not sufficient to reproduce the experimental binding behavior, as, for instance, sulfate was found to irreversibly leave the receptor **16** in the case of classical MD simulations.[293] In contrast, when using QM/MM simulations, which include charge-transfer interactions, the anion is kept within or at least above the cavity by virtue of charge-assisted hydrogen bonds with all four triazolium protons facing towards the anion.[293] Nonetheless, the charge assistance is an important feature leading to a high preference for the dianion sulfate over several monoanions (*e.g.* $K_a > 10^4$ M^{-1} for **16**·SO$_4$$^{2-}$ *vs.* K_a = 230 M^{-1} for **16**·Cl$^-$) in the highly competitive aqueous medium (d$_6$-DMSO/D$_2$O 1 : 1).[293]

Similarly, the binding stoichiometry can be controlled by the number of cationic charges of a cleft receptor, allowing the formation of a 2 : 1 complex with sulfate in the case of the mono(triazolium) receptor **17**, while a 1 : 1 complex was observed with the analogous bis(triazolium) receptor **18** (Fig. 21).[166]

The directionality of the hydrogen bonding with the triazolium may be optimized by placing EWGs at the triazolium ring in order to enhance charge-transfer and dipole–ion interactions, which are anisotropic and decline faster with increasing distance.[314] Alternatively, Ooi *et al.* demonstrated that a chiral triazolium-based catalyst (**19**) featuring an additional amide is capable of inducing high enantioselectivities in the asymmetric alkylation of oxindoles (Scheme 10).[284] Notably, dual hydrogen bonding *via* triazolium and amide was essential as the enantioselectivity dropped significantly if one of the hydrogen bond donors was blocked by substitution with a methyl group. Importantly, the strict enantiofacial discrimination, which is essential to achieve a high enantiomeric excess (ee), requires a permanent and intimate association of the prochiral oxindole enolate anion and the chiral counterion. This can be achieved under phase-transfer-catalysis conditions, *i.e.* the chiral triazolium cation is the only available countercation for the enolate, which reinforces the contact ion pair in the moderately polar solvent. Furthermore, an elaborated substitution pattern (in particular for the aryl substituents Ar^1 and Ar^2, *cf.* Scheme 10) was required to establish an anion binding site of pronounced asymmetry. Recently, the scope of reactions catalyzed by this type of amide-containing triazolium salt was extended to asymmetric Mannich reactions as well as asymmetric ring opening reactions of aziridines.[323,324] For this purpose, the stereoselectivity was improved by increasing the CH-acidity of the triazolium by the help of EWGs.

4.6. Halogen bonds

A supramolecular interaction analogous to the hydrogen bond (R–H⋯Y) is the interaction of an electron-deficient region of a halogen atom with a Lewis base, which is called the halogen bond (R–X⋯Y). Although rewarded with the Nobel Prize (Odd Hassel, 1969[325]) and well-known in crystal engineering thanks to the contributions by Metrangolo and Resnati *et al.*,[326–328] the relevance of halogen bonding in solution and its potential for, *e.g.*, anion recognition and catalysis was only recently recognized.[329,330] In analogy to hydrogen bonds, a halogen atom is donated by the so-called halogen bond donor (R–X), while it is accepted by the so-called halogen bond acceptor (E) – a nomenclature that is the reverse of the concomitant electron density acceptance by

Fig. 21 Triazole- and triazolium-based cleft and macrocyclic anion receptors and association constants with selected anions (R^1 = 2,6-dimethyl-4-bromophenyl, R^2 = 4-tolyl).[166,246,293]

15
Cl$^-$: K_a < 10 M^{-1} (d$_6$-DMSO)

16
Cl$^-$: K_a > 10^4 M^{-1} (d$_6$-DMSO)
Cl$^-$: K_a = 230 M^{-1} (d$_6$-DMSO/D$_2$O 1:1)
SO$_4$$^{2-}$: K_a > 10^4 M^{-1} (d$_6$-DMSO/D$_2$O 1:1)
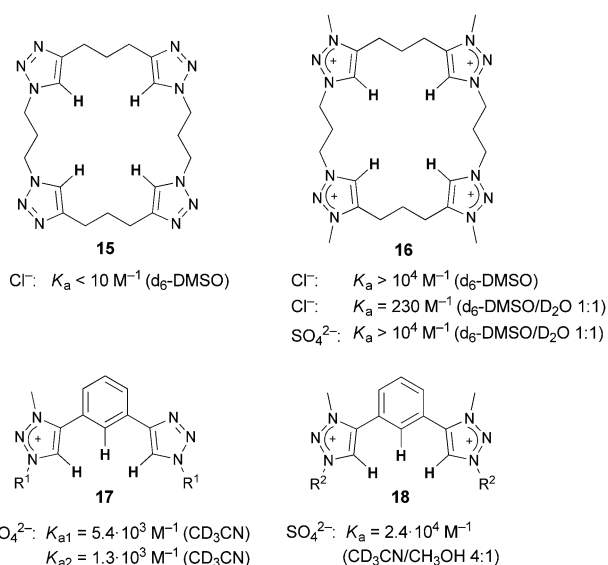
17
SO$_4$$^{2-}$: K_{a1} = 5.4·10^3 M^{-1} (CD$_3$CN)
  K_{a2} = 1.3·10^3 M^{-1} (CD$_3$CN)

18
SO$_4$$^{2-}$: K_a = 2.4·10^4 M^{-1}
(CD$_3$CN/CH$_3$OH 4:1)
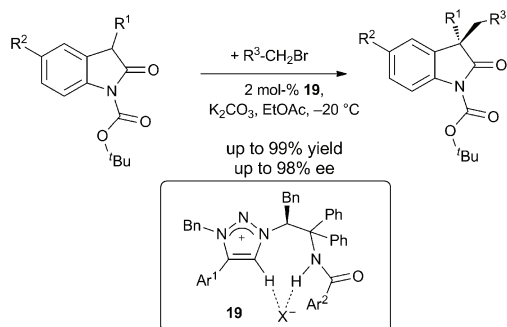
Scheme 10 Organocatalytic alkylation of *N*-Boc-protected oxindoles using a chiral triazolium-based phase-transfer catalyst.[284]

Fig. 22 Simplified molecular orbital scheme of an R–X bond to visualize the σ hole (unshared orbitals are omitted). The σ*(R–X) orbital is able to establish a hyperconjugative three-center, four-electron bond with an electron donor, R–X···Y.

R–X and donation by E.[331] Indeed, the electronegative halogen atom can feature an electropositive region, the so-called "σ hole", located at the opposite side of the R–X bond if R shows a sufficiently strong electron withdrawal. In line with an NBO population analysis, the halogen atoms (except F) show only minimal sp hybridization and the R–X bond involves essentially a single occupied p orbital of the halogen atom (Fig. 22).[331,332] If the effective electronegativity of R approaches the one of X, p-electron density is displaced significantly towards R and the halogen will contribute considerably to the σ*(R–X) orbital. Thus, p-electron depletion occurs at X opposed to the R–X bond, which is not compensated by the unshared s orbital as it is isotropically distributed, leading to a region of positive electrostatic potential allowing a charge-transfer interaction, n(Y) → σ*(R–X), with the donor (Y). The unshared p orbitals are orthogonal to the R–X bond and constitute an electron-rich belt with negative electrostatic potential. This model is able to explain the strict preference of the halogen bond angle, $\angle$(R–X···Y), to be very close to 180°, which was found crystallographically,[328] and the observed trend that the strength of the halogen bond, R–X···Y, increases in the order Cl < Br < I for the halogen-bond-donating atom X.

Similar to the hydrogen bond, the halogen bond is a combination of various interactions including polarization and dispersion interactions, with a dominant electrostatic interaction as well as a significant charge-transfer character (covalency).[329,333–335] For analogous systems, halogen bonds are usually stronger than hydrogen bonds;[334] note, however, that protic solvents are detrimental for halogen bonds.[336,337] Furthermore, the relative contributions of the attractive interactions depend on the actual halogen bond system resulting in a variable preference, *e.g.*, for either halides or oxyanions.[330,338–340] The significance of interactions that are not of electrostatic origin may be emphasized by the observation of unexpectedly strong halogen bonds in polar solvents like acetonitrile[336,337,340] as well as a high affinity for soft anions,[328–330] which is in marked contrast to hydrogen bonds. In analogy to the hydrogen bond, the halogen bond may be considered as a prereactive complex, eventually leading to a symmetrical halogen bond (*cf.* I$_3^-$)[329] or even to a chemical reaction (*cf.* *N*-halosuccinimides).[319,327] Ultimately, halogen bonds may be employed in cooperation with hydrogen bonds to control, *e.g.*, the selectivity
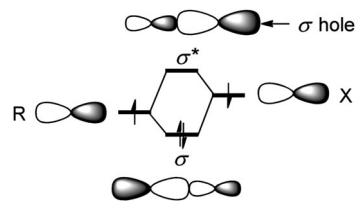
of anion receptors, although it should be noted that both interactions preferentially bind an anion in an orthogonal arrangement[341,342] and that the binding strength decreases much more sharply with a deviation from linearity for the halogen bond than for the hydrogen bond.[319,343,344]

4.7. Halo-1,2,3-triazoles

5-Halo-1,2,3-triazoles can be obtained by direct cycloaddition between organic azides and halo-alkynes or by trapping a Cu(I) triazolide with the corresponding electrophile (see Section 2.2). In analogy to the C–H bond polarization within 1,2,3-triazoles, a significant C–X bond polarization can be expected for 5-halo-1,2,3-triazoles owing to the presence of three nitrogen ring atoms, at least for X = I.

Very recently, Beer *et al.* reported picket-fence Zn(II) porphyrins featuring pendant 1,2,3-triazoles or 5-iodo-1,2,3-triazoles (Fig. 23) and systematically studied their anion binding.[340] While the hydrogen-bond- and the halogen-bond-based receptors showed essentially the same binding trends with halides, which might be dictated by auxiliary interactions with, *e.g.*, the Lewis-acidic Zn(II) center, the binding strength was significantly enhanced in the case of the halogen bond donor **20I**. Furthermore, it was demonstrated that the anion affinity in particular of the halogen-bond-based receptor increases in the solvent order chloroform < acetonitrile < acetone, *i.e.* with a decrease in the hydrogen-bond-donor strength of the solvent in line with a decreasing AN.[226,345]

4.8. Halo-1,2,3-triazolium salts

5-Halo-1,2,3-triazolium salts can be synthesized by methylation of the corresponding 5-halo-1,2,3-triazole using, *e.g.*,

E = I: **20I**	
X$^-$ = Cl$^-$:	K_a = 3592 (31) M^{-1}
X$^-$ = Br$^-$:	K_a = 1132 (11) M^{-1}
X$^-$ = I$^-$:	K_a = 305 (23) M^{-1}

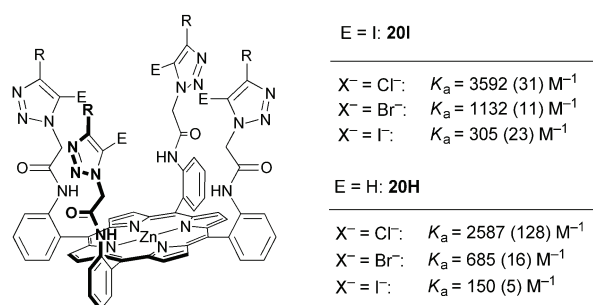| E = H: **20H**	
X$^-$ = Cl$^-$:	K_a = 2587 (128) M^{-1}
X$^-$ = Br$^-$:	K_a = 685 (16) M^{-1}
X$^-$ = I$^-$:	K_a = 150 (5) M^{-1}

Fig. 23 1,2,3-Triazole- and 5-iodo-1,2,3-triazole-containing anion receptors based on a picket-fence Zn(II) porphyrin (R = 4-*tert*-butylphenyl, association constants in CHCl$_3$).[340]

2540 | *Chem. Soc. Rev.*, 2014, **43**, 2522–2571

This journal is © The Royal Society of Chemistry 2014

trimethyloxonium tetrafluoroborate or methyl triflate as alkylating reagents (*vide supra*).[346,347] Alternatively, iodo-1,2,3-triazolium salts can be obtained by treating Ag(I)-1,2,3-triazolylidenes (see Section 5.4.2) with iodine.[348] Relative to the corresponding 5-halo-1,2,3-triazoles, the C–X bond polarization is expected to be enhanced for the halo-1,2,3-triazolium salts enabling strong halogen bonds accompanied by Coulomb interactions with anions.

Soon after the recent advent of halogen bonding in host–guest chemistry, Beer *et al.* demonstrated the potential of iodo-1,2,3-triazolium rings for anion recognition based on charge-assisted halogen bonds.[346] Using a template based on a combination of halogen and hydrogen bonds, a [2]rotaxane could be synthesized that showed strong halide binding in a highly competitive solvent mixture ($CDCl_3/CD_3OD/D_2O$ 45:45:10) with a remarkable halide preference following the order $Cl^- < Br^- < I^-$. For pseudorotaxane models with iodo-triazolium and triazolium threads (Scheme 11), a larger apparent association constant (K_{app}) for the simultaneous macrocycle threading and anion binding was found for the halogen bond system (**21I**) when compared to its hydrogen-bond-based analog (**21H**, both in chloroform). In both cases, a preference for bromide was given, although this was much more pronounced for the halogen bond. Notably, the anion preference within these restricted architectures is controlled by size complementarity between the host and guest as well as different levels of cooperativity. The latter are cooperations, firstly, between the hydrogen and halogen bonding[342] and, secondly, between the direct anion binding and the concomitant auxiliary interactions, like π interactions as well as hydrogen bonds between the remote methyl group of the azolium ring and the polyether backbone (*cf.* Scheme 11).[346] Nonetheless, the achieved nontrivial preference for soft anions is obviously promoted by the halogen bond, which emphasizes its potential for anion recognition.
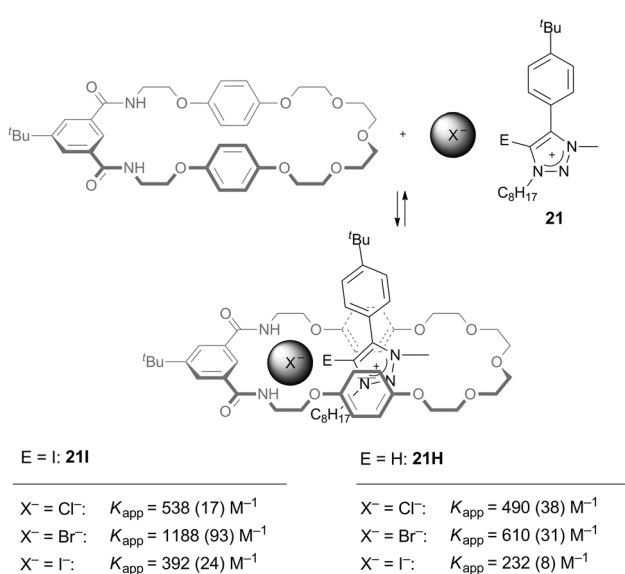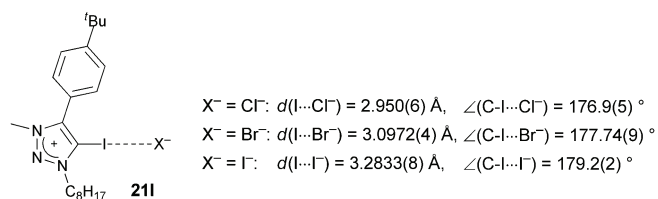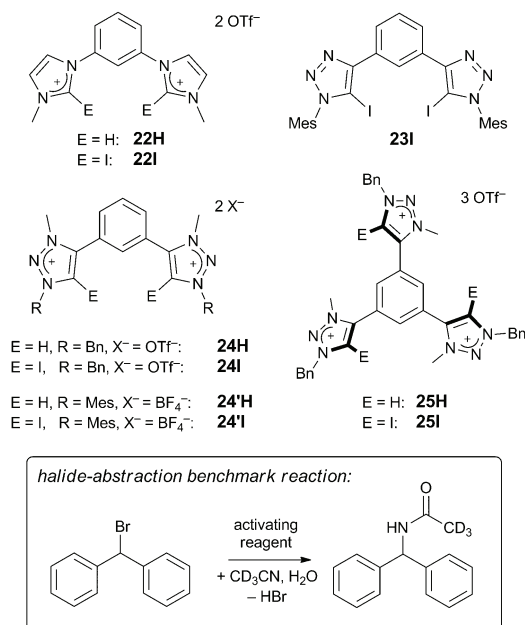

Fig. 24 Halogen-bond parameters in the solid state for iodo-triazolium halide complexes.[342]

For further information on anion templation and anion sensing using restricted architectures, the reader is referred to recent reviews by Beer *et al.*[208,210]

Further evidence for the ability of the iodo-triazolium to form strong charge-assisted halogen bonds is given by a crystallographic report by Beer *et al.*[342] The solid-state structures of a series of halide complexes with a iodo-triazolium (**21I**) revealed halogen bonds whose length corresponds to 80% of the sum of the van der Waals radii and which show almost linearity (Fig. 24). Interestingly, the observed halogen bonds are among the shortest in comparison to other iodine–halide halogen bonds, $C–I \cdots X^-$, and resemble the ones reported for an iodo-imidazolium chloride complex ($d(I \cdots Cl^-) = 2.9482(12)$ Å, $\angle (C–I \cdots Cl^-) = 177.65(13)°$) and iodide ($d(I \cdots I^-) = 3.28829(5)$ Å, $\angle (C–I \cdots I^-) = 177.56(8)$ °).[319] Additionally, if under-stoichiometric amounts of halides are present, coordination of a single halide by two iodo-triazolium halogen bond donors, $C–I \cdots X^- \cdots I–C$, was observed for X = Cl^- and I^-.[342] The angle of the bifurcated halogen bond, $\angle (I \cdots X^- \cdots I)$, was about 145° for Cl^- and about 80° for I^-. This is in line with other crystallographic reports where $\angle (I \cdots X^- \cdots I)$ was frequently close to 180° for Cl^- and Br^-, while for I^- the bond angle varies within the range of 80 to 180° with a slight preference for an orthogonal binding.[342] The larger angles observed for the complexes of smaller halides are explained by the shorter bond lengths resulting in more pronounced steric and electronic repulsion between the bulky halogen-bond-donating iodine atoms and the two cationic donors, respectively, at more acute angles. Accordingly, computations predict that $\angle (I \cdots X^- \cdots I)$ with neutral halogen bond donors is preferentially about 100° for the larger halides[349] and about 110° for the complexation of chloride, but a flat potential energy well for a widening of the bond angle is given.[338]

The complexation of halides by bi- and tridentate iodo-1,2,3-triazolium as well as by bidentate halo-imidazolium anion receptors was reported recently by Huber *et al.* (Scheme 12).[337,347] X-ray diffraction at single crystals of a complex between the bis(iodo-imidazolium) receptor **22I** and bromide revealed a bifurcated halogen bond with a bond angle $\angle (I \cdots Br^- \cdots I)$ of about 74° as well as a dihedral angle between the central phenyl ring and the imidazolium rings of about 60°.[337] A detailed calorimetric binding study revealed the formation of strong 1:1 complexes between **22I** and halides in acetonitrile (Table 4), while no complexation was observed by ITC with the analogous protic receptor **22H**. Although the association constant remained within the same order of magnitude for the different halides, a slight increase in the order $I^- < Br^- < Cl^-$ was observed. The binding enthalpy showed an inverse trend and successively decreased from iodide to chloride

Scheme 11 Halogen *vs.* hydrogen bonds in the formation of a pseudorotaxane (apparent association constants in $CDCl_3$).[346]

This journal is © The Royal Society of Chemistry 2014

Chem. Soc. Rev., 2014, **43**, 2522–2571 | **2541**

Scheme 12 Selected multidentate halogen and hydrogen bond donors (top) and halide–abstraction benchmark reaction (bottom).[337,347,348]

($\Delta H = -16.8$ kJ mol^{-1} for **22I·I$^-$** vs. $\Delta H = -13.5$ kJ mol^{-1} for **22I·Cl$^-$**), but this is overcompensated by an increasing entropic contribution ($T\Delta S = 14.6$ kJ mol^{-1} for **22I·I$^-$** vs. $T\Delta S = 19.7$ kJ mol^{-1} for **22I·Cl$^-$**). Apparently, the higher solvation enthalpy for the more charge-dense chloride lowers the effective binding enthalpy, while the liberation of solvent molecules upon binding promotes the anion complexation entropically. Notably, the anion affinity of the analogous bis(bromo-imidazolium) receptor was significantly reduced (e.g. $K_a = 1.3 \times 10^3$ M^{-1} for Cl$^-$) in line with a reduced polarization of the C–Br bond. Furthermore, a para-substituted bis(iodo-imidazolium) reference system showed a predominant monodentate binding of two halides with a significantly lower association constant (e.g. $K_a = 3.3 \times 10^4$ M^{-1} for Cl$^-$).[337]

An analogous ITC binding study for the bis(iodo-1,2,3-triazolium) receptor **24′I** (Table 4) revealed very similar binding strengths and trends, although a slightly weaker binding was observed throughout the series.[348] Consequently, halide polarization by a triazolium ring is weaker than the polarization by an imidazolium ring, which is expected based on the positioning of two electron-withdrawing nitrogen atoms adjacent to the C–X bond in the latter. As revealed by NMR binding studies in DMSO, the chloride affinity of the bis(iodo-1,2,3-triazolium) receptor **24′I** is significantly enhanced in comparison to the one of the charge-neutral bis(iodo-1,2,3-triazole) reference **23I** and the protic bis(1,2,3-triazolium) reference **24′H** (Table 4),[348]

which, again, emphasizes the great potential of charge-assisted halogen bonding for anion recognition.

The above-mentioned binding trends are in line with the results of a Ritter-type benchmark reaction when using the anion receptors as activating reagents (Scheme 12).[347] In this case, hydrogen or halogen bond formation facilitates the heterolytic C–Br bond cleavage resulting in the formation of a carbenium ion. According to the observed reactivities with the different activators, **24H**, **25H** ≪ **22I**, **24I** ≪ **25I**, the halogen bond donors perform superior to the halogen bond donors, while **25I** resulted in the highest reactivity, suggesting the formation of a trifurcated halogen bond. When using a less reactive test substrate ((1-bromoethyl)benzene), differences in reactivity were observed between activators **22I** and **24I** with the bis(iodo-imidazolium) receptor showing a slightly higher reactivity.[347]

In the end, triazolium-based halogen bond donors show great potential for application in anion recognition and beyond. In view of their synthetic flexibility, manipulation of the anion affinity via substituents at the triazolium ring and by construction of multidentate receptors is readily available. However, structural restrictions imposed by the bulkiness of the halogen-bond-donating atoms as well as by the strict linearity of the halogen bond have to be considered carefully.

5. 1,2,3-Triazoles in metal complexation

Virtually unlimited ligand architectures based on triazoles are available and myriads of applications of the triazole's coordination chemistry have been reported, covering metal ion sensing,[350–352] medicinal chemistry,[199] catalysis,[353–363] magnetic materials,[170,364–366] and photovoltaic[174,367–370] as well as electroluminescent devices.[371,372] In the following paragraphs, the focus will be on CuAAC-derived, 1,4-disubstituted 1H-1,2,3-triazoles and derivatives thereof, as these are certainly the most relevant target structures in view of their facile and modular synthesis allowing ready steric and electronic fine-tuning. Additionally, we will concentrate on the more established N3-coordination of the 1,2,3-triazole, but a comparison to the alternative N2-coordination is also provided. Later, the coordination behavior of the triazolate anion is briefly presented, followed by a more detailed discussion of the coordination via carbanionic, mesoionic carbene, and nitrenium donors of triazole-derivatives (Fig. 25). As we intended to impart general insights and trends, which may serve as a guideline for further applications, only selected references are discussed. Alternatively, an extensive overview of triazole ligands has been provided recently by

Table 4 Selected association constants[337,348]

Host	23I	24′H	24′I			22I		
Guest	Cl$^-$	Cl$^-$	Cl$^-$	Br$^-$	I$^-$	Cl$^-$	Br$^-$	I$^-$
K_{a1} [M^{-1}] by NMR (in d$_6$-DMSO)	20	100	440	—	—	—	—	—
$K_{a1}/10^5$ [M^{-1}] by ITC (in CH$_3$CN)	—	—	3.9	2.1	1.0	5.2	4.5	2.5
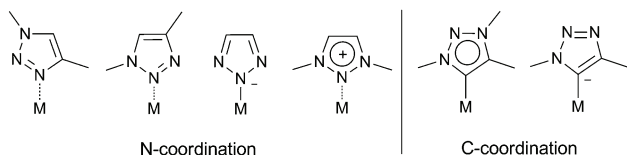
Fig. 25 Coordination modes of 1,2,3-triazoles and derivatives thereof.

Fig. 27 Selected AM1 frontier orbital energies.[131]

Crowley et al.,[373] while Schibli et al. reviewed this topic with an emphasis on medicinal chemistry.[374]

5.1. Triazoles as neutral nitrogen donors

5.1.1. The electronic nature of triazole ligands. The analysis of the contributions to a coordinative bond is not trivial and it has to be cautioned that a relative classification of σ and π effects based on experimental data can be misleading as in most cases only the net result of electrostatic and donor–acceptor interactions is observed. While, in principle, bond dissociation energies and individual binding contributions can be calculated by means of an energy decomposition analysis (EDA),[375] in our case only limited data is currently available.[169]

To assess the triazole's ability to interact with metal centers via σ donation and electrostatic interactions, the above-mentioned order of decreasing proton affinity (cf. Table 2), which correlates with a lowering of the σ lone pair energy, is recalled: imidazole > pyridine > 1H-1,2,3-triazole. This trend is also consistent with a decreasing NBO partial charge of the corresponding nitrogen donor (Fig. 26),[169,199,376] although it has to be cautioned that the partial charge is the net charge of the atom not accounting for anisotropic electron distribution,[377] while the electrostatic interactions with the metal are mainly due to an interaction with the ligand's σ lone pair.[375] Moving down the first group in the periodic table, the calculated relative alkali-metal-ion affinities in the gas phase for imidazole and triazole successively change in favor of the triazole.[149] While Li$^+$ is still significantly more strongly bound by the imidazole, the K$^+$ affinity is higher in the case of triazole.[149,202] The energy-optimized structures for the N3-bound Li$^+$ complex of triazole show a displacement of the Li$^+$ towards N2 to allow a better alignment with the dipole moment (cf. Fig. 26), which is not observed for the Li$^+$ imidazole complex.[149] For the larger K$^+$, this even allows additional stabilization by partial coordination to N2 (bridging) resulting in a cooperatively strengthened binding. However, this binding mode is unavailable in most chelating systems due to structural restraints, as concluded from the vast majority of crystallographic reports (vide infra), and does not reflect the intrinsic donor strength of N3. In addition, the calculated values cannot be confirmed experimentally
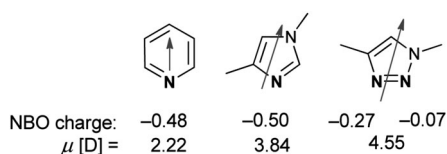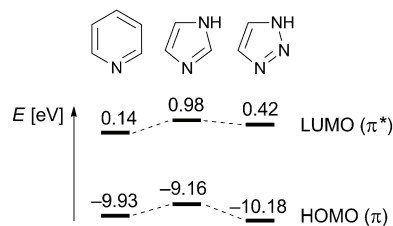
for the unsubstituted triazole due to its tautomerism (see Section 3.5).[149,151] On this basis, the triazole is concluded to be a weaker σ donor than pyridine and imidazole, which is reasonable regarding its high degree of aza substitution.[198]

Apart from metal ions with a closed d-shell, e.g. alkali metals, Ag(I), and Zn(II), for which the metal–ligand interactions are predominantly electrostatic in nature,[169,379,380] transition-metal ions with partially filled d orbitals allow strong σ and π interactions[381] leading to a significant covalent contribution to the coordinative bond.[382,383] Although the orbital coefficients will also play a role, the relative π-donor and π-acceptor properties of the triazole can be estimated by comparing the π and π* orbital energies with those of common donors such as pyridine and imidazole (Fig. 27 and Table 1).[131,144,384] Accordingly, pyridine is expected to be the stronger π acceptor than triazole, while imidazole is expected to be the strongest π donor.

A common yet ambiguous experimental technique to estimate the effective electron donation of a ligand, L, relies on the diagnostic stretching frequencies of carbonyl ligands bound to the metal complex fragment of interest, L–M–C≡O (cf. Tolman's electronic parameter, TEP).[385,386] Stronger σ donation from L strengthens the π back-donation from M into the π*(CO) orbital, which weakens, in turn, the C≡O bond (L–M=C=O). On the other hand, competitive π back-donation to L lowers the π back-donation to the CO ligand. Elliot et al. observed a marginally lower CO stretching frequency with Re(I) triazole complexes in comparison to their pyridine-analogs suggesting a slightly higher effective donor strength in the case of the triazole.[387] It has to be cautioned, however, that the apparently stronger donation is consistent with a weaker σ-donor strength combined with a weaker π-acceptor strength of the triazole, in other words, σ and π effects cannot be differentiated.[386]

In analogy to Lever's electrochemical parameter,[388] the relative σ-donor and π-acceptor strength of triazole and pyridine may alternatively be inferred from the response of the frontier orbital energies of Ru(II) polypyridyl complexes to the gradual replacement of the pyridines with triazoles.[168,250,389–392] In this kind of Ru(II) complexes, the highest occupied molecular orbitals are essentially metal d orbitals, while the lowest unoccupied molecular orbitals are mainly ligand π* orbitals in character, and metal d orbitals undergo π back-donation with low-lying π* ligand orbitals of appropriate symmetry. The lowest-energy electronic transitions are of almost pure metal-to-ligand charge-transfer (MLCT) character. Note that, for Ru(II) complexes, the initially formed singlet excited state immediately undergoes intersystem crossing and vibrational relaxation[393]

Fig. 26 Nitrogen NBO charges for selected donor atoms (bold)[169,199,376] as well as electric dipole moments (grey arrows).[44,140,378]

This journal is © The Royal Society of Chemistry 2014

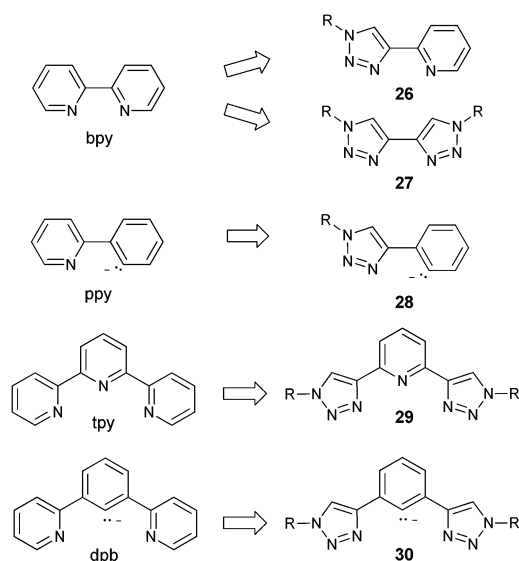Chem. Soc. Rev., 2014, 43, 2522–2571 | 2543

Fig. 28 Examples of bidentate and tridentate polypyridyl ligands and their cyclometalating counterparts as well as their triazole-analogs (note that the ligands are drawn as if coordinated).

resulting in the population of the lowest-energy triplet excited state, which is typically a triplet MLCT (^{3}MLCT) excited state.[394]

When comparing the homoleptic bis(tridenate) or tris(bidentate) Ru(II) complexes of either 2,2′-bipyridine (bpy) or 2,2′:6′,2″-terpyridine (tpy), $i.e.$ [Ru(bpy)$_3$]$^{2+}$ or [Ru(tpy)$_2$]$^{2+}$, with their triazole-containing counterparts, $i.e.$ [Ru(**26/27**)$_3$]$^{2+}$ [390–392] or [Ru(**29**)$_2$]$^{2+}$ [250] (Fig. 28), the replacement of pyridines by triazoles leads to a slight stabilization of the metal-based d orbitals and a pronounced destabilization of the ligand-based π* orbitals (Fig. 29) corresponding to an energetically raised ^{3}MLCT state. Experimentally, this is manifest in the shifts of the redox potentials, $i.e.$ a slightly more positive potential for the metal-based oxidation and a more negative potential for the ligand-based reduction, and in a
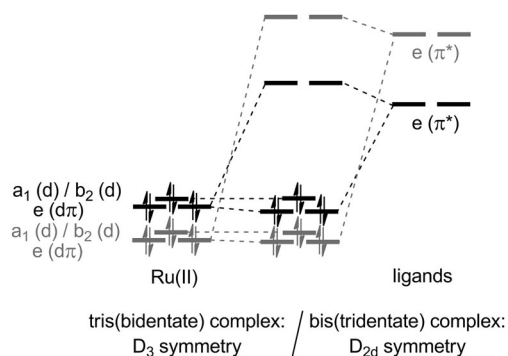
spectral blue shift of the MLCT absorption band.[168,250,389,390,392] This can be rationalized by the higher energy of the π* orbitals of the triazole-based ligand **27** ($cf.$ Fig. 27)[392] and, for ligands composed of both pyridine and triazole, **26** and **29**, additionally by the diminished π conjugation within the chelating ligand system (see Section 3.4).[250] On the other hand, the lowered energy of the occupied metal d orbitals can be ascribed to a weaker electrostatic repulsion between the metal electrons and electrons of the triazole ligands ($cf.$ Fig. 26), in particular the σ lone pair directed towards the metal center. In line with that, DFT calculations indicate that the σ lone pairs of ligand **27** are significantly more stabilized than the ones of bpy.[392]

As further consequence of the weaker σ donation by the triazole, the dσ* orbitals in the resulting complex are expected to be energetically lowered associated with a triplet metal-centered (^{3}MC) excited state of lower energy. For Ru(II) complexes, the latter is prone to radiationless deactivation, causing, if thermally accessible from the ^{3}MLCT, a shortening of the excited-state lifetime and a lowering of the luminescence quantum yield.[394] Exactly this scenario is observed for homoleptic Ru(II) complexes upon replacement of bpy and tpy by **26** and **29**, respectively.[250,389,390] Eventually, if all pyridines are replaced by triazoles, $i.e.$ in the case of [Ru(**27**)$_3$]$^{2+}$,[391,398] the lowest-energy excited state is no longer the ^{3}MLCT but the ^{3}MC instead.[392]

Furthermore, in the case of the heteroleptic Ru(II) complexes, [Ru(bpy)$_2$(**26/27**)]$^{2+}$ [390–392,399] and [Ru(bpy)(**26/27**)$_2$]$^{2+}$ [390–392] as well as [Ru(tpy)(**29**)]$^{2+}$,[168,389] the LUMO is located on the bpy or tpy ligand but it is destabilized relative to [Ru(bpy)$_3$]$^{2+}$ or [Ru(tpy)$_2$]$^{2+}$, respectively. This can be rationalized by an enhanced π back-donation to bpy or tpy in the heteroleptic complexes, $i.e.$ the pyridine-based ligands are of greater π-acceptor strength than their triazole-analogs.[168,392] The high energy of the triazole's π* orbitals is also reflected by the photophysical behavior of Re(I) complexes featuring triazole-containing ligands.[167,176,387,398,400,401]

In the case of cyclometalated Ir(III) and Ru(II) complexes, as a result of a repulsive interaction between an occupied metal d orbital and an energetically high π orbital of the anionic ligand (π donation), the HOMO is located on the metal and the cyclometalating ligand, while the LUMO is located on the charge-neutral polypyridyl ligand. After replacement of 2-phenylpyridine (Hppy) and 1,3-dipyridylbenzene (Hdpb) in [Ir(ppy)$_2$(bpy)]$^+$ and [Ru(dpb)(tpy)]$^+$ by **28**[402–404] and **30**,[168,367,405–407] respectively, the π system of the cyclometalating phenyl ring is less stabilized by the adjacent triazoles ($vide\ supra$), $i.e.$ the triazole-containing cyclometalating ligand is a stronger π donor. At the same time, the π back-bonding with the peripheral triazoles is less efficient. Consequently, the HOMO of the metal complex is higher in energy and the π back-donation into the polypyridyl ligand is reinforced, which leads to an energetically higher LUMO. As the LUMO destabilization is more pronounced than the HOMO destabilization, the energy gap is increased.[168,402,403] On the other hand, when replacing bpy with **26** in [Ir(ppy)$_2$(bpy)]$^+$,[408–411] the energy gap is increased mainly due to a direct LUMO destabilization in line with the energetically higher π* orbitals of the triazole ligand. Ultimately, when combining 1,2,3-triazole-containing

Fig. 29 Simplified MO scheme of [Ru(bpy)$_3$]$^{2+}$ or [Ru(tpy)$_2$]$^{2+}$ (black) and [Ru(**26/27**)$_3$]$^{2+}$ or [Ru(**29**)$_2$]$^{2+}$ (grey) illustrating the differences in π back-donation between the pyridine- and triazole-based ligands (σ interactions omitted for clarity; note that, in D_3-symmetric tris(bidentate) Ru(II) complexes, the LUMO is a non-interacting π*(a$_2$) ligand orbital (not shown), while in D_{2d}-symmetric bis(tridentate) Ru(II) complexes, the degenerate π*(e) ligand orbitals mostly represent the LUMO).[392,395–397]

cyclometalating and ancillary ligands, Ir(III)-based blue triplet emitters are obtained.[412,413]

In contrast to Ru(II) complexes, the energetical separation between e_g (dσ^*) and t_{2g} (dπ) orbitals (if O_h symmetry is assumed for simplicity) is small in Fe(II) complexes.[386] Accordingly, a transition from low spin (t_{2g}^6) to high spin ($t_{2g}^4 e_g^2$) was reported for bis(tridentate) Fe(II) complexes of triazole-containing ligands.[170,364] Among the most prominent Fe(II) complexes showing a spin-transition behavior are complexes of 2,6-bis(1H-pyrazol-1-yl)-pyridine ligands, which exhibit a spin crossover below room temperature.[414] Replacement of one[364] or both (29)[170] pyrazoles of the tridentate ligand framework by triazoles shifts the spin transition above room temperature, which is consistent with an increased ligand-field strength of the triazole-containing ligands causing a larger energy splitting between low-spin and high-spin states.[415] Based on the lower π^* orbital energy of the triazole in comparison to pyrazole (Table 1), this can be attributed to a higher π-acceptor strength of the former, which allows a better stabilization of the t_{2g} (dπ) orbitals. Accordingly, an even higher spin-transition temperature has been observed for Fe(II) complexes of 29, when the π-acceptor character of the ligand was increased by placing electron-withdrawing substituents at the triazoles.[170] In contrast, [Fe(tpy)$_2$]$^{2+}$ hardly undergoes spin transition, which can be ascribed to a larger e_g (dσ^*) destabilization and t_{2g} (dπ) stabilization due to a higher σ-donor and π-acceptor strength, respectively. Apart from electronic consequences when replacing pyridines with triazoles to give [Fe(29)$_2$]$^{2+}$, a reduced steric demand and, hence, an increased flexibility results (see Section 5.1.4). As for Fe(II) complexes of 2,6-bis(1H-pyrazol-1-yl)pyridines,[414,416] the triazole-containing analogs can undergo a stabilizing angular Jahn–Teller distortion in the high-spin state,[364] which is preserved in the solid state upon cooling, i.e. the high-spin configuration is trapped.[170] In the case of [Fe(tpy)$_2$]$^{2+}$, a lowering of the spin-transition temperature via a distortion of the complex requires external forces[417] or bulky substituents.[418] Consequently, the triazole-containing complexes structurally resemble the pyrazole-based Fe(II) complexes, while they impose a stronger ligand field, thus being electronically more related to [Fe(tpy)$_2$]$^{2+}$.[251]

Noteworthy, for Ni(II) complexes of bidentate ligands featuring triazole and pyridine donors (26), several computed bond indices indicate a stronger bond between the triazole and the metal.[419] Similarly, for a tris(bidentate) Ni(II) complex of 26, a slightly higher σ-donor strength has been deduced for triazole on the basis of a theoretical ligand field analysis.[420] However, these results are in contradiction with the experimental findings mentioned above and below.

In order to investigate the potential to influence the electronic properties of 1,2,3-triazole complexes by varying their N-substituent, Crowley et al. studied a series of Re(I) complexes bearing functionalized 1,2,3-triazole-containing ligands (cf. 26).[176] However, the photophysical and electrochemical properties of the complexes remained surprisingly constant despite the presence of either π-electron-withdrawing (4-nitrophenyl) or π-electron-donating (4-methoxyphenyl) substituents. Likewise,

the variation of the C-substituent within a series of Re(I) complexes featuring inverted pyridyl-1,2,3-triazole connectivity (see Section 5.1.5) only had a modest effect on the photophysical and electrochemical properties of the complexes.[421] This behavior is surprising, since, for uncomplexed 1,2,3-triazoles, extended conjugation of the HOMO and the LUMO onto the C- and the N-substituent, respectively, is expected (see Section 3.4).[158] Additionally, other examples have been reported where the variation of the substituents of the 1,2,3-triazole had a noticeable influence on the electronic properties of the metal complex,[422,423] although the effect is less pronounced than for pyridine.[170] Ultimately, the effect of varying substituents of 1,2,3-triazole ligands on the photophysical and electrochemical properties of the corresponding metal complexes can hardly be generalized as it depends, amongst others, on the localization of the frontier orbitals in the complex[175] and, thus, on the type of the ligand as well as on the metal center.

In conclusion, the analysis of the photophysical and electrochemical response in particular of Ru(II) polypyridyl complexes to the introduction of triazole-analogs as ligands reveals a weaker σ-donor and π-acceptor strength of the triazole relative to pyridine. Ultimately, the difference in electronic nature between triazole and pyridine ligands has important implications for the photophysical properties, e.g., of the corresponding Ru(II) or Ir(III) complexes, which is relevant for applications in photovoltaic[168,174,367] and electroluminescent devices[371,372,404,409,412,424] as well as photo-redox catalysis.[425] Furthermore, on account of the higher π-acceptor strength relative to pyrazole, triazoles can serve as valuable ligands in the design of magnetic materials.[170,364,365]

5.1.2. Stability of triazole-based coordination compounds. A particular problem arising for binding studies that compare ligands composed of different donor types is the potential interference from effects other than the intrinsic coordinative bond strength, e.g. differences in structural parameters, steric demands, and solvation enthalpy and entropy. Some of these points are addressed in the following, but in most cases "stronger binding" denotes "thermodynamically preferred". We thus selected examples that either show a high comparability due to their experimental design or that demonstrate the practical outcome when introducing triazoles into relevant chelating ligands. The latter is important since the triazole is particularly suited to construct various multidentate ligand systems in view of the high synthetic flexibility brought by click chemistry.

A direct demonstration of the relative bond strength of pyridine and triazole is provided by Benny et al. who used a tripodal ligand that features three different donor arms including a pyridine and a triazole donor (Scheme 13, top).[426] The ligand binds Re(I) or ^{99m}Tc(I) in a tridentate, facial coordination mode involving two arms only giving rise to intramolecular ligand competition. At high pH values, the triazole is replaced by a carboxylate (31b), while, at lower pH values, the carboxylate is cleaved and the dangling triazole arm can re-coordinate again (31a). This interconversion is reversible and can be monitored by ^{1}H NMR spectroscopy; however, no sign of pyridine decoordination was observed, which suggests a significantly more stable coordination in the case of the pyridine. Importantly, the
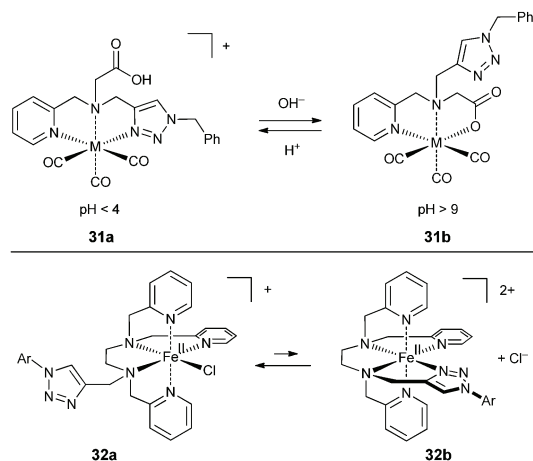
Scheme 13 Intramolecular ligand competition demonstrating the stronger coordination of pyridine over triazole (M = Re(I) and ^{99m}Tc(I), Ar = *p*-anisyl).[354,426]

intramolecular ligand exchange of either a pyridine or a triazole by the carboxylate minimizes interference from steric differences between pyridine and triazole (*vide infra*).

Similarly, Rebilly, Banse *et al.* reported an Fe(II) complex of a podand ligand building on an ethylenediamine fragment with three pyridines and one triazole as additional donors (**32b**, Scheme 13, bottom).[354] As inferred from UV-vis absorption and cyclic voltammetry experiments in acetonitrile, in the presence of one equivalent of chloride the triazole arm is mostly replaced by a chloro ligand (**32a**), which identifies the Fe(II)–triazole bond as weaker than the analogous Fe(II)–pyridine bond.

Reinaud *et al.* reported another test system consisting of a calix[6]arene decorated with either three triazoles, imidazoles, or pyridines (**33**, **34**, **35**, Fig. 30).[427] A varying coordination behavior depending on the nature of the metal was observed: for electron rich, soft metals, Cu(I) in this case, only a weak binding was found for the imidazole (**34**) and triazole ligand (**33**) in acetonitrile with the metal dynamically coordinating only two of three donors at once ("dancing"), suggesting that the coordination is not stabilized by strong π back-donation. If a strongly π-accepting carbonyl ligand is simultaneously coordinated to the Cu(I), the metal center is less electron-rich and the σ donation by imidazole or triazole becomes more important resulting in the coordination of all three N-donors, *i.e.* a cooperatively strengthened coordination is given. In contrast, coordination of three pyridines and neither "dancing" nor CO coordination was found for the Cu(I) complex of **35**, demonstrating the stronger π-accepting character of pyridine, which stabilizes the Cu(I) complex.[427,428] In comparison,
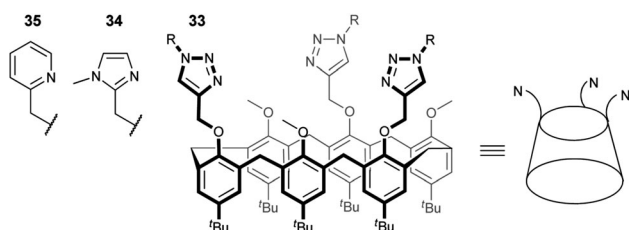

**Fig. 30** Pyridine-, imidazole-, and triazole-functionalized calix[6]arenes.[427]

when using an electron-poor and hard metal center like Zn(II), the imidazole complex is more stable than the pyridine complex as the stabilization mainly results from σ donation and electrostatic interactions (chloroform was used as solvent in this case). Apparently, the triazole complex is of intermediate stability as long as no electron-withdrawing substituents are attached to the triazole.[427] Since triazole is expected to be a less strong σ donor than pyridine, the increased stability of the Zn(II) triazole complex may originate from its larger dipole moment[198] (Fig. 26 and Table 1) or a partial bridging with N2[149] (*vide supra*) in this case. Noteworthy, in other Zn(II) complexes of podand ligands featuring pyridine and triazole donors, a weaker Zn(II)–triazole bond has been inferred.[429,430]

Besides the above mentioned flexible ligands, polydentate ligands that are composed of contiguous aromatic N-heterocycles represent another important ligand class including polypyridines (*cf.* Fig. 28). Hecht, Limberg *et al.* investigated the coordination behavior of a series of tpy-analogous 2,6-bis(1*H*-1,2,3-triazol-4-yl)pyridines (**29**) with Fe(II) using ITC (Table 5 and Scheme 14).[170] For 4-tolyl-N-substituted triazoles, depending on whether the substituent on the central pyridine ring is either electron-donating (R^1 = OTg with Tg = triethylene glycole) or electron-withdrawing (R^1 = COOTg), binding enthalpies of −64 and −62 kJ mol^{-1}, respectively, and cumulative association constants (β) of 1.4×10^8 and 6.1×10^7 M^{-2}, respectively, were determined for the formation of [Fe(**29**)$_2$](OTf)$_2$ in acetonitrile by successive addition of an Fe(II) triflate solution to the ligand solution. Furthermore, the possibility of controlling the binding enthalpy by variation of the triazole substituents was investigated using strongly electron-releasing and electron-withdrawing substituents like 4-(*N*,*N*-dimethylamino)phenyl and 4-nitrophenyl, respectively (Scheme 14 and Table 5). Accordingly, the binding enthalpies correlate linearly with Hammett's σ_{para} values[183] and are weakened if the triazoles are functionalized with EWGs suggesting that the binding strength predominantly results from σ donation with only little compensation by a simultaneously increased π back-donation. Furthermore, larger influences of the triazole substituents were observed in the case of an electron-rich central pyridine ring (R^1 = OTg) instead of an electron-poor pyridine (R^1 = COOTg) as binding enthalpies ranging from −55 to −76 kJ mol^{-1} and from −58 to −64 kJ mol^{-1}, respectively, were obtained.[170]

It is interesting to compare these thermodynamic parameters with the data for the Fe(II) complexation with tpy. By addition of an acetonitrile solution of Fe(II) perchlorate hexahydrate to the tpy ligand dissolved in the same solvent, the immediate formation of [Fe(tpy)$_2$](ClO$_4$)$_2$ is observed and a binding enthalpy of −160.7 kJ mol^{-1} was determined corresponding to a β of at least 10^{16} M^{-2}.[431,432] Notably, a different Fe(II) source was used in this case, although the effect of the weakly coordinating counterions (perchlorate *vs.* triflate) should be negligible in a strongly coordinating solvent like acetonitrile.[433] Furthermore, when dissolving a 1:2 mixture of [Fe(**29**)$_2$]$^{2+}$ and free **29** in acetonitrile, a single set of broad signals was observed in the ^{1}H NMR spectrum due to a ligand exchange faster than the NMR timescale (note that [Fe(**29**)$_2$]$^{2+}$ is a low-spin complex at ambient temperature). In contrast, for a 1:2 mixture of [Fe(tpy)$_2$]$^{2+}$ and free tpy, two distinct sets of tpy signals for

2546 | *Chem. Soc. Rev.*, 2014, **43**, 2522–2571

This journal is © The Royal Society of Chemistry 2014

Table 5 Thermodynamic parameters for the Fe(II) complexation with 2,6-bis(1H-1,2,3-triazol-4-yl)pyridine ligands (at 298 K, cf. Scheme 14)[170]

| R² =	R¹ = OTg				R¹ = COOTg			
	β [M⁻²]	ΔG [kJ mol⁻¹]	ΔH [kJ mol⁻¹]	$T\Delta S$ [kJ mol⁻¹]	β [M⁻²]	ΔG [kJ mol⁻¹]	ΔH [kJ mol⁻¹]	$T\Delta S$ [kJ mol⁻¹]
4-(N,N-Dimethylamino)phenyl	1.1×10^8	−45.8	−75.9	−30.1	6.2×10^7	−44.6	−64.1	−19.5
4-Tolyl	1.4×10^8	−46.5	−64.2	−17.7	6.1×10^7	−44.5	−61.7	−17.2
4-Nitrophenyl	3.0×10^7	−42.7	−54.8	−12.1	3.0×10^6	−37.0	−57.9	−20.9
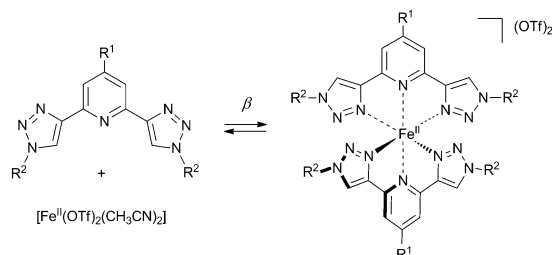
Scheme 14 Formation of bis(tridentate) Fe(II) complexes of 2,6-bis(1,2,3-triazol-4-yl)pyridine ligands (cf. Table 5).[170]

the bis(tridentate) complex and the free tpy ligand were observed with the expected 1:1 ratio (note that $K_2 \gg K_1$ for [Fe(tpy)₂]²⁺[434]), which is in line with a slow ligand exchange.[435] In dichloromethane, however, two signal sets were observed also for the triazole-system. Furthermore, addition of two equivalents of tpy to [Fe(**29**)₂]²⁺ in acetonitrile leads to the complete interconversion to [Fe(tpy)₂]²⁺ and uncomplexed **29**.[170] Moreover, for the formation of [Fe(**29**)₂](OTf)₂ in acetonitrile at 298 K, the entropic term ($T\Delta S$) is in the range of about −12 to −30 kJ mol⁻¹,[170] while it falls between −40 and −70 kJ mol⁻¹ for the formation of [Fe(tpy)₂](ClO₄)₂, if we assume $\beta = 10^{21}$ M⁻² as the higher[434] and $\beta = 10^{16}$ M⁻² as the lower limit and $\Delta H = -160.7$ kJ mol⁻¹.[431] Accordingly, the complexation is entropically less disfavored in the case of the triazole-containing ligand. It is tempting to speculate whether extensive interactions via hydrogen bonding and dipole–dipole interactions between the triazoles and the polar solvent (as discussed in the context of anion binding by triazoles, vide supra) may lower the complexation enthalpy,[154] while, on the other hand, the liberation of solvent molecules upon complex formation may support the complexation entropically.[436] Additionally, the more open coordination sphere due to the reduced steric demand of the triazole (see Section 5.1.4) may lead to a more severe solvent competition, i.e. a lower complex stability by perturbation of the coordination and an increased lability by allowing a more associative ligand exchange character (note that, however, Fe(II) usually shows a dissociative interchange mechanism).[439] Furthermore, structural constraints upon replacement of pyridines by triazoles, i.e. a more acute bite angle due to the replacement of six-membered by five-membered rings,[250] may further enhance the lability ("kinetic chelate strain effect").[437] Ultimately, other effects than the coordinative bond strength provided by the triazole may play an important role in the complexation thermodynamics and kinetics; however, without further experimental insights this remains speculative.

Similar to the bis(tridentate) Fe(II) complexes, Petitjean et al. observed much lower binding constants for the formation of bis(bidentate) Cu(I) complexes with 2-(1H-1-benzyl-1,2,3-triazol-4-yl)pyridine (**26**, cf. Fig. 28) in comparison with bpy.[438] UV-vis titration in acetonitrile/chloroform (1:1) of bpy and its triazole-analog with [Cu(CH₃CN)₄]BF₄ revealed a β of about 10^{10} M⁻² and 10^5 M⁻², respectively (corresponding to a ΔG of about −57 kJ mol⁻¹ and −29 kJ mol⁻¹, respectively).[438]

Nonetheless, in the case of multidentate ligands and metal centers that typically afford stable and inert complexes, e.g. Ru(II) and Ir(III),[439] the triazole can be conveniently used in place of other donors without overly compromising the complex stability. Accordingly, heteroleptic complexes of, e.g., Ru(II)[389,390] can be synthesized (vide supra), which requires slow ligand exchange kinetics. Furthermore, stable and inert high-molar-mass Ru(II) coordination polymers can be formed with ditopic tridentate ligands based on **29**.[440]

Although the above studies on multidentate ligands are of high practical relevance, an unstrained, monodentate coordination is more suitable to judge the individual coordination strength of the triazole. Van Koten, Klein Gebbink et al. elegantly used a cyclo-metalated Pt(II) N^C^N-pincer complex as probe,[441] which offers a single vacant coordination site where a ligand can coordinate in a labile fashion due to the trans effect imposed by the strong carbanionic donor.[442] Thus, by using equal amounts of a tetra-coordinate Pt(II) complex featuring a triazole-based reference ligand (**36a**) and a competitive ligand, the established equilibrium is a direct measure for the relative binding strength of both ligands (Scheme 15). Assuming that steric effects are negligible in this case, the binding strength of triazoles noticeably depends on the C- and N-substituents and increases in the order phenyl < H < benzyl < alkyl (cf. **36a**–**36d**). In the case of **36d**, the triazole approaches the binding strength provided by pyridine, while imidazole allows a superior binding over triazole and pyridine, i.e. the complete replacement of the triazole reference ligand by imidazole. The crystal structures of the Pt(II) complexes with triazoles **36a** and **36c** reveal a linear coordination via N3 with the triazole ring being twisted out of the plane of the N^C^N pincer ligand, which is expected to enable a rather weak π back-donation.[443] Assuming an out-of-plane arrangement also for the other aromatic ligands, the above ranking appears to be dictated by the σ-donor strength,[444] which is corroborated by the stronger binding of imidazole in comparison to pyridine (vide supra). Furthermore, the observed bond lengths between triazole and Pt(II) apparently correlate with the observed binding strengths, i.e. the Pt–N3(**36a**) bond is significantly longer than the Pt–N3(**36c**) bond (2.149(2) and 2.139(2) Å, respectively).[441] A similar trend has
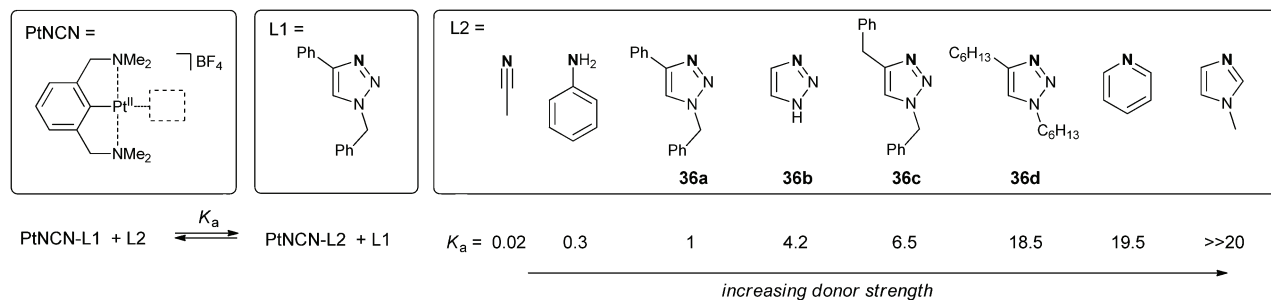
Scheme 15 Competitive binding strength of selected ligands (donor atoms in boldface, determined in d_6-acetone).[441]

also been observed for Pd(II) complexes.[445] The influence of the substituents is also reflected by the variation of the NBO charge of N3, which was calculated to be, *e.g.*, −0.28 and −0.22 in the case of a methyl and carboxy substituent, respectively, in the 4-position.[376]

5.1.3. Bond lengths. It is of importance to note that the bond strength–bond length correlation only holds for identical types of donors. Since various contributions act together in a (coordinative) bond, *e.g.*, σ- and π-orbital interactions as well as electrostatic interactions, the bond strength *cannot* be correlated with the bond length for different types of donors.[383,446,447]

When comparing analogous pyridine and triazole complexes, shorter bond lengths have been reported in the case of the triazole for a variety of ligand architectures and metal centers, *e.g.* monodentate complexes of Pt(II),[441,448] bidentate complexes of Ru(II)[423] and Ir(III),[372,449] and tridentate Ru(II)[168,170,250] complexes. The former suggests that this is not just due to structural restraints within a chelating ligand. Also if pyridine and triazole donors are combined within the same ligand, the same trend is observed for various transition metal complexes, *e.g.* of Ni(II),[420] Ru(II),[423] Pd(II),[165] Re(I),[167,176,401] Ir(III),[100] and Pt(II)[165] and even if the triazole is coordinated *via* N2,[421,445] which is a very weak donor (see Section 5.1.5). Occasionally, comparable metal–N bond lengths with pyridine and triazole have been reported for Cu(I),[438] Ni(II),[357] and Re(I)[387] complexes. By trend, however, the triazole affords shorter coordinative bond lengths than pyridine, but, with respect to the above binding studies, the shorter bond lengths do *not* imply a stronger coordination in this case.

Besides different steric demands[250] (see Section 5.1.4) and differences in electrostatic contributions (larger dipole moment but lower partial charge at the nitrogen donor for triazole), a potential explanation may be the difference in p character of the σ lone pair when comparing five- and six-membered-ring heterocycles. The more acute bond angle at the nitrogen donor in the five-membered ring (triazole = 108.9° *vs.* pyridine = 117.3°)[445] is expected to increase the s character of the in-plane σ lone pair,[450,451] which would reduce its size (orbital coefficient) and lower its energy.[446,452,453] A parallel trend is found for N-heterocyclic carbenes.[454] In addition, in the case of triazole, both N3 and N2 feature adjacent electron-withdrawing nitrogen atoms which may increase the p character of the ring N–N bonds while increasing the s character of the σ lone pair (*cf.* Bent's rule).[455] On the other hand, a larger p orbital contribution to the σ lone pair is anticipated for pyridine,

which would result in a more efficient charge transfer even at longer distances as well as an increased energy of the σ lone pair.[381]

5.1.4. Steric effects of triazole-based ligands. An exclusive feature of the 1,2,3-triazole in comparison to pyridine or imidazole is the presence of a nitrogen atom adjacent to the nitrogen donor reducing the steric demand of the ligand, which has important implications for the flexibility and the lability of the corresponding transition-metal complexes. In the following, we focus on the triazole's N3-donor noting that an analogous effect can be expected for coordination *via* N2, too.

Petitjean *et al.* investigated the redox behavior of Cu(I) complexes of the bpy-analog 2-(1H-1,2,3-triazol-4-yl)pyridine (**26**, Scheme 16).[438] In a weakly electron-donating/non-coordinating solvent like dichloromethane, the oxidation of $[\text{Cu}^{\text{I}}(\textbf{26})_2]^+$ requires a more positive potential than for $[\text{Cu}^{\text{I}}(\text{bpy})_2]^+$, which is expected on account of the weaker σ donation from the triazole (*vide supra*). Interestingly, in a strongly electron-donating/coordinating solvent like THF,[226] the redox potential of $[\text{Cu}^{\text{I}}(\textbf{26})_2]^+$ is significantly lowered (by almost 0.4 V) and even slightly below the potential of $[\text{Cu}^{\text{I}}(\text{bpy})_2]^+$. This can be attributed to the reduced steric demand of the triazole facilitating a structural transition from a tetrahedral to a square-planar coordination for $[\text{Cu}^{\text{II}}(\textbf{26})_2]^{2+}$, which is stabilized by coordination of solvent molecules in axial positions. In the resulting distorted
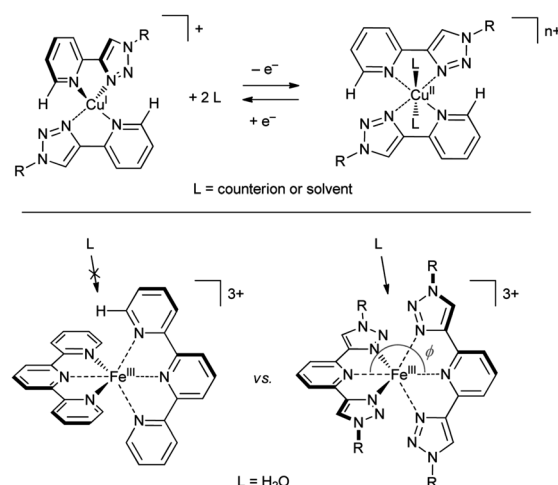
Scheme 16 Reduced steric demand of triazole-containing chelates in comparison to polypyridines.[250,438]

2548 | Chem. Soc. Rev., 2014, 43, 2522–2571

This journal is © The Royal Society of Chemistry 2014

octahedral coordination, the bidentate ligands occupy the equatorial positions in a mutual head-to-tail (*i.e.* antiparallel) arrangement[366,456,457] in order to avoid repulsion between the pyridines and, according to DFT calculations,[419] enable hydrogen bonding between the 6-proton of the pyridine and the 2-nitrogen of the triazole (*cf.* Scheme 16). The same antiparallel, planar arrangement of **26** was confirmed by single-crystal X-ray diffraction for Pd(II),[445] Ni(II),[357] and Zn(II)[419] complexes. In the case of $[Cu^{II}(bpy)_2]^{2+}$, in an energetically favorable in-plane coordination of two bpy ligands the 6,6′-protons of the different ligands would encounter, which is avoided by alternative octahedral or distorted trigonal-bipyramidal coordination.[458,459] In contrast, the Cu(I) complexes featuring triazole-based ligands allow a defined, redox-mediated switching from an orthogonal wrapping of both ligands around the metal center to an extended linear arrangement with respect to the triazole substituents, which makes them attractive for application in molecular machines.[438]

Also for bis(tridentate) Fe(II) complexes of 2,6-bis(1*H*-1,2,3-triazol-4-yl)pyridine ligands (**29**, Scheme 16), a different redox behavior than for the analogous tpy complex has been noted by Flood *et al.*[250] With an increasing amount of water in the electrolyte, the current of the reduction peak of the electrochemically generated $[Fe^{III}(29)_2]^{3+}$ is successively decreased, while a second reduction wave at much lower potentials is simultaneously built up. Thus, the formation of a seven-coordinate, aquated complex, $[Fe^{III}(29)_2H_2O]^{3+}$, has been proposed, which may additionally undergo a subsequent displacement of one of the triazole-arms; however, this process is fully reversible upon regeneration of the Fe(II) center. Notably, such redox behavior is not observed for $[Fe^{II}(tpy)_2]^{2+}$, which is apparently less susceptible to stabilization by an additional ligand in its oxidized Fe(III) state. This difference can be rationalized by the reduced steric demand of the triazole-ligand **29** causing a more exposed metal center as well as a shallower calculated potential-energy well for the angular distortion of a ligand plane (ϕ, *cf.* Scheme 16).[250]

For the above-mentioned Zn(II) complexes featuring calix[6]arene-based ligands studied by Reinaud *et al.* (Fig. 30), in the case of triazole arms (**33**), a more rapid exchange of guest ligands (G) bound within the cavity was observed than with imidazole arms (**34**, Fig. 31).[427] Again, the higher lability of the triazole-based system may be attributed to the triazole's reduced steric demand allowing the transient formation of a five-coordinate complex by remote coordination of, *e.g.*, a solvent molecule, thereby enabling a rapid guest-ligand exchange. This is corroborated by the observation that the guest ligand G is more weakly bound to Zn(II) in the case of the triazole system when compared to its imidazole counterpart, in other words, the remote coordination lowers the Lewis acidity of the Zn(II) center. In contrast, the imidazole features an α-CH-group preventing competitive remote coordination and associative ligand exchange.[427] Consequently, the more open coordination sphere brought about by the triazoles has important implications for both thermodynamics and kinetics of the corresponding coordination compounds.

5.1.5. Regular *vs.* inverse coordination. 1,4-Disubstituted 1*H*-1,2,3-triazoles offer two different nitrogen donors, which can coordinate individually or simultaneously in a bridging fashion.[91,169,366,460,461] A prime example for the latter is the dimeric Cu(I) complex of TBTA (Fig. 32), which is one of the most efficient CuAAC catalysts (see Section 2.2).[90,91] However, to understand the properties of both nitrogen donors, only individual coordination is considered in this paragraph.

In comparison to the "regular" coordination *via* the 3-nitrogen of the triazole, exploitation of the 2-nitrogen for metal coordination implies permutation of azide and alkyne building blocks and can thus be regarded as "inverse" connectivity (Fig. 33). Schibli *et al.* first directly compared the coordination *via* N3 (**37a**) and N2 (**37b**) using otherwise identical chelators in the formation of Re(I) and radiolabeled ^{99m}Tc(I) complexes.[199] The determined ^{99m}Tc-labelling capacities were much higher in the case of coordination *via* N3, which, in turn, was a littler lower than for the analogous *N*-methyl imidazole-based ligand, *i.e. N*-methyl histidine. The increased complex stability was attributed to the higher electron density at N3 (*vide infra*).[199] Consistently, for a Zn(II) triazole complex, DFT calculations indicate a stability that is 20% higher for the N3-coordination than for the N2-coordination.[462]
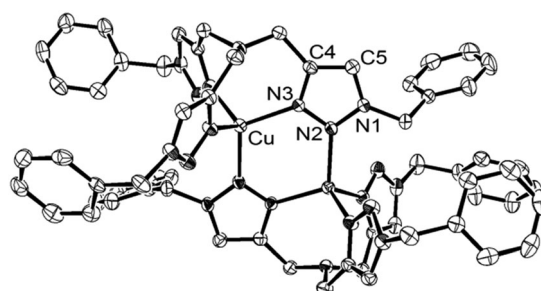
Fig. 32 Solid-state structure of a Cu(I) TBTA complex (thermal ellipsoids drawn at 50% probability level, solvent molecules, counterions, and hydrogen atoms omitted for clarity).[91]

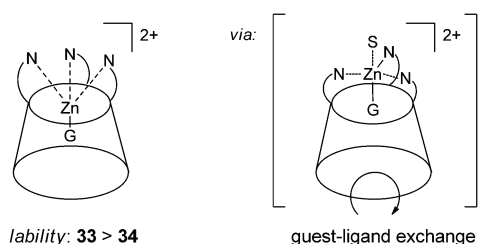*lability*: **33** > **34**   guest-ligand exchange

Fig. 31 Faster guest-ligand exchange on the triazole-based Zn(II) cavitands due to more open sterics facilitating an associative mechanism (S = residual H_2O in $CHCl_3$, *cf.* Fig. 30).[427]

37a   **37b**
"regular"   "inverse"
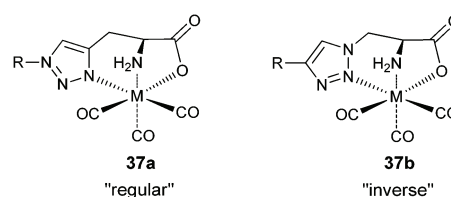
Fig. 33 "Regular" *vs.* "inverse" coordination (M = Re(I), ^{99m}Tc(I), R = various biomolecules).[199]

This journal is © The Royal Society of Chemistry 2014

Chem. Soc. Rev., 2014, **43**, 2522–2571 | 2549
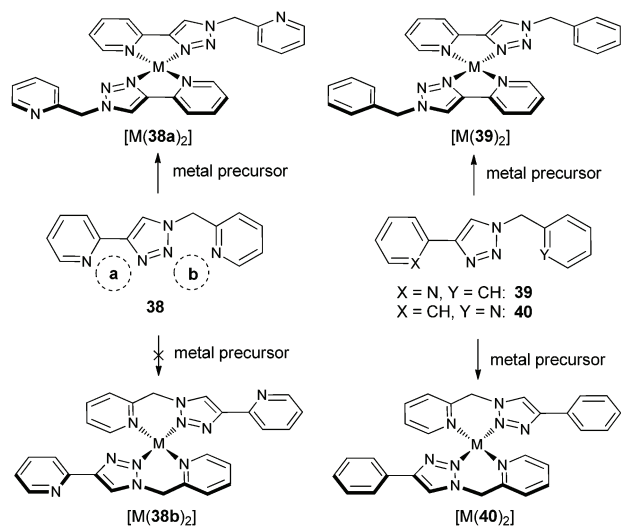
Scheme 17 Competitive binding study to demonstrate the stronger donation from the 3-nitrogen (the available binding sites of **38** are denoted with dashed circles, metal precursor = [Pd(CH$_3$CN)$_4$](BF$_4$)$_2$ or Cu(ClO$_4$)$_2$·6H$_2$O, M = Pd^{2+} or Cu(ClO$_4$)$_2$).[366,445]

The stronger binding by N3 was demonstrated directly in a competitive binding study with Pd(II) by Crowley et al. and with Cu(II) by Dalal, Shatruk, Zhu et al. (Scheme 17).[366,445] When employing a ligand that offers two binding sites involving either the N2 or N3 of the triazole along with a pyridine donor (**38**), solely an N3-bound, square-planar bis(bidentate) Pd(II) complex, [Pd(**38a**)$_2$]$^{2+}$, or a distorted octahedral Cu(II) complex with **38** occupying the equatorial positions, [Cu(**38a**)$_2$(ClO$_4$)$_2$], is obtained (Scheme 17, left). Formation of the N2-bound analogs is enabled if bidentate coordination via N3 is unavailable (**40**), and the complexes [Pd(**40**)$_2$]$^{2+}$ and [Cu(**40**)$_2$(ClO$_4$)$_2$] can be isolated (Scheme 17, right). When compared by means of DFT calculations, [Pd(**38a**)$_2$]$^{2+}$ is more stable in vacuum than the hypothetical [Pd(**38b**)$_2$]$^{2+}$ by about 80 kJ mol^{-1}.[445] In the case of the Cu(II) complexes, ITC experiments were conducted in acetonitrile at 298 K and the estimated cumulative association constant (β) for the formation of a 2:1 complex between Cu(ClO$_4$)$_2$ and **39** or **40** was about 100 times higher for [Cu(**39**)$_2$(ClO$_4$)$_2$] than for [Cu(**40**)$_2$(ClO$_4$)$_2$]. Interestingly, the entropic term ($T\Delta S$) of about -50 kJ mol^{-1} and -40 kJ mol^{-1}, respectively, represents a relatively high penalty, in particular for the formation of [Cu(**39**)$_2$(ClO$_4$)$_2$]. As a consequence, the binding Gibbs energies (ΔG) of about -40 kJ mol^{-1} and -30 kJ mol^{-1} for the Cu(II) complexation with **39** and **40**, respectively, are more similar than the binding enthalpies (ΔH) of about -90 kJ mol^{-1} and -70 kJ mol^{-1}, respectively. Importantly, the differences cannot be correlated solely with the involved donors N3 and N2 as the complexes differ in the size of the chelating ring. While in all cases the bidentate ligands adopt an antiparallel arrangement (vide supra), in the complexes of **40**, the methylene bridge of the six-membered-ring chelator enforces a twisted square-planar coordination[366,445,463] that potentially diminishes π interactions. Moreover, the methylene bridge can adopt a syn- or an anti-arrangement with both being in a dynamic

equilibrium as inferred from variable-temperature NMR experiments in the case of [Pd(**40**)$_2$]$^{2+}$.[464] The greater flexibility may also explain the smaller entropic penalty for the formation of [Cu(**40**)$_2$(ClO$_4$)$_2$]. Furthermore, in line with the above-mentioned influence of the triazole's substituents on the binding strength (cf. Scheme 15), for the N3- and N2-coordinated Pd(II) complexes a significantly shorter Pd–N(triazole) bond was observed when the respective N1- and C4-substituents were benzyl instead of phenyl.[445]

As for the latter examples, coordination via the triazole's N2 along with a pyridine donor often involves a six-membered-ring chelator featuring a methylene bridge between the two aromatic donors (cf. Scheme 17),[169,421,422,445,465] because it is synthetically more difficult to install the azide function at a pyridine ring, in particular multiple azides.[252,257] Nonetheless, a 2-(1H-1,2,3-triazol-1-yl)pyridine ligand featuring C–N connectivity has been presented as well,[174] which allows a better comparison to its counterpart with C–C connectivity (**26**). According to DFT calculations, the direct C–N connectivity allows an extension of the π^* orbitals over both triazole and pyridine (see Section 3.4).[174] Thus, a higher π-acceptor strength of the bidentate ligand coordinating via N2 is expected due to the energetically lowered π^* orbitals.

To gain deeper insights into the two N-coordination modes of the triazole, De Proft, Košmrlj et al. studied a series of transition-metal complexes of regular and inverse bidentate ligands (Fig. 34) both experimentally and theoretically.[169] Notably, the investigated ligands already represent a minimal ligand system, which cannot be further simplified since an auxiliary donor has to enforce the evidently weaker N2-coordination.[441] Experimentally, stable inverse complexes of Cu(II), Ag(I), Pd(II), Pt(II), and Ru(II) were obtained only with ligand **40**, but not with **41a**. For the regular ligand **41b**, at least the formation of a stable Pt(II) complex was observed.[169,376] While the partial charge (Fig. 34) only reflects the net charge of the atom,[377] still the interaction with the σ lone pair is expected to increase in the order N2 < N3 < pyridine < amine parallel to the increasing base strength (see Section 3.5).[226] Accordingly, the complex stability in this series is not governed by the σ-donor strength alone and the necessity of a pendant pyridine group (**40**) to achieve stable complexes can be ascribed to the π back-donation with the pyridine, which provides a stronger binding itself, but also makes the metal center more electrophilic and, hence, cooperatively strengthens the triazole's σ donation.[169,427]

Furthermore, model complexes of the above-mentioned metal centers featuring the bidentate ligand **40** or **41a/b** as well as additional ammine ligands (NH$_3$) were investigated theoretically.
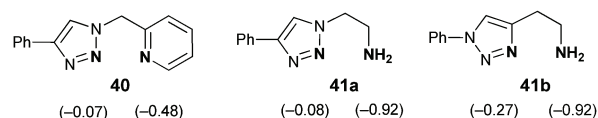

Fig. 34 Regular and inverse bidentate chelators examined in the complexation of Cu(II), Ag(I), Pd(II), Pt(II), and Ru(II) including the NBO charges of the different nitrogen donors (bold).[169]

2550 | Chem. Soc. Rev., 2014, 43, 2522–2571

This journal is © The Royal Society of Chemistry 2014

By the help of an EDA,[375] the contributions from orbital and electrostatic interactions to the attractive interactions were analyzed. However, as mentioned above, the very different σ-donor strengths of the involved donors are apparently levelled out and the π back-donation is determining for this series. In comparison to the uncoordinated triazole, the calculated NICS values (see Section 3.2) increase upon metal complexation, in particular for N3-coordination, which can be attributed to a delocalization of metal d electrons into π* orbitals of the ligand. Accordingly, coordination of the triazole *via* N3 allows a stronger π back-donation than for N2-coordination. This is in line with the experimental observation that **41b** affords a stable Pt(II) complex, while **41a** does not.[169]

5.2. 1,2,3-Triazolates as anionic nitrogen donors

If 1,2,3-triazoles are N-unsubstituted, they can serve as triazolato ligands after deprotonation. The resulting triazolate anion features three nitrogen donors, which allows various coordination modes including the formation of bi- and trimetallic complexes (Fig. 35). Here, we denote the huge variety of metal–ligand interactions offered by triazolate ligands, but a more detailed discussion would go beyond the scope of this review. Furthermore, the extensive metal–ligand interactions offered by the triazolate often lead to the formation of insoluble polymeric coordination compounds thus being rather a subject of crystal engineering. Accordingly, triazolato ligands can be exploited in the design of metal–organic frameworks (MOFs) and the reader is referred to a recent review by Gamez *et al.* of this particular field.[466]

If 1,2,3-triazolates are integrated in chelating ligands, a defined coordination *via* N1 to a single metal center is enabled.[467–469] For instance, bpy- and tpy-analog 1,2,3-triazolate-based ligands (**43** and **44**, Fig. 36) have been employed to obtain Ir(III) and Ru(II) complexes, respectively, that are suitable for applications in light-emitting diodes and dye-sensitized solar cells, respectively.[368,470] Depending on whether an internal or terminal alkyne is utilized, the ligands can be synthesized *via* thermal 1,3-dipolar cycloaddition or *via* CuAAC, respectively,[368] when using, *e.g.*, azidomethyl pivalate, which allows the cleavage of the N-substituent after the 1,2,3-triazole synthesis.[471] The 1,2,3-triazolate ligand can be reversibly converted into the corresponding 1H-1,2,3-triazole ligand by protonation. According to the response of the photophysical properties of the Ru(II) complex of **44** to protonation, *i.e.* 1H-1,2,3-triazole
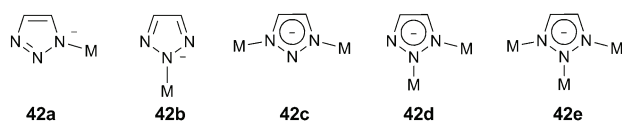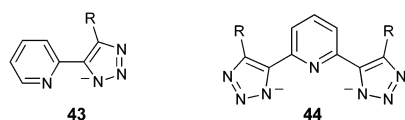
formation (*cf.* **29**), the 1,2,3-triazolate offers a significantly higher σ-donor and π-donor strength than the 1H-1,2,3-triazole.[368] Importantly, the 1,2,3-triazolate-based chelating ligands do not afford coordination isomers, which is in contrast to their 1,2,4-triazolate-analogs.[472]

Apart from the above examples, when coordinated to a single metal center as a monodentate ligand, the triazolate coordinates preferentially *via* N2 (**42b**), which is due to steric and electronic reasons (*cf.* the higher stability of the 2H-1,2,3-triazole discussed above). Alternatively, the triazolate can be directly formed with an azido ligand at the metal center with the N1-coordinated triazolate complex (**42a**) being the kinetic product and the N2-coordinated complex being thermodynamically more stable.[473–478]

In the case of bimetallic complexes, simultaneous coordination *via* N1 and N3 (distal, **42c**) is preferred over the coordination *via* N1/N3 and N2 (proximal, **42d**),[479,480] which is in analogy to the higher stability of 1,3H-1,2,3-triazolium salts and the preference for N3-coordination in the case of N1-substituted triazoles (*vide supra*). Still, formation of **42d** can be promoted by the formation of dimers[468,481] or if the two metal centers are held in proximity by an auxiliary bridging ligand.[479,482] Accordingly, for the latter, a transition from **42d** to **42c** is observed if the bridging coordination is broken by an additional ligand.[479] Interestingly, for a dinuclear Ru(II) complex of a 4,5-di(2-pyridyl)-1,2,3-triazolate ligand, which clearly adopts coordination mode **42c**, a strong electronic communication between the two metal centers was observed.[483]

Homo- and heterotrinuclear coordination compounds of type **42e** as well as clusters, coordination polymers, and metal–organic frameworks (MOFs) thereof assemble with various metal centers and the obtained materials can feature, for instance, interesting magnetic properties and high porosities.[484–489]

5.3. 1,2,3-Triazolides as carbanionic donors

A valuable, alternative coordination mode of 1,2,3-triazoles is the coordination *via* a carbanion in the 5-position. In order to differentiate, we want to use the term "triazolide"[81,100] for the carbanion in contrast to "triazolate" for the anionic nitrogen donors. As for other carbanionic donors,[490] a powerful σ and π donation can be expected, which is though tamed by the stabilizing nitrogen ring atoms as indicated by the higher CH-acidity of the 1,2,3-triazole relative to benzene (*cf.* Table 2). In contrast to the coordination *via* the triazole's nitrogen donors, the formation of triazolide complexes requires more challenging synthesis strategies, which are described in more detail in the following paragraph.

Notably, Cu(I) triazolides are intermediates in the catalytic cycle of the CuAAC (see Section 2.2).[81,82] They are labile and readily cleaved in protic media, which is essential for the CuAAC to proceed. Alternatively, the triazolide can be transmetalated from Cu(I) to transition metals that form more stable and inert complexes. As the probably most general approach, a two-step, one-pot procedure presented by Swager *et al.* can be applied (Scheme 18, top).[100] When using stoichiometric amounts of [Cu(CH$_3$CN)$_4$]PF$_6$, triethylamine as base, NaH as a proton scavenger, and THF as solvent, the CuAAC afforded the

Fig. 35 Selected interaction modes of a (symmetrical) 1,2,3-triazolate anion.

Fig. 36 1,2,3-Triazolate-based chelates (note that the ligands are drawn as if coordinated).[368,470]
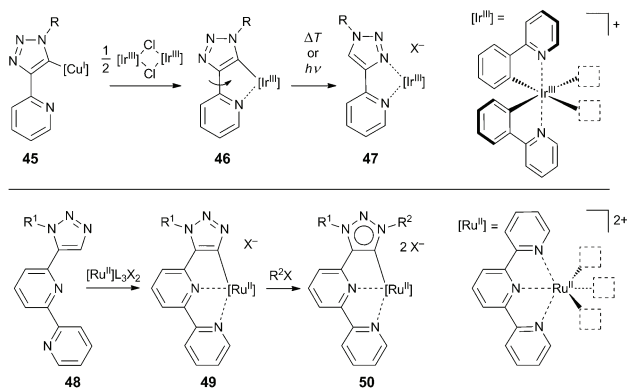
Scheme 18 Ir(III) triazolide synthesis *via* transmetalation from a Cu(I) triazolides and conversion to the corresponding triazole complex as the thermodynamic product (top).[100] Direct cyclometalation using a chelating ligand bearing a 1,5-disubstituted 1,2,3-triazole and post-complexation functionalization (L = CH₃CN, R² = Me or H, bottom).[369]

Cu(I)-coordinated triazolide **45** in high yields at ambient temperature. Subsequent addition of a suitable precursor, *e.g.* [Ir(2-phenylpyridine)₂(μ-Cl)], allowed the convenient preparation of the Ir(III) triazolide complex **46** by transmetalation.[100] Notably, the direct conversion of the free 2-(1*H*-1,2,3-triazol-4-yl)pyridine (**26**) only afforded the Ir(III) triazole complex **47** and no C–H activation was observed although this is common for Ir(III). Likewise, the triazolide Ir(III) complex **46** could be thermally or photochemically converted to the corresponding triazole complex **47** in the presence of a proton source (Scheme 18, top), presumably as the repulsive interaction between *trans*-aligned carbanions is avoided in the cationic N-bound complex.[491]

Alternatively, a chelating ligand featuring a 1,5-disubstituted triazole (**48**) can be used to circumvent the N-coordination of the 1,2,3-triazole[430] and, thereby, enable a direct cyclometalation by C–H activation at the triazole (Scheme 18, bottom).[369] Subsequently, the 1,2,3-triazolide complex (**49**) can be alkylated or reversibly protonated to obtain the corresponding 1,2,3-triazolylidene complex (**50**, *vide infra*).[369]

As mentioned above, transmetalation from Cu(I) triazolides usually requires aprotic conditions; however, this depends on the rate of the transmetalation step. Accordingly, the formation of a Re(I) triazolide by intramolecular transmetalation from the corresponding Cu(I) complex **51** in aqueous media (THF/water 4:1) was reported by Miguel *et al.* (Scheme 19).[492] When using
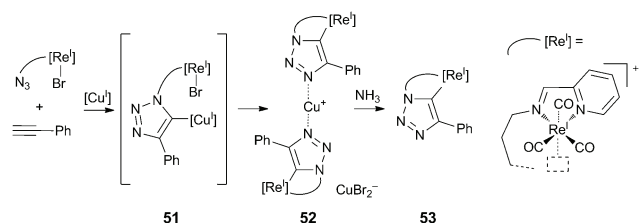
catalytic amounts of Cu(I) for the CuAAC, a Re(I) complex with a pendant, hydrolyzed triazole was obtained, while stoichiometric amounts allowed transmetalation of the triazolide to Re(I). Although an intramolecular transmetalation should be concentration-independent, a second metal center may assist the transmetalation by remote coordination to the triazolide and/or by halide abstraction from the Re(I). Under these conditions, the Re(I) triazolide is obtained as dimeric, Cu(I)-bridged, heterotrinuclear complex **52**. Subsequently, the free Re(I) triazolide complex **53** can be obtained by Cu(I) abstraction with ammonia and, again, the corresponding Re(I) triazolylidene complexes can be obtained by alkylation or by protonation. In comparison to the Re(I) triazolide complex, the Re(I)–C bond is slightly shorter in the Re(I) triazolylidene complex.[492] Notably, at elevated temperatures and when using an excess of acid, the Re(I)–C bond is cleaved (*vide infra*).

Depending on the ligand architecture, also 1,4-disubstituted triazoles may undergo a direct C–H activation. Gandelman *et al.* demonstrated that a thermodynamically favored pincer-type triazolide Pd(II) or Pt(II) complex (**56**) can be formed at elevated temperatures and in the presence of a proton scavenger *via* "rollover" cyclometalation[493] of a bidentate triazole complex (**55**), which initially forms as a kinetic product (Scheme 20).[494–497] Subsequently, the Pd(II) or Pt(II) triazolide complexes (**56**) can be converted into the corresponding triazolylidene complexes *via* alkylation (**57**).[497] Notably, when using pendant phosphine donors, the nucleophilic phosphorous(III) needs to be protected either as phosphine oxide or as borane adduct to prevent a Staudinger reaction with the azide.[494,498,499] Subsequent deprotection is achieved by reduction with trichlorosilane or addition of a sacrificial amine, respectively. Besides the direct C–H activation, the triazole can be deprotonated using *n*-butyl lithium followed by transmetalation to, *e.g.*, Pd(II).[495] Interestingly, the P^C^P-pincer ligand based on the five-member triazole ring (**54**) can apparently accommodate the Pt(II) center with less strain than the phenyl-based counterpart as indicated by the shorter Pt(II)–C bond lengths and smaller torsion of the donor arms in the complex of the former.[495] Moreover, in contrast to classical functionalization of a central ligand backbone to build up a pincer system, the implicit formation of the backbone upon "clicking" of different azide and alkyne building blocks greatly facilitates the synthesis of

Scheme 19 Formation of a Re(I) triazolide complex by intramolecular transmetalation.[492]
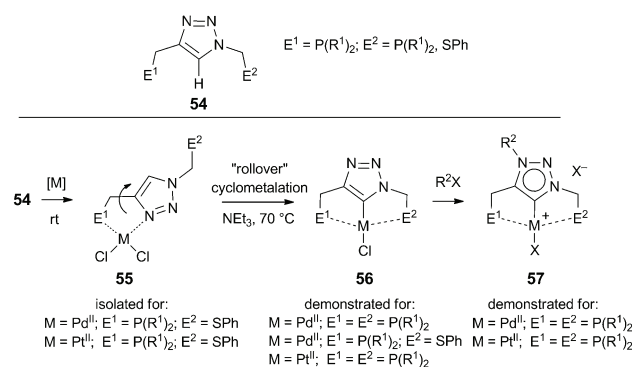
Scheme 20 Synthesis of triazolide pincer complexes and post-complexation functionalization.[495–497]
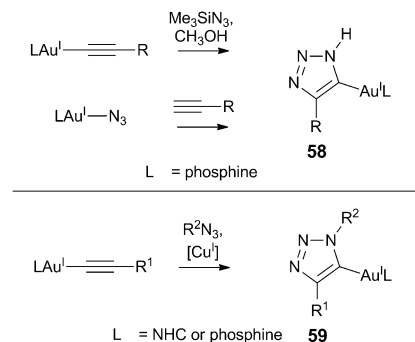
**Scheme 21** Direct formation of Au(I) triazolides from the corresponding azide and alkyne precursor complexes (in the case of **58**, the 1*H*-form is inferred from the solid state structure, but rapid tautomerization may occur in solution).[107,108,500]

Scheme 22 Cycloaddition between metal-coordinated alkynes and azides as inorganic click reaction ("iClick", R = aryl, L = phosphine).[172,502]

unsymmetrically substituted pincer ligands (**54**) with tailored steric demand and electronic properties.[494]

Apart from prior triazole formation and subsequent complex formation, cycloadditions involving metal azides and/or metal acetylides provide a direct access to 1,2,3-triazolide complexes.[477] As reported by Gray *et al.*, Au(I) acetylides can efficiently undergo (3+2) cycloaddition at ambient temperatures in toluene with *in situ* generated hydrazoic acid to form Au(I) complexes of 4-substituted 1*H*-1,2,3-triazolides (**58**, Scheme 21, top).[500] Notably, these Au(I) triazolide complexes are stable towards hydrolysis as they are formed in the presence of protic solvents and are protic species themselves. Mechanistically, the formation of a Au(I) azido complex is believed to be essential since it can be used directly as a reagent (Scheme 21, top) and is observed when Au(I) acetylides are combined with hydrazoic acid equivalents (trimethylsilyl azide in methanol), while non-hydrolyzable organic azides are not converted.[107,500] However, the carbophilic and π-acidic Au(I) is likely involved in the activation of the acetylide,[501] which would explain the formation of (C-coordinated) triazolide complexes (**58**) instead of (N-coordinated) triazolate complexes (**42a/b**, *vide supra*). Alternatively, organic azides can be reacted with Au(I) acetylides (**59**, Scheme 21, bottom) in the presence of catalytic amounts of Cu(I) even in aqueous media.[107,108] In analogy to the CuAAC (*cf.* Scheme 5),[82] the Cu(I) most likely π-coordinates at the Au(I) acetylide and subsequently mediates the cycloaddition with the organic azide, which allows the preservation of the Au(I)–C bond. It should be noted that Pt(II)-coordinated acetylides were not affected under CuAAC conditions.[180]

Furthermore, Veige *et al.* reported a clean cycloaddition between Au(I) azido and acetylide complexes at room temperature resulting in the corresponding C,N-coordinated bimetallic complex (Scheme 22, top), thus being termed inorganic click reaction ("iClick").[172] With respect to the isolobal relationship between a proton and Au(I), a 4-substituted 1*H*-1,2,3-triazole (**60a**), *i.e.* the "1,4-regioisomer", was obtained as the major product, as observed for the cycloaddition involving only a single Au(I)-coordinated reaction partner (*cf.* Scheme 21, top). This is in line with the regioselectivity of the CuAAC;[502] however, the mechanism of the Au(I)-promoted cycloaddition is not understood yet. Besides, traces of another product were observed, being
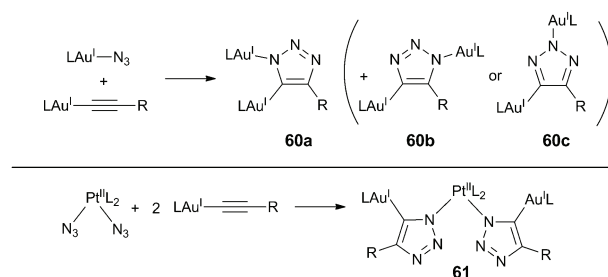
potentially the "1,5-regioisomer" (**60b**) or the 2*H*-1,2,3-triazole-analog (**60c**). While the partial formation of the latter (potentially being the thermodynamic product) would be plausible in view of the greater stability of the 2*H*-1,2,3-triazole (see Section 3.3) and N2-coordinated triazolates (*cf.* Fig. 35, **42b**), the concomitant C-coordination may cause a different coordination preference (*cf.* Scheme 21, **58**).[500] According to DFT calculations, the major product **60a** is more stable than the hypothetically formed **60b**, not least due to the more efficient HOMO delocalization onto the C-phenyl ring in the case of **60a**.

As mentioned above, various metal azides undergo cycloaddition with alkynes (see Section 5.2). Accordingly, the azide scope of the "iClick" reaction is not limited to Au(I) azido complexes. Recently, Veige *et al.* demonstrated that Pt(II) complexes bearing two azido ligands undergo cycloaddition with Au(I) acetylides, resulting in the formation of heterotrinuclear 1,2,3-triazolide complexes (**61**, Scheme 22, bottom).[502] Nonetheless, the reaction may suffer from azide-acetylide scrambling, with Pt(II) acetylides refusing to undergo cycloaddition. In any case, the formed 1,2,3-triazolides feature a Au(I)–C bond, suggesting the crucial role of Au(I) in the activation of the alkyne.[501]

To conclude, 1,2,3-triazolides are intriguing donors as their electronic properties can be strongly manipulated *via* protonation, alkylation, and metal coordination at the remote nitrogen. In the latter case, the 1,2,3-triazolides serve as bridging ligands, which can also result directly from a cycloaddition between individual azido and acetylide metal complexes.

5.4. 1,2,3-Triazolylidenes as mesoionic carbene ligands

N-heterocyclic carbenes (NHCs), *i.e.* heteroatom-stabilized, nucleophilic singlet carbenes, have found myriads of applications in coordination chemistry and (organo)catalysis.[300,503–508] The prototypical imidazol-2-ylidene, which could be isolated in its free from by Arduengo *et al.*,[504,509] was shown to be an excellent ligand allowing strong σ donation and moderate π back-donation and, thus, very stable metal–carbon bonds. Successively, the stabilizing effects within the parent imidazol-2-ylidene could be reduced to achieve even stronger electron donors than the classical NHCs.[510,511] Unexpectedly, Crabtree *et al.* discovered a C4-coordinated imidazolylidene, which was therefore called abnormal carbene.[512–515] Regarding the 1,2,3-triazole framework, although the nucleophilic character of deprotonated triazolium cations was discovered earlier by
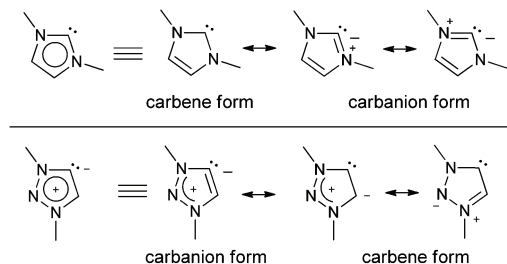
This journal is © The Royal Society of Chemistry 2014

Chem. Soc. Rev., 2014, **43**, 2522–2571 | **2553**

Fig. 37 Resonance hybrids and contributing structures of imidazol-2-ylidene (top) and 1,2,3-triazolylidene (bottom).

Begtrup,[516] their great potential as strongly σ-donating ligands was recognized much later by Albrecht *et al.*[283] In contrast to imidazolylidenes, solely the abnormal coordination mode is available for 1,2,3-triazolylidenes. The question arises, how the abnormal coordination mode impacts the electronic structure and if the term carbene is still justified. While normal NHCs are represented best by a neutral structure featuring a divalent carbon formally bearing an electron sextet, which is stabilized by virtue of ylidic (zwitterionic) contributing structures,[517] no reasonable charge-neutral structure can be drawn for abnormal carbenes (Fig. 37) suggesting the name mesoionic carbenes (MICs).[518,519] Despite the formal zwitterionic character of the latter,[520,521] the charge separation is diminished *via* delocalization within the aromatic system and, on account of the electron-withdrawing ring heteroatoms, significant contribution of a carbene structure can be expected (Fig. 37). A reinforced anionic character of MICs is expected nonetheless and the carbene character may be lowered, but the term carbene is still justified, not least because MICs essentially behave like NHC ligands, *i.e.* they are exceptionally strong σ donors and moderate π acceptors, which is in contrast to strongly σ- and π-donating carbanions including 1,2,3-triazolides (*vide supra*).[369]

The above points are discussed in more detail in the following chapter. In order to complete our survey on the triazole's manifold supramolecular interactions, we provide an overview of mesoionic carbenes derived from 1*H*-1,2,3-triazoles, namely 1,3-substituted 1,2,3-triazolylidenes. For further information including application in catalysis, the reader is referred to an early review by Crowley *et al.*[522] and a recent review by Albrecht *et al.*[297] Furthermore, reviews on abnormal carbenes have been presented by Albrecht *et al.*[513,515,523] and Crabtree.[514] According to the above explanations and in line with other authors, we omit the zwitterionic charges when drawing metal complexes of triazolylidenes and use both terms abnormal NHC and MIC.[514] Furthermore, it should be noted that referring to the carbene center as 4- or 5-position can be ambiguous and will thus be avoided if possible.[514]

5.4.1. Electronic properties of 1,2,3-triazolylidenes. The free 1,2,3-triazolylidene was unambiguously identified by single-crystal X-ray diffraction (Fig. 38). In comparison to the corresponding triazolium salt, the N1–C5–C4 bond angle is more acute (106° *vs.* 100°) and the N1–C5 and C4–C5 bonds are elongated in line with an increased s orbital contribution to the carbene lone pair, which is indicative of a singlet carbene and allows a better stabilization.[296,300,509,519] For triazolylidene
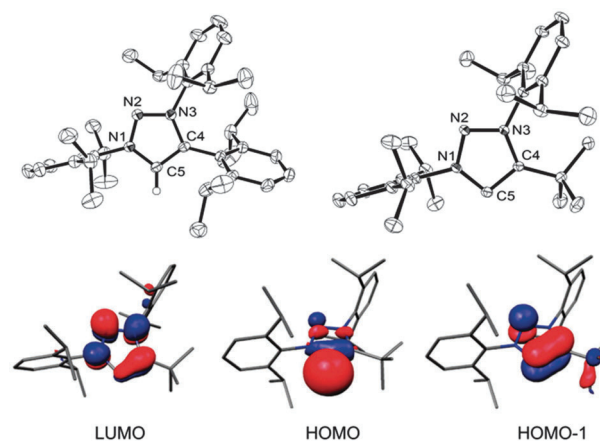

Fig. 38 Solid-state structure (thermal ellipsoids drawn at 50% probability level, counterion and protons, except for C5, omitted for clarity) of 1,3,4-tris(2,6-diisopropylphenyl)-1,2,3-triazolium (top left, N1–N2: 1.3201(16), N2–N3: 1.3278(16), N3–C4: 1.3819(16), C4–C5: 1.3713(19), C5–N1: 1.3523(17), ∠N1–C5–C4: 106.36(12)) and 4-*tert*-butyl-1,3-bis(2,6-diisopropylphenyl)-1,2,3-triazol-5-ylidene (top right, N1–N2: 1.3420(7), N2–N3: 1.3302(7), N3–C4: 1.3763(8), C4–C5: 1.4041(8), C5–N1: 1.3655(8), ∠N1–C5–C4: 100.21(5)) and frontier orbitals (BP86/def2-SVP) of the latter (bottom). Reprinted with permission from ref. 296. Copyright 2011 American Chemical Society.

metal complexes, the bond lengths and angles are in between those of triazolium and free triazolylidene (102°).[297] Furthermore, planarity and bond lengths between the values of single and double bonds suggest aromaticity.[296,519]

Consistently, DFT calculations predict a highly aromatic character and a large singlet–triplet energy gap (230 to 250 kJ mol^{-1}).[296,524] The frontier molecular orbitals of 1,2,3-triazolylidenes (Fig. 38)[296] are strikingly similar to those of, *e.g.*, imidazol-4-ylidenes and imidazol-2-ylidene.[382] Accordingly, the HOMO essentially represents the carbene's σ lone pair, while the HOMO−1 is part of the aromatic π system and receives significant contribution from the carbenic carbon atom. On the other hand, the LUMO is a π* orbital with a small orbital coefficient at the carbene center (note that the main π-accepting orbital may be a higher unoccupied orbital[525]).[296] Depending on the substitution pattern of the 1,2,3-triazolylidene, the partial charge of the carbenic carbon atom is in the range of −0.16 to −0.12, while the corresponding charges for imidazol-4-ylidene and imidazol-2-ylidene fall between −0.19 to −0.16 and −0.01 to 0.08, respectively.[296] These differences are more related to differences in polarization of the σ framework, as the carbene's p(π) population is very similar for, *e.g.*, 1,2,3-triazolylidenes and imidazoly-2-ylidenes (about 0.71 and 0.66 electrons, respectively).[524] While, by trend, mesoionic carbenes show a higher p(π) population, the similarity between both values demonstrates that normal and mesoionic carbenes are not fundamentally different.[524]

In line with that, energy partitioning by EDA for the corresponding metal complexes indicates only marginal differences in the nature of the bonding.[382,383,524] In general, the electrostatic interactions account for 50 to 70% of the total binding energy and are mainly ascribed to the strong interaction with the directed σ lone pair.[383,524,526,527] The covalent interactions in turn are dominated by a strong σ donation, but π interactions
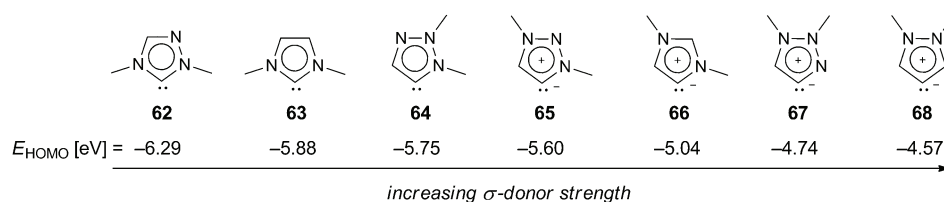
	62	**63**	**64**	**65**	**66**	**67**	**68**
E_{HOMO} [eV] =	−6.29	−5.88	−5.75	−5.60	−5.04	−4.74	−4.57

increasing σ-donor strength

Fig. 39 HOMO energies (B3LYP/aug-cc-pVTZ) of selected NHCs (**62**–**64**) and MICs (**65**–**68**).[524]

are in the range of 10 to 20% of the total orbital interaction energy and thus not negligible.[454,525,526,528,529] Consequently, the most important difference between the carbenes discussed herein is a variation in the σ-donor strength. As, for different NHCs and MICs, the first proton affinity correlates well with the energy of the HOMO, which, in turn, corresponds to the energy of the σ lone pair, the calculated HOMO energies can be used as a descriptor for the σ-donor strength.[524] Additionally, the HOMO energy correlates well with the total interaction energy with different metal centers, again confirming the pivotal role of the σ lone pair for the bonding.[383] As depicted in Fig. 39, the σ-donor strength depends mostly on the number of heteroatoms adjacent to the carbene, while a secondary effect is exerted by the number of nitrogen atoms in the ring. Accordingly, relative to **62** and **63**, whose carbene is stabilized by two neighboring (π-donating/σ-accepting) pyrrole-type nitrogen atoms, the shift of one (**64**–**66**) or both (**68**) adjacent nitrogen atoms to a remote position shows the most pronounced effect on the carbene's σ-donor strength. Additionally, on account of the higher nitrogen content, 1,2,4-triazolylidene **62** and 1,2,3-triazolylidene **65** are weaker donors than imidazol-2-ylidene **63** and imidazol-4-ylidenes **66**, respectively. The hypothetical 1,2,3-triazolylidene **67** is expected to have an even higher HOMO energy than the imidazole-4-ylidene **66**, which can be explained by the presence of a pyridyl-type nitrogen atom in the α position, giving rise to electronic repulsion between two adjacent σ lone pairs.[524]

The predicted increase of the σ-donor strength in the order **63** < **65** < **66** is in line with the trend obtained with an experimental ^{13}C NMR parameter suggested by Huynh et al.[444,530] Consistently, for complexes of derivatives of **63** and **66**, an increased metal d-electron energy has been determined for the latter by X-ray photoelectron spectroscopy (XPS).[520,531] Furthermore, if available, also experimentally[297] and computationally[532] determined TEP values are consistent with the above trend, except for **64** and **65**. In this case, the experimental TEP values suggest a slightly higher donor strength for a derivative of the normal 1,2,3-triazolylidene **64**.[297,533] However, it has to be cautioned that the TEP also depends on π interactions as well as on the steric demand of the used carbene ligand.
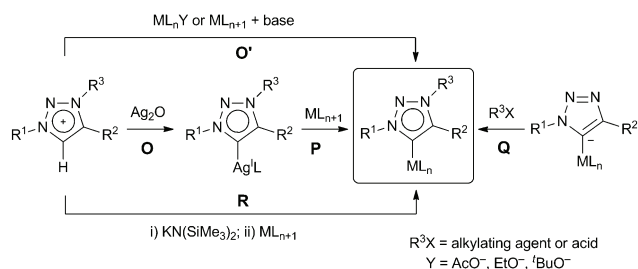
The successive increase in σ-donor strength upon gradual reduction of the heteroatom stabilization (Fig. 39) is roughly paralleled by a slight increase of the π donation and decrease of the π back-donation.[524] However, the trend is less clear than for the σ-donor strength and, additionally, only a minor contribution from π interactions to the total interaction energy is expected (*vide supra*). Ultimately, when comparing the ubiquitous imidazol-2-ylidene with the mesoionic 1,2,3-triazolylidenes, besides the significantly

higher σ-donor strength of the latter, an almost identical ability to undergo π donation and π back-donation is predicted by EDA,[524] which, again, emphasizes that the electronic properties of NHCs and MICs are not fundamentally different.

The very electron-rich σ lone pair of the 1,2,3-triazolylidene has a strong impact on the electrochemical and photophysical properties of Ru(II) complexes (*vide supra*). Consistent with the above conclusions, the Ru(III)/Ru(II) redox potentials are lower than for analogous imidazol-2-ylidene-based complexes.[534] Moreover, it has been demonstrated that 1,2,3-triazolylidenes are highly efficient in suppressing the radiationless deactivation in bis(tridentate) Ru(II) complexes by strongly destabilizing [3]MC excited states (see Section 5.1.1).[369,370,527,535]

In order to fully exploit the potential of mesoionic 1,2,3-triazolylidenes as powerful donors and readily functionalized ligand platforms, the ability to control the donor properties *via* the C- and N-substituents is of interest. On the basis of a ^{13}C NMR parameter,[444] a significant increase of the donor strength upon variation of the N-substituent next to the carbene in the order aryl < benzyl < alkyl has been reported.[530] In addition, also variation of the *para* substituent of phenyl rings attached to the 1,2,3-triazolylidene *via* the carbon atom results in a significant modulation of the electronic properties of the adjacent carbene center.[370] According to TEP, the N- and C-substituents have only a moderate influence on the donor strength of 1,2,3-triazolylidenes;[296,297,537] however, the response of the donor properties to variation of the substituents is comparable to the one of imidazol-2-ylidenes.[297,538] Still, this demonstrates the potential to fine-tune the ligand properties of triazolylidenes. For example, a significant improvement in catalytic activity upon replacement of an aryl ring with an alkyl chain as the C-substituent has been reported.[539]

Additionally, steric effects can influence the electronic characteristics of the carbene and the complex stability.[300,517,526,540] For instance, bulky substituents can cause a distortion of the carbonyl ligands[526] and enforce a torsion of the carbene ligand relative to the complex fragment, thus lowering the π interactions, which can lead to inconsistencies in the TEP (*vide supra*).[513] In this regard, it is important to note that, in contrast to imidazol-2-ylidenes, 1,2,3-triazolylidenes only require a single substituent adjacent to the carbene center.[296,513] Remarkably, the abnormal carbenes apparently do not undergo dimerization, most likely due to electrostatic repulsion resulting from the anionic character of the carbenic centers.[296,514,519] Thus, sterically relaxed C-unsubstituted carbenes can be employed, which might be beneficial for catalytic applications as π interactions are reinforced and the metal–carbon bond is more accessible.[296,513,519]

This journal is © The Royal Society of Chemistry 2014

Chem. Soc. Rev., 2014, **43**, 2522–2571 | **2555**

Scheme 23 Synthesis routes towards transition-metal 1,2,3-triazolylidene complexes.

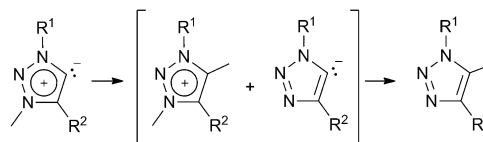Scheme 24 Decomposition of free 1,2,3-triazolylidenes.[296,519]

Furthermore, an additional metal coordination is enabled (see Section 5.4.4).

5.4.2. Synthesis of 1,2,3-triazolylidene metal complexes. In contrast to the formation of N-bound triazole metal complexes, the metal coordination of 1,2,3-triazolylidenes is less trivial and thus outlined in the following. Several synthesis routes are available (Scheme 23) starting in most cases from 1,2,3-triazolium salts (*vide supra*). A potential drawback may be the alkylation of nucleophiles other than the triazole in the synthesis of the triazolium salts, which can be circumvented by the use of protecting groups.[297,541] For instance, pyridines may be protected as N-oxide, as 1,2,3-triazoles are generally not selectively alkylated in the presence of the former.[287] Nonetheless, in the case of 1-(2-pyridyl)-1,2,3-triazoles and 2,6-bis(1,2,3-triazol-4-yl)pyridine (**29**), selective 1,2,3-triazole alkylation using methyl triflate[542] and trimethyloxonium tetra-fluoroborate,[527] respectively, was demonstrated.

A well-established and general method to achieve triazolylidene coordination is the metalation (**O**) with Ag$_2$O followed by transmetalation (**P**) of the triazolylidene to the desired transition metal (Scheme 23).[283,297,543,544] Triazolylidene complexes of Cu(I),[545,546] Rh(I),[283] Rh(III),[543] Ru(II),[283,287,527,534,543,547–550] Pd(II),[531,536,537,541,551–553] Pt(II),[543] Ir(I),[283,286] Ir(III),[286,550,554] and Au(I)[536,555,556] are available *via* this method. The Ag(I) triazolylidene formation may be promoted by addition of KBr.[557,558] Alternatively, transmetalation from Cu(I) complexes is possible.[559]

In some cases, direct metalation (**O'**) was achieved with metal precursors featuring basic anions, such as Pd(OAc)$_2$, at elevated temperatures, which allowed C–H activation *via* simultaneous deprotonation and metal coordination (Scheme 23).[283,537] Alternatively, alcoholate adducts were used in the case of Rh(I) or Ir(I).[560–562] Furthermore, PdCl$_2$ and triazolium salts afforded the corresponding triazolylidene complexes at elevated temperatures in the presence of K$_2$CO$_3$ and pyridine as solvent.[563] In this case, C–H activation at elevated temperatures and subsequent proton capture may be operative. For Cu(I), triazolylidene coordination was achieved with the triazolium salt in the presence of KO^{t}Bu at low temperatures.[564] In this case, metal coordination of the base and subsequent metathesis[565] is likely as KO^{t}Bu is supposed to not allow deprotonation of the used 1,3-dialkyl-1,2,3-triazolium salts (*vide infra*);[296,297] however, formation of free triazolylidene in lower concentrations and its capture by the metal precursor cannot be excluded.[304,566]

A completely different route proceeds *via* the transition-metal triazolide complex (*vide supra*) and the corresponding

triazolylidene complex is generated by alkylation or protonation (**Q**, Scheme 23).[369,492,497] The synthesis *via* oxidative addition of halo-triazolium salts has not been explored so far.[515]

In particular cases, the free triazolylidene (*vide infra*) could be generated in a prior step and, subsequently, coordination (**R**) to Ir(I) and Ru(II) was achieved.[296,519] Notably, the metalation–transmetalation sequence (**O**, **P**) circumvents the free triazolylidene, which, if N-alkylated, tends to undergo an alkyl shift to form the C-alkylated 1,2,3-triazole (Scheme 24).[296] Still, Bertrand *et al.* were able to isolate a moderately stable N-alkylated 1,2,3-triazolylidene after deprotonation with KN(SiMe$_3$)$_2$.[519] Alternatively, 1,3-diarylated 1,2,3-triazolium salts do not suffer from stability issues and are accessible directly *via* (3+2) cycloaddition between 1,3-diaza-2-azoniaallene salts and alkynes in moderate to good yields as reported by Jochims *et al.* (Scheme 25).[296,567] Prior to the alkyne addition, the 1,3-diaza-2-azoniaallene salt is generated *in situ* at low temperatures *via* chlorination and subsequent chloride abstraction. Following this synthesis route, Grubbs, Bertrand *et al.* could isolate free 1,3-diarylated 1,2,3-triazolylidenes after deprotonation of the corresponding 1,2,3-triazolium salts with, *e.g.*, KO^{t}Bu in THF.[296] In contrast, for 1,3-dialkyl triazolium salts, only N-dealkylation was observed with KO^{t}Bu. By using trimethylsilylacetylene or vinylbromide as an alkyne equivalent for the cycloaddition, even free C4-unsubstituted triazolylidenes were available after subsequent protodesilylation or dehydrohalogenation, respectively (*vide supra*).

In marked contrast to the relatively weak coordinative bond strength enabled by the triazole's nitrogen donors, the strong coordination of the triazolylidene renders already monodentate complexes stable and practically useful.[283,296,539,543,547] Nonetheless, chelating ligands offer more robust as well as highly defined complexes and click chemistry is particularly suited to modularly combine various donors in multidentate ligand architectures (Fig. 40). For instance, asymmetrically substituted pincer-type ligands featuring a central triazolylidene donor (**69**) are readily obtained.[494,497] Furthermore, 1,2,3-triazolylidene-containing alternatives to polypyridyl-type ligands like the
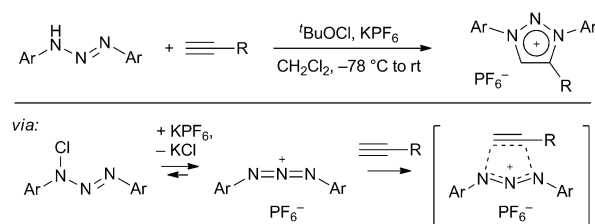
Scheme 25 Direct synthesis of 1,3-diaryl-1,2,3-triazolylidenes.[296]
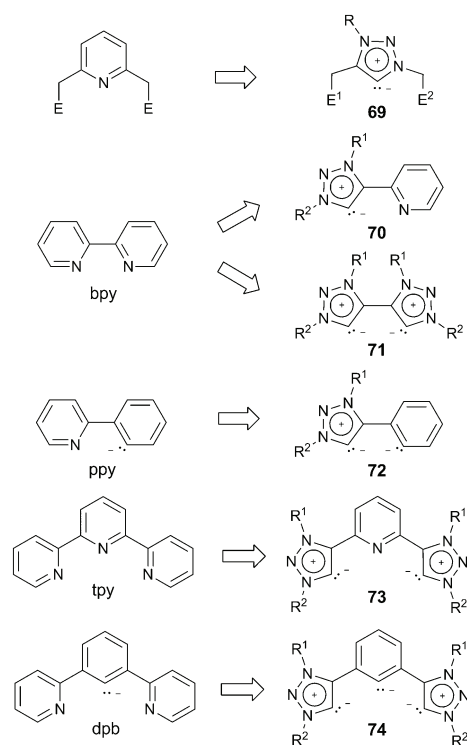
Fig. 40 Selected multidentate ligand architectures using the triazolylidene as a pyridine surrogate (note that the ligands are drawn as if coordinated).

Scheme 26 Synthesis of selected triazolylidene transition-metal complexes including direct or successive cyclometalation (cym = cymene).

bpy-analog ligands 70[287,534] and 71[296,550] as well as the tpy-analog ligand 73[369,370,527,535] have been presented. In the case of 70, additional N-alkylation and deprotonation of the pyridine affords a bidentate ligand featuring two different abnormal carbenes, namely pyridin-3-ylidene and 1,2,3-triazolylidene.[286,568,569] Additionally, an analog of ligand 70 featuring the pyridine as N-substituent of the 1,2,3-triazolylidene was reported.[295,542] Moreover, also ppy-analog, cyclometalating ligands (72) have been reported (*vide infra*).[537,543,548] On the other hand, cyclometalation of 74 involving the central carbanionic donor as known for the imidazol-2-ylidene-analog[570] has not been reported yet to the best of our knowledge. Alternatively, the bis(triazolylidene) ligands can serve as bridging ligands and homobimetallic complexes of 71 (resulting in axial chirality)[571] as well as of 74[555,557,561] and even heterobimetallic complexes of 74[561] have been reported. Furthermore, heterobimetallic complexes of dicarbenes composed of imidazol-2-ylidene and triazolylidene were reported,[562] and unsymmetrically substituted bis(triazolylidene) ligands 71 are available.[571–573]

5.4.3. Reactivity of 1,2,3-triazolylidenes. Triazolylidene complexes with high-valent, electrophilic metal centers tend to undergo spontaneous cyclometalation involving aryl wingtip groups of the triazolylidene ligand (Scheme 26), which has important implications for the synthesis of triazolylidene metal complexes and the design of corresponding catalysts.[297,537,543,548,554] Accordingly, upon triazolylidene transmetalation from a Ag(I) precursor, spontaneous cyclometalation was observed in the case of Ru(II), Rh(III), and Ir(III) (77), while only monocoordination of the
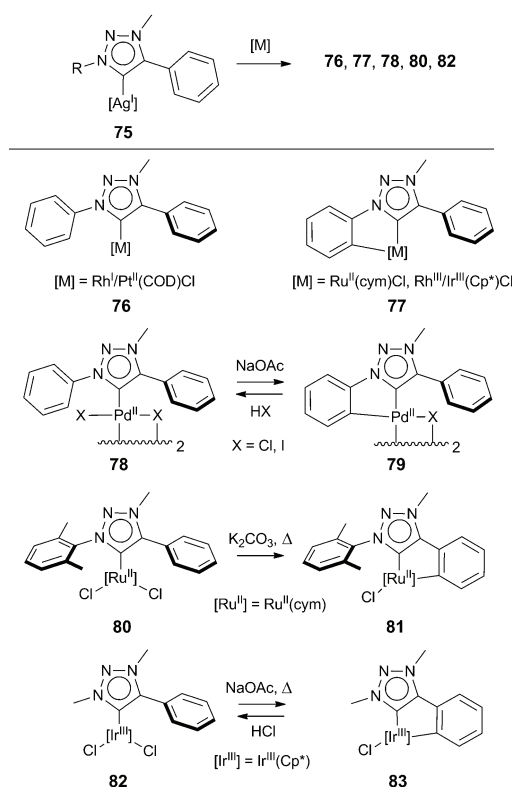
carbene ligand was achieved with Rh(I) and Pt(II) (76). Furthermore, oxidation of the Rh(I) complex induces cyclometalation.[543] Apparently, Pd(II) represents a borderline case as the isolated monocoordinated carbene complex 78 could be readily converted to the cyclometalated complex 79 when using NaOAc to assist the cyclometalation.[537,574] Formation of the metalacycle was found to be reversible and 78 was restored in the presence of HI or HCl, which further emphasizes the high stability of the triazolylidene–metal bond. In contrast, 76 did not undergo cyclometalation even under forcing conditions, while 77 withstood protonation. Importantly, the electrophilic C–H activation is chemoselective and exclusively affords cyclometalation at the N-linked phenyl rings.[543,548] Nonetheless, if this cyclometalation mode is unavailable, cyclometalation at the C-bound phenyl ring is achieved. However, C–H activation is less facile in this case, *i.e.* the monodentate carbene complexes of Ru(II) (80) and Ir(III) (82) could be isolated and cyclometalation required the presence of a base and elevated temperatures.[543,548,554] Likewise, cyclometalation could be reversed for the Ir(III) complex 83 with HCl. The observed chemoselectivity may be explained by a combination of electronic and steric factors: presumably, the weaker π conjugation of the triazolylidene π system with the N-substituent (see Section 3.4) causes the N-linked phenyl ring to be more electron-rich and, thus, more reactive in the electrophilic C–H activation, while repulsion between the C-linked phenyl ring and the N-methyl group hinders coplanarization and, thereby, the cyclometalation (note that the torsion of the C- and N-linked phenyl rings of 76 is

This journal is © The Royal Society of Chemistry 2014

Chem. Soc. Rev., 2014, 43, 2522–2571 | 2557

drawn according to its solid state structure).[543,548] Notably, although strongly depending on the metal center and not unknown for imidazol-2-ylidene complexes,[575] C–H activation is apparently facilitated in abnormal carbene complexes.[576]

The stability of triazolylidene metal complexes can hardly be generalized. On the one hand, a very strong complexation has been calculated for a Ru(II) complex featuring a chelating triazolylidene ligand (**73**),[527] the above-mentioned reactivity demonstrates an intriguing stability of the metal–triazolylidene bond in Ru(II), Rh(III), and Ir(III) complexes (**77**) against acids,[543] and Ru(II) and Ir(III) triazolylidene complexes even serve as efficient water-oxidation catalysts.[286,287] On the other hand, in certain cases, the displacement of monodentate triazolylidene ligands, induced either thermally or by acids or bases, is more easily achieved than for analogous imidazol-2-ylidene complexes. For instance, in the course of Suzuki and Heck cross-coupling reactions, the formation of Pd(0) nanoparticles from Pd(II) triazolylidene complexes was observed already at moderate temperatures.[297,551,563] Furthermore, for a Ru(II) ben-zylidene complex bearing both 1,2,3-triazolylidene and imidazol-2-ylidene, no catalytic activity in olefin metathesis was observed, but acid-induced triazolylidene cleavage generated a catalytic species with superior activity (Scheme 27, top).[577] In contrast, the analogous complex with two imidazol-2-ylidene ligands only showed a very slow conversion under identical conditions. The acid lability may be explained by protonation at N2 (note that a substantial second proton affinity for the N2-protonation has been predicted for 1,2,3-triazolylidenes),[296] which would strongly affect the triazolylidene donor strength (*cf.* Fig. 38).[296,577] The apparent contradiction with the afore-mentioned stability against acids may be attributed to the use of a C-unsubstituted triazolylidene in the latter case, which can be replaced more easily.[297] Note that a protonation of the carbon adjacent to the carbene is possible, but would not explain the pronounced labilization of the ligand (*vide infra*). For rather labile and less stable Cu(I) triazolylidene complexes, in the presence of CsOH, the formation of mesoionic oxides was observed (Scheme 27, bottom).[545] Alternatively, the mesoionic oxide can be obtained directly from the triazolium salt using CsOH, while degradation of the Cu(I) triazolylidene complex in the presence of water gave the free triazolium salt. Although the mechanism of this formal oxidation is unclear, oxygen is
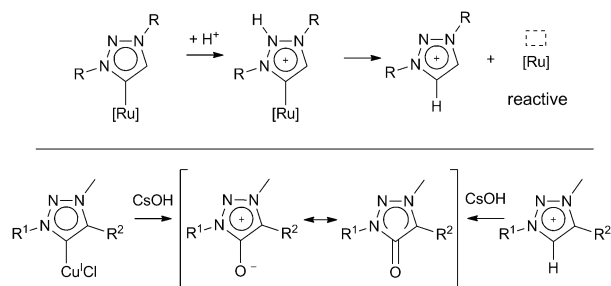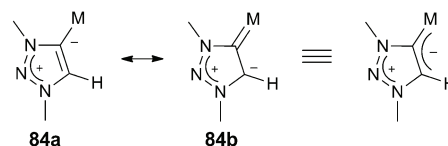
Fig. 41 The triazolylidene metal fragment as a "metala-allyl" system.

apparently not involved and hydroxide bases are required. Notably, base-induced N-dealkylation was observed as side reaction.[296,545]

Although the abnormal character is not the primary reason for the high donor strength of 1,2,3-triazolylidenes, it can become a striking feature in catalysis where it potentially allows the ligand to participate in substrate activation.[287,523,576,578] For the metal complex, a "metala-allyl" fragment is established, *i.e.* electronic flexibility is given as the triazolylidene can offer more anionic (**84a**) or carbenic character (**84b**) depending on the metal center and its oxidation state (Fig. 41 and *cf.* Fig. 37).[554] Thus, in Rh(III) complexes of the related abnormal imidazol-4-ylidene, a selective deuteration at the 5-position has been observed upon treatment with D_3PO_4.[576] Notably, deuteration was also observed after addition of $DSiEt_3$, which can be explained either by oxidative addition at the metal center and a subsequent 1,3-shift of the deuterium or, alternatively, by direct 1,3-addition of the Si–D σ bond across the "metala-allyl" fragment.[523,576,578]

The basic site of the ligand may furthermore allow reactions under base-free conditions.[546,547] A striking example is the performance of a Ru(II)–triazolylidene-based water-oxidation catalyst (Scheme 28).[287] In comparison to its imidazol-2-ylidene counterpart, the triazolylidene complex shows a super-ior stability and activity, thereby being among the most active ruthenium-based water-oxidation catalysts. This may be explained by the cooperativity and superior electron donation provided by the mesoionic carbene ligand: the triazolylidene may assist in the deprotonation of an aquo ligand to form a hydroxo ligand (**85a** to **85b**), which would facilitate the subse-quent oxidation by a sacrificial oxidant (*e.g.* a Ce(IV) complex), and, additionally, the generated Ru(IV) oxo complex (**86**) would be better stabilized.[579]

Consequently, the non-innocence of the abnormal carbene, *i.e.* its ability to efficiently shift electron density and protons to the adjacent carbon atom, emphasizes its potential for applications related to proton-coupled electron transfer (PCET).[297,523,579]

Scheme 27 Base- and acid-induced triazolylidene–metal bond cleavage as well as direct formation of mesoionic 1,2,3-triazolium-5-olate from 1,2,3-triazolium salts.[545,577]
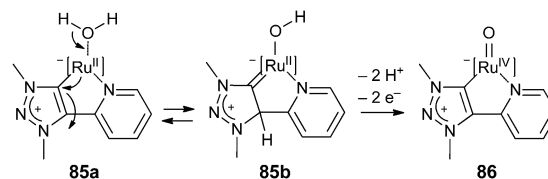

Scheme 28 Proposed initial step for the Ru(II)–triazolylidene-catalyzed water oxidation (the coordination sphere of the ruthenium center is completed with acetonitrile ligands).[287]
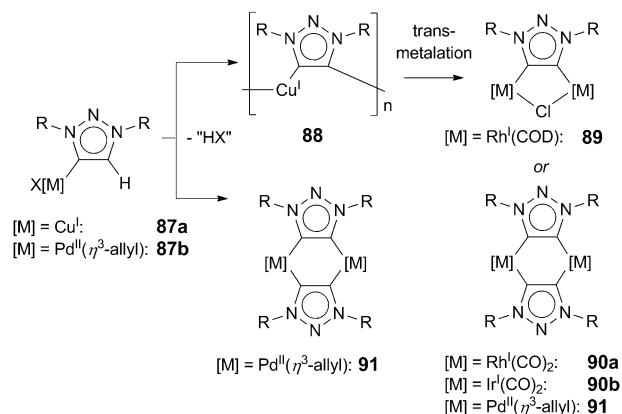
Scheme 29 Formation of bimetallic complexes of anionic 1,2,3-triazol-4,5-diylidenes (R = mesityl).[559]

Fig. 42 The 1,2,3-triazolium ion as an isoelectronic analog of the imidazol-2-ylidene.[581]

In general, the flexible synthesis, the electronic flexibility provided by the availability of carbanionic and carbenoid contributors, and the exceptionally high σ-donor strength open interesting perspectives for the application of triazolylidenes in catalysis. However, the above selection is only intended to provide an idea about the reactivity of triazolylidene complexes including their limitations and potential; applications in catalysis go beyond the scope of this review, but an overview thereof is provided elsewhere.[297,522,523]

5.4.4. 1,2,3-Triazol-4,5-diylidenes. Recently, Bertrand *et al.* demonstrated that, for example, Cu(I) (**87a**) and Pd(II) 1,2,3-triazolylidenes (**87b**) can undergo a second deprotonation using KN(SiMe$_3$)$_2$ to give oligomeric (**88**) or dimeric (**91**) complexes, respectively, with anionic 1,2,3-triazol-4,5-diylidenes as bridging ligands (Scheme 29).[559] The Cu(I) complex (**88**) can be further used as a transmetalating agent to obtain a greater variety of metal complexes (**89–91**).

In view of the single negative charge, the donor properties of the 1,2,3-triazol-4,5-diylidene dicarbene should fall in between the ones of the mesoionic 1,2,3-triazolylidene and the anionic 1,2,3-triazolide. Accordingly, while the Rh(I)–C bond lengths for the bimetallic Rh(I) complex **90a** and a monometallic Rh(I) complex bearing the bis(1,2,3-triazolylidene) **71** as well as additional carbonyl ligands are comparable, the CO stretching frequencies are lower for the bimetallic complex and more similar to the ones observed in a Rh(I) complex featuring an aromatic carbanionic donor.[559,560,580] Ultimately, the bridging dicarbene is an attractive ligand showing great potential to enable strong electronic communication and cooperativity between two metal centers, which suggests, amongst others, its application in bimetallic catalysis.[559]

5.5. 1,2,3-Triazolium ligands

Besides the formation of mesoionic 1,2,3-triazolylidenes by deprotonation of a 1,2,3-triazolium precursor, the 1,2,3-triazolium ion itself may serve as a carbene-analog ligand.[581,582] When considering the isoelectronic relationship between Arduengo-type imidazol-2-ylidenes and the 1,2,3-triazolium as well as the contributing structures of the latter (**92a–92c**, Fig. 42), the carbenoid character
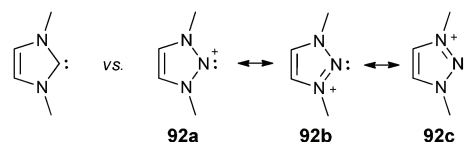
becomes obvious. Furthermore, as for the carbene center of the imidazol-2-ylidene, the nitrenium center features a singlet ground state, *i.e.* an unshared σ lone pair (note that a significant proton affinity was calculated for N2[296]) as well as a vacant p orbital, which is stabilized by the aromatic π system.[583]

Indeed, Gandelman *et al.* demonstrated that 1,2,3-triazolium ions supported by auxiliary phosphine donors within a P^N^P-pincer ligand are able to form stable Rh(I) (**93a** and **93b**, Fig. 43) and Ru(II) complexes.[581] The metal–nitrenium coordination was proven by single-crystal X-ray diffraction and, after ^{15}N-labeling in the 2-position, by the characteristic coupling with [103]Rh in the ^{15}N NMR spectrum. The high [15]N–[103]Rh coupling constant further indicates a high s character of the nitrenium σ lone pair as observed for NHCs.[509] Upon metal coordination, N–N bond elongation is observed, which is consistent with an increased contribution of the carbenoid structure (**92a**). In accord with DFT calculations, this can be ascribed to π back-donation from metal d orbitals into the nitrenium's vacant p orbital (Fig. 43) reducing the need for stabilization by the adjacent nitrogen atoms (**92b** and **92c**). For the square-planar Rh(I) complex featuring a carbonyl ligand *trans* to the nitrenium (**93a**, Fig. 43), a much higher carbonyl stretching frequency was observed than for analogous complexes with imidazol-2-ylidene- or pyridine-based pincer ligands, suggesting a weaker effective electron donation most likely due to a weak σ donation along with significant π back-donation. According to energy partitioning by a charge decomposition analysis, π back-donation (61 kJ mol^{-1}) affords a slightly higher contribution than the σ donation (58 kJ mol^{-1}) to the total interaction energy (196 kJ mol^{-1}) between an unsubstituted triazolium ring and a *trans*-[Rh^I(PH$_3$)$_2$Cl] fragment. The analogous interaction with imidazol-2-ylidene or pyridine is dominated by σ donation, in particular in the case of pyridine. Interestingly, the overall interaction energy with Rh(I) is higher in the case of the carbene (about 317 kJ mol^{-1}), while it is comparable for the nitrenium (196 kJ mol^{-1}) and the pyridine (191 kJ mol^{-1}). However, in contrast to pyridine, complexation of a nitrenium ligand in practice requires assistance by pendant donors (*cf.* **93**) presumably to overcome unfavorable complexation kinetics.[581] Nonetheless, the electrophilic nature of the nitrenium, *i.e.* its weak σ-donor and
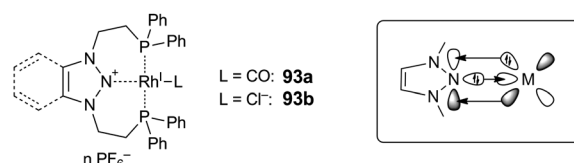
Fig. 43 Rh(I) 1,2,3-triazolium complex and illustration of the most relevant orbital interactions.[581,582]

This journal is © The Royal Society of Chemistry 2014

Chem. Soc. Rev., 2014, **43**, 2522–2571 | **2559**

relatively high π-acceptor strength, which is complementary to the nucleophilic nature of NHC ligands, may be beneficial in stabilizing electron-rich metal centers or generating electrophilic metal centers in the course of a catalytic cycle.[582]

6. Conclusion

As nitrogen-rich heterocycles, the 1,2,3-triazole and the related 1,2,3-triazolium feature highly polarized carbon atoms allowing the complexation of anions by (charge-assisted) hydrogen bonds, with hydrogen-bond-donor strengths approaching those of amides and imidazolium rings, respectively. Alternatively, the positively polarized carbon can, in turn, polarize a covalently attached halogen atom, thus enabling strong (charge-assisted) halogen bonds. The triazole polarization can be further enhanced by simultaneous metal coordination at the nitrogen atoms giving rise to cooperatively strengthened hydrogen bond donation. Furthermore, intramolecular hydrogen bond donation and/or acceptance can be exploited to design well-defined structures that show enhanced anion recognition or stimuli-responsiveness. Additionally, the preparation *via* click chemistry renders the triazole ring particularly suited for the construction of restricted architectures like macrocyclic anion receptors.

On the other hand, triazoles and triazolium salts provide access to carbanionic and mesoionic carbene donors, respectively, for the complexation of transition metals. The former 1,2,3-triazolide shows a strong electron donation though less strong than a phenyl anion due to heteroatom stabilization, which additionally allows switching of the donor characteristics by simultaneous protonation or metal coordination at the nitrogen ring atoms. The 1,2,3-triazolylidene shows superior σ donation to classical N-heterocyclic carbenes like imidazol-2-ylidene due to the remote positioning of stabilizing heteroatoms. As mesoionic carbene, the 1,2,3-triazolylidene offers a carbenoid character with variable carbanion contribution, which enables ligand cooperativity by virtue of a metala-allylic resonance. Accordingly, the 1,2,3-triazolylidene shows great potential for applications in transition-metal catalysis.

Apart from C-coordination, the triazole offers various N-coordination modes including anionic nitrogen donors, which allows the construction of multimetallic assemblies including metal–organic frameworks. The most commonly involved neutral N3-donor serves as a weaker σ donor than pyridine and imidazole and features intermediate π-acceptor strength between the weakly π-acidic imidazole and the more π-acidic pyridine. The actual coordination behavior depends, however, on the metal center and the substituents of the triazole. In addition, the triazole's reduced steric demand causes a more flexible coordination than pyridine. In combination with the facile ligand modification, this allows the design of dynamic coordination compounds, for instance transition-metal complexes featuring hemilabile ligands suitable for applications in catalysis. Provided that transition metals that afford stable and inert complexes are coordinated, triazole-containing ligands can be used as surrogates of polypyridyl ligands allowing rapid installation of

functional groups. Despite the potential to strongly influence the coordination strength, certain properties of the corresponding metal complex can be manipulated only to a very limited extent, as the triazole causes an interruption of the π conjugation. Furthermore, even the triazolium cation can coordinate to transition-metal centers, with the nitrenium donor serving as a weaker σ donor and a stronger π acceptor when compared to pyridine.

Ultimately, the ease of obtaining highly functionalized triazoles as well as the triazole's high degree of immanent functionality results in an enormous potential of this heterocycle, which has been demonstrated by successful applications, *e.g.*, in anion transport, sensing of anions and metal ions, molecular machines and switches, organocatalysis and transition-metal catalysis, or energy-conversion and magnetic materials.

Acknowledgements

Notes and references

1 H. C. Kolb, M. G. Finn and K. B. Sharpless, *Angew. Chem., Int. Ed.*, 2001, **40**, 2004–2021.
2 V. V. Rostovtsev, L. G. Green, V. V. Fokin and K. B. Sharpless, *Angew. Chem., Int. Ed.*, 2002, **41**, 2596–2599.
3 C. W. Tornøe, C. Christensen and M. Meldal, *J. Org. Chem.*, 2002, **67**, 3057–3064.
4 F. Schoenebeck, D. H. Ess, G. O. Jones and K. N. Houk, *J. Am. Chem. Soc.*, 2009, **131**, 8121–8133.
5 J. Lehn, *Science*, 1993, **260**, 1762–1763.
6 *Chem. Soc. Rev.*, 2010, **39**, 1221–1408.
7 *Top. Heterocycl. Chem.*, 2012, **28**, 1–232.
8 F. R. Benson and W. L. Savell, *Chem. Rev.*, 1950, **46**, 1–68.
9 T. L. Gilchrist and G. E. Gymer, in *Advances in Heterocyclic Chemistry*, ed. A. R. Katritzky and A. J. Boulton, Academic Press, 1974, pp. 33–85.
10 S. Rachwal and A. R. Katritzky, in *Comprehensive Heterocyclic Chemistry III*, ed. A. R. Katritzky, C. A. Ramsden, E. F. V. Scriven and R. J. K. Taylor, Elsevier, Oxford, 2008, pp. 1–158.
11 A. Michael, *J. Prakt. Chem.*, 1893, **48**, 94–95.
12 R. Huisgen, G. Szeimies and L. Möbius, *Chem. Ber.*, 1967, **100**, 2494–2507.
13 R. Huisgen, *Angew. Chem., Int. Ed. Engl.*, 1963, **2**, 565–598.
14 R. Huisgen, *Angew. Chem., Int. Ed. Engl.*, 1963, **2**, 633–645.
15 R. Huisgen, *Angew. Chem., Int. Ed. Engl.*, 1968, **7**, 321–328.
16 S. Bräse, C. Gil, K. Knepper and V. Zimmermann, *Angew. Chem., Int. Ed.*, 2005, **44**, 5188–5240.
17 K. N. Houk, J. Gonzalez and Y. Li, *Acc. Chem. Res.*, 1995, **28**, 81–90.
18 R. Huisgen, *J. Org. Chem.*, 1968, **33**, 2291–2297.
19 R. Huisgen, *J. Org. Chem.*, 1976, **41**, 403–419.

20 R. B. Woodward and R. Hoffmann, *Angew. Chem., Int. Ed. Engl.*, 1969, **8**, 781–853.

21 R. Sustmann, *Tetrahedron Lett.*, 1971, **12**, 2717–2720.

22 R. Sustmann and H. Trill, *Angew. Chem., Int. Ed. Engl.*, 1972, **11**, 838–840.

23 R. Sustmann, *Pure Appl. Chem.*, 1974, **40**, 569–593.

24 K. N. Houk, *Acc. Chem. Res.*, 1975, **8**, 361–369.

25 K. N. Houk, J. Sims, R. E. Duke, R. W. Strozier and J. K. George, *J. Am. Chem. Soc.*, 1973, **95**, 7287–7301.

26 K. N. Houk, J. Sims, C. R. Watts and L. J. Luskus, *J. Am. Chem. Soc.*, 1973, **95**, 7301–7315.

27 K. Fukui, *Science*, 1982, **218**, 747–754.

28 K. Fukui, T. Yonezawa and H. Shingu, *J. Chem. Phys.*, 1952, **20**, 722–725.

29 W. C. Herndon, *Chem. Rev.*, 1972, **72**, 157–179.

30 R. F. Hudson, *Angew. Chem., Int. Ed. Engl.*, 1973, **12**, 36–56.

31 G. Klopman, *J. Am. Chem. Soc.*, 1968, **90**, 223–234.

32 L. Salem, *J. Am. Chem. Soc.*, 1968, **90**, 553–566.

33 M. J. S. Dewar, *THEOCHEM*, 1989, **200**, 301–323.

34 W. Kirmse and L. Horner, *Liebigs Ann. Chem.*, 1958, **614**, 1–3.

35 Z. Li, T. S. Seo and J. Ju, *Tetrahedron Lett.*, 2004, **45**, 3143–3146.

36 F. Kloss, U. Köhn, B. O. Jahn, M. D. Hager, H. Görls and U. S. Schubert, *Chem.–Asian J.*, 2011, **6**, 2816–2824.

37 G. Molteni and A. Ponti, *Chem.–Eur. J.*, 2003, **9**, 2770–2774.

38 G. Molteni and A. Ponti, *ARKIVOC*, 2006, **xvi**, 49–55.

39 I. Fleming, *Frontier Orbitals and Organic Chemical Reactions*, John Wiley & Sons, Chichester, 1976.

40 P. Ykman, G. L'Abbé and G. Smets, *Tetrahedron*, 1971, **27**, 845–849.

41 M. E. Hermes and F. D. Marsh, *J. Am. Chem. Soc.*, 1967, **89**, 4760–4764.

42 G. Himbert and M. Regitz, *Liebigs Ann. Chem.*, 1973, **1973**, 1505–1529.

43 O. Dimroth, *Liebigs Ann. Chem.*, 1909, **364**, 183–226.

44 A. R. Katritzky, C. A. Ramsden, J. A. Joule and V. V. Zhdankin, *Handbook of Heterocyclic Chemistry*, Elsevier, Amsterdam, 3rd edn, 2010, pp. 473–604.

45 D. H. Ess, G. O. Jones and K. N. Houk, *Adv. Synth. Catal.*, 2006, **348**, 2337–2361.

46 R. G. Pearson, *J. Am. Chem. Soc.*, 1963, **85**, 3533–3539.

47 P. Geerlings and F. De Proft, *Phys. Chem. Chem. Phys.*, 2008, **10**, 3028–3042.

48 P. Geerlings, F. De Proft and W. Langenaeker, *Chem. Rev.*, 2003, **103**, 1793–1874.

49 R. G. Parr and W. Yang, *J. Am. Chem. Soc.*, 1984, **106**, 4049–4050.

50 A. K. Chandra, T. Uchimaru and M. T. Nguyen, *J. Chem. Soc., Perkin Trans. 2*, 1999, 2117–2121.

51 D. H. Ess and K. N. Houk, *J. Am. Chem. Soc.*, 2008, **130**, 10187–10198.

52 D. H. Ess and K. N. Houk, *J. Am. Chem. Soc.*, 2007, **129**, 10646–10647.

53 B. Braida, C. Walter, B. Engels and P. C. Hiberty, *J. Am. Chem. Soc.*, 2010, **132**, 7631–7637.

54 C. G. Gordon, J. L. Mackey, J. C. Jewett, E. M. Sletten, K. N. Houk and C. R. Bertozzi, *J. Am. Chem. Soc.*, 2012, **134**, 9199–9208.

55 G. Wittig and A. Krebs, *Chem. Ber.*, 1961, **94**, 3260–3275.

56 G. Himbert, D. Frank and M. Regitz, *Chem. Ber.*, 1976, **109**, 370–394.

57 S. J. Coats, J. S. Link, D. Gauthier and D. J. Hlasta, *Org. Lett.*, 2005, **7**, 1469–1472.

58 L. Birkofer, A. Ritter and H. Uhlenbrauck, *Chem. Ber.*, 1963, **96**, 3280–3288.

59 R. Breslow, *Acc. Chem. Res.*, 1991, **24**, 159–164.

60 U. M. Lindström, *Chem. Rev.*, 2002, **102**, 2751–2772.

61 D. W. C. MacMillan, *Nature*, 2008, **455**, 304–308.

62 M. Belkheira, D. El Abed, J.-M. Pons and C. Bressy, *Chem.–Eur. J.*, 2011, **17**, 12917–12921.

63 L. J. T. Danence, Y. Gao, M. Li, Y. Huang and J. Wang, *Chem.–Eur. J.*, 2011, **17**, 3584–3587.

64 D. B. Ramachary, K. Ramakumar and V. V. Narayana, *Chem.–Eur. J.*, 2008, **14**, 9143–9147.

65 L. Wang, S. Peng, L. J. T. Danence, Y. Gao and J. Wang, *Chem.–Eur. J.*, 2012, **18**, 6088–6093.

66 N. Seus, B. Goldani, E. J. Lenardão, L. Savegnago, M. W. Paixão and D. Alves, *Eur. J. Org. Chem.*, 2013, DOI: 10.1002/ejoc.201301547.

67 D. B. Ramachary and A. B. Shashank, *Chem.–Eur. J.*, 2013, **19**, 13175–13181.

68 D. K. J. Yeung, T. Gao, J. Huang, S. Sun, H. Guo and J. Wang, *Green Chem.*, 2013, **15**, 2384–2388.

69 A. Krasiński, V. V. Fokin and K. B. Sharpless, *Org. Lett.*, 2004, **6**, 1237–1240.

70 S. W. Kwok, J. R. Fotsing, R. J. Fraser, V. O. Rodionov and V. V. Fokin, *Org. Lett.*, 2010, **12**, 4217–4219.

71 W. S. Matthews, J. E. Bares, J. E. Bartmess, F. G. Bordwell, F. J. Cornforth, G. E. Drucker, Z. Margolin, R. J. McCallum, G. J. McCollum and N. R. Vanier, *J. Am. Chem. Soc.*, 1975, **97**, 7006–7014.

72 E. J. Corey and M. Chaykovsky, *J. Am. Chem. Soc.*, 1965, **87**, 1345–1353.

73 J. E. Hein and V. V. Fokin, *Chem. Soc. Rev.*, 2010, **39**, 1302–1315.

74 S. Díez-González, *Catal. Sci. Technol.*, 2011, **1**, 166–178.

75 M. Meldal and C. W. Tornøe, *Chem. Rev.*, 2008, **108**, 2952–3015.

76 V. D. Bock, H. Hiemstra and J. H. van Maarseveen, *Eur. J. Org. Chem.*, 2006, 51–68.

77 M. Ahlquist and V. V. Fokin, *Organometallics*, 2007, **26**, 4389–4391.

78 F. Himo, T. Lovell, R. Hilgraf, V. V. Rostovtsev, L. Noodleman, K. B. Sharpless and V. V. Fokin, *J. Am. Chem. Soc.*, 2005, **127**, 210–216.

79 B. F. Straub, *Chem. Commun.*, 2007, 3868–3870.

80 V. O. Rodionov, V. V. Fokin and M. G. Finn, *Angew. Chem., Int. Ed.*, 2005, **44**, 2210–2215.

81 C. Nolte, P. Mayer and B. F. Straub, *Angew. Chem., Int. Ed.*, 2007, **46**, 2101–2103.

82 B. T. Worrell, J. A. Malik and V. V. Fokin, *Science*, 2013, **340**, 457–460.

83 J. J. Eisch, H. Gopal and S.-G. Rhee, *J. Org. Chem.*, 1975, **40**, 2064–2069.

84 H. V. R. Dias, S. A. Polach, S.-K. Goh, E. F. Archibong and D. S. Marynick, *Inorg. Chem.*, 2000, **39**, 3894–3901.

85 J. P. Selegue, *Coord. Chem. Rev.*, 2004, **248**, 1543–1563.

86 M. Böhme, T. Wagener and G. Frenking, *J. Organomet. Chem.*, 1996, **520**, 31–43.

87 I. Marek, *Chem. Rev.*, 2000, **100**, 2887–2900.

88 E. Sperotto, G. P. M. van Klink, G. van Koten and J. G. de Vries, *Dalton Trans.*, 2010, **39**, 10338–10351.

89 G.-C. Kuang, P. M. Guha, W. S. Brotherton, J. T. Simmons, L. A. Stankee, B. T. Nguyen, R. J. Clark and L. Zhu, *J. Am. Chem. Soc.*, 2011, **133**, 13984–14001.

90 T. R. Chan, R. Hilgraf, K. B. Sharpless and V. V. Fokin, *Org. Lett.*, 2004, **6**, 2853–2855.

91 P. S. Donnelly, S. D. Zanatta, S. C. Zammit, J. M. White and S. J. Williams, *Chem. Commun.*, 2008, 2459–2461.

92 J. E. Hein, J. C. Tripp, L. B. Krasnova, K. B. Sharpless and V. V. Fokin, *Angew. Chem., Int. Ed.*, 2009, **48**, 8018–8021.

93 S. I. Presolski, V. Hong, S.-H. Cho and M. G. Finn, *J. Am. Chem. Soc.*, 2010, **132**, 14570–14576.

94 V. O. Rodionov, S. I. Presolski, S. Gardinier, Y.-H. Lim and M. G. Finn, *J. Am. Chem. Soc.*, 2007, **129**, 12696–12704.

95 B. M. Mykhalichko, O. N. Temkin and M. G. Mys'kiv, *Russ. Chem. Rev.*, 2000, **69**, 957–984.

96 Y. Angell and K. Burgess, *Angew. Chem., Int. Ed.*, 2007, **46**, 3649–3651.

97 J. González, V. M. Pérez, D. O. Jiménez, G. Lopez-Valdez, D. Corona and E. Cuevas-Yañez, *Tetrahedron Lett.*, 2011, **52**, 3514–3517.

98 S. Kamijo, T. Jin and Y. Yamamoto, *Tetrahedron Lett.*, 2004, **45**, 689–691.

99 Q. Cai, J. Yan and K. Ding, *Org. Lett.*, 2012, **14**, 3332–3335.

100 S. Liu, P. Müller, M. K. Takase and T. M. Swager, *Inorg. Chem.*, 2011, **50**, 7598–7609.

101 B. Wang, J. Zhang, X. Wang, N. Liu, W. Chen and Y. Hu, *J. Org. Chem.*, 2013, **78**, 10519–10523.

102 W. S. Brotherton, R. J. Clark and L. Zhu, *J. Org. Chem.*, 2012, **77**, 6443–6455.

103 L. Li, G. Zhang, A. Zhu and L. Zhang, *J. Org. Chem.*, 2008, **73**, 3630–3633.

104 L. Li, R. Li, A. Zhu, G. Zhang and L. Zhang, *Synlett*, 2011, 874, 878.

105 L. Ackermann and H. K. Potukuchi, *Org. Biomol. Chem.*, 2010, **8**, 4503–4513.

106 Y. Zhou, T. Lecourt and L. Micouin, *Angew. Chem., Int. Ed.*, 2010, **49**, 2607–2610.

107 D. V. Partyka, L. Gao, T. S. Teets, J. B. Updegraff, N. Deligonul and T. G. Gray, *Organometallics*, 2009, **28**, 6171–6182.

108 J. E. Heckler, N. Deligonul, A. L. Rheingold and T. Gray, *Chem. Commun.*, 2013, **49**, 5990–5992.

109 B. T. Worrell, S. P. Ellery and V. V. Fokin, *Angew. Chem., Int. Ed.*, 2013, **52**, 13037–13041.

110 B. H. M. Kuijpers, G. C. T. Dijkmans, S. Groothuys, P. J. L. M. Quaedflieg, R. H. Blaauw, F. L. van Delft and F. P. J. T. Rutjes, *Synlett*, 2005, 3059–3062.

111 C. Spiteri and J. E. Moses, *Angew. Chem., Int. Ed.*, 2010, **49**, 31–33.

112 S. Mignani, Y. Zhou, T. Lecourt and L. Micouin, *Top. Heterocycl. Chem.*, 2012, **28**, 1–48.

113 G.-C. Kuang, H. A. Michaels, J. T. Simmons, R. J. Clark and L. Zhu, *J. Org. Chem.*, 2010, **75**, 6540–6548.

114 C. Shao, G. Cheng, D. Su, J. Xu, X. Wang and Y. Hu, *Adv. Synth. Catal.*, 2010, **352**, 1587–1592.

115 N. Candelon, D. Lastecoueres, A. K. Diallo, J. Ruiz Aranzaes, D. Astruc and J.-M. Vincent, *Chem. Commun.*, 2008, 741–743.

116 S. Díez-González, A. Correa, L. Cavallo and S. P. Nolan, *Chem.–Eur. J.*, 2006, **12**, 7558–7564.

117 K. Kirchner, M. J. Calhorda, R. Schmid and L. F. Veiros, *J. Am. Chem. Soc.*, 2003, **125**, 11721–11729.

118 L. Zhang, X. Chen, P. Xue, H. H. Y. Sun, I. D. Williams, K. B. Sharpless, V. V. Fokin and G. Jia, *J. Am. Chem. Soc.*, 2005, **127**, 15998–15999.

119 B. C. Boren, S. Narayan, L. K. Rasmussen, L. Zhang, H. Zhao, Z. Lin, G. Jia and V. V. Fokin, *J. Am. Chem. Soc.*, 2008, **130**, 8923–8930.

120 L. K. Rasmussen, B. C. Boren and V. V. Fokin, *Org. Lett.*, 2007, **9**, 5337–5339.

121 D.-R. Hou, T.-C. Kuan, Y.-K. Li, R. Lee and K.-W. Huang, *Tetrahedron*, 2010, **66**, 9415–9420.

122 M. M. Majireck and S. M. Weinreb, *J. Org. Chem.*, 2006, **71**, 8680–8683.

123 S. Oppilliart, G. Mousseau, L. Zhang, G. Jia, P. Thuéry, B. Rousseau and J.-C. Cintrat, *Tetrahedron*, 2007, **63**, 8094–8098.

124 C.-T. Zhang, X. Zhang and F.-L. Qing, *Tetrahedron Lett.*, 2008, **49**, 3927–3930.

125 M. Lamberti, G. C. Fortman, A. Poater, J. Broggi, A. M. Z. Slawin, L. Cavallo and S. P. Nolan, *Organometallics*, 2012, **31**, 756–767.

126 D. S. Frohnapfel and J. L. Templeton, *Coord. Chem. Rev.*, 2000, **206–207**, 199–235.

127 V. C. Gibson, *Angew. Chem., Int. Ed. Engl.*, 1994, **33**, 1565–1572.

128 J.-M. Wu, W. Guo and C.-P. Li, *Acta Crystallogr., Sect. E: Struct. Rep. Online*, 2011, **67**, o1189.

129 W. Adam and A. Grimison, *Theor. Chim. Acta*, 1967, **7**, 342–351.

130 M. H. Palmer and S. Parsons, *Acta Crystallogr., Sect. C: Cryst. Struct. Commun.*, 1996, **52**, 2818–2822.

131 A. R. Katritzky, C. A. Ramsden, J. A. Joule and V. V. Zhdankin, *Handbook of Heterocyclic Chemistry*, Elsevier, Amsterdam, 3rd edn, 2010, pp. 139–209.

132 M. K. Cyrański, T. M. Krygowski, A. R. Katritzky and P. v. R. Schleyer, *J. Org. Chem.*, 2002, **67**, 1333–1338.

133 C. A. Ramsden, *Tetrahedron*, 2010, **66**, 2695–2699.

134 T. M. Krygowski and M. K. Cyrański, *Chem. Rev.*, 2001, **101**, 1385–1420.

135 T. M. Krygowski, M. K. Cyrański, Z. Czarnocki, G. Häfelinger and A. R. Katritzky, *Tetrahedron*, 2000, **56**, 1783–1796.

136 P. v. R. Schleyer, C. Maerker, A. Dransfeld, H. Jiao and N. J. R. v. E. Hommes, *J. Am. Chem. Soc.*, 1996, **118**, 6317–6318.

137 P. v. R. Schleyer, M. Manoharan, Z.-X. Wang, B. Kiran, H. Jiao, R. Puchta and N. J. R. van Eikema Hommes, *Org. Lett.*, 2001, **3**, 2465–2468.

138 Z. Chen, C. S. Wannere, C. Corminboeuf, R. Puchta and P. v. R. Schleyer, *Chem. Rev.*, 2005, **105**, 3842–3888.

139 P. v. R. Schleyer, *Chem. Rev.*, 2001, **101**, 1115–1118.

140 A. R. Katritzky, C. A. Ramsden, J. A. Joule and V. V. Zhdankin, *Handbook of Heterocyclic Chemistry*, Elsevier, Amsterdam, 3rd edn, 2010, pp. 37–86.

141 I. Alkorta and J. Elguero, *Magn. Reson. Chem.*, 2010, **48**, S32–S37.

142 M. K. Cyrański, P. v. R. Schleyer, T. M. Krygowski, H. Jiao and G. Hohlneicher, *Tetrahedron*, 2003, **59**, 1657–1665.

143 K. Jug, S. Chiodo, P. Calaminici, A. Avramopoulos and M. G. Papadopoulos, *J. Phys. Chem. A*, 2003, **107**, 4172–4183.

144 R. Vianello and Z. B. Maksić, *Mol. Phys.*, 2005, **103**, 209–219.

145 F. J. Weigert and J. D. Roberts, *J. Am. Chem. Soc.*, 1968, **90**, 3543–3549.

146 M. Begtrup, C. J. Nielsen, L. Nygaard, S. Samdal, C. E. Sjøgren and G. O. Sørensen, *Acta Chem. Scand., Ser. A*, 1988, **42**, 500–514.

147 G. Rauhut, *Phys. Chem. Chem. Phys.*, 2003, **5**, 791–800.

148 V. Jiménez and J. B. Alderete, *THEOCHEM*, 2006, **775**, 1–7.

149 M. T. Rodgers and P. B. Armentrout, *Int. J. Mass Spectrom.*, 1999, **185–187**, 359–380.

150 I. Alkorta and J. Elguero, *J. Chem. Soc., Perkin Trans. 2*, 1998, 2497–2504.

151 J. Catalán, M. Sánchez-Cabezudo, J. L. G. De Paz, J. Elguero, R. W. Taft and F. Anvia, *J. Comput. Chem.*, 1989, **10**, 426–433.

152 J. Luis, M. Abboud, C. Foces-Foces, R. Notario, R. E. Trifonov, A. P. Volovodenko, V. A. Ostrovskii, I. Alkorta and J. Elguero, *Eur. J. Org. Chem.*, 2001, 3013–3024.

153 M. H. Palmer, S. V. Hoffmann, N. C. Jones, A. R. Head and D. L. Lichtenberger, *J. Chem. Phys.*, 2011, **134**, 084309.

154 F. Tomas, J. L. M. Abboud, J. Laynez, R. Notario, L. Santos, S. O. Nilsson, J. Catalan, R. M. Claramunt and J. Elguero, *J. Am. Chem. Soc.*, 1989, **111**, 7348–7353.

155 J. Kalisiak, K. B. Sharpless and V. V. Fokin, *Org. Lett.*, 2008, **10**, 3171–3174.

156 R. Westlund, E. Glimsdal, M. Lindgren, R. Vestberg, C. Hawker, C. Lopes and E. Malmstrom, *J. Mater. Chem.*, 2008, **18**, 166–175.

157 D. J. V. C. van Steenis, O. R. P. David, G. P. F. van Strijdonck, J. H. van Maarseveen and J. N. H. Reek, *Chem. Commun.*, 2005, 4333–4335.

158 S. Bakbak, P. J. Leech, B. E. Carson, S. Saxena, W. P. King and U. H. F. Bunz, *Macromolecules*, 2006, **39**, 6793–6795.

159 T. Yamamoto, Y. Yamagata, R. Yamashita, M. Abla, H. Fukumoto and T.-A. Koizumi, *Synth. Met.*, 2012, **162**, 2406–2413.

160 C. Curutchet, J. Poater, M. Solà and J. Elguero, *J. Phys. Chem. A*, 2011, **115**, 8571–8577.

161 W.-Y. Hung, G.-M. Tu, S.-W. Chen and Y. Chi, *J. Mater. Chem.*, 2012, **22**, 5410–5418.

162 P. D. Jarowski, Y.-L. Wu, W. B. Schweizer and F. Diederich, *Org. Lett.*, 2008, **10**, 3347–3350.

163 A. R. Waterloo, S. Kunakom, F. Hampel and R. R. Tykwinski, *Macromol. Chem. Phys.*, 2012, **213**, 1020–1032.

164 Y. Han and H. V. Huynh, *Dalton Trans.*, 2011, **40**, 2141–2147.

165 D. Schweinfurth, R. Pattacini, S. Strobel and B. Sarkar, *Dalton Trans.*, 2009, 9291–9297.

166 B. Schulze, C. Friebe, M. D. Hager, W. Günther, U. Köhn, B. O. Jahn, H. Görls and U. S. Schubert, *Org. Lett.*, 2010, **12**, 2710–2713.

167 M. Obata, A. Kitamura, A. Mori, C. Kameyama, J. A. Czaplewska, R. Tanaka, I. Kinoshita, T. Kusumoto, H. Hashimoto, M. Harada, Y. Mikata, T. Funabiki and S. Yano, *Dalton Trans.*, 2008, 3292–3300.

168 B. Schulze, D. Escudero, C. Friebe, R. Siebert, H. Görls, S. Sinn, M. Thomas, S. Mai, J. Popp, B. Dietzek, L. González and U. S. Schubert, *Chem.–Eur. J.*, 2012, **18**, 4010–4025.

169 D. Urankar, B. Pinter, A. Pevec, F. De Proft, I. Turel and J. Košmrlj, *Inorg. Chem.*, 2010, **49**, 4820–4829.

170 M. Ostermeier, M.-A. Berlin, R. M. Meudtner, S. Demeshko, F. Meyer, C. Limberg and S. Hecht, *Chem.–Eur. J.*, 2010, **16**, 10202–10213.

171 A. Wild, C. Friebe, A. Winter, M. D. Hager, U.-W. Grummt and U. S. Schubert, *Eur. J. Org. Chem.*, 2010, 1859–1868.

172 T. J. Del Castillo, S. Sarkar, K. A. Abboud and A. S. Veige, *Dalton Trans.*, 2011, **40**, 8140–8144.

173 A.-S. Cornec, C. Baudequin, C. Fiol-Petit, N. Plé, G. Dupas and Y. Ramondenc, *Eur. J. Org. Chem.*, 2013, 1908–1915.

174 I. Stengel, A. Mishra, N. Pootrakulchote, S.-J. Moon, S. M. Zakeeruddin, M. Grätzel and P. Bäuerle, *J. Mater. Chem.*, 2011, **21**, 3726–3734.

175 G. F. Manbeck, W. W. Brennessel and R. Eisenberg, *Inorg. Chem.*, 2011, **50**, 3431–3441.

176 T. Y. Kim, A. B. S. Elliott, K. J. Shaffer, C. John McAdam, K. C. Gordon and J. D. Crowley, *Polyhedron*, 2013, **52**, 1391–1398.

177 P. D. Zoon, I. H. M. van Stokkum, M. Parent, O. Mongin, M. Blanchard-Desce and A. M. Brouwer, *Phys. Chem. Chem. Phys.*, 2010, **12**, 2706–2715.

178 M. Parent, O. Mongin, K. Kamada, C. Katan and M. Blanchard-Desce, *Chem. Commun.*, 2005, 2029–2031.

179 D. Schweinfurth, K. I. Hardcastle and U. H. F. Bunz, *Chem. Commun.*, 2008, 2203–2205.

180 I. Stengel, C. A. Strassert, E. A. Plummer, C.-H. Chien, L. De Cola and P. Bäuerle, *Eur. J. Inorg. Chem.*, 2012, 1795–1809.

181 Z. Zhou and C. J. Fahrni, *J. Am. Chem. Soc.*, 2004, **126**, 8862–8863.

182 G. Nagarjuna, S. Yurt, K. G. Jadhav and D. Venkataraman, *Macromolecules*, 2010, **43**, 8045–8050.

183 C. Hansch, A. Leo and R. W. Taft, *Chem. Rev.*, 1991, **91**, 165–195.

184 P. Shieh, M. J. Hangauer and C. R. Bertozzi, *J. Am. Chem. Soc.*, 2012, **134**, 17428–17431.

185 S. Potratz, A. Mishra and P. Bäuerle, *Beilstein J. Org. Chem.*, 2012, **8**, 683–692.

186 C. A. Ramsden, *Chem. Soc. Rev.*, 1994, **23**, 111–118.

187 A. R. Katritzky, C. A. Ramsden, J. A. Joule and V. V. Zhdankin, *Handbook of Heterocyclic Chemistry*, Elsevier, Amsterdam, 3rd edn, 2010, pp. 87–138.

188 M. P. Cassidy, J. Raushel and V. V. Fokin, *Angew. Chem., Int. Ed.*, 2006, **45**, 3154–3157.

189 T. Horneff, S. Chuprakov, N. Chernyak, V. Gevorgyan and V. V. Fokin, *J. Am. Chem. Soc.*, 2008, **130**, 14972–14974.

190 I. Bae, H. Han and S. Chang, *J. Am. Chem. Soc.*, 2005, **127**, 2038–2039.

191 M. Whiting and V. V. Fokin, *Angew. Chem., Int. Ed.*, 2006, **45**, 3157–3161.

192 V. E. Matulis, Y. S. Halauko, O. A. Ivashkevich and P. N. Gaponik, *THEOCHEM*, 2009, **909**, 19–24.

193 K. Shen, Y. Fu, J.-N. Li, L. Liu and Q.-X. Guo, *Tetrahedron*, 2007, **63**, 1568–1576.

194 R. W. Taft, F. Anvia, M. Taagepera, J. Catalan and J. Elguero, *J. Am. Chem. Soc.*, 1986, **108**, 3237–3239.

195 J. Catalán, R. M. Claramunt, J. Elguero, J. Laynez, M. Menéndez, F. Anvia, J. H. Quian, M. Taagepera and R. W. Taft, *J. Am. Chem. Soc.*, 1988, **110**, 4105–4111.

196 I. Jano, *J. Phys. Chem.*, 1991, **95**, 7694–7699.

197 S. Cradock, R. H. Findlay and M. H. Palmer, *Tetrahedron*, 1973, **29**, 2173–2181.

198 N. Kovačević and A. Kokalj, *J. Phys. Chem. C*, 2011, **115**, 24189–24197.

199 T. L. Mindt, H. Struthers, L. Brans, T. Anguelov, C. Schweinsberg, V. Maes, D. Tourwé and R. Schibli, *J. Am. Chem. Soc.*, 2006, **128**, 15096–15097.

200 Z. Zhou, S. Li, Y. Zhang, M. Liu and W. Li, *J. Am. Chem. Soc.*, 2005, **127**, 10824–10825.

201 Z. Zhou, R. Liu, J. Wang, S. Li, M. Liu and J.-L. Brédas, *J. Phys. Chem. A*, 2006, **110**, 2322–2324.

202 J. K.-C. Lau, C. H. S. Wong, P. S. Ng, F. M. Siu, N. L. Ma and C. W. Tsang, *Chem.–Eur. J.*, 2003, **9**, 3383–3396.

203 E. R. Kay, D. A. Leigh and F. Zerbetto, *Angew. Chem., Int. Ed.*, 2007, **46**, 72–191.

204 A. C. Fahrenbach and J. F. Stoddart, *Chem.–Asian J.*, 2011, **6**, 2660–2669.

205 P. R. Schreiner, *Chem. Soc. Rev.*, 2003, **32**, 289–296.

206 A. G. Doyle and E. N. Jacobsen, *Chem. Rev.*, 2007, **107**, 5713–5743.

207 P. D. Beer and P. A. Gale, *Angew. Chem., Int. Ed.*, 2001, **40**, 486–516.

208 A. Caballero, F. Zapata and P. D. Beer, *Coord. Chem. Rev.*, 2013, **257**, 2434–2455.

209 M. D. Lankshear and P. D. Beer, *Coord. Chem. Rev.*, 2006, **250**, 3142–3160.

210 G. T. Spence and P. D. Beer, *Acc. Chem. Res.*, 2013, **46**, 571–586.

211 E. Arunan, G. R. Desiraju, R. A. Klein, J. Sadlej, S. Scheiner, I. Alkorta, D. C. Clary, R. H. Crabtree, J. J. Dannenberg, P. Hobza, H. G. Kjaergaard, A. C. Legon, B. Mennucci and D. J. Nesbitt, *Pure Appl. Chem.*, 2011, **83**, 1637–1641.

212 G. R. Desiraju, *Angew. Chem., Int. Ed.*, 2011, **50**, 52–59.

213 G. R. Desiraju, *Acc. Chem. Res.*, 2002, **35**, 565–573.

214 P. Gilli, L. Pretto, V. Bertolasi and G. Gilli, *Acc. Chem. Res.*, 2009, **42**, 33–44.

215 S. J. Grabowski, *Chem. Rev.*, 2011, **111**, 2597–2625.

216 P. Gilli, V. Bertolasi, V. Ferretti and G. Gilli, *J. Am. Chem. Soc.*, 1994, **116**, 909–915.

217 T. Steiner, *Angew. Chem., Int. Ed.*, 2002, **41**, 48–76.

218 L. J. Prins, D. N. Reinhoudt and P. Timmerman, *Angew. Chem., Int. Ed.*, 2001, **40**, 2382–2426.

219 T. H. Rehm and C. Schmuck, *Chem. Soc. Rev.*, 2010, **39**, 3597–3611.

220 K. Hirose, *J. Inclusion Phenom. Macrocyclic Chem.*, 2001, **39**, 193–209.

221 P. Thordarson, *Chem. Soc. Rev.*, 2011, **40**, 1305–1323.

222 F. P. Schmidtchen, *Analytical Methods in Supramolecular Chemistry*, Wiley-VCH Verlag GmbH & Co. KGaA, 2012, pp. 67–103.

223 J. L. Sessler, D. E. Gross, W.-S. Cho, V. M. Lynch, F. P. Schmidtchen, G. W. Bates, M. E. Light and P. A. Gale, *J. Am. Chem. Soc.*, 2006, **128**, 12281–12288.

224 F. P. Schmidtchen, *Chem. Soc. Rev.*, 2010, **39**, 3916–3935.

225 F. P. Schmidtchen, *Coord. Chem. Rev.*, 2006, **250**, 2918–2928.

226 V. Gutmann, *Coord. Chem. Rev.*, 1976, **18**, 225–255.

227 V. S. Bryantsev and B. P. Hay, *Org. Lett.*, 2005, **7**, 5031–5034.

228 K. P. McDonald, Y. Hua and A. H. Flood, *Top. Heterocycl. Chem.*, 2010, **24**, 341–366.

229 B. P. Hay and V. S. Bryantsev, *Chem. Commun.*, 2008, 2417–2428.

230 V. R. Pedireddi and G. R. Desiraju, *J. Chem. Soc., Chem. Commun.*, 1992, 988–990.

231 R. Vargas, J. Garza, D. A. Dixon and B. P. Hay, *J. Am. Chem. Soc.*, 2000, **122**, 4750–4755.

232 K. P. McDonald, R. O. Ramabhadran, S. Lee, K. Raghavachari and A. H. Flood, *Org. Lett.*, 2011, **13**, 6260–6263.

233 J. L. Sessler, J. Cai, H.-Y. Gong, X. Yang, J. F. Arambula and B. P. Hay, *J. Am. Chem. Soc.*, 2010, **132**, 14058–14060.

234 S. Defazio, G. Tamasi and R. Cini, *C. R. Chim.*, 2005, **8**, 1584–1609.

235 D.-W. Yoon, D. E. Gross, V. M. Lynch, J. L. Sessler, B. P. Hay and C.-H. Lee, *Angew. Chem., Int. Ed.*, 2008, **47**, 5038–5042.

236 H. Lumbroso, *J. Mol. Struct.*, 1991, **244**, 259–276.

237 F. G. Bordwell, J. A. Harrelson and T. Y. Lynch, *J. Org. Chem.*, 1990, **55**, 3337–3341.

238 F. G. Bordwell, *Acc. Chem. Res.*, 1988, **21**, 456–463.

239 A. E. Reed, L. A. Curtiss and F. Weinhold, *Chem. Rev.*, 1988, **88**, 899–926.

240 F. G. Bordwell and G. Z. Ji, *J. Am. Chem. Soc.*, 1991, **113**, 8398–8401.

241 G. Lauri and P. A. Bartlett, *J. Comput. Aided Mol. Des.*, 1994, **8**, 51–66.

242 B. P. Hay, *Chem. Soc. Rev.*, 2010, **39**, 3700–3708.

243 S. Kubik, C. Reyheller and S. Stüwe, *J. Inclusion Phenom. Macrocyclic Chem.*, 2005, **52**, 137–187.

2564 | *Chem. Soc. Rev.*, 2014, **43**, 2522–2571

This journal is © The Royal Society of Chemistry 2014

244 F. P. Schmidtchen and M. Berger, *Chem. Rev.*, 1997, **97**, 1609–1646.

245 K. Kavallieratos, S. R. de Gala, D. J. Austin and R. H. Crabtree, *J. Am. Chem. Soc.*, 1997, **119**, 2325–2326.

246 S. Lee, Y. Hua, H. Park and A. H. Flood, *Org. Lett.*, 2010, **12**, 2100–2102.

247 N. G. White and P. D. Beer, *Chem. Commun.*, 2012, **48**, 8499–8501.

248 S. C. Picot, B. R. Mullaney and P. D. Beer, *Chem.–Eur. J.*, 2012, **18**, 6230–6237.

249 I. A. W. Filot, A. R. A. Palmans, P. A. J. Hilbers, R. A. van Santen, E. A. Pidko and T. F. A. de Greef, *J. Phys. Chem. B*, 2010, **114**, 13667–13674.

250 Y. Li, J. C. Huffman and A. H. Flood, *Chem. Commun.*, 2007, 2692–2694.

251 R. M. Meudtner, M. Ostermeier, R. Goddard, C. Limberg and S. Hecht, *Chem.–Eur. J.*, 2007, **13**, 9834–9840.

252 T. Merckx, P. Verwilst and W. Dehaen, *Tetrahedron Lett.*, 2013, **54**, 4237–4240.

253 L. Piot, R. M. Meudtner, T. El Malah, S. Hecht and P. Samorì, *Chem.–Eur. J.*, 2009, **15**, 4788–4792.

254 R. M. Meudtner and S. Hecht, *Angew. Chem., Int. Ed.*, 2008, **47**, 4926–4930.

255 R. M. Meudtner and S. Hecht, *Macromol. Rapid Commun.*, 2008, **29**, 347–351.

256 Y. Wang, F. Li, Y. Han, F. Wang and H. Jiang, *Chem.–Eur. J.*, 2009, **15**, 9424–9433.

257 D. Zornik, R. M. Meudtner, T. El Malah, C. M. Thiele and S. Hecht, *Chem.–Eur. J.*, 2011, **17**, 1473–1484.

258 Y.-Y. Zhu, G.-T. Wang, R.-X. Wang and Z.-T. Li, *Cryst. Growth Des.*, 2009, **9**, 4778–4783.

259 C.-F. Wu, X. Zhao, W.-X. Lan, C. Cao, J.-T. Liu, X.-K. Jiang and Z.-T. Li, *J. Org. Chem.*, 2012, **77**, 4261–4270.

260 B.-Y. Lu, Z.-M. Li, Y.-Y. Zhu, X. Zhao and Z.-T. Li, *Tetrahedron*, 2012, **68**, 8857–8862.

261 L.-Y. You, S.-G. Chen, X. Zhao, Y. Liu, W.-X. Lan, Y. Zhang, H.-J. Lu, C.-Y. Cao and Z.-T. Li, *Angew. Chem., Int. Ed.*, 2012, **51**, 1657–1661.

262 T. Pirali, S. Gatti, R. Di Brisco, S. Tacchi, R. Zaninetti, E. Brunelli, A. Massarotti, G. Sorba, P. L. Canonico, L. Moro, A. A. Genazzani, G. C. Tron and R. A. Billington, *ChemMedChem*, 2007, **2**, 437–440.

263 H. Juwarker, J. M. Lenhardt, J. C. Castillo, E. Zhao, S. Krishnamurthy, R. M. Jamiolkowski, K.-H. Kim and S. L. Craig, *J. Org. Chem.*, 2009, **74**, 8924–8934.

264 M. Mammen, E. I. Shakhnovich and G. M. Whitesides, *J. Org. Chem.*, 1998, **63**, 3168–3175.

265 I. Bandyopadhyay, K. Raghavachari and A. H. Flood, *ChemPhysChem*, 2009, **10**, 2535–2540.

266 Y. Hua and A. H. Flood, *Chem. Soc. Rev.*, 2010, **39**, 1262–1271.

267 Y. Hua, R. O. Ramabhadran, J. A. Karty, K. Raghavachari and A. H. Flood, *Chem. Commun.*, 2011, **47**, 5979–5981.

268 Y. Hua, R. O. Ramabhadran, E. O. Uduehi, J. A. Karty, K. Raghavachari and A. H. Flood, *Chem.–Eur. J.*, 2011, **17**, 312–321.

269 S. Lee and A. Flood, *Top. Heterocycl. Chem.*, 2012, **28**, 1–23.

270 Y. Li and A. H. Flood, *J. Am. Chem. Soc.*, 2008, **130**, 12111–12122.

271 Y. Li and A. H. Flood, *Angew. Chem., Int. Ed.*, 2008, **47**, 2649–2652.

272 K. P. McDonald, Y. Hua, S. Lee and A. H. Flood, *Chem. Commun.*, 2012, **48**, 5065–5075.

273 R. O. Ramabhadran, Y. Hua, Y.-j. Li, A. H. Flood and K. Raghavachari, *Chem.–Eur. J.*, 2011, **17**, 9123–9129.

274 H. Juwarker, J. M. Lenhardt, D. M. Pham and S. L. Craig, *Angew. Chem., Int. Ed.*, 2008, **47**, 3740–3743.

275 B. L. Vallee and R. J. Williams, *Proc. Natl. Acad. Sci. U. S. A.*, 1968, **59**, 498–505.

276 C. Cui, S. J. Cho and K. S. Kim, *J. Phys. Chem. A*, 1998, **102**, 1119–1123.

277 E. M. Zahran, Y. Hua, Y. Li, A. H. Flood and L. G. Bachas, *Anal. Chem.*, 2010, **82**, 368–375.

278 D. A. Leigh, C. C. Robertson, A. M. Z. Slawin and P. I. T. Thomson, *J. Am. Chem. Soc.*, 2013, **135**, 9939–9943.

279 V. Haridas, S. Sahu, P. P. Praveen Kumar and A. R. Sapala, *RSC Adv.*, 2012, **2**, 12594–12605.

280 J. M. Aizpurua, R. M. Fratila, Z. Monasterio, N. Pérez-Esnaola, E. Andreieff, A. Irastorza and M. Sagartzazu-Aizpurua, *New J. Chem.*, 2014, DOI: 10.1039/C3NJ00667K.

281 A. Kumar and P. S. Pandey, *Org. Lett.*, 2007, **10**, 165–168.

282 R. K. Chhatra, A. Kumar and P. S. Pandey, *J. Org. Chem.*, 2011, **76**, 9086–9089.

283 P. Mathew, A. Neels and M. Albrecht, *J. Am. Chem. Soc.*, 2008, **130**, 13534–13535.

284 K. Ohmatsu, M. Kiyokawa and T. Ooi, *J. Am. Chem. Soc.*, 2011, **133**, 1307–1309.

285 Q.-Y. Cao, T. Pradhan, M. H. Lee, K. No and J. S. Kim, *Analyst*, 2012, **137**, 4454–4457.

286 R. Lalrempuia, N. D. McDaniel, H. Müller-Bunz, S. Bernhard and M. Albrecht, *Angew. Chem., Int. Ed.*, 2010, **49**, 9765–9768.

287 L. Bernet, R. Lalrempuia, W. Ghattas, H. Mueller-Bunz, L. Vigara, A. Llobet and M. Albrecht, *Chem. Commun.*, 2011, **47**, 8058–8060.

288 S. Sanghi, E. Willett, C. Versek, M. Tuominen and E. B. Coughlin, *RSC Adv.*, 2012, **2**, 848–853.

289 K. M. Mullen, J. Mercurio, C. J. Serpell and P. D. Beer, *Angew. Chem., Int. Ed.*, 2009, **48**, 4781–4784.

290 L. C. Gilday, N. G. White and P. D. Beer, *Dalton Trans.*, 2012, **41**, 7092–7097.

291 G. T. Spence, M. B. Pitak and P. D. Beer, *Chem.–Eur. J.*, 2012, **18**, 7100–7108.

292 N. G. White and P. D. Beer, *Beilstein J. Org. Chem.*, 2012, **8**, 246–252.

293 N. G. White, S. Carvalho, V. Felix and P. D. Beer, *Org. Biomol. Chem.*, 2012, **10**, 6951–6959.

294 Q.-Y. Cao, Z.-C. Wang, M. Li and J.-H. Liu, *Tetrahedron Lett.*, 2013, **54**, 3933–3936.

295 M. Delgado-Rebollo, D. Canseco-Gonzalez, M. Hollering, H. Mueller-Bunz and M. Albrecht, *Dalton Trans.*, 2014, DOI: 10.1039/C3DT53052C.

This journal is © The Royal Society of Chemistry 2014

Chem. Soc. Rev., 2014, **43**, 2522–2571 | **2565**

296 J. Bouffard, B. K. Keitz, R. Tonner, G. Guisado-Barrios, G. Frenking, R. H. Grubbs and G. Bertrand, *Organometallics*, 2011, **30**, 2617–2627.

297 K. F. Donnelly, A. Petronilho and M. Albrecht, *Chem. Commun.*, 2013, 1145–1159.

298 Y. Chu, H. Deng and J.-P. Cheng, *J. Org. Chem.*, 2007, **72**, 7790–7793.

299 E. M. Higgins, J. A. Sherwood, A. G. Lindsay, J. Armstrong, R. S. Massey, R. W. Alder and A. C. O'Donoghue, *Chem. Commun.*, 2011, **47**, 1559–1561.

300 T. Dröge and F. Glorius, *Angew. Chem., Int. Ed.*, 2010, **49**, 6940–6952.

301 R. S. Massey, C. J. Collett, A. G. Lindsay, A. D. Smith and A. C. O'Donoghue, *J. Am. Chem. Soc.*, 2012, **134**, 20421–20432.

302 P. A. Hunt, B. Kirchner and T. Welton, *Chem.–Eur. J.*, 2006, **12**, 6762–6775.

303 C. Caumes, O. Roy, S. Faure and C. Taillefumier, *J. Am. Chem. Soc.*, 2012, **134**, 9553–9556.

304 B. Sui, B. Kim, Y. Zhang, A. Frazer and K. D. Belfield, *ACS Appl. Mater. Interfaces*, 2013, **5**, 2920–2923.

305 M. Begtrup, *Acta Chem. Scand.*, 1971, **25**, 249–259.

306 M. N. Kobrak and H. Li, *Phys. Chem. Chem. Phys.*, 2010, **12**, 1922–1932.

307 K. Wendler, S. Zahn, F. Dommert, R. Berger, C. Holm, B. Kirchner and L. Delle Site, *J. Chem. Theory Comput.*, 2011, **7**, 3040–3044.

308 C. Krekeler, F. Dommert, J. Schmidt, Y. Y. Zhao, C. Holm, R. Berger and L. Delle Site, *Phys. Chem. Chem. Phys.*, 2010, **12**, 1817–1821.

309 C. Krekeler, J. Schmidt, Y. Y. Zhao, B. Qiao, R. Berger, C. Holm and L. D. Site, *J. Chem. Phys.*, 2008, **129**, 174503–174507.

310 J. Schmidt, C. Krekeler, F. Dommert, Y. Zhao, R. Berger, L. D. Site and C. Holm, *J. Phys. Chem. B*, 2010, **114**, 6150–6155.

311 K. Wendler, F. Dommert, Y. Y. Zhao, R. Berger, C. Holm and L. Delle Site, *Faraday Discuss.*, 2012, **154**, 111–132.

312 J. Cai, B. P. Hay, N. J. Young, X. Yang and J. Sessler, *Chem. Sci.*, 2013, **4**, 1560–1567.

313 H. Boroudjerdi, Y. W. Kim, A. Naji, R. R. Netz, X. Schlagberger and A. Serr, *Phys. Rep.*, 2005, **416**, 129–199.

314 H. Ihm, S. Yun, H. G. Kim, J. K. Kim and K. S. Kim, *Org. Lett.*, 2002, **4**, 2897–2900.

315 K. Sato, S. Arai and T. Yamagishi, *Tetrahedron Lett.*, 1999, **40**, 5219–5222.

316 G. Boche, P. Andrews, K. Harms, M. Marsch, K. S. Rangappa, M. Schimeczek and C. Willeke, *J. Am. Chem. Soc.*, 1996, **118**, 4925–4930.

317 S. Tsuzuki, H. Tokuda and M. Mikami, *Phys. Chem. Chem. Phys.*, 2007, **9**, 4780–4784.

318 G. T. Spence, C. J. Serpell, J. Sardinha, P. J. Costa, V. Félix and P. D. Beer, *Chem.–Eur. J.*, 2011, **17**, 12955–12966.

319 A. Caballero, S. Bennett, C. J. Serpell and P. D. Beer, *CrystEngComm*, 2013, **15**, 3076–3081.

320 J. Yoon, S. K. Kim, N. J. Singh and K. S. Kim, *Chem. Soc. Rev.*, 2006, **35**, 355–360.

321 B. Dietrich, M. W. Hosseini, J. M. Lehn and R. B. Sessions, *J. Am. Chem. Soc.*, 1981, **103**, 1282–1283.

322 P. Arranz, A. Bencini, A. Bianchi, P. Diaz, E. García-España, C. Giorgi, S. V. Luis, M. Querol and B. Valtancoli, *J. Chem. Soc., Perkin Trans. 2*, 2001, 1765–1770.

323 K. Ohmatsu, A. Goto and T. Ooi, *Chem. Commun.*, 2012, **48**, 7913–7915.

324 K. Ohmatsu, Y. Hamajima and T. Ooi, *J. Am. Chem. Soc.*, 2012, **134**, 8794–8797.

325 O. Hassel, *Science*, 1970, **170**, 497–502.

326 G. Cavallo, P. Metrangolo, T. Pilati, G. Resnati, M. Sansotera and G. Terraneo, *Chem. Soc. Rev.*, 2010, **39**, 3772–3783.

327 P. Metrangolo, F. Meyer, T. Pilati, G. Resnati and G. Terraneo, *Angew. Chem., Int. Ed.*, 2008, **47**, 6114–6127.

328 P. Metrangolo, H. Neukirch, T. Pilati and G. Resnati, *Acc. Chem. Res.*, 2005, **38**, 386–395.

329 M. Erdelyi, *Chem. Soc. Rev.*, 2012, **41**, 3547–3557.

330 T. M. Beale, M. G. Chudzinski, M. G. Sarwar and M. S. Taylor, *Chem. Soc. Rev.*, 2013, **42**, 1667–1680.

331 P. Politzer, P. Lane, M. Concha, Y. Ma and J. Murray, *J. Mol. Model.*, 2007, **13**, 305–311.

332 T. Clark, M. Hennemann, J. Murray and P. Politzer, *J. Mol. Model.*, 2007, **13**, 291–296.

333 K. E. Riley and P. Hobza, *J. Chem. Theory Comput.*, 2008, **4**, 232–242.

334 N. J. M. Amezaga, S. C. Pamies, N. l. M. Peruchena and G. L. Sosa, *J. Phys. Chem. A*, 2010, **114**, 552–562.

335 B. Pinter, N. Nagels, W. A. Herrebout and F. De Proft, *Chem.–Eur. J.*, 2013, **19**, 519–530.

336 M. G. Sarwar, B. Dragisic, L. J. Salsberg, C. Gouliaras and M. S. Taylor, *J. Am. Chem. Soc.*, 2010, **132**, 1646–1653.

337 S. M. Walter, F. Kniep, L. Rout, F. P. Schmidtchen, E. Herdtweck and S. M. Huber, *J. Am. Chem. Soc.*, 2012, **134**, 8507–8512.

338 M. G. Sarwar, B. Dragisić, E. Dimitrijević and M. S. Taylor, *Chem.–Eur. J.*, 2013, **19**, 2050–2058.

339 M. Cametti, K. Raatikainen, P. Metrangolo, T. Pilati, G. Terraneo and G. Resnati, *Org. Biomol. Chem.*, 2012, **10**, 1329–1333.

340 L. C. Gilday, N. G. White and P. D. Beer, *Dalton Trans.*, 2013, **42**, 15766–15773.

341 A. R. Voth, P. Khuu, K. Oishi and P. S. Ho, *Nat. Chem.*, 2009, **1**, 74–79.

342 N. L. Kilah, M. D. Wise and P. D. Beer, *Cryst. Growth Des.*, 2011, **11**, 4565–4571.

343 M. G. Chudzinski, C. A. McClary and M. S. Taylor, *J. Am. Chem. Soc.*, 2011, **133**, 10559–10567.

344 C. J. Serpell, N. L. Kilah, P. J. Costa, V. Félix and P. D. Beer, *Angew. Chem., Int. Ed.*, 2010, **49**, 5322–5326.

345 N. G. White, A. Caballero and P. D. Beer, *CrystEngComm*, 2014, DOI: 10.1039/C3CE41944D.

346 N. L. Kilah, M. D. Wise, C. J. Serpell, A. L. Thompson, N. G. White, K. E. Christensen and P. D. Beer, *J. Am. Chem. Soc.*, 2010, **132**, 11893–11895.

347 F. Kniep, L. Rout, S. M. Walter, H. K. V. Bensch, S. H. Jungbauer, E. Herdtweck and S. M. Huber, *Chem. Commun.*, 2012, **48**, 9299–9301.

348 R. Tepper, B. Schulze, M. Jäger, C. Friebe, D. Scharf, H. Görls and U. S. Schubert, manuscript in preparation.

349 Q.-C. Shi, Y.-X. Lu, J.-C. Fan, J.-W. Zou and Y.-H. Wang, *THEOCHEM*, 2008, **853**, 39–44.

350 M. Watkinson, *Top. Heterocycl. Chem.*, 2012, **28**, 1–28.

351 Y. H. Lau, P. J. Rutledge, M. Watkinson and M. H. Todd, *Chem. Soc. Rev.*, 2011, **40**, 2848–2866.

352 J. J. Bryant and U. H. F. Bunz, *Chem.–Asian J.*, 2013, **8**, 1354–1367.

353 W. Yan, X. Ye, N. G. Akhmedov, J. L. Petersen and X. Shi, *Org. Lett.*, 2012, **14**, 2358–2361.

354 N. Ségaud, J.-N. Rebilly, K. Sénéchal-David, R. Guillot, L. Billon, J.-P. Baltaze, J. Farjon, O. Reinaud and F. Banse, *Inorg. Chem.*, 2013, **52**, 691–700.

355 C. Hua, K. Q. Vuong, M. Bhadbhade and B. A. Messerle, *Organometallics*, 2012, **31**, 1790–1800.

356 C. M. Wong, K. Q. Vuong, M. R. D. Gatus, C. Hua, M. Bhadbhade and B. A. Messerle, *Organometallics*, 2012, **31**, 7500–7510.

357 D. Schweinfurth, C.-Y. Su, S.-C. Wei, P. Braunstein and B. Sarkar, *Dalton Trans.*, 2012, **41**, 12984–12990.

358 K. E. Djernes, O. Moshe, M. Mettry, D. D. Richards and R. J. Hooley, *Org. Lett.*, 2012, **14**, 788–791.

359 D. Wang, D. Denux, J. Ruiz and D. Astruc, *Adv. Synth. Catal.*, 2013, **355**, 129–142.

360 C. Ornelas, J. R. Aranzaes, L. Salmon and D. Astruc, *Chem.–Eur. J.*, 2008, **14**, 50–64.

361 G. Zhang, Y. Wang, X. Wen, C. Ding and Y. Li, *Chem. Commun.*, 2012, **48**, 2979–2981.

362 E. Hao, Z. Wang, L. Jiao and S. Wang, *Dalton Trans.*, 2010, **39**, 2660–2666.

363 E. Amadio, M. Bertoldini, A. Scrivanti, G. Chessa, V. Beghetto, U. Matteoli, R. Bertani and A. Dolmella, *Inorg. Chim. Acta*, 2011, **370**, 388–393.

364 N. Chandrasekhar and R. Chandrasekar, *Dalton Trans.*, 2010, **39**, 9872–9878.

365 D. Schweinfurth, F. Weisser, D. Bubrin, L. Bogani and B. Sarkar, *Inorg. Chem.*, 2011, **50**, 6114–6121.

366 P. M. Guha, H. Phan, J. S. Kinyon, W. S. Brotherton, K. Sreenath, J. T. Simmons, Z. Wang, R. J. Clark, N. S. Dalal, M. Shatruk and L. Zhu, *Inorg. Chem.*, 2012, **51**, 3465–3477.

367 B. Schulze, D. G. Brown, K. C. D. Robson, C. Friebe, M. Jäger, E. Birckner, C. P. Berlinguette and U. S. Schubert, *Chem.–Eur. J.*, 2013, **19**, 14171–14180.

368 S. Sinn, B. Schulze, C. Friebe, D. G. Brown, M. Jäger, J. Kübel, B. Dietzek, C. P. Berlinguette and U. S. Schubert, *Inorg. Chem.*, 2014, DOI: 10.1021/ic402701v.

369 S. Sinn, B. Schulze, C. Friebe, D. G. Brown, M. Jäger, E. Altuntaş, J. Kübel, O. Guntner, B. Dietzek, C. P. Berlinguette and U. S. Schubert, *Inorg. Chem.*, 2014, DOI: 10.1021/ic402702z.

370 D. G. Brown, P. A. Schauer, J. Borau-Garcia, B. R. Fancy and C. P. Berlinguette, *J. Am. Chem. Soc.*, 2013, **135**, 1692–1695.

371 J. M. Fernández-Hernández, C.-H. Yang, J. I. Beltrán, V. Lemaur, F. Polo, R. Fröhlich, J. Cornil and L. De Cola, *J. Am. Chem. Soc.*, 2011, **133**, 10543–10558.

372 J. M. Fernández-Hernández, J. I. Beltrán, V. Lemaur, M.-D. Gálvez-López, C.-H. Chien, F. Polo, E. Orselli, R. Fröhlich, J. Cornil and L. De Cola, *Inorg. Chem.*, 2013, **52**, 1812–1824.

373 J. D. Crowley and D. A. McMorran, *Top. Heterocycl. Chem.*, 2012, **28**, 1–53.

374 H. Struthers, T. L. Mindt and R. Schibli, *Dalton Trans.*, 2010, **39**, 675–696.

375 G. Frenking, K. Wichmann, N. Fröhlich, C. Loschen, M. Lein, J. Frunzke and V. M. Rayón, *Coord. Chem. Rev.*, 2003, **238–239**, 55–82.

376 A. Maisonial, P. Serafin, M. Traïkia, E. Debiton, V. Théry, D. J. Aitken, P. Lemoine, B. Viossat and A. Gautier, *Eur. J. Inorg. Chem.*, 2008, 298–305.

377 G. Frenking, *J. Organomet. Chem.*, 2001, **635**, 9–23.

378 H. Huang and M. T. Rodgers, *J. Phys. Chem. A*, 2002, **106**, 4277–4289.

379 P. Su and H. Li, *J. Chem. Phys.*, 2009, **131**, 014102.

380 E. D. Glendening, *J. Am. Chem. Soc.*, 1996, **118**, 2473–2482.

381 G. Frenking and N. Fröhlich, *Chem. Rev.*, 2000, **100**, 717–774.

382 R. Tonner, G. Heydenrych and G. Frenking, *Chem.–Asian J.*, 2007, **2**, 1555–1567.

383 G. Heydenrych, M. von Hopffgarten, E. Stander, O. Schuster, H. G. Raubenheimer and G. Frenking, *Eur. J. Inorg. Chem.*, 2009, 1892–1904.

384 K. Tamao, M. Uchida, T. Izumizawa, K. Furukawa and S. Yamaguchi, *J. Am. Chem. Soc.*, 1996, **118**, 11974–11975.

385 C. A. Tolman, *Chem. Rev.*, 1977, **77**, 313–348.

386 J. E. Huheey, E. A. Keiter and R. L. Keiter, *Inorganic Chemistry: Principles of Structure and Reactivity*, HarperCollins College Publishers, New York, 1993.

387 B. S. Uppal, R. K. Booth, N. Ali, C. Lockwood, C. R. Rice and P. I. P. Elliott, *Dalton Trans.*, 2011, **40**, 7610–7616.

388 A. B. P. Lever, *Inorg. Chem.*, 1990, **29**, 1271–1285.

389 B. Schulze, C. Friebe, M. D. Hager, A. Winter, R. Hoogenboom, H. Görls and U. S. Schubert, *Dalton Trans.*, 2009, 787–794.

390 B. Happ, C. Friebe, A. Winter, M. D. Hager, R. Hoogenboom and U. S. Schubert, *Chem.–Asian J.*, 2009, **4**, 154–163.

391 J. T. Fletcher, B. J. Bumgarner, N. D. Engels and D. A. Skoglund, *Organometallics*, 2008, **27**, 5430–5433.

392 C. E. Welby, S. Grkinic, A. Zahid, B. S. Uppal, E. A. Gibson, C. R. Rice and P. I. P. Elliott, *Dalton Trans.*, 2012, **41**, 7637–7646.

393 N. H. Damrauer, G. Cerullo, A. Yeh, T. R. Boussie, C. V. Shank and J. K. McCusker, *Science*, 1997, **275**, 54–57.

394 A. Juris, V. Balzani, F. Barigelletti, S. Campagna, P. Belser and A. von Zelewsky, *Coord. Chem. Rev.*, 1988, **84**, 85–277.

395 F. Alary, J. L. Heully, L. Bijeire and P. Vicendo, *Inorg. Chem.*, 2007, **46**, 3154–3165.

396 S. H. Wadman, M. Lutz, D. M. Tooke, A. L. Spek, F. Hartl, R. W. A. Havenith, G. P. M. van Klink and G. van Koten, *Inorg. Chem.*, 2009, **48**, 1887–1900.

397 O. A. Borg, S. S. M. C. Godinho, M. J. Lundqvist, S. Lunell and P. Persson, *J. Phys. Chem. A*, 2008, **112**, 4470–4476.

398 U. Monkowius, S. Ritter, B. König, M. Zabel and H. Yersin, *Eur. J. Inorg. Chem.*, 2007, 4597–4606.

399 S. Hohloch, D. Schweinfurth, F. Weisser, F. Ehret, N. Deibel, M. Sommer and B. Sarkar, *Dalton Trans.*, 2014, DOI: 10.1039/C3DT52898G.

400 A. Boulay, A. Seridi, C. Zedde, S. Ladeira, C. Picard, L. Maron and E. Benoist, *Eur. J. Inorg. Chem.*, 2010, 5058–5062.

401 M. Wolff, L. Munoz, A. Francois, C. Carrayon, A. Seridi, N. Saffon, C. Picard, B. Machura and E. Benoist, *Dalton Trans.*, 2013, **42**, 7019–7031.

402 B. Beyer, C. Ulbricht, D. Escudero, C. Friebe, A. Winter, L. González and U. S. Schubert, *Organometallics*, 2009, **28**, 5478–5488.

403 S. Ladouceur, D. Fortin and E. Zysman-Colman, *Inorg. Chem.*, 2011, **50**, 11514–11526.

404 K. N. Swanick, S. Ladouceur, E. Zysman-Colman and Z. Ding, *Chem. Commun.*, 2012, **48**, 3179–3181.

405 W.-W. Yang, L. Wang, Y.-W. Zhong and J. Yao, *Organometallics*, 2011, **30**, 2236–2240.

406 W. Yang and Y. Zhong, *Chin. J. Chem.*, 2013, **31**, 329–338.

407 C. Friebe, B. Schulze, H. Görls, M. Jäger and U. S. Schubert, *Chem.–Eur. J.*, 2014, DOI: 10.1002/chem.201301439.

408 S. Zanarini, M. Felici, G. Valenti, M. Marcaccio, L. Prodi, S. Bonacchi, P. Contreras-Carballada, R. M. Williams, M. C. Feiters, R. J. M. Nolte, L. De Cola and F. Paolucci, *Chem.–Eur. J.*, 2011, **17**, 4640–4647.

409 M. Mydlak, C. Bizzarri, D. Hartmann, W. Sarfert, G. Schmid and L. De Cola, *Adv. Funct. Mater.*, 2010, **20**, 1812–1820.

410 A. Maity, J.-S. Choi, T. S. Teets, N. Deligonul, A. J. Berdis and T. G. Gray, *Chem.–Eur. J.*, 2013, **19**, 15924–15932.

411 M. Juricek, M. Felici, P. Contreras-Carballada, J. Lauko, S. R. Bou, P. H. J. Kouwer, A. M. Brouwer and A. E. Rowan, *J. Mater. Chem.*, 2011, **21**, 2104–2111.

412 J. M. Fernández-Hernández, S. Ladouceur, Y. Shen, A. Iordache, X. Wang, L. Donato, S. Gallagher-Duval, M. de Anda Villa, J. D. Slinker, L. De Cola and E. Zysman-Colman, *J. Mater. Chem. C*, 2013, **1**, 7440–7452.

413 L. Donato, P. Abel and E. Zysman-Colman, *Dalton Trans.*, 2013, **42**, 8402–8412.

414 M. A. Halcrow, *Coord. Chem. Rev.*, 2009, **253**, 2493–2514.

415 P. Gütlich, A. Hauser and H. Spiering, *Angew. Chem., Int. Ed. Engl.*, 1994, **33**, 2024–2054.

416 A. B. Gaspar, M. Seredyuk and P. Gütlich, *Coord. Chem. Rev.*, 2009, **253**, 2399–2413.

417 Y. Bodenthin, U. Pietsch, H. Möhwald and D. G. Kurth, *J. Am. Chem. Soc.*, 2005, **127**, 3110–3114.

418 E. C. Constable, G. Baum, E. Bill, R. Dyson, R. van Eldik, D. Fenske, S. Kaderli, D. Morris, A. Neubrand, M. Neuburger, D. R. Smith, K. Wieghardt, M. Zehnder and A. D. Zuberbühler, *Chem.–Eur. J.*, 1999, **5**, 498–508.

419 T. Romero, R. l. A. Orenes, A. Espinosa, A. Tárraga and P. Molina, *Inorg. Chem.*, 2011, **50**, 8214–8224.

420 D. Schweinfurth, J. Krzystek, I. Schapiro, S. Demeshko, J. Klein, J. Telser, A. Ozarowski, C.-Y. Su, F. Meyer, M. Atanasov, F. Neese and B. Sarkar, *Inorg. Chem.*, 2013, **52**, 6880–6892.

421 C. B. Anderson, A. B. S. Elliott, C. J. McAdam, K. C. Gordon and J. D. Crowley, *Organometallics*, 2013, **32**, 788–797.

422 C. B. Anderson, A. B. S. Elliott, J. E. M. Lewis, C. J. McAdam, K. C. Gordon and J. D. Crowley, *Dalton Trans.*, 2012, **41**, 14625–14632.

423 B. Happ, D. Escudero, M. D. Hager, C. Friebe, A. Winter, H. Görls, E. Altuntaş, L. González and U. S. Schubert, *J. Org. Chem.*, 2010, **75**, 4025–4038.

424 K. N. Swanick, S. Ladouceur, E. Zysman-Colman and Z. Ding, *Angew. Chem., Int. Ed.*, 2012, **51**, 11079–11082.

425 A. Mattiuzzi, I. Jabin, C. Moucheron and A. Kirsch-De Mesmaeker, *Dalton Trans.*, 2011, **40**, 7395–7402.

426 S. C. Bottorff, A. L. Moore, A. R. Wemple, D.-K. Bučar, L. R. MacGillivray and P. D. Benny, *Inorg. Chem.*, 2013, **52**, 2939–2950.

427 B. Colasson, N. Le Poul, Y. Le Mest and O. Reinaud, *Inorg. Chem.*, 2011, **50**, 10985–10993.

428 S. Blanchard, L. Le Clainche, M.-N. Rager, B. Chansou, J.-P. Tuchagues, A. F. Duprat, Y. Le Mest and O. Reinaud, *Angew. Chem., Int. Ed.*, 1998, **37**, 2732–2735.

429 H. A. Michaels, C. S. Murphy, R. J. Clark, M. W. Davidson and L. Zhu, *Inorg. Chem.*, 2010, **49**, 4278–4287.

430 J. T. Simmons, J. R. Allen, D. R. Morris, R. J. Clark, C. W. Levenson, M. W. Davidson and L. Zhu, *Inorg. Chem.*, 2013, **52**, 5838–5850.

431 R. Dobrawa, P. Ballester, R. Saha-Möller Chantu and F. Würthner, *Metal-Containing and Metallosupramolecular Polymers and Materials*, American Chemical Society, 2006, pp. 43–62.

432 R. Dobrawa, M. Lysetska, P. Ballester, M. Grüne and F. Würthner, *Macromolecules*, 2005, **38**, 1315–1325.

433 K. S. Hagen, *Inorg. Chem.*, 2000, **39**, 5867–5869.

434 R. H. Holyer, C. D. Hubbard, S. F. A. Kettle and R. G. Wilkins, *Inorg. Chem.*, 1966, **5**, 622–625.

435 R. Hogg and R. G. Wilkins, *J. Chem. Soc.*, 1962, 341–350.

436 B. B. Beele, E. Rudiger, F. Schworer, U. Mullich, A. Geist and P. J. Panak, *Dalton Trans.*, 2013, **42**, 12139–12147.

437 S. Aizawa, K. Matsuda, T. Tajima, M. Maeda, T. Sugata and S. Funahashi, *Inorg. Chem.*, 1995, **34**, 2042–2047.

438 O. Fleischel, N. Wu and A. Petitjean, *Chem. Commun.*, 2010, **46**, 8454–8456.

439 D. T. Richens, *Chem. Rev.*, 2005, **105**, 1961–2002.

440 B. Schulze, C. Friebe, S. Hoeppener, G. M. Pavlov, A. Winter, M. D. Hager and U. S. Schubert, *Macromol. Rapid Commun.*, 2012, **33**, 597–602.

441 B. M. J. M. Suijkerbuijk, B. N. H. Aerts, H. P. Dijkstra, M. Lutz, A. L. Spek, G. van Koten and R. J. M. Klein Gebbink, *Dalton Trans.*, 2007, 1273–1276.

442 M. Schmülling, D. M. Grove, G. van Koten, R. van Eldik, N. Veldman and A. L. Spek, *Organometallics*, 1996, **15**, 1384–1391.

443 G. Frenking, M. Solà and S. F. Vyboishchikov, *J. Organomet. Chem.*, 2005, **690**, 6178–6204.

444 H. V. Huynh, Y. Han, R. Jothibasu and J. A. Yang, *Organometallics*, 2009, **28**, 5395–5404.

445 K. J. Kilpin, E. L. Gavey, C. J. McAdam, C. B. Anderson, S. J. Lind, C. C. Keep, K. C. Gordon and J. D. Crowley, *Inorg. Chem.*, 2011, **50**, 6334–6346.

2568 | *Chem. Soc. Rev.*, 2014, **43**, 2522–2571

This journal is © The Royal Society of Chemistry 2014

446 G. Frenking, K. Wichmann, N. Fröhlich, J. Grobe, W. Golla, D. L. Van, B. Krebs and M. Läge, *Organometallics*, 2002, **21**, 2921–2930.

447 M. Kaupp, B. Metz and H. Stoll, *Angew. Chem., Int. Ed.*, 2000, **39**, 4607–4609.

448 H. Jude, J. A. Krause Bauer and W. B. Connick, *Inorg. Chem.*, 2003, **43**, 725–733.

449 K. Hasan and E. Zysman-Colman, *Inorg. Chem.*, 2012, **51**, 12560–12564.

450 K. Nielsen and I. Søtofte, *Acta Chem. Scand.*, 1985, **A39**, 259–271.

451 K. Nielsen, I. Søtofte and H. Johansen, *Acta Chem. Scand.*, 1993, **47**, 943–949.

452 K. Yoshikawa, M. Hashimoto and I. Morishima, *J. Am. Chem. Soc.*, 1974, **96**, 288–289.

453 S. F. Nelsen, *J. Org. Chem.*, 1984, **49**, 1891–1897.

454 A. Comas-Vives and J. N. Harvey, *Eur. J. Inorg. Chem.*, 2011, 5025–5035.

455 H. A. Bent, *Chem. Rev.*, 1961, **61**, 275–311.

456 L. P. Battaglia, M. Carcelli, F. Ferraro, L. Mavilla, C. Pelizzi and G. Pelizzi, *J. Chem. Soc., Dalton Trans.*, 1994, 2651–2654.

457 E. Manoj, M. R. P. Kurup, R. P. John, M. Nethaji and A. Punnoose, *Inorg. Chem. Commun.*, 2009, **12**, 952–955.

458 C. J. Simmons, B. J. Hathaway, K. Amornjarusiri, B. D. Santarsiero and A. Clearfield, *J. Am. Chem. Soc.*, 1987, **109**, 1947–1958.

459 M.-M. Yu, Y.-N. Zhang and L.-H. Wei, *Acta Crystallogr., Sect. E: Struct. Rep. Online*, 2007, **63**, m2380.

460 D. Urankar, A. Pevec, I. Turel and J. Košmrlj, *Cryst. Growth Des.*, 2010, **10**, 4920–4927.

461 J. D. Crowley, P. H. Bandeen and L. R. Hanton, *Polyhedron*, 2010, **29**, 70–83.

462 A. Bastero, D. Font and M. A. Pericàs, *J. Org. Chem.*, 2007, **72**, 2460–2468.

463 Y. Fu, Y. Liu, X. Fu, L. Zou, H. Li, M. Li, X. Chen and J. Qin, *Chin. J. Chem.*, 2010, **28**, 2226–2232.

464 B. Pinter, A. Demšar, D. Urankar, F. De Proft and J. Košmrlj, *Polyhedron*, 2011, **30**, 2368–2373.

465 W. S. Brotherton, P. M. Guha, H. Phan, R. J. Clark, M. Shatruk and L. Zhu, *Dalton Trans.*, 2011, **40**, 3655–3665.

466 G. Aromí, L. A. Barrios, O. Roubeau and P. Gamez, *Coord. Chem. Rev.*, 2011, **255**, 485–546.

467 A. L. Rheingold, L. M. Liable-Sands and S. Trofimenko, *Angew. Chem., Int. Ed.*, 2000, **39**, 3321–3324.

468 J. Alcántara-Garciá, V. Jancik, J. Barroso, S. Hidalgo-Bonilla, R. Cea-Olivares, R. A. Toscano and M. Moya-Cabrera, *Inorg. Chem.*, 2009, **48**, 5874–5883.

469 M. Tropiano, C. J. Record, E. Morris, H. S. Rai, C. Allain and S. Faulkner, *Organometallics*, 2012, **31**, 5673–5676.

470 E. Orselli, R. Q. Albuquerque, P. M. Fransen, R. Fröhlich, H. M. Janssen and L. De Cola, *J. Mater. Chem.*, 2008, **18**, 4579–4590.

471 J. C. Loren, A. Krasiński, V. V. Fokin and K. B. Sharpless, *Synlett*, 2005, 2847–2850.

472 M. Duati, S. Tasca, F. C. Lynch, H. Bohlen, J. G. Vos, S. Stagni and M. D. Ward, *Inorg. Chem.*, 2003, **42**, 8377–8384.

473 T. Kemmerich, J. H. Nelson, N. E. Takach, H. Boebme, B. Jablonski and W. Beck, *Inorg. Chem.*, 1982, **21**, 1226–1232.

474 G. Q. Li and M. Orchin, *J. Organomet. Chem.*, 1997, **535**, 43–47.

475 C.-W. Chang and G.-H. Lee, *Organometallics*, 2003, **22**, 3107–3116.

476 E. Evangelio, N. P. Rath and L. M. Mirica, *Dalton Trans.*, 2012, **41**, 8010–8021.

477 L. Casarrubios, M. C. de la Torre and M. A. Sierra, *Chem.–Eur. J.*, 2013, **19**, 3534–3541.

478 T. Cruchter, K. Harms and E. Meggers, *Chem.–Eur. J.*, 2013, **19**, 16682–16689.

479 S. Komeda, M. Lutz, A. L. Spek, Y. Yamanaka, T. Sato, M. Chikuma and J. Reedijk, *J. Am. Chem. Soc.*, 2002, **124**, 4738–4746.

480 A. Magistrato, P. Ruggerone, K. Spiegel, P. Carloni and J. Reedijk, *J. Phys. Chem. B*, 2005, **110**, 3604–3613.

481 J. A. Balanta-Díaz, M. Moya-Cabrera, V. Jancik, L. W. Pineda-Cedeño, R. A. Toscano and R. Cea-Olivares, *Inorg. Chem.*, 2009, **48**, 2518–2525.

482 W.-Y. Gao, W. Yan, R. Cai, L. Meng, A. Salas, X.-S. Wang, L. Wojtas, X. Shi and S. Ma, *Inorg. Chem.*, 2012, **51**, 4423–4425.

483 C. Richardson, C. M. Fitchett, F. R. Keene and P. J. Steel, *Dalton Trans.*, 2008, 2534–2537.

484 M. Grzywa, D. Denysenko, J. Hanss, E.-W. Scheidt, W. Scherer, M. Weil and D. Volkmer, *Dalton Trans.*, 2012, **41**, 4239–4248.

485 Y.-Y. Liu, M. Grzywa, M. Tonigold, G. Sastre, T. Schuttrigkeit, N. S. Leeson and D. Volkmer, *Dalton Trans.*, 2011, **40**, 5926–5938.

486 F. Gándara, F. J. Uribe-Romo, D. K. Britt, H. Furukawa, L. Lei, R. Cheng, X. Duan, M. O'Keeffe and O. M. Yaghi, *Chem.–Eur. J.*, 2012, **18**, 10595–10601.

487 J. C. Rybak, L. V. Meyer, J. Wagenhöfer, G. Sextl and K. Müller-Buschbaum, *Inorg. Chem.*, 2012, **51**, 13204–13213.

488 J. Xiao, B.-Y. Liu, G. Wei and X.-C. Huang, *Inorg. Chem.*, 2011, **50**, 11032–11038.

489 R. Shaw, R. H. Laye, L. F. Jones, D. M. Low, C. Talbot-Eeckelaers, Q. Wei, C. J. Milios, S. Teat, M. Helliwell, J. Raftery, M. Evangelisti, M. Affronte, D. Collison, E. K. Brechin and E. J. L. McInnes, *Inorg. Chem.*, 2007, **46**, 4968–4978.

490 M. Albrecht, *Chem. Rev.*, 2009, **110**, 576–623.

491 B. Pinter, V. Van Speybroeck, M. Waroquier, P. Geerlings and F. De Proft, *Phys. Chem. Chem. Phys.*, 2013, **15**, 17354–17365.

492 C. M. Álvarez, L. A. García-Escudero, R. García-Rodriguez and D. Miguel, *Chem. Commun.*, 2012, **48**, 7209–7211.

493 B. Butschke and H. Schwarz, *Chem. Sci.*, 2012, **3**, 308–326.

494 E. M. Schuster, M. Botoshansky and M. Gandelman, *Angew. Chem., Int. Ed.*, 2008, **47**, 4555–4558.

495 E. M. Schuster, M. Botoshansky and M. Gandelman, *Organometallics*, 2009, **28**, 7001–7005.

496 E. M. Schuster, G. Nisnevich, M. Botoshansky and M. Gandelman, *Organometallics*, 2009, **28**, 5025–5031.

497 E. M. Schuster, M. Botoshansky and M. Gandelman, *Dalton Trans.*, 2011, **40**, 8764–8767.

498 R. J. Detz, S. A. Heras, R. de Gelder, P. W. N. M. van Leeuwen, H. Hiemstra, J. N. H. Reek and J. H. van Maarseveen, *Org. Lett.*, 2006, **8**, 3227–3230.

499 M. Köhn and R. Breinbauer, *Angew. Chem., Int. Ed.*, 2004, **43**, 3106–3116.

500 D. V. Partyka, J. B. Updegraff, M. Zeller, A. D. Hunter and T. G. Gray, *Organometallics*, 2007, **26**, 183–186.

501 A. Fürstner and P. W. Davies, *Angew. Chem., Int. Ed.*, 2007, **46**, 3410–3449.

502 A. R. Powers, X. Yang, T. J. Del Castillo, I. Ghiviriga, K. A. Abboud and A. S. Veige, *Dalton Trans.*, 2013, **42**, 14963–14966.

503 A. J. Arduengo, F. Davidson, H. V. R. Dias, J. R. Goerlich, D. Khasnis, W. J. Marshall and T. K. Prakasha, *J. Am. Chem. Soc.*, 1997, **119**, 12742–12749.

504 A. J. Arduengo, R. L. Harlow and M. Kline, *J. Am. Chem. Soc.*, 1991, **113**, 361–363.

505 W. A. Herrmann and C. Köcher, *Angew. Chem., Int. Ed. Engl.*, 1997, **36**, 2162–2187.

506 S. Díez-González, N. Marion and S. P. Nolan, *Chem. Rev.*, 2009, **109**, 3612–3676.

507 D. Enders, O. Niemeier and A. Henseler, *Chem. Rev.*, 2007, **107**, 5606–5655.

508 L. Mercs and M. Albrecht, *Chem. Soc. Rev.*, 2010, **39**, 1903–1912.

509 A. J. Arduengo, *Acc. Chem. Res.*, 1999, **32**, 913–921.

510 D. Bourissou, O. Guerret, F. P. Gabbaï and G. Bertrand, *Chem. Rev.*, 2000, **100**, 39–92.

511 D. Martin, M. Melaimi, M. Soleilhavoup and G. Bertrand, *Organometallics*, 2011, **30**, 5304–5313.

512 S. Gründemann, A. Kovacevic, M. Albrecht, J. W. Faller Robert and H. Crabtree, *Chem. Commun.*, 2001, 2274–2275.

513 M. Albrecht, *Chem. Commun.*, 2008, 3601–3610.

514 R. H. Crabtree, *Coord. Chem. Rev.*, 2013, **257**, 755–766.

515 O. Schuster, L. Yang, H. G. Raubenheimer and M. Albrecht, *Chem. Rev.*, 2009, **109**, 3445–3478.

516 M. Begtrup, *J. Chem. Soc., Chem. Commun.*, 1975, 334–335.

517 S. Díez-González and S. P. Nolan, *Coord. Chem. Rev.*, 2007, **251**, 874–883.

518 S. Araki, Y. Wanibe, F. Uno, A. Morikawa, K. Yamamoto, K. Chiba and Y. Butsugan, *Chem. Ber.*, 1993, **126**, 1149–1155.

519 G. Guisado-Barrios, J. Bouffard, B. Donnadieu and G. Bertrand, *Angew. Chem., Int. Ed.*, 2010, **49**, 4759–4762.

520 M. Heckenroth, A. Neels, M. G. Garnier, P. Aebi, A. W. Ehlers and M. Albrecht, *Chem.–Eur. J.*, 2009, **15**, 9375–9386.

521 V. Lavallo, C. A. Dyker, B. Donnadieu and G. Bertrand, *Angew. Chem., Int. Ed.*, 2009, **48**, 1540–1542.

522 J. D. Crowley, A.-L. Lee and K. J. Kilpin, *Aust. J. Chem.*, 2011, **64**, 1118–1132.

523 A. Krüger and M. Albrecht, *Aust. J. Chem.*, 2011, **64**, 1113–1117.

524 J. C. Bernhammer, G. Frison and H. V. Huynh, *Chem.–Eur. J.*, 2013, **19**, 12892–12905.

525 U. Radius and F. M. Bickelhaupt, *Coord. Chem. Rev.*, 2009, **253**, 678–686.

526 H. Jacobsen, A. Correa, A. Poater, C. Costabile and L. Cavallo, *Coord. Chem. Rev.*, 2009, **253**, 687–703.

527 B. Schulze, D. Escudero, C. Friebe, R. Siebert, H. Görls, U. Köhn, E. Altuntas, A. Baumgaertel, M. D. Hager, A. Winter, B. Dietzek, J. Popp, L. González and U. S. Schubert, *Chem.–Eur. J.*, 2011, **17**, 5494–5498.

528 X. Hu, I. Castro-Rodriguez, K. Olsen and K. Meyer, *Organometallics*, 2004, **23**, 755–764.

529 H. Jacobsen, A. Correa, C. Costabile and L. Cavallo, *J. Organomet. Chem.*, 2006, **691**, 4350–4358.

530 D. Yuan and H. V. Huynh, *Organometallics*, 2011, **31**, 405–412.

531 T. Terashima, S. Inomata, K. Ogata and S. Fukuzawa, *Eur. J. Inorg. Chem.*, 2012, 1387–1393.

532 D. G. Gusev, *Organometallics*, 2009, **28**, 6458–6461.

533 L.-A. Schaper, K. Ofele, R. Kadyrov, B. Bechlars, M. Drees, M. Cokoja, W. A. Herrmann and F. E. Kuhn, *Chem. Commun.*, 2012, **48**, 3857–3859.

534 V. Leigh, W. Ghattas, R. Lalrempuia, H. Müller-Bunz, M. T. Pryce and M. Albrecht, *Inorg. Chem.*, 2013, **52**, 5395–5402.

535 D. G. Brown, N. Sanguantrakun, B. Schulze, U. S. Schubert and C. P. Berlinguette, *J. Am. Chem. Soc.*, 2012, **134**, 12354–12357.

536 J. R. Wright, P. C. Young, N. T. Lucas, A.-L. Lee and J. D. Crowley, *Organometallics*, 2013, **32**, 7065–7076.

537 A. l. Poulain, D. Canseco-Gonzalez, R. Hynes-Roche, H. Müller-Bunz, O. Schuster, H. Stoeckli-Evans, A. Neels and M. Albrecht, *Organometallics*, 2011, **30**, 1021–1029.

538 G. Ung and G. Bertrand, *Chem.–Eur. J.*, 2011, **17**, 8269–8272.

539 D. Canseco-Gonzalez and M. Albrecht, *Dalton Trans.*, 2013, **42**, 7424–7432.

540 O. Kühl, *Coord. Chem. Rev.*, 2009, **253**, 2481–2492.

541 T. Karthikeyan and S. Sankararaman, *Tetrahedron Lett.*, 2009, **50**, 5834–5837.

542 A. Bolje and J. Košmrlj, *Org. Lett.*, 2013, **15**, 5084–5087.

543 K. F. Donnelly, R. Lalrempuia, H. Müller-Bunz and M. Albrecht, *Organometallics*, 2012, **31**, 8414–8419.

544 J. C. Y. Lin, R. T. W. Huang, C. S. Lee, A. Bhattacharyya, W. S. Hwang and I. J. B. Lin, *Chem. Rev.*, 2009, **109**, 3561–3598.

545 A. Petronilho, H. Müller-Bunz and M. Albrecht, *Chem. Commun.*, 2012, **48**, 6499–6501.

546 T. Nakamura, T. Terashima, K. Ogata and S. Fukuzawa, *Org. Lett.*, 2011, **13**, 620–623.

547 A. Prades, E. Peris and M. Albrecht, *Organometallics*, 2011, **30**, 1162–1167.

548 K. Ogata, S. Inomata and S. Fukuzawa, *Dalton Trans.*, 2013, **42**, 2362–2365.

549 J. Cai, X. Yang, K. Arumugam, C. W. Bielawski and J. L. Sessler, *Organometallics*, 2011, **30**, 5033–5037.

550 S. Hohloch, L. Suntrup and B. Sarkar, *Organometallics*, 2013, **32**, 7376–7385.

2570 | *Chem. Soc. Rev.*, 2014, **43**, 2522–2571

This journal is © The Royal Society of Chemistry 2014

551 D. Canseco-Gonzalez, A. Gniewek, M. Szulmanowicz, H. Müller-Bunz, A. M. Trzeciak and M. Albrecht, *Chem.– Eur. J.*, 2012, **18**, 6055–6062.

552 R. Saravanakumar, V. Ramkumar and S. Sankararaman, *Organometallics*, 2011, **30**, 1689–1694.

553 R. Saravanakumar, V. Ramkumar and S. Sankararaman, *J. Organomet. Chem.*, 2013, **736**, 36–41.

554 A. Petronilho, M. Rahman, J. A. Woods, H. Al-Sayyed, H. Müller-Bunz, D. J. MacElroy, S. Bernhard and M. Albrecht, *Dalton Trans.*, 2012, **41**, 13074–13080.

555 K. J. Kilpin, U. S. D. Paul, A.-L. Lee and J. D. Crowley, *Chem. Commun.*, 2011, **47**, 328–330.

556 D. Canseco-Gonzalez, A. Petronilho, H. Mueller-Bunz, K. Ohmatsu, T. Ooi and M. Albrecht, *J. Am. Chem. Soc.*, 2013, **135**, 13193–13203.

557 E. C. Keske, O. V. Zenkina, R. Wang and C. M. Crudden, *Organometallics*, 2011, **31**, 456–461.

558 M. Iglesias, D. J. Beetstra, J. C. Knight, L.-L. Ooi, A. Stasch, S. Coles, L. Male, M. B. Hursthouse, K. J. Cavell, A. Dervisi and I. A. Fallis, *Organometallics*, 2008, **27**, 3279–3289.

559 X. Yan, J. Bouffard, G. Guisado-Barrios, B. Donnadieu and G. Bertrand, *Chem.–Eur. J.*, 2012, **18**, 14627–14631.

560 G. Guisado-Barrios, J. Bouffard, B. Donnadieu and G. Bertrand, *Organometallics*, 2011, **30**, 6017–6021.

561 M. T. Zamora, M. J. Ferguson and M. Cowie, *Organometallics*, 2012, **31**, 5384–5395.

562 M. T. Zamora, M. J. Ferguson, R. McDonald and M. Cowie, *Organometallics*, 2012, **31**, 5463–5477.

563 E. C. Keske, O. V. Zenkina, R. Wang and C. M. Crudden, *Organometallics*, 2012, **31**, 6215–6221.

564 S. Hohloch, C.-Y. Su and B. Sarkar, *Eur. J. Inorg. Chem.*, 2011, 3067–3075.

565 Z. Lin, *Coord. Chem. Rev.*, 2007, **251**, 2280–2291.

566 O. Holloczki, D. Gerhard, K. Massone, L. Szarvas, B. Nemeth, T. Veszpremi and L. Nyulaszi, *New J. Chem.*, 2010, **34**, 3004–3009.

567 W. Wirschun, M. Winkler, K. Lutz and J. C. Jochims, *J. Chem. Soc., Perkin Trans. 1*, 1998, 1755–1762.

568 R. Lalrempuia, H. Müller-Bunz and M. Albrecht, *Angew. Chem., Int. Ed.*, 2011, **50**, 9969–9972.

569 A. Petronilho, J. A. Woods, S. Bernhard and M. Albrecht, *Eur. J. Inorg. Chem.*, 2013, DOI: 10.1002/ejic.201300843.

570 M. Raynal, R. Pattacini, C. S. J. Cazin, C. Vallée, H. Olivier-Bourbigou and P. Braunstein, *Organometallics*, 2009, **28**, 4028–4047.

571 J. M. Aizpurua, M. Sagartzazu-Aizpurua, Z. Monasterio, I. Azcune, C. Mendicute, J. I. Miranda, E. García-Lecina, A. Altube and R. M. Fratila, *Org. Lett.*, 2012, **14**, 1866–1868.

572 J. M. Aizpurua, I. Azcune, R. M. Fratila, E. Balentova, M. Sagartzazu-Aizpurua and J. I. Miranda, *Org. Lett.*, 2010, **12**, 1584–1587.

573 J. M. Aizpurua, M. Sagartzazu-Aizpurua, I. Azcune, J. I. Miranda, Z. Monasterio, E. García-Lecina and R. M. Fratila, *Synthesis*, 2011, 2737–2742.

574 I. Fabre, N. von Wolff, G. Le Duc, E. Ferrer Flegeau, C. Bruneau, P. H. Dixneuf and A. Jutand, *Chem.–Eur. J.*, 2013, **19**, 7595–7604.

575 C. M. Crudden and D. P. Allen, *Coord. Chem. Rev.*, 2004, **248**, 2247–2273.

576 A. Krüger, L. J. L. Häller, H. Müller-Bunz, O. Serada, A. Neels, S. A. Macgregor and M. Albrecht, *Dalton Trans.*, 2011, **40**, 9911–9920.

577 B. K. Keitz, J. Bouffard, G. Bertrand and R. H. Grubbs, *J. Am. Chem. Soc.*, 2011, **133**, 8498–8501.

578 A. Krüger and M. Albrecht, *Chem.–Eur. J.*, 2012, **18**, 652–658.

579 C. J. Gagliardi, A. K. Vannucci, J. J. Concepcion, Z. Chen and T. J. Meyer, *Energy Environ. Sci.*, 2012, **5**, 7704–7717.

580 G. van Koten, J. T. B. H. Jastrzebski and J. G. Noltes, *J. Organomet. Chem.*, 1978, **148**, 317–325.

581 Y. Tulchinsky, M. A. Iron, M. Botoshansky and M. Gandelman, *Nat. Chem.*, 2011, **3**, 525–531.

582 J. Choudhury, *Angew. Chem., Int. Ed.*, 2011, **50**, 10772–10774.

583 S. McIlroy, C. J. Cramer and D. E. Falvey, *Org. Lett.*, 2000, **2**, 2451–2454.

This journal is © The Royal Society of Chemistry 2014

Chem. Soc. Rev., 2014, **43**, 2522–2571 | **2571**

Publication A2:

"Anion complexation by triazolium 'ligands': Mono- and bis-tridentate complexes of sulfate"

B. Schulze, C. Friebe, M. D. Hager, W. Günther, U. Köhn, B. O. Jahn, H. Görls, U. S. Schubert

Anion Complexation by Triazolium "Ligands": Mono- and Bis-tridentate Complexes of Sulfate

Benjamin Schulze,[†] Christian Friebe,[†] Martin D. Hager,[†] Wolfgang Günther,[†]
Uwe Köhn,[†] Burkhard O. Jahn,[†] Helmar Görls,[‡] and Ulrich S. Schubert*,[†,§]

*Laboratory of Organic and Macromolecular Chemistry, Friedrich-Schiller-University
Jena, Humboldtstr. 10, 07743 Jena, Germany, Laboratory of Inorganic and Analytic
Chemistry, Friedrich-Schiller-University Jena, Lessing-Str. 8, 07743 Jena, Germany,
and Laboratory for Macromolecular Chemistry and Nanoscience, Eindhoven
University of Technology, P.O. Box 513, 5600 MB Eindhoven, The Netherlands*

ulrich.schubert@uni-jena.de

ABSTRACT
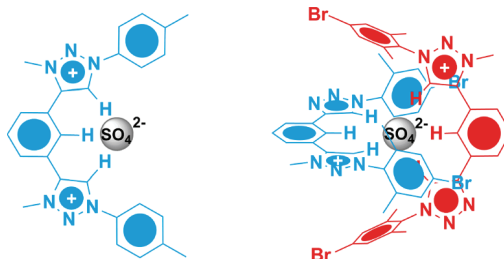
By utilizing click chemistry and methylation, the triazolium motif was employed to design tridentate "ligands" that bind by electron acception instead of electron donation. As electronically inverted ligands they are able to complex sulfate ions by hydrogen bonding and electrostatic interactions. The formation of mono- or bis-tridentate complexes could be achieved by controlling the degree of methylation with the appropriate reagents and was proven by NMR spectroscopy and computational methods.

In supramolecular chemistry, pincer-type ligands have attracted particular interest as exemplarily shown by terpyridine. Consequently, the copper(I)-catalyzed azide alkyne 1,3-dipolar cycloaddition (CuAAC)—one of the prime examples of the concept of highly efficient and modular reactions named click chemistry[1]—has been applied in the synthesis of analogous tridentate ligands, the so-called tripy,[2] coordinating metal ions via triazoles. Recently, click chemistry was successfully applied in anion coordination, and the triazole

and triazolium moieties have been shown to act as efficient C−H hydrogen bond donors as well.[3] We intended to expand the scope of tridentate "clicked" ligands in terms of anion complexation by hydrogen bonding and electrostatic interactions. Since anions can be structured, biorelevant, and nucleophilic, the respective ligands might have potential for template-directed assembling, sensing and recognition of anions, and organocatalysis.[4] Furthermore, they show a dynamic coordination behavior that allows fast switching processes and stimuli responses, respectively.

So far, triazoles have been employed in anion recognition

[†] Laboratory of Organic and Macromolecular Chemistry, Friedrich-Schiller-University Jena.

[‡] Laboratory of Inorganic and Analytic Chemistry, Friedrich-Schiller-University Jena.

[§] Eindhoven University of Technology.

(1) (a) Kolb, H. C.; Finn, M. G.; Sharpless, K. B. *Angew. Chem., Int. Ed.* **2001**, *40*, 2004. (b) Tornøe, C. W.; Meldal, M. *Chem. Rev.* **2008**, *108*, 2952.

(2) (a) Li, Y.; Huffman, J. C.; Flood, A. H. *Chem. Commun.* **2007**, 2692. (b) Meudtner, R. M.; Ostermeier, M.; Goddard, R.; Limberg, C.; Hecht, S. *Chem.—Eur. J.* **2007**, *13*, 9834. (c) Schulze, B.; Friebe, C.; Hager, M. D.; Winter, A.; Hoogenboom, R.; Görls, H.; Schubert, U. S. *Dalton Trans.* **2009**, 787.

in terms of triazolophanes[3a–c] and triazole foldamers[3d–f] where a lot of weak C−H···X interactions were accumulated. Very recently, the anion binding capacity was enhanced by preorganization to form a neutral tridentate hydrogen bond donor.[5] Alternatively, triazolium salts with strongly increased CH-acidity have been used as anion receptors[6] and within the template synthesis of a [2]rotaxane.[7] Furthermore, a [2]catenane has been synthesized by using pyridinium nicotinamide as hydrogen bond donor and sulfate as the templating anion.[8] Both templates were primarily based on hydrogen bonds as well as electrostatic interactions, but required elegantly designed second sphere interactions such as additional hydrogen bonds and π-stacking.[9] There are further interesting examples of 2:1 sulfate complexes, but the ligand syntheses lack facility.[10]

Our approach is to use strong hydrogen bonding as well as electrostatic interactions offered by the triazolium moieties. A direct motivation was to make use of the functional groups that are readily installed within the ligand synthesis by CuAAC, but that point in opposite directions in a metal complex (Scheme 1). Essentially, coordination via the

Scheme 1. Classical and Electronically Inverted Ligands
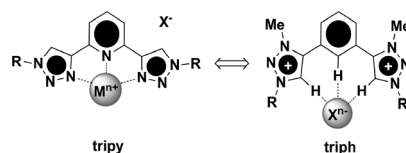
triazole or triazolium protons would lead to functional groups pointing in the same direction and the choice of a tetrahedral anion might allow the formation of an octahedral bis-tridentate complex that can be considered as a *directed* template. Thereby, a singly charged ligand should support the formation of a charge neutral bis-complex with a doubly charged anion.

The synthesis of the building blocks **1** and **2** could be achieved most easily under click conditions (Scheme 2).[1a]

(3) (a) Li, Y.; Flood, A. H. *Angew. Chem., Int. Ed.* **2008**, *47*, 2649. (b) Li, Y.; Flood, A. H. *J. Am. Chem. Soc.* **2008**, *130*, 12111. (c) Li, Y.; Pink, M.; Karty, J. A.; Flood, A. H. *J. Am. Chem. Soc.* **2008**, *130*, 17293. (d) Juwarker, H.; Lenhardt, J. M.; Pham, D. M.; Craig, S. L. *Angew. Chem., Int. Ed.* **2008**, *47*, 3740. (e) Juwarker, H.; Lenhardt, J. M.; Castillo, J. C.; Zhao, E.; Krishnamurthy, S.; Jamiolkowski, R. M.; Kim, K.-H.; Craig, S. L. *J. Org. Chem.* **2009**, *74*, 8924. (f) Meudtner, R. M.; Hecht, S. *Angew. Chem., Int. Ed.* **2008**, *47*, 4926.
(4) (a) Beer, P. D.; Gale, P. A. *Angew. Chem., Int. Ed.* **2001**, *40*, 486. (b) Lankshear, M. D.; Beer, P. D. *Coord. Chem. Rev.* **2006**, *250*, 3142. (c) Schreiner, P. R. *Chem. Soc. Rev.* **2003**, *32*, 289.
(5) Lee, S.; Hua, Y.; Park, H.; Flood, A. H. *Org. Lett.* **2010**, *1*, 2100.
(6) Kumar, A.; Pandey, P. S. *Org. Lett.* **2008**, *10*, 165.
(7) Mullen, K. M.; Mercurio, J.; Serpell, C. S.; Beer, P. D. *Angew. Chem., Int. Ed.* **2009**, *48*, 4781.
(8) Huang, B.; Santos, S. M.; Felix, V.; Beer, P. D. *Chem. Commun.* **2008**, 4610.
(9) Sambrook, M. R.; Beer, P. D.; Wisner, J. A.; Paul, R. L.; Cowley, A. R.; Szemes, F.; Drew, M. G. B. *J. Am. Chem. Soc.* **2005**, *127*, 2292.
(10) (a) Chmielewski, M. J.; Zhao, L.; Brown, A.; Curiel, D.; Sambrook, M. R.; Thompson, A. L.; Santos, S. M.; Felix, V.; Davis, J. J.; Beer, P. D. *Chem. Commun.* **2008**, 3154. (b) Kobiro, K.; Inoue, Y. *J. Am. Chem. Soc.* **2003**, *125*, 421.

Scheme 2. Synthesis of the Anion Coordinating Ligands
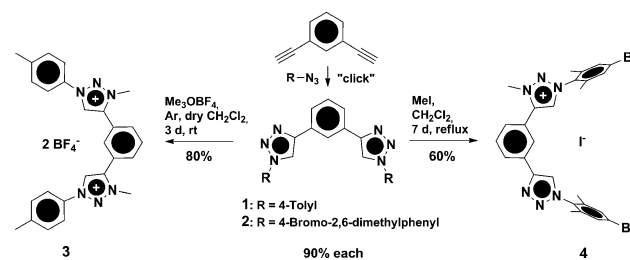
The "activation" for the sulfate complexation could be performed selectively by choosing the appropriate reagents. Methyl iodide just leads to single methylation, while Meerwein's salt easily affords double methylation.

The degree of methylation of **3** and **4** was proven unambiguously by single crystal X-ray diffraction (Figure 1). In the solid state, no tridentate interactions could be found
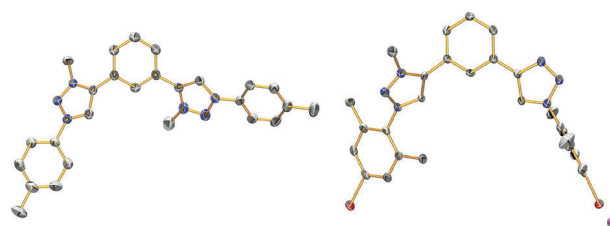
Figure 1. Solid-state structures of **3** (left) and **4** (right) (ellipsoids at 50% propability level; hydrogen atoms, solvents molecules, and tetrafluoroborate anion omitted for clarity).

with the given counterions tetrafluoroborate and iodide, respectively. While ligand **4** features already a *syn-syn* conformation with respect to the potential hydrogen-bonding protons, ligand **3** shows an *anti-syn* conformation but can easily flip in solution since **3** shows at least C_2-symmetry in ^{1}H NMR experiments. However, due to the steric demand in particular of the methyl groups, the triazolium rings are twisted out of plane by 33° for **3** and 38° for **4** in the free ligand, respectively.

The anion coordination behavior of **3** and **4** could be determined qualitatively and quantitatively. A continuous variation plot (Job plot) of **3** and tetrabutylammonium sulfate (TBA$_2$SO$_4$) obtained from ^{1}H NMR spectroscopy revealed the formation of a 1:1 complex.[12] For solubility reasons, acetonitrile-d_3/methanol 4:1 was used as solvent mixture with nondeuterated methanol, since the triazolium protons rapidly undergo deuterium exchange as they are strongly CH-acidic. The association constant of the 1:1 complex could be obtained by ^{1}H NMR titration of **3** with TBA$_2$SO$_4$ (Figure 2) and by analyzing the relatively large triazolium proton downfield shift with the WinEQNMR2 software[11] and was

(11) Hynes, M. J. *J. Chem. Soc., Dalton Trans.* **1993**, 311.
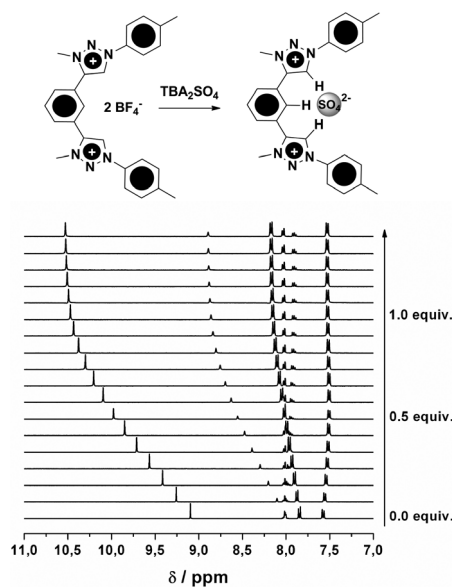
Figure 2. ^{1}H NMR spectra of **3** upon titration with tetrabutyl-ammonium sulfate (TBA$_2$SO$_4$) in acetonitrile-d_3/methanol 4:1 at 298 K.

Figure 4. ^{1}H NMR spectra of **4** upon titration with tetrabutyl-ammonium sulfate (TBA$_2$SO$_4$) in acetonitrile-d_3 at 298 K.

determined to be log $K = 4.39 \pm 0.28$ or $K \approx 24,000$ M^{-1}, respectively.[12]

The concentration-weighted shift of a single signal for the free ligand *and* the complex results from an exchange faster than the NMR time scale. The large binding constant and the fact that the maximum shift, i.e., the full complexation, is nearly reached after the addition of 1 equiv of TBA$_2$SO$_4$ demonstrate a relatively strong sulfate binding even in the presence of methanol. The symmetry within the spectrum and the protons that are involved in the hydrogen bonding indicate a tridentate complexation as depicted in Figure 2.

The Job plot of **4** with sulfate (Figure 3) in acetonitrile-d_3 reveals the formation of a 2:1 complex beside a 1:1 complex.

Figure 3. Continuous variation plot (Job plot) of **4** and TBA$_2$SO$_4$ obtained from ^{1}H NMR spectroscopy (aromatic 4-bromo-2,6-dimethylphenyl protons).

The ^{1}H NMR titration experiment (Figure 4) supports these findings: the aromatic protons of the quasi-mesityl substit-

(12) See Supporting Information.

uents are shifted to higher field with a maximum shift at 0.5 equiv of TBA$_2$SO$_4$ and recover in the course of the titration, whereas the triazole, phenyl, and triazolium signals are downfield-shifted only. Obviously, the protons of the outer phenyl rings selectively respond to the complexation in a bis-tridentate fashion and remain nearly unchanged in the free ligand and in the 1:1 complex. The signals involved in the hydrogen bonding respond similarly on both coordination modes, but with a less pronounced downfield shift for the 2:1 complex since the two ligands compete in binding to the same anion. By titration of TBA$_2$SO$_4$ with **4**, the order of the formed complexes is changed, and thus also the shifts of protons participating in hydogen bonds show a characteristic migration resulting from an initial 1:1 complexation and the successive formation of a 2:1 complex.[12] Again, the set of protons that contribute to the hydrogen bonding can only be explained by a tridentate coordination in each case.

The association constants could be calculated by fitting the titration curve of the aromatic 4-bromo-2,6-dimethylphenyl protons with the WinEQNMR2 software[11] and were determined to be log $K_1 = 3.73 \pm 0.07$ ($K_1 \approx 5,400$ M^{-1}), log $K_2 = 3.1 \pm 0.2$ ($K_2 = 1,300$ M^{-1}), and log $K_1 K_2 = 6.84 \pm 0.15$ ($K_1 K_2 \approx 7,000,000$ M^{-2}).[12] Again, the overall sulfate binding is relatively strong, and the difference of K_1 and K_2 reflects qualitatively the same coordination behavior as in terpyridine complexes of zinc(II), i.e., a 2:1 stoichiometry of host to guest yields a 2:1:1 ratio of 2:1 complex to 1:1 complex to free ligand. With respect to the ligand, the ratio is 4:1:1, and a maximum yield of 70% can be expected from a template synthesis in acetonitrile at a concentration of 10^{-3} M if dynamic effects are negligible as found in the report of Beer and co-workers.[8] This might be improved by removing the iodide with silver sulfate and by using a less polar solvent such as dichloromethane to provoke the formation of the uncharged bis-complex.
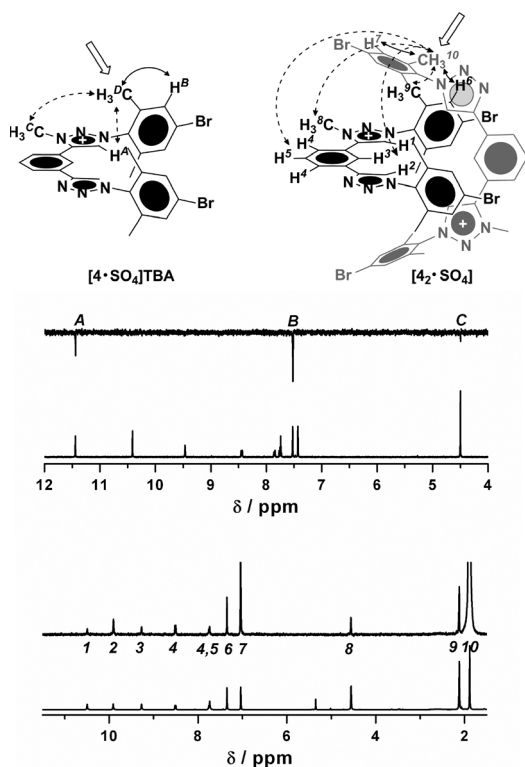
Figure 5. Selective NOESY spectra for [4·SO$_4$]TBA (top, acetonitrile-d_3) and [4$_2$·SO$_4$] (bottom, dichloromethane-d_2) (sulfate omitted; the excited protons are marked with a hollow arrow, and strong and medium NOESY contacts are indicated with solid and dashed arrows, respectively).

To prove a bis-tridentate coordination suitable for templation in solution, selective NOESY experiments were conducted (Figure 5). Therefore, [4$_2$·SO$_4$] was prepared using 4·I and Ag$_2$SO$_4$, whereas [4·SO$_4$]TBA was obtained from a 1:10 mixture of 4·I and TBA$_2$SO$_4$. The methyl groups of the quasi-mesityl substituents, which are not equivalent because of the single site methylation, were excited, and the NOE contacts were recorded.

For the 1:1 complex, only a strong contact to the adjacent aromatic proton and medium contacts to the aromatic and aliphatic triazolium protons on the same side of the molecule were visible. In contrast, the 2:1 complex showed contacts to the central phenyl ring and the other end of the molecule, which is only possible if two ligands arrange in the desired orthogonal fashion. In addition, the phase is inverted due to a doubled molar mass.

To consolidate the indirect image of the bis-tridentate complex obtained by NMR investigations, although crystallization attempts failed, and to exclude packing effects, we conducted DFT calculations (B3LYP/SVP).[12] The results are depicted in Figure 6 and are consistent with the experimental
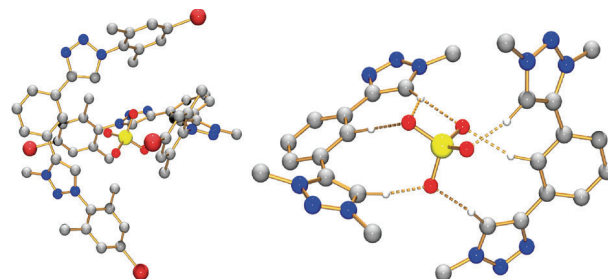
Figure 6. Calculated most stable structure for [4$_2$·SO$_4$]. Left: arrangement of the ligands. Right: hydrogen bonds, substituents omitted for clarity.

findings of a 2:1 complex. As one could expect from the distortion in the crystal structures of the ligands due to the triazolium methyl groups, the sulfate is complexed less ideally but still in the desired way to serve as template.

In conclusion, we applied the facile "click" synthesis with the structural benefits of the triazole and triazolium moieties, respectively, to design tridentate ligands that allow the formation of relatively stable complexes with sulfate ions. The formation of mono- and bis-complexes could be controlled by the number of triazolium moieties within the tridentate ligand. In particular, the formation of a bis-tridentate complex of sulfate could be proven that meets the demands for a [2]catenane template.

Supporting Information Available: Experimental details, spectral data, NMR spectra, binding studies, X-ray data and DFT calculation data. This material is available free of charge via the Internet at http://pubs.acs.org.

OL100776X

Publication A3:

"A heteroleptic *bis*(tridentate) ruthenium(II) complex of a click-derived abnormal carbene pincer ligand with potential for photosensitizer application"

B. Schulze, D. Escudero, C. Friebe, R. Siebert, H. Görls, U. Köhn, E. Altuntaş, A. Baumgaertel, M. D. Hager, A. Winter, B. Dietzek, J. Popp, L. González, U. S. Schubert
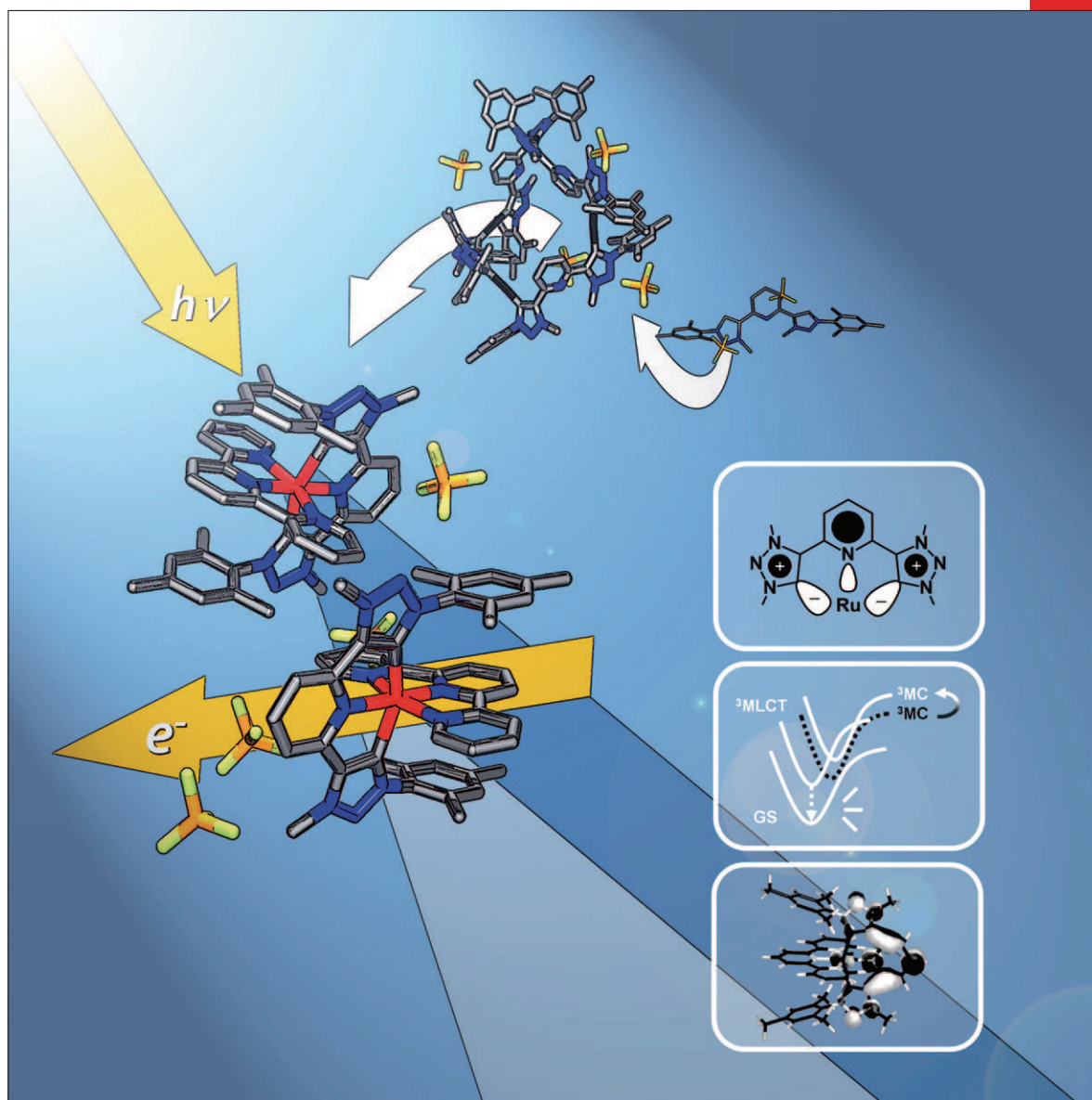
IYC 2011
International Year of
CHEMISTRY

A Journal of

ChemPubSoc
Europe

Supported by
ACES

More than just a click…

… 1,2,3-triazoles not only serve as linkers, they also provide access to 1,2,3-triazolylidenes that are powerful mesoionic carbene donors. In their Communication on page 5494 ff., L. González, U. S. Schubert et al. report on a heteroleptic ruthenium(II) complex of a new tridentate triazolylidene ligand. The complex features great potential for photosensitizer applications and is studied by experimental and computational methods.

www.chemeurj.org

Back Cover

Benjamin Schulze, Daniel Escudero, Christian Friebe, Ronald Siebert, Helmar Görls, Uwe Köhn, Esra Altuntas, Anja Baumgaertel, Martin D. Hager, Andreas Winter, Benjamin Dietzek, Jürgen Popp, Leticia González*, and Ulrich S. Schubert*

More than just a click…

… 1,2,3-triazoles not only serve as linkers, they also provide access to 1,2,3-triazolyli-denes that are powerful mesoionic carbene donors. In their Communication on page 5494 ff., L. González, U. S. Schubert et al. report on a heteroleptic ruthenium(II) complex of a new tridentate triazolylidene ligand. The complex features great potential for photosensitizer applications and is studied by experimental and computational methods.

A Heteroleptic Bis(tridentate) Ruthenium(II) Complex of a Click-Derived Abnormal Carbene Pincer Ligand with Potential for Photosensitzer Application

Benjamin Schulze,[a] Daniel Escudero,[b] Christian Friebe,[a] Ronald Siebert,[c] Helmar Görls,[d] Uwe Köhn,[a] Esra Altuntas,[a] Anja Baumgaertel,[a] Martin D. Hager,[a] Andreas Winter,[a] Benjamin Dietzek,[c] Jürgen Popp,[c] Leticia González,*[b] and Ulrich S. Schubert*[a]

Ruthenium(II) polypyridyl complexes have received particular interest with respect to photosensitizer applications, because they are stable and inert complexes that show a defined metal-to-ligand charge transfer (MLCT).[1] A central dilemma is that trisbidentate complexes (e.g., of 2,2′-bipyridine, bpy) show long excited-state lifetimes, whereas bis(tridentate) complexes (e.g., of 2,2′:6′,2″-terpyridine, tpy) allow the isomer-free construction of linear assemblies for vectorial electron-transfer processes.[2] The quest of diminishing the fast radiationless deactivation of the ^{3}MLCT state through the triplet metal-centered state (^{3}MC) of bis(tridentate) ruthenium(II) polypyridyl complexes[3] has motivated numerous approaches[4–6] that aim at ^{3}MLCT lowering or ^{3}MC raising or both. Ideally, electronic manipulations are realized by direct incorporation of stronger donors, that is, by cyclometalation[7] or coordination through anionic N-heterocycles[8] and N-heterocyclic carbenes (NHCs).[9] Thereby, strong σ and π donation by coordination through anionic carbon or nitrogen donors lead to a destabilized ground state and, thus, a lowered ^{3}MLCT, resulting in a radiationless deactivation governed by the energy-gap law[10] and a low driving force for the potential electron-transfer processes. In contrast, classical NHC ligands are strong, charge-neutral σ donors and π acceptors, thus causing a favorable ^{3}MC destabilization, but also undesirably blue-shifted MLCT transitions. Alternatively, the expansion to six-membered ring chelators[6] leads to excellent excited-state lifetimes by a more favorable bite angle, but can also cause the formation of isomers (*fac*, *mer*) that show very different properties and that are hard to separate.

In this regard, abnormal or mesoionic carbene ligands[11] provide superior σ-donating and only moderate π-accepting properties that ideally would lead to strongly destabilized ^{3}MC states and a maintained ^{3}MLCT energy. 1,2,3-Triazolylidenes match these demands and are readily accessible by modular click chemistry. Herein we present a heteroleptic bis(tridentate) ruthenium(II) complex (RuCNC) of the new 2′,6′-bis(1-mesityl-3-methyl-1,2,3-triazol-4-yl-5-idene)pyridine (CNC) ligand and the parent tpy. A heteroleptic complex with tpy is particularly interesting, because it preserves the elaborated terpyridine chemistry, including a variety of ruthenium precursors, allows for asymmetric functionalization, and includes a reference ligand. The electronic and optical properties of RuCNC were investigated by experimental and theoretical studies.

The synthesis of RuCNC was achieved under mild reaction conditions with a high selectivity and reasonable yield (Scheme 1). For the preparation of 2′,6′-bis(1-mesityl-3-methyl-1,2,3-triazolium-4-yl)pyridine tetrafluoroborate (H$_2$CNC), the parent click-derived 2′,6′-bis(1-mesityl-1,2,3-triazol-4-yl)pyridine (tripy)[12] could be methylated selectively with Meerwein's salt[13] as evidenced by single-crystal X-ray diffraction (Figure 1), spectroscopic, and spectrometric methods. Because free 1,2,3-triazolylidenes undergo a 5–3 methyl shift,[11] a stable silver(I)-precursor (AgCNC) was

[a] Dipl.-Chem. B. Schulze, Dipl.-Chem. C. Friebe, Dr. U. Köhn,
E. Altuntas, Dipl.-Chem. A. Baumgaertel, Dr. M. D. Hager,
Dr. A. Winter, Prof. Dr. U. S. Schubert
Laboratory of Organic and Macromolecular Chemistry (IOMC)
Jena Center for Soft Matter (JCSM)
Friedrich-Schiller-University Jena
Humboldtstr. 10, 07743 Jena (Germany)
Fax: (+49) 3641948202
E-mail: ulrich.schubert@uni-jena.de

[b] D. Escudero, Prof. Dr. L. González
Laboratory of Theoretical Chemistry
Jena Center for Soft Matter (JCSM)
Friedrich-Schiller-University Jena
Helmholtzweg 4, 07743 Jena (Germany)
Fax: (+49) 3641948302
E-mail: leticia.gonzalez@uni-jena.de

[c] Dipl.-Chem. R. Siebert, Dr. B. Dietzek, Prof. Dr. J. Popp
Institute of Physical Chemistry and Abbe Center of Photonics
Jena Center for Soft Matter (JCSM)
Friedrich-Schiller-University Jena
Helmholtzweg 4, 07743 Jena (Germany)
and
Institute of Photonic Technology Jena
Albert-Einstein-Straße 9, 07745 Jena (Germany)

[d] Dr. H. Görls
Laboratory of Inorganic and Analytic Chemistry
Friedrich-Schiller-University Jena
Lessingstr. 8, 07743 Jena (Germany)

Supporting information for this article is available on the WWW under http://dx.doi.org/10.1002/chem.201100045.
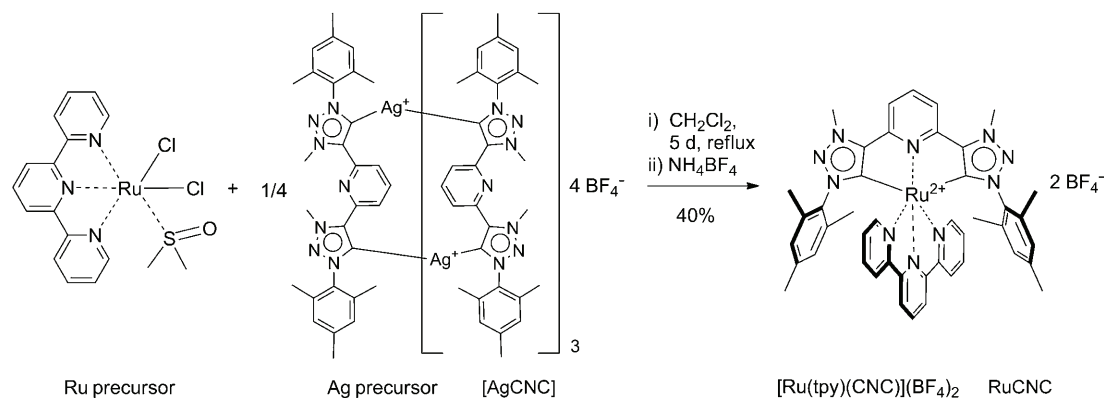
Scheme 1. Schematic representation of the synthesis RuCNC.
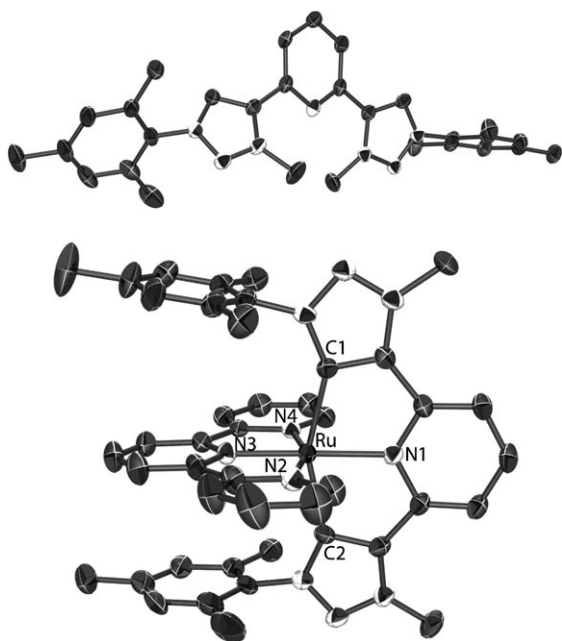
Figure 1. Solid-state structures of H$_2$CNC (top) and RuCNC (bottom, ellipsoids at 50% probability level; hydrogen atoms, solvents molecules, and tetrafluoroborate anions are omitted for clarity). Selected bond lengths (Å) and angles (°) of RuCNC: Ru−C1, 2.058(4); Ru−C2, 2.051(4); Ru−N1, 2.083(4); Ru−N2, 2.068(4); Ru−N3, 1.962(4); Ru−N4, 2.052(4); C1-Ru-C2, 154.34(17); N2-Ru-N4, 158.25(15); N1-Ru-N3, 178.48(15).

prepared by utilizing silver(I) oxide. ESI-ToF MS, MALDI-ToF MS, and MS/MS measurements revealed isotopically resolved peaks of up to tetrameric cycles (see Figure S36 in the Supporting Information for an optimized structure of the tetrameric complex).[14] In the milder ESI MS, mainly the 4:4 complex, beside 3:3 and 1:1 fragments, were observed. Diffusion-ordered NMR-spectroscopy (DOSY) measurements proved the uniformity of the proton signals and the formation of a higher aggregate. In the ^{13}C NMR spectra, the abnormal carbene signals appeared with a typical $^{107/109}$Ag coupling at around 170 ppm that was shifted to higher field by 10 ppm compared with a silver complex of a normal imidazolylidene carbene with a carbon sextet.[14] For

the subsequent transmetalation, common ruthenium(II) and ruthenium(III) monocomplexes of tpy were tested, but only cis-[Ru(tpy)(DMSO)Cl$_2$][15] proved to be a sufficiently selective and reactive precursor. Single crystals of RuCNC suitable for X-ray diffraction were grown by vapor diffusion of diethyl ether into a methanolic solution (Figure 1). The C,N,C-pincer coordination as well as an intramolecular tweezer-like π stacking was clearly confirmed. The ruthenium–carbon bond lengths are identical to those reported for a related heteroleptic ruthenium(II) complex of the classical 2′,6′-bis(3-methylimidazol-1-yl-2-idene)pyridine and terpyridine, other bond lengths are comparable and the bite angles are slightly larger.[9] The identity and purity of the complex were proven by MS and various NMR techniques. The triazolium protons vanished and characteristic high-field shifts due to the π stacking were visible in the ^{1}H NMR spectrum. Furthermore, a strong low-field shift to around 185 ppm can be observed for the coordinating carbons in the ^{13}C NMR spectrum, but again less pronounced than for classical NHC ligands.[9]

The UV/Vis absorption spectrum of RuCNC shows a typical MLCT transition, but, due to the reduced symmetry of the heteroleptic complex, it exhibits a comparatively low extinction coefficient and a band splitting. The absorption profile is similar to the related heteroleptic complex with N,N,N-bound tripy.[12] Noteworthy, the MLCT absorption is only marginally blue-shifted in comparison to the parent [Ru(tpy)$_2$](PF$_6$)$_2$ (see above and Table 1). The room-temperature emission measurement revealed an intense red and unstructured emission with quantum yields close to the [Ru(bpy)$_3$](PF$_6$)$_2$ reference value (Table 1). Furthermore, the emission showed a slow and monoexponential decay, thus arising from a single phosphorescent triplet state (Figure 2). The excited-state lifetime of 633 ns can almost compete with [Ru(bpy)$_3$](PF$_6$)$_2$ and is 2500 times longer than for [Ru(tpy)$_2$](PF$_6$)$_2$.

In comparison to ruthenium(II) complexes of charge-neutral polypyridyl ligands, the redox potentials show a cathodic shift, most likely due to the anionic carbon of the mesoionic carbene, but a similar energy gap. The HOMO and LUMO energies calculated from the cyclovoltammetry results

Table 1. Selected photophysical and electrochemical data.

	[Ru(tpy)$_2$](PF$_6$)$_2$	[Ru(bpy)$_3$](PF$_6$)$_2$	RuCNC
λ_{max}^{Abs} [nm][a]	474	450	463
ε [10^4 M^{-1} cm^{-1}][a]	1.8	1.4	1.0
λ_{ma}^{Em} [nm]	–	597	643 (634)[b]
τ [ns]	0.21[c]	860;[d] 680[d,e]	633; 615[e]
Φ_{PL} [%]	–	6.2[f]	4.4;[g] 5.5[e,g]
$E_{1/2}^{Ox}$ [V][h]	0.90	0.90	0.60
$E_{1/2}^{Red}$ [V][h]	−1.64	−1.71	−1.95
E_{LUMO} [eV][i]	−3.20	−3.28	−2.70
E_{HOMO} [eV][i]	−5.71	−5.70	−5.38

Measured in deaerated acetonitrile at 298 K, unless stated otherwise. [a] Maximum of the MLCT band. [b] Theoretical predicted AEE value (PCM-B3LYP/6-31G*). [c] Measured in butyronitrile at 290 K; from ref. [3a]. [d] From ref. [16]. [e] Measured in deaerated CH$_2$Cl$_2$. [f] From ref. [17a]. [g] Against [Ru(bpy)$_3$](PF$_6$)$_2$ as standard. [h] Measured in CH$_3$CN containing 0.1 M NBu$_4$PF$_6$ and with Fc/Fc$^+$ as a reference. [i] Calculated by using $E^{LUMO/HOMO} = [-(E_{onset}^{Red/Ox} - E_{onset}^{Fc/Fc+}) - 4.8]$ eV.
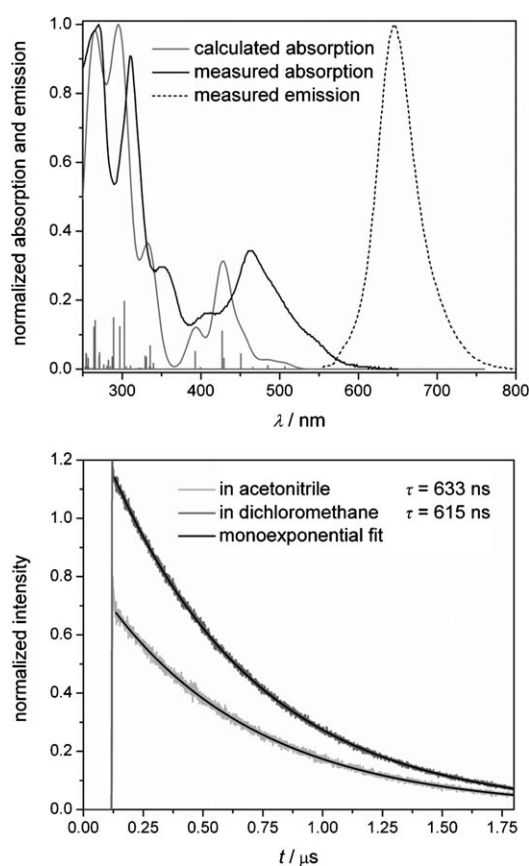
Figure 2. Calculated and measured UV/Vis absorption and measured emission spectra (top). Emission decay (bottom).

(Table 1) are raised in energy and, additionally, the oxidation appears to be reversible. To obtain a more detailed insight into the oxidation process, UV/Vis spectroelectrochemical experiments were executed (see Figure S31 in the Supporting Information). Several isosbestic points suggest the presence of only two species and, thus, a well-defined oxidation process. The most obvious spectral change is the strong decrease of the MLCT bands at 463, 410, and 352 nm, con-

sistent with the assignment of the oxidation process as a ruthenium(II)/ruthenium(III) transition. Additionally, a weak and broad band at around 600 to 800 nm appears, most likely due to ligand-to-metal charge transfer (LMCT, $\pi \rightarrow$ d) transitions, whereas the bands below 330 nm, in the region dominated by ligand-centered (LC) transitions, appear essentially unchanged. Remarkably, the reduction of the oxidized species regenerates the parent complex quantitatively. This highlights the potential of RuCNC to act as an electron donor.

To understand the electronic properties and the bonding of the abnormal carbene ligand to the ruthenium center, energy-decomposition analysis (EDA)[18] was performed (see computational details in the Supporting Information). The EDA (BP86-ZORA/TZP) calculation revealed that the interaction energy between the carbene and the ruthenium(II)–tpy fragment is −256 kcal mol^{-1}. Former EDA calculations on ruthenium complexes of normal (C2-bound) and abnormal (C4-bound) imidazolylidenes revealed interaction energies of −60 to −70 kcal mol^{-1} for a single ruthenium–carbene bond.[19] Assuming these values for a tridentate system still leaves a significant energy difference, this means that CNC enables very strong ruthenium—abnormal carbene bonds. The global interaction energy stems roughly 1:1 from covalent and ionic interactions due to the mesoionic character of the carbene donor ligand. Concerning the covalency of the bond, strong σ-donating as well as π-accepting interactions contribute to the global energy (see Figure S37 and Table S3 in the Supporting Information). Furthermore, time-dependent DFT (TD-DFT) calculations in the presence of acetonitrile (PCM-TD-B3LYP/6-31G*) were performed to rationalize the absorption and emission spectra. The geometry-optimization calculations show that the HOMOs are centered on the ruthenium, whereas the LUMOs are localized on both ligands (Figure 3b). Thus, several transitions, mainly of MLCT character and directed towards both ligands, are observable in the visible region of the absorption spectrum (see Figure 3a and Table S4 in the Supporting In-
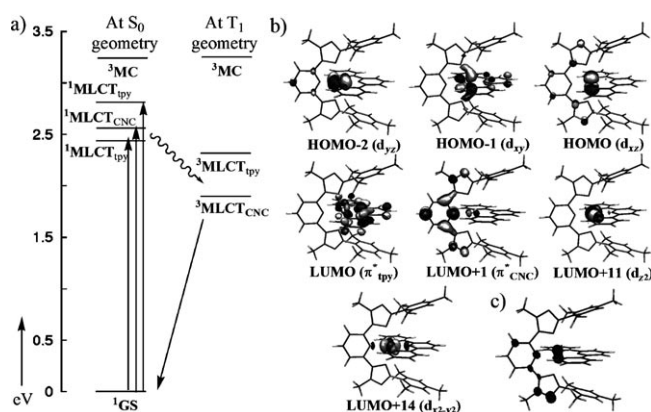
Figure 3. a) Energy-level scheme of the lowest excited states of RuCNC at both the S$_0$- and T$_1$-optimized geometries (GS = ground state). b) Most relevant Kohn–Sham orbitals computed at the PCM-B3LYP/6-31G* level of theory. c) Spin-density plot of the T$_1$ state.

formation). The calculated UV/Vis spectrum is slightly blue-shifted in comparison with the measured spectrum, but both are consistent in shape (see Figure 2). Also, the computed emission maximum is in good agreement with the experiment (see the value of the theoretical predicted adiabatic electronic emission, AEE, in Table 1). Thereby, the longest-wavelength [1]MLCT absorption involves the tpy ligand, whereas, the [3]MLCT emission originates from the carbene ligand after redistribution of electron density in the course of vibrational relaxation and intersystem crossing. The MLCT nature of the T_1 state was confirmed by spin-density analysis (see Figure 3c). Remarkably, due to the strong σ donation, the [3]MC states are of very high energies, 32 kcal mol^{-1} above the [3]MLCT, thus hardly populated thermally and therefore, the radiationless deactivation is suppressed efficiently (see Figure 3a and Table S5). Oppositely, for the parent compound [Ru(tpy)$_2$]$^{2+}$, it was found, with the help of ΔDFT calculations, that the [3]MC state is even 4 kcal mol^{-1} lower in energy than the [3]MLCT.[6f]

In conclusion, click chemistry and subsequent methylation was employed to introduce tridentate 2′,6′-bis(1,2,3-triazolylidene)pyridine ligands with mesoionic carbene donors. Ruthenium(II) complexation was achieved by transmetalation from a tetrameric silver(I) cycle. Due to the superior σ donation of the mesoionic carbene, the heteroleptic ruthenium(II) complex of the new ligand and the parent terpyridine possesses promising photophysical and electrochemical properties with respect to photosensitizer applications. As a bis(tridentate), heteroleptic system, the complex allows for the construction of isomer-free, linear, and asymmetric substituted assemblies.

Experimental Section

Experimental and computational details are provided in the Supporting Information. CCDC-787332 (H$_2$CNC) and -787333 (RuCNC) contain the supplementary crystallographic data for this paper. These data can be obtained free of charge from The Cambridge Crystallographic Data Centre via www.ccdc.cam.ac.uk/data_request/cif.

Acknowledgements

Keywords: carbenes · click chemistry · computational chemistry · photosensitizer · ruthenium

[1] a) A. Juris, V. Balzani, F. Barigelletti, S. Campagna, P. Belser, A. von Zelewsky, *Coord. Chem. Rev.* **1988**, *84*, 85–277; b) J.-P. Sauvage, J.-P. Collin, J.-C. Chambron, S. Guillerez, C. Coudret, V. Balzani, F. Barigelletti, L. De Cola, L. Flamigni, *Chem. Rev.* **1994**, *94*, 993–1019.

[2] a) E. A. Medlycott, G. S. Hanan, *Chem. Soc. Rev.* **2005**, *34*, 133–142; b) E. A. Medlycott, G. S. Hanan, *Coord. Chem. Rev.* **2006**, *250*, 1763–1782.

[3] a) D. W. Fink, W. E. Ohnesorge, *J. Am. Chem. Soc.* **1969**, *91*, 4995–4998; b) A. Amini, A. Harriman, A. Mayeux, *Phys. Chem. Chem. Phys.* **2004**, *6*, 1157–1164.

[4] For the multichromophore approach, see: a) J. Wang, G. S. Hanan, F. Loiseau, S. Campagna, *Chem. Commun.* **2004**, 2068–2069; b) J. H. Wang, Y. Q. Fang, L. Bourget-Merie, M. I. J. Poison, G. S. Hanan, A. Juris, F. Loiseau, S. Campagna, *Chem. Eur. J.* **2006**, *12*, 8539–8548.

[5] For electronic manipulations, see: a) M. Maestri, N. Armaroli, V. Balzani, E. C. Constable, A. M. W. Cargill Thompson, *Inorg. Chem.* **1995**, *34*, 2759–2767; b) Y.-Q. Fang, N. J. Taylor, G. S. Hanan, F. Loiseau, R. Passalacqua, S. Campagna, H. Nierengarten, A. V. Dorsselaer, *J. Am. Chem. Soc.* **2002**, *124*, 7912–7913; c) R. Siebert, A. Winter, B. Dietzek, U. S. Schubert, J. Popp, *Macromol. Rapid Commun.* **2010**, *31*, 883–888.

[6] For structural manipulations, see: a) L. Hammarström, O. Johansson, *Coord. Chem. Rev.* **2010**, *254*, 2546–2559; b) M. Abrahamsson, M. Jäger, T. Österman, L. Eriksson, P. Persson, H.-C. Becker, O. Johansson, L. Hammarström, *J. Am. Chem. Soc.* **2006**, *128*, 12616–12617; c) M. Abrahamsson, M. Jäger, R. J. Kumar, T. Österman, P. Persson, H.-C. Becker, O. Johansson, L. Hammarström, *J. Am. Chem. Soc.* **2008**, *130*, 15533–15542; d) F. Schramm, V. Meded, H. Fliegl, K. Fink, O. Fuhr, Z. Qu, W. Klopper, S. Finn, T. E. Keyes, M. Ruben, *Inorg. Chem.* **2009**, *48*, 5677–5684; e) A. Breivogel, C. Förster, K. Heinze, *Inorg. Chem.* **2010**, *49*, 7052–7056; f) O. Anders Borg, S. S. M. C. Godinho, M. J. Lundqvist, S. Lunell, P. Persson, *J. Phys. Chem. A* **2008**, *112*, 4470–4476; as apparent from the last reference, an ideal octahedral symmetry avoids admixing of ruthenium(II) d orbitals to the LUMO; this lowers the probability of the [3]MLCT-to-[3]MC transition and, consequently, the energy of the MC state becomes less crucial.

[7] a) J.-P. Collin, M. Beley, J.-P. Sauvage, F. Barigelletti, *Inorg. Chim. Acta* **1991**, *186*, 91–93; b) S. H. Wadman, M. Lutz, D. M. Tooke, A. L. Spek, F. Hartl, R. W. A. Havenith, G. P. M. van Klink, G. van Koten, *Inorg. Chem.* **2009**, *48*, 1887–1900; c) M. Jäger, A. Smeigh, F. Lombeck, H. Görls, J.-P. Collin, J.-P. Sauvage, L. Hammarström, O. Johansson, *Inorg. Chem.* **2010**, *49*, 374–376; d) P. G. Bomben, K. C. D. Robson, P. A. Sedach, C. P. Berlinguette, *Inorg. Chem.* **2009**, *48*, 9631–9643.

[8] a) M. Duati, S. Fanni, J. G. Vos, *Inorg. Chem. Commun.* **2000**, *3*, 68–70; b) M. Duati, S. Tasca, F. C. Lynch, H. Bohlen, J. G. Vos, *Inorg. Chem.* **2003**, *42*, 8377–8384.

[9] a) S. U. Son, K. H. Park, Y.-S. Lee, B. Y. Kim, C. H. Choi, M. S. Lah, Y. H. Jang, D.-J. Jang, Y. K. Chung, *Inorg. Chem.* **2004**, *43*, 6896–6898; b) H.-J. Park, K. H. Kim, S. Y. Choi, H.-M. Kim, W. I. Lee, Y. K. Kang, Y. K. Chung, *Inorg. Chem.* **2010**, *49*, 7340–7352.

[10] a) R. Englman, J. Jortner, *Mol. Phys.* **1970**, *18*, 145–164; b) J. V. Caspar, B. P. Sullivan, E. M. Kober, T. J. Meyer, *Chem. Phys. Lett.* **1982**, *91*, 91–95.

[11] a) P. Mathew, A. Neels, M. Albrecht, *J. Am. Chem. Soc.* **2008**, *130*, 13534–13535; b) G. Guisado-Barrios, J. Bouffard, B. Donnadieu, G. Bertrand, *Angew. Chem.* **2010**, *122*, 4869–4872; *Angew. Chem. Int. Ed.* **2010**, *49*, 4759–4762; c) O. Schuster, L. Yang, H. G. Raubenheimer, M. Albrecht, *Chem. Rev.* **2009**, *109*, 3445–3478; d) R. Lalrempuia, N. D. McDaniel, H. Müller-Bunz, S. Bernhard, M. Albrecht, *Angew. Chem.* **2010**, *122*, 9959–9962; *Angew. Chem. Int. Ed.* **2010**, *49*, 9765–9768.

[12] a) Y. Li, J. C. Huffman, A. H. Flood, *Chem. Commun.* **2007**, 2692–2694; b) R. M. Meudtner, M. Ostermeier, R. Goddard, C. Limberg, S. Hecht, *Chem. Eur. J.* **2007**, *13*, 9834–9840; c) B. Schulze, C. Friebe, M. D. Hager, A. Winter, R. Hoogenboom, H. Görls, U. S. Schubert, *Dalton Trans.* **2009**, 787–794; d) M. Ostermeier, M.-A. Berlin, R. M. Meudtner, S. Demeshko, F. Meyer, C. Limberg, S. Hecht, *Chem. Eur. J.* **2010**, *16*, 10202–10213.

[13] a) B. Schulze, C. Friebe, M. D. Hager, W. Günther, U. Köhn, B. O. Jahn, H. Görls, U. S. Schubert, *Org. Lett.* **2010**, *12*, 2710–2713;

b) K. J. Kilpin, U. S. D. Paul, A.-L. Lee, J. D. Crowley, *Chem. Commun.* **2011**, *47*, 328–330; c) K. M. Mullen, J. Mercurio, C. J. Serpell, P. D. Beer, *Angew. Chem.* **2009**, *121*, 4875–4878; *Angew. Chem. Int. Ed.* **2009**, *48*, 4781–4784; d) T. Karthikeyan, S. Sankararaman, *Tetrahedron Lett.* **2009**, *50*, 5834–5837.

[14] a) M. L. Gower, J. D. Crowley, *Dalton Trans.* **2010**, *39*, 2371–2378; b) C. Radloff, H.-Y. Gong, C. Schulte to Brinke, T. Pape, V. M. Lynch, J. L. Sessler, F. E. Hahn, *Chem. Eur. J.* **2010**, *16*, 13077–13081.

[15] R. Ziessel, V. Grosshenny, M. Hissler, C. Stroh, *Inorg. Chem.* **2004**, *43*, 4262–4271.

[16] B. Durham, J. V. Caspar, J. K. Nagle, T. J. Meyer, *J. Am. Chem. Soc.* **1982**, *104*, 4803–4810.

[17] a) J. M. Calvert, J. V. Caspar, R. A. Binstead, T. D. Westmoreland, T. J. Meyer, *J. Am. Chem. Soc.* **1982**, *104*, 6620–6627; b) K. Suzuki, A. Kobayashi, S. Kaneko, K. Takehira, T. Yoshihara, H. Ishida, Y. Shiina, S. Oishic, S. Tobita, *Phys. Chem. Chem. Phys.* **2009**, *11*, 9850–9860. The second reference reported the photoluminescence quantum yield of $[Ru(bpy)_3](PF_6)_2$ to be 9.2%. According to that, the quantum yields of RuCNC would be 6.5 and 8.2%, respectively.

[18] a) F. M. Bickelhaupt, E. J. Baerends, *Kohn–Sham Density Functional Theory: Predicting and Understanding Chemistry in Reviews in Computational Chemistry, Vol. 15* (Eds.: K. B. Lipkowitz, D. B. Boyd), Wiley-VCH, Weinheim, **2000**, pp. 1–86; b) M. Lein, G. Frenking in *Theory and Applications of Computational Chemistry: The First 40 Years* (Eds.: C. E. Dykstra, G. Frenking, K. S. Kim, G. E. Scuseria), Elsevier, Amsterdam, **2005**, pp. 291–367.

[19] a) R. Tonner, G. Heydenrych, G. Frenking, *Chem. Asian J.* **2007**, *2*, 1555–1567; b) N. S. Antonova, J. J. Carbó, J. M. Poblet, *Organometallics* **2009**, *28*, 4283–4287.

Publication A4:

"Physicochemical analysis of ruthenium(II) sensitizers of 1,2,3-triazole-derived mesoionic carbene and cyclometalating ligands"

S. Sinn, B. Schulze, C. Friebe, D. G. Brown, M. Jäger, E. Altuntaş, J. Kübel, O. Guntner, B. Dietzek, C. P. Berlinguette, U. S. Schubert

Physicochemical Analysis of Ruthenium(II) Sensitizers of 1,2,3-Triazole-Derived Mesoionic Carbene and Cyclometalating Ligands

Stephan Sinn,[†,§] Benjamin Schulze,[†,§] Christian Friebe,[†,§] Douglas G. Brown,[‡] Michael Jäger,[†,§] Esra Altuntaş,[†,§] Joachim Kübel,[#,⊥] Oliver Guntner,[#] Curtis P. Berlinguette,*[‡,∥] Benjamin Dietzek,*[#,⊥,§] and Ulrich S. Schubert*[†,§]

[†]Laboratory of Organic and Macromolecular Chemistry (IOMC), Friedrich Schiller University Jena, Humboldtstr. 10, 07743 Jena, Germany

[§]Jena Center for Soft Matter (JCSM), Friedrich Schiller University Jena, Philosophenweg 7, 07743 Jena, Germany

[‡]Department of Chemistry, University of Calgary, 2500 University Drive N.W., Calgary, Alberta, Canada T2N 1N4

[∥]Department of Chemistry, The University of British Columbia, 2036 Main Mall, Vancouver, British Columbia, Canada V6T 1Z1

[#]Institute of Physical Chemistry (IPC) and Abbe Center of Photonics, Friedrich Schiller University Jena, Helmholtzweg 4, 07743 Jena, Germany

[⊥]Leibniz Institute of Photonic Technology (IPHT), Albert-Einstein-Str. 9, 07745 Jena, Germany

Ⓢ Supporting Information

ABSTRACT: A series of heteroleptic bis(tridentate) ruthenium(II) complexes bearing ligands featuring 1,2,3-triazolide and 1,2,3-triazolylidene units are presented. The synthesis of the C^N^N-coordinated ruthenium(II) triazolide complex is achieved by direct C−H activation, which is enabled by the use of a 1,5-disubstituted triazole. By postcomplexation alkylation, the ruthenium(II) 1,2,3-triazolide complex can be converted to the corresponding 1,2,3-triazolylidene complex. Additionally, a ruthenium(II) complex featuring a C^N^C-coordinating bis(1,2,3-triazolylidene)pyridine ligand is prepared via transmetalation from a silver(I) triazolylidene precursor. The electronic consequences of the carbanion and mesoionic carbene donors are studied both experimentally and computationally. The presented complexes exhibit a broad absorption in the visible region as well as long lifetimes of the charge-separated excited state suggesting their application in photoredox catalysis and photovoltaics. Testing of the dyes in a conventional dye-sensitized solar cell (DSSC) generates, however, only modest power conversion efficiencies (PCEs).

■ INTRODUCTION

Ruthenium(II) polypyridyl complexes are promising candidates for the utilization of solar energy by means of photoredox catalysis,[1−5] artificial photosynthesis,[6] and photovoltaic applications like dye-sensitized solar cells (DSSCs),[7−9] as they allow for a light-driven charge separation by a metal-to-ligand charge transfer (MLCT).[10] To exploit the charge-separated triplet excited state (³MLCT), photo- and redox-stability as well as

sufficiently long excited-state lifetimes are required. Bis-(tridentate) ruthenium(II) complexes, e.g., [Ru(tpy)₂]²⁺ (tpy = 2,2′:6′,2″-terpyridine), offer a high stability and allow for isomer-free functionalization, but usually suffer from short-lived excited states owing to a rapid deactivation via an energetically

low lying triplet metal-centered excited state (^{3}MC). The latter is caused by the nonideal bite angle of the tpy ligand, which weakens the σ donation from the outer pyridine rings and, therefore, lowers the energy of the corresponding σ-antibonding orbitals, which are mainly of $d_{x^2-y^2}$ character.[11,12] Different strategies have been developed during the past decades to overcome the poor photophysical properties that are typical for $[Ru(tpy)_2]^{2+}$ including structural[13] and electronic[14,15] manipulations. The latter usually involve an increase of the σ-donor strength by introducing, for instance, carbanionic or carbene donors in the peripheral positions of the tridentate ligand, which help to destabilize the ^{3}MC. Additionally, a decelerated radiationless deactivation of the ^{3}MLCT via the ^{3}MC in organometallic ruthenium(II) complexes may be caused not only by a higher energy barrier, but also by a lower pre-exponential factor.[16,17]

When comparing the electronic effects of carbanion and carbene donors, the repulsive $d(\pi)-p(\pi)$ interaction between the metal center and the carbanion raises the energy of the ^{3}MLCT and, to a greater extent, that of the ground state (GS) resulting in a small ^{3}MLCT–^{3}MC energy gap. The latter enables efficient light harvesting in the DSSC,[7,18] but shortens the excited-state lifetimes by virtue of the energy-gap law.[11,19−23] Additionally, as the ^{3}MLCT is destabilized, the ^{3}MLCT–^{3}MC energy separation is lowered, which facilitates the nonradiative deactivation via the ^{3}MC. In contrast, charge-neutral N-heterocyclic carbenes (NHCs) like imidazol-2-ylidenes and mesoionic carbenes (MICs) such as 1,2,3-triazolylidenes allow for significant ^{3}MC destabilization, while the GS and ^{3}MLCT energies are less affected, which results in significantly prolonged excited-state lifetimes.[24] Recently, we could demonstrate that the exploitation of the superior σ donation provided by 1,2,3-triazolylidenes allows for the design of bis(tridentate) ruthenium(II) complexes with excited-state lifetimes of up to several microseconds.[25−27]

In this work, we present the photophysical and electrochemical properties of a series of heteroleptic bis(tridentate) ruthenium(II) complexes of 1,2,3-triazole-derived ligands that involve either anionic 1,2,3-triazolide or mesoionic 1,2,3-triazolylidene donors (Figure 1).[28] Relative to the N-coordination of the triazole via its 3-nitrogen, the C-coordination of the triazolide or triazolylidene enables significantly stronger σ donation.[29,30] Thereby, the anionic triazolide additionally acts as a π donor, owing to the high energy of the π system. In contrast, the π and π^* orbitals of the mesoionic 1,2,3-triazolylidene are lower in energy resulting in a weakened π donation and strengthened π back-donation (Figure 2).[25] Beside the fundamental properties, we were interested in the viability of these dyes for application in the DSSC, as the long excited-state lifetimes of the mesoionic carbene complexes (2c, 3c) might enable high electron injection efficiencies with a low injection driving force, i.e., with a low energy loss.[31,32] Furthermore, electron donation from phenyl anions within cyclometalated ruthenium(II) complexes can afford Ru(III)/Ru(II) redox potentials that are too low to allow for efficient dye regeneration. In these cases, the installation of electron-withdrawing groups may be necessary in order to increase the redox potential.[33,34] In this regard, we were interested in whether the intrinsically stabilized carbanion of the anionic 1,2,3-triazolide donor (1c) can serve as a valuable alternative.
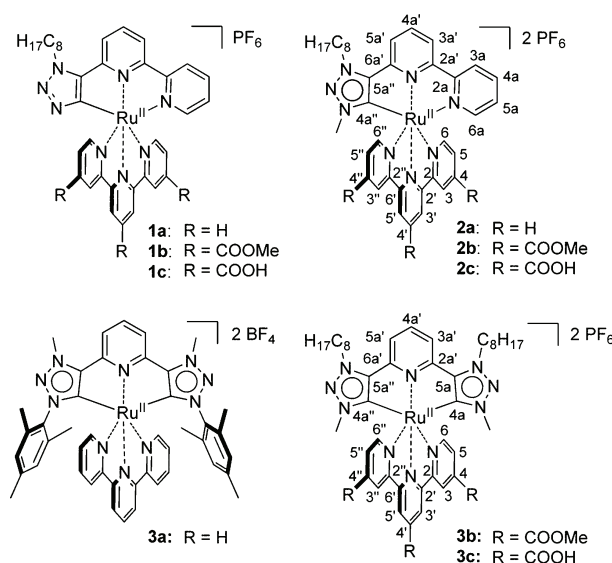
Figure 1. Ruthenium(II) complexes studied in this work. Numbering schemes for the complexes and the corresponding ligands.
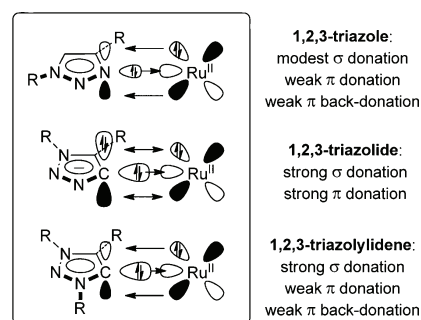
Figure 2. Illustration of the electronic differences between 1,2,3-triazolide and 1,2,3-triazolylidene donors. Note that the π donation is repulsive (cf. 1,2,3-triazolide).

1,2,3-Triazole-derived ligands can be readily synthesized and functionalized via catalyzed azide−alkyne cycloaddition reactions.[30,35,36] We chose the ruthenium-catalyzed version to selectively obtain the 1,5-disubstituted triazole.[37] In contrast to the 1,4-disubstituted triazole, the 1,5-regioisomer exclusively affords the cyclometalated complex, because the alternative tridentate coordination via the 3-nitrogen of the triazole is blocked (Figure 3).[38] Additionally, as the corresponding
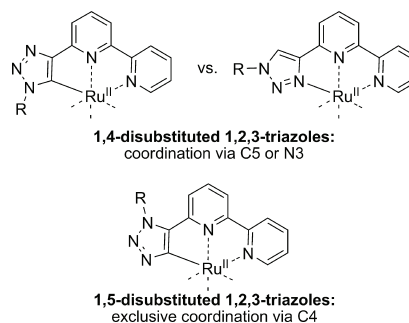
Figure 3. Implications of the ligand design for the ruthenium(II) coordination.

Scheme 1. Synthesis Routes Towards the Ruthenium(II) Complexes 1a–1c, 2a–2c, and 3a–3c[a]
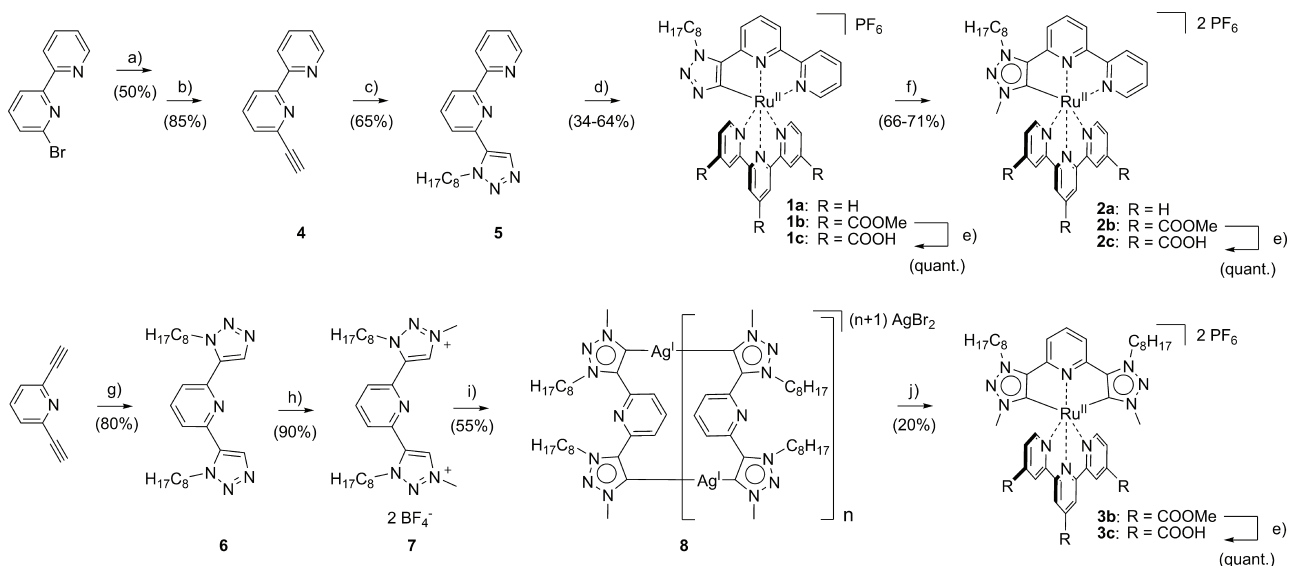
[a](a) Trimethylsilylacetylene, Pd(PPh₃)₄, CuI, THF, diisopropylamine, rt, 3 d; (b) KF, THF/MeOH, rt, 24 h; (c) *n*-octyl azide, RuCp*(PPh₃)₂Cl, 1,4-dioxane, 60 °C, microwave, 3 h; (d) [Ru^II(tpy)(MeCN)₃](PF₆)₂ or [Ru^II(tcmtpy)(MeCN)₃](PF₆)₂, MeOH (+ 2,6-lutidine) or DMF, 160 °C, microwave, 30 min; (e) DMF/NEt₃/H₂O, reflux, 48 h; (f) MeI, CHCl₃, 70 °C, 48 h; (g) *n*-octyl azide, RuCp*(PPh₃)₂Cl, 1,4-dioxane, 60 °C, microwave, 3 h; (h) Me₃O⁺BF₄⁻, CH₂Cl₂, rt, 48 h; (i) Ag₂O, KBr, MeCN, rt, 96 h; (j) Ru(tcmtpy)(DMSO)Cl₂, CH₂Cl₂, 70 °C, 24 h.

triazolide and triazolylidene complexes are supposed to be anchored to TiO₂ via the tpy ligand, substituents on the triazole ring will point away from the semiconductor surface in case of the 1,5-regioisomer offering the installation of hydrophobic alkyl chains to increase the solubility of the dyes, suppress water-induced dye-desorption, and potentially reduce recombination reactions in the DSSC.[39,40]

■ RESULTS AND DISCUSSION

Synthesis. The alkyne building block 6-ethynyl-2,2′-bipyridine and 2,6-diethynylpyridine[41] were obtained via a Sonogashira cross-coupling reaction. To ensure the selective formation of 1,5-disubstituted triazoles, RuCp*(PPh₃)₂Cl (Cp* = pentamethylcyclopentadienyl) was chosen as catalyst for the subsequent azide–alkyne cycloaddition[42–44] with *n*-octyl azide, which afforded the 1,2,3-triazole frameworks 5 and 6 in good yields (Scheme 1). Methylation of 6 was accomplished using Meerwein's reagent as reported previously.[25] In view of the wide scope of available azides and the potential to use substituted alkynyl-pyridine building blocks, modularly functionalized ligands are thus available.

The cyclometalated complexes 1a and 1b were obtained in good yields by converting ligand 5 with [Ru^II(tpy)(MeCN)₃]-(PF₆)₂ and [Ru^II(tcmtpy)(MeCN)₃](PF₆)₂ (tcmtpy = trimethyl-2,2′:6′,2″-terpyridine-4,4′,4″-tricarboxylate), respectively, under microwave irradiation in ethanol or DMF.[16,18] As a partial alkylation of the triazolide was already encountered under the acidic reaction conditions when alcohols were used as solvents, either 2,6-lutidine was added or DMF was used instead of the alcohol. Formation of 2a and 2b was achieved conveniently by alkylation of the respective 1,2,3-triazolide complexes 1a and 1b using methyl iodide.[45] The changes in the ¹³C NMR spectral shifts of the ruthenium(II)-coordinated carbon atom upon alkylation were only marginal; however, the formation of the anticipated product was proven by 2D NMR techniques as well as mass spectrometry. Additionally, selective

NOESY measurements were performed (see the SI), revealing a correlation between the α-CH₂ protons of the alkyl chain and the central pyridine ring, while no correlation was found for the methyl groups in line with the anticipated substitution pattern.

In contrast to the aforementioned 1,2,3-triazolylidene formation at the complex, the bis(triazolylidene) complex 3b was synthesized via preparation of a silver(I) 1,2,3-triazolylidene complex and subsequent transmetalation using *cis*-Ru(tcmtpy)(DMSO)Cl₂, as reported for the synthesis of 3a and derivatives thereof.[25,26] For the formation of the silver(I) precursor by reacting the triazolium salt 7 with Ag₂O, KBr had to be added to increase the reactivity of Ag₂O,[46] as the acidity of the alkyl-substituted triazolium salt is lower than that of previously used aryl-substituted analogues.[30,47] The saponification of the esters 1b–3b was achieved in good yields by heating the corresponding complexes in DMF/NEt₃/H₂O (3:1:1 *v/v/v*) according to literature protocols.[34,48,49]

Computational Methods. In order to gain a deeper insight into the photophysical and electrochemical properties of the complexes, density functional theory (DFT) and time-dependent (TD) DFT calculations have been carried out for the methyl-ester-substituted complexes. Octyl chains have been replaced by methyl groups (1b′–3b′) to shorten the computation time.

The relevant molecular orbitals, depicted in Table S1, reflect the electronic effects of the employed ligands. Due to the strong σ- and π-donating character of the anionic ligand of 1b′, the HOMO is constituted of ruthenium d orbitals and triazolide π orbitals, while the LUMO is predominantly composed of tpy π* orbitals. As a result of the electronic repulsion between the π orbitals of the triazolide and occupied metal d orbitals (π donation), the HOMO is strongly destabilized, which, in turn, leads to an increased π back-donation toward the tpy and, hence, the LUMO is destabilized as well, although to a lesser extent. Consequently, 1b′ features a relatively narrow HOMO–LUMO gap. In contrast, the HOMO of 2b′ is 0.6 eV lower in
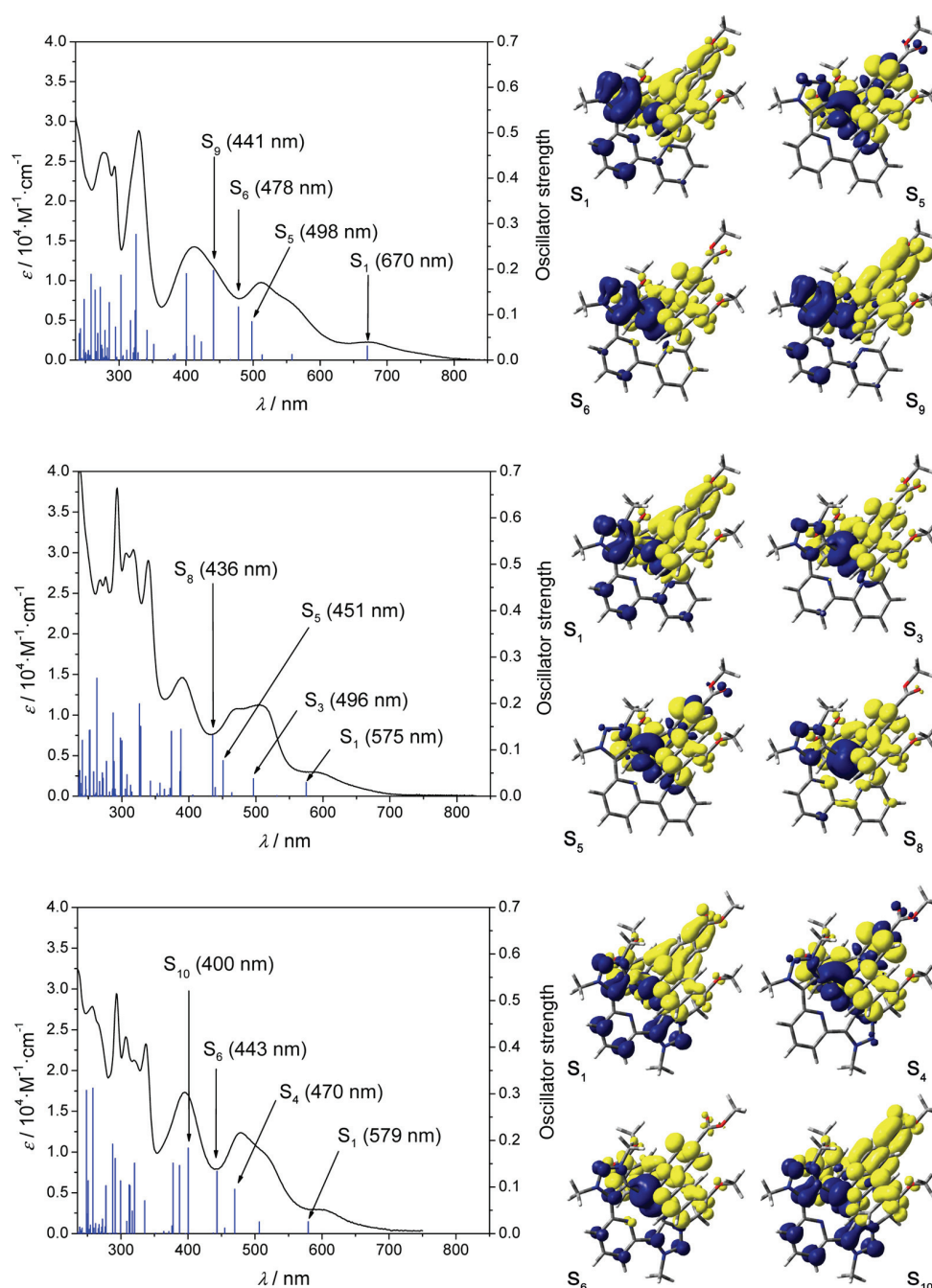
Figure 4. Calculated electronic singlet−singlet transitions and experimental UV−vis absorption spectra for the ester-substituted complexes (left, from top to bottom: **1b′**−**3b′**) and corresponding EDDM plots (right, blue = depletion of electron density, yellow = accumulation of electron density, isovalue = 0.001). Molecular orbitals involved in the transition are depicted in Table S1.

energy due to the moderate π-accepting character of the mesoionic carbene.[25] On account of the less electron-rich metal center, the destabilization of the tpy-based LUMO is also less pronounced resulting in a HOMO−LUMO gap of **2b′** that is, all in all, 0.3 eV larger than for **1b′**. Introduction of a second 1,2,3-triazolylidene donor (**3b′**) further increases the σ donation and, thus, the HOMO and LUMO destabilization, although the energy gap remains constant.

Electron-density difference maps (EDDMs), which display the depletion and accumulation of electron density during an

electronic transition, have been calculated for the relevant transitions in the visible-light region (Figure 4, Tables S2−4). Importantly, the calculated transitions are in good correlation with the experimental UV−vis spectra (vide infra). For **1b′**, the longest-wavelength transition involves a charge transfer from the HOMO, located on the ruthenium(II) center and the cyclometalating ligand, more precisely the triazolide ring, to the LUMO, which spreads over the tpy ligand. The corresponding transition is thus best described as a mixed metal-to-ligand charge transfer (MLCT) and ligand-to-ligand charge transfer
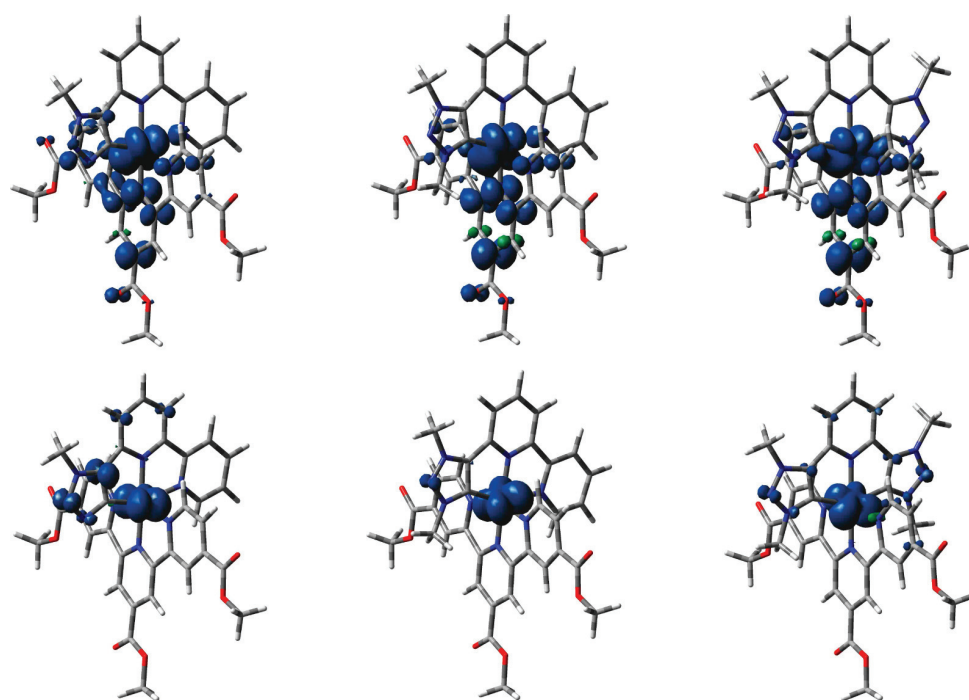
Figure 5. Spin-density plots (isovalue = 0.004) of the lowest-energy triplet excited state (top) and the singly oxidized GS (bottom) of the ester-substituted complexes (from left to right: **1b′−3b′**). Color code: Carbon, gray; hydrogen, white; nitrogen, blue; oxygen, red; ruthenium, cyan.

(LLCT), i.e., a metal-ligand-to-ligand charge-transfer (MLLCT) transition; however, the term MLCT is kept in the following (Figure 4, population of S_1).[50] The transitions at shorter wavelengths (between 350 and 600 nm) exhibit MLCT character with varying LLCT contributions (e.g., population of S_5, S_6, S_9). Certain transitions at ∼400 nm likewise show mixed MLCT and intraligand charge-transfer (ILCT) character involving the cyclometalating ligand, while absorption bands below 350 nm can be assigned to ligand-centered (LC) and metal-centered (MC) transitions. However, after internal conversion (IC), ultrafast intersystem crossing (ISC), and vibrational relaxation, the lowest-energy triplet excited-state is populated, which is expected to be a ^{3}MLCT featuring singly occupied molecular orbitals (SOMOs) located on the metal center/the anionic triazolide ring and the tpy ligand (vide infra). For the mesoionic carbene complexes **2b′** and **3b′**, the EDDM plots reveal a similar behavior as for **1b′**. The lowest-energy transitions involve a charge transfer from the HOMO, which is located on the carbene ligand and the metal, to the LUMO, located on the tpy ligand. Other transitions with high oscillator strengths in the visible region are of MLCT character involving lower occupied orbitals as well as higher unoccupied orbitals and are mostly directed toward the tpy ligand (Figure 4). Again, some MLCT transitions at shorter wavelengths are directed toward the carbene ligand and LC as well as MC transitions occur in the UV region.

Since we had previously encountered that the ISC is accompanied by a charge transfer from the tpy ligand to the carbene ligand in case of **3a**,[25] we also included a calculation of the spin-density distribution in the ^{3}MLCT for **1b′−3b′** (Figure 5). Owing to the stabilization of the π* orbitals of the tpy ligand by the carboxymethyl groups, the initial electron transfer to the tpy is preserved in the lowest-energy ^{3}MLCT. With respect to application in DSSCs, the anchoring groups are

therefore properly placed to allow for electron injection into TiO₂ (vide infra).

Furthermore, we calculated the spin-density distribution of the oxidized complexes (**1b′⁺−3b′⁺**, Figure 5), as this allows for an assessment of the localization of the electron hole remaining after the injection of an excited electron into the TiO₂. Similar to the HOMO distribution of **1b′** (Table S1), the cyclometalated ruthenium(III) complex **1b′⁺** shows significant spin density on the anionic triazolide ring, in contrast to the mesoionic carbene complexes. This finding is discussed below.

Photophysical Properties. The UV−vis absorption and emission spectra of the new complexes are depicted in Figures S12−S19, complemented with data for complex **3a**,[25] and the data is summarized in Table 1. In comparison to the parent homoleptic complex of tpy, [Ru(tpy)₂](PF₆)₂, the mesoionic carbene complexes **2a** and **3a** show MLCT maxima and absorption onsets at similar wavelengths but with lower extinction coefficients. Analogous behavior was reported recently for a tris(bidentate) ruthenium(II) complex featuring a 1,2,3-triazolylidene when compared to its polypyridyl counterpart [Ru(bpy)₃](PF₆)₂ (bpy = 2,2′-bipyridine).[51]

In contrast, the anionic triazolide of complex **1a** induces a bathochromic shift, in line with the DFT calculations (vide supra). In comparison to the analogous C^N^N-cyclometalated complex that features a phenyl anion as donor,[54,55] the bathochromic shift is less pronounced, which is expected based on the intrinsic lowering of the triazolide's electron donation by the ring nitrogen atoms.

The attachment of electron-withdrawing ester groups on the tpy (**1b−3b**) causes a bathochromic shift of the MLCT bands and absorption onsets due to the stabilization of tpy-based π* orbitals. Furthermore, the ester groups increase the extinction coefficients (Table 1). However, the bathochromic shifts are

Table 1. Photophysical Data of the Complexes

complex	λ_{abs} /nm ($\varepsilon/10^3$ M^{-1} cm^{-1})$^{a-c}$	λ_{em} /nm (λ_{exc} /nm); $\Phi_{PL}/\%^{b,d}$	τ / ns^{b,c}
[Ru(tpy)$_2$] (PF$_6$)$_2$	520 (4.7), 475 (14.7), 308 (63.4), 274 (37.3)	–	0.21^e
1a	619s (2.7), 505 (12.1), 386 (9.5), 316 (35.9)	730 (500); 0.2	35
1aH	542s (2.1), 476 (10.7), 400s (3.2), 310 (44.6)	648 (470); 1.8	47
2a	545s (2.7), 480 (10.4), 400 (4.5), 310 (40.4)	650 (478); 0.82	45
3a^f	539 (3.0), 463 (10.5), 405 (5), 353 (9), 311 (28)	643 (463); 4.4	633
1b	672 (3.0), 556s (8.9), 512 (10.9), 414 (16.8), 329 (33.5)	~ 800 (670); <10^{-2}	50
1bH	593 (2.8), 507 (10.8), 472 (10.2), 388 (13.9), 339 (26.4)	706 (510); 2.2	71
2b	593 (3.0), 503 (11.3), 471 (10.8), 391 (14.6), 339 (29.0)	703 (590); 3.0	133
3b	603 (3.0), 516s (9.7), 478 (12.3), 395 (17.3), 337 (23.3)	716 (600); 9.0	297
1c	626 (2.2), 530s (8.4), 499 (10.6), 400 (10.1), 323 (29.4)^g	736 (500)^g	54^g
2c	566 (2.9), 493 (11.7), 460s (10.5), 399 (6.2), 321 (35.1)^g	671 (490)^g	117^g
3c	571 (2.6), 495 (10.5), 467 (11.6), 376 (8.7), 328 (26.4)^g	674 (500)^g	410, 306^g

^{a}s = shoulder. ^{b}Measured in MeCN unless stated otherwise. ^{c}Air-equilibrated solution. ^{d}Determined using [Ru(dqp)$_2$](PF$_6$)$_2$ in MeOH/EtOH 1:4 (ΦPL = 2.0%)^{52} as reference; solutions were purged with N$_2$. ^{e}Taken from ref 53; measured in deaerated butyronitrile. ^{f}Taken from ref 25; measured in deaerated MeCN. ^{g}Measured in MeOH.

less pronounced for the complexes featuring free carboxylic acids (**1c**–**3c**) or TiO$_2$-anchored carboxylates (vide infra).

The E_{0-0} values follow the above-mentioned trends and are similar for the triazolylidene complexes, while they are significantly smaller for the 1,2,3-triazolide complexes (Table 2). Implications for the design of DSSCs thereof will be discussed later.

The cyclometalated ruthenium(II) complex **1a** is weakly emissive at room temperature in acetonitrile solution with slightly higher quantum yields (Φ_{PL} = 0.2%) than for ruthenium(II) complexes featuring cyclometalating phenyl rings.[16,54,55] The emission maximum at 723 nm is hypsochromically shifted relative to the emission maximum at about 800 nm observed for analogous ruthenium(II) complexes bearing a C^N^N-cyclometalating 6-phenyl-2,2′-bipyridine ligand,[54,55] which is again ascribed to the high degree of *aza* substitution within the 1,2,3-triazole ring lowering the GS destabilization. The excited-state lifetime was measured to be 35 ns, which is slightly shorter than for analogous ruthenium-(II) complexes featuring a cyclometalating phenyl ring instead of the triazolide.[55] For **1b** and **1c**, prolonged excited-state lifetimes of 50 and 54 ns, respectively, were measured, which is attributed to a stabilization of the ^{3}MLCT and, thus, an increased energy separation between the ^{3}MLCT and the ^{3}MC. As reported earlier,[25–27] the introduction of 1,2,3-triazolylidenes as powerful σ donors enables a strong destabilization of the ^{3}MC relative to the ^{3}MLCT and, thus, the suppression of the radiationless deactivation via the ^{3}MC. In contrast to the cyclometalated complexes **1a** and **1b**, the GS and ^{3}MLCT destabilization is expected to be less pronounced due to the weaker π donation from the 1,2,3-triazolylidene. Consequently, the ^{3}MLCT−^{3}MC separation as well as the GS−^{3}MLCT gap is increased giving rise to longer-lived excited states and higher emission quantum yields. Indeed, **2a** and **2b** show excited-state lifetimes of 45 and 133 ns as well as phosphorescence quantum yields of 0.8% and 3.0%, respectively. Again, the electron-withdrawing ester groups further diminish the radiationless deactivation as they increase the ^{3}MLCT−^{3}MC energy separation by lowering the ^{3}MLCT energy. Even longer excited-state lifetimes (297 ns) and remarkably high phosphorescence quantum yields (9.0%) were measured for **3b** suggesting potential application in electroluminescence devices.[17,56–59] In comparison to the previously reported complex **3a**,[25] a shorter excited-state lifetime has been measured for **3b**, which is attributed to the use of air-equilibrated solvents for the

Table 2. Electrochemical Data of the Complexes

complex	$E_{1/2,ox}$ /V^{a-c}	$E_{1/2,red}$ /V^{a-c}	E_{S*} /V^{a,d}	E_{0-0} /eV^{b,e}
[Ru(tpy)$_2$](PF$_6$)$_2$	0.90^{25}	−1.64^{25}	–	–
1a	0.25	−1.93		1.88
1aH	0.67	–^{f}	−1.44	2.11
2a	0.70	−1.75	−1.40	2.10
3a	0.60	−1.95	−1.49	2.09
1b	0.47	−1.51		1.67
1bH	0.86	–^{f}	−1.02	1.88
2b	0.87	−1.35	−1.00	1.87
3b	0.73	−1.47	−1.12	1.85
1c	0.40 (1.03)^g	–	−1.43 (−0.80)	1.83^h
2c	0.84 (1.47)^g	–	−1.13 (−0.50)	1.97^h
3c	0.66 (1.29)^g	–	−1.31 (−0.68)	1.97^h
N749	0.16 (0.85)^i	–	−1.42 (−0.73)	1.58^i

^{a}Referenced vs. Fc$^+$/Fc (vs. NHE). ^{b}Measured in MeCN solution unless stated otherwise. ^{c}Determined by cyclic voltammetry experiments using Bu$_4$NPF$_6$ as supporting electrolyte, unless stated otherwise; conversion to NHE scale by addition of 0.63 V^{61} and 0.69 V^{62} when the measurement was done in MeCN and DMF/MeOH (4:1 v/v), respectively. ^{d}Calculated using $E_{S*} = E_{1/2, ox} - E_{0-0}$.[63] ^{e}Determined at the intersection of the absorption and emission spectra with the latter being normalized with respect to the lowest-energy absorption. ^{f}Could not be measured due to proton reduction with the added acid. ^{g}Determined by square-wave voltammetry with the complex-anchored TiO$_2$ anode as the working electrode immersed in MeCN containing Bu$_4$NPF$_6$ as supporting electrolyte; OMFc$^+$/OMFc was used as internal standard; conversion to Fc$^+$/Fc-scale by subtraction of 0.4 V and to NHE scale by addition of 0.23 V, i.e., E vs. Fc$^+$/Fc + 0.63 = E vs. NHE.[61,62,64] ^{h}Measured in MeOH solution. ^{i}Measured in DMF/MeOH (4:1 v/v) solution.

lifetime measurements. Also for the designated photosensitizers featuring free carboxylic acids, **2c** and **3c**, long excited-state lifetimes of 117 and 306 ns, respectively, have been measured in methanol solution despite the presence of oxygen in the solvent. Accordingly, oxygen exclusion is not required during the DSSC fabrication.

An interesting feature of the complexes **1a**−**1c** is the reversible switchability of the ligand's donor properties between the anionic triazolide and an *N*-protonated triazolide ring, i.e., a mesoionic 1,2,3-triazolylidene,[60] as exemplarily shown for **1a** in Figure 6. The optical properties of the protonated forms, **1aH**
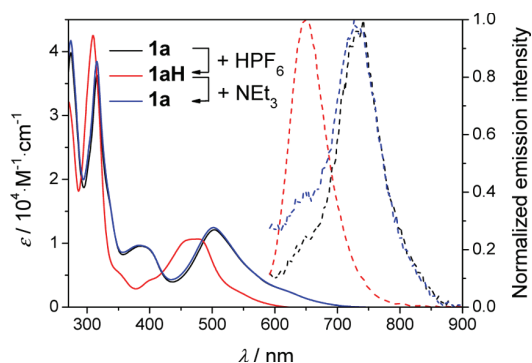

Figure 6. UV−vis spectral changes upon protonation and deprotonation of **1a** and **1aH**, respectively.

and **1bH**, resemble those of **2a** and **2b**, respectively (Table 1). In the case of **2b**, however, the lifetimes are still significantly longer than for the corresponding complex **1bH**.

Electrochemical Properties. The redox behavior of the presented ruthenium(II) complexes (Table 2) follows the electronic and structural trends as discussed for the computational results and the photophysical properties. Accordingly, the Ru(III)/Ru(II) redox potentials are the lowest for the complexes **1a**−**1c** (0.25, 0.47, and 0.40 V vs. Fc$^+$/Fc, respectively), intermediate for **3a**−**3c** (0.60, 0.73, and 0.66 V vs. Fc$^+$/Fc, respectively), and highest for **2a**−**2c** (0.70, 0.87, and 0.84 V vs. Fc$^+$/Fc, respectively), reflecting the electron donation by the anionic triazolide and the mesoionic triazolylidene donors. Importantly, the ruthenium-based redox process is fully reversible (Figure S20−S22). The tpy-based reduction follows the same trend: the more electron-rich the metal center, the more negative the redox potentials. This is attributed to a progressive destabilization of the tpy-based LUMO through π back-donation. In case of **3a**, however, the redox potential is even more negative than for **1a**, which might be rationalized by the close proximity between the mesityl moieties and the tpy plane giving rise to enhanced electronic repulsion upon tpy-based reduction. Similarly to the reduction process, the excited-state redox potentials (E_{S*}) show a successive cathodic shift as the effective donor strength of the ligands increases (Table 2). Furthermore, the direct LUMO and indirect HOMO stabilization is stronger for the ester-functionalized complexes than for the complexes featuring carboxylic acid groups. Again, the electronic properties of the protonated cyclometalated complexes **1aH** and **1bH** resemble those of the carbene analogs **2a** and **2b**.

As a consequence of the strong σ donation from the 1,2,3-triazolylidenes and the strong σ and π donation from the 1,2,3-triazolide, the Ru(III)/Ru(II)-based redox process of **1a**−**3a**

occurs at redox potentials that are significantly cathodically shifted relative to the parent $[Ru(tpy)_2]^{2+}$ (0.90 V vs. Fc$^+$/Fc).[25] Even for **2b**, featuring only a single 1,2,3-triazolylidene donor but three strongly electron-withdrawing −COOMe groups on the tpy ligand, the redox potential for the first oxidation is still slightly lower than for $[Ru(tpy)_2]^{2+}$. Also, for bis(tridentate) ruthenium(II) complexes featuring imidazol-2-ylidene-based ligands, the oxidation is facilitated relative to the tpy-analogous complexes.[24,65,66] On the other hand, a ruthenium(II) complex featuring a 2,6-bis(imidazol-2-ylidene)-pyridine and a 2,2′:6′,2′′-terpyridine-4′-carboxylic acid ligand was reported to exhibit a metal-based redox process at 1.15 V vs. Fc$^+$/Fc,[67] which is remarkably dissimilar to the data measured for **3c** (0.66 V vs. Fc$^+$/Fc). Nonetheless, the higher donor strength of the 1,2,3-triazolylidene relative to imidazol-2-ylidene,[47,68] caused by the remote positioning of ring nitrogen atoms,[29,30,47,69] is expected to result in cathodically shifted ground- and excited-state redox potentials for the corresponding ruthenium(II) complexes. Accordingly, for a series of tris(bidentate) ruthenium(II) complexes containing either an imidazol-2-ylidene or a 1,2,3-triazolylidene, the latter showed a 140 mV less positive redox potential for the ruthenium-based oxidation process.[51] In comparison to **1a**, the C^N^N-coordinated ruthenium(II) complex featuring a cyclometalating phenyl ring shows a 100 mV lower Ru(III)/Ru(II)-based redox potential,[54] which reflects the weaker electron donation by the 1,2,3-triazolide.

Dye-Sensitized Solar Cells. In order to evaluate the performance of the presented triazolide and triazolylidene ruthenium(II) complexes in the DSSC, commercially available test cells with transparent TiO$_2$ anodes (12-μm-thick layer of 20 nm TiO$_2$ particles, 0.88 cm^2 active area) were used and assembled according to standard literature procedures.[70] A cell containing **N749** ($[Ru(Htctpy)(NCS)_3](NBu_4)_3$ with Htctpy = 2,2′:6′,2′′-terpyridine-4′-carboxylic acid-4,4′′-dicarboxylate)[71] as sensitizer and a I$_3^-$/I$^-$-based electrolyte with a typical lithium iodide concentration of 0.1 M was included as internal standard.[72] In view of the less negative excited-state redox potentials of some of the new ruthenium(II) sensitizers (Figure 7) and in order to get an idea about their ability to achieve high incident photon-to-current efficiencies (IPCEs), an increased lithium iodide concentration of 1 M was used to lower the TiO$_2$ conduction band and, thereby, facilitate the electron injection
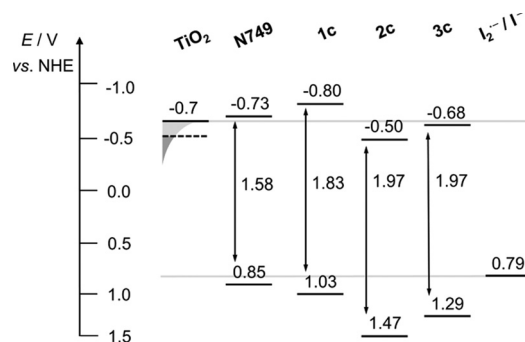

Figure 7. Comparison of the excited-state and ground-state redox potentials (values refer to the NHE scale, cf. Table 2) with the relevant redox potential of the electrolyte and the conduction band edge (solid line) as well as the appropriate position of the Fermi level (dashed line) of TiO$_2$.

into TiO_2 (vide infra).[31,73,74] However, the performance in the DSSC of **1c−3c** is clearly inferior to **N749** (Table 3).

Table 3. Selected DSSC Data for the Ru(II) Complexes Measured under AM1.5 Light Conditions

dye	$c(Li^+)$ /M	V_{OC} /V	J_{SC} /mAcm^{-2}	FF	PCE/%
1c	1	0.44	5.0	0.61	1.4
2c	1	0.38	1.9	0.61	0.5
3c	1	0.42	3.7	0.61	1.0
N749	0.1	0.69	11.6	0.62	5.1

Notably, the energy gaps of the presented sensitizers, which are larger than that of **N749** (Figure 7), cannot explain the significantly lower photocurrents on their own, as the integrated products of the absorbance of the dye-loaded TiO_2 films (see Figure S27) and the AM1.5 solar photon flux (with $\lambda > 400$ nm)[18,75] reveal overall light-harvesting capabilities relative to **N749** of 65%, 85%, and 77% for **1c**, **2c**, and **3c**, respectively.

In the case of **2c**, the excited-state redox potential (vide supra) lies considerably below the potential of the TiO_2 conduction band (Figure 7), which suppresses electron injection, in line with the low J_{sc} and IPCE values (Figures S28 and S29). In contrast, for **1c** and **3c**, injection problems should not be encountered due to the similar excited-state redox potentials of **1c**, **3c**, and **N749** (Figure 7), the prolonged lifetimes, particularly of **3c** (306 ns in methanol vs. 30 ns for **N749** in ethanol), and the high lithium concentration (1 M). Noteworthy, for osmium(II) sensitizers that feature a significantly lower excited-state redox potential than **N749**, high injection efficiencies had been achieved with a moderately increased lithium iodide concentration (0.6 M).[76] Inefficient dye regeneration might be another potential explanation. While it has been inferred that an electron hole on the dye that is exposed toward the electrolyte facilitates the dye regeneration by enabling an intimate contact with iodide,[86,88,89] for **2b′** and **3b′** (Figure 5, bottom), only marginal spin density is located on the ligand in the oxidized ground state according to the DFT calculations. Thus, although the positively shifted Ru(III)/Ru(II) redox potential provides a large regeneration driving force, the regeneration kinetics might be slow allowing for competitive backward electron transfer.[77,78]

Since not only the J_{sc} but also the V_{oc} values are quite low, even for the 1 M LiI additive, we suspect that an enhanced recombination of electrons in the TiO_2 conduction band with the oxidized dye is the main origin of the low PCE and IPCE values. Additionally, unfavorable interactions between the sensitizer and iodine could provoke recombination reactions with the electrolyte.[79−81] Furthermore, the long alkyl chains could also, in principle, slow down the regeneration kinetics; however, even lower PCEs have been observed with other ruthenium(II) carbene complexes devoid of alkyl chains,[27,67] while high PCEs have been achieved with sensitizers bearing even longer alkyl chains.[82,83]

In contrast to the carbene complexes, for the cyclometalated complex **1c**, a significant portion of the electron hole is located on the cyclometalating ligand (Figure 5). In line with the above mentioned argument, this is expected to facilitate dye regeneration. Indeed, **1c** shows the highest photocurrents despite its lower light-harvesting capabilities (vide supra). Still, the PCE and IPCE values of the cyclometalated complex **1c** are inferior to other photosensitizers featuring a carbanionic phenyl ring,[18,33,49,84,85] which may be attributed partly to a diminished electron injection on account of the less negative excited-state redox potential[86] and/or recombination reactions due to dye-iodine interaction.[79−81] Additionally, a partial lithium or proton coordination at the 3-nitrogen of the triazolide ring would render the electronic properties of **1c** similar to **2c** (vide supra).[60] While a protonation is unlikely due to the presence of 0.5 M 4-*tert*-butylpyridine in the electrolyte, and although UV−vis absorption and CV measurements with **1c** in acetonitrile solution containing either 1 M $LiClO_4$ or 1 M Bu_4NClO_4 did not indicate any interaction between **1c** and Li^+, it cannot be ruled out that the triazolide is affected in the working device.

Ultimately, as the sensitizers **1c** and **3c** do not show obvious molecular design drawbacks, we tentatively ascribe the comparably low PCE and IPCE values to unfavorable interactions between the sensitizer and the electrolyte and inefficient regeneration, respectively. Prospectively, **3c** might allow significantly improved IPCEs using electrolytes based on cobalt(III)/cobalt(II) polypyridyl complexes or ferrocenium/ferrocene, which would additionally allow the exploitation of the high Ru(III)/Ru(II) redox potential of the mesoionic carbene complex potentially leading to high V_{oc} values.[87−89]

■ CONCLUSION

A series of new bis(tridentate) ruthenium(II) complexes featuring ligands with anionic triazolide and mesoionic triazolylidene donors is presented. The σ and π donation from the triazolide carbanion is lowered in comparison to a phenyl anion due to the stabilization by three ring nitrogen atoms. The mesoionic carbenes are very strong σ donors but weak π donors resulting in a larger energy gap, more positive redox potentials, and a negligible ligand contribution to the HOMO in comparison to the triazolide complex. The 1,2,3-triazolide complexes can be reversibly switched to the corresponding 1,2,3-triazolylidene complexes by protonation. The emission of red light with relatively high photo-luminescence quantum yields of the triazolylidene complexes suggests a potential application in electroluminescence devices. The presented ruthenium(II) complexes can be readily functionalized and show a broad absorption of visible light resulting in the formation of charge-separated excited states that feature relatively long lifetimes, in particular, in the case of the 1,2,3-triazolylidene complexes. These attractive photo-physical properties suggest the application as photoredox catalysts or as photosensitizers for DSSC applications. The potential for the latter was investigated, but the achieved J_{sc} and V_{oc} values were relatively low, which is tentatively attributed to less efficient electron injection and/or dye regeneration.

■ EXPERIMENTAL SECTION

$[Ru^{II}(tpy)(MeCN)_3](PF_6)_2$, $[Ru^{II}(tcmtpy)(MeCN)_3](PF_6)_2$, 2,6-di-ethynylpyridine, and *n*-octyl azide were synthesized according to literature procedures.[16,41,90,91] Methanol was dried by distillation over magnesium and kept under nitrogen using standard Schlenk techniques. Anhydrous (99.8%) *N,N*-dimethylformamide (DMF) and $RuCp^*(PPh_3)_2Cl$ were purchased from Sigma-Aldrich. 4,4′,4″-Tricarboxymethyl-2,2′:6′,2″-terpyridine (tcmtpy) was purchased from hetcat. $[Ru(Htctpy)(NCS)_3](NBu_4)_3$ (**N749** or black dye; Htctpy = 2,2′:6′,2″-terpyridine-4′-carboxylic acid-4,4″-dicarboxylate) was purchased from Solaronix. All other chemicals were purchased from commercial suppliers and used as received. All reactions were performed in oven-dried flasks and were monitored by thin-layer chromatography (TLC) (silica gel on aluminum sheets with fluorescent dye F254, Merck KGaA). Microwave reactions were

2090

dx.doi.org/10.1021/ic402702z | *Inorg. Chem.* 2014, 53, 2083−2095

carried out using a Biotage Initiator Microwave synthesizer. NMR spectra have been recorded on a Bruker AVANCE 250 MHz, AVANCE 300 MHz, or AVANCE 400 MHz instrument in deuterated solvents (euriso-top) at 25 °C. ^{1}H and ^{13}C resonances were assigned using appropriate 2D correlation spectra. Chemical shifts are reported in ppm using the solvent as internal standard. Matrix-assisted laser desorption-ionization time-of-flight (MALDI-TOF) mass spectra were obtained using an Ultraflex III TOF/TOF mass spectrometer with dithranol as matrix in reflector mode. High resolution electrospray ionization quadrupole time-of-flight mass spectrometry (ESI-Q-TOF MS) was performed on an ESI-Q-TOF-MS microTOF QII (Bruker Daltonics) mass spectrometer. UV/vis absorption spectra were recorded on a Perkin-Elmer Lambda 750 UV/vis spectrophotometer, emission spectra on a Jasco FP6500. Measurements were carried out using 10^{-6} M solutions of respective solvents (spectroscopy grade) in 1 cm quartz cuvettes or on dye-loaded, transparent TiO$_2$ anodes (12 μm thick, 0.88 cm^2 active area, see Cell Fabrication) at room temperature. Lifetime measurements were mostly obtained by time-correlated single-photon counting utlizling a Titan:Sapphire laser (Tsunami, Newport Spectra-Physics GmbH) as light source.[92] The repetition rate was set to 400 kHz (pulse generator, Model 3980) and the 500 nm pump beam created by a second harmonic generator from Newport Spectra-Physics GmbH. The emission is detected by a Becker & Hickel PMC-100-4 photon-counting module. Samples are prepared to yield an optical density of 0.1 at the excitation wavelength. Cyclic voltammetry measurements were performed on a Metrohm Autolab PGSTAT30 potentiostat with a standard three-electrode configuration using a graphite-disk working electrode, a platinum-rod auxiliary electrode, and a Ag/AgCl reference electrode; scan rates from 50 to 500 mV·s^{-1} were applied. The experiments were carried out in degassed solvents (spectroscopy grade) containing 0.1 M Bu$_4$NPF$_6$ salt (dried previously by heating at 110 °C and storing under vacuum). At the end of each measurement, ferrocene was added as an internal standard. All calculations are based on density functional theory (DFT). The geometries of the singlet ground state, the singly oxidized ground state, and the lowest triplet excited state have been optimized for all the ruthenium(II) complexes, presented herein. The hybrid functional B3LYP[93,94] has been selected in combination with the 6-31G* basis set for all atoms. To reproduce the measured absorption UV−vis spectrum, the lowest-lying 75 vertical singlet electronic excitation energies were calculated using time-dependent DFT (TD-DFT) at the S$_0$ optimized geometry. The TD-DFT calculations were performed in solution using acetonitrile as solvent with the polarization continuum model and with the same functional and basis set as in the optimizations.[95,96] All these calculations were performed with the *Gaussian09* program package.[97] The analysis of the EDDM calculations were performed by *GaussSum2.2*.[98] Electron density difference maps (density isovalue = 0.001), Kohn−Sham orbitals (MO isovalue = 0.04), and spin-density calculations (density isovalue = 0.004) were visualized by *GaussView5.0.8*.[97]

Synthesis of Ru(tcmtpy)(DMSO)Cl$_2$. Ru(DMSO)$_4$Cl$_2$ (1.2 g, 2.6 mmol), tcmtpy (391 mg, 0.96 mmol), and LiCl[99] (190 mg, 4.49 mmol) were suspended in 80 mL deaerated EtOH and the mixture was refluxed under a nitrogen atmosphere. After 5 h, the full conversion of tcmtpy was confirmed by TLC and the reaction mixture was allowed to cool to room temperature. The solvent was evaporated in vacuo and the remaining solid was suspended in H$_2$O, filtered, and washed with H$_2$O (3 × 3 mL), EtOH (2 × 3 mL), and Et$_2$O (3 × 3 mL) to yield 406 mg (0.62 mmol, 64%) of a purple solid. The product was stored under a nitrogen atmosphere in the fridge. ^{1}H NMR (300 MHz, DMSO-d$_6$) δ = 9.24 (d, J = 5.6 Hz, 2H, $H^{6,6''}$), 9.20 (s, 2H, $H^{3,3''}$), 9.17 (s, 2H, $H^{3',5'}$), 8.29 (d, J = 4.5 Hz, 2H, $H^{5,5''}$), 4.06 (s, 3H, C$^{4'}$−COOCH$_3$), 4.02 (s, 6H, C$^{4,4''}$−COOCH$_3$), 2.62−2.53 (m, 6H, DMSO-d$_6$) ppm; ^{13}C NMR (63 MHz, DMSO-d$_6$) δ = 164.5 (C$^{4'}$−COOMe), 164.2 (C$^{4,4''}$−COOCH$_3$), 160.1 (C$^{2,2''}$), 159.4 (C$^{2',6'}$), 153.8 (C$^{6,6''}$), 137.6 (C$^{4,4''}$), 133.7 (C$^{4'}$), 127.1 (C$^{5,5''}$), 122.7 (C$^{3',5'}$), 122.3 (C$^{3,3''}$), 53.2 (C$^{4,4'/4''}$−COOCH$_3$), 41.6 ppm.

Synthesis of 6-(Trimethylsilyl ethynyl)-2,2′-bipyridine. Under a nitrogen atmosphere, 6-bromo-2,2′-bipyridine (2 g, 8.51 mmol), Pd(PPh$_3$)$_4$ (479 mg, 0.41 mmol, 5 mol %), CuI (180 mg, 0.95 mmol,

11 mol %) were suspended in a mixture of dry and nitrogen-purged THF (35 mL) and diisopropylamine (4 mL). While stirring, trimethylsilylacetylene (2.5 mL, 17.87 mmol, 2 equiv) was added dropwise at room temperature. After stirring for 24 h at room temperature, additional trimethylsilylacetylene (1 mL) was added. After additional 96 h, the full conversion was confirmed by GC-MS and TLC. After addition of aq. EDTA (1 mL, 35%) and H$_2$O, the crude product was extracted with CH$_2$Cl$_2$ and subjected to column chromatography (silica, CH$_2$Cl$_2$/MeOH, 99:1 or alumina, CH$_2$Cl$_2$) to obtain 1.01 g (4.01 mmol, 47%) of a colorless solid. ^{1}H NMR (400 MHz, CD$_2$Cl$_2$) δ = 8.65 (dd, ^3J = 3.9, ^4J = 0.8 Hz, 1H, H^{6a}), 8.47−8.35 (m, 2H, $H^{3a,3a'}$), 7.90−7.74 (m, 2H, $H^{4a,4a'}$), 7.48 (d, ^3J = 7.7 Hz, 1H, H^{5a}), 7.39−7.28 (m, 1H, H^{5a}), 0.33 (s, 9H) ppm; ^{13}C NMR (100 MHz, CD$_2$Cl$_2$) δ = 156.8 (C$^{2a'}$), 155.7 (C^{2a}), 149.5 (C$^{6a'}$), 142.7 (C$^{6a'}$), 137.4 (C$^{4a'}$), 137.3 (C^{4a}), 127.8 (C^{5a}), 124.4 (C$^{5a'}$), 121.4 (C^{3a}), 120.8 (C$^{3a'}$), 104.4 (C^{tert}), 94.5 (Si−C^{tert}), −0.2 ppm (Si−CH$_3$); MS (HR ESI-Q-TOF): calcd. for C$_{15}$H$_{16}$N$_2$SiNa ([M + Na]$^+$): m/z = 275.0975; found: m/z = 275.1023.

Synthesis of 4. 6-(Trimethylsilyl ethynyl)-2,2′-bipyridine (1 g, 3.96 mmol) was dissolved in THF/MeOH (1:1, 100 mL) and the resulting solution was purged with nitrogen. The solution was stirred at room temperature under a nitrogen atmosphere and KF (460 mg, 7.92 mmol, 2 equiv) was added portionwise. The reaction mixture was stirred under light exclusion at room temperature. After 24 h, the full conversion was confirmed by TLC (alumina, n-hexane/CH$_2$Cl$_2$, 2:1) and all volatiles were evaporated in vacuo. After purification by column chromatography (silica, CH$_2$Cl$_2$/MeOH, 99:1), 600 mg (3.33 mmol, 84%) of a colorless solid were obtained. ^{1}H NMR (400 MHz, CD$_2$Cl$_2$) δ = 8.66 (d, ^3J = 4.1 Hz, 1H, H^{6a}), 8.43 (dd, ^3J = 8.0, ^4J = 2.1 Hz, 2H, $H^{3a,3a'}$), 7.88−7.77 (m, 2H, $H^{4a,4a'}$), 7.51 (dd, ^3J = 7.6, ^4J = 0.8 Hz, 1H, H^{5a}), 7.38−7.29 (m, 1H, H^{5a}), 3.23 (s, 1H, C^{tert}CH) ppm; ^{13}C NMR (100 MHz, CD$_2$Cl$_2$) δ = 156.9 (C$^{2a'}$), 155.6 (C^{2a}), 149.5 (C^{6a}), 141.9 (C$^{6a'}$), 137.5 (C$^{4a'}$), 137.3 (C^{4a}), 127.9 (C^{5a}), 124.5 (C$^{5a'}$), 121.4 (C^{3a}), 121.2 (C$^{3a'}$), 83.3 (C^{tert}), 76.8 ppm (C^{tert}CH); MS (HR ESI-Q-TOF): calcd. for C$_{12}$H$_8$N$_2$Na ([M + Na]$^+$): m/z = 203.058; found: m/z = 203.0618.

Synthesis of 5. 4 (79 mg, 0.44 mmol), n-octyl azide (150 mg, 0.97 mmol, 2.2 equiv), and RuCp*(PPh$_3$)$_2$Cl (7.3 mg, 0.009 mmol, 2 mol %) were suspended in dry and nitrogen-purged 1,4-dioxane (3.4 mL). Subsequently, the reaction mixture was heated to 60 °C for 3 h in the microwave reactor and the full conversion was confirmed by TLC (alumina, n-hexane/CH$_2$Cl$_2$, 1:1). The crude product mixture was subjected to column chromatography (silica, CHCl$_3$). After evaporation of the solvent, the remaining solid was suspended in hot n-hexane and filtered. The filtrate was concentrated and, after additional purification by column chromatography (alumina, n-hexane/CH$_2$Cl$_2$, 1:1) and removal of the solvent, 96.2 mg (0.29 mmol, 65%) of a yellow solid were obtained. ^{1}H NMR (250 MHz, CD$_2$Cl$_2$) δ = 8.70 (d, ^3J = 4.7 Hz, 1H, H^{6a}), 8.48 (d, ^3J = 8.0 Hz, 1H, $H^{3a'}$), 8.37 (d, ^3J = 8.0 Hz, 1H, H^{3a}), 8.01 (s, 1H, $H^{4a''}$), 7.95 (t, ^3J = 7.9 Hz, 1H, $H^{4a'}$), 7.86 (t, ^3J = 7.7 Hz, 1H, H^{4a}), 7.66 (d, ^3J = 7.8 Hz, 1H, $H^{5a'}$), 7.37 (t, ^3J = 6.17 Hz, 1H, H^{5a}), 4.96 (t, ^3J = 7.6 Hz, 2H, N−CH$_2$−), 2.05−1.85 (m, 2H, N−CH$_2$−CH$_2$−), 1.20 (s, 10H, −CH$_2$−), 0.83 (t, ^3J = 6.6 Hz, 3H, −CH$_3$) ppm; ^{13}C NMR (63 MHz, CD$_2$Cl$_2$) δ = 156.2 (C$^{2a'}$), 155.4 (C^{2a}), 149.3 (C^{6a}), 146.7 (C$^{6a'}$), 138.1 (C$^{4a'}$), 136.8 (C^{4a}), 135.5 (C$^{5a''}$), 133.5 (C$^{4a''}$), 124.1 (C^{5a}), 122.8 (C$^{5a'}$), 120.7 (C^{3a}), 120.4 (C$^{3a'}$), 50.1 (N−CH$_2$−), 31.7 (−CH$_2$−), 30.4 (−CH$_2$−), 29.1 (−CH$_2$−), 29.1 (−CH$_2$−), 26.5 (−CH$_2$−), 22.5 (−CH$_2$−), 13.8 (−CH$_3$) ppm; MS (HR ESI-Q-TOF): calcd. for C$_{20}$H$_{34}$N$_4$O$_7$SNa ([M + Na]$^+$): m/z = 336.2183; found: m/z = 336.2165.

Synthesis of 6. n-Octyl azide (1.28 g, 8.24 mmol, 4.4 equiv), 2,6-diethynylpyridine (240 mg, 1.89 mmol), and RuCp*(PPh$_3$)$_2$Cl (30 mg, 0.04 mmol, 2 mol %) were dissolved in dry and nitrogen-purged 1,4-dioxane (9 mL). Subsequently, the reaction mixture was heated to 60 °C for 3 h in the microwave reactor and the full conversion of the alkyne was confirmed by TLC (alumina, CH$_2$Cl$_2$). The solvent was evaporated in vacuo and the crude product mixture was subjected to column chromatography (alumina, CH$_2$Cl$_2$/n-hexane, 3:1) to yield 665 mg (1.52 mmol, 81%) of a colorless solid. ^{1}H NMR (250 MHz, CD$_2$Cl$_2$) δ = 7.97 (s, 2H, $H^{4a,4a''}$), 7.96 (t, 1H, ^3J = 7.9 Hz, $H^{4a'}$), 7.62

(d, ^3J = 7.9 Hz, 2H, $H^{3a',5a'}$), 4.75 (t, ^3J = 7.3 Hz, 4H, N−CH$_2$−), 1.94−1.67 (m, 4H, N−CH$_2$−CH$_2$−), 1.22 (d, ^3J = 23.3 Hz, 20H, −CH$_2$−), 0.84 (t, ^3J = 6.7 Hz, 6H, −CH$_3$) ppm; ^{13}C NMR (63 MHz, CD$_2$Cl$_2$) δ = 148.1 ($C^{2a',6a'}$), 138.9 ($C^{4a'}$), 135.8 ($C^{5a,5a''}$), 134.4 ($C^{4a,4a''}$), 123.3 ($C^{3a',5a'}$), 49.9 (N−CH$_2$−), 32.0 (−CH$_2$−), 30.6 (−CH$_2$−), 29.4 (−CH$_2$−), 29.3 (−CH$_2$−), 26.8 (−CH$_2$−), 22.9 (−CH$_2$−), 14.2 (−CH$_3$) ppm; MS (HR ESI-Q-TOF): calcd. for C$_{25}$H$_{39}$N$_7$Na ([M + Na]$^+$): m/z = 460.3159; found: m/z = 460.3157; Elem. anal. calcd. for C$_{21}$H$_{31}$N$_7$ (437.62): C, 68.61%; H, 8.98%; N, 22.40%, found: C, 68.25%; H, 9.74%; N, 22.61%.

Synthesis of 7. In accordance with the literature,[25] **6** (319 mg, 0.73 mmol) was reacted with trimethyloxonium tetrafluoroborate (580 mg, 3.92 mmol, 5 equiv) in dry CH$_2$Cl$_2$ (6.8 mL) at room temperature for 48 h. The full conversion was confirmed by TLC (alumina, CH$_2$Cl$_2$) and MeOH (3 mL) was added dropwise to the reaction mixture. Subsequently, all volatiles were evaporated in vacuo and the resulting liquid was purified by column chromatography (alumina, MeCN/CH$_2$Cl$_2$, 3:1) to yield 423 mg (0.66 mmol, 90%) of a yellow oil. ^{1}H NMR (400 MHz, CD$_2$Cl$_2$) δ = 9.03 (s, 2H, $H^{4a,4a''}$), 8.18 (d, ^3J = 8.9 Hz, 1H, $H^{4a'}$), 8.13−8.07 (m, 2H, $H^{3a',5a'}$), 4.86 (t, ^3J = 7.3 Hz, 4H, N−CH$_2$−), 4.43 (s, 6H, N−CH$_3$), 2.08−1.86 (m, 4H, N−CH$_2$−CH$_2$−), 1.53−1.00 (m, 20H, −CH$_2$−), 0.86 (t, J = 6.9 Hz, 6H, −CH$_3$) ppm; ^{13}C NMR (101 MHz, CD$_2$Cl$_2$) δ = 143.9 ($C^{2a',6a'}$), 141.2 ($C^{4a'}$), 140.3 ($C^{5a,5a''}$), 132.0 ($C^{4a,4a''}$), 127.7 ($C^{3a',5a'}$), 54.4 (N−CH$_2$−), 54.2 (−CH$_2$−), 54.1 (−CH$_2$−), 53.8 (−CH$_2$−), 53.5 (−CH$_2$−), 53.3 (−CH$_2$−), 40.9 (−CH$_2$−), 32.0 (−CH$_2$−), 29.3 (−CH$_2$−), 29.3 (−CH$_2$−), 29.2 (−CH$_2$−), 26.5 (−CH$_2$−), 22.9 (−CH$_2$−), 14.2 (−CH$_3$) ppm; MS (HR ESI-Q-TOF): calcd. for C$_{27}$H$_{45}$N$_7$BF$_4$ ([M − BF$_4$]$^{2+}$): m/z = 554.3765; found: m/z = 554.3755.

Synthesis of 8. **7** (234 mg, 0.37 mmol), KBr[46] (640 mg, 5.38 mmol, 15 equiv), and freshly prepared Ag$_2$O (700 mg, 3 mmol, 8 equiv) were suspended in dry and nitrogen-purged MeCN (15 mL). After stirring for 6 d under light exclusion at room temperature, the crude reaction mixture was diluted with dry CH$_2$Cl$_2$ and filtered over a Celite plug. Subsequently, all volatiles were evaporated in vacuo and the remaining solid was dissolved in CH$_2$Cl$_2$ and precipitated into n-hexane. The formed precipitate was filtered, washed with n-hexane, and rinsed with CH$_2$Cl$_2$. After evaporation of the solvent in vacuo, 264.4 mg (0.2 mmol, 55%) of a gold-brown solid were obtained. ^{1}H NMR (250 MHz, CD$_2$Cl$_2$) δ = 8.19−8.04 (m, 3H, $H^{3a',4a',5a'}$), 4.66 (t, ^3J = 7.3 Hz, 4H, N−CH$_2$−), 4.30 (s, 6H, N−CH$_3$), 1.81 (s, 4H, N−CH$_2$−CH$_2$−), 1.21 (d, J = 24.0 Hz, 20H, −CH$_2$−), 0.85 (t, J = 6.8 Hz, 6H, −CH$_3$) ppm; ^{13}C NMR (100 MHz, CD$_2$Cl$_2$) δ = 173.2, 172.2, 168.3, 148.2, 146.5, 143.6, 139.7, 125.8, 51.8, 43.6, 32.0, 29.9, 29.3, 29.1, 27.7, 26.56, 22.9, 14.2, ppm; MS (HR ESI-Q-TOF): calcd. for C$_{54}$H$_{86}$Ag$_2$N$_{14}$ ([dimer − 2AgBr$_2$]$^{2+}$): m/z = 573.2704; found: m/z = 573.2685; MS (ESI-TOF, negative mode): calcd. for AgBr$_2$ (counter-ion): m/z = 266.7397; found: m/z = 266.7403.

Synthesis of 1a. [Ru(tpy)(MeCN)$_3$] (PF$_6$)$_2$ (20 mg, 0.03 mmol), **5** (9 mg, 0.03 mmol), and 2,6-lutidine (15 μL, 0.129 mmol, 5 equiv) were dissolved in dry and nitrogen-purged MeOH (1 mL). Subsequently, the reaction mixture was heated to 130 °C for 30 min in the microwave reactor. After the full conversion of [Ru(tpy)-(MeCN)$_3$](PF$_6$)$_2$ was confirmed by TLC (silica, MeCN/H$_2$O/aq KNO$_3$, 40:4:1), the crude product mixture was dropped into aq. NH$_4$PF$_6$. The formed precipitate was filtered, washed with H$_2$O, and rinsed with MeCN. After purification by column chromatography (alumina, CH$_2$Cl$_2$/MeCN, 4:1), 10 mg (0.01 mmol, 64%) of a violet solid were obtained. ^{1}H NMR (600 MHz, CD$_3$CN) δ = 8.55 (d, ^3J = 8.1 Hz, 2H, $H^{3',5'}$), 8.41 (d, ^3J = 8.2 Hz, 1H, H^{3a}), 8.36 (d, ^3J = 8.1 Hz, 2H, $H^{3,3''}$), 8.29 (d, ^3J = 7.9 Hz, 1H, H^{5a}), 8.08 (t, ^3J = 8.0 Hz, 1H, $H^{4a'}$), 8.04 (t, ^3J = 8.1 Hz, 1H, $H^{4'}$), 8.01 (d, ^3J = 8.0 Hz, 1H, $H^{3a'}$), 7.83 (t, ^3J = 7.8 Hz, 1H, H^{4a}), 7.75 (t, ^3J = 7.9 Hz, 2H, $H^{4,4''}$), 7.37 (d, ^3J = 5.3 Hz, 1H, $H^{6a'}$), 7.35 (d, ^3J = 5.4 Hz, 2H, $H^{6,6''}$), 7.10−7.03 (m, 3H, $H^{5,5'',5a}$), 4.65 (t, ^3J = 7.1 Hz, 2H, N−CH$_2$−), 1.92−1.85 (m, 2H, N−CH$_2$−CH$_2$−), 1.42−1.13 (m, 10H, −CH$_2$−), 0.84 (t, J = 7.2 Hz, 3H, −CH$_3$) ppm; ^{13}C NMR (150 MHz, CD$_3$CN) δ = 177.8 (Ru−C), 158.3 ($C^{2,2''}$), 156.9 ($C^{2a'}$), 156.8 (C^{2a}), 155.3 ($C^{2',6'}$), 153.82 ($C^{6a'}$), 152.2 ($C^{6,6''}$), 151.4 (C^{6a}), 140.8 ($C^{5a'}$), 138.3 (C^{4a}), 136.4 ($C^{4a'}$), 136.2 ($C^{4,4''}$), 131.1 ($C^{4'}$), 127.3 ($C^{5,5''}$), 127.2 (C^{5a}), 124.4 (C^{3a}),

123.9 ($C^{3,3''}$), 122.9 ($C^{3',5'}$), 119.1 ($C^{3a'}$), 118.8 ($C^{5a'}$), 50.1 (N−CH$_2$−), 32.4 (−CH$_2$−), 30.7 (−CH$_2$−), 29.9 (−CH$_2$−), 29.7 (−CH$_2$−), 27.1 (−CH$_2$−), 23.3 (−CH$_2$−), 14.4 (−CH$_3$) ppm; MS (HR ESI-Q-TOF): calcd. for C$_{35}$H$_{35}$N$_8$Ru ([M − PF$_6$]$^+$): m/z = 669.2031; found: m/z = 669.2016.

Synthesis of 2a. A microwave vial was charged with **1a** (6.3 mg, 0.01 mmol), MeI (1.5 μL, 0.024 mmol, 3 equiv), and dry CHCl$_3$ (0.6 mL). The vial was capped and heated to 70 °C for 24 h while stirring using an oil bath. The full conversion was confirmed by TLC (silica, MeCN/H$_2$O/aq.KNO$_3$, 40:4:1). All volatiles were evaporated in vacuo and the remaining solid was dissolved in MeCN, and dropped into aq. NH$_4$PF$_6$. The formed precipitate was filtered, washed with H$_2$O, and dried to yield 5.0 mg (0.005 mmol, 66%) of a red solid. ^{1}H NMR (600 MHz, CD$_3$CN) δ = 8.63 (d, ^3J = 8.1 Hz, 2H, $H^{3',5'}$), 8.50 (d, ^3J = 7.4 Hz, 1H, $H^{5a'}$), 8.47 (d, ^3J = 8.1 Hz, 1H, H^{3a}), 8.41 (d, ^3J = 8.1 Hz, 2H, $H^{3,3''}$), 8.29−8.21 (m, 3H, $H^{4',3a',4a'}$), 7.92 (t, ^3J = 7.8 Hz, 1H, H^{4a}), 7.87 (t, ^3J = 7.2 Hz, 2H, $H^{4,4''}$), 7.40 (d, ^3J = 5.3 Hz, 1H, H^{6a}), 7.29 (d, ^3J = 5.3 Hz, 2H, $H^{6,6''}$), 7.18 (d, ^3J = 6.5 Hz, 1H, H^{5a}), 7.12 (t, ^3J = 6.6 Hz, 2H, $H^{5,5''}$), 4.76 (t, ^3J = 7.2 Hz, 2H, N−CH$_2$−), 3.06 (s, 3H, N−CH$_3$), 2.03−1.97 (m, 2H, N−CH$_2$−CH$_2$−),1.39−1.32 (m, 2H, N−CH$_2$−CH$_2$−CH$_2$), 1.32−1.16 (m, 8H, −CH$_2$−), 0.85 (t, ^3J = 7.1 Hz, 3H, −CH$_3$) ppm; ^{13}C NMR (75 MHz, CD$_3$CN) δ = 176.6 (Ru−C), 158.2 ($C^{2,2''}$), 157.7 ($C^{2a'}$), 156.7 (C^{2a}), 155.73 ($C^{2',6'}$), 153.2 ($C^{6,6''}$), 151.3 (C^{6a}), 151.0 ($C^{6a'}$), 146.7 ($C^{5a''}$), 139.2 (C^{4a}), 137.9 ($C^{4,4'}$), 137.1 ($C^{4a'}$), 134.8 ($C^{4'}$), 128.1 (C^{5a}), 128.0 ($C^{5,5''}$), 125.1 (C^{3a}), 124.8 ($C^{3,3''}$), 124.1 ($C^{3',5'}$), 122.0 ($C^{5a'}$), 121.9 ($C^{3a'}$), 52.9 (N−CH$_2$−), 39.6 (−CH$_2$−), 32.3 (−CH$_2$−), 29.7 (−CH$_2$−), 29.5 (−CH$_2$−), 29.4 (−CH$_2$−), 26.7 (−CH$_2$−), 23.2 (−CH$_2$−), 14.3 (−CH$_3$) ppm; MS (HR ESI-Q-TOF): calcd. for C$_{36}$H$_{38}$N$_8$Ru ([M − 2PF$_6$]$^{2+}$): m/z = 342.1122; found: m/z = 342.1131.

Synthesis of 1b. [Ru(tcmtpy)(MeCN)$_3$](PF$_6$)$_2$ (62.5 mg, 0.07 mmol) and **5** (21.5 mg, 0.06) were dissolved in dry and nitrogen-purged DMF (2 mL). The reaction mixture was heated to 160 °C for 30 min in the microwave reactor. The full conversion of **5** was confirmed by TLC (alumina, CH$_2$Cl$_2$). The crude reaction mixture was precipitated in aq. NH$_4$PF$_6$, washed with H$_2$O, rinsed with MeCN and, subsequently, purified by column chromatography (silica, MeCN/H$_2$O/aq. KNO$_3$, 100:4:1). After anion exchange to PF$_6^-$, 21.3 mg (0.02 mmol, 34%) of a brown solid were obtained. ^{1}H NMR (400 MHz, CD$_2$Cl$_2$) δ = 9.12 (s, 2H, $H^{3',5'}$), 8.90 (d, ^4J = 1.1 Hz, 2H, $H^{3,3''}$), 8.47 (d, ^3J = 8.0 Hz, 1H, $H^{3a'}$), 8.43 (d, ^3J = 8.2 Hz, 1H, H^{3a}), 8.35 (t, ^3J = 8.1 Hz, 1H, $H^{4a'}$), 8.17 (d, ^3J = 8.0 Hz, 1H, $H^{5a'}$), 7.91 (dt, ^3J = 8.0, ^4J = 1.5 Hz, 1H, H^{4a}), 7.66 (dd, ^3J = 5.8, ^4J = 1.7 Hz, 2H, $H^{5,5''}$), 7.50 (d, ^3J = 5.8 Hz, 2H, $H^{6,6''}$), 7.21 (d, ^3J = 4.6 Hz, 1H, H^{6a}), 7.15 (t, ^3J = 6.5 Hz, 1H, H^{5a}), 4.79 (t, ^3J = 7.4 Hz, 2H, N−CH$_2$−), 4.17 (s, 3H, C$^{4'}$−COOCH$_3$), 3.96 (s, 6H, C$^{4,4''}$−COOCH$_3$), 2.11−1.99 (m, 2H, N−CH$_2$−CH$_2$−), 1.58−1.09 (m, 10H, −CH$_2$−), 0.86 (t, ^3J = 6.9 Hz, 3H, −CH$_3$) ppm; ^{13}C NMR (100 MHz, CD$_2$Cl$_2$) δ = 173.2 (Ru−C), 164.7 (C$^{4'}$−COOMe), 164.0 (C$^{4,4''}$−COOMe), 158.2 ($C^{2,2''}$), 156.3 ($C^{2a'}$), 155.8 (C^{2a}), 155.1 ($C^{2',6'}$), 152.5 ($C^{6,6''}$), 150.5 ($C^{6a,6a'}$), 143.4 ($C^{5a''}$), 139.0 (C^{4a}), 138.2 ($C^{4a'}$), 138.0 ($C^{4,4''}$), 134.5 ($C^{4'}$), 127.8 (C^{5a}), 126.8 ($C^{5,5''}$), 124.8 (C^{3a}), 123.0 ($C^{3,3''}$), 122.8 ($C^{3',5'}$), 120.9 ($C^{3a'}$), 120.7 ($C^{5a'}$), 53.7 (N−CH$_2$−), 53.5 (−CH$_2$−), 52.2 (−CH$_2$−), 32.0 (−CH$_2$−), 29.5 (−CH$_2$−), 29.4 (−CH$_2$−), 29.3 (−CH$_2$−), 26.7 (−CH$_2$−), 22.9 (−CH$_2$−), 14.2 (−CH$_3$) ppm; MS (HR ESI-Q-TOF): calcd. for C$_{41}$H$_{41}$N$_8$O$_6$Ru ([M − PF$_6$]$^+$): m/z = 843.2198; found: m/z = 843.2204.

Synthesis of 2b. Following the same procedure as described for **2a**, **1b** (7.8 mg, 0.01 mmol) and MeI (1.5 μL, 0.02 mmol, 3 equiv) were reacted in dry CHCl$_3$ (0.6 mL) at 70 °C for 48 h. After anion exchange to PF$_6^-$, 6.5 mg (0.01 mmol, 71%) of a brown solid were obtained. ^{1}H NMR (400 MHz, CD$_2$Cl$_2$) δ = 9.22 (s, 2H, $H^{3',5'}$), 8.96 (d, ^4J = 1.2 Hz, 2H, $H^{3,3''}$), 8.51 (d, ^3J = 8.1 Hz, 1H, $H^{3a'}$), 8.47−8.36 (m, 2H, $H^{3a,4a'}$), 8.27 (d, ^3J = 8.0 Hz, 1H, H^{4a}), 8.06−7.86 (m, 1H, H^{4a}), 7.76 (dd, ^3J = 5.8, ^4J = 1.6 Hz, 2H, $H^{5,5''}$), 7.61 (d, ^3J = 5.8 Hz, 2H, $H^{6,6''}$), 7.27 (d, ^3J = 4.7 Hz, 1H, H^{6a}), 7.23−7.13 (m, 1H, H^{5a}), 4.82 (t, ^3J = 7.5 Hz, 2H, N−CH$_2$−), 4.20 (s, 3H, C$^{4'}$−COOCH$_3$), 3.97 (s, 6H, C$^{4,4''}$−COOCH$_3$), 3.08 (s, 3H), 2.17−2.02 (m, 2H, N−CH$_2$−CH$_2$−), 1.50−1.18 (m, 10H, −CH$_2$−), 0.86 (t, ^3J = 6.9 Hz, 3H, −CH$_3$) ppm; ^{13}C NMR (100 MHz, CD$_2$Cl$_2$) δ = 173.6 (Ru−C), 164.4

($C^{4\prime}$−COOMe), 163.9 ($C^{4,4\prime\prime}$−COOMe), 157.4 ($C^{2,2\prime\prime}$), 156.3 ($C^{2a\prime}$), 155.6 (C^{2a}), 155.4 ($C^{2\prime,6\prime}$), 153.5 ($C^{6,6\prime\prime}$), 150.8 (C^{6a}), 149.7 ($C^{6a\prime}$), 146.1 ($C^{5a\prime\prime}$), 139.3 (C^{4a}), 138.7 ($C^{4a\prime,4,4\prime\prime}$), 135.4 ($C^{4\prime}$), 128.3 ($C^{5a}$), 127.8 ($C^{5,5\prime\prime}$), 124.9 ($C^{3a}$), 123.4 ($C^{3,3\prime\prime}$), 123.2 ($C^{3\prime,5\prime}$), 122.2 ($C^{5a\prime}$), 121.9 ($C^{3a}$), 54.0 (N−$CH_2$−), 53.8 (−$CH_2$−), 53.0 (−$CH_2$−), 39.4 (−$CH_2$−), 36.5 (−$CH_2$−), 32.0 (−$CH_2$−), 29.3 (−$CH_2$−), 29.2 (−$CH_2$−), 28.8 (−$CH_2$−), 26.1 (−$CH_2$−), 22.9 (−$CH_2$−), 14.2 (−$CH_3$) ppm; MS (HR ESI-Q-TOF): calcd. for $C_{42}H_{44}N_8O_6Ru$ ([M − $2PF_6$]$^{2+}$): m/z = 429.1214; found: m/z = 429.1203.

Synthesis of 3b. Under a nitrogen atmosphere, a microwave vial was charged with **8** (52 mg, 0.06 mmol), Ru(tcmtpy)(DMSO)Cl_2 (41 mg, 0.06 mmol), and dry and nitrogen-purged CH_2Cl_2 (9 mL). The vial was capped and heated to 70 °C for 24 h while stirring using an oil bath. The reaction mixture was allowed to cool to room temperature and the solvent was evaporated. The remaining solid was dissolved in MeCN, followed by the precipitation in aq. NH_4PF_6, filtration, washing with H_2O, and rinsing with MeCN. The crude product was subjected to column chromatography (silica, MeCN/H_2O/aq. KNO$_3$, 100:2:1) and the anion was exchanged to PF_6^- again. After precipitation into diethyl ether from a concentrated MeCN solution, filtration, washing with diethyl ether, rinsing with MeCN, and evaporation of all volatiles in vacuo, 13 mg (0.01 mmol, 21%) of a brown solid were obtained. ^{1}H NMR (400 MHz, CD_2Cl_2) δ = 9.16 (s, 2H, $H^{3\prime,5\prime}$), 8.96 (d, ^4J = 1.1 Hz, 2H, $H^{3,3\prime\prime}$), 8.32 (t, ^3J = 8.2 Hz, 1H, $H^{4a\prime}$), 8.01 (d, ^3J = 8.2 Hz, 2H, $H^{3a\prime,5a\prime}$), 7.79 (dd, ^3J = 5.8, ^4J = 1.7 Hz, 2H, $H^{5,5\prime\prime}$), 7.75 (d, ^3J = 5.8 Hz, 2H, $H^{6,6\prime\prime}$), 4.77 (t, ^3J = 7.5 Hz, 4H, N−CH_2−), 4.19 (s, 3H, $C^{4\prime}$−COOCH_3), 3.99 (s, 6H, $C^{4,4\prime\prime}$−COOCH_3), 3.00 (s, 6H, N−CH_3), 2.12−2.01 (m, 4H, N−CH_2−CH_2−), 1.48−1.19 (m, 20H, −CH_2−), 0.86 (t, ^3J = 6.9 Hz, 6H, −CH_3) ppm; ^{13}C NMR (100 MHz, CD_2Cl_2) δ = 179.7 (Ru−C), 164.7 ($C^{4\prime}$−COOMe), 164.2 ($C^{4,4\prime\prime}$−COOMe), 156.4 ($C^{2,2\prime\prime}$), 154.3 ($C^{2\prime,6\prime}$), 154.0 ($C^{5,5\prime\prime}$), 151.1 ($C^{2a\prime,6a\prime}$), 145.8 ($C^{4a\prime}$), 139.3 ($C^{5a,5a\prime\prime}$), 137.6 ($C^{4,4\prime\prime}$), 132.8 ($C^{4\prime}$), 127.3 ($C^{6,6\prime\prime}$), 122.9 ($C^{3,3\prime\prime}$), 122.2 ($C^{3\prime,5\prime}$), 119.8 ($C^{3a\prime,5a\prime}$), 54.2 (N−CH_2−), 53.7 (−CH_2−), 52.8 (−CH_2−), 39.4 (−CH_2−), 32.0 (−CH_2−), 29.4 (−CH_2−), 29.2 (−CH_2−), 28.9 (−CH_2−), 26.7 (−CH_2−), 22.9 (−CH_2−), 14.2 (−CH_3) ppm; MS (HR ESI-Q-TOF): calcd. for $C_{48}H_{60}N_{10}O_6Ru$ ([M − $2PF_6$]$^{2+}$): m/z = 487.1871; found: m/z = 487.1848.

General Procedure for the Saponification of the Complexes 1−3b. According to the literature,[49] the ester-substituted complex was suspended in a DMF/NEt$_3$/H_2O (3:1:1, $v/v/v$, 2 mL) and heated to reflux for 24 to 48 h under a nitrogen atmosphere. After the full conversion was confirmed by MALDI-TOF MS, the solvents were evaporated in vacuo and the remaining solid was suspended in CH_2Cl_2. After collection of the solid using a centrifuge, the solvent was decanted and the remaining solvent was dried in vacuo.

Synthesis of 1c. 1b (21.3 mg, 0.022 mmol) was reacted for 48 h to yield 16.1 mg (0.017 mmol, 79%) of a black solid. ^{1}H NMR (400 MHz, CD_3CN) δ = 9.21 (s, 2H), 9.01 (s, 2H), 8.75−8.61 (m, 2H), 8.48−8.33 (m, 2H), 7.99 (t, ^3J = 8.9 Hz, 1H), 7.60 (d, ^3J = 5.6 Hz, 2H), 7.55 (d, ^3J = 4.1 Hz, 1H), 7.48 (d, ^3J = 5.6 Hz, 2H), 7.26 (t, ^3J = 5.7 Hz, 1H), 2.16−2.04 (m, 2H), 1.32 (s, 10H), 0.97−0.82 (m, 3H); MS (MALDI-TOF): calcd. for $C_{38}H_{35}N_8O_6Ru$ (M − PF_6]$^+$): m/z = 801.174; found: m/z = 801.252.

Synthesis of 2c. 2b (16 mg, 0.014 mmol) was reacted for 24 h to yield 11.4 mg (0.012 mmol, 85%) of a black solid. ^{1}H NMR (400 MHz, MeOD) δ = 9.33 (s, 2H), 9.08 (s, 2H), 8.77 (d, ^3J = 8.1 Hz, 1H), 8.70 (d, ^3J = 8.0 Hz, 1H), 8.53−8.39 (m, 2H), 8.02 (t, ^3J = 7.2 Hz, 1H), 7.68 (d, ^3J = 4.2 Hz, 2H), 7.59−7.51 (m, 3H), 7.28 (t, ^3J = 6.6 Hz, 1H), 3.20 (s, 3H), 2.19−2.02 (m, 2H), 1.52−1.18 (m, 10H), 0.88 (t, ^3J = 7.1 Hz, 3H). MS (MALDI-TOF): calcd. for $C_{39}H_{38}N_8O_6Ru$ ([M − $2PF_6$]$^+$): m/z = 816.196; found: m/z = 816.354.

Synthesis of 3c. 3b (20.6 mg, 0.016 mmol) was reacted for 48 h to yield 15.3 mg (0.014 mmol, 87%) of a deep brown solid. ^{1}H NMR (400 MHz, CD_3CN) δ = 9.25 (s, 2H), 9.05 (s, 2H), 8.32 (t, ^3J = 8.1 Hz, 1H), 8.23 (d, ^3J = 8.2 Hz, 2H), 7.66 (d, ^3J = 4.3 Hz, 2H), 7.60 (d, ^3J = 5.8 Hz, 2H), 3.15 (s, 6H), 2.15−2.03 (m, 4H), 1.51−1.17 (m, 20H), 0.88 (t, ^3J = 6.9 Hz, 6H); MS (MALDI-TOF): calcd. for

$C_{45}H_{54}N_{10}O_6Ru$ ([M − $2PF_6$]$^+$): m/z = 932.327; found: m/z = 932.463.

Cell Fabrication. Photoanodes were prefabricated by Dyesol, Inc. (Australia) with a screenprintable TiO_2 paste (18-NRT, Dyesol). The active area of the TiO_2 electrode is 0.88 cm^2 with a thickness of 12 μm (18-NRT) on fluorine-doped tin-oxide (FTO; TEC15 (15 Ω cm^{-2})). TiO_2 substrates were treated with $TiCl_4$(aq) (0.05 M) at 70 °C for 30 min and subsequently rinsed with H_2O and EtOH and dried prior to heating. The electrodes were heated to 450 °C for 20 min under ambient atmosphere and allowed to cool to 80 °C before dipping into the dye solution. The anode was soaked overnight for 16 h in anhydrous methanol and ethanol containing ∼0.25 mM **1c**−**3c** and **N749**, respectively. The stained films were rinsed copiously with the solvent they were dipped in and subsequently dried. The cells were fabricated using a Pt-coated counter-electrode (FTO TEC-15 (15 Ω cm^{-2})) and sandwiched with a 30 μm Surlyn (Dupont) gasket by resistive heating. The acetonitrile-based electrolytes contained 0.1 M guanidinium thiocyanate (GuSCN), 0.5 M 4-*tert*-butylpyridine (TBP), 0.06 M iodine, 0.6 M 1,3-dimethylimidazolium iodide (DMII), and either 1 M (**1c**−**3c**) or 0.1 M (**N749**) LiI. The electrolyte was introduced to the void via vacuum backfilling through a hole in the counter electrode. The hole was sealed with an aluminum-backed Bynel foil (Dyesol). After sealing, silver bus bars were added to all cells.[70]

■ ASSOCIATED CONTENT

Ⓢ Supporting Information

Figures S1−S83: Additional computational, photophysical, and electrochemical data as well as NMR, ESI-TOF MS and MALDI-TOF MS spectra. This material is available free of charge via the Internet at http://pubs.acs.org.

■ AUTHOR INFORMATION

Corresponding Authors
*E-mail: cberling@chem.ubc.ca.
*E-mail: benjamin.dietzek@uni-jena.de.
*E-mail: ulrich.schubert@uni-jena.de.

Notes
The authors declare no competing financial interest.

■ ACKNOWLEDGMENTS

■ REFERENCES

(1) Prier, C. K.; Rankic, D. A.; MacMillan, D. W. C. *Chem. Rev.* **2013**, *113*, 5322.
(2) Tschierlei, S.; Karnahl, M.; Presselt, M.; Dietzek, B.; Guthmuller, J.; González, L.; Schmitt, M.; Rau, S.; Popp, J. *Angew. Chem., Int. Ed.* **2010**, *49*, 3981.
(3) Narayanam, J. M. R.; Stephenson, C. R. J. *Chem. Soc. Rev.* **2011**, *40*, 102.
(4) Zeitler, K. *Angew. Chem., Int. Ed.* **2009**, *48*, 9785.
(5) Tucker, J. W.; Stephenson, C. R. J. *J. Org. Chem.* **2012**, *77*, 1617.
(6) Alstrum-Acevedo, J. H.; Brennaman, M. K.; Meyer, T. J. *Inorg. Chem.* **2005**, *44*, 6802.
(7) Bomben, P. G.; Robson, K. C. D.; Koivisto, B. D.; Berlinguette, C. P. *Coord. Chem. Rev.* **2012**, *256*, 1438.
(8) Robson, K. C. D.; Bomben, P. G.; Berlinguette, C. P. *Dalton Trans.* **2012**, *41*, 7814.

(9) Yin, J.-F.; Velayudham, M.; Bhattacharya, D.; Lin, H.-C.; Lu, K.-L. *Coord. Chem. Rev.* **2012**, *256*, 3008.

(10) Juris, A.; Balzani, V.; Barigelletti, F.; Campagna, S.; Belser, P.; von Zelewsky, A. *Coord. Chem. Rev.* **1988**, *84*, 85.

(11) Sauvage, J.-P.; Collin, J.-P.; Chambron, J.-C.; Guillerez, S.; Coudret, C.; Balzani, V.; Barigelletti, F.; De Cola, L.; Flamigni, L. *Chem. Rev.* **1994**, *94*, 993.

(12) Borg, O. A.; Godinho, S. S. M. C.; Lundqvist, M. J.; Lunell, S.; Persson, P. *J. Phys. Chem. A* **2008**, *112*, 4470.

(13) Hammarström, L.; Johansson, O. *Coord. Chem. Rev.* **2010**, *254*, 2546.

(14) Medlycott, E. A.; Hanan, G. S. *Chem. Soc. Rev.* **2005**, *34*, 133.

(15) Medlycott, E. A.; Hanan, G. S. *Coord. Chem. Rev.* **2006**, *250*, 1763.

(16) Schulze, B.; Escudero, D.; Friebe, C.; Siebert, R.; Görls, H.; Sinn, S.; Thomas, M.; Mai, S.; Popp, J.; Dietzek, B.; González, L.; Schubert, U. S. *Chem.—Eur. J.* **2012**, *18*, 4010.

(17) Costa, R. D.; Ortí, E.; Bolink, H. J.; Monti, F.; Accorsi, G.; Armaroli, N. *Angew. Chem., Int. Ed.* **2012**, *51*, 8178.

(18) Schulze, B.; Brown, D. G.; Robson, K. C. D.; Friebe, C.; Jäger, M.; Birckner, E.; Berlinguette, C. P.; Schubert, U. S. *Chem.—Eur. J.* **2013**, *19*, 14171.

(19) Caspar, J. V.; Sullivan, B. P.; Kober, E. M.; Meyer, T. J. *Chem. Phys. Lett.* **1982**, *91*, 91.

(20) Wächtler, M.; Maiuri, M.; Brida, D.; Popp, J.; Rau, S.; Cerullo, G.; Dietzek, B. *ChemPhysChem* **2013**, *14*, 2973.

(21) Kalyanasundaram, K.; Nazeeruddin, M. K. *Chem. Phys. Lett.* **1992**, *193*, 292.

(22) Lees, A. J. *Chem. Rev.* **1987**, *87*, 711.

(23) Jayabharathi, J.; Thanikachalam, V.; Srinivasan, N.; Perumal, M. V. *Spectrochim. Acta, Part A* **2011**, *79*, 338.

(24) Son, S. U.; Park, K. H.; Lee, Y.-S.; Kim, B. Y.; Choi, C. H.; Lah, M. S.; Jang, Y. H.; Jang, D.-J.; Chung, Y. K. *Inorg. Chem.* **2004**, *43*, 6896.

(25) Schulze, B.; Escudero, D.; Friebe, C.; Siebert, R.; Görls, H.; Köhn, U.; Altuntas, E.; Baumgaertel, A.; Hager, M. D.; Winter, A.; Dietzek, B.; Popp, J.; González, L.; Schubert, U. S. *Chem.—Eur. J.* **2011**, *17*, 5494.

(26) Gentilini, D.; Gagliardi, A.; Auf der Maur, M.; Vesce, L.; D'Ercole, D.; Brown, T. M.; Reale, A.; Di Carlo, A. *J. Phys. Chem. C* **2012**, *116*, 1151.

(27) Brown, D. G.; Schauer, P. A.; Borau-Garcia, J.; Fancy, B. R.; Berlinguette, C. P. *J. Am. Chem. Soc.* **2013**, *135*, 1692.

(28) Note that the numeration of the 1,3-triazolylidene ring used in this article follows the priority of the *N*-substituents of the triazole, which differs from the usually employed synthetic route via the copper(I)-catalyzed azide−alkyne cycloaddition. To avoid ambiguities, we avoid an indication of the carbene position (C4 or C5) and only use the term 1,2,3-triazolylidene throughout this article except for the NMR assignment.

(29) Schuster, O.; Yang, L.; Raubenheimer, H. G.; Albrecht, M. *Chem. Rev.* **2009**, *109*, 3445.

(30) Schulze, B.; Schubert, U. S. *Chem. Soc. Rev.*, in press, DOI: 10.1039/c3cs60386e.

(31) Bai, Y.; Zhang, J.; Wang, Y.; Zhang, M.; Wang, P. *Langmuir* **2011**, *27*, 4749.

(32) Juozapavicius, M.; Kaucikas, M.; van Thor, J. J.; O'Regan, B. C. *J. Phys. Chem. C* **2013**, *117*, 116.

(33) Bessho, T.; Yoneda, E.; Yum, J.-H.; Guglielmi, M.; Tavernelli, I.; Imai, H.; Rothlisberger, U.; Nazeeruddin, M. K.; Grätzel, M. *J. Am. Chem. Soc.* **2009**, *131*, 5930.

(34) Bomben, P. G.; Thériault, K. D.; Berlinguette, C. P. *Eur. J. Inorg. Chem.* **2011**, 1806.

(35) Struthers, H.; Mindt, T. L.; Schibli, R. *Dalton Trans.* **2010**, *39*, 675.

(36) Crowley, J. D.; McMorran, D. A. In *Topics in Heterocyclic Chemistry: Click Triazoles*; Košmrlj, J., Ed.; Springer: Berlin, 2012; Vol. 28, p 31.

(37) Zhang, L.; Chen, X.; Xue, P.; Sun, H. H. Y.; Williams, I. D.; Sharpless, K. B.; Fokin, V. V.; Jia, G. *J. Am. Chem. Soc.* **2005**, *127*, 15998.

(38) Liu, S.; Müller, P.; Takase, M. K.; Swager, T. M. *Inorg. Chem.* **2011**, *50*, 7598.

(39) Wang, M.; Moon, S.-J.; Zhou, D.; Le Formal, F.; Cevey-Ha, N.-L.; Humphry-Baker, R.; Grätzel, C.; Wang, P.; Zakeeruddin, S. M.; Grätzel, M. *Adv. Funct. Mater.* **2010**, *20*, 1821.

(40) Klein, C.; Nazeeruddin, M. K.; Di Censo, D.; Liska, P.; Grätzel, M. *Inorg. Chem.* **2004**, *43*, 4216.

(41) Shin, Y.; Fryxell, G. E.; Johnson, C. A., II; Haley, M. M. *Chem. Mater.* **2008**, *20*, 981.

(42) Lamberti, M.; Fortman, G. C.; Poater, A.; Broggi, J.; Slawin, A. M. Z.; Cavallo, L.; Nolan, S. P. *Organometallics* **2012**, *31*, 756.

(43) Boren, B. C.; Narayan, S.; Rasmussen, L. K.; Zhang, L.; Zhao, H.; Lin, Z.; Jia, G.; Fokin, V. V. *J. Am. Chem. Soc.* **2008**, *130*, 8923.

(44) Rasmussen, L. K.; Boren, B. C.; Fokin, V. V. *Org. Lett.* **2007**, *9*, 5337.

(45) Schuster, E. M.; Botoshansky, M.; Gandelman, M. *Dalton Trans.* **2011**, *40*, 8764.

(46) Keske, E. C.; Zenkina, O. V.; Wang, R.; Crudden, C. M. *Organometallics* **2012**, *31*, 456.

(47) Donnelly, K. F.; Petronilho, A.; Albrecht, M. *Chem. Commun.* **2013**, *49*, 1145.

(48) Wadman, S. H.; Kroon, J. M.; Bakker, K.; Havenith, R. W. A.; van Klink, G. P. M.; van Koten, G. *Organometallics* **2010**, *29*, 1569.

(49) Robson, K. C. D.; Koivisto, B. D.; Yella, A.; Sporinova, B.; Nazeeruddin, M. K.; Baumgartner, T.; Grätzel, M.; Berlinguette, C. P. *Inorg. Chem.* **2011**, *50*, 5494.

(50) Bomben, P. G.; Robson, K. C. D.; Sedach, P. A.; Berlinguette, C. P. *Inorg. Chem.* **2009**, *48*, 9631.

(51) Leigh, V.; Ghattas, W.; Lalrempuia, R.; Müller-Bunz, H.; Pryce, M. T.; Albrecht, M. *Inorg. Chem.* **2013**, *52*, 5395.

(52) Abrahamsson, M.; Jäger, M.; Österman, T.; Eriksson, L.; Persson, P.; Becker, H.-C.; Johansson, O.; Hammarström, L. *J. Am. Chem. Soc.* **2006**, *128*, 12616.

(53) Amini, A.; Harriman, A.; Mayeux, A. *Phys. Chem. Chem. Phys.* **2004**, *5*, 1157.

(54) Wadman, S. H.; Lutz, M.; Tooke, D. M.; Spek, A. L.; Hartl, F.; Havenith, R. W. A.; van Klink, G. P. M.; van Koten, G. *Inorg. Chem.* **2009**, *48*, 1887.

(55) Collin, J.-P.; Beley, M.; Sauvage, J.-P.; Barigelletti, F. *Inorg. Chim. Acta* **1991**, *186*, 91.

(56) Chou, P.-T.; Chi, Y. *Eur. J. Inorg. Chem.* **2006**, 3319.

(57) Armstrong, N. R.; Wightman, R. M.; Gross, E. M. *Annu. Rev. Phys. Chem.* **2001**, *52*, 391.

(58) Chou, P.-T.; Chi, Y. *Chem.—Eur. J.* **2007**, *13*, 380.

(59) Abruña, H. D. *J. Electrochem. Soc.* **1985**, *132*, 842.

(60) Álvarez, C. M.; García-Escudero, L. A.; García-Rodríguez, R.; Miguel, D. *Chem. Commun.* **2012**, *48*, 7209.

(61) Pavlishchuk, V. V.; Addison, A. W. *Inorg. Chim. Acta* **2000**, *298*, 97.

(62) Connelly, N. G.; Geiger, W. E. *Chem. Rev.* **1996**, *96*, 877.

(63) Hagfeldt, A.; Boschloo, G.; Sun, L.; Kloo, L.; Pettersson, H. *Chem. Rev.* **2010**, *110*, 6595.

(64) Bietti, M.; DiLabio, G. A.; Lanzalunga, O.; Salamone, M. *J. Org. Chem.* **2010**, *75*, 5875.

(65) Park, H.-J.; Yoo, S.; Shin, I.-S.; Chung, Y. K.; Kim, J. *Electroanalysis* **2013**, *25*, 1111.

(66) Park, H.-J.; Chung, Y. K. *Dalton Trans.* **2012**, *41*, 5678.

(67) Park, H.-J.; Kim, K. H.; Choi, S. Y.; Kim, H.-M.; Lee, W. I.; Kang, Y. K.; Chung, Y. K. *Inorg. Chem.* **2010**, *49*, 7340.

(68) Gusev, D. G. *Organometallics* **2009**, *28*, 6458.

(69) Crabtree, R. H. *Coord. Chem. Rev.* **2013**, *257*, 755.

(70) Bomben, P. G.; Borau-Garcia, J.; Berlinguette, C. P. *Chem. Commun.* **2012**, *48*, 5599.

(71) Nazeeruddin, M. K.; Péchy, P.; Renouard, T.; Zakeeruddin, S. M.; Humphry-Baker, R.; Comte, P.; Liska, P.; Cevey, L.; Costa, E.;

Shklover, V.; Spiccia, L.; Deacon, G. B.; Bignozzi, C. A.; Grätzel, M. *J. Am. Chem. Soc.* **2001**, *123*, 1613.

(72) Chiba, Y.; Islam, A.; Watanabe, Y.; Komiya, R.; Koide, N.; Han, L. *Jpn. J. Appl. Phys.* **2006**, *45*, L638.

(73) Jennings, J. R.; Wang, Q. *J. Phys. Chem. C* **2009**, *114*, 1715.

(74) Onicha, A. C.; Castellano, F. N. *J. Phys. Chem. C* **2010**, *114*, 6831.

(75) Hasan, K.; Zysman-Colman, E. *Inorg. Chem.* **2012**, *51*, 12560.

(76) Wu, K.-L.; Ho, S.-T.; Chou, C.-C.; Chang, Y.-C.; Pan, H.-A.; Chi, Y.; Chou, P.-T. *Angew. Chem., Int. Ed.* **2012**, *51*, 5642.

(77) Clifford, J. N.; Palomares, E.; Nazeeruddin, M. K.; Grätzel, M.; Durrant, J. R. *J. Phys. Chem. C* **2007**, *111*, 6561.

(78) Jennings, J. R.; Liu, Y.; Wang, Q. *J. Phys. Chem. C* **2011**, *115*, 15109.

(79) Li, X.; Reynal, A.; Barnes, P.; Humphry-Baker, R.; Zakeeruddin, S. M.; De Angelis, F.; O'Regan, B. C. *Phys. Chem. Chem. Phys.* **2012**, *14*, 15421.

(80) Reynal, A.; Forneli, A.; Martinez-Ferrero, E.; Sánchez-Díaz, A.; Vidal-Ferran, A.; O'Regan, B. C.; Palomares, E. *J. Am. Chem. Soc.* **2008**, *130*, 13558.

(81) Richards, C. E.; Anderson, A. Y.; Martiniani, S.; Law, C.; O'Regan, B. C. *J. Phys. Chem. Lett.* **2012**, *3*, 1980.

(82) Polander, L. E.; Yella, A.; Curchod, B. F. E.; Ashari Astani, N.; Teuscher, J.; Scopelliti, R.; Gao, P.; Mathew, S.; Moser, J.-E.; Tavernelli, I.; Rothlisberger, U.; Grätzel, M.; Nazeeruddin, M. K.; Frey, J. *Angew. Chem., Int. Ed.* **2013**, *52*, 8731.

(83) Mori, S. N.; Kubo, W.; Kanzaki, T.; Masaki, N.; Wada, Y.; Yanagida, S. *J. Phys. Chem. C* **2007**, *111*, 3522.

(84) Wadman, S. H.; Kroon, J. M.; Bakker, K.; Lutz, M.; Spek, A. L.; van Klink, G. P. M.; van Koten, G. *Chem. Commun* **2007**, 1907.

(85) Kisserwan, H.; Kamar, A.; Shoker, T.; Ghaddar, T. H. *Dalton Trans.* **2012**, *41*, 10643.

(86) Lin, H.-W.; Wang, Y.-S.; Huang, Z.-Y.; Lin, Y.-M.; Chen, C.-W.; Yang, S.-H.; Wu, K.-L.; Chi, Y.; Liu, S.-H.; Chou, P.-T. *Phys. Chem. Chem. Phys.* **2012**, *14*, 14190.

(87) Hamann, T. W. *Dalton Trans.* **2012**, *41*, 3111.

(88) Ondersma, J. W.; Hamann, T. W. *Coord. Chem. Rev.* **2013**, *257*, 1533.

(89) Daeneke, T.; Mozer, A. J.; Uemura, Y.; Makuta, S.; Fekete, M.; Tachibana, Y.; Koumura, N.; Bach, U.; Spiccia, L. *J. Am. Chem. Soc.* **2012**, *134*, 16925.

(90) Alvarez, S. G.; Alvarez, M. T. *Synthesis* **1997**, 413.

(91) Park, S. H. *Bull. Korean Chem. Soc.* **2003**, *24*, 253.

(92) Siebert, R.; Hunger, C.; Guthmuller, J.; Schlütter, F.; Winter, A.; Schubert, U. S.; González, L.; Dietzek, B.; Popp, J. *J. Phys. Chem. C* **2011**, *115*, 12677.

(93) Becke, A. D. *J. Chem. Phys.* **1993**, *98*, 5648.

(94) Lee, C.; Yang, W.; Parr, R. G. *Phys. Rev. B* **1988**, *37*, 785.

(95) Mennucci, B.; Tomasi, J. *J. Chem. Phys.* **1997**, *106*, 5151.

(96) Cossi, M.; Barone, V.; Mennucci, B.; Tomasi, J. *Chem. Phys. Lett.* **1998**, *286*, 253.

(97) Frisch, M. J.; Trucks, G. W.; Schlegel, H. B.; Scuseria, G. E.; Robb, M. A.; Cheeseman, J. R.; Scalmani, G.; Barone, V.; Mennucci, B.; Petersson, G. A.; Nakatsuji, H.; Caricato, M.; Li, X.; Hratchian, H. P.; Izmaylov, A. F.; Bloino, J.; Zheng, G.; Sonnenberg, J. L.; Hada, M.; Ehara, M.; Toyota, K.; Fukuda, R.; Hasegawa, J.; Ishida, M.; Nakajima, T.; Honda, Y.; Kitao, O.; Nakai, H.; Vreven, T.; Montgomery, J. A.; Peralta, J. E.; Ogliaro, F.; Bearpark, M.; Heyd, J. J.; Brothers, E.; Kudin, K. N.; Staroverov, V. N.; Kobayashi, R.; Normand, J.; Raghavachari, K.; Rendell, A.; Burant, J. C.; Iyengar, S. S.; Tomasi, J.; Cossi, M.; Rega, N.; Millam, J. M.; Klene, M.; Knox, J. E.; Cross, J. B.; Bakken, V.; Adamo, C.; Jaramillo, J.; Gomperts, R.; Stratmann, R. E.; Yazyev, O.; Austin, A. J.; Cammi, R.; Pomelli, C.; Ochterski, J. W.; Martin, R. L.; Morokuma, K.; Zakrzewski, V. G.; Voth, G. A.; Salvador, P.; Dannenberg, J. J.; Dapprich, S.; Daniels, A. D.; Foresman, J. B.; Ortiz, J. V.; Cioslowski, J.; Fox, D. J., *Gaussian 09*, Revision B.01; Gaussian Inc., Wallingford, CT, 2009.

(98) O'Boyle, N. M.; Tenderholt, A. L.; Langner, K. M. *J. Comput. Chem.* **2008**, *29*, 839.

(99) Wolpher, H.; Sinha, S.; Pan, J.; Johansson, A.; Lundqvist, M. J.; Persson, P.; Lomoth, R.; Bergquist, J.; Sun, L.; Sundström, V.; Åkermark, B.; Polívka, T. *Inorg. Chem.* **2007**, *46*, 638.

Publication A5:

"Ruthenium(II) photosensitizers of tridentate click-derived cyclometalating ligands: A joint experimental and computational study"

B. Schulze, D. Escudero, C. Friebe, R. Siebert, H. Görls, S. Sinn, M. Thomas, S. Mai, J. Popp, B. Dietzek, L. González, U. S. Schubert
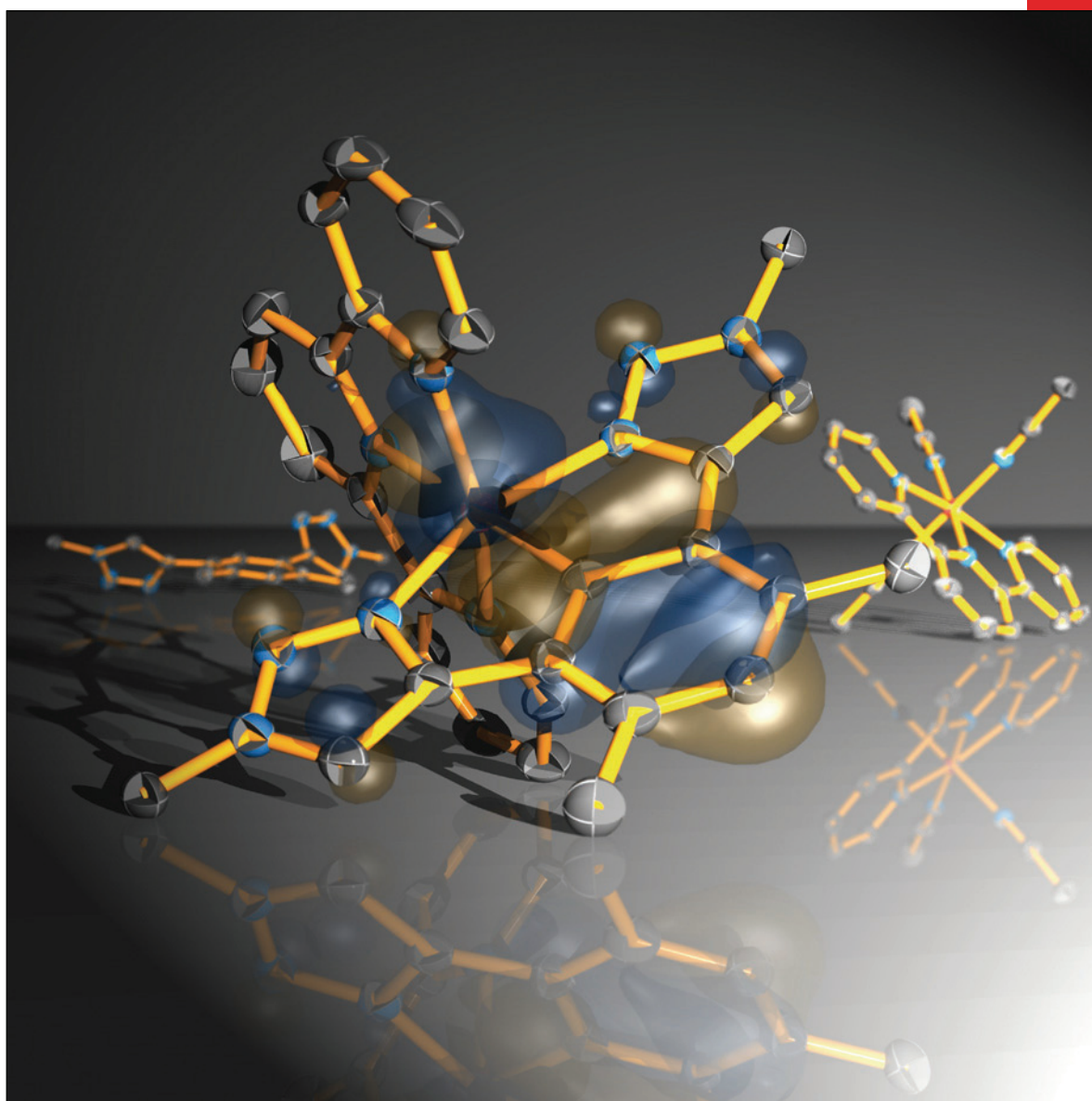
Review
Directed Remote Aromatic Metalations:
Mechanisms and Driving Forces
D. Tilly, J. Magolan and J. Mortier

A Journal of

**ChemPubSoc
Europe**

Supported by
ACES

A photosensitizer exhibition…

… of ruthenium(II) complexes featuring click-derived tridentate cyclometalating ligands is reported. Systematic structural manipulations and detailed electrochemical, photophysical, and computational investigations have been performed, allowing a deeper understanding and revealing great potential for application in dye-sensitized solar cells. For more details, see the Full Paper by U. S. Schubert, B. Dietzek, L. González et al. on page 4010 ff.
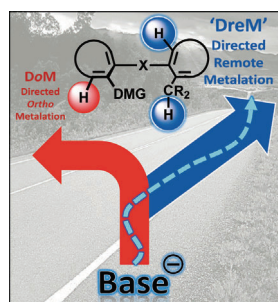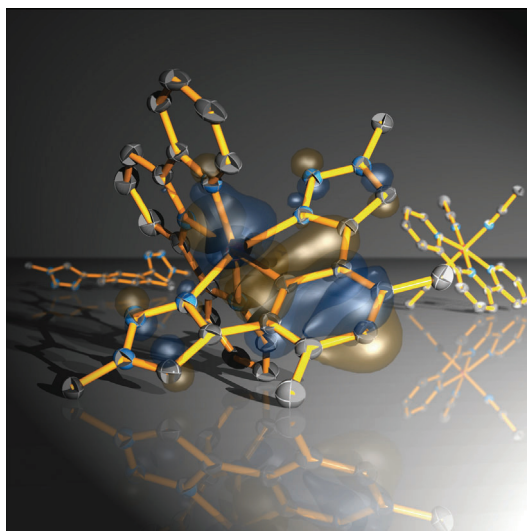
Directed Metalation

The synthetic utility of directed remote aromatic metalations (DreM) is an outcome of good reaction yields and unique reactivity that can be complementarity to Friedel–Crafts transformations. Mechanisms, driving forces, and parameters influencing remote metalations are discussed in the Review on page 3804 ff. by D. Tilly, J. Magolan, and J. Mortier.

Polyoxometalates

$Na_9(NH_4)_5[\{(B-\alpha-PW_9O_{34})Co_3(OH)(H_2O)_2(O_3PC(O)-(C_3H_6NH_3)PO_3)\}_2Co]\cdot35\,H_2O$ represents a rare example of a 3D polyanionic SMM (single-molecule magnet), but overall is also the first hybrid SMM POM characterized to date. Importantly, its stability in aqueous solution has been demonstrated by using electronic absorption spectroscopy, electrochemical measurements, and multinuclear NMR experiments. For more details, see the Communication by P. Mialane, B. Keita et al. on page 3845 ff.
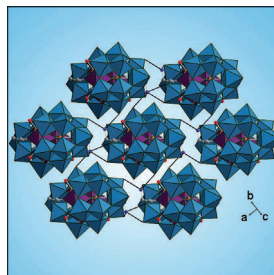
Molecular Dynamics

A non-damaging method is described to determine the configuration of nitrotyrosine residues of native proteins in solution. A ^{15}N-tagged nitro group and the adjacent aromatic proton were detected by using HSQC NMR spectroscopy optimized for ^3J(N−H) couplings. This method enabled the detection of four out of five nitrated residues and further, determined the configuration of each nitrotyrosine residue in the modified proteins and their different dynamic behaviour in the protein environment. For further details, see the Full Paper by Díaz-Moreno et al. on page 3872 ff.
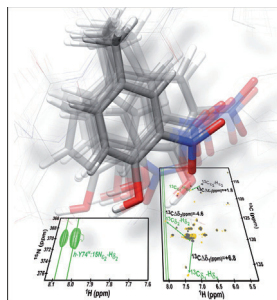
GDCh — GERMANY
KNCV — NETHERLANDS
KVCV — BELGIUM
ITALY
Société Chimique de France — FRANCE
Real Sociedad Española de Química — SPAIN
Sociedade Portuguesa de Química — PORTUGAL
GREECE
CSCH — CZECH REPUBLIC
PTCh — POLAND
Svenska Kemistsamfundet — SWEDEN
MKE — HUNGARY
GÖCH — AUSTRIA
ChemPubSoc Europe

Supported by
ACES

Chemistry—A European Journal is jointly owned by the 14 Chemical Societies shown above and published by Wiley-VCH. This group of Societies has banded together as Chemistry Publishing Society (ChemPubSoc) Europe for its combined publishing activities. The journal is also supported by the Asian Chemical Editorial Society (ACES).

VIP

Ruthenium(II) Photosensitizers of Tridentate Click-Derived Cyclometalating Ligands: A Joint Experimental and Computational Study

Benjamin Schulze,[a, b] Daniel Escudero,[b, c] Christian Friebe,[a, b] Ronald Siebert,[b, d] Helmar Görls,[e] Stephan Sinn,[a, b] Martin Thomas,[b, c] Sebastian Mai,[b, c] Jürgen Popp,[b, d] Benjamin Dietzek,*[b, d] Leticia González,*[b, c, f] and Ulrich S. Schubert*[a, b]

Abstract: A systematic series of heteroleptic bis(tridentate)ruthenium(II) complexes of click-derived 1,3-bis(1,2,3-triazol-4-yl)benzene N^C^N-coordinating ligands was synthesized, analyzed by single crystal X-ray diffraction, investigated photophysically and electrochemically, and studied by computational methods. The presented comprehensive characterization allows a more detailed understanding of the radiationless deactivation mechanisms. Furthermore, we provide a fully optimized synthesis and systematic variations towards redox-matched, broadly and intensely absorbing, cyclometalated ruthenium(II) complexes. Most of them show a weak room-temperature emission and a prolonged excited-state lifetime. They display a broad absorption up to 700 nm and high molar extinction coefficients up to $20\,000\,\mathrm{M^{-1}\,cm^{-1}}$ of the metal-to-ligand charge transfer bands, resulting in a black color. Thus, the complexes reveal great potential for dye-sensitized solar-cell applications.

Keywords: click chemistry · computational methods · cyclometalation · photosensitizers · ruthenium

[a] B. Schulze, C. Friebe, S. Sinn, Prof. Dr. U. S. Schubert
Laboratory of Organic and Macromolecular Chemistry (IOMC)
Friedrich-Schiller-University Jena
Humboldtstr. 10, 07743 Jena (Germany)
Fax: (+49) 3641948202
E-mail: ulrich.schubert@uni-jena.de

[b] B. Schulze, Dr. D. Escudero, C. Friebe, Dr. R. Siebert, S. Sinn,
M. Thomas, S. Mai, Prof. Dr. J. Popp, Prof. Dr. B. Dietzek,
Prof. Dr. L. González, Prof. Dr. U. S. Schubert
Jena Center for Soft Matter (JCSM)
Friedrich-Schiller-University Jena
Humboldtstr. 10, 07743 Jena (Germany)

[c] Dr. D. Escudero, M. Thomas, S. Mai, Prof. Dr. L. González
Laboratory of Theoretical Chemistry
Friedrich-Schiller-University Jena
Helmholtzweg 4, 07743 Jena (Germany)

[d] Dr. R. Siebert, Prof. Dr. J. Popp, Prof. Dr. B. Dietzek
Institute of Physical Chemistry and Abbe Center of Photonics
Friedrich-Schiller-University Jena
Helmholtzweg 4, 07743 Jena (Germany)
and Institute of Photonic Technology Jena
Albert-Einstein-Straße 9, 07745 Jena (Germany)
Fax: (+49) 3641206399
E-mail: benjamin.dietzek@uni-jena.de

[e] Dr. H. Görls
Laboratory of Inorganic and Analytic Chemistry
Friedrich-Schiller-University Jena
Lessingstr. 8, 07743 Jena (Germany)

[f] Prof. Dr. L. González
Current address: Prof. Dr. L. González
Institute of Theoretical Chemistry, University of Vienna
Währinger Str. 17, 1090 Vienna (Austria)
Fax: (+43) 1427752793
E-mail: leticia.gonzalez@univie.ac.at

Introduction

Ruthenium(II) polypyridyl complexes are highly prominent in photochemistry, since they allow for a light-driven charge separation in which the ligand becomes photoreduced while the metal is photooxidized and both can undergo subsequent redox reactions in terms of artificial photosynthesis. This metal-to-ligand charge transfer (MLCT) can be fine-tuned by the ligand properties to optimize the photophysical and electrochemical properties. To allow homogeneous, diffusion-controlled photocatalysis, a long excited-state lifetime is most important. A central dilemma is that, in contrast to tris(bidentate) ruthenium(II) complexes, bis(tridentate) ones are more stable and allow an isomer-free functionalization, but typically show only short excited-state lifetimes.[1] Various optimization strategies to prolong the excited-state lifetime have been developed.[2] The use of very strong, anionic donors causes slightly prolonged lifetimes, and moreover, interesting properties such as a broadened and red-shifted absorption of visible light and a directed MLCT transition.

An application for which these features become most important and the lifetimes are not that crucial, due to immobilization of the complexes and fast electron injection into the semiconductor, is the dye-sensitized solar cell (DSSC), developed by O'Regan and Grätzel in 1991.[3] The DSSC applies the principles of natural photosynthesis, namely the spatial separation of the basic functions that are light-driven charge separation and charge transport, and, therefore, allows for modular manipulations of the light-harvesting dyes. Here, the almost pure, and thus predictable and tunable MLCT and reversible redox behavior made RuII polypyridyl complexes the most attractive candidates. In particu-

lar, Ru^{II} complexes featuring thiocyanate ligands like the red (N3, N719) and black dyes (N749) still display the benchmark with about 11% solar-cell efficiency.[4] Their anionic, strong σ- and π-donating thiocyanate ligand enables panchromatic absorption and efficient electron injection into the semiconductor. However, at the same time the main drawback of the classical Ru^{II} dyes is the monodentate thiocyanate ligand limiting their stability and prohibiting further functionalization that could improve the light harvesting. Consequently, Ru^{II} complexes possessing aromatic carbanion donors that essentially adopt the function of the thiocyanate have been employed in DSSCs with great success.[5] When embedded within a multidentate ligand, this cyclometalation[6] allows for higher stability and ligand functionalization to optimize the photophysical and electrochemical properties.

Recently, click-derived[7] ligands have been successfully used as analogues of polypyridyl ligands, in particular of 2,2′:6′,2″-terpyridine (tpy).[8] We were interested in extending this analogy to tridentate cyclometalating polypyridyl ligands, namely 1,3-dipyridylbenzene (dpbH).[9] In this context, we present a new and systematic series of click-derived, tridentate, cyclometalated Ru^{II} complexes[10] that was studied in detail by experimental and computational methods to elucidate the potential for dye-sensitized solar-cell application.[11] Thereby, the combination of theoretical investigations and photophysical as well as electrochemical studies enables a consistent and emergent explanatory picture of the new dyes.

Results and Discussion

Syntheses: A fully optimized synthetic procedure is presented for the new cyclometalated complexes as well as for a non-cyclometalated model complex.[8d] The optimization, the design strategy and an exemplary synthetic procedure are explained in the following. For synthetic details, the reader is referred to the Supporting Information.

The ligands were obtained from aryl azides and diethynylbenzene building blocks in good yields using standard click conditions. For the sake of blocking alternative, bidentate coordinations that were observed in initial attempts, methyl groups were placed at strategic positions when possible and reasonable.[12] Therefore, o-xylene was chosen as the central ring as well as mesityl moieties for the clicked-on functionalities (Scheme 1).
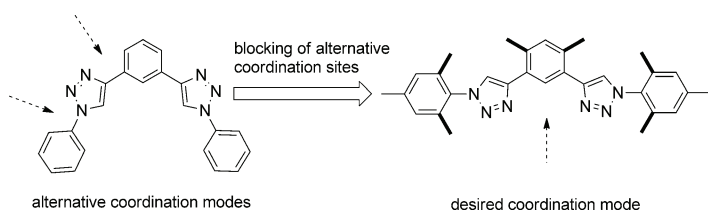
Scheme 1. Schematic illustration of the optimization strategy.

Furthermore, mesityl was chosen as substituent for further reasons: 1) it enables both good solubility and good crystallization behavior, 2) it is electronically decoupled due to its orthogonality and therefore a reasonable electronic reference, 3) it allows for eased NMR interpretations, and 4) it is readily available from mesityl amine through diazotization/azidation and can be considered as a safe azide. The diethynylbenzene building blocks were synthesized under standard Sonogashira conditions with additional LiCl[13] starting from functionalized dibromobenzenes (Scheme 2).
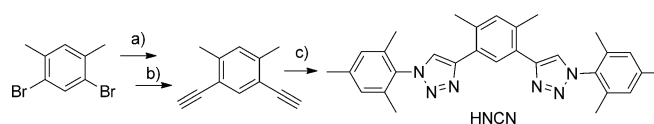
Scheme 2. Exemplary synthesis of the cyclometalating ligands: a) [Pd-(PPh$_3$)$_4$], LiCl, CuI, TMS-CCH, NEt$_3$, PhMe, 50 °C, 72 h; b) KF, THF/MeOH (1:1); 50% over 2 steps; c) CuSO$_4$·5H$_2$O, NaAsc., MesN$_3$, CH$_2$Cl$_2$/EtOH/H$_2$O (1:2:1), 60 °C, 12 h, 90%.

In one case, σ-accepting fluoro substituents replace the methyl groups in the position *meta* to the carbanion to allow blocking as well as electronic fine-tuning.[5c,e,12] In the case of 1,3,5-tribromobenzene, 2-methylbut-3-yn-2-ol was chosen as protected alkyne to ease the chromatographic separation.[14] After deprotection and cycloaddition, the according 5-bromo-1,3-bis(triazolyl)benzene allows further ligand-functionalizations by cross-coupling methods in an important position. The subsequent installation of a chromophore at the *para* position of the cyclometalating ring, for example, thiophene, would extend the conjugated system and increase the light absorptivity. Similarly, the mesityl azide reference was changed once to 9-(4-azidophenyl)-3,6-di-*tert*-butyl-9H-carbazole to install an organic chromophore at the complex periphery as light-harvesting antenna.[15] In this case, the conjugation through the triazole ring is not expected[16] and the increase of light harvesting would be additive only. However, although click chemistry provides facile functionalization within the ligand formation, leading to modular and higher functionalized complexes, we kept the mesityl moiety as reference in all other cases to discuss the more pronounced influences of substituents directly attached to the cyclometalating phenyl ring or the opposed ligand (Scheme 3). In addition, it is questionable if the overall device efficiency profits from the increased absorptivity due to the carbazoles or if it drops due to lowered dye coverage on the semiconductor surface.

To facilitate the coordination and cyclometalation, the common [Ru^{III}(tpy)Cl$_3$] precursor can be activated in situ by halide abstraction with a silver(I) salt in a weakly coordinating solvent. However, it is known that silver(I) can oxidize the product yielding a homocoupled dimer[9a] and therefore needs to be filtered off after the activation step. Still, application of a Ru^{III} precursor includes a reduction step towards Ru^{II} after coordination that is normally achieved by alcohols or amines. Since the cyclometalated complexes are oxidized
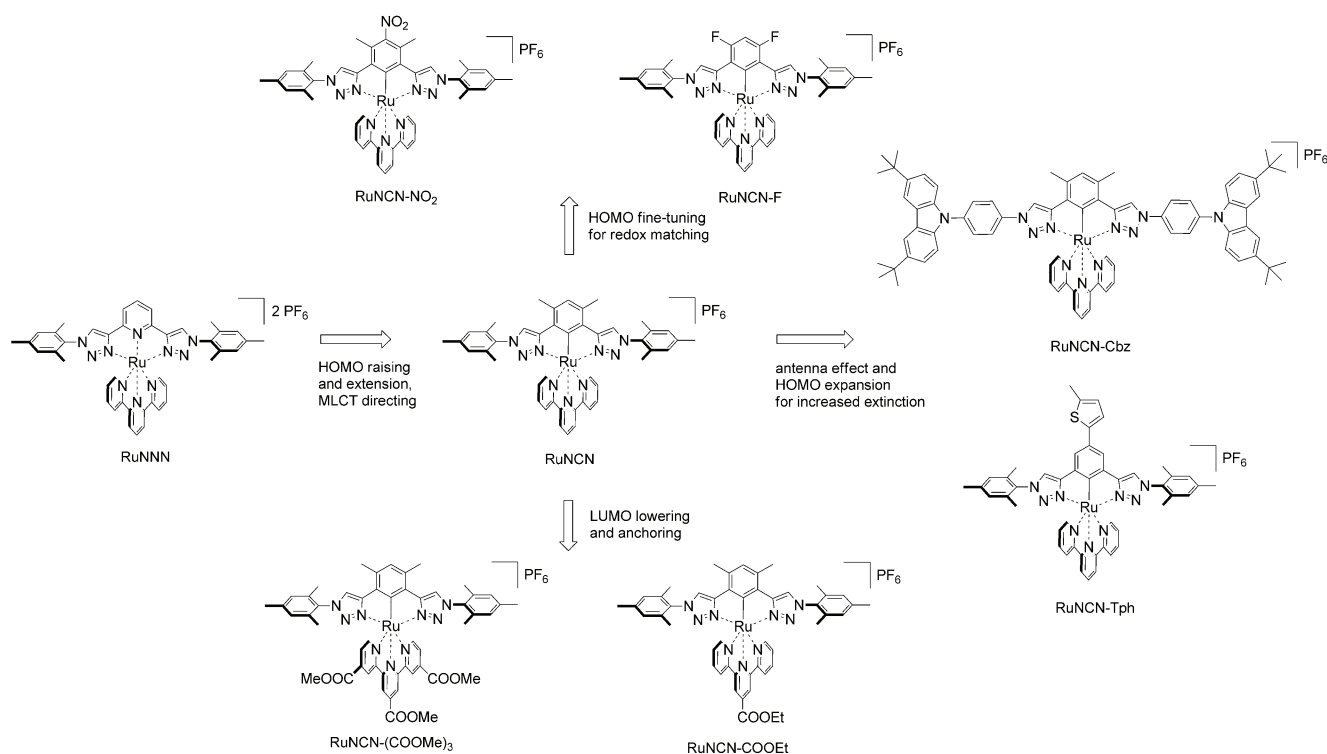
Scheme 3. Design strategy and overview of the synthesized ruthenium(II) complexes.

easily, the product is achieved either as Ru^{III} complex or it already underwent side reactions in the position *para* to the cyclometalation that has significant radical character within the Ru^{III} complex. This drawback can be overcome by the use of [Ru^{II}(tpy)(CH$_3$CN)$_3$][PF$_6$]$_2$ as precursor (see Scheme 4 for a representative example).[17] In fact, it is
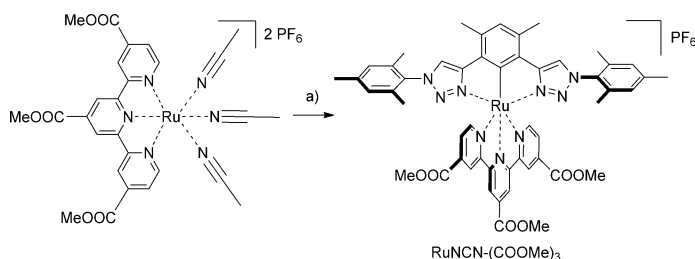
Scheme 4. Exemplary synthesis of the cyclometalated ruthenium(II) complexes: a) HNCN, methanol, microwave, 30 min., 160 °C, 50 %.

easily synthesized from [Ru^{III}(tpy)Cl$_3$] in acetonitrile/ethanol/water using AgNO$_3$ and, in contrast to [Ru^{III}(tpy)Cl$_3$], it can be purified completely, thus simplifying the subsequent complexation. In more detail, after removal of the AgCl by filtration over celite, the product can be isolated either by column chromatography or directly by vapor diffusion of diethyl ether into a concentrated acetonitrile solution yielding large, even X-ray-quality crystals (see the Supporting Information). The subsequent cyclometalation was performed

under oxygen-free conditions in a closed vial using an alcohol as solvent and microwave heating to 160 °C for 30 min. Isolation of the product by a combination of column chromatography and crystallization afforded the desired complexes, in most cases as X-ray-quality crystals (Figure 1 and the Supporting Information) and in reasonable yields varying from 40 to 70 % (Scheme 4 and the Supporting Information), depending, amongst others, on whether all strategic methyl groups were present.

Since cyclometalated complexes are very electron-rich in the position *para* to the carbanion, they enable targeted homocoupling and post-complexation functionalizations in the presence of oxidants, electrophiles, or both.[18] This allowed the introduction of a nitro group under Menke conditions and, thereby, the respective manipulation of the carbanion donation by a σ- and π-accepting group in turn.[5d]

The installation of the anchoring carboxylic acid functions for the DSSC was achieved simply by using ester functionalized ligands and saponification[5e,f] subsequent to the complexation. Thus, the intermediate, highly soluble, ester-functionalized complexes could be purified and studied, since they are seen as models for the final complexes adsorbed to TiO$_2$.[5k]

Crystal structures: Single crystals of the ligands HNCN and HNCN-F as well as of the three Ru^{II} precursors and of RuNNN, RuNCN, RuNCN-NO$_2$, RuNCN-F and RuNCN-Tph could be grown and characterized successfully by X-ray diffraction (Figure 1 and the Supporting Information). The systematic variation allows for comparison although only
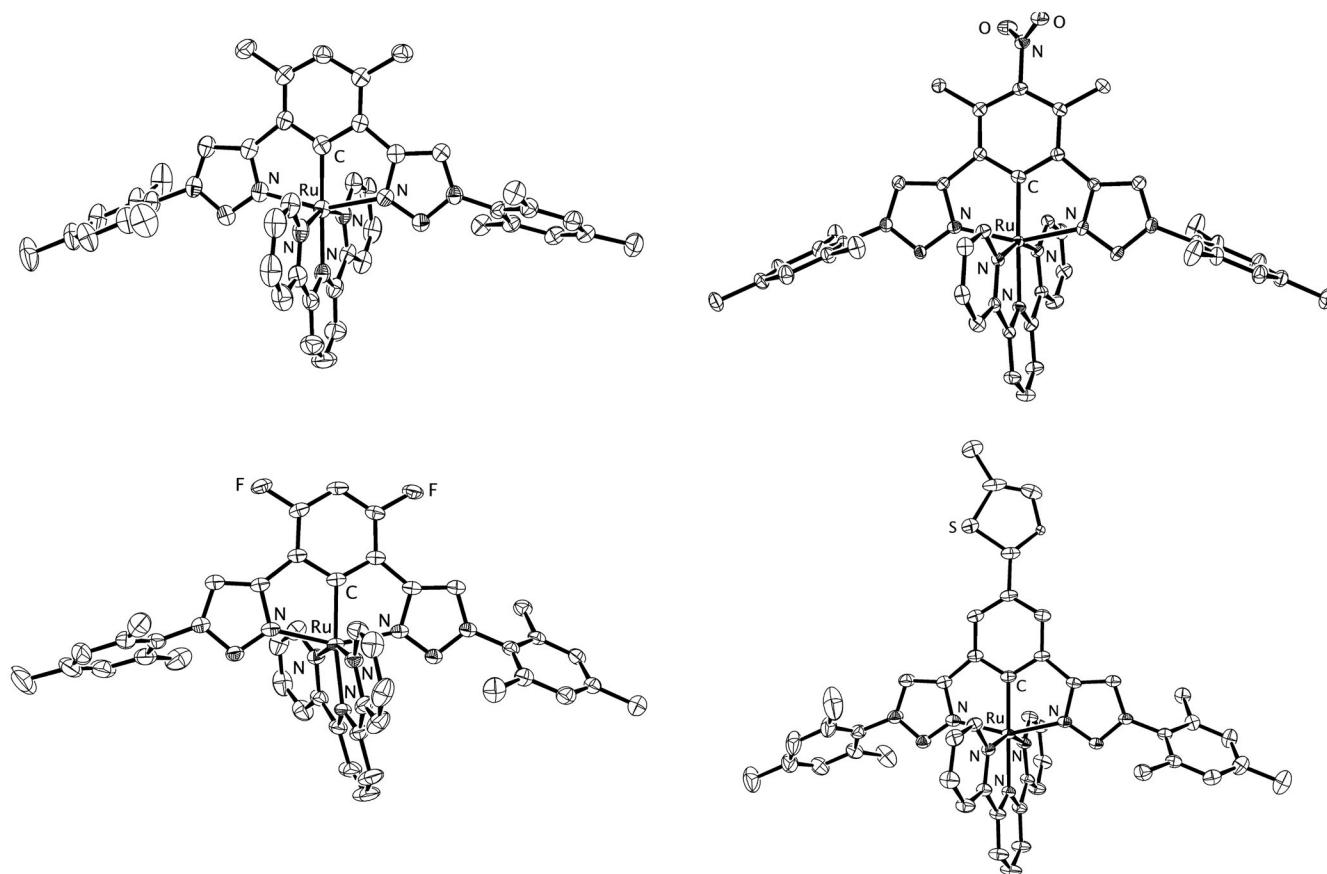
Figure 1. Solid-state structures of RuNCN (top left), RuNCN-NO$_2$ (top right), RuNCN-F (bottom left) and RuNCN-Tph (bottom right) (50 % probability level; counterions, hydrogen atoms and solvent molecules omitted for clarity).

the most pronounced changes are discussed to beware of packing effects (note the strong distortion within RuNCN-F).

The mesityl–triazole torsion angle of the complex series varies between 60° and 90°. The thiophene–phenyl torsion angle in RuNCN-Tph was determined to be 30.7°, thus being in good agreement with the calculated value of 30.2° (see Scheme S9 in the Supporting Information) and allowing for partial extension of the conjugation into the thiophene ring.

The replacement of a dative Ru–N bond of the polypyridyl-type complex RuNNN by a covalent, organometallic Ru–C bond within the cyclometalated RuNCN complex leads to a bond shortening from 2.02 to 1.98 Å, caused by the very good σ donation and additional π donation as well as by electrostatic interactions with the anionic, aromatic carbon donor. Furthermore, the adjacent triazole N–Ru bonds are slightly elongated, most likely due to a declined σ orbital overlap by the smaller bite angle. As a consequence of the good electron donation ability of the carbanion, the opposed Ru–N bond becomes elongated from 1.97 to 2.01 Å which is well-known as *trans* influence. Furthermore, the outer pyridine N–Ru bonds are shortened as result of increased π back donation from the more electron-rich Ru^{II} metal center in the cyclometalated complex (Figure 2 and
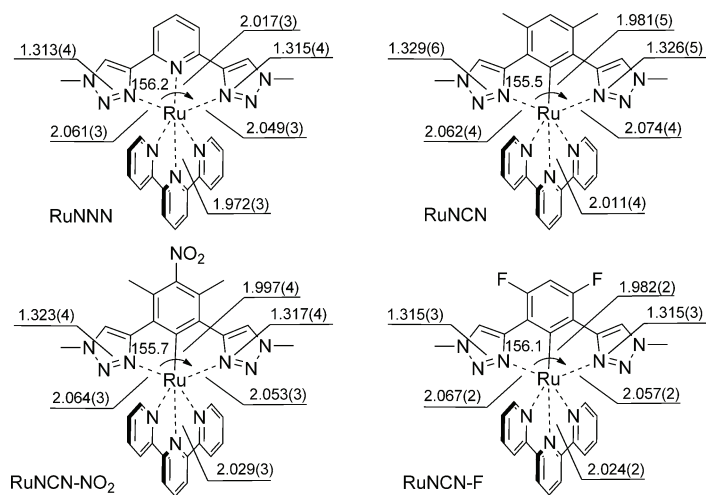
Figure 2. Selected bond lengths (Å) and angles (°) of RuNNN, RuNCN, RuNCN-NO$_2$ and RuNCN-F.

Scheme 5). Also within the triazole ring, the N^2–N^3 double bond is elongated as a consequence of the increased π back donation into π* orbitals.

For RuNCN-NO$_2$, upon installing an electron-withdrawing group, namely a nitro group that is capable of withdrawal
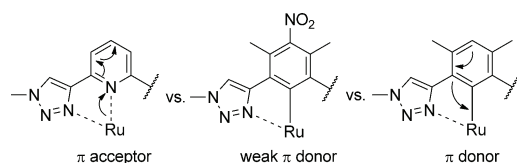
Scheme 5. Schematic representation of the electronic consequences of the cyclometalation and an electron-withdrawing group.

through the σ and π system, most of the consequences of the cyclometalation are less pronounced than for RuNCN. Even though the π-accepting capability might be reduced due to the dihedral angle of 51.8° (51.6° calculated, see Scheme S9 in the Supporting Information) with the central phenyl ring due to repulsion with the *ortho*-methyl groups, there is a distinct influence on the π system that strongly reduces the π-donation ability of the cyclometalating carbanion in the *para* position. Consequently, the Ru−C bond is elongated to 2.00 Å (Figure 2 and Scheme 5). In particular in comparison to RuNCN-F, the fluoro substituents that are strongly σ-accepting, but whose moderate π-donation ability does not affect the carbanion because they are in *meta* positions, still allow a very short Ru−C bond of 1.98 Å. Also the changes in bond lengths within the central phenyl ring are consistent with a participation of a chinoid resonance structure in RuNCN-NO$_2$. The successive reduction of the electron donation of the carbanion by the fluoro and nitro substituents is demonstrated by the shortening of the triazole N^2=N^3 double bond due to decreased π back donation. Also the Ru−N bond *trans* to the carbanion is further elongated for the same reason.

Apparently, the fluoro substituent mostly influences the σ donation and might lower the energy of the π system indirectly (inductive effect), while the nitro group causes an additional polarization of the π system that strongly weakens the π donation (mesomeric effect) but to a less extent the σ donation. This is consistent with the electrochemical data: for RuNCN-F only the HOMO is stabilized, located on the Ru^{II} metal center and the fluoro-substituted cyclometalating phenyl ring as well, while RuNCN-NO$_2$ shows an additional LUMO stabilization that is mediated through the aromatic π system/Ru^{II} d orbitals, since the LUMO is located on the opposed tpy ligand.

Interestingly, within all investigated solid-state structures of triazole-containing ruthenium(II) complexes (see Figure S143 in the Supporting Information), short-contact interactions of the triazole with either the counterions or the solvent are present. Triazoles and triazolium salts are known to allow hydrogen bonding as well as electrostatic interactions.[19] Similar to triazolium salts, a ruthenium-coordinated triazole is expected to be more polarized than a free triazole. Preliminary results indicate an interaction of the ruthenium(II)-coordinated triazole with iodide (see Figure S144 in the Supporting Information). The question, if hydrogen bonds/electrostatic interactions might allow the preorganization of the redox mediator in a position favorable for ruthenium(III) reduction, will be targeted in the future.

DFT calculations: As a basis for a deeper understanding of the photophysical and electrochemical properties of the presented Ru^{II} complexes, namely to gain insight into detailed structure–property relations, density functional theory (DFT) calculations, and time-dependent (TD) DFT calculations have been performed.

Whilst the description of the UV/Vis characteristics of these complexes is nowadays close to routine, the description of non-adiabatic events occurring after light excitation is more troublesome. Their description would in principle require the use of multiconfigurational methods in combination with a proper description of spin-orbit coupling (SOC) effects. Unfortunately, these methods are practically unaffordable for Ru^{II}–polypyridyl dyes.[20] Therefore, Δ-SCF-DFT (SCF=self-consistent field) and TDDFT methods remain as valuable alternatives to obtain qualitative and even quantitative information about Ru^{II} complexes and many examples are found in the literature.[21] DFT calculations provide the geometries and energies of the ground and lowest excited states of each symmetry and spin, whilst information on the higher excited states (i.e., energies, oscillator strengths and associated character of the excitations) can be obtained with the help of TDDFT calculations.

In order to understand the deactivation mechanisms after light excitation for RuNNN and RuNCN, their most relevant structures involved, namely the singlet ground state (S$_0$) as well as the most stable ^{3}MLCT and triplet metal-centered (^{3}MC) excited state, were optimized. As known for Ru^{II}–polypyridyl complexes, after excitation of the ^{1}MLCT manifold, ultrafast inter-system crossing (ISC) occurs within less than 100 fs, leading to the formation of the ^{3}MLCT states with near-unity quantum yield. Among the subsequent radiative and non-radiative processes, radiationless deactivation through thermal population of ^{3}MC states is supposed to determine the ^{3}MLCT lifetime.[1,2] Thus, in addition to the location of the ^{3}MLCT and ^{3}MC states, crossing points between the S$_0$ and the ^{3}MC potential energy surface determine the non-adiabatic population transfer, as has been recently stated by Boggio-Pasqua et al. for similar Ru^{II}–polypyridyl complexes.[22]

The electronic nature of the lowest-energy triplet excited states of RuNCN has been confirmed by analysis of the spin density distributions (Figure 3). The most stable ^{3}MLCT state indeed displays unpaired electrons within a Ru 4d$_{yz}$ orbital and a π* orbital of the tpy ligand, while only Ru-based 4d orbitals are involved in the ^{3}MC state. The main geometrical features of both the optimized ^{3}MLCT and ^{3}MC structures for RuNNN and RuNCN are given in Scheme S9 and S10 in the Supporting Information. In comparison to the S$_0$ geometry, the ^{3}MLCT and also the ^{3}MC geometries of each complex show a weakening of the coordination, attributed to the population of antibonding orbitals, either π* or "e$_g$*", as well as to the weakened π back bonding with the formally oxidized Ru "t$_{2g}$" orbitals. In the ^{3}MC structures the tpy coordination is even distorted (see exemplarily the ^{3}MC structure of RuNCN in Figure 3) due to the weakening, not only of the π back donation but also of the σ donation by the
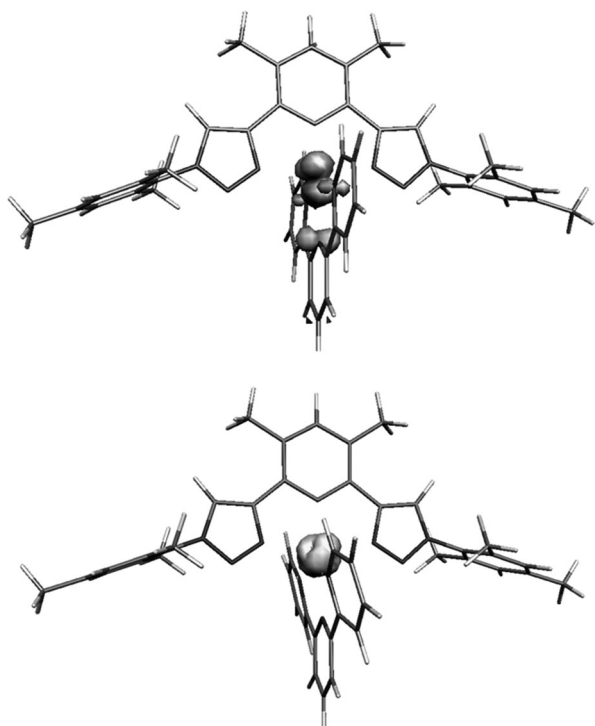
Figure 3. Spin density distribution of the energy optimized ^{3}MLCT (top) and ^{3}MC (bottom) geometries of RuNCN.

population of the "e_g*" levels. Thus, repulsive interactions are avoided by ligand distortion, hence lowering the energy of the ^{3}MC state. This is important, since in the ^{3}MLCT geometry, due to the strong effective σ donation, the unoccupied, antibonding metal d orbitals are located at high ener-

gies (see below and Figure 4), while in the ^{3}MC geometry, in which these orbitals are occupied, the destabilizing effects are less pronounced (see the photophysical model section below). Furthermore, while the tridentate ligand is only distorted, a monodentate ligand, such as thiocyanate, can be cleaved off. For all other compounds, only the S_0 and the lowest ^{3}MLCT states were optimized and the main geometrical features are given in the Supporting Information.

To understand the substituent effects on the photophysical properties, the relevant frontier Kohn–Sham orbitals are plotted in Figure 4. For RuNCN, π donation destabilizes the HOMO that is composed of Ru d_{yz} and NCN π orbitals. In contrast, for RuNNN the HOMO is less destabilized and almost of pure Ru d_{xz} character; only a weak π donation contributes to the HOMO−1, which is therefore lower in energy. In both complexes, the LUMO is formed by the same π* orbital of the tpy ligand; however, the strongly destabilized HOMO of RuNCN causes an additional indirect LUMO destabilization through the π back donation. Because the LUMO destabilization is less pronounced than for the HOMO, the resulting energy gap is much smaller for RuNCN. A further effect of the strong electron donation within RuNCN is the strongly destabilized "e_g*" orbitals in terms of a strong ligand field. Thus, the d_{z^2} orbital is the LUMO+8 in RuNNN, being 1.9 eV higher in energy than the LUMO, while in RuNCN it is the LUMO+14 with an energy difference of 2.3 eV. This demonstrates that cyclometalation indeed enables destabilization of orbitals that are populated in ^{3}MC states and that are relevant for the radiationless deactivation. However, the actual electronic situation at the ^{3}MC geometry might be different as mentioned above. Therefore, although the ^{3}MC stabilization might be
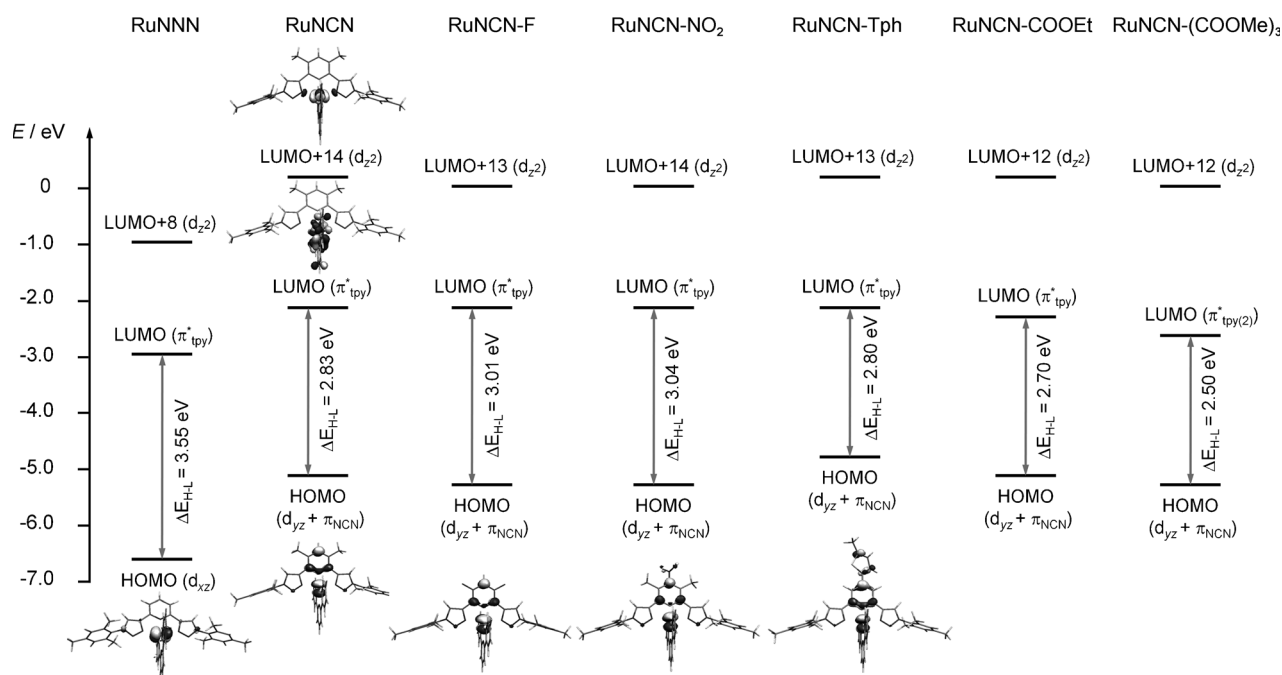
Figure 4. Selected PCM-B3LYP/6-31G* Kohn–Sham orbitals and energy level scheme for the Kohn–Sham orbitals of the Ru^{II} complexes.

helpful, it does not necessarily cause a suppression of the thermal population of the ^{3}MC from the ^{3}MLCT states (this issue will be discussed in more detail in the photophysical model section below).

Figure 4 also shows the HOMO orbitals of RuNCN-F, RuNCN-NO$_2$ and RuNCN-Tph. The introduction of an electron-withdrawing fluoro or nitro group directly attached to the HOMO site leads to HOMO stabilization, since the electronic repulsion and electron donation of the carbanion donor is tempered, but also because the aromatic system, which forms a part of the HOMO itself, is stabilized. In case of RuNCN-Tph, the HOMO and LUMO are slightly destabilized due to electron donation from the thiophene moiety, while the energy gap remains constant. Importantly, the conjugation of the HOMO is extended onto the thiophene ring, which should give rise to an increased light absorptivity (see the photophysical properties). Apparently, stabilization due to extension of the conjugation is overcompensated by electron donation of the thiophene. For complexes of ester-functionalized tpy ligands, the HOMO is slightly stabilized because of the increased π acidity of the ligand. Since they are directly attached to the LUMO site, the LUMO level is strongly stabilized by their electron withdrawal, resulting in smaller energy gaps, in particular for RuNCN-(COOMe)$_3$. Furthermore, the LUMO, which is not shown for these complexes, is the same orbital throughout the whole series and differs only in energy. As an exception, in RuNCN-(COOMe)$_3$ the LUMO is a different orbital that is however located on the tpy ligand.

Photophysical properties: A key feature of designated photo-redoxactive Ru^{II} complexes, in particular when aiming at a potential application in dye-sensitized solar cells, is their photophysical behavior. Thus, UV/Vis absorption and emission spectrum measurements as well as photoluminescence quantum yield (Φ_{PL}) and lifetime determinations were executed. Additionally, PCM-TD-B3LYP (PCM = polarizable continuum model) vertical excitations were computed for all the complexes except for RuNCN-Cbz (see the Supporting Information for computational details).

First of all, the free cyclometalating ligands were characterized. Their UV/Vis spectra show a strong absorption peak at around 240 nm with extinction coefficients of 36 000–140 000 M^{-1} cm^{-1}. Additional bands are located at about 295 nm with weak intensities of 1100 and 4600 M^{-1} cm^{-1} for HNCN and HNCN-F, respectively. In contrast, HNCN-Cbz and HNCN-Tph, possessing additional chromophores, exhibit strong absorption peaks beyond 290 nm, with ε values of 58 000 and 46 300 M^{-1} cm^{-1} for HNCN-Cbz and 15 400 M^{-1} cm^{-1} for HNCN-Tph. All ligands are fluorescent, showing emission bands at 325 (HNCN, HNCN-F), 367 (HNCN-Tph), and 404 nm (HNCN-Cbz) (see the Supporting Information).

The absorption and emission features as well as the computed transitions of the studied Ru^{II} complexes are shown in Figure 5 and Table 1. For the assignment of the PCM-TD-B3LYP excitations, see Tables S4–S10 in the Supporting In-

formation. Firstly, the comparison of the parent cyclometalated complex RuNCN with its non-cyclometalated counterpart RuNNN reveals the strong influence of the carbanion donor on the UV/Vis absorption properties. A significant bathochromic shift of the MLCT maxima from 428 to 532 nm, corresponding to 4500 cm^{-1}, is observed upon cyclometalation and well reproduced by the performed calculations. Additionally, an extension of the absorption from 550 to 650 nm is observed that can be explained by destabilization of the Ru-4d orbitals in the RuNCN complex. Indeed, the electronic excitations responsible for these bands involve mainly these orbitals (Table S4 in the Supporting Information). Furthermore, since RuNCN possesses an organometallic, covalent bond, the HOMO is composed of Ru-d orbitals as well as π orbitals of the cyclometalating ligand, while the LUMO (and higher unoccupied molecular orbitals) is π*-tpy-based. Thus, if the anchoring groups are installed at the tpy acceptor ligand, the transition dipole moment is directed towards the semiconductor surface by the distinct push–pull effect.[5a] Since these transitions exhibit partial ligand-to-ligand charge-transfer (LLCT) character, they can be described as metal/ligand-to-ligand charge-transfer (MLLCT) excitations. This underlines the feasibility of directly influencing the HOMO by manipulation of the cyclometalating ligand, although usually the MLCT declaration is kept in literature.[5f,j] Furthermore, the MLCT bands are broadened and even split because of the electronic asymmetry that breaks the orbital degeneracy. Thus, the shorter wavelength transitions around 400 nm exhibit MLCT, MLLCT, and admixed MC character (see S$_6$, S$_{14}$ and S$_{17}$ in Table S4 in the Supporting Information). In the UV region, the high-energy transitions are mainly of π–π* character (see S$_{34}$ and S$_{41}$). However, after thermal relaxation in terms of Kasha's rule, the transferred charge will reside on the acceptor ligand. As a further result of the strong anionic carbon donor, a weak room-temperature emission at 751 nm (Φ_{PL}: 0.006 %) was observed for RuNCN (see the photophysical model below).[6a]

To understand the influence of the triazole moiety, a comparison referring to the corresponding Ru^{II} complexes of pyridine analogues, namely 2,2′:6′,2′′-terpyridine and 1,3-dipyridylbenzene, is helpful. When compared to [Ru(tpy)$_2$]-[PF$_6$]$_2$, the analogous but heteroleptic RuNNN shows a broadened and blue-shifted absorption. Also the emission at 77 K, which is similar in shape for both, is blue-shifted from 603 to 574 nm. According to the calculations, the emitting state is of ^{3}MLCT character and tpy-based (see the DFT calculation above). Additionally, the computed emission maxima (adiabatic emission energies obtained with Δ-SCF approach, see the Supporting Information for details), are given in Table 1 and correlate well with the experimental data. The absorption spectra of [Ru(tpy)(dpb)]PF$_6$ and RuNCN are similar,[5j] except for a slight hypsochromic shift that is observed in the absorption and emission spectra of RuNCN. Interestingly, although still weak, the emission is slightly increased for RuNCN, most likely because of the higher emission energy in accordance with the energy-gap
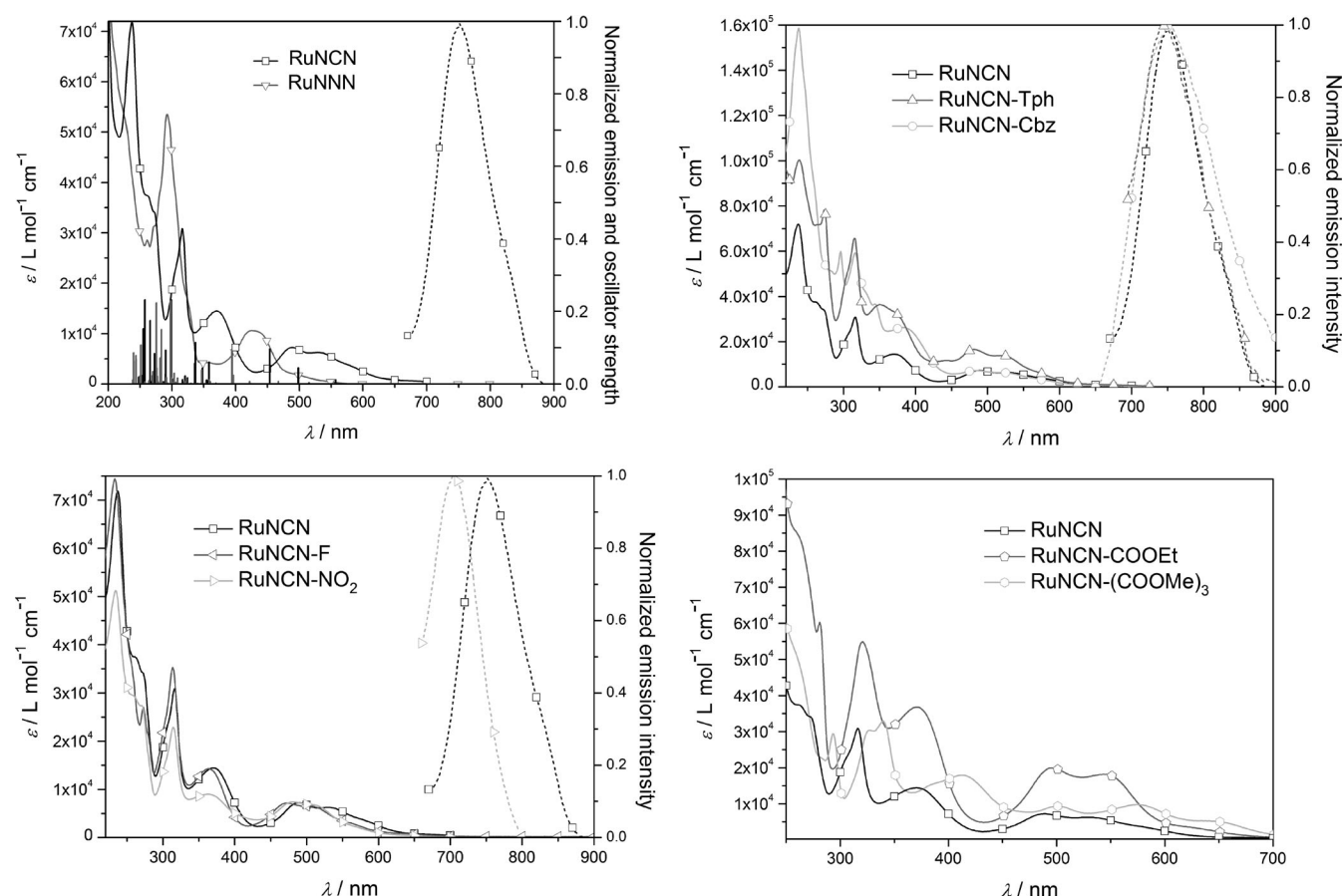
Figure 5. UV/Vis absorption and emission spectra of the investigated ruthenium(II) complexes (10^{-6} M in CH_3CN). For RuNCN and RuNNN, the PCM-TD-DFT/6-31G* computed vertical excitations are superimposed. Solid lines represent the measured curve and symbols are only used for assignment.

law. Furthermore, the extinction coefficients are lowered for RuNCN, attributed to the shorter conjugation that is only partially extended into the triazole.[8a]

To allow for HOMO fine-tuning (see the electrochemical properties below), electron-withdrawing groups, namely nitro and fluoro substituents, were installed at the central phenyl ring. Consequently, a slight hypsochromic shift ($700\ cm^{-1}$) of the MLCT features in the UV/Vis absorption spectrum was observed due to HOMO stabilization. Accordingly, a room-temperature emission can be observed for RuNCN-NO$_2$ that is blue-shifted by $870\ cm^{-1}$ (Φ_{PL}: 0.010%). In contrast, RuNCN-F features no measurable photoluminescence (see the temperature-dependent lifetime measurements below). Besides, the π-accepting nitro group, *para* to the Ru—C bond, leads to a decrease of the extinction coefficient by a third compared to the parent RuNCN complex, attributed to interference with the push–pull polarization.

To increase the extinction coefficients, additional chromophores were attached[5d–g,15,23] either directly to the central phenyl ring or as clicked-on antennas. The thiophene moiety that was installed *para* to the Ru—C bond increases the extinction coefficients over the whole UV/Vis absorption spectrum, including the highest wavelength absorption that grows from $7300\ M^{-1}cm^{-1}$ for RuNCN to $16\,500\ M^{-1}cm^{-1}$.

Evidently, this is due to extension of the HOMO and, thus, expansion of the optical cross section (see DFT calculations and Figure 4).[5d] In contrast, the attachment of the carbazole moiety provides an additional but separated chromophore that is not in conjugation with the cyclometalated phenyl ring.[16] Thereby, the extinction coefficients below 450 nm double with respect to RuNCN, because the carbazole participates in LC transitions, while the absorption bands beyond 450 nm, in analogy to RuNCN assigned mainly to $d_{Ru}/\pi_{NCN} \rightarrow \pi^*_{tpy}$ transitions, remain unchanged in shape and intensity. Furthermore, the room-temperature emission of RuNCN was preserved, thus no additional quenching pathways are introduced; instead, the emission intensity was even slightly increased (Table 1).

For the immobilization on the semiconductor surface in DSSCs, carboxylic groups on the acceptor ligand are necessary. Beside their function as anchoring groups, they also strongly influence the photophysical properties as additional electron-withdrawing groups. Here, the ester-functionalized complexes were seen as models for the TiO$_2$-bound dyes.[5k] The introduction of a single carboxylic ester at the 4′-position of the terpyridine causes a stabilization of the π^*_{tpy}-based LUMO (Figure 4) and an enhanced transition dipole moment, thus leading to a slight bathochromic shift by about $500\ cm^{-1}$ as well as a tripled extinction coefficient in

Table 1. Photophysical data of the complexes.

Complex	298 K				77 K		k_r+k_1 [s^{-1}][f]	k_2 [s^{-1}]	k_3 [s^{-1}]	ΔE_2 [cm^{-1}]	ΔE_3 [cm^{-1}]
	λ_{max}^{abs} [nm] (ε [10^3 M^{-1}·cm^{-1}][a,b]	λ_{max}^{em} [nm][a,c,d]	Φ_{PL} 10^{-5}[a,e]	τ [ns]	λ_{max}^{em} [nm][d]	τ [µs]					
RuNNN	325 (sh), 428 (10.6), 500 (1.8)	– (545)	–	–	574	14	–	–	–	–	–
[Ru(tpy)$_2$][PF$_6$]$_2$[5j,30]	308 (63.4), 475 (14.7)	–	–	0.25	603	–	6.5×10^4	2.0×10^{13}	2.1×10^7	1700	720
RuNCN	371 (14.5), 488 (7.3), 532 (6.3)	751 (827)	6.1	4.1	719	4.1	2.44×10^5	1.1×10^{12}	3.11×10^8	1830	350
[Ru(tpy)(dpb)]PF$_6$[5j]	424 (9.6), 499 (14.4), ≈540 (≈10)	781	0.9	–	–	–	–	–	–	–	–
[Ru(ttpy)(dpb)]PF$_6$[g]	504 (10.8), 550 (8.3)	784	4.5	4.5	752	0.48	–	–	–	–	–
RuNCN-F	363 (14.3), 473 (7.2), 507 (6.5)	–	–	0.5[h]	661	5.8	1.72×10^5	9.74×10^{11}	–	1290	–
RuNCN-NO$_2$	365 (9.0), 483 (7.4), 511 (6.8)	705 (759)	10.0	5.3	667	5.2	1.92×10^5	6.63×10^{11}	–	1395	–
RuNCN-Cbz	384 (26.2), 485 (7.3), 523 (6.3)	750	25.0	6.7[h]	712	4.5	2.22×10^5	2.04×10^{11}	1.33×10^8	1570	270
RuNCN-Tph	350 (36.4), 482 (16.5), 518 (13.8)	745 (802)	5.3	4.1[h]	722	4.3	2.33×10^5	1.89×10^{11}	1.42×10^8	1452	240
RuNCN-COOEt	372 (36.8), 495 (19.9), 546 (18.2)	– (941)[d]	–[d]	–[d]	–[d]	–[d]	–	–	–	–	–
RuNCN-COOH	373 (22.0), 491 (10.5), 532 (10.5)	–	–	12.3	745	5.7	1.75×10^5	2.02×10^{10}	–	1135	–
RuNCN-(COOMe)$_3$	413 (17.9), 500 (9.4), 574 (9.8), 641 (5.3)	– (1032)[d]	–[d]	–[d]	–[d]	–[d]	–	–	–	–	–
RuNCN-(COOH)$_3$	398 (8.7), 497 (5.0), 572 (5.3), 641 (3.2)	–[d]	–[d]	–[d]	–[d]	–[d]	–	–	–	–	–

[a] Measured 10^{-6} M in deaerated CH$_3$CN. [b] sh=shoulder. [c] In brackets: Adiabatic emission energy values (ΔSCF-PCM-DFT/6-31G*). [d] The detector limit is at 800 nm. [e] Determined using [Ru(dqp)$_2$][PF$_6$]$_2$ in MeOH/EtOH (1:4; $\Phi_{PL}=2.0\%$)[31] as a reference. [f] The sum of k_r and k_1 is the reciprocal of the 77 K lifetime. [g] ttpy=4'-tolyl-tpy, from reference [32], note that the 4'-tolyl substituent stabilizes the ^{3}MLCT and thereby prolongs the excited state lifetime.[33] [h] Extrapolated from the temperature-dependent phosphorescence lifetime measurements.

the visible region. When carboxylic ester groups are attached to the *para* positions of all three pyridine moieties of the terpyridine ligand, namely for RuNCN-(COOMe)$_3$, the absorption is again significantly red-shifted (by 3000 cm^{-1}) and additionally broadened, hence covering almost the whole visible spectrum and causing a black color of the complex. The main visible absorption features are slightly more intense and separated, but they reflect the same transitions as in RuNCN, which becomes evident in comparison to a 77 K excitation spectrum of RuNCN (see Figure S118 in the Supporting Information). A photoluminescence of the complexes bearing carboxylic ester groups was not observed, most likely due to the low energy gap according to the energy-gap law (see below) or the reduced spectrometer sensitivity at low emission energies.[24] The drop in extinction and the slight blue shift of the saponified complexes, RuNCN-COOH and RuNCN-(COOH)$_3$, are attributed to the lowered electron acception that causes a decreasing polarization and LUMO stabilization.

77 K emission spectroscopy: As all presented coordination compounds show either no or only a weak emission at room temperature, owing to the presence of several non-radiative deactivation pathways that will be discussed in detail later, the exact energy of the lowest-lying excited state is challenging to determine. Emission spectroscopy at low temperatures can enable the determination of these energies if the dominant non-radiative channels are thermally activated.

All the investigated complexes, except RuNCN-COOEt, RuNCN-(COOH)$_3$ and RuNCN-(COOMe)$_3$, are emissive at 77 K and show bandshapes typical for ruthenium coordination compounds, namely an intense 0–0 transition that is accompanied by a weaker vibronic satellite (Figure 6, see Fig-
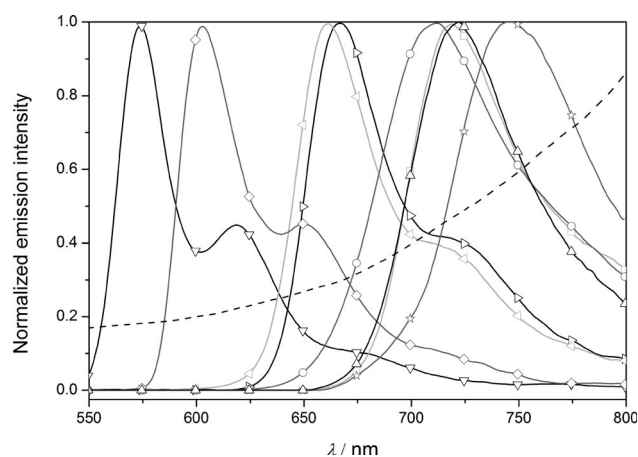
Figure 6. Emission spectra of the complexes: RuNNN ($\triangledown$), [Ru^{II}(tpy)$_2$] ($\diamond$), RuNCN-F ($\triangleleft$), RuNCN-NO$_2$ ($\triangleright$), RuNCN-Cbz ($\circ$), RuNCN ($\square$), RuNCN-Tph ($\triangle$) and RuNCN-COOH ($\star$) in *n*-butyronitrile glass at 77 K. The spectral resolution decreases at higher wavelengths due to a decreasing spectrometer sensitivity (spectrometer response is given as a dashed line). Solid lines represent the measured curve and symbols are only used for assignment, a color figure is given in the Supporting Information (Figure S119).

ure S118 in the Supporting Information for excitation spectra). The emission maxima are summarized in Table 1. We note that the emission at 77 K is blue-shifted compared to the respective room-temperature emission, because the rigid solvent matrix at low temperatures prevents solvent reorganization and thus avoids the stabilization of the more polar charge-separated excited state (rigidochromic effect).[25] Still, the comparison of the emission spectra at 77 K reveals a strong bathochromic shift of 3520 cm^{-1} relative to the non-cyclometalated RuNNN caused by the strong HOMO destabilization in RuNCN. The functionalization of the NCN ligand with the slightly electron-donating thiophene causes no further HOMO destabilization, which might be attributed to the dihedral angle of around 30° which diminishes the conjugation.[26] In contrast, the functionalization of the NCN ligand with electron-withdrawing groups results in a HOMO stabilization, and thus a blue shift of the emission maximum of about 1130 cm^{-1} with respect to RuNCN.

Functionalization of the tpy ligand with carboxylic acid esters or free carboxylic acids causes a LUMO stabilization and, as a consequence, a red-shifted absorption and emission. However, it was only possible to measure the emission spectra at 77 K for RuNCN-COOH, which is red-shifted by 490 cm^{-1} relative to RuNCN. We note that the detector is less sensitive in the near-infrared region as demonstrated by the response function in Figure 6. A theoretically predicted emission of RuNCN-(COOMe)$_3$ above 1000 nm (Table 1) would thus not be detectable with our measurement setup.

Another important excited-state parameter is its lifetime, which, in contrast to the emission quantum yield, truly reflects the stability of the excited state. Therefore, emission lifetimes were determined at both room temperature and 77 K (Table 1). As a main result, the emission lifetime decreases with decreasing emission energy. Assuming that thermally activated radiationless deactivation pathways are frozen at 77 K, this can be explained by the energy-gap law.[27] Usually, it can be observed only within a series of very similar complexes or in different solvents,[28] since other effects, such as delocalization and rigidity, may interfere so that long excited-state lifetimes and small energy gaps do not exclude each other.[29] Accordingly, RuNCN-COOH has a longer lifetime than RuNCN (Table 1), which is attributed to the modification of the acceptor ligand.

Temperature-dependent lifetime measurements: To gain detailed insight into the deactivation dynamics of the lowest-lying excited state and the stabilizing/destabilizing effects of different substitution patterns, temperature-dependent lifetime measurements were carried out between 300 and 160 K.[34] The results of these experiments are depicted in Figure 7.

In general, the investigated cyclometalated complexes reveal a steady rise of the emission lifetime with decreasing temperature. However, depending on the specific substitution pattern, the slope of the lifetime increase varies. Similar to the emission spectra at 77 K, the complexes RuNCN-F
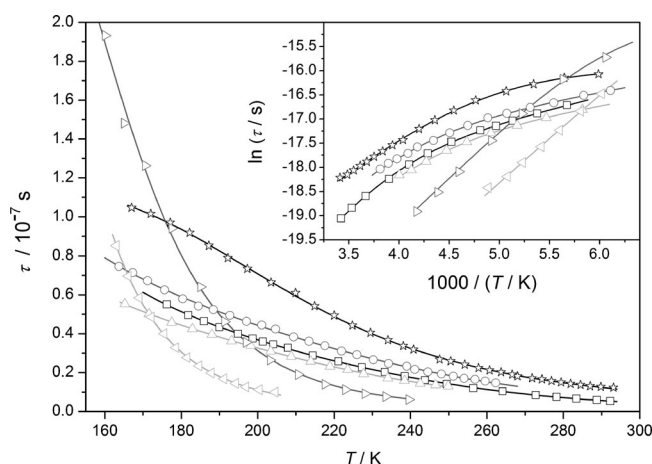
Figure 7. Temperature-dependent emission lifetimes for the complexes: RuNCN-F (◁), RuNCN-NO$_2$ (▷), RuNCN-Cbz (○), RuNCN (□), RuNCN-Tph (△) and RuNCN-COOH (☆) in *n*-butyronitrile. Symbols correspond to measured lifetimes and solid lines represent a non-linear fit according to equation 1 (RuNCN-COOH, RuNCN-F and RuNCN-NO$_2$) or equation 2 (RuNCN, RuNCN-Cbz and RuNCN-Tph). A color figure is given in the Supporting Information (Figure S120).

and RuNCN-NO$_2$ show a different behavior compared to RuNCN, RuNCN-Cbz, and RuNCN-Tph. In detail, for the last three complexes the lifetime starts to increase at higher temperatures and shows a reduced slope than for RuNCN-F and RuNCN-NO$_2$, thus being shorter-lived at 77 K. In accordance with the literature, the excited-state lifetime at higher temperatures is determined by thermal deactivation via ^{3}MC states.[1,2] Evidently, the electron-withdrawing groups reduce the donor strength of the carbanion and therefore lower the ^{3}MC states. Consequently, thermal deactivation is facilitated, which can be quantified by fitting an Arrhenius expression to the experimental data [Eqs. (1) or (2)]. Thus, fundamental information about thermally activated, non-radiative deactivation channels can be obtained, for example, their rate constants and activation energies.

$$\tau(T) = \frac{1}{k_r + \sum k_{nr}} = \frac{1}{k_r + k_1 + k_2 \exp(-\Delta E_2/k_B T)} \quad (1)$$

$$\tau(T) = \frac{1}{k_r + \sum k_{nr}} =$$
$$\frac{1}{k_r + k_1 + k_2 \exp(-\Delta E_2/k_B T) + k_3 \exp(-\Delta E_3/k_B T)} \quad (2)$$

For RuNCN, RuNCN-Cbz, and RuNCN-Tph, two thermally activated (k_2, ΔE_2 and k_3, ΔE_3) and one non-activated decay channel (k_1),[35] in addition to the radiative one (k_r), are necessary to fit the equation to the data [Eq. (2)]. In contrast, for RuNCN-F and RuNCN-NO$_2$ a model of three channels (a radiative, a non-activated, and a thermally activated non-radiative one) is sufficient to reproduce the data [Eq. (1)]. In principle, there should be a third dark channel for the last two complexes, but due to its low activation energy it is not visible in the experimental temperature

range between 300 and 160 K. The results obtained by analyzing the temperature-dependent lifetime data are summarized in Table 1.

The first activated decay channel (k_2, ΔE_2) is assigned to the transition from the emitting ^{3}MLCT to the S_0 via the ^{3}MC excited state.[36] Compared to [Ru(tpy)$_2$]$^{2+}$ and other complexes of functionalized terpyridines, this activation energy is remarkably low (see the discussion of the ^{3}MC geometry in the DFT section).[30,34] We postulate that the room-temperature emission and prolonged excited-state lifetimes, which were observed despite similar or lower activation energies for the ^{3}MLCT–^{3}MC internal conversion than in [Ru(tpy)$_2$]$^{2+}$, are caused by a weaker coupling of the ^{3}MC and the ground state.[36] This is substantiated by small k_2 rate constants (10^{11}–10^{12} vs. 1.7×10^{13} s^{-1} in case of [Ru(tpy)$_2$]$^{2+}$). To the best of our knowledge, such a temperature-dependent excited-state lifetime measurement has been performed the first time for cyclometalated ruthenium(II) complexes. In principle, we would expect a similar behavior for [Ru(tpy)(dpb)]$^+$ or analogous complexes.

Furthermore, for RuNCN-F and RuNCN-NO$_2$ lower ΔE_2 values were obtained, supporting the assumption of a decreased ^{3}MC destabilization, but k_2 is again small and even smaller for RuNCN-NO$_2$. When comparing RuNCN-F and RuNCN-NO$_2$, the fluoro substituent mainly lowers the ^{3}MC energy, which is therefore closer to the ^{3}MLCT state. In contrast, the π-accepting nitro group *para* to the carbanion also affects the ^{3}MLCT energy (see the LUMO energy in Table 2) resulting in a larger observed ^{3}MLCT–^{3}MC barrier that allows for room-temperature emission. This is also reflected by the displacement of the RuNCN-F curve to lower temperatures (Figure 7).

Despite this good correlation between structure and excited-state dynamics, the temperature-dependent emission properties of RuNCN-COOH need to be discussed separately. Within the whole series, its activation energy for the ^{3}MLCT–^{3}MC internal conversion is the least. Nevertheless, a room-temperature lifetime of 12.3 ns could be measured, which is remarkably high in comparison with the other complexes discussed herein. This can only be explained by the relatively low transition rate for this process, which is one order of magnitude smaller than in the other complexes. Apparently, here the absence of a detectable room-tempera-

ture emission might be due to experimental limitations and does not necessarily mean short excited-state lifetimes.

The second activated decay channel (k_3, ΔE_3) can be attributed to internal conversion (IC) to an energetically slightly higher-lying MLCT state of increased singlet character (MLCT′), which is also a common feature for ruthenium polypyridyl dyes.[30,37]

Electrochemistry: Crucial for the potentially photo-redoxactive Ru^{II} complexes, in particular with respect to photovoltaic applications, are their electrochemical properties. Thus, the reversibility of the redox processes and the location of the oxidation and reduction potentials in comparison to the I$_3^-$/I$^-$ couple and the TiO$_2$ conduction band, respectively, are highly important. Consequently, cyclic voltammetry (CV) measurements were carried out and related results are presented in Figures 8 and 9, Table 2, and the Supporting Information.

Analyzing the influence of cyclometalation by comparing RuNCN to RuNNN shows a strong cathodic shift of the oxidation potential of 900 mV due to the strong σ and π donation as well as electronic repulsion caused by the carbanion.[6a] Based on the calculations (see above), the first oxidation of RuNCN is not only metal-, but also ligand-based, and corresponds to a transition from d$_{Ru}$/π_{NCN}^+ to d$_{Ru}$/$\pi_{NCN}^{2+·}$ transition. Also the first reduction process, located on the terpyridine ligand, is shifted towards lower potentials by 260 mV, owing to increased π back donation from the more electron-rich Ru^{II} center.[5j] Both oxidation and reduction process of the RuNCN complex are fully reversible under cyclic voltammetric conditions. Nevertheless, reversibility was investigated in a more detailed fashion by UV/Vis spectroelectrochemical means (see below).

Again, a comparison of the triazole-containing complexes with their pyridine counterparts allows for a relative classification of electronic properties of the ligands. In comparison to the RuNNN-analogous [Ru(tpy)$_2$][PF$_6$]$_2$, the substitution of a terpyridine ligand by the click-derived 2,6-bis(1,2,3-triazol-4-yl)pyridine leads to a metal-based HOMO of lower energy and tpy-based LUMO of higher energy, indicating a weaker σ-donor and π-acceptor strength of the triazole-containing ligand that would allow the tpy to predominate the π back donation.[8a–d] In contrast, when comparing

Table 2. Electrochemical data of the complexes.

Complex	$E_{1/2}^{ox}$ [V] (i_{pa}/i_{pc}, ΔE_p [mV])[a]	$E_{1/2}^{red}$ [V] (i_{pa}/i_{pc}, ΔE_p [mV])[a]	E_{S*}(ox) [V][d]	E_{HOMO} [eV][c]	E_{LUMO} [eV][c]	$E_{gap,el}$ [eV]	$E_{gap,opt}$ [eV]
RuNNN	0.98 (1.1, 74)	−1.72 (0.9, 80)	−1.22	−5.78	−3.22	2.56	2.20
[Ru(tpy)$_2$][PF$_6$]$_2$[5j]	0.89 (64)	−1.66 (63)	–	–	–	–	–
RuNCN	0.08 (1.0, 67)	−1.98 (1.0, 71)	−1.83	−4.88	−2.91	1.97	1.91
[Ru(tpy)(dpb)]PF$_6$[5j]	0.12 (62)	−1.95 (63)	–	–	–	–	–
RuNCN-F	0.31 (1.0, 74)	−1.95 (1.0, 79)	−1.67	−5.12	−2.97	2.15	1.98
RuNCN-NO$_2$	0.26 (1.0, 76)	−1.82 (1.0, 88)	−1.77	−5.07	−3.11	1.96	2.03
RuNCN-Cbz	0.10 (1.0, 83)	−1.97 (irrev.)[b]	−1.84	−4.89	−3.00	1.89	1.94
RuNCN-Tph	0.07 (1.0, 69)	−1.97 (irrev.)[b]	−1.93	−4.87	−2.93	1.94	2.00
RuNCN-COOEt	0.16 (1.0, 70)	−1.79 (1.1, 80)	−1.74	−4.96	−3.14	1.82	1.90
RuNCN-(COOMe)$_3$	0.26 (1.0, 71)	−1.56 (1.0, 71)	−1.51	−5.06	−3.37	1.69	1.77

[a] Measured in CH$_3$CN with 0.1 M Bu$_4$NPF$_6$; with respect to Fc/Fc$^+$ as a reference. [b] Irreversible process; $E_{1/2}$ received from DPP. [c] Calculated by using $E_{LUMO/HOMO} = [-(E_{onset}^{red/ox} - E_{onset}^{Fc/Fc^+}) - 4.8]$ eV. [d] Calculated using $E_S = E_{1/2}^{ox} - E_{gap,opt}$.[3b]
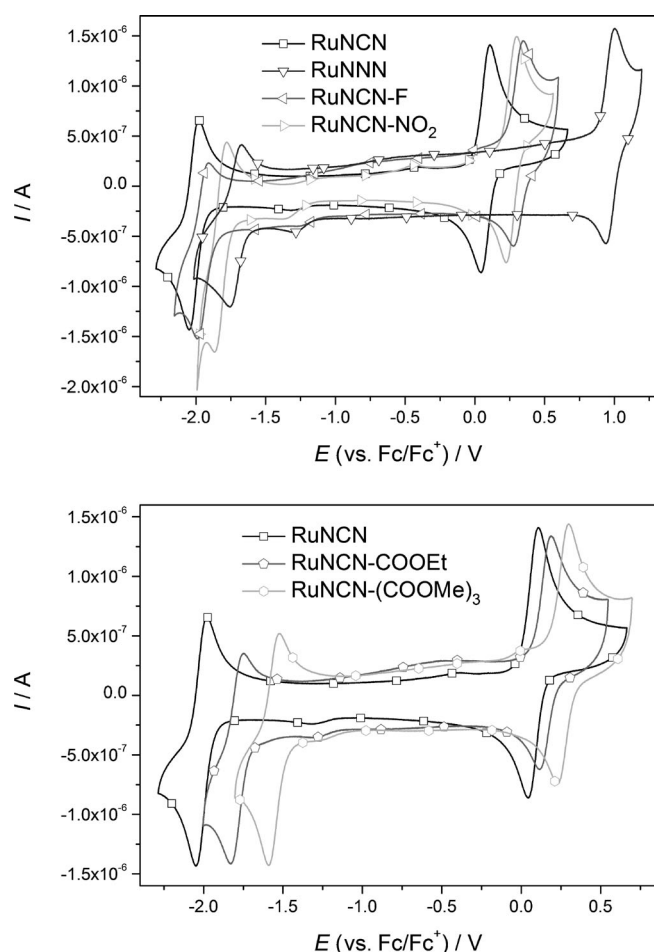
Figure 8. Cyclovoltammetric spectra of the cyclometalated ruthenium(II) complexes and RuNNN as a reference (10^{-5} M in CH$_3$CN with 0.1 M Bu$_4$NPF$_6$). Solid lines represent the measured curve and symbols are only used for assignment.
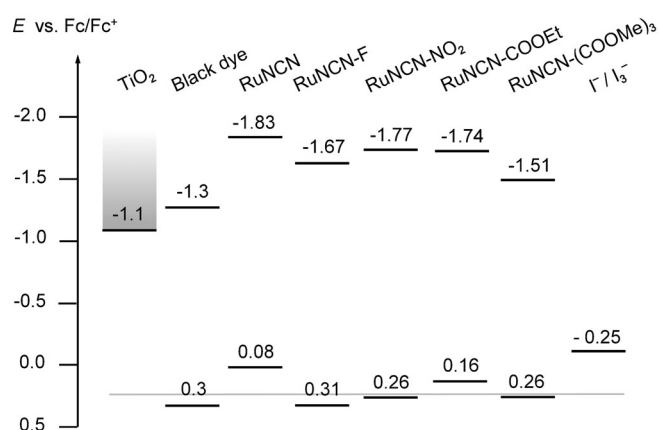

Figure 9. Comparison of the excited-state and ground-state oxidation potentials with the TiO$_2$ conducting band and the I$^-$/I$_3^-$ redox couple, respectively. The grey line indicates a potential that ensures enough driving force for the dye regeneration.[3b,5i] The actual TiO$_2$ conducting band edge depends on the electrolyte composition and is therefore drawn diffusely.[38]

RuNCN with the analogous [Ru(tpy)(dpb)]PF$_6$, for the click-derived complex the oxidation and reduction potentials are cathodically shifted. Evidently, the triazole-containing cyclometalating ligand is a stronger π donor increasing the electron density on the Ru^{II}/NCN-based HOMO and, through increased π back donation from the more electron-rich Ru^{II} to the tpy ligand, the energy of the tpy-based LUMO. This is most likely due to weaker stabilization of the carbanion by the triazole in terms of its electron excess and shorter conjugation length.[8a] Additionally, for the same reason as for RuNNN, the lower π acceptor strength of the triazole-containing cyclometalating ligand, when compared to its pyridine analogue, might cause the HOMO and tpy-based LUMO of higher energy. Consequently, the more negative excited-state oxidation potential (Figure 9, Table 2) should increase the driving force for the electron injection into the TiO$_2$ conducting band or would allow for a higher TiO$_2$ conducting band, which can be achieved by a different electrolyte composition,[38] and therefore higher cell voltages. At the same time, the lower oxidation potential would lower the driving force for the regeneration of the photooxidized dye (Figure 9). In consistence with the blue shift of absorption and emission, which correspond to the optical gap, the electrochemical HOMO–LUMO gap of RuNCN is increased in comparison with [Ru(tpy)(dpb)]PF$_6$.

To still allow efficient dye regeneration, a fine-tuning of the oxidation potential was achieved by installing electron-withdrawing fluoro and nitro groups on the cyclometalated phenyl ring.[5c–e] Thus, the HOMO is stabilized and the oxidation shows an anodic shift by 230 and 180 mV, respectively, to be about 0.5 V more positive than the I$^-$/I$_3^-$ redox couple and, thereby, ensure enough driving force for the dye reduction.[3b,5c,e,i,39] In the case of RuNCN-F, the reduction potential remains nearly unchanged, while for RuNCN-NO$_2$ a distinct anodic shift from -1.98 to -1.82 V is observed. Most likely, the strong π-accepting nitro group weakens the π donation of the *para*-carbanion and, thereby, the π back donation to the terpyridine. A more detailed discussion of the electronic effects of nitro and fluoro substituents on a cyclometalated phenyl ring depending on their positions can be taken from the literature.[5d,40]

Introduction of the carbazole and thiophene moieties affects the oxidation and reduction potentials only marginally, but leads to irreversibility of the reduction process under CV conditions in both cases. However, only the dye oxidation and subsequent reduction is the operative process in DSSCs and this process still is reversible. We note that a strategic methyl group was placed in the 5-position of the thiophene to avoid any following reactions, such as radical dimerizations.[41]

Electrochemical investigations on the ester-substituted complexes RuNCN-COOEt and RuNCN-(COOMe)$_3$ showed significant anodic shifts of the reduction potentials about 190 and 430 mV, respectively, due to stabilization of the LUMO, which is tpy-based. Still, enough driving force for a fast electron injection would be given. Furthermore, since the π-accepting esters are in *para* position, they in-

crease the overall π-acceptor strength of the polypyridyl ligand, causing a small anodic shift of the oxidation of 80 and 180 mV, respectively. Thus, the oxidation potential of RuNCN-(COOMe)$_3$ would enable efficient regeneration. However, the strongly electron-withdrawing carboxylic ester can only be seen as approximation of TiO$_2$-adsorbed carboxylic acids[5k] and the actual electronic situation depends on the protonation state of the adsorbed complex (see pK_a determinations in the Supporting Information).[42] Therefore, although electron-withdrawing, the anchoring carboxylic acids most likely will have to be combined with above-mentioned strategies to lower the oxidation potential directly.[5c,e,i] Consequently, the RuNCN complexes are basically applicable in established DSSCs.

UV/Vis spectroelectrochemical analysis: To obtain a more detailed insight into the electrochemistry of the presented cyclometalated Ru^{II} systems, mainly with regard to reversibility and redox stability, UV/Vis spectroelectrochemical experiments were performed (see Figure 10 for RuNCN and Figures S122–S128 in the Supporting Information for the remaining complexes).
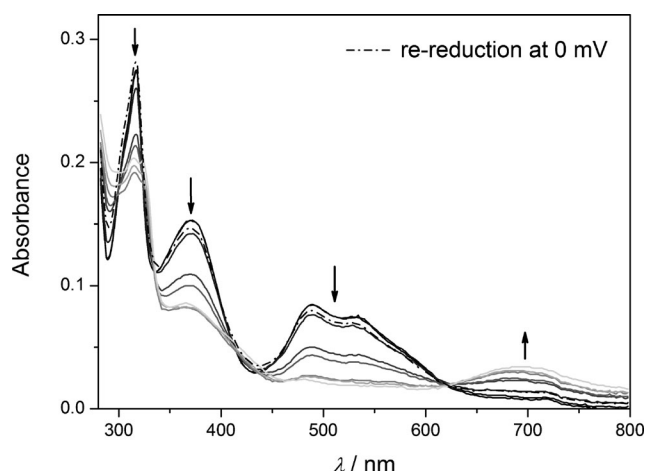

Figure 10. UV/Vis spectroelectrochemical investigation on the oxidation process of RuNCN (voltage varied between 400 and 1000 mV vs. Ag/AgCl; 10^{-5} M in CH$_3$CN with 0.1 M Bu$_4$NPF$_6$).

In general, the oxidation processes show several isosbestic points, indicating the temporary presence of only two species to ultimately form the singly oxidized complex in a well-defined reaction. The most evident changes during oxidation are the decrease of MLCT and MLLCT bands between 350 and 600 nm, caused by depopulation of the d$_{Ru}$/π$_{NCN}$ HOMO, and the appearance of additional, broad peaks between 600 and 850 nm (up to 1000 nm in case of RuNCN-(COOMe)$_3$), most likely attributed to emerging LMCT (π$_{NCN}$→d$_{Ru}$) or LMLCT (π$_{NCN}$→d$_{Ru}$/π$_{NCN}$·) transitions. Here, the fluoro-substituted RuNCN-F represents an exception that shows no changes beyond 600 nm (Figure S123 in the Supporting Information), probably because of a very low transition dipole moment. Accordingly, for

RuNCN-NO$_2$ the arising transition is very weak. In contrast, the thiophene-containing complex RuNCN-Tph exhibits the appearance of two intense absorption peaks around 450 and 900 nm (Figure S126 in the Supporting Information), which can be likely assigned to a mixed MC/MLCT (MMLCT, d$_{Ru}$→d$_{Ru}$/π$_{NCN}$·), MLCT (d$_{Ru}$→π*$_{NCN}$), or LMLCT transitions that would possess large orbital contributions of the thiophene. Remarkably, the reductions of all oxidized species recreate the original spectra almost completely, thus confirming that the oxidation processes are fully reversible even under these demanding conditions under which the complexes are oxidized for a long time.

The first reductions (studied only for the complexes showing reversible reduction under CV conditions, see the Supporting Information), being located on the terpyridine ligand (tpy→tpy·$^-$), reveal a less-defined spectral change in spectroelectrochemical measurements. Again, an absorbance decrease in the MLCT/MLLCT region can be observed, caused by the population of a π*$_{tpy}$ orbital that acts as the acceptor within the longest-wavelength transition processes. Additionally, the absorbance also increases at around 450 nm and several changes occur in the UV region of the spectrum, both originating from appearing, disappearing, or shifted LC and LLCT transitions. In contrast to the oxidation described above, recreation of the initial complex is not successful in most cases, which is likely due to following reactions. As an exception, RuNCN-(COOMe)$_3$, which possesses three electron-withdrawing ester groups at the terpyridine ligand that enable an enhanced stabilization of the electron-rich tpy·$^-$ moiety, allows the nearly full regeneration by re-oxidation.

Photophysical model: Cyclometalated polypyridyl Ru^{II} complexes have been known for some time,[6,9a] but it was only quite recently that they have been applied to the field of dye-sensitized solar cells.[5] Although there has been elaborated research on photoactive electron-transfer assemblies, such as homo- and heteronuclear dyads, for the prototypical bis(tridentate), heteroleptic Ru^{II} complex of terpyridine and its cyclometalated analogue 1,3-dipyridylbenzene, a detailed investigation on the excited-state processes is missing up to date.[32,43] Only a simplified, qualitative explanation of its photophysical properties by relative energies of the S$_0$, the lowest ^{3}MLCT state and the ^{3}MC state has been reported.[6a,32] According to that, the lifetime of the charge-separated excited-state is determined by the ^{3}MLCT–^{3}MC energy difference, since the metal-centered excited state shows a strong coupling to the ground state and therefore causes a rapid relaxation once the ^{3}MC state is populated. This is plausible because antibonding orbitals are occupied in the ^{3}MC state, which shows a displacement that typically matches the ground-state geometry at high-energy vibrations; in other words, the transition is highly probable because of a large Franck–Condon factor (strong coupling case of displaced oscillators).[44] Alternatively, the fast decay to the ground state can be explained in a classical picture assuming the surfaces show a nearly barrierless crossing.[45]

However, we emphasize that the ^3MC–S_0 intersystem crossing not only depends on the ^3MC, but also on the S_0 potential energy surface, which itself is strongly influenced by the electronic nature of the ligand. Thus, several Ru^{II} complexes have been reported, for example, $Ru(bpy)_2(CN)_2$, that show a weaker ^3MC–S_0 coupling.[36] Despite these studies, the prolonged excited-state lifetime of the cyclometalated [Ru(tpy)-(dpb)]$^+$ in comparison to [Ru(tpy)$_2$]$^{2+}$ has only been attributed to the ^3MC destabilization by the carbanion so far.

Nonetheless, temperature-dependent emission lifetime measurements reveal a similar and even lowered activation barrier for the population of the ^3MC state within the RuNCN series compared to [Ru(tpy)$_2$]$^{2+}$. At the same time, the non-radiative deactivation rate constant of RuNCN is orders of magnitude smaller than for [Ru(tpy)$_2$]$^+$.[30] We expect a similar behaviour for the analogous [Ru(tpy)-(dpb)]$^+$ complex.

Consequently, Δ-SCF calculations were performed to gain a deeper understanding of the photophysics. In Figure 11 the schematic potential energy surfaces for the complexes RuNCN and RuNNN are depicted. The diabatic energies (DE) are obtained as the energetic differences between the energy minima of the optimized geometries, while the adiabatic energies (AE) are obtained as the actual energy differences at the ^3MLCT and the ^3MC optimized geometries. As shown in Figure 11, the ^3MLCT and ^3MC minima are almost

isoenergetic for RuNCN, while for RuNNN the ^3MC minimum is lower in energy than the ^3MLCT one. This is in agreement with a destabilized ^3MC state for RuNCN as a result of the cyclometalation. As an additional consequence, the S_0 is destabilized as well and both ^3MLCT and ^3MC states appear at lower energies relative to the S_0. However, for the thermal ^3MLCT–^3MC internal conversion, the energy barrier and the respective ^3MLCT–^3MC conversion rate (see ΔE_2 and k_2 in the temperature-dependent lifetime measurements) are determining. Usually, the subsequent ^3MC–S_0 intersystem crossing rate is the limiting rate. Thus, referring to the experimental ^3MLCT–^3MC energy barrier, which is lower for RuNCN than for [Ru(tpy)$_2$]$^{2+}$, and the nonetheless prolonged excited-state lifetimes, we postulate a weaker ^3MC–S_0 coupling. In agreement with previous reports,[46] we conclude that the ^3MC–S_0 intersystem crossing occurs at high energies on the potential energy surfaces for RuNCN, while for RuNNN and [Ru(tpy)$_2$]$^{2+}$ this ^3MC–S_0 intersystem crossing point is at low energies and thus readily accessible. This is plausible, since the covalent binding of the cyclometalating ligand has a significant influence on both electronic structure and geometry already of the S_0 affecting also the ^3MC–S_0 coupling.

Still, the lifetime of cyclometalated complexes is relatively short and the quantum yield is low in comparison to [Ru-(bpy)$_3$]$^{2+}$, for example, because of the S_0 destabilization. The resulting small S_0–^3MLCT energy gap leads to a more probable thermally non-activated, radiationless deactivation due to an increased Franck–Condon overlap of the S_0 and ^3MLCT vibrational wave functions. The observed decrease of the excited-state lifetime with decreasing emission energy is in accordance with the already mentioned energy-gap law.[27]

Conclusion

A systematically modified series of new ruthenium(II) complexes of click-derived tridentate cyclometalating ligands aimed towards the application in dye-sensitized solar cells was investigated. An optimized synthetic route was established. The presented cyclometalated ruthenium(II) polypyridyl complexes feature all benefits of established Ru^{II} thiocyanate dyes:

1) The HOMO is raised in energy causing a small energy gap and, therefore, a strongly red-shifted absorption.
2) The strong electron donation destabilizes ^3MC states and thus offers prolonged excited-state lifetimes.
3) The HOMO is extended to the cyclometalating ligand that facilitates the dye regeneration.
4) The LUMO is located on the opposite, anchoring ligand. Consequently, the charge transfer is directed towards the semiconductor surface.
5) At the same time, the anchoring groups, namely the carboxylic acid functions, strongly lower the LUMO energy, resulting in a panchromatic shift and intense absorption
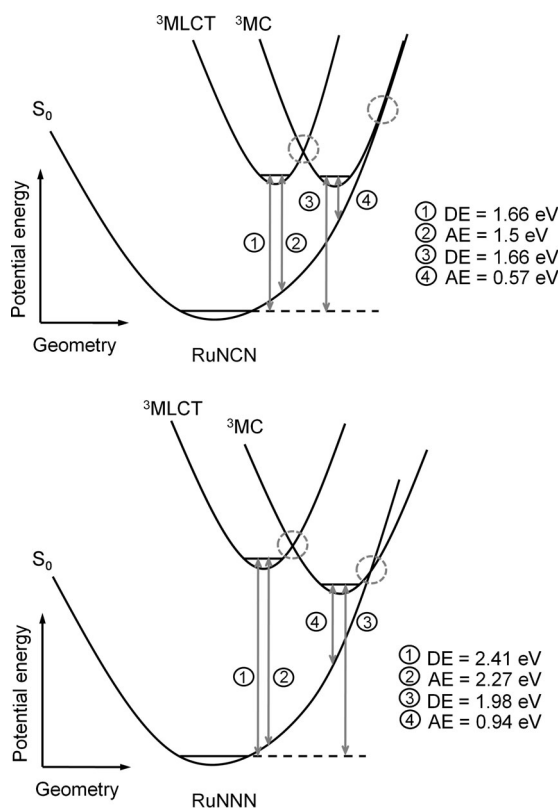

Figure 11. Proposed potential energy surfaces (the MLCT′ is omitted for clarity) including adiabatic (AE) and diabatic energies (DE) at the ΔSCF-PCM-DFT/6-31G* level of theory for the complexes RuNCN (top) and RuNNN (bottom).

For RuNCN:
① DE = 1.66 eV
② AE = 1.5 eV
③ DE = 1.66 eV
④ AE = 0.57 eV

For RuNNN:
① DE = 2.41 eV
② AE = 2.27 eV
③ DE = 1.98 eV
④ AE = 0.94 eV

due to the pronounced push–pull effect that heightens the oscillator strengths and the extinction coefficients.

Additionally, the cyclometalated complexes offer further advantages that are essentially absent in thiocyanate complexes:

6) The electronic functions of the monodentate thiocyanate ligands are adopted by a multidentate ligand thus preventing photochemical ligand loss and offering higher long-term stability.

7) Since the HOMO is extended to the cyclometalating ligand, the optoelectronic properties can be optimized by ligand functionalization. Thus, redox-matching with the electrolyte and improvement of the light harvesting are enabled.

Moreover, the complexes of triazole-containing tridentate cyclometalating ligands offer potential advantages over their pyridyl analogues:

8) The stronger effective electron donation allows for longer excited-state lifetimes.

9) Their ligands can be readily and modularly functionalized.

A potential drawback might be the lower extinction coefficients, although strategies to increase them have been demonstrated. Still, the determined optoelectronic properties strongly encourage us to test the presented type of complex in a dye-sensitized solar cell. Also, a potential iodide–triazole interaction shall be investigated in the future.

As a result of the combined efforts of experimental and computational methods, a detailed understanding of the photophysical properties is provided, in particular of the crucial radiationless deactivation process of cyclometalated ruthenium(II) complexes.

Experimental Section

Extensive experimental details are given in the Supporting Information. These include synthetic procedures, UV/Vis absorption and emission, CV, NMR and ESI-Tof MS spectra, further solid-state structures and a more detailed discussion thereof, as well as computational details. CCDC-848606 (HNCN), CCDC-848607 (HNCN-F), CCDC-848608 ([Ru-(tpy)(CH$_3$CN)$_3$][PF$_6$]$_2$), CCDC-848609 ([Ru(tpy-COOEt)(CH$_3$CN)$_3$]-[PF$_6$]$_2$), CCDC-848610 ([Ru(tpy-(COOMe)$_3$)(CH$_3$CN)$_3$][PF$_6$]$_2$), CCDC-848611 (RuNNN), CCDC-848612 (RuNCN), CCDC-848613 (RuNCN-NO$_2$), CCDC-848614 (RuNCN-F), and CCDC-848615 (RuNCN-Tph) contain the supplementary crystallographic data for this paper. These data can be obtained free of charge from The Cambridge Crystallographic Data Centre via www.ccdc.cam.ac.uk/data_request/cif.

Acknowledgements

[1] a) A. Juris, V. Balzani, F. Barigelletti, S. Campagna, P. Belser, A. von Zelewsky, *Coord. Chem. Rev.* **1988**, *84*, 85–277; b) J. P. Sauvage, J. P. Collin, J. C. Chambron, S. Guillerez, C. Coudret, V. Balzani, F. Barigelletti, L. De Cola, L. Flamigni, *Chem. Rev.* **1994**, *94*, 993–1019.

[2] a) L. Hammarström, O. Johansson, *Coord. Chem. Rev.* **2010**, *254*, 2546–2559; b) E. A. Medlycott, G. S. Hanan, *Chem. Soc. Rev.* **2005**, *34*, 133–142; c) E. A. Medlycott, G. S. Hanan, *Coord. Chem. Rev.* **2006**, *250*, 1763–1782.

[3] a) B. O'Regan, M. Grätzel, *Nature* **1991**, *353*, 737–740; b) A. Hagfeldt, G. Boschloo, L. Sun, L. Kloo, H. Pettersson, *Chem. Rev.* **2010**, *110*, 6595–6663.

[4] a) M. K. Nazeeruddin, A. Kay, I. Rodicio, R. Humphry-Baker, E. Mueller, P. Liska, N. Vlachopoulos, M. Grätzel, *J. Am. Chem. Soc.* **1993**, *115*, 6382–6390; b) M. K. Nazeeruddin, P. Péchy, T. Renouard, S. M. Zakeeruddin, R. Humphry-Baker, P. Comte, P. Liska, L. Cevey, E. Costa, V. Shklover, L. Spiccia, G. B. Deacon, C. A. Bignozzi, M. Grätzel, *J. Am. Chem. Soc.* **2001**, *123*, 1613–1624; c) H. Tributsch, *Coord. Chem. Rev.* **2004**, *248*, 1511–1530.

[5] a) P. G. Bomben, K. C. D. Robson, P. A. Sedach, C. P. Berlinguette, *Inorg. Chem.* **2009**, *48*, 9631–9643; b) B. D. Koivisto, K. C. D. Robson, C. P. Berlinguette, *Inorg. Chem.* **2009**, *48*, 9644–9652; c) T. Bessho, E. Yoneda, J.-H. Yum, M. Guglielmi, I. Tavernelli, H. Imai, U. Rothlisberger, M. K. Nazeeruddin, M. Grätzel, *J. Am. Chem. Soc.* **2009**, *131*, 5930–5934; d) P. G. Bomben, B. D. Koivisto, C. P. Berlinguette, *Inorg. Chem.* **2010**, *49*, 4960–4971; e) P. G. Bomben, K. D. Thériault, C. P. Berlinguette, *Eur. J. Inorg. Chem.* **2011**, 1806–1814; f) K. C. D. Robson, B. D. Koivisto, A. Yella, B. Sporinova, M. K. Nazeeruddin, T. Baumgartner, M. Grätzel, C. P. Berlinguette, *Inorg. Chem.* **2011**, *50*, 5494–5508; g) K. C. D. Robson, B. Sporinova, B. D. Koivisto, E. Schott, D. G. Brown, C. P. Berlinguette, *Inorg. Chem.* **2011**, *50*, 6019–6028; h) S. H. Wadman, J. M. Kroon, K. Bakker, M. Lutz, A. L. Spek, G. P. M. van Klink, G. van Koten, *Chem. Commun.* **2007**, 1907–1909; i) P. G. Bomben, T. J. Gordon, E. Schott, C. P. Berlinguette, *Angew. Chem.* **2011**, *123*, 10870–10873; *Angew. Chem. Int. Ed.* **2011**, *50*, 10682–10685; j) S. H. Wadman, M. Lutz, D. M. Tooke, A. L. Spek, F. Hartl, R. W. A. Havenith, G. P. M. van Klink, G. van Koten, *Inorg. Chem.* **2009**, *48*, 1887–1900; k) S. H. Wadman, J. M. Kroon, K. Bakker, R. W. A. Havenith, G. P. M. van Klink, G. van Koten, *Organometallics* **2010**, *29*, 1569–1579.

[6] a) J.-P. Collin, M. Beley, J.-P. Sauvage, F. Barigelletti, *Inorg. Chim. Acta* **1991**, *186*, 91–93; b) E. C. Constable, J. M. Holmes, *J. Organomet. Chem.* **1986**, *301*, 203–208.

[7] H. C. Kolb, M. G. Finn, K. B. Sharpless, *Angew. Chem.* **2001**, *113*, 2056–2075; *Angew. Chem. Int. Ed.* **2001**, *40*, 2004–2021.

[8] a) Y. Li, J. C. Huffman, A. H. Flood, *Chem. Commun.* **2007**, 2692–2694; b) R. M. Meudtner, M. Ostermeier, R. Goddard, C. Limberg, S. Hecht, *Chem. Eur. J.* **2007**, *13*, 9834–9840; c) M. Ostermeier, M.-A. Berlin, R. M. Meudtner, S. Demeshko, F. Meyer, C. Limberg, S. Hecht, *Chem. Eur. J.* **2010**, *16*, 10202–10213; d) B. Schulze, C. Friebe, M. D. Hager, A. Winter, R. Hoogenboom, H. Görls, U. S. Schubert, *Dalton Trans.* **2009**, 787–794; e) B. Happ, C. Friebe, A. Winter, M. D. Hager, R. Hoogenboom, U. S. Schubert, *Chem. Asian J.* **2009**, *4*, 154–163; f) B. Schulze, D. Escudero, C. Friebe, R. Siebert, H. Görls, U. Köhn, E. Altuntas, A. Baumgaertel, M. D. Hager, A. Winter, B. Dietzek, J. Popp, L. González, U. S. Schubert, *Chem. Eur. J.* **2011**, *17*, 5494–5498.

[9] a) M. Beley, J. P. Collin, R. Louis, B. Metz, J. P. Sauvage, *J. Am. Chem. Soc.* **1991**, *113*, 8521–8522; b) J. A. G. Williams, *Chem. Soc. Rev.* **2009**, *38*, 1783–1801; c) B. Beyer, C. Ulbricht, D. Escudero, C.

Friebe, A. Winter, L. González, U. S. Schubert, *Organometallics* **2009**, *28*, 5478–5488.

[10] While this manuscript was in preparation, a communication by Zhong, Yao et al. already introduced this type of click-derived NCN-cyclometalated Ru[II] complex. However, only a basic characterization was provided and the synthesis was not optimized. W.-W. Yang, L. Wang, Y.-W. Zhong, J. Yao, *Organometallics* **2011**, *30*, 2236–2240.

[11] Very recently, the use of a 1,2,3-triazolylpyridine within a classical Ru[II]–thiocyanate complex demonstrated the potential of a click-derived ligand for solar-cell applications. I. Stengel, A. Mishra, N. Pootrakulchote, S.-J. Moon, S. M. Zakeeruddin, M. Grätzel, P. Bauerle, *J. Mater. Chem.* **2011**, *21*, 3726–3734.

[12] A. J. Wilkinson, H. Puschmann, J. A. K. Howard, C. E. Foster, J. A. G. Williams, *Inorg. Chem.* **2006**, *45*, 8685–8699.

[13] C. Amatore, A. Jutand, *Acc. Chem. Res.* **2000**, *33*, 314–321.

[14] J. G. Rodríguez, T. Laparra, *Tetrahedron* **2009**, *65*, 2551–2555.

[15] a) C. Y. Chen, H. C. Lu, C. G. Wu, J. G. Chen, K. C. Ho, *Adv. Funct. Mater.* **2007**, *17*, 29–36; b) C. Y. Chen, S. J. Wu, J. Y. Li, C. G. Wu, J. G. Chen, K. C. Ho, *Adv. Mater.* **2007**, *19*, 3888–3891; c) C.-Y. Chen, J.-G. Chen, S.-J. Wu, J.-Y. Li, C.-G. Wu, K.-C. Ho, *Angew. Chem.* **2008**, *120*, 7452–7455; *Angew. Chem. Int. Ed.* **2008**, *47*, 7342–7345; d) C.-Y. Chen, S.-J. Wu, C.-G. Wu, J.-G. Chen, K.-C. Ho, *Angew. Chem.* **2006**, *118*, 5954–5957; *Angew. Chem. Int. Ed.* **2006**, *45*, 5822–5825; e) C.-C. Chou, K.-L. Wu, Y. Chi, W.-P. Hu, S. J. Yu, G.-H. Lee, C.-L. Lin, P.-T. Chou, *Angew. Chem.* **2011**, *123*, 2102–2106; *Angew. Chem. Int. Ed.* **2011**, *50*, 2054–2058; f) F. Gao, Y. Wang, D. Shi, J. Zhang, M. Wang, X. Jing, R. Humphry-Baker, P. Wang, S. M. Zakeeruddin, M. Grätzel, *J. Am. Chem. Soc.* **2008**, *130*, 10720–10728; g) F. Gao, Y. Wang, J. Zhang, D. Shi, M. Wang, R. Humphry-Baker, P. Wang, S. M. Zakeeruddin, M. Grätzel, *Chem. Commun.* **2008**, 2635–2637; h) N. Hirata, J.-J. Lagref, E. J. Palomares, J. R. Durrant, M. K. Nazeeruddin, M. Gratzel, D. Di Censo, *Chem. Eur. J.* **2004**, *10*, 595–602.

[16] R. Westlund, E. Glimsdal, M. Lindgren, R. Vestberg, C. Hawker, C. Lopes, E. Malmström, *J. Mater. Chem.* **2008**, *18*, 166–175.

[17] a) M. Jäger, R. J. Kumar, H. Görls, J. Bergquist, O. Johansson, *Inorg. Chem.* **2009**, *48*, 3228–3238; b) H. F. Suen, S. W. Wilson, M. Pomerantz, J. L. Walsh, *Inorg. Chem.* **1989**, *28*, 786–791.

[18] M. Gagliardo, D. J. M. Snelders, P. A. Chase, R. J. M. Klein Gebbink, G. P. M. van Klink, G. van Koten, *Angew. Chem.* **2007**, *119*, 8710–8726; *Angew. Chem. Int. Ed.* **2007**, *46*, 8558–8573.

[19] a) Y. Li, A. H. Flood, *Angew. Chem.* **2008**, *120*, 2689–2692; *Angew. Chem. Int. Ed.* **2008**, *47*, 2649–2652; b) Y. Li, A. H. Flood, *J. Am. Chem. Soc.* **2008**, *130*, 12111–12122; c) S. Liu, P. Müller, M. K. Takase, T. M. Swager, *Inorg. Chem.* **2011**, *50*, 7598–7609; d) B. Schulze, C. Friebe, M. D. Hager, W. Günther, U. Köhn, B. O. Jahn, H. Görls, U. S. Schubert, *Org. Lett.* **2010**, *12*, 2710–2713.

[20] L. González, D. Escudero, L. Serrano-Andrés, *ChemPhysChem.* **2012**, *13*, 28–51.

[21] a) B. Happ, D. Escudero, M. D. Hager, C. Friebe, A. Winter, H. Görls, E. Altuntaş, L. González, U. S. Schubert, *J. Org. Chem.* **2010**, *75*, 4025–4038; b) A. Vlček Jr., S. Záliš, *Coord. Chem. Rev.* **2007**, *251*, 258–287; c) M.-F. Charlot, A. Aukauloo, *J. Phys. Chem. A* **2007**, *111*, 11661–11672.

[22] J. Heully, F. Alary, M. Boggio-Pasqua, *J. Chem. Phys.* **2009**, *131*, 184308.

[23] a) K. C. D. Robson, B. D. Koivisto, T. J. Gordon, T. Baumgartner, C. P. Berlinguette, *Inorg. Chem.* **2010**, *49*, 5335–5337; b) R. Siebert, A. Winter, B. Dietzek, U. S. Schubert, J. Popp, *Macromol. Rapid Commun.* **2010**, *31*, 883–888.

[24] R. Englman, J. Jortner, *Mol. Phys.* **1970**, *18*, 145–164.

[25] a) F. Barigelletti, P. Belser, A. Von Zelewsky, A. Juris, V. Balzani, *J. Phys. Chem.* **1985**, *89*, 3680–3684; b) M. Wrighton, D. L. Morse, *J. Am. Chem. Soc.* **1974**, *96*, 998–1003.

[26] a) M. Presselt, B. Dietzek, M. Schmitt, J. Popp, A. Winter, M. Chiper, C. Friebe, U. S. Schubert, *J. Phys. Chem. C* **2008**, *112*, 18651–18660; b) M. Presselt, B. Dietzek, M. Schmitt, S. Rau, A. Winter, M. Jäger, U. S. Schubert, J. Popp, *J. Phys. Chem. A* **2010**, *114*, 13163–13174.

[27] a) J. V. Caspar, T. J. Meyer, *J. Phys. Chem.* **1983**, *87*, 952–957; b) K. R. Barqawi, Z. Murtaza, T. J. Meyer, *J. Phys. Chem.* **1991**, *95*, 47–50; c) J. V. Caspar, E. M. Kober, B. P. Sullivan, T. J. Meyer, *J. Am. Chem. Soc.* **1982**, *104*, 630–632.

[28] J. V. Caspar, B. P. Sullivan, E. M. Kober, T. J. Meyer, *Chem. Phys. Lett.* **1982**, *91*, 91–95.

[29] J. A. Treadway, B. Loeb, R. Lopez, P. A. Anderson, F. R. Keene, T. J. Meyer, *Inorg. Chem.* **1996**, *35*, 2242–2246.

[30] A. C. Benniston, G. Chapman, A. Harriman, M. Mehrabi, C. A. Sams, *Inorg. Chem.* **2004**, *43*, 4227–4233.

[31] M. Abrahamsson, M. Jäger, R. J. Kumar, T. Österman, P. Persson, H.-C. Becker, O. Johansson, L. Hammarström, *J. Am. Chem. Soc.* **2008**, *130*, 15533–15542.

[32] M. Beley, S. Chodorowski, J.-P. Collin, J.-P. Sauvage, L. Flamigni, F. Barigelletti, *Inorg. Chem.* **1994**, *33*, 2543–2547.

[33] C. R. Hecker, A. K. I. Gushurst, D. R. McMillin, *Inorg. Chem.* **1991**, *30*, 538–541.

[34] a) R. Siebert, C. Hunger, J. Guthmuller, F. Schlütter, A. Winter, U. S. Schubert, L. González, B. Dietzek, J. Popp, *J. Phys. Chem. C* **2011**, *115*, 12677–12688; b) R. Siebert, A. Winter, U. S. Schubert, B. Dietzek, J. Popp, *Phys. Chem. Chem. Phys.* **2011**, *13*, 1606–1617.

[35] As a non-radiative temperature-independent channel is assumed to contribute to the excited-state dynamics the experimental phosphorescence rate at 77 K can be expressed as $1/\tau_{77K} = k_r + k_1$.

[36] a) G. H. Allen, R. P. White, D. P. Rillema, T. J. Meyer, *J. Am. Chem. Soc.* **1984**, *106*, 2613–2620; b) W. F. Wacholtz, R. A. Auerbach, R. H. Schmehl, *Inorg. Chem.* **1986**, *25*, 227–234; c) F. Barigelletti, A. Juris, V. Balzani, P. Belser, A. Von Zelewsky, *J. Phys. Chem.* **1987**, *91*, 1095–1098; d) A. Islam, N. Ikeda, A. Yoshimura, T. Ohno, *Inorg. Chem.* **1998**, *37*, 3093–3098.

[37] a) B. J. Coe, D. W. Thompson, C. T. Culbertson, J. R. Schoonover, T. J. Meyer, *Inorg. Chem.* **1995**, *34*, 3385–3395; b) R. S. Lumpkin, E. M. Kober, L. A. Worl, Z. Murtaza, T. J. Meyer, *J. Phys. Chem.* **1990**, *94*, 239–243; c) M. Sykora, J. R. Kincaid, *Inorg. Chem.* **1995**, *34*, 5852–5856; d) H. Yersin, E. Gallhuber, A. Vogler, H. Kunkely, *J. Am. Chem. Soc.* **1983**, *105*, 4155–4156.

[38] B. Enright, G. Redmond, D. Fitzmaurice, *J. Phys. Chem.* **1994**, *98*, 6195–6200.

[39] G. Boschloo, A. Hagfeldt, *Acc. Chem. Res.* **2009**, *42*, 1819–1826.

[40] Z. Wang, E. Turner, V. Mahoney, S. Madakuni, T. Groy, J. Li, *Inorg. Chem.* **2010**, *49*, 11276–11286.

[41] J. Heinze, B. A. Frontana-Uribe, S. Ludwigs, *Chem. Rev.* **2010**, *110*, 4724–4771.

[42] Y. Tachibana, M. K. Nazeeruddin, M. Grätzel, D. R. Klug, J. R. Durrant, *Chem. Phys.* **2002**, *285*, 127–132.

[43] M. Beley, J. P. Collin, J. P. Sauvage, *Inorg. Chem.* **1993**, *32*, 4539–4543.

[44] K. Freed, J. Jortner, *J. Chem. Phys.* **1970**, *52*, 6272–6291.

[45] J. H. Alstrum-Acevedo, M. K. Brennaman, T. J. Meyer, *Inorg. Chem.* **2005**, *44*, 6802–6827.

[46] I. M. Dixon, F. Alary, J.-L. Heully, *Dalton Trans.* **2010**, *39*, 10959–10966.

Publication A6:

"A heteroleptic *bis*(tridentate) ruthenium(II) platform featuring an anionic 1,2,3-triazolate-based ligand for application in the dye-sensitized solar cell"

S. Sinn, B. Schulze, C. Friebe, D. G. Brown, M. Jäger, J. Kübel, B. Dietzek, C. P. Berlinguette, U. S. Schubert

A Heteroleptic Bis(tridentate) Ruthenium(II) Platform Featuring an Anionic 1,2,3-Triazolate-Based Ligand for Application in the Dye-Sensitized Solar Cell

Stephan Sinn,[†,‡,△] Benjamin Schulze,[†,‡,△] Christian Friebe,[†,‡] Douglas G. Brown,[§] Michael Jäger,[†,‡] Joachim Kübel,[⊥,∇] Benjamin Dietzek,[⊥,∇,‡,*] Curtis P. Berlinguette,[§,∥,*] and Ulrich S. Schubert[†,‡,*]

[†]Laboratory of Organic and Macromolecular Chemistry (IOMC), Friedrich Schiller University Jena, Humboldtstr. 10, 07743 Jena, Germany

[‡]Jena Center for Soft Matter (JCSM), Friedrich Schiller University Jena, Philosophenweg 7, 07743 Jena, Germany

[§]Department of Chemistry, University of Calgary, 2500 University Drive N.W., Calgary, Alberta, Canada T2N 1N4

[∥]Department of Chemistry, The University of British Columbia, 2036 Main Mall, Vancouver, British Columbia, Canada V6T 1Z1

[⊥]Institute of Physical Chemistry (IPC) and Abbe Center of Photonics, Friedrich Schiller University Jena, Helmholtzweg 4, 07743 Jena, Germany

[∇]Leibniz Institute of Photonic Technology (IPHT), Albert-Einstein-Str. 9, 07745 Jena, Germany

ⓢ *Supporting Information*

ABSTRACT: A series of bis(tridentate) ruthenium(II) complexes featuring new anionic 1,2,3-triazolate-based tridentate ligands and 2,2′:6′,2′′-terpyridine is presented. For a complex equipped with carboxy anchoring groups, the performance in a dye-sensitized solar cell is evaluated. The title complexes are readily synthesized and can be decorated with alkyl chains utilizing azide−alkyne cycloaddition methods, in order to improve the device stability and allow the use of alternative electrolytes. On account of the strong electron donation from the 1,2,3-triazolates, the complexes exhibit a broad metal-to-ligand charge-transfer absorption (up to 700 nm), leading to an electron transfer toward the anchoring ligand. The lifetimes of the charge-separated excited states are in the range of 50 to 80 ns. In addition, the ground- and excited-state redox potentials are appropriate for the application in dye-sensitized solar cells, as demonstrated by power conversion efficiencies of up to 4.9% (vs 6.1% for **N749**).
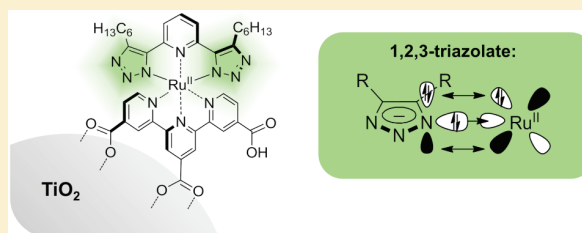
■ INTRODUCTION

Dye-sensitized solar cells (DSSCs) rely on the sensitization of a wide-band-gap semiconductor such as TiO_2 with dye molecules. The sensitizer needs to be photo- and redox-stable, absorb as much light as possible, and feature excited- and ground-state redox potentials that allow for efficient electron injection into the conduction band of the semiconductor and subsequent regeneration by the electrolyte, respectively.[1,2] Meanwhile, power conversion efficiencies (PCEs) of up to 12.3% have been achieved with molecular dyes[3] and ruthenium(II) polypyridyl complexes featuring thiocyanato ligands, such as $(NBu_4)_3[Ru(Htctpy)(NCS)_3]$ (**N749** or black dye; Htctpy = 2,2′:6′,2′′-terpyridine-4′-carboxylic acid-4,4′′-dicarboxylate) (Figure 1), are among the most efficient sensitizers, with PCEs up to 11.4%.[4−7] However, the monodentate thiocyanato ligands preclude further optimization *via* ligand functionalization and limit the lifetime of DSSCs, as they can decoordinate easily.[8,9] Consequently, the thiocyanate ligands have been replaced by anionic multidentate ligands including anionic phenyl rings,[10−16] tetrazolates,[17] 1,2,4-triazolates,[18−20] and pyrazolates,[20−23] enabling an improved

long-term stability and similar or higher PCEs compared to thiocyanate-based benchmark dyes.[24] Moreover, these chelating ligands enable the introduction of hydrophobic alkyl chains and additional chromophores to further improve the DSSC life span[18,25−27] and the light-harvesting capability, respectively.[24]

Chou and co-workers presented ruthenium(II) dyes featuring functionalized dianionic 2,6-bis(5-pyrazolyl)pyridine ligands (Figure 1), which achieved remarkable PCEs of 9.1% (TF-1) and 10.7% (TF-2, vs 9.2% for **N749**) in the DSSC.[23] Building on these promising results, we present herein a series of heteroleptic bis(tridentate) ruthenium(II) complexes containing anionic 1,2,3-triazolates as thiocyanate surrogates (Figure 1). This approach benefits from a very simple ligand synthesis *via* azide−alkyne cycloaddition, which also allows the ready installation of alkyl chains. In comparison to the parent, charge-neutral 1,2,3-triazoles,[28−30] the σ lone pair and the π system of anionic triazolates are raised in energy, resulting in an enhanced σ- and π-donor strength. Furthermore, the use of

Figure 1. Schematic representation of the ruthenium(II) complexes **1** and **2a−2c** and related literature examples.[4,23]
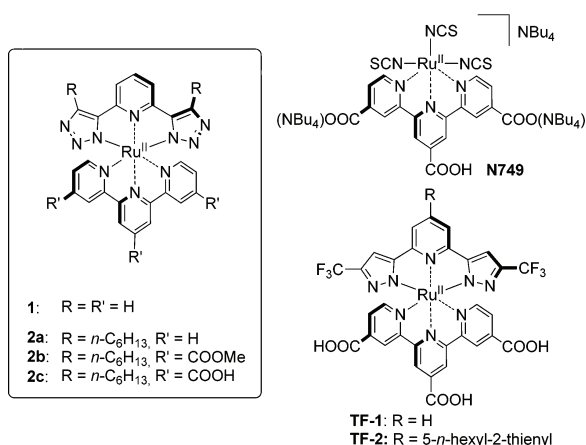
1,2,3-triazolates circumvents the formation of coordination isomers, which plague analogous 1,2,4-triazolate-based ruthenium(II) complexes (Figure 2),[31] and, in contrast to related pyrazolate complexes,[23] no electron-withdrawing groups need to be installed to raise the Ru(III)/Ru(II) redox potential, due to the higher degree of *aza* substitution of the 1,2,3-triazolate.
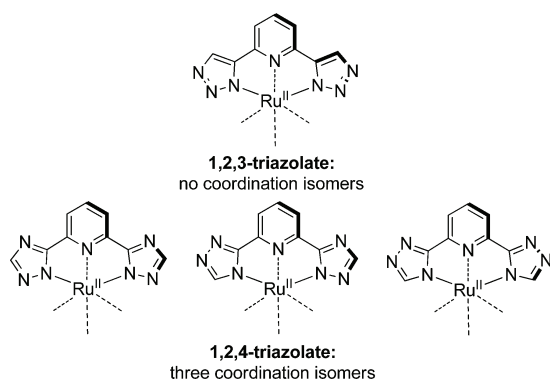
Figure 2. Schematic illustration of the formation of isomeric ruthenium(II) complexes with tridentate ligands based on 1,2,4-triazolates.

■ RESULTS AND DISCUSSION

Synthesis. The 2,6-bis(1,2,3-triazol-4-yl)pyridine ligands were synthesized either *via* Cu(I)-catalyzed azide−alkyne cycloaddition, using *in situ* generated hydroxymethyl azide,[32] followed by a base-induced cleavage of formaldehyde, or, in the case of the internal alkyne (see Scheme 1 and the Supporting Information (SI)), *via* a thermal azide−alkyne cycloaddition with azidomethyl pivalate.[33] For the latter, the cycloadduct is obtained as a statistically distributed mixture; however, after cleavage in basic media and subsequent reprotonation, the free NH-triazole is obtained, which undergoes rapid tautomerization.[30] The corresponding ruthenium(II) complexes were obtained in good yields utilizing [Ru^{II}(tpy)(MeCN)$_3$](PF$_6$)$_2$ (tpy = 2,2′:6′,2″-terpyridine) or [Ru^{II}(tcmtpy)(MeCN)$_3$]-(PF$_6$)$_2$ (tcmtpy = 4,4′,4″-tricarboxymethyl-2,2′:6′,2″-terpyridine; see Scheme 1 and the SI) as precursor.[34] The subsequent saponification of **2b** was achieved as described previously.[12]

Scheme 1. Schematic Representation of the Synthesis of Complexes 1 and 2a−2c, and the Numbering Scheme of the Studied Complexes[a]
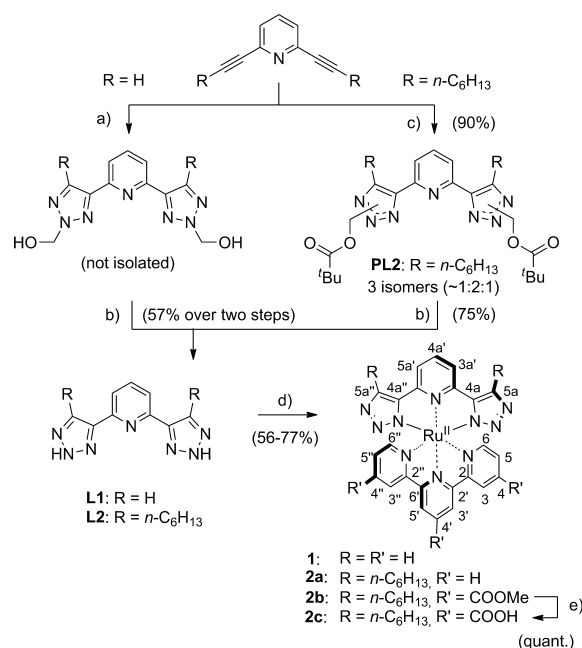
[a]Conditions: (a) HCHO$_{aq}$, AcOH, NaN$_3$, CuSO$_4$, sodium ascorbate, dioxane, rt, 24 h. (b) NaOH, MeOH/H$_2$O, rt, 24 h. (c) Azidomethyl pivalate, 100 °C, 72 h. (d) [Ru^{II}(tpy)(MeCN)$_3$](PF$_6$)$_2$ or [Ru^{II}(tcmtpy)(MeCN)$_3$](PF$_6$)$_2$, alcohol, or triethylene glycol dimethyl ether, 150 °C, 30 min, microwave irradiation. (e) DMF/NEt$_3$/H$_2$O (3:1:1 *v/v/v*).

The solubilities of the charge-neutral complexes are expectedly low; however, the introduction of the alkyl chains (**2a−2c**) improves the solubility, allowing the investigation of the photophysical and electrochemical properties (*vide infra*).

Computational Methods. To enable a deeper understanding of the electronic properties of the new ruthenium(II) complexes, density functional theory (DFT) calculations have been performed for **2a−2c** (note that the hexyl chains have been replaced by methyl groups to shorten the computing time). Additionally, the electronic properties of the fully deprotonated form of **2c** (**2c′**) were calculated, while the electronic excitations for **2c** were computed with the help of time-dependent (TD) DFT.[23] The calculations revealed that the highest occupied molecular orbital (HOMO) of the complexes is composed of a metal d orbital and π orbitals located on the triazolate rings, which is expected in view of the electron-rich π system of the anionic ring.[18,22,24] As a result of the electron repulsion between the anionic ligand and the metal center, the HOMO is strongly destabilized in comparison to polypyridyl complexes such as [Ru(tpy)$_2$](PF$_6$)$_2$. For **2a−2c**, the lowest unoccupied molecular orbital (LUMO) is mainly composed of π* orbitals of the terpyridine ligand (Table S2). Relative to **2a**, the HOMO and, in particular, the LUMO of **2b** are stabilized due to the electron-withdrawing −COOMe groups, resulting in a significantly smaller HOMO−LUMO gap. The −COOH anchoring groups of **2c** have a similar effect on the frontier orbitals energies. In contrast, when compared to **2a**, the HOMO and LUMO of the fully deprotonated complex **2c′** are destabilized and the HOMO−LUMO gap is slightly larger

1638

dx.doi.org/10.1021/ic402701v | *Inorg. Chem.* 2014, 53, 1637−1645

(Figure S11), which is attributed to the electron-donating effect of the −COO⁻ groups. The most relevant electronic transitions of **2c** are displayed in Figure 3 along with the corresponding

Figure 3. Top: Experimental UV−vis absorption spectrum of **2c** adsorbed on TiO₂ (12 μm thick, transparent film, active area of 0.88 cm²) and calculated vertical singlet−singlet transitions of **2c**. Bottom: Corresponding EDDM plots (blue and yellow represent depletion and accumulation, respectively, of electron density upon electronic excitation, isovalue = 0.001) and spin-density plot of the oxidized ground state (bottom right, isovalue = 0.004) of **2c**. Color code: carbon, gray; hydrogen, white; oxygen, red;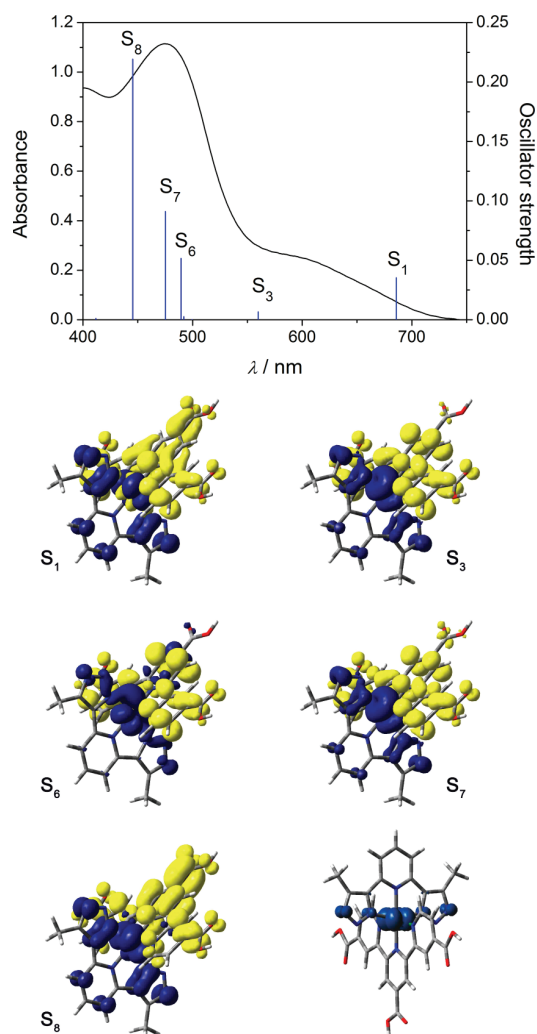 nitrogen, blue; ruthenium, cyan. Note that the tpy ligand is functionalized with carboxy groups, which are known to electronically resemble Ti(IV)-coordinated carboxylates.[35]

electron-density difference maps (EDDM). The computed electronic excitations are in good agreement with the experimental UV−vis absorption spectrum (*vide infra*). The lowest-energy absorption (population of S₁) is a pure HOMO−LUMO transition, which can thus be assigned to a metal-to-ligand charge transfer (MLCT) with some ligand-to-ligand charge-transfer (LLCT) character. Also the other electronic transitions in the visible-light region are of MLCT character with varying LLCT contribution (Figure 3, population of S₃, S₆, S₇, and S₈). As the electron transfer is directed toward the

anchoring tctpy ligand in each case, **2c** features an excited-state electronic structure suitable for electron injection into TiO₂.[36] To allow the estimation of the "hole distribution" resulting after photo-oxidation, the spin-density distribution was calculated for the oxidized complex. As a result, the hole is shared by the metal and the anionic ligand, which is believed to facilitate the sensitizer regeneration.[37,38]

Photophysics and Electrochemistry. The photophysical and electrochemical properties of the complexes are in line with the computational results. The increased σ- and π-donor strength of the anionic 1,2,3-triazolates relative to the neutral 1,2,3-triazoles[31,34,39] causes a destabilization of the metal d orbitals, resulting in a cathodically shifted Ru(III)/Ru(II) redox couple as well as bathochromically shifted MLCT transitions (Table 1). Consequently, a weak, plateau-like absorption band that extends to very long wavelengths is observed (Figures 4 and 5), which is typical for bis(tridentate) ruthenium(II) complexes featuring azolate donors.[21,23,31,40]

As the 1,2,3-triazolate rings of the ruthenium(II) complexes feature additional nitrogen donors, the complexes can be protonated (Figure 4) with the properties of the resulting complexes reflecting those of analogous 1,2,3-triazole ruthenium(II) complexes.[34,39] The protonation was investigated in more detail by UV−vis acid−base titration of **1** (Figures S1−S3). Within the studied pH range from 0 to 12, only one spectral change around pH 4 to 5 occurs; no isosbestic points are present, which indicates that there are more than two species involved. The first and second protonation of the triazolate ligand of **1** occur most likely both within the narrow pH window of 4 to 5, and thus, only a single pK_a value of about 4.7 could be determined (Figures S1 and S2). Furthermore, a weak emission appears upon increasing the pH value, which can be attributed to an increased destabilization of the deactivating triplet metal-centered (³MC) excited states relative to the ³MLCT state.[31,40,41] Accordingly, the excited-state lifetimes of **2a** (54 ns, Table 1) and **2c** (83 ns) are significantly prolonged relative to those of the related [Ru(tpy)₂](PF₆)₂ complex (0.21 ns)[42] and sufficiently long (>10 ns) to enable efficient electron injection into TiO₂ given that injection occurs on the picosecond time scale.[43] Comparison with analogous heteroleptic bis(tridentate) ruthenium(II) complexes featuring 1,2,4-triazolates or tetrazolates shows that **1** is less basic than the 1,2,4-triazolate complex but more basic than the tetrazolate counterpart.[31] Apparently, the cumulative arrangement of the nitrogen atoms within the 1,2,3-triazolate lowers the base strength relative to the 1,2,4-triazolate.[44] The corresponding excited-state lifetimes are slightly prolonged with increasing azolate donor strength.[31] Furthermore, in view of the similar excited-state lifetimes that are observed with related tris-(bidentate) ruthenium(II) complexes featuring imidazolates,[45] the excited-state decay of the deprotonated complexes appears to be governed by the energy-gap law.[46]

As mentioned above, the −COOMe groups cause a LUMO stabilization and, by increasing the π acidity of the tpy ligand, also a minor stabilization of the HOMO of **2b**. In the case of **2c**, the tctpy ligand (tctpy = 2,2′:6′,2″-terpyridine-4,4′,4″-tricarboxylic acid) features three successive deprotonation steps with corresponding pK_a values of approximately 1.2, 3.1, and 5.5.[4,34] In view of the above-mentioned pK_a values for the first and second protonation steps of the triazolate ligand of **1** (about 4.7), complex **2c** is expected to form a zwitterion in solution with two protons of the three carboxylic acid groups

Table 1. Photophysical and Electrochemical Data of Selected Ruthenium(II) Complexes

complex	λ_{Abs}/nm (ε /10^3 M^{-1} cm^{-1})	λ_{Em} (λ_{Ex})/nm	Φ_{PL}/%[a]	τ/ns[b]	$E_{1/2,ox}$/V vs Fc^+/Fc (vs NHE)[c]	E_{S^*}/V vs Fc^+/Fc (vs NHE)[d]	E_{0-0}/eV[e]
1[f]	661s (0.3), 600s (0.8), 482 (5.2), 370 (5.2), 316 (29.9)	705 (490)	0.55	g	g	g	1.85
2a[f]	662 (0.7), 608 (0.9), 487 (5.6), 389 (4.4), 319 (30.5)	719 (490)	0.35	54	0.20 (0.83)	−1.60 (−0.97)	1.80
2b[f]	742 (2.3), 673 (2.7), 507 (8.9), 448 (10.7), 397 (13.7), 323 (28.7)	h	h	h	0.46 (1.09)		
2c	651(1.2), 602(2.1), 479(11.0), 388 (10.9), 320 (40.9)[i,j]	698 (480)[i,j]		83[i,j]	0.23 (0.86)[k]	−1.63 (−1.00)	1.86[j]
N749	620(6.5), 585(6.0), 420(10.5), 329(18.5)[l]	820[l]		30[m]	0.16 (0.85)[l]	−1.40 (−0.71)	1.58

[a]Determined using $[Ru(dqp)_2](PF_6)_2$ (in MeOH/EtOH 1:4, Φ_{PL} = 2.0%)[48] as reference; solutions were purged with N_2. [b]Air-equilibrated solution. [c]Unless stated otherwise, redox half-wave potentials were determined by cyclic voltammetry using Bu_4NPF_6 as the supporting electrolyte and Fc^+/Fc as the internal standard; conversion to NHE scale by addition of 0.63 V[49] and 0.69 V[50] when the measurement was done in MeCN and DMF/MeOH (4:1 v/v), respectively. [d]Calculated using $E_{S^*} = E_{1/2,ox} - E_{0-0}$.[2] [e]Determined at the intersection of the absorption and emission spectra with the latter being normalized with respect to the lowest-energy absorption. [f]Measured in MeCN containing 0.5 M NEt_3. [g]Not measured due to low solubility. [h]Not observed with the used instrumental setup. [i]Measured in MeOH containing 0.5 M NEt_3. [j]Fully deprotonated species, see text. [k]Determined by square-wave voltammetry with the complex-anchored TiO_2 anode as the working electrode immersed in MeCN containing 0.5 M pyridine and 0.1 M Bu_4NPF_6 as the supporting electrolyte. [l]Measured in DMF/MeOH (4:1 v/v). [m]Measured in EtOH, taken from ref 4.
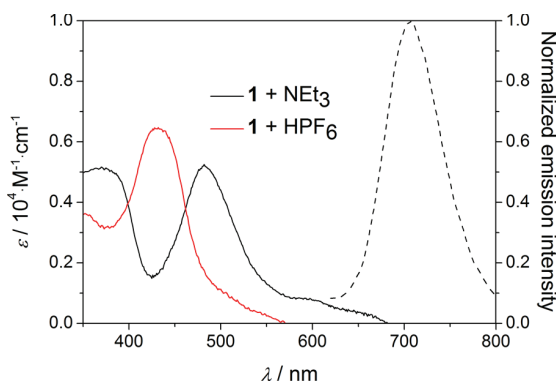
Figure 4. UV−vis absorption (solid) and room-temperature emission (dashed) spectra of **1** in the presence of NEt_3 and HPF_6 in MeCN.
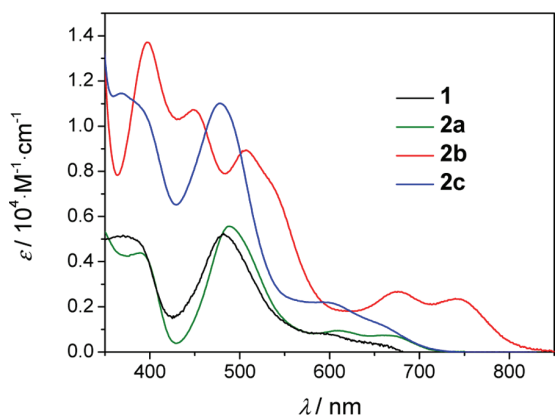
Figure 5. UV−vis absorption spectra of **1**, **2a**, **2b** (in MeCN + 0.5 M NEt_3), and **2c** (in MeOH + 0.5 M NEt_3).

being transferred to the triazolate rings. Thus, to provide a defined protonation state, the photophysical properties were determined in MeOH solution containing 0.5 M NEt_3 in order to ensure the complete deprotonation of the 1,2,3-triazolates. The UV−vis absorption and emission maxima are slightly hypsochromically shifted relative to **2a**, which is attributed to the LUMO destabilization by the three carboxylates. Notably, the E_{0-0} value determined for **2c** in solution (1.86 eV, Table 1) is therefore overestimated, which becomes obvious in view of

the onset of the incident photon-to-current efficiency (IPCE) spectrum (*vide infra*), which occurs at 700 nm; that is, the E_{0-0} value for **2c** featuring TiO_2-coordinated carboxylates is at least 1.77 eV.

Importantly, due to the presence of 0.5 M 4-*tert*-butylpyridine (tBP) in the DSSC electrolyte (*vide infra*), the two triazolates of **2c** are deprotonated under working conditions. This assessment is corroborated by the measurement of the Ru(III)/Ru(II) redox potential of **2c** by square-wave voltammetry in acetonitrile containing 0.5 M pyridine with a **2c**-anchored TiO_2 anode as the working electrode. The measured value of 0.86 V vs NHE is between the redox potentials of **2a** and **2b** and considerably less positive than that for the analogous complex featuring charge-neutral 1,2,3-triazoles (1.61 V vs NHE),[34,39] which supports the presence of two anionic triazolates. Notably, the redox potential of **2c** is sufficiently high to ensure efficient regeneration by the relevant $I_2^{•-}$/I^- redox couple (0.79 V vs NHE).[47] Despite the above-mentioned difficulties to accurately determine the E_{0-0} value, a lower limit of the excited-state redox potential of **2c** can be determined from the ground-state redox potential and the minimum E_{0-0} value, which corresponds to the onset in the IPCE spectrum (750 nm or 1.65 eV). On this basis, the excited-state redox potential is at least −0.79 V vs NHE, which is sufficiently more negative than the conduction band edge of TiO_2 (ca. −0.7 V vs NHE)[43] and should enable efficient electron injection into the semiconductor.

Dye-Sensitized Solar Cells. To investigate the performance of **2c** in the DSSC, commercially available test cells were assembled according to literature procedures (*vide infra*)[51] and an electrolyte composition typically used for **N749** was chosen.[5] The obtained parameters are reported in Table 2. Under identical conditions, the PCEs of **2c** and **N749** are 4.0% and 6.1%, respectively. The lower V_{OC} and J_{SC} achieved with **2c** (Figure 6) were expected in view of the higher degree of protonation, which lowers the TiO_2 conduction-band energy,[35] and the lower light-harvesting capability. However, the IPCE spectrum not only reflects the inferior light harvesting at longer wavelengths but also reveals a lower IPCE maximum (Figure 7). When coadsorbed with chenodeoxycholic acid (cheno), **2c** allows a slightly higher V_{OC} and a significantly improved J_{SC}, in line with much higher IPCE values, resulting in a promising PCE of 4.9%. The significant enhancement of the photocurrent in the presence of cheno suggests that the relatively low IPCE

Table 2. Selected DSSC Data for the Ruthenium(II) Complexes Measured under AM1.5 Light Conditions[a]

dye	cheno	V_{oc}/V	J_{sc}/ mA cm^{-2}	FF	PCE/%
2c	no	0.61	8.9	0.70	4.0
2c	yes	0.62	11.8	0.63	4.9
N749	no	0.69	12.7	0.66	6.1

[a]Conditions: TiO$_2$ layer thickness of 12 μm (20 nm particles) + 3 μm (400 nm particles), active area of 0.28 cm^2; acetonitrile-based electrolyte containing 0.6 M 1,3-dimethylimidazolium iodide, 0.06 M I$_2$, 0.1 M LiI, 0.5 M tBP, and 0.1 M guanidinium thiocyanate.
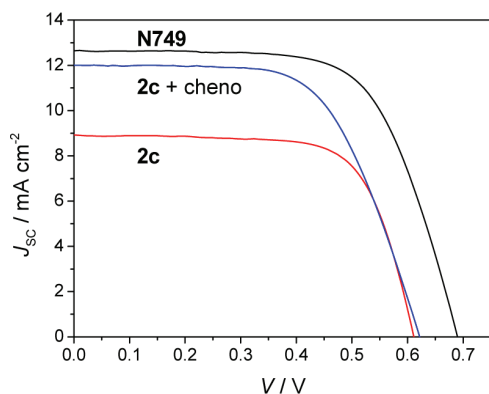
Figure 6. Selected J−V curves of **2c** and **N749** (see Table 2 for conditions).
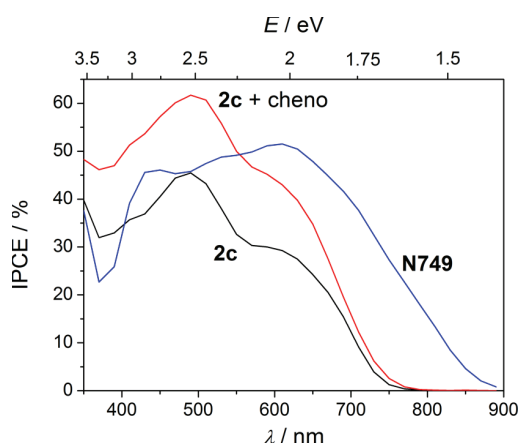
Figure 7. Photocurrent action spectra of **2c** and **N749**.

values observed in the absence of cheno are not caused by inefficient regeneration or injection but rather by more pronounced recombination reactions (*vide infra*). Similarly, it was reported that the PCE achieved with **N749** could be increased from 4.3 to 4.7% by coadsorption with cheno, although the higher PCE is mostly a result of an increased voltage.[52]

To better understand the effect of cheno, electrochemical impedance spectroscopy was performed (Figure S8).[16,51,53−56] A secondary effect is the lowering of the transport resistance (R_t), which is usually caused by a lowered TiO$_2$ conduction-band energy.[53] This effect may be ascribed to a reduced accessibility of the TiO$_2$ surface for the tBP electrolyte additive,[16] which is known to raise the conduction band.[57] The expected concomitant lowering of the recombination or charge-transfer resistance (R_{ct}) is apparently overcompensated

by the lowered recombination tendency (*cf.* Table 2) as the TiO$_2$ surface passivation is improved by cheno. Accordingly, the V_{oc} is slightly enhanced by cheno. As a further result of the lowered R_t and the increased R_{ct}, the injected electrons can be collected much more efficiently, which is reflected by a normalized diffusion length well above 1[53] if **2c** is coadsorbed with cheno (Figure S8), which is in line with a higher J_{sc}. Without cheno, **N749** allows a higher R_{ct} than **2c**, which leads to an intermediate normalized diffusion length when compared to **2c** with and without cheno (Figure S8). The slightly higher recombination tendency for the sensitizer **2c** suggests a less effective surface coverage than for **N749** and/or interactions between iodine and **2c**. Nonetheless, **2c** is not expected to leave larger voids on the TiO$_2$ surface, since, even in the absence of cheno, a promising performance (J_{sc} = 6.2 mA cm^{-2}, V_{oc} = 0.70 V, FF = 0.58, PCE = 2.7%) was achieved in an initial attempt using a [Co^{III}(bpy)$_3$](PF$_6$)$_3$/[Co^{II}(bpy)$_3$](PF$_6$)$_2$-containing electrolyte[14,58] (see SI). This is attributed to the decoration of **2c** with hexyl chains allowing a more effective protection of the TiO$_2$ surface from the bulky redox mediator and, thus, a diminution of recombination reactions, which are typically observed when using thiocyanate-based benchmark dyes and the same Co(III)/Co(II)-based redox shuttle.[14,59]

■ CONCLUSION

The new heteroleptic bis(tridentate) ruthenium(II) complex featuring 1,2,3-triazolates was accessed by a facile and modular synthesis and possesses photophysical and electrochemical properties suitable for DSSC application. In comparison to ruthenium(II) polypyridyl complexes ([Ru(tpy)$_2$](PF$_6$)$_2$), the presented compounds exhibit prolonged excited-state lifetimes and room-temperature emission. A promising DSSC performance was achieved with different types of electrolytes. Prospectively, the thiocyanate-free, bis(tridentate) sensitizer platform should enable an extended DSSC life span[18] and offers the potential to optimize the light-harvesting capability *via* attachment of additional chromophores at the central pyridine ring of the anionic ligand.[12,23]

■ EXPERIMENTAL SECTION

[Ru^{II}(tpy)(MeCN)$_3$](PF$_6$)$_2$,[34] [Ru^{II}(tcmtpy)(MeCN)$_3$](PF$_6$)$_2$,[34] 2,6-diethynylpyridine,[60] and azidomethyl pivalate[33] were synthesized according to literature procedures. Dry toluene was obtained from a Pure Solv MD-4-EN solvent purification system (Innovative Technologies Inc.). Triethylamine was dried over KOH. Methanol was dried by distillation over magnesium and kept under nitrogen using standard Schlenk techniques. Tcmtpy was purchased from hetcat. [Ru(Htctpy)(NCS)$_3$](NBu$_4$)$_3$ was purchased from Solaronix. All other chemicals were purchased from commercial suppliers and used as received. All reactions were performed in oven-dried flasks and were monitored by thin-layer chromatography (TLC) (silica gel on aluminum sheets with fluorescent dye F254, Merck KGaA). Microwave reactions were carried out using a Biotage Initiator Microwave synthesizer. NMR spectra have been recorded on a Bruker AVANCE 250 MHz, AVANCE 300 MHz or AVANCE 400 MHz instrument in deuterated solvents (euriso-top) at 25 °C. ^{1}H and ^{13}C resonances were assigned using appropriate 2D correlation spectra. Chemical shifts are reported in ppm using the solvent as internal standard. Matrix-assisted laser desorption-ionization time-of-flight (MALDI-TOF) mass spectra were obtained using an Ultraflex III TOF/TOF mass spectrometer with dithranol as matrix in reflector mode. High-resolution electro-spray-ionization time-of-flight mass spectrometry (ESI-Q-TOF MS) was performed on an ESI-(Q)-TOF-MS microTOF II (Bruker Daltonics) mass spectrometer. UV−vis absorption spectra were recorded on a Perkin-Elmer Lambda 750 UV/vis spectrophotometer,

and emission spectra on a Jasco FP6500. Measurements were carried out using 10^{-6} M solutions of respective solvents (spectroscopy grade) in 1 cm quartz cuvettes or on dye-loaded, transparent TiO_2 anodes (12 μm thick, 0.88 cm^2 active area, see the Cell Fabrication) at room temperature. Acid−base titration was carried out in aqueous solution containing Britton−Robinson buffer (0.04 M phosphoric acid, 0.04 M acetic acid, 0.04 M boronic acid).[61] The pH value was adjusted using 2 M aqueous solutions of hydrochloric acid and sodium hydroxide. The resulting spectral behavior was monitored recording UV−vis absorption and emission spectra at distinct pH values. The variation of absorbance and emission intensity was analyzed for selected wavelengths by fitting a sigmoidal Boltzmann function to the experimental data; the obtained turning points represent the pK_a values. Emission lifetimes are mostly obtained by time-correlated single-photon counting. Here, a Titan:Sapphire laser (Tsunami, Newport Spectra-Physics GmbH) is used as the light source. The repetition rate is reduced to 400 kHz by a pulse selector (model 3980, Newport Spectra-Physics GmbH). Afterwards, the fundamental beam of the Ti-Sapphire oscillator is frequency doubled in a second harmonic generator (Newport Spectra-Physics GmbH) to create the 500-nm pump beam. The emission is detected by a Becker & Hickel PMC-100-4 photon-counting module. For these measurements the instrumental response function was on the order of several nanoseconds due to filter fluorescence. Thus, for lifetime determination the first 10−15 ns after excitation were consequently ignored. In most cases a monoexponential fitting was carried out with the rest of the data points. However, both models yield the same numerical data for the respective longer lifetime being the subject of the discussion. Since the lifetimes reported are significantly longer than the instrumental response, we claim our results with a typical uncertainty of 10%. For some measurements, excitation was carried out at 390 nm and emission was detected by a Hamamatsu HPDTA streak camera *via* a suitable spectrograph. Here, the decay curves were obtained as the spectral integral, as no spectral relaxation was observed. Samples are prepared to yield an optical density of 0.1 at the excitation wavelength. Cyclic voltammetry measurements were performed on a Metrohm Autolab PGSTAT30 potentiostat with a standard three-electrode configuration using a graphite-disk working electrode, a platinum-rod auxiliary electrode, and a Ag/AgCl reference electrode; scan rates from 50 to 500 mV·s^{-1} were applied. The experiments were carried out in degassed solvents (spectroscopy grade) containing 0.1 M Bu_4NPF_6 salt (dried previously by heating at 110 °C and storing under vacuum). At the end of each measurement, ferrocene was added as an internal standard. All calculations are based on density functional theory (DFT). The geometries of the singlet ground state and the singly oxidized ground state have been optimized for all the ruthenium(II) complexes, presented herein. The hybrid functional B3LYP[62,63] has been selected in combination with the 6-31G* basis set for all atoms. To reproduce the measured absorption UV−vis spectrum, the lowest-lying 75 vertical singlet electronic excitation energies were calculated using time-dependent DFT (TD-DFT) at the S_0 optimized geometry. The TD-DFT calculations were performed in solution using acetonitrile as solvent with the polarization continuum model and with the same functional and basis set as in the optimizations.[64,65] All these calculations were performed with the Gaussian09 program package.[66] The analysis of the EDDM calculations were performed by GaussSum2.2.[67] Electron-density difference maps (density isovalue = 0.001), Kohn−Sham orbitals (MO isovalue = 0.04), and spin-density calculations (density isovalue = 0.004) were visualized by Gauss-View5.0.8.[66]

Cell Fabrication. Photoanodes were prefabricated by Dyesol, Inc. (Australia) with a screen-printable TiO_2 paste (18-NRT, Dyesol). The active area of the TiO_2 electrode is 0.28 cm^2 with a thickness of 12 μm (18-NRT) and 3 μm (WER4-O) on fluorine-doped tin-oxide (FTO; TEC15 (15 Ω cm^{-2})). TiO_2 substrates were treated with $TiCl_4$(aq) (0.05 M) at 70 °C for 30 min and subsequently rinsed with H_2O and EtOH and dried prior to heating. The electrodes were heated to 450 °C for 20 min under ambient atmosphere and allowed to cool to 80 °C before dipping into the dye solution. The anode was soaked overnight for 16 h in a methanol and ethanol solution (~0.25 mM)

containing the dyes **2c** and **N749**, respectively. The stained films were rinsed copiously with the solvent they were dipped in and subsequently dried. The cells were fabricated using a Pt-coated counter electrode (FTO TEC-15 (15 Ω cm^{-2})) that was heated to 450 °C for 15 min under ambient atmosphere and allowed to cool to room temperature prior to the assembling. Both electrodes were sandwiched with a 30 μm Surlyn (Dupont) gasket by resistive heating. An acetonitrile electrolyte solution, El 1 (0.6 M 1,3-dimethylimidazolium iodide (DMII), 0.06 M I_2, 0.1 M LiI, 0.5 M 4-*tert*-butylpyridine (tBP), and 0.1 M guanidinium thiocyanate (GuSCN)), El 2 (0.21 M [Co(bpy)$_3$](PF$_6$)$_2$, 0.033 M [Co(bpy)$_3$](PF$_6$)$_3$, 0.1 M LiClO$_4$, 0.5 M tBP), was introduced to the void *via* vacuum backfilling through a hole in the counter electrode. The hole was sealed with an aluminum-backed Bynel foil (Dyesol). After sealing, silver bus bars were added to all cells.[51,14]

Cell Characterization. Photovoltaic measurements were recorded with a Newport Oriel solar simulator (model 9225A1) equipped with a class A 150 W xenon light source powered by a Newport power supply (model 69907). The light output (area = 5 cm × 5 cm) was calibrated to AM 1.5 using a Newport Oriel correction filter to reduce the spectral mismatch in the region of 350−700 nm to less than 1.5%. The power output of the lamp was measured to 1 Sun (100 mW cm^{-2}) using a certified Si reference cell. The current−voltage ($I–V$) characteristic of each cell was obtained by applying an external potential bias to the cell and measuring the generated photocurrent with a Keithley digital source meter (model 2400). All cells were measured without a mask. IPCE measurements were performed on a QEX7 Solar Cell Spectral Response Measurement System from PV Instruments, Inc. The system was calibrated with a photodiode that was calibrated against NIST standard I755 with transfer uncertainty less than 0.5% between 400 and 1,000 nm and less than 1% at all other wavelengths. All measurements were carried out in AC mode at 4 Hz chopping frequency under a bias light between 0.01 and 0.1 sun. The system was calibrated and operated in Beam Power mode. Electrochemical impedance spectroscopy (EIS) was performed on a Gamry EIS300 potentiostat. All EIS experiments were performed in the dark and scanned the frequency range from 100 kHz to 0.5 Hz with a 10 mV voltage modulation applied to the bias.[51]

Synthesis of L1. According to the literature,[32,33] a mixture of aqueous HCHO (37%, 1.2 mL, 13.6 mmol), concentrated AcOH (96%, 0.14 mL, 2.1 mmol), and 1,4-dioxane (1.2 mL) was stirred at room temperature for 15 min. After the addition of sodium azide (153.3 mg, 2.36 mmol) and 2,6-diethynylpyridine (100 mg, 0.79 mmol), the mixture was stirred at room temperature for additional 10 min. Subsequently, concentrated aqueous solutions, first of sodium ascorbate (63 mg, 0.32 mmol) and then of $CuSO_4$ (13 mg, 0.08 mmol), were added and the resulting mixture was stirred at room temperature for 24 h. After the complete conversion of the alkyne was confirmed by TLC, EDTA was added (30 mg, 0.1 mmol), and stirring was maintained for 2h. After addition of an excess of water, the resulting suspension was filtered and washed with a minimal amount of water, and the obtained solid was kept. Additionally, the filtrate was extracted 3 times with ethyl acetate, and the organic solvent was removed *in vacuo*. The obtained solids were combined, MeOH/H_2O (1:1, 6 mL), solid NaOH (140 mg, 3.5 mmol) was added, and the mixture was stirred at room temperature for 24 h. After neutralization with 1 M HCl (3.5 mL) and addition of H_2O (30 mL), the formed precipitate was filtered, washed with water, and dried *in vacuo* to yield 128 mg (0.6 mmol, 76%) of a white solid. ^{1}H NMR (400 MHz, DMSO-d_6, ppm) δ = 15.37 (s, 2H, N*H*), 8.53 (s, 2H, N^{trz}−*H*), 8.29−7.67 (m, 3H, *H*$^{3a',4a',5a'}$). ^{13}C NMR (100 MHz, DMSO-d_6, ppm) δ = 149.37, 145.43, 138.27, 128.43, 118.98 MS (MALDI-TOF, dithranol): calcd for $C_{22}H_{29}N$ ([M + H]$^+$): m/z = 214.0834; found: m/z = 214.0640.

Synthesis of 2,6-Di(oct-1-yn-1-yl)pyridine. Under a nitrogen atmosphere, 2,6-dibromopyridine (2.34 g, 9.87 mmol), Pd(PPh$_3$)$_4$ (583 mg, 0.51 mmol, 5 mol-%), and CuI (101.2 mg, 0.53 mmol, 5 mol-%) were suspended in deaerated toluene/triethylamine (4:1, *v/v* 53 mL). The resulting suspension was additionally purged with nitrogen. Subsequently, 1-octyne (4.15 mL, 27.87 mmol, 2.8 equiv)

was added dropwise at room temperature to the stirred suspension. The reaction mixture was heated to 55 °C with an oil bath, and the reaction was monitored by GC-MS. After 72 h, the reaction mixture was allowed to cool to room temperature and filtered, and the remaining solid was washed with toluene. The filtrate was evaporated *in vacuo*, and the obtained solid was dissolved in CH_2Cl_2 and extracted with aqueous NH_4Cl to remove Cu(I). The organic phase was dried over Na_2SO_4, concentrated *in vacuo*, and purified by column chromatography (silica, CH_2Cl_2/n-hexane 1:1; R_f = 0.4). The solvents were evaporated *in vacuo* to yield 2.07 g (7.00 mmol, 71%) of a yellow oil. ^{1}H NMR (250 MHz, CD_2Cl_2, ppm) δ = 7.53 (t, ^3J = 7.8 Hz, 1H, $H^{4a'}$), 7.23 (d, ^3J = 7.8 Hz, 2H, $H^{3a',5a'}$), 2.42 (t, ^3J = 7.0 Hz, 4H, CC–CH_2–CH_2–), 1.71–1.53 (m, 4H, CC–CH_2–CH_2–), 1.53–1.19 (m, 12H, –CH_2–), 0.90 (t, ^3J = 6.6 Hz, 6H, CH_3); ^{13}C NMR (63 MHz, CD_2Cl_2, ppm) δ = 144.3, 136.5, 125.7, 91.3, 80.5, 31.8, 29.1, 28.8, 22.9, 19.6, 14.2 ppm; MS (HR ESI-Q-TOF): calcd for $C_{22}H_{29}N$ ([M + H]$^+$): m/z = 296.2371; found: m/z = 296.2460.

Synthesis of PL2. A 20 mL microwave vial was charged with 2,6-di(oct-1-yn-1-yl)pyridine (1.27 g, 4.29 mmol) and azidomethyl pivalate (1.67 g, 10.65 mmol, 2.5 equiv). The vial was capped and heated to 100 °C in an oil bath for 72 h. The completion of the reaction was confirmed by TLC (alumina, CH_2Cl_2) and GC-MS. All volatiles were removed *in vacuo*, and the remaining solid was subjected to column chromatography (alumina, CH_2Cl_2/n-hexane, 3:1). All product fractions (irrespective of the regioisomer) were combined to yield 1.99 g (3.27 mmol, 76%) of a brown oil. For the NMR analysis, the asymmetric product (see Scheme 1) was used exemplarily. ^{1}H NMR (250 MHz, CD_2Cl_2, ppm) δ = 8.28 (d, ^3J = 8.0 Hz, 1H, $H^{3a'}$), 7.94 (t, ^3J = 7.9 Hz, 1H, $H^{4a'}$), 7.38 (d, ^3J = 7.6 Hz, 1H, $H^{5a'}$), 6.44 (s, 2H, N–CH_2–O), 6.27 (s, 2H, N^{trz}–CH_2–O), 3.33–2.99 (m, 2H, C^{5a}–CH_2–CH_2), 2.88–2.67 (m, 2H, C$^{5a''}$–CH_2–CH_2), 1.79–1.45 (m, 4H, C$^{5a,5a''}$–CH_2–CH_2), 1.35–1.07 (m, 21H, CH_2, $H^{tert\text{-}butyl}$), 0.96 (s, 9H, –CH_3), 0.92–0.59 (m, 6H, $H^{tert\text{-}butyl}$); ^{13}C NMR (63 MHz, CD_2Cl_2, ppm) δ = 177.1, 176.7, 152.9, 147.2, 147.1, 143.0, 138.4, 138.0, 133.5, 123.4, 121.5, 70.3, 69.1, 39.1, 38.9, 31.8, 31.7, 29.6, 29.4, 29.2, 29.2, 27.0, 26.8, 25.5, 23.5, 22.9, 22.8, 14.2, 14.1; MS (HR ESI-Q-TOF): calcd for $C_{33}H_{52}N_7O_4$ ([M + H]$^+$): m/z = 610.4081; found: m/z = 610.4084.

Synthesis of L2. According to the literature,[33] PL2 (1.4 g, 2.29 mmol) and NaOH (210 mg, 5.25 mmol, 4.4 equiv) were dissolved in $MeOH/H_2O$ (1:1, v/v 30 mL) and the mixture was stirred at room temperature. The full conversion of the educt was determined by TLC (alumina, CH_2Cl_2). After 24 h, the reaction mixture was dropped into HCl_{aq} (0.175 M) and, subsequently, neutralized with $NaHCO_3$. The precipitated product was filtered, washed with water, and dried *in vacuo* to yield 650 mg (1.71 mmol, 74%) of a colorless solid. ^{1}H NMR (250 MHz, DMSO-d_6, ppm) δ = 15.20 (s, 1H, N–H), 14.80 (s, 1H, N–H), 7.93 (m, 3H, $H^{3a',4a',5a'}$), 3.26–2.88 (m, 4H, C$^{5a,5a''}$–CH_2–), 1.80–1.43 (m, 4H, C$^{5a,5a''}$–CH_2–CH_2–), 1.38–1.04 (m, 12H, –CH_2–), 0.85–0.63 (m, 6H, –CH_3). ^{13}C NMR (63 MHz, DMSO-d_6, ppm) δ = 151.6, 151.1, 145.2, 142.7, 141.1, 137.6, 135.9, 120.4, 112.0, 119.7, 119.3, 31.0, 30.9, 28.2, 25.2, 22.8, 21.9, 13.8; MS (HR ESI-Q-TOF): calcd for $C_{21}H_{31}N_7Na$ ([M + Na]$^+$): m/z = 404.2538; found: m/z = 404.2513. Elem. anal. calcd for $C_{21}H_{31}N_7$ (381.52): C, 66.11%; H, 8.19%; N, 25.70%; found: C, 64.93%; H, 8.78%; N, 25.82%.

Synthesis of 1. A 10 mL microwave vial was charged with L1 (50 mg, 0.23 mmol), [Ru(tpy)(MeCN)$_3$](PF$_6$)$_2$ (175 mg, 0.23 mmol), and EtOH (8 mL). The vial was capped and the suspension was purged with nitrogen for 10 min. Subsequently, the mixture was heated to 150 °C for 30 min in the microwave reactor. NEt$_3$ (1 mL) was added to the reaction mixture to complete the precipitation. The dark precipitate was filtered and washed thoroughly with MeOH/NEt$_3$ (9:1, v/v) and, subsequently, with CH_2Cl_2. The obtained solid was allowed to dry upon standing, yielding 99 mg (0.18 mmol, 77%) of a dark brown solid. Due to the low solubility of the charge-neutral complex, some drops of trifluoroacetic acid (TFA) were added for the NMR analysis. A ^{13}C NMR spectrum could not be recorded, owing to the low solubility. ^{1}H NMR (400 MHz, CD_2Cl_2 + CF_3COOH, ppm) δ = 8.68 (s, 2H, $H^{5a,5a''}$), 8.48 (d, ^3J = 8.1, 2H, $H^{3',5'}$), 8.40–8.21 (m, 6H,

$H^{3a',4a',5a', 4', 3,3''}$), 7.91 (td, ^3J = 7.9 Hz, ^4J = 1.5 Hz, 2H, $H^{4,4''}$), 7.29 (d, ^3J = 4.9 Hz, 2H, $H^{6,6''}$), 7.18 (ddd, ^3J = 7.5, 5.5 Hz, ^4J = 1.2 Hz, 2H, $H^{5,5''}$); MS (MALDI-TOF, dithranol): calcd for $C_{36}H_{41}N_{10}Ru$ ([M + H]$^+$): m/z = 547.0691; found: m/z = 547.0840.

Note: Under the reaction conditions, a partial triazole *N*-alkylation,[68] presumably due to the formation of a carbenium ion from the alcohol solvent under the acidic reaction conditions was observed; however, the minor side product was easily removed by trituration of the reaction mixture with MeOH/NEt$_3$ (9:1, v/v). Nonetheless, TEGDME was chosen as solvent in case of **2b** (*vide infra*) in order to circumvent this side reaction.

Synthesis of 2a. A 20 mL microwave vial was charged with L2 (160 mg, 0.419 mmol), [Ru(tpy)(MeCN)$_3$](PF$_6$)$_2$ (313 mg, 0.419 mmol), and EtOH (17 mL). The vial was capped and the suspension purged with nitrogen for 10 min. Subsequently, the mixture was heated to 160 °C for 30 min in the microwave reactor. The full conversion of the precursor was proven by TLC (silica, MeCN/H$_2$O/ aq KNO$_3$ 40:4:1). NEt$_3$ was added to the crude product mixture to ensure complete deprotonation. Afterwards, the black solid was filtered and thoroughly washed with EtOH/NEt$_3$ (9:1, v/v). The solid was dried and suspended in MeOH/NEt$_3$ (9:1, v/v), filtered, washed again with MeOH/NEt$_3$ (9:1, v/v), and dried to yield 215 mg (0.301 mmol, 72%) of a black solid. Due to the low solubility of the charge-neutral complex, TFA was added for NMR analysis. ^{1}H NMR (400 MHz, CD_2Cl_2 + CF_3COOH, ppm) δ = 8.45 (d, ^3J = 8.1 Hz, 2H, $H^{3',5'}$), 8.32–8.19 (m, 4H, $H^{3,3'',4',4a'}$), 8.04 (d, ^3J = 8.1 Hz, 2H, $H^{3a',5a'}$), 7.87 (t, ^3J = 7.8 Hz, 2H, $H^{4,4''}$), 7.26 (d, ^3J = 5.1 Hz, 2H, $H^{6, 6''}$), 7.15 (d, ^3J = 6.4 Hz, 2H, $H^{5, 5''}$), 3.23–3.04 (m, 4H, C$^{5a,5a''}$–CH_2–), 1.86–1.64 (m, 4H, C$^{5a,5a''}$–CH_2–CH_2–), 1.48–1.17 (m, 12H, –CH_2–), 1.04–0.77 (m, 6H, –CH_3); ^{13}C NMR (100 MHz, CD_2Cl_2 + CF_3COOH, ppm) δ = 159.0, 156.7, 152.0, 151.2, 144.1, 141.1, 138.1, 137.1, 135.8, 127.6, 124.1, 122.7, 118.6, 31.5, 29.1, 28.6, 24.0, 22.8, 14.0; MS (HR ESI-Q-TOF): calcd for $C_{36}H_{41}N_{10}Ru$ ([M + H]$^+$): m/z = 715.2550; found: m/z = 715.2328.

Synthesis of 2b. A 10 mL microwave vial was loaded with [Ru(tcmtpy)(MeCN)$_3$](PF$_6$)$_2$ (80 mg, 0.086 mmol), L2 (33 mg, 0.086 mmol), and TEGDME (4.8 mL) The vial was capped, and the solution was purged with nitrogen for 10 min. Subsequently, the reaction mixture was heated to 150 °C for 30 min in the microwave reactor. After the full conversion of [Ru(tcmtpy)(MeCN)$_3$](PF$_6$)$_2$ was confirmed by TLC (silica, MeCN/H$_2$O/aq KNO$_3$ 40:4:1), the reaction mixture was dropped into H$_2$O and the precipitate was filtered, washed with H$_2$O, rinsed with MeCN, and subjected to column chromatography (silica, MeCN/MeOH 9:1). Subsequently, the product was precipitated in H$_2$O from a concentrated MeCN solution, additionally washed with H$_2$O, and rinsed with MeCN. After evaporation of the solvent *in vacuo*, 44 mg (0.049 mmol, 58%) of a red solid were obtained. ^{1}H NMR (400 MHz, CD_2Cl_2, ppm) δ = 9.08 (s, 2H, $H^{3',5'}$), 8.85 (s, 2H, $H^{3,3''}$), 8.04 (t, J = 7.9 Hz, 1H, $H^{4a'}$), 7.71 (d, J = 8.0 Hz, 2H, $H^{3a',5a'}$), 7.62 (d, J = 4.3 Hz, 2H, $H^{5,5''}$), 7.58 (d, J = 5.8 Hz, 2H, $H^{6,6''}$), 4.16 (s, 3H, –COOCH$_3$′), 3.95 (s, 6H, –COOCH$_3$), 2.94 (t, 4H, C$^{5a,5a''}$–CH_2–), 1.75–1.62 (m, 4H, C$^{5a,5a''}$–CH_2–CH_2–), 1.34 (m, 12H, –CH_2–), 0.87 (d, J = 6.5 Hz, 6H, –CH_3); ^{13}C NMR (100 MHz, CD_2Cl_2, ppm) δ = 165.1, 164.2, 159.6, 157.3, 152.4, 152.0, 146.8, 141.0, 137.2, 136.8, 132.4, 126.3, 122.2, 121.5, 114.7, 53.5, 53.4, 32.0, 29.8, 29.6, 26.9, 23.0, 14.2; MS (HR ESI-Q-TOF): calcd for $C_{42}H_{47}N_{10}O_6Ru$ ([M + H]$^+$): m/z = 889.2730; found: m/z = 889.2861.

Synthesis of 2c. According to the literature,[12,69] **2b** (30 mg, 0.03 mmol) was suspended in DMF/NEt$_3$/H$_2$O (3:1:1, v/v 3 mL) and heated to reflux under a nitrogen atmosphere. After 36 h, the full conversion was confirmed with MS (MALDI ToF) and the solvents were evaporated *in vacuo*. The resultant solid was suspended in CH_2Cl_2 and collected by centrifugation. The solvent was decanted, and this procedure was repeated twice with CH_2Cl_2 and once with MeOH. The remaining solid was dried *in vacuo* to obtain 16 mg (0.02 mmol, 56%) of a brown solid. ^{1}H NMR (400 MHz, MeOD, ppm) δ = 9.23 (s, 2H, $H^{3',5'}$), 9.02 (s, 2H, $H^{3,3''}$), 8.36 (t, J = 7.9 Hz, 1H, $H^{4a'}$), 8.22 (d, J = 8.1 Hz, 2H, $H^{3a',5a'}$), 7.70 (d, J = 5.7 Hz, 2H, $H^{5,5''}$), 7.58 (d, J = 5.5 Hz, 2H, $H^{6,6''}$), 3.19–3.10 (m, 4H, C$^{5a,5a''}$–CH_2–), 1.84–

1.72 (m, 4H, $C^{5a,5a''}-CH_2-CH_2-$), 1.48−1.25 (m, 12H, $-CH_2-$), 0.88 (t, J = 7.0 Hz, 6H, $-CH_3$); MS (MALDI-TOF, dithranol): calcd for $C_{39}H_{40}N_{10}O_6Ru$ ([M + H]$^+$): m/z = 847.2780; found: m/z = 847.2221.

ASSOCIATED CONTENT

Ⓢ Supporting Information

Additional computational, photophysical, electrochemical, and EIS data as well as NMR and MS spectra. This material is available free of charge *via* the Internet at http://pubs.acs.org.

AUTHOR INFORMATION

Corresponding Author

*E-mail: benjamin.dietzek@uni-jena.de (B.D.), cberling@chem.ubc.ca (C.P.B.), ulrich.schubert@uni-jena.de (U.S.S.).

Author Contributions

△S.S. and B.S. contributed equally to this work.

Notes

The authors declare no competing financial interests.

ACKNOWLEDGMENTS

REFERENCES

(1) O'Regan, B.; Grätzel, M. *Nature* **1991**, *353*, 737.

(2) Hagfeldt, A.; Boschloo, G.; Sun, L.; Kloo, L.; Pettersson, H. *Chem. Rev.* **2010**, *110*, 6595.

(3) Yella, A.; Lee, H.-W.; Tsao, H. N.; Yi, C.; Chandiran, A. K.; Nazeeruddin, M. K.; Diau, E. W.-G.; Yeh, C.-Y.; Zakeeruddin, S. M.; Grätzel, M. *Science* **2011**, *334*, 629.

(4) Nazeeruddin, M. K.; Péchy, P.; Renouard, T.; Zakeeruddin, S. M.; Humphry-Baker, R.; Comte, P.; Liska, P.; Cevey, L.; Costa, E.; Shklover, V.; Spiccia, L.; Deacon, G. B.; Bignozzi, C. A.; Grätzel, M. *J. Am. Chem. Soc.* **2001**, *123*, 1613.

(5) Chiba, Y.; Islam, A.; Watanabe, Y.; Komiya, R.; Koide, N.; Han, L. *Jpn. J. Appl. Phys.* **2006**, *45*, L638.

(6) Reynal, A.; Palomares, E. *Eur. J. Inorg. Chem.* **2011**, 4509.

(7) Han, L.; Islam, A.; Chen, H.; Malapaka, C.; Chiranjeevi, B.; Zhang, S.; Yang, X.; Yanagida, M. *Energy Environ. Sci.* **2012**, *5*, 6057.

(8) Nour-Mohhamadi, F.; Nguyen, S. D.; Boschloo, G.; Hagfeldt, A.; Lund, T. *J. Phys. Chem. B* **2005**, *109*, 22413.

(9) Nguyen, P. T.; Degn, R.; Nguyen, H. T.; Lund, T. *Sol. Energy Mater. Sol. Cells* **2009**, *93*, 1939.

(10) Bessho, T.; Yoneda, E.; Yum, J.-H.; Guglielmi, M.; Tavernelli, I.; Imai, H.; Rothlisberger, U.; Nazeeruddin, M. K.; Grätzel, M. *J. Am. Chem. Soc.* **2009**, *131*, 5930.

(11) Wadman, S. H.; Kroon, J. M.; Bakker, K.; Lutz, M.; Spek, A. L.; van Klink, G. P. M.; van Koten, G. *Chem. Commun.* **2007**, 1907.

(12) Robson, K. C. D.; Koivisto, B. D.; Yella, A.; Sporinova, B.; Nazeeruddin, M. K.; Baumgartner, T.; Grätzel, M.; Berlinguette, C. P. *Inorg. Chem.* **2011**, *50*, 5494.

(13) Pogozhev, D. V.; Bezdek, M. J.; Schauer, P. A.; Berlinguette, C. P. *Inorg. Chem.* **2013**, *52*, 3001.

(14) Bomben, P. G.; Gordon, T. J.; Schott, E.; Berlinguette, C. P. *Angew. Chem., Int. Ed.* **2011**, *50*, 10682.

(15) Kisserwan, H.; Ghaddar, T. H. *Dalton Trans.* **2011**, *40*, 3877.

(16) Schulze, B.; Brown, D. G.; Robson, K. C. D.; Friebe, C.; Jäger, M.; Birckner, E.; Berlinguette, C. P.; Schubert, U. S. *Chem.—Eur. J.* **2013**, *19*, 14171.

(17) Dragonetti, C.; Colombo, A.; Magni, M.; Mussini, P.; Nisic, F.; Roberto, D.; Ugo, R.; Valore, A.; Valsecchi, A.; Salvatori, P.; Lobello, M. G.; De Angelis, F. *Inorg. Chem.* **2013**, *52*, 10723.

(18) Hsu, C.-W.; Ho, S.-T.; Wu, K.-L.; Chi, Y.; Liu, S.-H.; Chou, P.-T. *Energy Environ. Sci.* **2012**, *5*, 7549.

(19) Yeh, H.-H.; Ho, S.-T.; Chi, Y.; Clifford, J. N.; Palomares, E.; Liu, S.-H.; Chou, P.-T. *J. Mater. Chem. A* **2013**, *1*, 7681.

(20) Wang, S.-W.; Wu, K.-L.; Ghadiri, E.; Lobello, M. G.; Ho, S.-T.; Chi, Y.; Moser, J.-E.; De Angelis, F.; Grätzel, M.; Nazeeruddin, M. K. *Chem. Sci.* **2013**, *4*, 2423.

(21) Wu, K.-L.; Li, C.-H.; Chi, Y.; Clifford, J. N.; Cabau, L.; Palomares, E.; Cheng, Y.-M.; Pan, H.-A.; Chou, P.-T. *J. Am. Chem. Soc.* **2012**, *134*, 7488.

(22) Wu, K.-L.; Hsu, H.-C.; Chen, K.; Chi, Y.; Chung, M.-W.; Liu, W.-H.; Chou, P.-T. *Chem. Commun.* **2010**, *46*, 5124.

(23) Chou, C.-C.; Wu, K.-L.; Chi, Y.; Hu, W.-P.; Yu, S. J.; Lee, G.-H.; Lin, C.-L.; Chou, P.-T. *Angew. Chem., Int. Ed.* **2011**, *50*, 2054.

(24) Bomben, P. G.; Robson, K. C. D.; Koivisto, B. D.; Berlinguette, C. P. *Coord. Chem. Rev.* **2012**, *256*, 1438.

(25) Wang, M.; Moon, S.-J.; Zhou, D.; Le Formal, F.; Cevey-Ha, N.-L.; Humphry-Baker, R.; Grätzel, C.; Wang, P.; Zakeeruddin, S. M.; Grätzel, M. *Adv. Funct. Mater.* **2010**, *20*, 1821.

(26) Wang, P.; Zakeeruddin, S. M.; Moser, J. E.; Nazeeruddin, M. K.; Sekiguchi, T.; Grätzel, M. *Nat. Mater.* **2003**, *2*, 402.

(27) Zakeeruddin, S. M.; Nazeeruddin, M. K.; Humphry-Baker, R.; Péchy, P.; Quagliotto, P.; Barolo, C.; Viscardi, G.; Grätzel, M. *Langmuir* **2002**, *18*, 952.

(28) Crowley, J. D.; McMorran, D. A. In *Topics in Heterocyclic Chemistry: Click Triazoles*; Košmrlj, J., Ed.; Springer: Berlin Heidelberg, 2012; Vol. 28, p 31.

(29) Struthers, H.; Mindt, T. L.; Schibli, R. *Dalton Trans.* **2010**, *39*, 675.

(30) Schulze, B.; Schubert, U. S. *Chem. Soc. Rev.*, in press, DOI: 10.1039/c3cs60386e.

(31) Duati, M.; Tasca, S.; Lynch, F. C.; Bohlen, H.; Vos, J. G.; Stagni, S.; Ward, M. D. *Inorg. Chem.* **2003**, *42*, 8377.

(32) Kalisiak, J.; Sharpless, K. B.; Fokin, V. V. *Org. Lett.* **2008**, *10*, 3171.

(33) Loren, J. C.; Krasiński, A.; Fokin, V. V.; Sharpless, K. B. *Synlett* **2005**, 2847.

(34) Schulze, B.; Escudero, D.; Friebe, C.; Siebert, R.; Görls, H.; Sinn, S.; Thomas, M.; Mai, S.; Popp, J.; Dietzek, B.; González, L.; Schubert, U. S. *Chem.—Eur. J.* **2012**, *18*, 4010.

(35) Nazeeruddin, M. K.; Humphry-Baker, R.; Liska, P.; Grätzel, M. *J. Phys. Chem. B* **2003**, *107*, 8981.

(36) Benkö, G.; Kallioinen, J.; Myllyperkiö, P.; Trif, F.; Korppi-Tommola, J. E. I.; Yartsev, A. P.; Sundström, V. *J. Phys. Chem. B* **2004**, *108*, 2862.

(37) Clifford, J. N.; Palomares, E.; Nazeeruddin, M. K.; Grätzel, M.; Durrant, J. R. *J. Phys. Chem. C* **2007**, *111*, 6561.

(38) Jeon, J.; Goddard, W. A., III; Kim, H. *J. Am. Chem. Soc.* **2013**, *135*, 2431.

(39) Schulze, B.; Friebe, C.; Hager, M. D.; Winter, A.; Hoogenboom, R.; Görls, H.; Schubert, U. S. *Dalton Trans.* **2009**, 787.

(40) Duati, M.; Fanni, S.; Vos, J. G. *Inorg. Chem. Commun.* **2000**, *3*, 68.

(41) Buchanan, B. E.; Vos, J. G.; Kaneko, M.; van der Putten, W. J. M.; Kelly, J. M.; Hage, R.; de Graaff, R. A. G.; Prins, R.; Haasnoot, J. G.; Reedijk, J. *J. Chem. Soc., Dalton Trans.* **1990**, 2425.

(42) Amini, A.; Harriman, A.; Mayeux, A. *Phys. Chem. Chem. Phys.* **2004**, *6*, 1157.

(43) Listorti, A.; O'Regan, B.; Durrant, J. R. *Chem. Mater.* **2011**, *23*, 3381.

(44) Katritzky, A. R.; Ramsden, C. A.; Joule, J. A.; Zhdankin, V. V. In *Handbook of Heterocyclic Chemistry*, 3rd ed; Elsevier: Amsterdam, 2010; p 473.

(45) Lancaster, K. M.; Gerken, J. B.; Durrell, A. C.; Palmer, J. H.; Gray, H. B. *Coord. Chem. Rev.* **2010**, *254*, 1803.

(46) Thompson, D. W.; Ito, A.; Meyer, T. J. *Pure Appl. Chem.* **2013**, *85*, 1257.

(47) Boschloo, G.; Gibson, E. A.; Hagfeldt, A. *J. Phys. Chem. Lett.* **2011**, *2*, 3016.

(48) Abrahamsson, M.; Jäger, M.; Österman, T.; Eriksson, L.; Persson, P.; Becker, H.-C.; Johansson, O.; Hammarström, L. *J. Am. Chem. Soc.* **2006**, *128*, 12616.

(49) Pavlishchuk, V. V.; Addison, A. W. *Inorg. Chim. Acta* **2000**, *298*, 97.

(50) Connelly, N. G.; Geiger, W. E. *Chem. Rev.* **1996**, *96*, 877.

(51) Bomben, P. G.; Borau-Garcia, J.; Berlinguette, C. P. *Chem. Commun.* **2012**, *48*, 5599.

(52) Lee, K.-M.; Suryanarayanan, V.; Ho, K.-C.; Justin Thomas, K. R.; Lin, J. T. *Sol. Energy Mater. Sol. Cells* **2007**, *91*, 1426.

(53) Fabregat-Santiago, F.; Bisquert, J.; Garcia-Belmonte, G.; Boschloo, G.; Hagfeldt, A. *Sol. Energy Mater. Sol. Cells* **2005**, *87*, 117.

(54) Bisquert, J. *Phys. Chem. Chem. Phys.* **2003**, *5*, 5360.

(55) Bisquert, J.; Fabregat-Santiago, F. In *Dye-sensitized Solar Cells*, 1st ed.; Kalyanasundaram, K., Ed.; EPFL Press: Lausanne, 2010; p 457.

(56) Fabregat-Santiago, F.; Garcia-Belmonte, G.; Mora-Seró, I.; Bisquert, J. *Phys. Chem. Chem. Phys.* **2011**, *13*, 9083.

(57) Yu, Z.; Vlachopoulos, N.; Gorlov, M.; Kloo, L. *Dalton Trans.* **2011**, *40*, 10289.

(58) Hamann, T. W. *Dalton Trans.* **2012**, *41*, 3111.

(59) Klahr, B. M.; Hamann, T. W. *J. Phys. Chem. C* **2009**, *113*, 14040.

(60) Shin, Y.; Fryxell, G. E.; Johnson, C. A., II; Haley, M. M. *Chem. Mater.* **2008**, *20*, 981.

(61) Britton, H. T. S.; Robinson, R. A. *J. Chem. Soc.* **1931**, 1456.

(62) Becke, A. D. *J. Chem. Phys.* **1993**, *98*, 5648.

(63) Lee, C.; Yang, W.; Parr, R. G. *Phys. Rev. B* **1988**, *37*, 785.

(64) Mennucci, B.; Tomasi, J. *J. Chem. Phys.* **1997**, *106*, 5151.

(65) Cossi, M.; Barone, V.; Mennucci, B.; Tomasi, J. *Chem. Phys. Lett.* **1998**, *286*, 253.

(66) Frisch, M. J.; Trucks, G. W.; Schlegel, H. B.; Scuseria, G. E.; Robb, M. A.; Cheeseman, J. R.; Scalmani, G.; Barone, V.; Mennucci, B.; Petersson, G. A.; Nakatsuji, H.; Caricato, M.; Li, X.; Hratchian, H. P.; Izmaylov, A. F.; Bloino, J.; Zheng, G.; Sonnenberg, J. L.; Hada, M.; Ehara, M.; Toyota, K.; Fukuda, R.; Hasegawa, J.; Ishida, M.; Nakajima, T.; Honda, Y.; Kitao, O.; Nakai, H.; Vreven, T.; Montgomery, J. A.; Peralta, J. E.; Ogliaro, F.; Bearpark, M.; Heyd, J. J.; Brothers, E.; Kudin, K. N.; Staroverov, V. N.; Kobayashi, R.; Normand, J.; Raghavachari, K.; Rendell, A.; Burant, J. C.; Iyengar, S. S.; Tomasi, J.; Cossi, M.; Rega, N.; Millam, J. M.; Klene, M.; Knox, J. E.; Cross, J. B.; Bakken, V.; Adamo, C.; Jaramillo, J.; Gomperts, R.; Stratmann, R. E.; Yazyev, O.; Austin, A. J.; Cammi, R.; Pomelli, C.; Ochterski, J. W.; Martin, R. L.; Morokuma, K.; Zakrzewski, V. G.; Voth, G. A.; Salvador, P.; Dannenberg, J. J.; Dapprich, S.; Daniels, A. D.; Farkas; Foresman, J. B.; Ortiz, J. V.; Cioslowski, J.; Fox, D. J., *Gaussian 09*, Revision B.01; Gaussian Inc.: Wallingford, CT, 2009.

(67) O'Boyle, N. M.; Tenderholt, A. L.; Langner, K. M. *J. Comput. Chem.* **2008**, *29*, 839.

(68) Timokhin, B. V.; Golubin, A. I.; Vysotskaya, O. V.; Kron, V. A.; Oparina, L. A.; Gusarova, N. K.; Trofimov, B. A. *Chem. Heterocycl. Compd.* **2002**, *38*, 981.

(69) Bomben, P. G.; Thériault, K. D.; Berlinguette, C. P. *Eur. J. Inorg. Chem.* **2011**, 1806.

Publication A7:

"Cyclometalated ruthenium(II) complexes featuring tridentate click-derived ligands for dye-sensitized solar cell applications"

B. Schulze, D. G. Brown, K. C. D. Robson, C. Friebe, M. Jäger, E. Birckner, C. P. Berlinguette, U. S. Schubert

Chem. Eur. J. **2013**, *19*, 14171−14180.
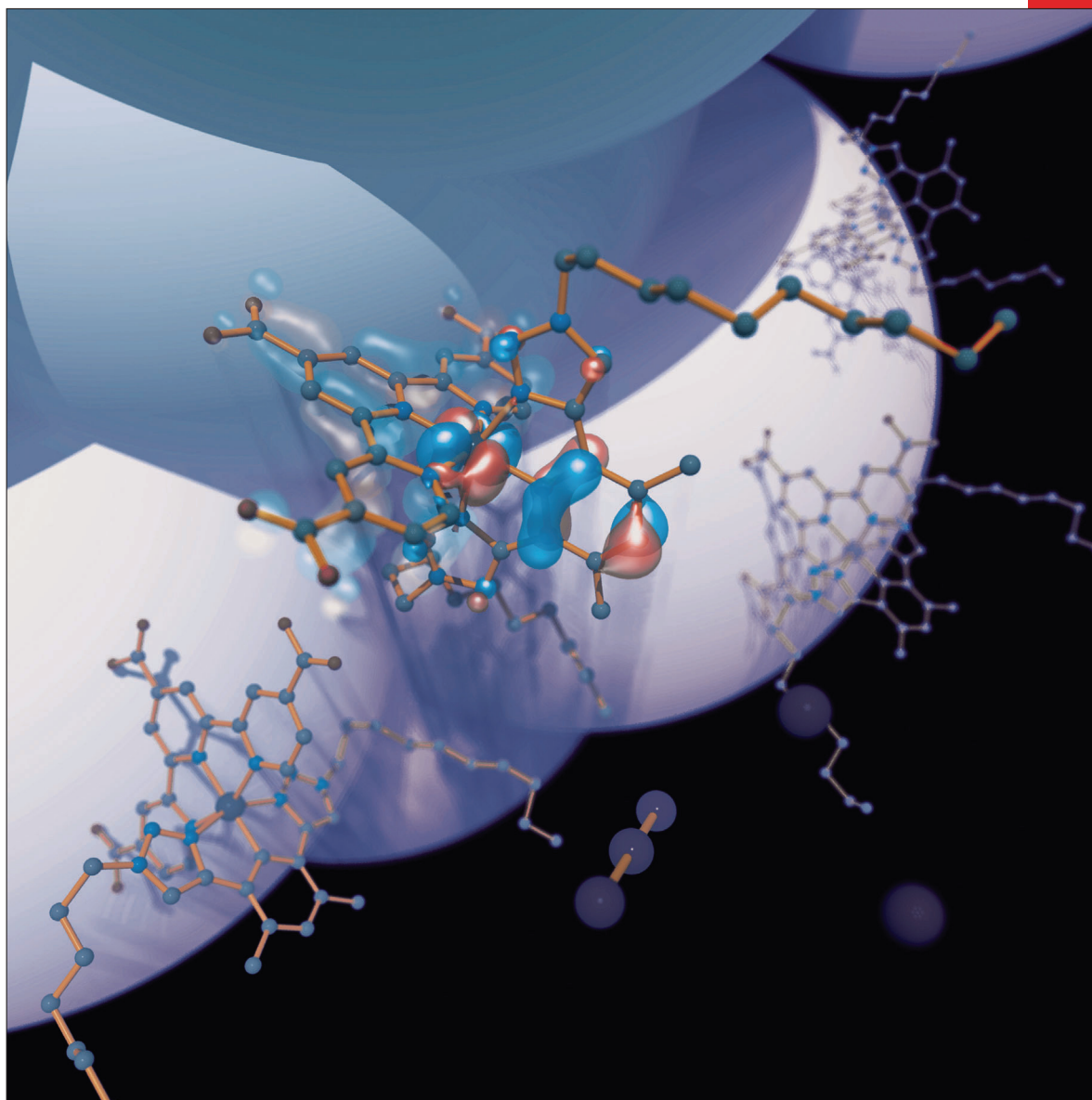
Compounds to dye for? …

… A series of 1,2,3-triazole-containing cyclometalated ruthenium(II) sensitizers is presented. The click-derived complexes are readily functionalized with alkyl chains and enable promising power conversion efficiencies in the dye-sensitized solar cell approaching the values achieved with a thiocyanate-containing benchmark sensitizer. For more details, see the Full Paper by C. P. Berlinguette, U. S. Schubert, et al. on page 14171 ff.

Cyclometalated Ruthenium(II) Complexes Featuring Tridentate Click-Derived Ligands for Dye-Sensitized Solar Cell Applications

Benjamin Schulze,[a, b] Douglas G. Brown,[c] Kiyoshi C. D. Robson,[c] Christian Friebe,[a, b] Michael Jäger,[a, b] Eckhard Birckner,[d] Curtis P. Berlinguette,*[c] and Ulrich S. Schubert *[a, b]

Abstract: A series of heteroleptic bis-(tridentate) Ru^{II} complexes featuring N^C^N-cyclometalating ligands is presented. The 1,2,3-triazole-containing tridentate ligands are readily functionalized with hydrophobic side chains by means of click chemistry and the corresponding cyclometalated Ru^{II} complexes are easily synthesized. The performance of these thiocyanate-free complexes in a dye-sensitized solar cell was tested and a power conversion efficiency (PCE) of up to 4.0 % (J_{sc} = 8.1 mA cm^{-2}, V_{oc} = 0.66 V, FF = 0.70) was achieved, while the black dye ((NBu$_4$)$_3$[Ru(Htctpy)(NCS)$_3$]; Htctpy = 2,2':6',2''-terpyridine-4'-carboxylic acid-4,4''-dicarboxylate) showed 5.2 % (J_{sc} = 10.7 mA cm^{-2}, V_{oc} = 0.69 V, FF = 0.69) under comparable conditions. When co-adsorbed with chenodeoxycholic acid, the PCE of the best cyclometalated dye could be improved to 4.5 % (J_{sc} = 9.4 mA cm^{-2}, V_{oc} = 0.65 V, FF = 0.70). The PCEs correlate well with the light-harvesting capabilities of the dyes, while a comparable incident photon-to-current efficiency was achieved with the cyclometalated dye and the black dye. Regeneration appeared to be efficient in the parent dye, despite the high energy of the highest occupied molecular orbital. The device performance was investigated in more detail by electrochemical impedance spectroscopy. Ultimately, a promising Ru^{II} sensitizer platform is presented that features a highly functionalizable "click"-derived cyclometalating ligand.

Keywords: click chemistry · cyclometalation · dye-sensitized solar cell · ruthenium · thiocyanate-free

Introduction

The photoactive material within a conventional dye-sensitized solar cell (DSSC) is a sensitizer adsorbed onto a nanocrystalline, semiconducting TiO$_2$ surface.[1] Upon light excitation, the sensitizer injects an electron into the conduction band of the semiconductor and is regenerated by a redox mediator. Consequently, the light-driven charge separation and subsequent charge transport are separated, which isolates the optimization of light harvesting to a molecular design level. Molecular engineering enables the systematic fine-tuning of the photophysical properties, but at the same time requires a highly photo/redox-stable dye. Furthermore, the efficiency of electron injection and subsequent dye regeneration relies on kinetic competition between charge separation and recombination, which, amongst others, relies on the appropriate positioning of the involved energy levels.[2]

Polypyridyl Ru^{II} complexes are well-suited for application in DSSCs because of their redox stability and tunable metal-to-ligand charge-transfer (MLCT) absorption band.[3] By the use of strong σ- and π-donating ligands (e.g., thiocyanate), this MLCT band can be extended to the near-infrared region to better overlap with the solar spectrum.[4] Careful design of the complexes can enforce an MLCT transition that involves the transfer of an electron from the metal to the anchoring ligand, which is critical for sensitizing TiO$_2$. In view of this overarching principle, the vast majority of Ru^{II} sensitizers in the literature is based on (NBu$_4$)$_2$[Ru(Hdcbpy)$_2$(NCS)$_2$] (**N719**; Hdcbpy = 2,2'-bipyridine-4-carboxylic acid-4'-carboxylate)[5] or (NBu$_4$)$_3$[Ru(Htctpy)(NCS)$_3$] (**N749** or black dye; Htctpy = 2,2':6',2''-terpyridine-4'-carboxylic acid-4,4''-dicarboxylate)[4b] (Figure 1); both dyes still serve as important benchmarks with reported power conversion efficiencies (PCEs) of up to 11.1 % under optimized conditions.[6] The thiocyanato ligand, however,

[a] B. Schulze, C. Friebe, Dr. M. Jäger, Prof. Dr. U. S. Schubert
Laboratory of Organic and Macromolecular Chemistry (IOMC)
Friedrich Schiller University Jena
Humboldtstr. 10, 07743 Jena (Germany)
Fax: (+49) 3641 948202
E-mail: ulrich.schubert@uni-jena.de

[b] B. Schulze, C. Friebe, Dr. M. Jäger, Prof. Dr. U. S. Schubert
Jena Center for Soft Matter (JCSM)
Friedrich Schiller University Jena
Philosophenweg 7, 07743 Jena (Germany)

[c] D. G. Brown, Dr. K. C. D. Robson, Prof. Dr. C. P. Berlinguette
Department of Chemistry
University of Calgary
2500 University Drive N.W., Calgary T2N 1N4, (Canada)
E-mail: cberling@ucalgary.ca

[d] Dr. E. Birckner
Institute of Physical Chemistry
Friedrich Schiller University Jena
Lessingstr. 10, 07743 Jena (Germany)

Figure 1. Schematic representation of the benchmark dye **N749**, of a related cyclometalated analogue **T4**, and of the target structures of this work.

cannot be chemically modified and can be displaced in a working solar cell, thus compromising the lifetime of the device.[7] Consequently, the NCS⁻ groups were replaced by an anionic chelating ligand to improve the stability of the complex by virtue of the chelate effect. Moreover, these aromatic donor ligands enable the accurate optimization of the photophysical and electrochemical properties by attachment of additional chromophores and electron-donating or -withdrawing substituents.[8] Despite prototypical cyclometalated RuII complexes being documented long ago,[9] it was only recently that such complexes were shown to produce PCEs in DSSC applications that are comparable to **N719** and **N749**.[10]

There are particular advantages to developing bis(tridentate) RuII complexes (e.g., a higher stability than their tris-(bidentate) counterparts).[11] While the vast majority of DSSC sensitizers contain polypyridyl ligands, it has been demonstrated that 1,2,3-triazoles can serve as useful analogues of these systems.[12] Motivated by a high PCE of 8.3% for (NBu₄)[Ru(Htctpy)(dpb)] (**T4**; Hdpb = 1,3-di(2-pyridyl)benzene) (vs. 9.0% achieved with **N719** under iden-

tical conditions),[10g] we sought to examine the viability of triazole-based analogues as useful sensitizer platforms. One of the distinct advantages of 1,3-bis(1,2,3-triazol-4-yl)benzene (cf. Figure 1) is that it is amenable to functionalization by means of its synthesis based on the facile copper(I)-catalyzed azide–alkyne 1,3-dipolar cycloaddition (CuAAC),[13] which is the prime example of the concept of click reactions.[14] The ligand can be easily equipped with hydrophobic alkyl chains, which are known to improve the thermal and long-term stability of a DSSC by preventing water-induced dye desorption,[15] while also enabling the use of alternative electrolytes.[16] Furthermore, the electronic properties of RuII complexes can be acutely affected through the judicious attachment of substituents to the triazoles[12c] and, moreover, we demonstrated recently that analogous RuII complexes with clicked-on thiophene moieties can successfully undergo anodic electropolymerization to enable the deposition of photoredoxactive films.[17]

This study continues our recent physicochemical analysis of a series of related RuII complexes featuring the 1,3-bis(1,2,3-triazol-4-yl)benzene cyclometalating ligand[12d] by demonstrating their performance in the DSSC. This study also includes a series of sensitizers bearing aptly positioned electron-withdrawing groups (EWGs) in view of the need to maintain a highest occupied molecular orbital (HOMO) of sufficiently low energy to accommodate regeneration of the photo-oxidized sensitizer by the electrolyte.[8e]

Results and Discussion

Synthesis: Aligned with our previous reports,[12d–f] the synthesis of the alkyl-functionalized tridentate ligands was readily achieved by CuAAC. In a simple two-step one-pot procedure, the *n*-decyl azide is generated first and subsequently reacted with an alkyne building block under typical CuAAC conditions to afford the tridentate ligands with good yields. The cyclometalation step was conducted in either methanol or *N,N*-dimethylformamide (DMF) at elevated temperatures, while exposed to microwave irradiation (Scheme 1). The use of [RuII(tcmtpy)(MeCN)₃](PF₆)₂ (tcmtpy = 4,4′,4″-

Scheme 1. Schematic representation of the synthesis of the RuII sensitizers: a) C₁₀H₂₁N₃, CuSO₄·5H₂O, sodium ascorbate, EtOH/H₂O (2:1, v/v), 50°C, 2 h, 81 to 85%; b) methanol or DMF, 150 to 160°C, 30 to 60 min, 56 to 60%; c) Cu(NO₃)₂, CH₂Cl₂/methanol (2:1, v/v), 40°C, 18 h, 87%; d) DMF/NEt₃/H₂O (3:1:1, v/v), 80°C, 24 h, 95 to 98%.

tricarboxymethyl-2,2′:6′,2″-terpyridine) afforded the desired cyclometalated product with fair yields after a simple chromatographic purification. The high reactivity and selectivity are attributed to weakly coordinated solvent ligands and the circumvention of a Ru^{III} intermediate, respectively.[12d] Additionally, the methyl and fluoro groups on the central phenyl ring prevent competitive bidentate cyclometalation and, thus, simplify the purification of the desired product.[12d] The ester derivatives of the Ru^{II} complexes were isolated, because they provide higher solubility and thermal stability than their acid analogues, which facilitates separation and characterization of the compounds. Methanol was the solvent of choice to avoid transesterification/saponification and to promote the cyclometalation process.[8f,12d,18] A partial replacement by a methoxy group was, however, observed in cases in which fluoro-substituted ligands were used, leading to inseparable mixtures. In this case, DMF was found to be a valuable alternative, because it precludes saponification as well as undesirable reactions involving the replacement of a fluoro substituent, and the high polarity of the solvent assists the cyclometalation step.[8f] The solubility of the ligand is also enhanced in DMF, which is particularly useful for the complexes bearing hydrophobic ligands.[19]

The anionic aryl ring enables facile post-complexation functionalization of the formed Ru^{II} complexes *para* to the Ru−C bond.[20] In order to attenuate electron donation from the carbanion, a nitro group could be installed using Cu-(NO$_3$)$_2$, while bromo substituents could be introduced using *N*-bromosuccinimide (NBS, see the Supporting Information) enabling subsequent cross-coupling reactions.[21]

The free carboxylic acids of the cyclometalated complexes were obtained by saponifying the corresponding esters at elevated temperatures in DMF/water/triethylamine (3:1:1, v/v/v).[8e,10d] After washing with dichloromethane, the cyclometalated sensitizers were obtained as zwitterionic species, as confirmed by elemental analyses. The solubility of the complexes was sufficient to prepare a 0.25 mM staining solution in DMF/methanol (4:1, v/v). The synthetic procedures and analytical data are given in the Supporting Information.

Photophysical properties: The absorption behavior of a parent series of heteroleptic Ru^{II} complexes featuring cyclometalating 1,3-bis(1,2,3-triazol-4-yl)benzene ligands was previously described in detail.[12d] To allow a deeper understanding of photophysical properties of the Ru^{II} complexes presented herein, density functional theory (DFT) and time-dependent DFT (TD-DFT) calculations were performed (see the Supporting Information). The calculated vertical singlet transitions are in reasonable agreement with the experimental absorption spectra. For **RuNCN** (Figure 2 and Figure S38 in the Supporting Information) and **RuNCN-F** (Figure S39 in the Supporting Information), all vertical singlet transitions in the visible-light region are mainly of MLCT character with varying ligand-to-ligand charge-transfer (LLCT) contributions (MLLCT), that is, they essentially involve a charge transfer from the metal center (and in some cases the cyclometalating ligand) to the anchoring
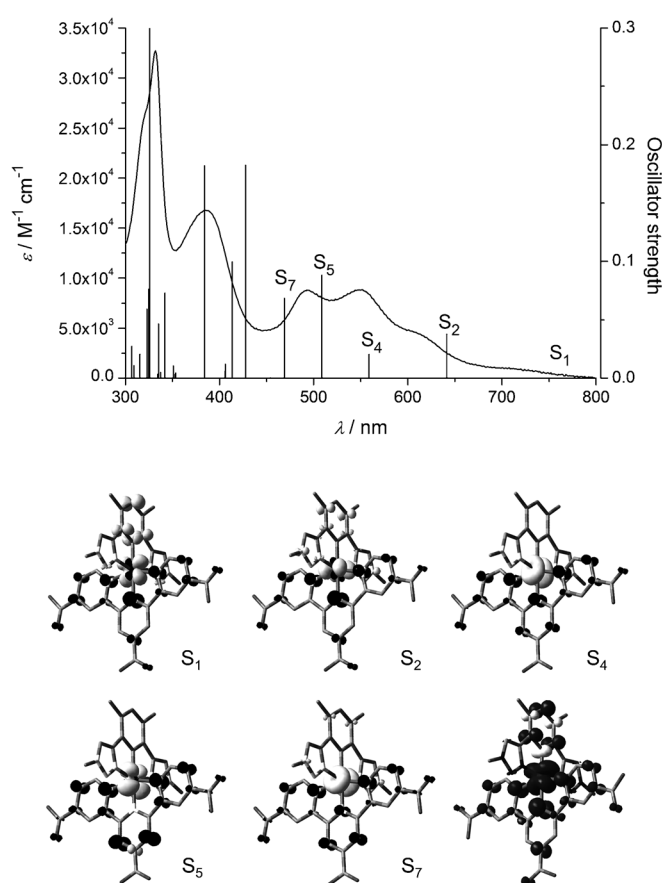

Figure 2. Experimental UV/Vis absorption (in DMF/methanol, 4:1 v/v) and calculated vertical singlet transitions (top), selected electron-density difference maps (bottom, white = depletion, black = accumulation, isovalue 0.004), and spin-density distribution of the ^{3}MLCT state (bottom right, isovalue 0.004) of **RuNCN** (the decyl chains have been replaced by a methyl group and the tpy ligand features three carboxylic acid functions).

tctpy ligand. Thereby, the lowest energy transition (S$_1$), which is an almost pure HOMO–LUMO transition, is not allowed and only a weak shoulder is observed in the experimental spectrum. In the case of **RuNCN-NO$_2$**, the LUMO+ 2 features significant contribution from the nitro group resulting in an intense MLCT transition at about 470 nm, directed from the metal center towards both the tctpy ligand and the nitro group (Figure S40 in the Supporting Information, S$_6$). In addition, a charge-transfer transition from the metal center mainly to the nitro group is predicted at about 430 nm (Figure S40 in the Supporting Information, S$_8$). However, after internal conversion (IC), ultrafast intersystem crossing (ISC), and vibrational relaxation, the lowest-energy ^{3}MLCT excited state will be populated[22] and the localization of the transferred charge on the anchoring tctpy ligand in the ^{3}MLCT state was confirmed for all three complexes by calculation of the spin-density distribution (Figure 2 and Figure S37 in the Supporting Information). Consequently, the anchoring carboxylic acids are adequately installed on the tpy ligand to enable electron injection into TiO$_2$.

The experimental UV/Vis absorption and emission spectra of the ruthenium complexes under consideration are displayed in Figure 3 and summarized in Table 1. In comparison to the ester-functionalized precursors, the complexes that feature more weakly electron-withdrawing carboxylic
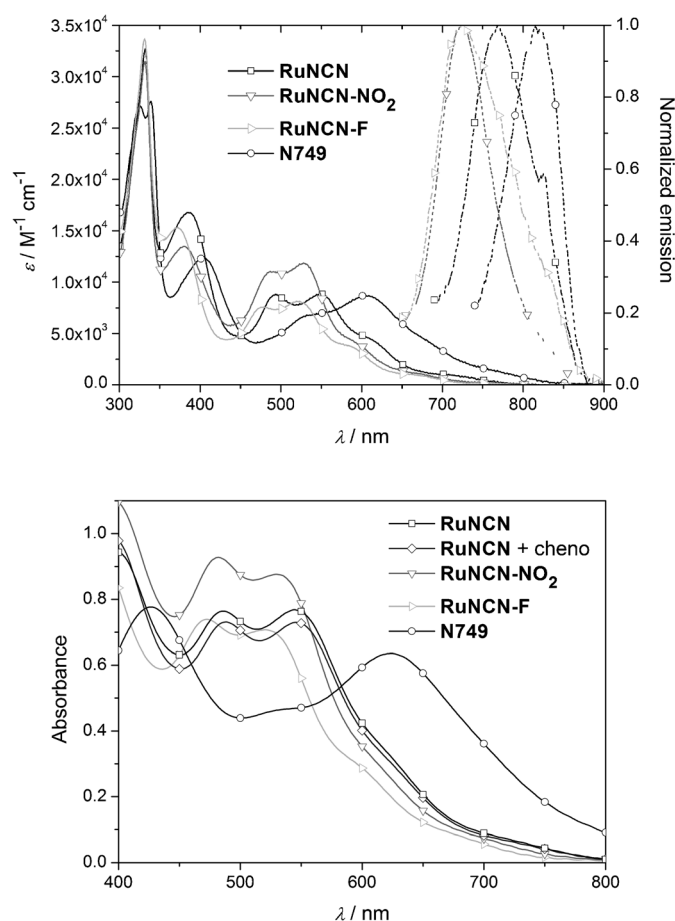

Figure 3. Top: UV/Vis absorption (solid) and emission (dashed, uncorrected for detector response) spectra of selected complexes recorded in DMF/methanol (4:1 v/v). Bottom: UV/Vis absorption of the complexes adsorbed on TiO₂ (12 μm thick transparent TiO₂ with an active area of 0.88 cm²). The lines represent the measured curve and symbols are used for assignment only.

acids (more precisely, two carboxylic acids and one carboxylate) show a hypsochromic shift in the electronic absorption and emission spectra, which is more pronounced in DMF/methanol (4:1, v/v) than in methanol (see Figure S28 in the Supporting Information). The differences between the solvent systems may be attributed to stronger hydrogen-bond interactions with the carboxylates/carboxylic acids in pure methanol. Upon functionalization of the central cyclometalating phenyl ring with electron-withdrawing groups, the HOMO destabilization by the carbanion is reduced, resulting in a further hypsochromic shift of the MLCT features corresponding to 0.07 to 0.10 eV. The nitro group causes a slightly smaller hypsochromic shift than the fluoro substituents, which contrasts a related series of tris(bidentate) Ru^{II} complexes bearing the same substitution patterns.[8c] This difference is ascribed to steric repulsion between the adjacent methyl groups, which induces a dihedral angle between the nitro group and the phenyl ring of about 50° diminishing conjugation and, hence, the π-accepting character of the nitro group.[12d] The **RuNCN** and **RuNCN-F** complexes show moderate extinction coefficients in the MLCT region (about 9000 and 8000 M^{-1} cm^{-1}, respectively, see Table 1), while for **RuNCN-NO$_2$**, the extinction coefficient in the MLCT maximum is increased by about 30% relative to **RuNCN** (about 12 000 M^{-1} cm^{-1}) in line with the DFT-calculated participation of the nitro group in the HOMO and, in particular, the LUMO + 2 (vide supra, Tables S1 and S4 in the Supporting Information).

In comparison to **N749**, the MLCT maximum of **RuNCN** has a comparable extinction coefficient, but is hypsochromically shifted from 605 to 552 nm (corresponding to 0.2 eV) in DMF/methanol (4:1, v/v). To assess the light-harvesting capabilities of the cyclometalated dyes relative to **N749**, the product of $\varepsilon(\lambda)$ (with $\lambda > 400$ nm) and the AM 1.5 solar photon flux was integrated.[25] Ideally, **RuNCN** would allow for 80% of the theoretical current achievable with **N749**, while **RuNCN-F** would only allow about 60% of **N749** and 75% of **RuNCN** due to its blue-shifted absorption. For **RuNCN-NO$_2$**, the spectral blue shift is compensated by the increased molar absorptivity yielding an overall light-harvesting capability equal to the one of **RuNCN**. Prospectively, the molar extinction coefficients could be improved by in-

Table 1. Selected data of the Ru^{II} complexes.

	λ_{max}^{abs} [nm] (ε [×10³ M^{-1} cm^{-1}])	λ_{max}^{em} [nm]	τ [ns]	E_{0-0} [eV][a]	$E_{1/2}$ [V] vs. Fc$^+$/Fc (vs. NHE)[b]	E^* [V] vs. Fc$^+$/Fc (vs. NHE)[c]
RuNCN-Me	419 (15.3), 507 (8.2), 581 (7.8), 660 (4.2)[d]	_[e]	_[e]	_[f]	0.24 (0.87)[d]	_[f]
RuNCN-NO$_2$-Me	407 (16.6), 497 (10.2), 560 (8.9), 638 (sh, 4.4)[d]	815[d]	_[f]	1.61[d]	0.41 (1.04)[d]	−1.20 (−0.57)
RuNCN-F-Me	401 (17.0), 492 (9.4), 554 (9.2), 635 (4.8)[d]	800[d]	_[f]	1.62[d]	0.46 (1.09)[d]	−1.16 (−0.53)
RuNCN	386 (16.8), 493 (8.9), 552 (8.9), 610 (sh, 4.5)[g]	768[g]	16.1,[h] 16.7[i]	1.68[g]	0.11 (0.80)[g]	−1.57 (−0.88)
RuNCN-NO$_2$	380 (13.5), 487 (11.0), 528 (11.9), 591 (sh, 4.2)[g]	725[g]	11.0,[h] 11.7[i]	1.78[g]	0.30 (0.99)[g]	−1.48 (−0.79)
RuNCN-F	373 (15.3), 477 (7.6), 522 (8.1), 580 (sh, 3.8)[g]	723[g]	4.5,[h] 4.9[i]	1.79[g]	0.37 (1.06)[g]	−1.42 (−0.73)
N749	403 (12.3), 528 (sh, 6.7), 605 (8.7)[g]	820[g]	30[j]	1.58[g]	0.16 (0.85)[g]	−1.42 (−0.73)

[a] Determined at the intersection of the absorption and emission with the latter being normalized to the lowest-energy absorption. [b] Determined by cyclic voltammetry using NBu₄PF₆ as supporting electrolyte, conversion to NHE scale by addition of 0.63 V[48] and 0.69 V[49] when the measurement was done in MeCN and DMF/methanol (4:1, v/v), respectively. Notably, the latter value accounts for pure DMF and thus only allows an approximate conversion to the NHE scale. [c] Calculated using $E^* = E_{1/2} - E_{0-0}$.[1b] [d] Measured in MeCN. [e] Not detectable. [f] Not determined. [g] Measured in DMF/methanol (4:1 v/v). [h] Measured in aerated DMF/methanol (4:1 v/v). [i] Measured in nitrogen-sparged DMF/methanol (4:1 v/v). [j] Measured in EtOH, taken from ref. [4b].

stallation of additional chromophores at the cyclometalating phenyl ring.[8a,b,12d]

The absorption profiles of the complexes anchored to transparent TiO$_2$ anodes are also provided in Figure 3. Assuming that the extinction coefficients do not change upon anchoring of the dyes onto TiO$_2$, the dye uptake of the cyclometalated sensitizers is comparable to **N749**. Also, when **RuNCN** was co-adsorbed with chenodeoxycholic acid (cheno), the absorbance was maintained at the same level.

The optical energy gap, E_{0-0}, which is required to determine the excited-state redox potential (vide infra), was estimated from the intersection of the absorption and emission with the latter being normalized to the lowest-energy absorption corresponding to the HOMO–LUMO transition (vide supra). The energy gap of 1.58 eV for **N749** was determined to be the smallest of the dyes studied, as those of **RuNCN**, **RuNCN-NO$_2$**, and **RuNCN-F** were 1.68, 1.78, and 1.79 eV, respectively. Furthermore, when comparing the absorption profiles in DMF/methanol (4:1, v/v) solution with the ones of dye-loaded transparent TiO$_2$ films (see Figure S28 in the Supporting Information), the energy gap for the cyclometalated dyes remained static, while a slight bathochromic shift is observed for **N749** upon anchoring.[26]

The cyclometalated complexes were found to be very weak emitters with emission maxima between 720 and 770 nm. As the lifetime of the charge-separated excited state is crucial due to kinetic competition between electron injection and decay to the ground state,[2a] excited-state lifetimes were determined by using time-correlated single-photon counting (TCSPC, see Figure S29 in the Supporting Information). By applying a monoexponential fit, lifetimes of 4.9, 11.7, and 16.7 ns were obtained for **RuNCN-F**, **RuNCN-NO$_2$**, and **RuNCN**, respectively, in nitrogen-sparged DMF/methanol (4:1 v/v), which are typical values for cyclometalated bis(tridentate) Ru^{II} complexes.[10] In air-equilibrated DMF/methanol (4:1 v/v) solution, the excited-state lifetimes of the cyclometalated sensitizers are only marginally shorter (see Table 1). The observation of the shortest lifetime for **RuNCN-F** is in line with our previous study and is attributed to a small energy separation between the emitting ^{3}MLCT state and the deactivating ^{3}MC state.[12d] All lifetimes are shorter than for **N749** (30 ns), but, except for **RuNCN-F**, sufficiently long to allow for almost quantitative electron injection if the injection occurs within 100 ps.[2a] Nonetheless, the injection can be much faster and even with an excited-state lifetime of 1 ns, apparently no injection problems were encountered in a series of related complexes.[10]

Electrochemical behavior: The cyclic voltammetry of related complexes was reported in a previous study.[12d] These experiments, as well as spectroelectrochemistry experiments in which the complexes were oxidized for hours, showed that the metal-based redox process was fully reversible for this kind of Ru^{II} complex.

The destabilization of the HOMO in cyclometalated Ru^{II} complexes causes a negative shift for the Ru^{III}/Ru^{II} redox process, which may compromise the dye regeneration if an iodide-based electrolyte is used.[8e,10b,f] Consequently, a redox potential of about 0.9 V versus NHE has been suggested as a guideline to guarantee efficient regeneration,[8e,10b,m,n] which accounts for the relevant I$_2$$^{•-}$/I$^-$ redox couple of a I$_3$$^-$/I$^-$-based electrolyte located at 0.79 V versus NHE (Figure 4).[27] Nonetheless, dyes with redox potentials less
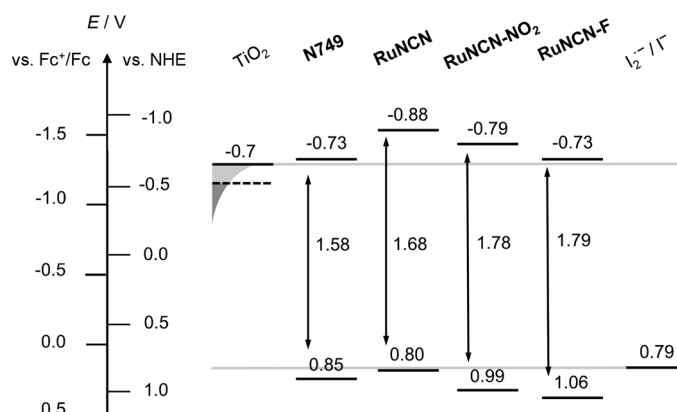

Figure 4. Comparison of the excited-state and ground-state redox potentials (values refer to the NHE scale) with the relevant redox potential of the electrolyte and the conduction band edge (solid line) as well as the approximate position of the TiO$_2$ quasi Fermi level (dashed line).

positive than 0.85 V versus NHE can function properly in a DSSC.[28] For **RuNCN**, a Ru^{III}/Ru^{II} redox potential of 0.11 V versus Fc$^+$/Fc (0.80 V vs. NHE) was measured, while for **RuNCN-F** and **RuNCN-NO$_2$**, $E_{1/2}$ values of 0.30 V versus Fc$^+$/Fc (0.99 V vs. NHE) and 0.37 V versus Fc$^+$/Fc (1.06 V vs. NHE), respectively, were measured in DMF/methanol (4:1 v/v).[29] The positively shifted potentials for the latter are a consequence of the electron-withdrawing substituents, while for the parent **RuNCN** complex, the Ru^{III}/Ru^{II}-based redox process occurs at a critically low potential. Additionally, square-wave voltammetry experiments in acetonitrile with the complex-anchored TiO$_2$ anode as the working electrode were undertaken as these conditions are closest to later working conditions;[10] however, the measured redox potentials (see the Supporting Information) are comparable to the cyclic voltammetry results. As an internal reference, the redox potential of **N749** was measured in DMF/methanol (4:1 v/v) to give a value of 0.16 V versus Fc$^+$/Fc (0.85 V vs. NHE), which is 50 mV more positive than for **RuNCN**.[30] For comparison, while regeneration problems for a dye having a redox potential 40 mV lower than **N749** have been reported,[31] there are examples of well-functioning dyes with even 50 to 60 mV less positive redox potentials relative to **N749**.[28b,32] Ultimately, even if the redox potential is accurately determined, the regeneration efficiency may depend on the individual molecular structure and some dye–electrolyte interactions have been proposed.[10n,33] At this point, it remains unclear whether **RuNCN** will allow efficient regeneration by the I$_3$$^-$/I$^-$-based electrolyte.[34]

The excited-state redox potentials were calculated from the Ru^{III}/Ru^{II} redox potentials and the optical energy gap E_{0-0} (Table 1).[1b] The complexes show excited-state redox potentials between -1.42 V versus Fc^+/Fc (-0.73 V vs. NHE) and -1.57 V versus Fc^+/Fc (-0.88 V vs. NHE) and are therefore more negative than the conduction band edge of TiO_2 located at -1.3 V versus Fc^+/Fc (-0.7 V vs. NHE) allowing, in principle, for efficient electron injection (Figure 4).[35]

Photovoltaic performance: To test the PCE of the presented cyclometalated dyes in DSSCs, commercially available test cells with transparent TiO_2 anodes (20 nm particles, 12 μm thickness, 0.28 or 0.88 cm² active area) were used and assembled according to standard literature procedures (see the Supporting Information), and directly compared to **N749**. Notably, since the square-cell type (0.88 cm²) was used up during the experiments, the measurements were continued with spot cells of identical transparent TiO_2, but with a smaller area (0.28 cm²). However, only small differences in current or voltage between the used square and spot cells were noted, except for the fill factor (FF), which is generally higher for the smaller cells.

An established acetonitrile-based electrolyte solution was chosen, containing 0.05 M iodine, guanidinium thiocyanate (0.1 M), 4-*tert*-butylpyridine (TBP; 0.5 M), and varying concentrations of dimethylimidazolium iodide (DMII) and lithium or sodium iodide (Table 2, Figure 5).[33d] Starting with a sodium-containing electrolyte[10c,36] (0.6 M NaI, El 1a), a PCE of about 2% was obtained throughout the series. As regeneration problems were suspected for **RuNCN**, the effective iodide concentration was increased[37] (1.0 M DMII, El 1b), which significantly improved the J_{sc} resulting in a PCE of 3.0%. Subsequently, an electrolyte with a high lithium concentration (1.0 M, El 2) was used to facilitate both electron injection[38] and dye regeneration,[39] which provided an estimation of the photocurrents attainable with the cyclometalated dyes. For **RuNCN**, again the J_{sc} was significantly im-

Figure 5. Selected $J–V$ curves for two different electrolytes (El 1a, dashed, and El 2, solid) using the square cell (0.88 cm²) except for the combination **RuNCN-F** and El 2, for which the spot cell (0.28 cm²) was used. The lines represent the measured curve and symbols are used for assignment only.

proved relative to the sodium-containing electrolytes (9.2 mA cm⁻²), while for **RuNCN-NO₂** and **RuNCN-F**, only a slight improvement in J_{sc} was achieved resulting in much inferior values (6.3 and 5.8 mA cm⁻², respectively). The extent of current improvement for these last complexes is in the range observed for benchmark dyes.[38] This behavior suggests that the excited-state redox potential is sufficiently high, which is consistent with the above-mentioned estimations (Figure 4). For **RuNCN-F**, the low photocurrents are thus mainly ascribed to the lower light-harvesting ability, which was estimated to be only 75% of **RuNCN** (vide supra). In contrast, **RuNCN-NO₂** should be a light harvester as good as **RuNCN** and the lower photocurrents as well as the comparatively lower V_{oc} values (about 80 mV less than for **RuNCN** and **RuNCN-F**) are attributed to enhanced recombinations (vide infra).[40]

As an internal reference, the performance of **N749** was measured using a typical electrolyte composition containing 0.1 M LiI (El 3, Table 2).[6] The same electrolyte was tested for **RuNCN** as this dye clearly shows the best performance within the series. In Figure 6, the $J–V$ curves and the incident photon-to-current efficiency (IPCE) spectra for **RuNCN** and **N749** measured under identical conditions are provided. In this direct comparison, two benefits of **N749** become clear. Firstly, **N749** produces a higher current (10.7 vs. 8.1 mA cm⁻²), which is ascribed mainly to the better red- to near IR-response as evident from the IPCE traces (Figure 6, right). Note that the estimated light-harvesting ability of **RuNCN** amounts to 80% of the one of **N749** (vide supra). Secondly, **N749** allows for a higher voltage (0.69 vs. 0.66 V), which is attributed to its doubly deprotonated form and anionic charge leading to a higher TiO_2 conduction band.[41] Consequently, **N749** achieves a PCE of 5.1%, while **RuNCN** affords 4.0% under identical conditions. It should be noted that under these conditions, the PCE for **RuNCN** is apparently not limited by inefficient regeneration. The superior performance achieved with electrolytes containing

Table 2. Selected data of the Ru^{II} complexes measured under AM 1.5 light conditions.

	Area [cm²][a]	Electrolyte[b]	V_{oc} [V]	J_{sc} [mA cm⁻²]	FF	η [%]
RuNCN	0.88	El 1a	0.62	5.7	0.61	2.2
	0.88	El 1b	0.62	7.4	0.62	3.0
	0.88	El 2	0.57	9.2	0.61	3.4
	0.28	El 3	0.66	8.1	0.70	4.0
	0.28	El 3[c]	0.65	9.4	0.70	4.5
RuNCN-NO₂	0.88	El 1a	0.57	5.5	0.56	1.8
	0.88	El 2	0.49	6.3	0.58	1.9
RuNCN-F	0.88	El 1a	0.63	5.4	0.56	2.0
	0.28	El 2	0.57	5.8	0.70	2.5
N749	0.88	El 3	0.69	11.6	0.62	5.1
	0.28	El 3	0.69	10.7	0.69	5.2

[a] 0.88 cm² refers to the square cell type, 0.28 cm² refers to the spot cell type, 12 μm active, transparent TiO_2 for both. [b] Electrolyte abbreviations: El 1a: 0.6 M NaI, 0.6 M DMII; El 1b: 0.6 M NaI, 1.0 M DMII; El 2: 1.0 M LiI, 0.6 M DMII; El 3: 0.1 M LiI, 0.6 M DMII. [c] Co-adsorbed with cheno.
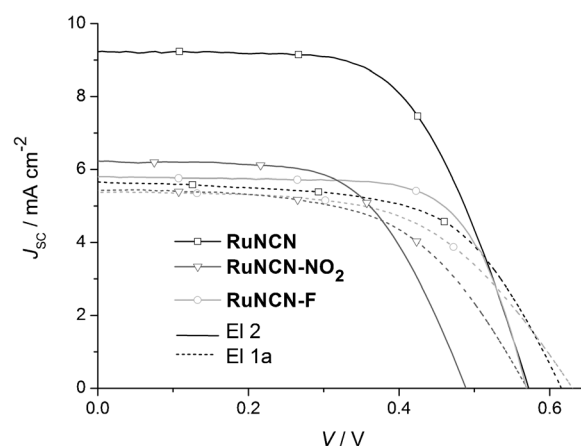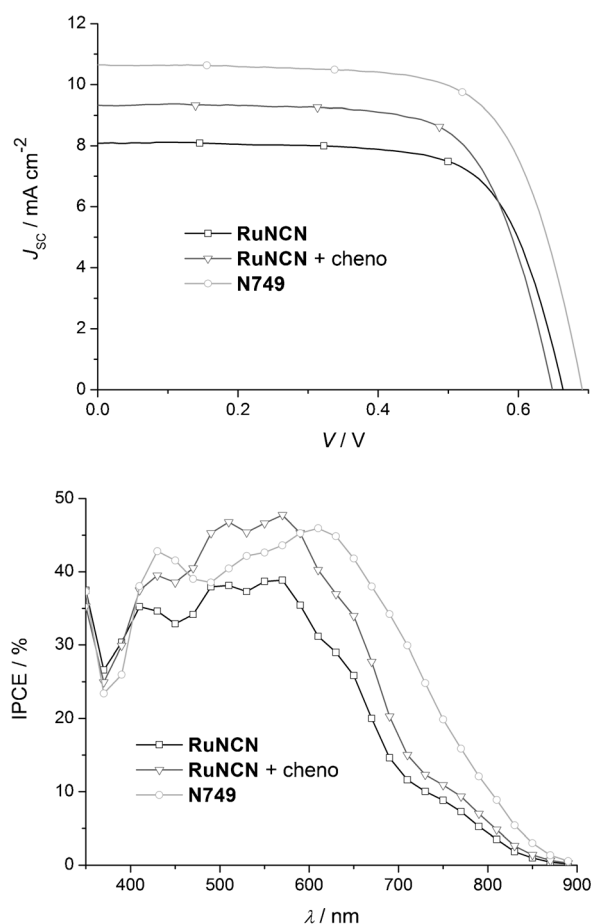
FULL PAPER

Figure 6. Top: **RuNCN** with and without cheno co-adsorbent versus **N749** without cheno under otherwise identical conditions (El 3, 0.28 cm^2). Bottom: Photocurrent action spectra. Note that symbols represent datapoints in the photocurrent action spectra, while they are used for assignment only in the *J–V* curves.

Li$^+$ instead of Na$^+$ (Figure 5) indicates that the dye regeneration kinetics need to be enhanced by increasing the near-surface iodide concentration with the help of charge-dense cations.[39] However, a 0.1 M lithium concentration is sufficient,[42] which still allows reasonably high voltages and commonly results in the best overall performance as the electron injection is facilitated as well.[43]

For **RuNCN**, using the best electrolyte composition (El 3), the influence of the cheno co-adsorbent was tested (Table 2, Figure 6) to gain information about the dye's ability to protect the TiO$_2$ surface from the electrolyte and, thereby, prevent recombinations.[44] The J_{sc} values could be further improved (9.4 vs. 8.1 mA cm^{-2}), although the V_{oc} decreased slightly (0.65 vs. 0.66 V). The observed improvement in the IPCE spectrum (Figure 6) suggests that the charge collection efficiency is enhanced by the help of cheno and **RuNCN** achieves a plateau value as high as for **N749**. Notably, it was reported that the PCE achieved with **N749** could be increased from 4.3 to 4.7 % by co-adsorption with cheno,[45] presumably because **N749** is unable to create a complete monolayer[4b] and, thus, it inadequately shields the TiO$_2$ sur-

face from the electrolyte. The effect of cheno will be discussed in more detail below.

Electrochemical impedance spectroscopy: In order to better understand the origins of the differences between the achieved device performances, electrochemical impedance spectroscopy (EIS)[15d, 46] was performed for selected cells. A forward bias was therefore applied in the dark causing electron injection into TiO$_2$, electron interception by iodine or triiodide at the TiO$_2$/electrolyte interface and electron abstraction from iodide at the counter electrode.[15d] To distinguish between the individual processes, the impedance data were modeled with an appropriate transmission line (Figure S33 in the Supporting Information) to obtain three key parameters: the transport resistance within TiO$_2$ (R_t), the recombination or charge-transfer resistance (R_{ct}) at the TiO$_2$/electrolyte interface and the recombination or charge-transfer capacitance (C_{ct}) at the TiO$_2$/electrolyte interface. Since the density of available states increases exponentially as the Fermi level (which depends on the applied potential) approaches the conduction band, R_t and R_{ct} decrease, while C_{ct} increases at higher applied voltages (see the Supporting Information).[46a,c] The measurements were thus conducted at different potentials and the parameters were plotted against the applied potentials to visualize the differences independently of the V_{oc} values of the different devices.[15d,46a,47] To achieve a good device performance, R_t should be low, while R_{ct} and C_{ct} should be high. Thereby, a higher conduction band energy results in a lower electron population of the conduction band (Boltzman statistics) and, hence, lower recombination and transport rates corresponding to higher R_{ct} and R_t values.[46a] On the other hand, R_{ct} and C_{ct} are lowered with increasing conduction band energy as the recombination driving force increases.[38,46a] Furthermore, R_{ct} and C_{ct} are increased if the TiO$_2$ surface is protected against the electrolyte by the adsorbed dye (TBP) and cheno, while they are lowered in case of interactions between the sensitizer and iodine. The conduction band energy can be increased by TBP and lowered by cationic additives. Ultimately, if $R_t < R_{ct}$, then the normalized diffusion length (L_d/L) is greater than 1, which means that the electron lifetime is longer than the electron transit time within TiO$_2$ and the charges can thus be efficiently collected at the anode resulting in higher J_{sc} values under illumination.[46a] In case of illumination under open-circuit conditions, the photocurrent generation is fully compensated by recombination reactions,[38,48] in other words, a higher R_{ct} is a prerequisite to achieve higher V_{oc} values.

Firstly, two different electrolytes containing either sodium (EL 1a) or lithium salts (El 2) were compared for **RuNCN** (Figure S34 in the Supporting Information). Using identical cell types, electrolyte El 1a (0.6 M NaI) leads to a higher R_t and lower C_{ct} than El 2 (1.0 M LiI), which is in line with a higher conduction band energy and, hence, a lower electron population of the conduction band.[46a] For the same reason, R_{ct} is increased although this benefit is partially offset by an increased recombination driving force.[38,46a] Still, the higher

R_{ct} leads to diminished recombination reactions and, thus, enables a higher V_{oc} in case of El 1a. As a further result, for El 2, R_t is smaller than R_{ct} throughout the measured potential range, which allows a more efficient charge collection and higher J_{sc} values under illumination than for El 1a.

The comparison between the devices based on **RuNCN-NO$_2$** and **RuNCN-F** under identical conditions (El 1a, square cell) reveals a lower R_{ct} and C_{ct} for **RuNCN-NO$_2$**, while R_t is comparable for both dyes (Figure S35 in the Supporting Information). Accordingly, the higher V_{oc} and J_{sc} values achieved with **RuNCN-F** can be ascribed to less pronounced recombination reactions. In view of the essentially identical molecular structures and anchoring modes of both dyes, this is attributed to enhanced recombination reactions due to interactions between the nitro group and iodine.[40]

The effect of the cheno co-adsorbent on devices based on **RuNCN** and El 3 is demonstrated in Figure S36 in the Supporting Information. In the absence of cheno, R_t and R_{ct} increase, although to a lesser extent in case of R_{ct}, while C_{ct} is lowered. This scenario qualitatively reflects the trends as observed with **RuNCN** for the different electrolytes (vide supra) and is ascribed to a higher conduction band energy when cheno is absent. Presumably, TBP is more hindered in reaching the TiO$_2$ surface in the presence of the cheno coadsorbent, resulting in a lowered conduction-band-lifting effect of the TBP additive. Additionally, a better TiO$_2$ surface passivation in the presence of cheno might cause a relative enhancement of R_{ct} and C_{ct}. However, this effect appears to have a minor contribution as R_{ct} is still lower than for **RuNCN** without cheno. Ultimately, while the R_{ct} values for **RuNCN** with and without cheno are almost equal, the lower R_t in the presence of the co-adsorbent enables a more efficient charge collection in line with higher J_{sc} values. On the other hand, the slightly lower V_{oc} observed for **RuNCN** with cheno is related to a slightly lower R_{ct}.

When comparing the devices constructed with **N749** and with **RuNCN** (both without cheno, Figure S36 in the Supporting Information), the R_t and C_{ct} values are equal, while R_{ct} is higher in case of **N749**. While a higher conduction band energy and, therefore, a higher R_t is expected for **N749** in view of its lower charge and lower degree of protonation, it has to be noted that the dependency of R_t solely on the conduction band energy is only valid for very similar sensitizers, that is, the electron diffusion, which follows an electron-hopping mechanism by means of trapping and detrapping,[49] might depend also on the sensitizer. Still, a higher conduction band might be reflected by the higher R_{ct} for **N749**; however, the dissimilarities between **RuNCN** and **N749** preclude an unambiguous interpretation of the impedance data. Ultimately, in view of the equal R_t values obtained with **N749** and **RuNCN**, the lower recombination tendency in case of **N749** enables both a higher V_{oc} as well as a higher J_{sc} in line with a longer normalized diffusion length.

Conclusion

The performance of a series of click-derived bis(tridentate) cyclometalated Ru^{II} complexes in the DSSC has been investigated. The parent **RuNCN** dye devoid of electron-withdrawing groups revealed the best results: The IPCE values are comparable to **N749** and the achieved PCE corresponds to 80 % of the value of **N749**, which correlates well with the individual light-harvesting capabilities. Despite the high HOMO energy of the parent photosensitizer, its regeneration appeared to be efficient when lithium-containing electrolytes are used. In contrast, the *meta*-difluoro substitution pattern, which is often used to lower the HOMO energy, showed a detrimental effect on the light-harvesting properties and resulted in an inferior performance. Consequently, a promising thiocyanate-free Ru^{II} photosensitizer platform is presented, which shows great potential for further improvement in view of its rapidly synthesized and highly functionalizable cyclometalating ligand. As demonstrated, hydrophobic alkyl chains can most easily be introduced and are expected to be beneficial for the long-term stability and allow for alternative electrolytes. Additional chromophores can, in principle, be installed on the cyclometalated phenyl ring to further optimize the light harvesting in the future.

Experimental Section

Experimental and computational details are given in the Supporting Information. These include synthetic procedures, further computational, photophysical and electrochemical data, NMR and MS spectra as well as EIS data.

Acknowledgements

[1] a) B. O'Regan, M. Grätzel, *Nature* **1991**, *353*, 737–740; b) A. Hagfeldt, G. Boschloo, L. Sun, L. Kloo, H. Pettersson, *Chem. Rev.* **2010**, *110*, 6595–6663; c) S. Ardo, G. J. Meyer, *Chem. Soc. Rev.* **2009**, *38*, 115–164; d) N. Robertson, *Angew. Chem.* **2006**, *118*, 2398–2405; *Angew. Chem. Int. Ed.* **2006**, *45*, 2338–2345; e) M. Grätzel, *Acc. Chem. Res.* **2009**, *42*, 1788–1798.

[2] a) A. Listorti, B. O'Regan, J. R. Durrant, *Chem. Mater.* **2011**, *23*, 3381–3399; b) B. C. O'Regan, J. R. Durrant, *Acc. Chem. Res.* **2009**, *42*, 1799–1808.

[3] a) A. Juris, V. Balzani, F. Barigelletti, S. Campagna, P. Belser, A. von Zelewsky, *Coord. Chem. Rev.* **1988**, *84*, 85–277; b) J.-P. Sauvage, J.-P. Collin, J.-C. Chambron, S. Guillerez, C. Coudret, V. Balzani, F. Barigelletti, L. De Cola, L. Flamigni, *Chem. Rev.* **1994**, *94*, 993–1019; c) A. Reynal, E. Palomares, *Eur. J. Inorg. Chem.* **2011**, 4509–4526.

[4] a) M. K. Nazeeruddin, P. Péchy, M. Grätzel, *Chem. Commun.* **1997**, 1705–1706; b) M. K. Nazeeruddin, P. Péchy, T. Renouard, S. M. Za-keeruddin, R. Humphry-Baker, P. Comte, P. Liska, L. Cevey, E. Costa, V. Shklover, L. Spiccia, G. B. Deacon, C. A. Bignozzi, M. Grätzel, *J. Am. Chem. Soc.* **2001**, *123*, 1613–1624.

[5] M. K. Nazeeruddin, S. M. Zakeeruddin, R. Humphry-Baker, M. Jir-ousek, P. Liska, N. Vlachopoulos, V. Shklover, C.-H. Fischer, M. Grätzel, *Inorg. Chem.* **1999**, *38*, 6298–6305.

[6] Y. Chiba, A. Islam, Y. Watanabe, R. Komiya, N. Koide, L. Han, *Jpn. J. Appl. Phys.* **2006**, *45*, L638–L640.

[7] F. Nour-Mohhamadi, S. D. Nguyen, G. Boschloo, A. Hagfeldt, T. Lund, *J. Phys. Chem. B* **2005**, *109*, 22413–22419.

[8] a) B. D. Koivisto, K. C. D. Robson, C. P. Berlinguette, *Inorg. Chem.* **2009**, *48*, 9644–9652; b) K. C. D. Robson, B. D. Koivisto, T. J. Gordon, T. Baumgartner, C. P. Berlinguette, *Inorg. Chem.* **2010**, *49*, 5335–5337; c) P. G. Bomben, B. D. Koivisto, C. P. Berlinguette, *Inorg. Chem.* **2010**, *49*, 4960–4971; d) P. G. Bomben, K. C. D. Robson, P. A. Sedach, C. P. Berlinguette, *Inorg. Chem.* **2009**, *48*, 9631–9643; e) P. G. Bomben, K. D. Thériault, C. P. Berlinguette, *Eur. J. Inorg. Chem.* **2011**, 1806–1814; f) S. H. Wadman, M. Lutz, D. M. Tooke, A. L. Spek, F. Hartl, R. W. A. Havenith, G. P. M. van Klink, G. van Koten, *Inorg. Chem.* **2009**, *48*, 1887–1900; g) I. M. Dixon, F. Alary, J.-L. Heully, *Dalton Trans.* **2010**, *39*, 10959–10966; h) H. C. Zhao, J. P. Harney, Y.-T. Huang, J.-H. Yum, M. K. Nazeer-uddin, M. Grätzel, M.-K. Tsai, J. Rochford, *Inorg. Chem.* **2012**, *51*, 1–3.

[9] a) P. Reveco, R. H. Schmehl, W. R. Cherry, F. R. Fronczek, J. Selbin, *Inorg. Chem.* **1985**, *24*, 4078–4082; b) E. C. Constable, J. M. Holmes, *J. Organomet. Chem.* **1986**, *301*, 203–208; c) M. Beley, S. Chodorow-ski, J.-P. Collin, J.-P. Sauvage, L. Flamigni, F. Barigelletti, *Inorg. Chem.* **1994**, *33*, 2543–2547; d) M. Beley, J.-P. Collin, J.-P. Sauvage, *Inorg. Chem.* **1993**, *32*, 4539–4543; e) J.-P. Collin, M. Beley, J.-P. Sauvage, F. Barigelletti, *Inorg. Chim. Acta* **1991**, *186*, 91–93.

[10] a) P. G. Bomben, J. Borau-Garcia, C. P. Berlinguette, *Chem. Commun.* **2012**, *48*, 5599–5601; b) P. G. Bomben, T. J. Gordon, E. Schott, C. P. Berlinguette, *Angew. Chem.* **2011**, *123*, 10870–10873; *Angew. Chem. Int. Ed.* **2011**, *50*, 10682–10685; c) K. C. D. Robson, B. D. Koivisto, A. Yella, B. Sporinova, M. K. Nazeeruddin, T. Baum-gartner, M. Grätzel, C. P. Berlinguette, *Inorg. Chem.* **2011**, *50*, 5494–5508; d) S. H. Wadman, J. M. Kroon, K. Bakker, R. W. A. Havenith, G. P. M. van Klink, G. van Koten, *Organometallics* **2010**, *29*, 1569–1579; e) S. H. Wadman, J. M. Kroon, K. Bakker, M. Lutz, A. L. Spek, G. P. M. van Klink, G. van Koten, *Chem. Commun.* **2007**, 1907–1909; f) T. Bessho, E. Yoneda, J.-H. Yum, M. Guglielmi, I. Tavernelli, H. Imai, U. Rothlisberger, M. K. Nazeeruddin, M. Grät-zel, *J. Am. Chem. Soc.* **2009**, *131*, 5930–5934; g) E. Yoneda, M. Grätzel, M. K. Nazeeruddin, Eur. Pat. Appl. (2009), EP 2036955; h) K.-L. Wu, H.-C. Hsu, K. Chen, Y. Chi, M.-W. Chung, W.-H. Liu, P.-T. Chou, *Chem. Commun.* **2010**, *46*, 5124–5126; i) H. Kisserwan, T. H. Ghaddar, *Dalton Trans.* **2011**, *40*, 3877–3884; j) C.-C. Chou, K.-L. Wu, Y. Chi, W.-P. Hu, S. J. Yu, G.-H. Lee, C.-L. Lin, P.-T. Chou, *Angew. Chem.* **2011**, *123*, 2102–2106; *Angew. Chem. Int. Ed.* **2011**, *50*, 2054–2058; k) K.-L. Wu, C.-H. Li, Y. Chi, J. N. Clifford, L. Cabau, E. Palomares, Y.-M. Cheng, H.-A. Pan, P.-T. Chou, *J. Am. Chem. Soc.* **2012**, *134*, 7488–7496; l) H. Kisserwan, A. Kamar, T. Shoker, T. H. Ghaddar, *Dalton Trans.* **2012**, *41*, 10643–10651; m) P. G. Bomben, K. C. D. Robson, B. D. Koivisto, C. P. Berlingu-ette, *Coord. Chem. Rev.* **2012**, *256*, 1438–1450; n) K. C. D. Robson, P. G. Bomben, C. P. Berlinguette, *Dalton Trans.* **2012**, *41*, 7814–7829.

[11] a) E. A. Medlycott, G. S. Hanan, *Chem. Soc. Rev.* **2005**, *34*, 133–142; b) E. A. Medlycott, G. S. Hanan, *Coord. Chem. Rev.* **2006**, *250*, 1763–1782.

[12] a) Y. Li, J. C. Huffman, A. H. Flood, *Chem. Commun.* **2007**, 2692–2694; b) R. M. Meudtner, M. Ostermeier, R. Goddard, C. Limberg, S. Hecht, *Chem. Eur. J.* **2007**, *13*, 9834–9840; c) M. Ostermeier, M.-A. Berlin, R. M. Meudtner, S. Demeshko, F. Meyer, C. Limberg, S. Hecht, *Chem. Eur. J.* **2010**, *16*, 10202–10213; d) B. Schulze, D. Esco-dero, C. Friebe, R. Siebert, H. Görls, S. Sinn, M. Thomas, S. Mai, J. Popp, B. Dietzek, L. González, U. S. Schubert, *Chem. Eur. J.* **2012**,

18, 4010–4025; e) B. Schulze, C. Friebe, M. D. Hager, A. Winter, R. Hoogenboom, H. Görls, U. S. Schubert, *Dalton Trans.* **2009**, 787–794; f) B. Schulze, C. Friebe, S. Hoeppener, G. M. Pavlov, A. Winter, M. D. Hager, U. S. Schubert, *Macromol. Rapid Commun.* **2012**, *33*, 597–602; g) W.-W. Yang, L. Wang, Y.-W. Zhong, J. Yao, *Organome-tallics* **2011**, *30*, 2236–2240; h) I. Stengel, A. Mishra, N. Pootraku-lchote, S.-J. Moon, S. M. Zakeeruddin, M. Grätzel, P. Bäuerle, *J. Mater. Chem.* **2011**, *21*, 3726–3734.

[13] a) C. W. Tornøe, C. Christensen, M. Meldal, *J. Org. Chem.* **2002**, *67*, 3057–3064; b) V. V. Rostovtsev, L. G. Green, V. V. Fokin, K. B. Sharpless, *Angew. Chem.* **2002**, *114*, 2708–2711; *Angew. Chem. Int. Ed.* **2002**, *41*, 2596–2599.

[14] a) H. C. Kolb, M. G. Finn, K. B. Sharpless, *Angew. Chem.* **2001**, *113*, 2056–2075; *Angew. Chem. Int. Ed.* **2001**, *40*, 2004–2021; b) D. Four-nier, R. Hoogenboom, U. S. Schubert, *Chem. Soc. Rev.* **2007**, *36*, 1369–1380.

[15] a) C. Klein, M. K. Nazeeruddin, D. Di Censo, P. Liska, M. Grätzel, *Inorg. Chem.* **2004**, *43*, 4216–4226; b) P. Wang, S. M. Zakeeruddin, J. E. Moser, M. K. Nazeeruddin, T. Sekiguchi, M. Grätzel, *Nat. Mater.* **2003**, *2*, 402–407; c) S. M. Zakeeruddin, M. K. Nazeeruddin, R. Humphry-Baker, P. Péchy, P. Quagliotto, C. Barolo, G. Viscardi, M. Grätzel, *Langmuir* **2002**, *18*, 952–954; d) Q. Wang, J.-E. Moser, M. Grätzel, *J. Phys. Chem. B* **2005**, *109*, 14945–14953.

[16] L. E. Polander, A. Yella, B. F. E. Curchod, N. Ashari Astani, J. Teuscher, R. Scopelliti, P. Gao, S. Mathew, J.-E. Moser, I. Tavernelli, U. Rothlisberger, M. Grätzel, M. K. Nazeeruddin, J. Frey, *Angew. Chem.* **2013**, *125*, 8893–8897.

[17] C. Friebe, B. Schulze, H. Görls, M. Jäger, U. S. Schubert, *Chem. Eur. J.* DOI: 10.1002/chem.201301439.

[18] E. C. Constable, M. J. Hannon, *Inorg. Chim. Acta* **1993**, *211*, 101–110.

[19] K. C. D. Robson, B. D. Koivisto, C. P. Berlinguette, *Inorg. Chem.* **2012**, *51*, 1501–1507.

[20] a) M. Gagliardo, D. J. M. Snelders, P. A. Chase, R. J. M. Klein Geb-bink, G. P. M. van Klink, G. van Koten, *Angew. Chem.* **2007**, *119*, 8710–8726; *Angew. Chem. Int. Ed.* **2007**, *46*, 8558–8573; b) S. H. Wadman, R. W. A. Havenith, M. Lutz, A. L. Spek, G. P. M. van Klink, G. van Koten, *J. Am. Chem. Soc.* **2010**, *132*, 1914–1924.

[21] C. Coudret, S. Fraysse, J.-P. Launay, *Chem. Commun.* **1998**, 663–664.

[22] N. H. Damrauer, G. Cerullo, A. Yeh, T. R. Boussie, C. V. Shank, J. K. McCusker, *Science* **1997**, *275*, 54–57.

[23] V. V. Pavlishchuk, A. W. Addison, *Inorg. Chim. Acta* **2000**, *298*, 97–102.

[24] N. G. Connelly, W. E. Geiger, *Chem. Rev.* **1996**, *96*, 877–910.

[25] K. Hasan, E. Zysman-Colman, *Inorg. Chem.* **2012**, *51*, 12560–12564.

[26] This effect causes another slight improvement of the above estima-tion of the light-harvesting capability for **N749**. The difference in be-havior may be associated with the degree of protonation, that is, the two carboxylates of **N749** (with non-coordinating Bu$_4$N$^+$) become more electron-accepting and hence LUMO-stabilizing upon coordi-nation to Ti^{4+}, which is consistent with the bathochromically shifted MLCT maxima for the doubly or fully protonated form of **N749**. See reference [4b].

[27] a) G. Boschloo, E. A. Gibson, A. Hagfeldt, *J. Phys. Chem. Lett.* **2011**, *2*, 3016–3020; b) G. Boschloo, A. Hagfeldt, *Acc. Chem. Res.* **2009**, *42*, 1819–1826; c) J. G. Rowley, B. H. Farnum, S. Ardo, G. J. Meyer, *J. Phys. Chem. Lett.* **2010**, *1*, 3132–3140.

[28] a) A. Yella, H.-W. Lee, H. N. Tsao, C. Yi, A. K. Chandiran, M. K. Nazeeruddin, E. W.-G. Diau, C.-Y. Yeh, S. M. Zakeeruddin, M. Grätzel, *Science* **2011**, *334*, 629–634; b) S.-H. Yang, K.-L. Wu, Y. Chi, Y.-M. Cheng, P.-T. Chou, *Angew. Chem.* **2011**, *123*, 8420–8424; *Angew. Chem. Int. Ed.* **2011**, *50*, 8270–8274.

[29] In the DSSC literature, redox potentials are often referenced to the (aqueous) NHE scale, while the experiments were mostly conducted in organic solvents using Fc$^+$/Fc as an internal reference. Notably, the Fc$^+$/Fc couple is widely solvent-independent and inconsistent conversion numbers to the NHE scale are applied, which makes it reasonable to compare directly the experimental values referring to

Fc[+]/Fc in line with IUPAC recommendations. However, we provide the potentials against the traditional NHE scale here as well. See references [23,24] and G. Gritzner, J. Kuta, *Pure Appl. Chem.* **1984**, *56*, 461–466.

[30] Notably, the Ru[III]/Ru[II] redox couple strongly depends on the solvent environment/measuring conditions and values ranging from 0.86 V to 0.89 V vs. NHE are reported for **N749**. See references [4b,10k].

[31] C.-W. Hsu, S.-T. Ho, K.-L. Wu, Y. Chi, S.-H. Liu, P.-T. Chou, *Energy Environ. Sci.* **2012**, *5*, 7549–7554.

[32] M. Kimura, J. Masuo, Y. Tohata, K. Obuchi, N. Masaki, T. N. Murakami, N. Koumura, K. Hara, A. Fukui, R. Yamanaka, S. Mori, *Chem. Eur. J.* **2013**, *19*, 1028–1034.

[33] a) T. Privalov, G. Boschloo, A. Hagfeldt, P. H. Svensson, L. Kloo, *J. Phys. Chem. C* **2009**, *113*, 783–790; b) J. N. Clifford, E. Palomares, M. K. Nazeeruddin, M. Grätzel, J. R. Durrant, *J. Phys. Chem. C* **2007**, *111*, 6561–6567; c) H. Kusama, K. Sayama, *J. Phys. Chem. C* **2012**, *116*, 1493–1502; d) Z. Yu, N. Vlachopoulos, M. Gorlov, L. Kloo, *Dalton Trans.* **2011**, *40*, 10289–10303.

[34] Given the high reactivity of the position *para* to the Ru—C bond (note that also the benzylic position on the cyclometalated phenyl ring is reactive), a potential iodination under working conditions cannot be excluded. A derivative of **RuNCN-Me** featuring mesityl substituents instead of decyl chains (see reference [12d]) was iodinated in the position *para* to the Ru—C bond using *N*-iodosuccinimide resulting in a 50 mV anodic shift of the Ru[III]/Ru[II] redox potential (see Figure S32 in the Supporting Information). Accordingly, a potential iodination of **RuNCN** under working conditions can be expected to shift the Ru[III]/Ru[II] redox couple to about 0.85 V versus NHE thus providing sufficient regeneration driving force. This behaviour may apply for other cyclometalated dyes as well, but further studies are required to verify this hypothesis.

[35] Often a value of −0.5 V versus NHE is quoted, which rather corresponds to the quasi Fermi level and limits the V_{oc}. However, the injection is limited by the conduction band edge located at −0.7 V versus NHE; see reference [2a] and the comment therein.

[36] H. Wang, L. M. Peter, *J. Phys. Chem. C* **2012**, *116*, 10468–10475.

[37] A. C. Onicha, F. N. Castellano, *J. Phys. Chem. C* **2010**, *114*, 6831–6840.

[38] Y. Bai, J. Zhang, Y. Wang, M. Zhang, P. Wang, *Langmuir* **2011**, *27*, 4749–4755.

[39] S. Pelet, J.-E. Moser, M. Grätzel, *J. Phys. Chem. B* **2000**, *104*, 1791–1795.

[40] A. Reynal, A. Forneli, E. Martinez-Ferrero, A. Sánchez-Díaz, A. Vidal-Ferran, B. C. O'Regan, E. Palomares, *J. Am. Chem. Soc.* **2008**, *130*, 13558–13567.

[41] a) M. K. Nazeeruddin, R. Humphry-Baker, P. Liska, M. Grätzel, *J. Phys. Chem. B* **2003**, *107*, 8981–8987; b) S.-H. Liu, H. Fu, Y.-M. Cheng, K.-L. Wu, S.-T. Ho, Y. Chi, P.-T. Chou, *J. Phys. Chem. C* **2012**, *116*, 16338–16345; c) F. De Angelis, S. Fantacci, A. Selloni, M. K. Nazeeruddin, M. Grätzel, *J. Phys. Chem. C* **2010**, *114*, 6054–6061.

[42] It has been reported that the reversal of the TiO₂ ζ-potential from negative to positive values occurs at concentrations one order of magnitude lower for the more charge-dense Li^{+} when compared to Na^{+} (see reference [39]). As a result of the positively charged surface, the near-surface concentration of iodide is increased and the dye regeneration kinetics are improved abruptly. A potential coordination of Li^{+} to the vacant 2-nitrogen of the 1,2,3-triazole and a concomitant increase of the redox potential can be excluded since no changes in the Ru[III]/Ru[II] couple were observed for **RuNCN-Me** in the presence of 0.1 M Li[+] in acetonitrile (0.1 M LiClO₄ vs. 0.1 M NBu₄ClO₄ as supporting electrolyte). Notably, the ester derivative was used to avoid interactions with the carboxylic acid/carboxylates and provide sufficient solubility in acetonitrile.

[43] S. E. Koops, B. C. O'Regan, P. R. F. Barnes, J. R. Durrant, *J. Am. Chem. Soc.* **2009**, *131*, 4808–4818.

[44] T. Daeneke, T.-H. Kwon, A. B. Holmes, N. W. Duffy, U. Bach, L. Spiccia, *Nat. Chem.* **2011**, *3*, 211–215; additionally, cheno may suppress the formation of aggregates, which can potentially lower the J_{sc}, see: Z.-S. Wang, Y. Cui, Y. Dan-oh, C. Kasada, A. Shinpo, K. Hara, *J. Phys. Chem. C* **2007**, *111*, 7224–7230. However, this effect is rather unlikely given the bulkiness of the presented sensitizers.

[45] K.-M. Lee, V. Suryanarayanan, K.-C. Ho, K. R. J. Thomas, J. T. Lin, *Sol. Energy Mater. Sol. Cells* **2007**, *91*, 1426–1431.

[46] a) F. Fabregat-Santiago, J. Bisquert, G. Garcia-Belmonte, G. Boschloo, A. Hagfeldt, *Sol. Energy Mater. Sol. Cells* **2005**, *87*, 117–131; b) F. Fabregat-Santiago, G. Garcia-Belmonte, I. Mora-Seró, J. Bisquert, *Phys. Chem. Chem. Phys.* **2011**, *13*, 9083–9118; c) J. Bisquert, F. Fabregat-Santiago in *Dye-sensitized Solar Cells*, 1st ed. (Ed.: K. Kalyanasundaram), EPFL Press, Lausanne, **2010**, pp. 457–554.

[47] Q. Wang, S. Ito, M. Grätzel, F. Fabregat-Santiago, I. Mora-Seró, J. Bisquert, T. Bessho, H. Imai, *J. Phys. Chem. B* **2006**, *110*, 25210–25221.

[48] J. Bisquert, I. Mora-Seró, *J. Phys. Chem. Lett.* **2010**, *1*, 450–456.

[49] a) J. Nelson, *Phys. Rev. B* **1999**, *59*, 15374–15380; b) J. Bisquert, D. Cahen, G. Hodes, S. Rühle, A. Zaban, *J. Phys. Chem. B* **2004**, *108*, 8106–8118.

Publication A8:

"Designing cyclometalated ruthenium(II) complexes for anodic electropolymerization"

C. Friebe, B. Schulze, H. Görls, M. Jäger, U. S. Schubert

Electropolymerization

Designing Cyclometalated Ruthenium(II) Complexes for Anodic Electropolymerization

Christian Friebe,[a, b] Benjamin Schulze,[a, b] Helmar Görls,[c] Michael Jäger,[a, b] and Ulrich S. Schubert*[a, b]

Abstract: The anodic electropolymerization of thiophene-functionalized cyclometalated ruthenium(II) complexes is shown for the first time. Oxidative decomposition reactions can be overcome by modification of the involved redox potentials through the introduction of electron-withdrawing substituents, namely nitro groups, at the cyclometalating phenyl ring. The generated functionalized ruthenium(II) complexes allow the electrochemical preparation of thin polymer films, which show a broad UV/Vis absorption as well as reversible redox switchability. The presented complexes are promising candidates for future photovoltaic applications based on photo-redox-active films.

Introduction

The ruthenium(II)-polypyridyl motif represents a highly favorable building block with regard to applications as photosensitizer units (e.g., in solar cells, light-driven catalysis, and water splitting).[1] In particular, the incorporation of strong electron-donating ligands enables the formation of ruthenium(II) complexes providing long excited-state lifetimes and broad absorption features, both of which are crucial for an efficient photosensitizer dye.[2] Thereby, ruthenium(II) complexes that contain thiocyanate ligands have been applied very successfully.[3] However, the monodentate thiocyanates cause a lowered complex stability and impede further functionalization with regard to dye optimization. Hence, alternative polydentate ligands that feature strong electron donors, namely anionic carbon[4] and nitrogen[5] atoms as well as classical[6] and mesoionic[7] N-heterocyclic carbenes, were designed for sensitizer applications. In this context, we recently presented a series of complexes based on a cyclometalating, tridentate ligand possessing 1,2,3-triazole moieties, which were introduced through copper(I)-catalyzed azide–alkyne 1,3-dipolar cycloaddition

(CuAAC),[8] allowing the facile assembly of functionalized ligands. The complexes showed prolonged excited-state lifetimes, redox stability, and suitability for application in dye-sensitized solar cells.[4a, 9]

Most photosensitizer applications require the processing of the dye in thin films to allow light absorption as well as efficient charge transfer to the affiliated reaction site. Thereby, an instrumentally simple technique for the formation of defined layers is electropolymerization, i.e., the formation of insoluble polymers through the coupling of electrochemically generated monomer radicals on an electrode surface.[10] In this way, different ruthenium(II) complexes of polypyridyl-type ligands have already been used successfully to form polymeric coatings.[11] Recently, cyclometalated systems were also polymerized through electrochemical reduction,[12] and, very recently, through an anodic approach.[13] However, successful oxidative electropolymerization of cyclometalated ruthenium(II) complexes was reported only rarely in the literature, although the anodic polymerization allows the usage of aromatic electropolymerizable units such as thiophene, 3,4-ethylenedioxythiophene (EDOT), and pyrrole. These enable the assembly of metallopolymers[14] that feature π-conjugated spacer units, providing additional chromophores and potentially enabling an intramolecular electron transfer after photo-oxidation of the complex.[15] This, in turn, leads to more efficient UV/Vis absorption and extended charge separation, respectively. A potential challenge is the high reactivity of the electron-rich central phenyl ring of the cyclometalating ligand, which possesses a high spin density, possibly leading to electrochemical coupling.[16] Nevertheless, redox stability could be shown in UV/Vis/NIR spectroelectrochemical experiments, at least for the first oxidized state.[4a] Still, the electron-rich aromatic moiety may give rise to side reactions or decomposition under the highly positive potentials required for the electropolymerization.

In this work, we present the preparation and electrochemical polymerization of ruthenium(II) complexes based on 1,2,3-tria-

[a] Dr. C. Friebe,+ B. Schulze,+ Dr. M. Jäger, Prof. Dr. U. S. Schubert
Laboratory of Organic and Macromolecular Chemistry (IOMC)
Friedrich Schiller University Jena
Humboldtstr. 10, 07743 Jena (Germany)
E-mail: ulrich.schubert@uni-jena.de

[b] Dr. C. Friebe,+ B. Schulze,+ Dr. M. Jäger, Prof. Dr. U. S. Schubert
Jena Center for Soft Matter (JCSM)
Friedrich Schiller University Jena
Philosophenweg 7, 07743 Jena (Germany)

[c] Dr. H. Görls
Laboratory of Inorganic and Analytical Chemistry
Friedrich Schiller University Jena
Humboldtstr. 8, 07743 Jena (Germany)

[+] These authors contributed equally to this work.

Supporting information for this article is available on the WWW under
http://dx.doi.org/10.1002/chem.201301439.

zole-containing cyclometalating ligands. Two structural motifs are introduced, varying in the presence and absence of methyl groups at the linking phenyl rings, which prevent and allow, respectively, a coplanarization of the phenylthienyl and the central, metal-coordinating triazole moieties, and thus, may affect the extent of π conjugation between thiophene and triazole. However, electronic coupling through the triazole is not expected.[17] The synthesized monomer complexes were fully characterized, with the prepared polymer films studied through cyclic voltammetry, UV/Vis absorption spectroscopy, and UV/Vis/NIR spectroelectrochemistry. Furthermore, supporting computational calculations based on density functional theory (DFT) were performed to gain further insight into the electrochemical behavior.

Results and Discussion

Synthesis and electrochemical behavior of thiophene-equipped complexes

As a first survey of the ability of the cyclometalated ruthenium(II) complexes to undergo anodic electropolymerization, two complexes possessing 4-(2-thienyl)phenyl moieties at the triazole rings were synthesized (Scheme 1) and studied through electrochemical means.

To allow a rapid and modular access to the thiophene-functionalized 1,3-bis(1,2,3-triazol-4-yl)benzene (N^CH^N) ligands, we rely on a click-derived triazole-based framework. It has been demonstrated that the involved triazole units can be used as analogues for pyridine donors.[18] Initial attempts to couple 2-thienylboronic acid directly to the corresponding bromo-functionalized N^CH^N ligand framework through Suzuki cross-coupling were not successful (sluggish reaction, intractable reaction mixtures). Likewise, attempted cyclometalation using a bromo-functionalized N^CH^N ligand to install the thiophene after complexation was precluded by partial debromination resulting in an inseparable mixture of complexes.[19] The alternative approach, that is, installing the thio-

phene on an azide-functionalized bromobenzene first, afforded the desired 2-(4-azidophenyl)thiophene building blocks in reasonable yields. Notably, the Suzuki cross-coupling tolerated the presence of aryl azides despite their known tendency to form phosphazides and phosphimines with free or coordinated phosphines of the palladium catalyst.[20] The subsequent CuAAC afforded the thiophene-containing N^CH^N ligands in good yields. In contrast to the initially attempted cross-coupling method, the CuAAC greatly simplifies the purification because the educt and byproducts are removed readily, which is particularly important in the case of low product solubility, for example, for **HTph** (Scheme 1). For **HTphMe**, the solubility is much higher owing to the steric interactions between the triazoles and the *ortho* methyl groups of the outer phenyl rings, which enforce a twisting out of plane and thereby preclude π stacking. As a result, single crystals suitable for X-ray diffraction could be grown through vapor diffusion of diethyl ether into a concentrated dichloromethane solution (see Figure S42, Supporting Information). The cyclometalation was achieved in fair yields by using $[Ru^{II}(tpy)(CH_3CN)_3][PF_6]_2$ (tpy = 2,2':6',2''-terpyridine) as the precursor.[4a]

Subsequently, the monomer complexes were characterized electrochemically; the obtained cyclic voltammograms (CVs) and differential pulse voltammograms (DPVs) are depicted in the Supporting Information (Figures S45 and S46), and the first redox potential values are given in Table 1. The CVs of **RuTph** and **RuTphMe** reveal a reversible first oxidation process with a half-wave potential of 0.10 V, which is assigned to the depopulation of a mixed ruthenium- and cyclometalating-ligand-based orbital on the basis of previous computational investigations on related systems.[4a] In the region around 1.1 to 1.4 V, further oxidation processes appear, including thienyl radical cation formation, which is crucial for the electropolymerization. Thereby, the thienyl-based signals possess a significantly larger peak current than the first redox processes. This is attributed to a lack of electronic coupling, because the 1,2,3-triazole is known to interrupt π conjugation,[17] leading to simultaneous oxidation of both thiophene moieties at the same redox po-
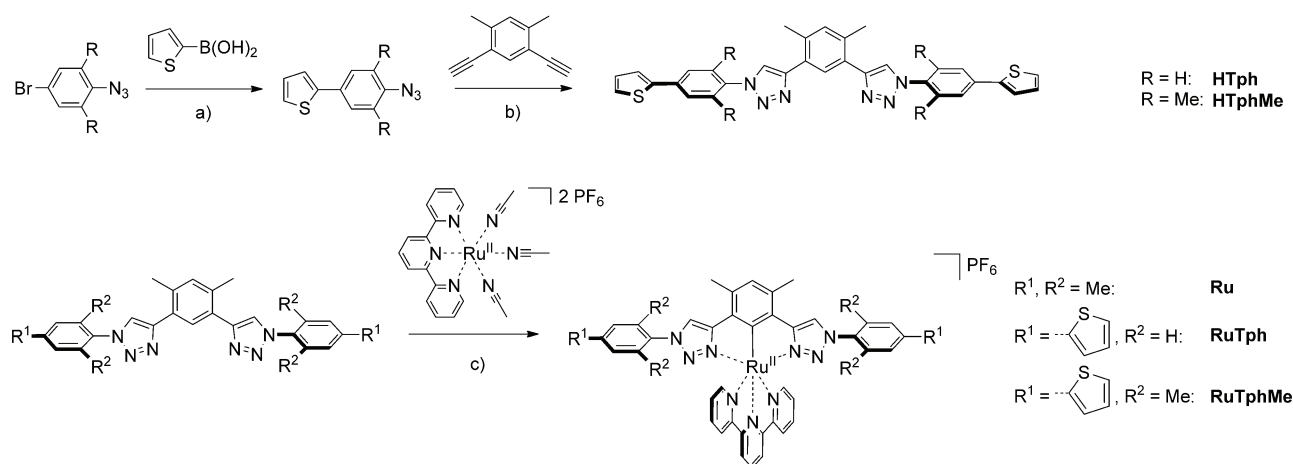
Scheme 1. Synthesis of the thiophene-containing cyclometalated ruthenium(II) complexes: a) Pd(PPh₃)₄, K₂CO₃, DMF, 50 °C, 12 h, 40 %; b) CuSO₄·5 H₂O, NaAsc., CH₂Cl₂/EtOH/H₂O (1:2:1), 50 °C, 12 h, 70 %; c) EtOH/toluene (1:1) or DMF, 140 to 160 °C, 30 to 120 min, 50 %. **Ru** was prepared previously in an analogous synthesis.[4a]

Table 1. Electrochemical characteristics of the monomer complexes (10^{-4} M in CH_2Cl_2 with 0.1 M Bu_4NPF_6).

Complex	$E_{1/2}$ [V] (i_{pa}/i_{pc}, ΔE_p [mV])[a]	
	$+1 \rightarrow +2$	$+1 \rightarrow 0$
RuTph	0.10 (1.05, 65)	−2.12 (irrev.)[b]
RuTphMe	0.10 (1.0, 74)	−2.17 (irrev.)[b]
RuTphNO₂	0.29 (1.0, 67)	−1.87 (1.0, 75)
RuTphMeNO₂	0.31 (1.0, 72)	−1.88 (1.05, 78)

[a] Potentials vs. Fc⁺/Fc. [b] Peak potential of the cathodic wave.

tential. The first, ligand-based reduction appears at −2.04 V for **RuTph** and −2.06 V for **RuTphMe**, and is irreversible in both cases.

The electropolymerization experiments were performed potentiodynamically in different solvents using 0.1 M Bu_4NPF_6 as the electrolyte. The first studies were executed in acetonitrile. With the inclusion of the higher oxidation processes at 1.2 to 1.4 V in the potential cycling, both **RuTph** and **RuTphMe** show a rapid decrease in all redox signals, indicating decomposition of the complexes (see Figure S47, Supporting Information). Because changing the potential range or scan rate did not lead to successful polymerization, the solvent was changed to dichloromethane, which has a lower nucleophilicity than acetonitrile, possibly leading to a diminished rate of side reactions[10] (see Figure S48 and Figure 1 as an example for **RuTphMe**). For **RuTph**, the cyclovoltammetric development is divided into two phases: During the first eleven cycles, an increase in the original Ru^{III}/Ru^{II}-based redox signal occurs, indicating the formation of the desired polymer, which is, however, accompanied by additional signals arising at around −0.1 and 0.9 V, suggesting the formation of byproducts. After the eleventh cycle, the redox signals in the region between −0.4 and 0.4 V start to decrease, which is probably because of the electrochemical decomposition of the formed compounds. For **RuTphMe**, likewise, additional redox processes appear at around −0.2 V, but already during the third cycle, the signal decrease begins. In addition, further studies involving the use
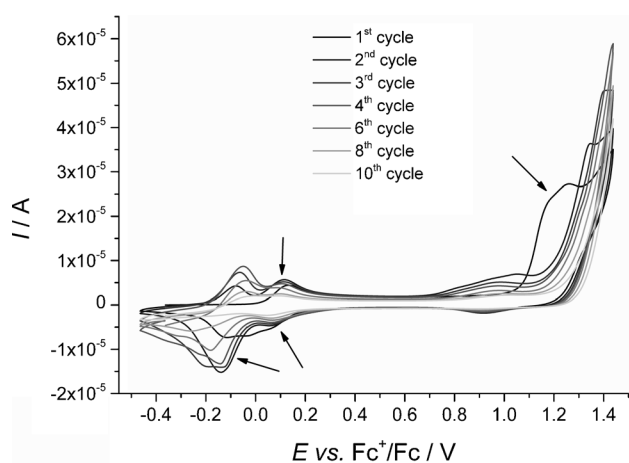
of Lewis acids (e.g., $BF_3 \cdot OEt_2$, borate esters)[21] or weak bases (e.g., water, 2,6-di-*tert*-butylpyridine),[10] did not result in successful electropolymerization. $BF_3 \cdot OEt_2$ in acetonitrile even caused the displacement of the cyclometalating ligand, leading to the undesired recovery of the [Ru^{II}(tpy)(CH$_3$CN)$_3$]$^{2+}$ precursor species (see Figures S43 and S49, Supporting Information).

We assumed that the decomposition is caused by an inherent electrochemical process of the complexes. This assumption is supported by comparison of the cyclic voltammograms of the thienyl-equipped system with those of its parent complex devoid of thiophene units (**Ru**, Figure 2). The latter system reveals an additional, irreversible redox process, which is in the same potential range as the oxidation of the thienyl moeities. Thus, oxidation of the thienyl units would not be possible without inducing an irreversible oxidation reaction of the central complex moiety.

Synthesis and electrochemical behavior of redox-modified nitro-complexes

To overcome the problem of electrochemical decomposition, we attempted to shift the respective redox potential beyond the thiophene-related one. Therefore, a nitro group was introduced at the 4-position of the central phenyl ring of the cyclometalating ligand to increase the redox potentials as observable for the respective thiophene-free parent complex (**RuNO₂**, Figure 2).
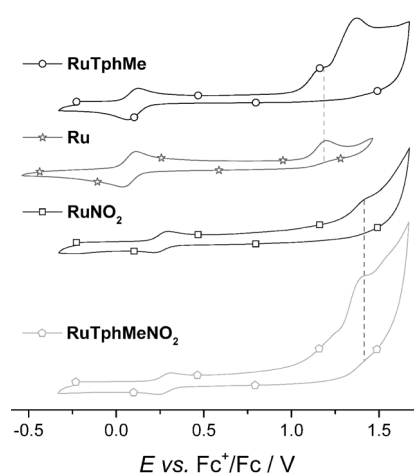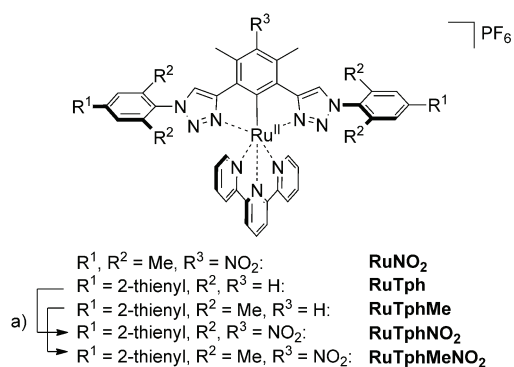

Figure 2. Cyclic voltammograms depicting the oxidation processes of **RuTphMe** and **RuTphMeNO₂** in comparison with the parent **Ru** and **RuNO₂** (10^{-4} M in CH_3CN with 0.1 M Bu_4NPF_6).

The nitro group was attached directly on the cyclometalating phenyl ring using $Cu(NO_3)_2$ (Scheme 2). Here, the common Menke conditions[4a, 22] had to be attenuated to prevent the nitration of the thiophene moiety.[23] In fact, even if a high excess of $Cu(NO_3)_2$ is used in dichloromethane/methanol as a solvent mixture, only the nitration on the cyclometalating phenyl ring is observed, which underlines the high reactivity in the position *para* to the carbanion and, conversely, the ease of manipulating the carbanion donation in cyclometalated com-

Figure 1. CV development during electropolymerization attempt for **RuTphMe** in CH_2Cl_2 (10^{-4} M with 0.1 M Bu_4NPF_6).

Scheme 2. Synthesis of the nitro-functionalized thiophene-containing cyclo-metalated ruthenium(II) complexes: a) Cu(NO$_3$)$_2$, CH$_2$Cl$_2$/MeOH (2:1 to 3:1), RT, 96 h, 67 to 85%. **RuNO$_2$** was prepared previously in an analogous synthesis.[4a]

plexes. The pure complexes were obtained after counterion exchange to hexafluorophosphate and crystallization through vapor diffusion of diethyl ether into a concentrated DMF solution. The desired nitro-functionalization was proven unambiguously by single-crystal X-ray diffraction in case of **RuTphMeNO$_2$** (Figure 3).[24] The bond lengths and bite angles as well as the dihedral angles of the nitro group relative to the central
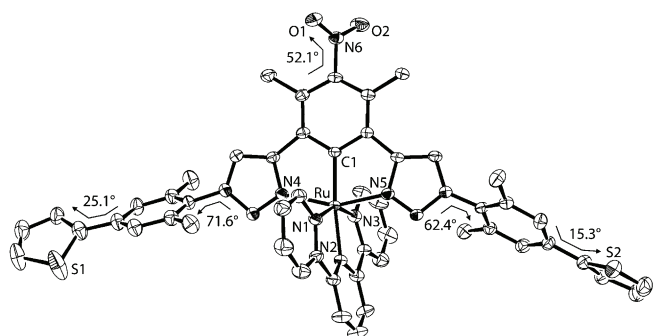
Figure 3. ORTEP plot[24] of **RuTphMeNO$_2$**: thermal ellipsoids drawn at 50% probability level; solvent molecules, counterion, and hydrogen atoms omitted for clarity. Disorder of a thiophene omitted for clarity. Selected bond lengths (Å) and angles (°): Ru–C1, 1.981(4); Ru–N1, 2.085(4); Ru–N2, 2.032(3); Ru–N3, 2.075(4); Ru–N4, 2.082(3); Ru–N5, 2.052(3); N4-Ru-N5, 155.56(13); N1-Ru-N3, 155.89(14).

phenyl ring (52°) and of the mesityl ring relative to the triazole (62–72°) are comparable to the previously reported crystallographic data.[4a] Accordingly, the electron-withdrawing character of the nitro group is attenuated, and the π conjugation between the complex and the *N*-substituents of the triazole is broken. Note also that the π conjugation into the triazoles for **RuTph** is only weak as indicated by DFT calculations (vide infra), which is in line with the literature reports.[17] On the other hand, the small torsion between thiophene and mesityl allows extended conjugation, which may give rise to an additional chromophore after the electropolymerization (vide infra). In addition, a bromo function was introduced to the central phenyl

ring of **RuTph** by using CuBr$_2$ in dichloromethane/methanol,[25] with the aim of blocking the reactive *para* position of the central phenyl ring, but maintaining the oxidation potential at a reasonably constant value. However, as for the nonbrominated species, the electropolymerization control experiments resulted in nondefined electrochemical processes (see Figure S50, Supporting Information), thus ruling out potential side reactions that are related to the reactive position *para* to the carbanion.

Electrochemical characterization of **RuTphMeNO$_2$** and **RuTphNO$_2$** showed that both the first oxidation and first reduction potentials are shifted anodically by about 200 mV (see Table 1) because of the electron-withdrawing influence of the nitro group. As for their nitro-free counterparts, the first, reversible anodic signal is assigned to oxidation of the ruthenium(II)/cyclometalating-ligand moiety.[4a] Importantly, as intended, the second oxidation is achieved more easily than the irreversible oxidation of the parent **RuNO$_2$** complex (see Figure 2). Hence, this redox process is assigned to the thienyl-based oxidation, which should, in turn, enable electrochemical polymerization without decomposition. In contrast to the preceding complexes, the first reduction is reversible, and a further process occurs at −2.10 V.

In addition, DFT calculations were executed to examine the energies and spin-density distributions of the singly and doubly oxidized states of the four complexes (see Figure 4 and Figures S68 to S77 in the Supporting Information). First, the assignment of the first oxidation to a metal- and cyclometalating-ligand-based process is confirmed for all the complexes. The second oxidation process may formally lead to a singlet or triplet state, depending on whether the removed electron has
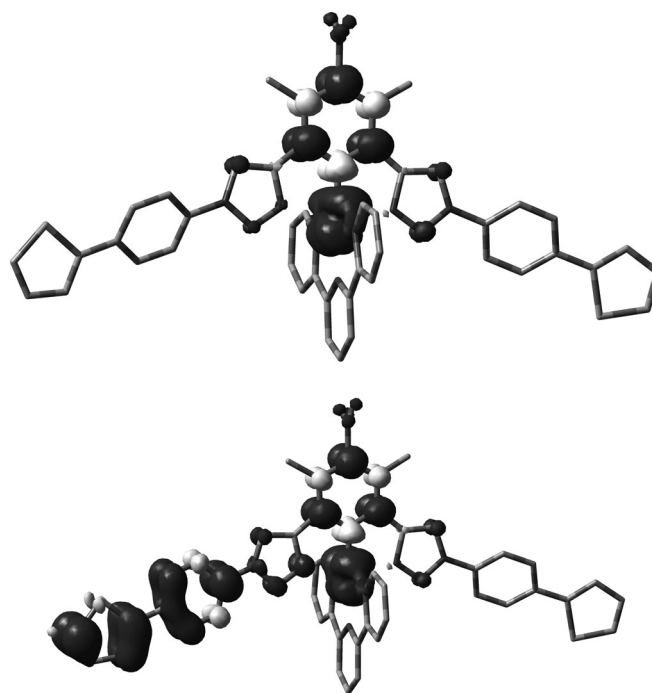

Figure 4. Spin density of singly oxidized (top) and doubly oxidized triplet (bottom) states of **RuTphNO$_2$** (dark and light regions indicate excess of alpha and beta spin, respectively; iso value 0.002).

alpha or beta spin, respectively. The singlet (closed shell) configuration affords a metal–cyclometalating-ligand-based oxidation, which requires a potential that is shifted anodically by 1.33 to 1.55 V in comparison with the first oxidation process. Whereas the triplet configuration of the parent complexes **Ru** and **RuNO$_2$** displays a small stabilization relative to the singlet configuration, the thiophene-containing complexes reveal the localization of the second spin on one phenylthienyl unit, causing a potential difference of only 0.80 to 1.15 V compared with the first oxidation. Notably, the computed second oxidation should be regarded as an upper limit, considering the artificial stabilization of extended π-systems,[26] the effect of the surrounding charges,[27] and the challenges involved in treating spin–spin interactions accurately,[28] which become particularly important in strongly coupled open-shell systems.[29] The introduction of the nitro substituent leads to an anodic shift of the calculated metal–cyclometalating-ligand-based redox potentials by approximately 0.25 V, whereas the thiophene-based oxidation remains almost unchanged. Hence, the calculations support the observed electrochemical behavior of the systems upon nitration, but cannot definitely support the electrochemical decomposition of the thiophene-equipped complexes through an irreversible oxidation of the central complex fragment. However, the observed deviations between experimental data and calculations for the model complex **Ru**, namely the difference for the second oxidation, must also be taken into account for the thiophene-functionalized complexes.

The electropolymerization of **RuTphMeNO$_2$** in dichloromethane was studied, and the respective cyclic voltammograms are shown in Figure 5. The peak current of the first oxidation of the complex increases during the first five to ten cycles, as
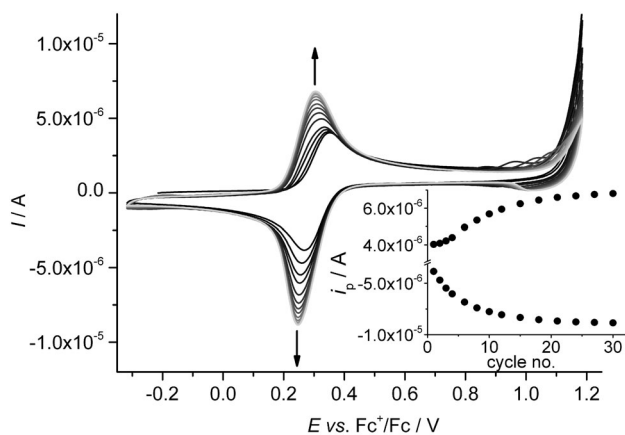

Figure 6. CVs of **RuTphMeNO$_2$** films showing the first oxidation process at different scan rates. Inset: Relationship between peak currents and applied scan rate. (Film on glassy-carbon disk electrode in CH$_2$Cl$_2$ with 0.1 M Bu$_4$NPF$_6$.)

voltammetry (depicted in Figure 6) and UV/Vis spectroscopy (vide infra) was possible. The CV shows a reversible first oxidation with a half-wave potential of 0.28 V, which is slightly shifted cathodically compared with the dissolved monomer complex. Furthermore, the peak current grows linearly with increasing scan rate up to 500 mV s^{-1}, indicating the formation of conductive films with only weakly diffusion-controlled charge migration.[10,31]

In a similar manner, anodic polymerization was also attempted for the nonmethylated congener **RuTphNO$_2$**. Notably, only relatively low concentrations (around 50 µg mL^{-1} or 5×10^{-5} M) could be applied because of the poor solubility of the complex. However, in contrast to its methylated counterpart, a linear increase with a steady slope of the monitored peak current was observed within the 30 cycles conducted (Figure 7),[32] and a surface coverage of $\Gamma = 2 \times 10^{-9}$ mol cm^{-2} was obtained. Additional signals appeared at 0.45 and −0.05 V, which are tentatively assigned to radicals that were not incorporated into the polymer. Comparable features had already been observed in former electropolymerization studies.[19] The

Figure 5. CV and peak-current development during the electropolymerization of **RuTphMeNO$_2$** in CH$_2$Cl$_2$ (10^{-4} M with 0.1 M Bu$_4$NPF$_6$).

expected for a successful electropolymerization. However, the slope is comparatively low, indicating a low polymerization rate, and decreases afterwards, reaching a plateau at the twentieth cycle.[30] Hence, the obtained films are very thin (the apparent surface coverage was determined to be only $\Gamma = 1 \times 10^{-9}$ mol cm^{-2}). Nevertheless, their characterization by cyclic
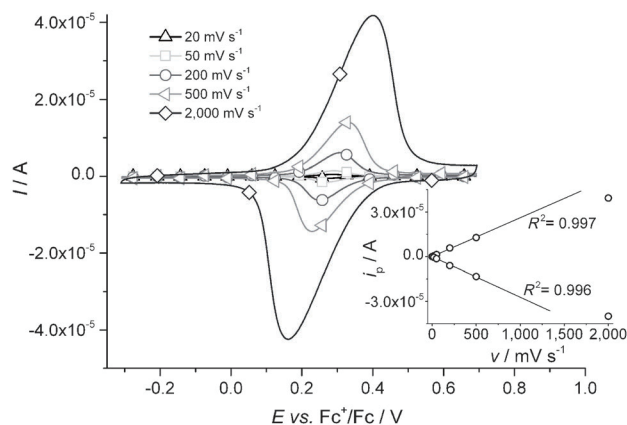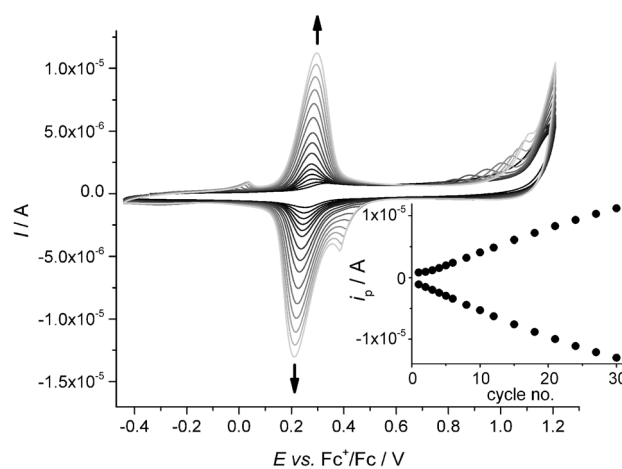

Figure 7. CV and peak-current development during the electropolymerization of **RuTphNO$_2$** in CH$_2$Cl$_2$ (10^{-5} M with 0.1 M Bu$_4$NPF$_6$).

CVs of the obtained thin polymer films displayed a reversible redox signal at 0.25 V, which is slightly shifted cathodically with respect to both its corresponding monomer and the **RuTphMeNO$_2$** polymer film. As for the latter, the peak-current/scan-rate relationship shows linear behavior up to 500 mVs^{-1} (Figure 8). Notably, the accompanying signals at 0.45 and −0.05 V are not present in the film CVs, supporting their assignment to species that were not incorporated.
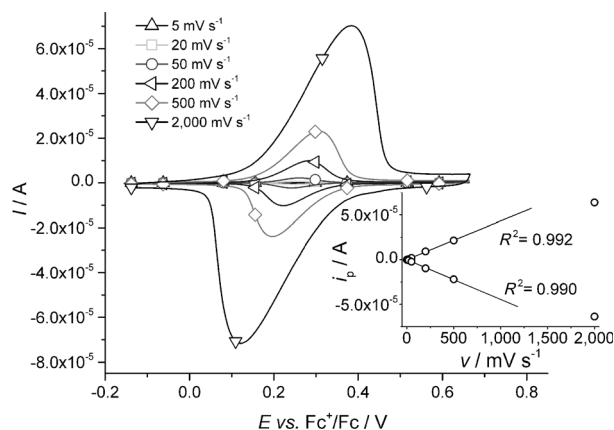

Figure 8. CVs of **RuTphNO$_2$** films showing the first oxidation process at different scan rates. Inset: Relationship between peak currents and applied scan rate. (Film on glassy-carbon disk electrode in CH$_2$Cl$_2$ with 0.1 M Bu$_4$NPF$_6$.)

In addition, electropolymerization studies on the nitro-functionalized complexes using higher vertex potentials were performed, which resulted in a nondefined reaction process, as already observed for the non-nitro species (Figures S52 and S53, Supporting Information). Thus, the enhanced electropolymerization ability upon nitro-functionalization can indeed be attributed to shifted redox potentials, but not to a blocking of reactive sites.

Copolymerization experiments

For further enhancement of the electropolymerization performance of the **RuTphMeNO$_2$** complex, copolymerization with 3,4-ethylenedioxythiophene (EDOT) as a co-monomer was attempted. The ruthenium(II) complexes are diluted within the resulting copolymers, thus undesirable side reactions between the metal complexes are expected to be diminished. Hence, different complex/EDOT ratios were used to identify the EDOT content that leads to improved electropolymerization. The resulting CVs during the potentiodynamic anodic polymerization experiments are shown for a molar ratio of 1:1 in Figure 9 (see Figure S54 for ratios of 5:1, 2:1, and 1:5). With a 5:1 ratio, no improvement in the polymerization process is noticeable at all. As for the pure complex, the peak-current development shows an interruption around the fifteenth cycle. However, an additional plateau arises between −0.2 and 0.6 V, which is assigned to the formation of poly(3,4-ethylenedioxythiophene) (PEDOT) chains (see Figure S58 for comparison). For a molar ratio of 2:1, enhanced PEDOT generation is observable, but the slope
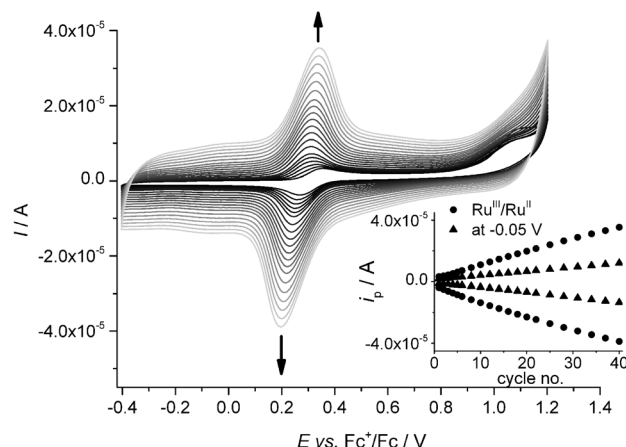

Figure 9. CV and peak-current development during the co-electropolymerization of **RuTphMeNO$_2$** with EDOT in CH$_2$Cl$_2$ (10^{-4} M with 0.1 M Bu$_4$NPF$_6$) using a molar ratio of 1:1.

of the Ru^{III}/Ru^{II}-based peak-current increase is still reduced after 15 cycles, and the further current development parallels the pure PEDOT-based one. This indicates that only PEDOT is formed from that cycle on, and that the ruthenium(II) complex is no longer included. Eventually, an increase in the EDOT molar ratio to 1:1 leads to significantly improved polymerization. The Ru^{III}/Ru^{II}-related current increases linearly at least up to the fortieth cycle with a larger slope than the PEDOT-related current, indicating that the ruthenium(II) moiety is still incorporated into the generated copolymer. A similar behavior was observed for an excess of EDOT, namely for a ruthenium(II)-complex/EDOT ratio of 1:5, with a higher current for the PEDOT-related background, as expected. In this way, copolymer films containing the cyclometalated ruthenium(II) complex were prepared and characterized. Cyclic voltammetry revealed a reversible oxidation process for both the 1:1 and 1:5 copolymers at around 0.27 V accompanied by a broad, undefined redox current assigned to the electrochemical doping of PEDOT chains. In both cases, the peak-current/scan-rate relationship is linear up to 500 mVs^{-1} (Figures 10 and S56), and apparent surface coverages of 5×10^{-9} and 8×10^{-9} mol cm^{-2} (with respect to the complex moieties) were determined for the 1:1 and 1:5 ratios, respectively.

As for its methylated analogue, copolymers of **RuTphNO$_2$** and EDOT were prepared electrochemically with molar ratios of 1:1 and 1:5 (see Figure S55, Supporting Information). For the equimolar ratio, only marginal differences, namely a small current plateau between −0.2 and 0.5 V, occur in comparison with the homopolymerization. This behavior can probably be attributed to the very low concentration (below 10^{-4} M) of EDOT, which is required because of the low complex solubility. In contrast, a fivefold EDOT excess leads to the distinct formation of PEDOT moieties, as indicated by the development of a broad current plateau. As for **RuTphMeNO$_2$**, the peak current corresponding to the Ru^{III}/Ru^{II} redox couple increases faster than the subjacent PEDOT-related current, showing that both the ruthenium(II) complex and EDOT are copolymerized. Subsequent electrochemical characterization confirmed these find-
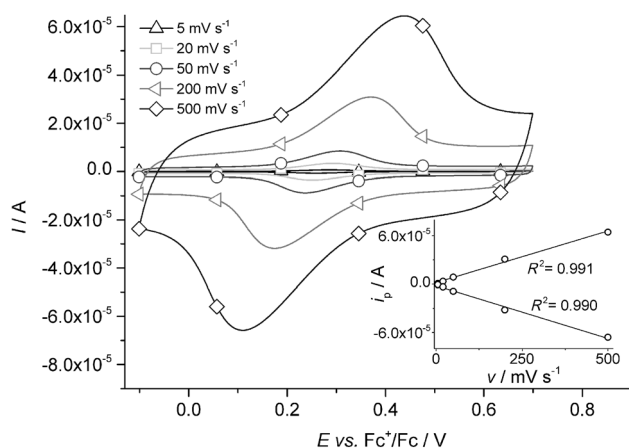
Figure 10. CVs of electropolymerized copolymer films from **RuTphMeNO$_2$** and EDOT showing the first oxidation process at different scan rates and relationship between peak currents and applied scan rate (films on glassy-carbon disk electrode in CH$_2$Cl$_2$ with 0.1 M Bu$_4$NPF$_6$) for a molar ratio of 1:1.

ings. The cyclic voltammogram of the 1:1 polymer (Figure S57, Supporting Information) resembles in principle the homopolymer with only small deviations, whereas the films from the higher EDOT ratio show significant PEDOT influence, that is, a broad, underlying current plateau. Analysis of the Ru^{III}/Ru^{II}-related current revealed an apparent surface coverage of approximately 2×10^{-9} mol cm^{-2} in both cases.

UV/Vis spectroscopy and UV/Vis/NIR spectroelectrochemistry

The UV/Vis absorption and emission features of the monomer complexes are depicted in Table 2 and the Supporting Information (Figure S59). The absorption spectra exhibit a set of bands

Table 2. UV/Vis spectroscopic characteristics of the monomer complexes (10^{-6} M in CH$_2$Cl$_2$).

Complex	λ_{Abs} [nm] (ε [10^3 M^{-1} cm^{-1}])[a]	λ_{Em} [nm]
RuTph	685s (0.7), 586s (5.0), 533 (9.5), 491 (11.0), 388 (43.8)	733
RuTphMe	689s (0.8), 590s (5.5), 536 (10.5), 491 (12.8), 372 (32.1)	743
RuTphNO$_2$	645s (0.7), 570s (4.0), 507 (11.8), 479 (13.7), 389 (36.3)	689
RuTphMeNO$_2$	642s (0.7), 560s (5.6), 515 (14.3), 482 (16.5), 361 (26.1)	690
[a] s: shoulder.		

between 450 and 700 nm, which are assigned to metal-to-ligand and metal/ligand-to-ligand charge-transfer (MLCT and MLLCT, respectively) transitions.[4a] The introduction of nitro groups causes a blueshift of these bands owing to the electron-withdrawing nature of the nitro group, which gives rise to a stabilization of the HOMOs, located on the cyclometalating ligand and the metal.[4a] An additional band can be found at around 400 nm. Here, the introduction of methyl groups at the

phenyl spacer moieties causes a hypsochromic shift as well as a decreasing extinction coefficient. This is probably because of diminished π conjugation within the triazole-phenyl fragment owing to steric hindrance by the methyl groups, precluding coplanarization. Emission measurements revealed room-temperature photoluminescence at around 740 nm for the nitro-free **RuTph** and **RuTphMe**, whereas the emission maxima for the nitro-substituted species are, as expected, blueshifted by about 900 to 1000 cm^{-1}.

Comparison of the UV/Vis absorption spectrum of the **RuTphMeNO$_2$** polymer film with that of the monomer complex shows only a negligible redshift of the MLCT maximum of 110 cm^{-1} from 520 nm for the dropcasted monomer film to 523 nm for the polymer, accompanied by a broadening and a loss of structural features for the MLCT band (Figure 11, top). Additionally, an intense peak arises at 341 nm, which is assigned to $\pi\pi^*$ transitions that are located on the bis(phenylth-
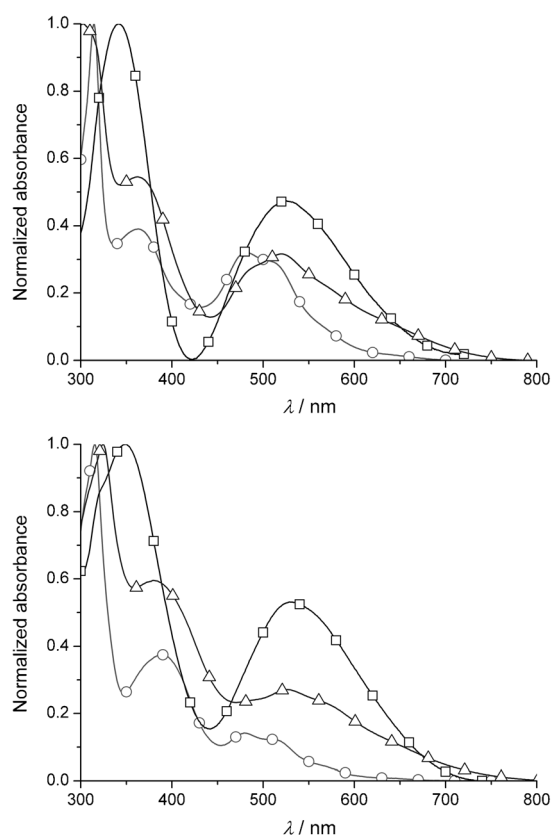

Figure 11. UV/Vis absorption spectra of electropolymerized films (□) from **RuTphMeNO$_2$** (top) and **RuTphNO$_2$** (bottom) in comparison with the dropcasted monomer (△) (films on ITO-coated glass) and the dissolved monomer (○) (10^{-6} M in CH$_2$Cl$_2$).

ienyl) moiety,[33] which is present in the polymer but not in the monomer, and thus confirms the coupling of the monomer complexes. Unfortunately, spectroelectrochemical investigations could not be executed because the obtained films were too thin to give an observable absorption signal within the used setup.

For the polymer film from **RuTphNO$_2$**, the UV/Vis absorption results exhibit a prominent, MLCT-based band at 531 nm,

slightly redshifted by 220 cm⁻¹ with respect to the monomer film (525 nm) (Figure 11, bottom) and by 290 cm⁻¹ compared with the methylated analogue, suggesting a higher degree of conjugation in the nonmethylated polymer. Likewise, the additional band that is present in the UV region, assigned to bis(phenylthienyl) units[33] formed through the polymerization, is redshifted by 590 cm⁻¹ to 348 nm. Furthermore, UV/Vis/NIR spectroelectrochemical studies on the polymer film were performed and an example is shown in Figure 12. The spectral
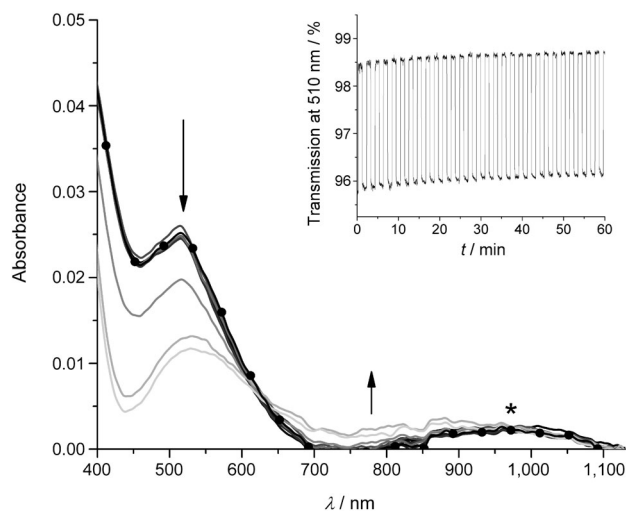

Figure 12. Change in the UV/Vis absorption spectrum of an electropolymerized film of **RuTphNO₂** during the oxidation and re-reduction (●) process. (Note that the underlying absorbance between 800 an 1100 nm (*) is attributed to the ITO substrate.) Inset: Change of transmission at 510 nm over 30 cycles of switching between initial and oxidized state. (Film on ITO-coated glass in CH₂Cl₂ with 0.1 M Bu₄NPF₆.)

changes during the oxidation process with a half-wave potential of 0.25 V resemble in principle the characteristic features observed for the present cyclometalated ruthenium(II) complex moiety, namely a bleaching of the MLCT absorption and the rise of a broad and weak band between 700 and 900 nm, which is assigned to ligand-to-metal charge-transfer (LMCT) transitions.[4a] Repeated switching between the initial and oxidized state turned out to be reversible for at least the 30 cycles that were run, proving the redox stability of the prepared polymer film, and revealed switching times (defined as the time necessary to undergo 95% of the full transmission change[34]) of 1.8 s.

The UV/Vis absorption spectra of the 1:1 and 1:5 copolymer films of **RuTphMeNO₂** show absorption maxima at 523 nm and 341 nm, accompanied by a broad band in the NIR region (see Figure S60, Supporting Information). With increasing EDOT ratio, the relative intensity of the latter rises; this is attributed to the growing content of PEDOT moieties, which exhibit a strong NIR absorption (see Figure S62 for comparison). Simultaneously, the band at 341 nm, which is related to the bis(phenylthienyl) moieties, decreases with respect to the MLCT absorption because the bis(thienyl) bridges are replaced by oligo-EDOT blocks for the copolymers. UV/Vis/NIR spectroelec-

trochemical studies of the copolymer films showed a combination of **Ru** and PEDOT characteristics (see Figures S63 to S66, Supporting Information): The disappearance of the MLCT band between 400 and 600 nm, and the rise of a broad, intense band in the NIR region, respectively. In the long-wavelength visible-light region, the behavior of the metal complex, that is, the formation of a new LMCT absorption band, is dominant. Notably, for the 1:1 copolymer, the PEDOT-based NIR absorption is blueshifted with respect to the 1:5 copolymer, indicating the presence of shorter oligo-EDOT chains, which possess a smaller conjugated π system, whereas the 1:5 system exhibits an NIR absorption maximum similar to the pure PEDOT reference, indicating that the maximum conjugation length is already achieved. The application of a re-reducing potential led to the recovery of the initial spectrum in both cases, and similarly, monitoring of the UV/Vis transmission while repeatedly changing between the oxidizing and re-reducing potentials showed a reversible redox switchability for at least 30 cycles.

The UV/Vis absorption spectrum of the **RuTphNO₂** 1:1 copolymer (see Figure S61, Supporting Information) is basically the same as that of the homopolymer. In contrast, the film of the 1:5 copolymer shows an enhanced absorption in the NIR region, characteristic of PEDOT. Remarkably, in contrast to its methylated counterpart, a notable redshift of 1300 cm⁻¹ between the homopolymer and the 1:5 copolymer appears for the absorption band around 520 nm, due to an overlap with the PEDOT-based absorption (see Figure S67, Supporting Information). UV/Vis/NIR spectroelectrochemical studies on the copolymer films revealed the typical spectral changes during oxidation. For the 1:1 copolymer, as soon as the oxidation of the metal center begins, the MLCT absorption band at around 500 nm vanishes, whereas a very broad, weak absorption arises beyond 600 nm. In contrast to the homopolymer (vide supra), the latter spans the region up to 1600 nm, and is attributed to the incorporated oligo-EDOT chains. However, their influence is significantly smaller than for the 1:1 copolymer of the methylated analog. An isosbestic point at 590 nm, which is not present for the other copolymer studies, supports the presence of only one electro-optically determinant species, namely the ruthenium(II) complex, whereas the other copolymers show significant features of both metal complex and PEDOT. In the case of the 1:5 copolymer, both the metal complex moiety and PEDOT chains determine the spectra; a decrease in the complex MLCT absorption between 400 and 600 nm is accompanied by the emergence of a strong NIR absorption peaking at 1350 nm. Re-reduction of the 1:1 and 1:5 copolymer films recovered the initial UV/Vis/NIR absorption spectra, demonstrating the redox stability of the systems. However, for the 1:5 copolymer, repetitive switching of the redox state over 30 cycles showed a diminishing of the maximum absorption change to 95% of the initial value, which could not be observed for the other systems.

Conclusion

Oxidative electrochemical polymerization can be applied successfully to incorporate electron-rich ruthenium(II) complexes

of cyclometalating, 1,2,3-triazole-based polypyridyl-type ligands equipped with electropolymerizable thiophene moieties into polymeric thin-film coatings. The use of nonfunctionalized thiophene-containing complexes leads to decomposition reactions during the electropolymerization process, which are attributed to an irreversible second oxidation of the electron-rich central complex fragment. The subsequent selective introduction of a nitro group at the phenyl ring causes an anodic shift of the decomposition-related redox potential, but not of the thiophene-assigned one. Hence, the maximum potential during the potentiodynamic polymerization can be chosen such that the generation of thienyl radicals, which are crucial for the formation of the polymer chains, is possible, without degradation of the complex fragment. The problem of undesired side reactions is expected to be a general issue for the oxidative electropolymerization of cyclometalated complexes, so this approach is believed to be a generally applicable strategy for the processing of cyclometalated ruthenium(II)-polypyridyl systems. Alternatively, the incorporation of 3,4-ethylenedioxythiophene (EDOT) moieties instead of the thiophene groups into the ruthenium(II) complex represents a possible future approach for an improved electropolymerization, because the oxidation potential required for radical formation would be lowered. Besides modifications of the metal complexes themselves, an additional comonomer can be used to enhance the polymerization performance further. Consequently, EDOT was utilized to form copolymers with different monomer ratios.

The obtained homopolymer films show UV/Vis absorption up to 700 nm as well as stable redox switchability associated with electrochromicity. The copolymers exhibit UV/Vis absorption that is expanded to the NIR region, which is attributed to the incorporated oligo-/poly-EDOT chains, as well as reversible electrochemical and spectroelectrochemical behavior, reflecting the mixed characteristics of the ruthenium(II) and EDOT moieties.

In summary, a method has been presented for the generation of conductive photo-redox-active and -stable films featuring a low energy gap, which are believed to have great potential for applications in photovoltaic and electrochromic devices.

Experimental Section

General methods, detailed synthetic procedures, and further electrochemical and photophysical data can be found in the Supporting Information. CCDC-929252 (**HTphMe**), 929253 ([Ru^{II}(tpy)-(CH$_3$CN)$_3$][BF$_4$]$_2$), and 929254 (**RuTphMeNO$_2$**) contain the supplementary crystallographic data for this paper. These data can be obtained free of charge from The Cambridge Crystallographic Data Centre via www.ccdc.cam.ac.uk/data_request/cif.

Acknowledgements

[1] a) J.-P. Sauvage, J.-P. Collin, J.-C. Chambron, S. Guillerez, C. Coudret, V. Balzani, F. Barigelletti, L. De Cola, L. Flamigni, *Chem. Rev.* **1994**, *94*, 993–1019; b) A. Juris, V. Balzani, F. Barigelletti, S. Campagna, P. Belser, A. von Zelewsky, *Coord. Chem. Rev.* **1988**, *84*, 85–277; c) T. J. Meyer, *Pure Appl. Chem.* **1986**, *58*, 1193–1206.

[2] K. Kalyanasundaram, M. Grätzel, *Coord. Chem. Rev.* **1998**, *177*, 347–414.

[3] a) A. Hagfeldt, G. Boschloo, L. Sun, L. Kloo, H. Pettersson, *Chem. Rev.* **2010**, *110*, 6595–6663; b) H. Tributsch, *Coord. Chem. Rev.* **2004**, *248*, 1511–1530; c) M. K. Nazeeruddin, P. Péchy, T. Renouard, S. M. Zakeeruddin, R. Humphry-Baker, P. Comte, P. Liska, L. Cevey, E. Costa, V. Shklover, L. Spiccia, G. B. Deacon, C. A. Bignozzi, M. Grätzel, *J. Am. Chem. Soc.* **2001**, *123*, 1613–1624; d) M. K. Nazeeruddin, A. Kay, I. Rodicio, R. Humphry-Baker, E. Müller, P. Liska, N. Vlachopoulos, M. Grätzel, *J. Am. Chem. Soc.* **1993**, *115*, 6382–6390; e) B. O'Regan, M. Grätzel, *Nature* **1991**, *353*, 737–740.

[4] a) B. Schulze, D. Escudero, C. Friebe, R. Siebert, H. Görls, S. Sinn, M. Thomas, S. Mai, J. Popp, B. Dietzek, L. González, U. S. Schubert, *Chem. Eur. J.* **2012**, *18*, 4010–4025; b) K. C. D. Robson, B. D. Koivisto, A. Yella, B. Sporinova, M. K. Nazeeruddin, T. Baumgartner, M. Grätzel, C. P. Berlinguette, *Inorg. Chem.* **2011**, *50*, 5494–5508; c) P. G. Bomben, T. J. Gordon, E. Schott, C. P. Berlinguette, *Angew. Chem.* **2011**, *123*, 10870–10873; *Angew. Chem. Int. Ed.* **2011**, *50*, 10682–10685; d) T. Bessho, E. Yoneda, J.-H. Yum, M. Guglielmi, I. Tavernelli, H. Imai, U. Rothlisberger, M. K. Nazeeruddin, M. Grätzel, *J. Am. Chem. Soc.* **2009**, *131*, 5930–5934; e) Y. Eiji, M. Grätzel, M. K. Nazeeruddin, Eur. Pat. Appl., EP 2036955, **2009**; f) S. H. Wadman, J. M. Kroon, K. Bakker, M. Lutz, A. L. Spek, G. P. M. van Klink, G. van Koten, *Chem. Commun.* **2007**, 1907–1909.

[5] a) C.-C. Chou, K.-L. Wu, Y. Chi, W.-P. Hu, S. J. Yu, G.-H. Lee, C.-L. Lin, P.-T. Chou, *Angew. Chem.* **2011**, *123*, 2102–2106; *Angew. Chem. Int. Ed.* **2011**, *50*, 2054–2058; b) K.-L. Wu, H.-C. Hsu, K. Chen, Y. Chi, M.-W. Chung, W.-H. Liu, P.-T. Chou, *Chem. Commun.* **2010**, *46*, 5124–5126.

[6] a) H.-J. Park, K. H. Kim, S. Y. Choi, H.-M. Kim, W. I. Lee, Y. K. Kang, Y. K. Chung, *Inorg. Chem.* **2010**, *49*, 7340–7352; b) S. U. Son, K. H. Park, Y.-S. Lee, B. Y. Kim, C. H. Choi, M. S. Lah, Y. H. Jang, D.-J. Jang, Y. K. Chung, *Inorg. Chem.* **2004**, *43*, 6896–6898.

[7] a) D. G. Brown, N. Sanguantrakun, B. Schulze, U. S. Schubert, C. P. Berlinguette, *J. Am. Chem. Soc.* **2012**, *134*, 12354–12357; b) B. Schulze, D. Escudero, C. Friebe, R. Siebert, H. Görls, U. Köhn, E. Altuntas, A. Baumgaertel, M. D. Hager, A. Winter, B. Dietzek, J. Popp, L. González, U. S. Schubert, *Chem. Eur. J.* **2011**, *17*, 5494–5498; c) O. Schuster, L. Yang, H. G. Raubenheimer, M. Albrecht, *Chem. Rev.* **2009**, *109*, 3445–3478.

[8] a) J. E. Hein, V. V. Fokin, *Chem. Soc. Rev.* **2010**, *39*, 1302–1315; b) M. Meldal, C. W. Tornøe, *Chem. Rev.* **2008**, *108*, 2952–3015.

[9] a) B. Schulze, D. G. Brown, K. C. D. Robson, C. Friebe, M. Jäger, E. Birckner, C. P. Berlinguette, U. S. Schubert, *Chem. Eur. J.* **2013**, *19*, 14171–14180; b) W. Yang, Y. Zhong, *Chin. J. Chem.* **2013**, *31*, 329–338; c) W.-W. Yang, L. Wang, Y.-W. Zhong, J. Yao, *Organometallics* **2011**, *30*, 2236–2240.

[10] J. Heinze, B. A. Frontana-Uribe, S. Ludwigs, *Chem. Rev.* **2010**, *110*, 4724–4771.

[11] a) X. J. Zhu, B. J. Holliday, *Macromol. Rapid Commun.* **2010**, *31*, 904–909; b) J. Hjelm, R. W. Handel, A. Hagfeldt, E. C. Constable, C. E. Housecroft, R. J. Forster, *Inorg. Chem.* **2005**, *44*, 1073–1081; c) J. A. Moss, J. C. Yang, J. M. Stipkala, X. Wen, C. A. Bignozzi, G. J. Meyer, T. J. Meyer, *Inorg. Chem.* **2004**, *43*, 1784–1792; d) R. M. Leasure, T. Kajita, T. J. Meyer, *Inorg. Chem.* **1996**, *35*, 5962–5963; e) C. P. Horwitz, Q. Zuo, *Inorg. Chem.* **1992**, *31*, 1607–1613; f) T. F. Guarr, F. C. Anson, *J. Phys. Chem.* **1987**, *91*, 4037–4043; g) C. D. Ellis, L. D. Margerum, R. W. Murray, T. J. Meyer, *Inorg.*

Chem. **1983**, *22*, 1283 – 1291; h) P. Denisevich, H. D. Abruña, C. R. Leidner, T. J. Meyer, R. W. Murray, *Inorg. Chem.* **1982**, *21*, 2153 – 2161.

[12] a) C.-J. Yao, J. Yao, Y.-W. Zhong, *Inorg. Chem.* **2012**, *51*, 6259 – 6263; b) C.-J. Yao, Y.-W. Zhong, H.-J. Nie, H. D. Abruña, J. Yao, *J. Am. Chem. Soc.* **2011**, *133*, 20720 – 20723.

[13] C.-J. Yao, Y.-W. Zhong, J. Yao, *Inorg. Chem.* **2013**, *52*, 10000 – 10008.

[14] a) C. Friebe, M. D. Hager, A. Winter, U. S. Schubert, *Adv. Mater.* **2012**, *24*, 332 – 345; b) W. K. Chan, *Coord. Chem. Rev.* **2007**, *251*, 2104 – 2118; c) M. O. Wolf, *J. Inorg. Organomet. Polym. Mater.* **2006**, *16*, 189 – 199; d) Y. Liu, Y. Li, K. S. Schanze, *J. Photochem. Photobiol. C* **2002**, *3*, 1 – 23; e) T. Hirao, *Coord. Chem. Rev.* **2002**, *226*, 81 – 91; f) P. G. Pickup, *J. Mater. Chem.* **1999**, *9*, 1641 – 1653.

[15] K. Hu, K. C. D. Robson, P. G. Johansson, C. P. Berlinguette, G. J. Meyer, *J. Am. Chem. Soc.* **2012**, *134*, 8352 – 8355.

[16] a) W.-W. Yang, J. Yao, Y.-W. Zhong, *Organometallics* **2012**, *31*, 1035 – 1041; b) M. Beley, S. Chodorowski, J.-P. Collin, J.-P. Sauvage, L. Flamigni, F. Barigelletti, *Inorg. Chem.* **1994**, *33*, 2543 – 2547; c) M. Beley, J.-P. Collin, R. Louis, B. Metz, J.-P. Sauvage, *J. Am. Chem. Soc.* **1991**, *113*, 8521 – 8522.

[17] a) S. Potratz, A. Mishra, P. Bäuerle, *Beilstein J. Org. Chem.* **2012**, *8*, 683 – 692; b) I. Stengel, C. A. Strassert, E. A. Plummer, C.-H. Chien, L. De Cola, P. Bäuerle, *Eur. J. Inorg. Chem.* **2012**, 1795 – 1809; c) A. Wild, C. Friebe, A. Winter, M. D. Hager, U.-W. Grummt, U. S. Schubert, *Eur. J. Org. Chem.* **2010**, 1859 – 1868.

[18] J. D. Crowley, D. A. McMorran in *Click Triazoles: Topics in Heterocyclic Chemistry, Vol. 28* (Ed.: J. Košmrlj), Springer, Berlin/Heidelberg, **2012**, p. 31 – 83.

[19] C. Friebe, H. Görls, M. Jäger, U. S. Schubert, *Eur. J. Inorg. Chem.* **2013**, 4191 – 4202.

[20] M. Lamberti, G. C. Fortman, A. Poater, J. Broggi, A. M. Z. Slawin, L. Cavallo, S. P. Nolan, *Organometallics* **2012**, *31*, 756 – 767.

[21] a) W. Chen, G. Xue, *Prog. Polym. Sci.* **2005**, *30*, 783 – 811; b) S. Jin, G. Xue, *Macromolecules* **1997**, *30*, 5753 – 5757.

[22] M. Gagliardo, D. J. M. Snelders, P. A. Chase, R. J. M. Klein Gebbink, G. P. M. van Klink, G. van Koten, *Angew. Chem.* **2007**, *119*, 8710 – 8726; *Angew. Chem. Int. Ed.* **2007**, *46*, 8558 – 8573.

[23] A. R. Katritzky, E. F. V. Scriven, S. Majumder, R. G. Akhmedova, N. G. Akhmedov, A. V. Vakulenko, *ARKIVOC* **2005**, 179 – 191.

[24] L. J. Farrugia, *J. Appl. Crystallogr.* **1997**, *30*, 565.

[25] S. H. Wadman, R. W. A. Havenith, M. Lutz, A. L. Spek, G. P. M. van Klink, G. van Koten, *J. Am. Chem. Soc.* **2010**, *132*, 1914 – 1924.

[26] M. Lundberg, P. E. M. Siegbahn, *J. Chem. Phys.* **2005**, *122*, 224103.

[27] M. L. Naklicki, S. I. Gorelsky, W. Kaim, B. Sarkar, R. J. Crutchley, *Inorg. Chem.* **2012**, *51*, 1400 – 1407.

[28] A. J. Cohen, P. Mori-Sánchez, W. Yang, *Science* **2008**, *321*, 792 – 794.

[29] D. H. Ess, T. C. Cook, *J. Phys. Chem. A* **2012**, *116*, 4922 – 4929.

[30] Notably, it was observed that even small leftovers of DMF inhibit the electropolymerization. Hence, they had to be removed thoroughly by repeated suspension in CH_3CN or CH_2Cl_2 and subsequent precipitation with diethyl ether.

[31] A. J. Bard, L. R. Faulkner, *Electrochemical Methods*, 2nd ed., John Wiley & Sons, Inc., New York, **2001**.

[32] Note that comparative experiments with low concentrations for **RuTph-MeNO₂** resulted likewise in a limited polymerization ability as for the described studies with higher concentrations (see the Supporting Information).

[33] J. J. Apperloo, L. B. Groenendaal, H. Verheyen, M. Jayakannan, R. A. J. Janssen, A. Dkhissi, D. Beljonne, R. Lazzaroni, J.-L. Brédas, *Chem. Eur. J.* **2002**, *8*, 2384—2396.

[34] C. L. Gaupp, D. M. Welsh, R. D. Rauh, J. R. Reynolds, *Chem. Mater.* **2002**, *14*, 3964—3970.